

AD-A244 401



CONTRACTOR REPORT BRL-CR-678

BRL

RAREFACTION WAVE ELIMINATOR DESIGN STUDY

ROBERT L. GUICE
APPLIED RESEARCH ASSOCIATES

JAMES BUTZ
ADA TECHNOLOGIES, INC.

JAMES GOTTLIEB
UNIVERSITY OF TORONTO
INSTITUTE FOR AEROSPACE STUDIES

DTIC
ELECTE
JAN 13 1992
S B D

DECEMBER 1991

APPROVED FOR PUBLIC RELEASE; DISTRIBUTION IS UNLIMITED.

92-01025


U.S. ARMY LABORATORY COMMAND

BALLISTIC RESEARCH LABORATORY
ABERDEEN PROVING GROUND, MARYLAND

NOTICES

Destroy this report when it is no longer needed. DO NOT return it to the originator.

Additional copies of this report may be obtained from the National Technical Information Service, U.S. Department of Commerce, 5285 Port Royal Road, Springfield, VA 22161.

The findings of this report are not to be construed as an official Department of the Army position, unless so designated by other authorized documents.

The use of trade names or manufacturers' names in this report does not constitute indorsement of any commercial product.

UNCLASSIFIED

REPORT DOCUMENT PAGE			Form Approved OMB No. 0704-0188
Public reporting burden for this collection of information is estimated to average 1 hour per response, including the time for reviewing instructions, searching existing data sources, gathering and maintaining the data needed, and completing and reviewing the collection of information. Send comments regarding this burden estimate or any other aspect of this collection of information, including suggestions for reducing this burden, to Washington Headquarters Services, Directorate for Information Operations and Reports, 1215 Jefferson Davis Highway, Suite 1204, Arlington, VA 22202-4302, and to the Office of Management and Budget, Paperwork Reduction Project (0704-0188), Washington, DC 20503.			
1. AGENCY USE ONLY (Leave blank)	2. REPORT DATE December 1991	3. REPORT TYPE AND DATES COVERED Final 18 Sep 1987 to 15 Jul 1989	
4. TITLE AND SUBTITLE Rarefaction Wave Eliminator Design Study		5. FUNDING NUMBERS PR: 1L162120AH25	
6. AUTHOR(S) Robert L. Guice, James Butz*, James Gottlieb**		8. PERFORMING ORGANIZATION REPORT NUMBER 5462	
7. PERFORMING ORGANIZATION NAME(S) AND ADDRESS(ES) Applied Research Associates, Inc. 7114 W. Jefferson Ave., Suite 305 Lakewood, Colorado 80235			
9. SPONSORING/MONITORING AGENCY NAME(S) AND ADDRESS(ES) U.S. Army Ballistic Research Laboratory SLCBL-DD-T Aberdeen Proving Ground, Maryland 21005-5066		10. SPONSORING/MONITORING AGENCY REPORT NUMBER BRL-CR-678	
11. SUPPLEMENTARY NOTES Work performed under Contract No. DAAA15-87-C-0086 * James Butz of ADA Technologies, Inc.; **James Gottlieb of UTIAS			
12a. DISTRIBUTION/AVAILABILITY STATEMENT Approved for public release; distribution is unlimited.		12b. DISTRIBUTION CODE	
13. ABSTRACT (Maximum 200 words) Active and passive Rarefaction Wave Eliminators (RWE) were investigated for use on a small shock tube. An active RWE with rotation louvers for a modest size BRL shock tube was designed, with the open area versus time setting based on requirements from free-jet theory and the Random-Choice Method. This design yielded a device which met the operational requirements of completely closing within the 30 ms time duration of the positive phase of the simulated blast wave, and thereafter opened for the negative phase. The RWE was installed and tested at three blast wave overpressures. The results with the RWE are compared to those for both an open channel end and an extended channel on the shock tube, in order to evaluate the RWE performance. The experimental results showed that the preprogrammed theoretical area closing function was fairly accurate, especially at the lower overpressure levels. The predicted area setting is not accurate for the first few milliseconds after the shock arrives at the RWE, when the shock-induced outflow is inherently unsteady prior to the establishment of a semi quasi-steady jet outflow. Extrapolation of the small scale RWE design was made to the Large Blast and Thermal Simulator concept as well as the determination of preliminary costs.			
14. SUBJECT TERMS Unsteady Flow Blast Simulators Shock Tubes Gas Dynamics Computerized Simulation Fluid Dynamics Rarefaction Wave Elimination Wave Propagation Blast Waves		15. NUMBER OF PAGES 325	
17. SECURITY CLASSIFICATION OF REPORT UNCLASSIFIED		16. PRICE CODE	
		20. LIMITATION OF ABSTRACT UL	
18. SECURITY CLASSIFICATION OF THIS PAGE UNCLASSIFIED		19. SECURITY CLASSIFICATION OF ABSTRACT UNCLASSIFIED	

NSN 7540-01-280-5500

Standard Form 298 (Rev. 2-89)
Prescribed by ANSI Std. Z39-18 298-102

Best Available Copy UNCLASSIFIED

INTENTIONALLY LEFT BLANK.

TABLE OF CONTENTS

	<u>Page</u>
INTRODUCTION	1
BACKGROUND	9
OBJECTIVES	11
NUMERICAL PREDICTION OF BLAST-SIMULATOR FLOWS	13
Initial Geometrical Model of Blast Simulator	13
Revised Geometrical Model of the Blast Simulator	22
Equations Governing Blast-Simulator Flows	25
Discharge Coefficient for Louvered Reflection Eliminators	26
Numerical Solutions of Blast-Simulator Flows	37
1/57TH SCALE SHOCK TUBE DESCRIPTION	39
1/57TH SCALE RWE DESIGN	41
Approach	41
Louver Dimensions	41
Calculation of Power Requirements	43
Louver Stress	45
System Layout and Component Selection	46
1/57th SCALE RWE CONSTRUCTION	53
1/57th SCALE RWE OPERATION	61
Motion Control Algorithms	61
Preparation of Motion Profile Data Sets	61
Servomotor Control Software Development	64
EXPERIMENTAL PROGRAM	67
Shock Tube Calibration	67
Optical Tracker	70
RWE Tests	70
1/57th Scale Results	76
Design Modifications	81
FULL SCALE RWE DESIGN	83
Operational Description of the LB/TS	83
Selected Design	85
Rotating Louver Justification	86
Side Vent Configuration	87
Power Calculations and Impact on Design	87
Hydraulic Design Parameters	89
Structural Design	89

TABLE OF CONTENTS (continued)

	<u>Page</u>
FULL SCALE RWE DESIGN (continued)	
Optimization of the Louver Cross Section	90
Offset of Adjacent Louvers	94
Operating Mechanism	96
Structural Analysis	96
RWE Carriage	101
RWE Support Beams	101
Design of the Hydraulic Power System for the Full Scale RWE	104
Guidelines	104
Hydraulic Component Selection	105
Servo Actuator	105
Accumulator	107
Pump	107
Hydraulic Tubing	107
FULL SCALE RWE OPERATION	109
ESTIMATED FULL SCALE RWE COSTS	111
PASSIVE RWE DEVELOPMENT	113
CONCLUSIONS	115
RECOMMENDATIONS	117
REFERENCES	119
APPENDIX A - INITIAL RCM CALCULATIONAL RESULTS	121
APPENDIX B - IMPROVED DRIVER RCM CALCULATIONAL RESULTS	173
APPENDIX C - COMPARATIVE TEST RESULTS FROM SHOCK TUBE CALIBRATION AND RWE TESTS	209
APPENDIX D - TEST DATA AND RCM CALCULATION COMPARISONS	273
APPENDIX E - DISCHARGE COEFFICIENT FOR FLOWS THROUGH LOUVERS	299
APPENDIX F - LISTING OF THE ELIM CODE	309
APPENDIX G - CONSTRUCTION DRAWINGS AND PHOTOGRAPHS OF THE 1/57TH SCALE RWE	317

LIST OF FIGURES

<u>Figure</u>		<u>Page</u>
1	French (CEG) Large Blast Simulator (LBS) facility	2
2	U.S. Large Blast and Thermal Simulator (LB/TS) facility concept . .	3
3	Operational envelope of the RWE	4
4	Typical wave diagram in an open ended shock tube	6
5	Waveform comparisons	7
6	BRL 1/57th scale LB/TS geometry for unheated driver experiments . .	14
7	Expanded view of the throat section of the blast-wave simulator, showing the differences between the simulator drawing and model . .	15
8	Time histories at location 1.828 m	17
9	Time histories at location 2.295 m	18
10	Time histories at location 2.815 m	19
11	Time histories at location 6.139 m	20
12	Spatial distributions at time 0.000 to 180.000	21
13	Driver of the BRL 1/57 scale blast-wave simulator	23
14	RCM calculational results from modeled driver	24
15	Illustration of quasisteady flow through the louvers of the reflection eliminator	28
16	Illustration of the similarity between the flows through the louvers and the flows in ducts ending with a slot formed by an angled flap	29
17	Sketches of a subsonic jet (a), sonic jet (b), supersonic jet (c) from a sharp-edged slot or orifice at the end of a duct, showing the jet contraction	31
18	Sketches of an on-axis end jet (a), off-axis end jet (b), and off-axis side jet (c)	34
19	Contraction coefficient C_d as a function of the pressure ratio $1 - P_{atm}/P_s$ and the area ratio A_d/A_e	35
20	Contraction coefficient C_d as a function of the pressure ratio $1 - P_{atm}/P_s$ and the area ratio A_d/A_e , for two different end angles of 45° and 90°	36

LIST OF FIGURES

<u>Figure</u>		<u>Page</u>
21	1/57th scale RWE louver geometry	42
22	Gear train showing direction of rotation	47
23a	Angular acceleration profile for 1/57th scale RWE	49
23b	Angular velocity profile for 1/57th scale RWE	50
24	End view of 1/57th scale RWE	54
25	Side view of 1/57th scale RWE	55
26	Top view of 1/57th scale RWE	57
27	1/57th scale RWE louver	58
28	Environmental housing of gear train	60
29	1/57th scale RWE control schematic	62
30	Various shock tube configurations for 1/57th scale RWE tests . . .	68
31	Estimation of closing function based on test data	72
32	Experimental closure rate comparisons at 3 pressures	73
33	Closure rate comparisons at 103.3 kPa	74
34	Theoretical closure rate comparisons at 3 pressures	75
35	Results from 34.5 kPa pressure tests	77
36	Results from 68.9 kPa pressure tests	79
37	Results from 103.3 kPa pressure tests	80
38	Illustration of physical flow phenomena	84
39	LB/TS RWE cross section showing side and end vents	88
40	Rotating louver power comparison of alternate designs	91
41	LB/TS RWE rotating louver cross section	93
42	Louver offset position projections	95
43	Bending along axis of a typical louver	97

LIST OF FIGURES

<u>Figure</u>		<u>Page</u>
44	Bending on cross section of typical louver	99
45	Bending stress for fixed and active RWEs	100
46	Bending stress versus louver position	102
47	Hydraulic system concept schematic	106



Accession For	
NTIS GRA&I	<input checked="" type="checkbox"/>
DTIC TAB	<input type="checkbox"/>
Unannounced	<input type="checkbox"/>
Justification	
By	
Distribution/	
Availability Codes	
Dist	Avail and/or Special
A-1	

INTENTIONALLY LEFT BLANK.

LIST OF TABLES

<u>Table</u>	<u>Page</u>
1 1/57th Scale Shock Tube Driver Section Configurations to Produce Various Blast Waves at the Test Section	16
2 Power and Torque Requirements	44
3 Simulator and 1/57th RWE Inertia	51
4 Material Factors of Safety for Gears	52
5 Shock Tube Calibration Configuration	67
6 Pressure Gage Locations	69
7 Shock Tube Calibration Driver Conditions	69
8 Support Beams for the LB/TS Reflected Wave Eliminator	103
9 Estimated Costs	111

INTENTIONALLY LEFT BLANK.

INTRODUCTION

At present the blast simulation capability of the U.S. Armed Forces is limited to the lower end of the yield range required for testing of full-scale military equipment. Because the current free-field tests with high explosives are laborious to set up, very time consuming, and expensive, a reusable blast simulator is preferable. The blast and thermal effects of nuclear explosions can indeed be simulated in shock tubes of special design, called Large Blast and Thermal Simulators (LB/TS). Such facilities exist in Great Britain and in France (Fig. 1) but not in the United States. In response to the problems of full scale nuclear blast and thermal simulation, the Defense Audit Service has recommended that the Defense Nuclear Agency (DNA) develop an LB/TS. The U.S. Army Ballistic Research Laboratory (BRL) has taken the lead role in the research of LB/TS designs on behalf of the U.S. Army Harry Diamond Laboratory. This effort is part of a continuing program to develop a practical LB/TS design.

An LB/TS is basically a large shock tube in which military systems and civil defense structures could be tested on nearly a full scale. The main differences from conventional shock tubes are (a) the manner in which the shock is produced, and (b) the test environment that is generated, i.e., a heat wave followed by a decaying blast wave. A schematic layout of the proposed U.S. facility is shown in Figure 2. The current U.S. LB/TS design has nine high-pressure steel driver tubes (1) of 1.83m diameter each of which is anchored in a large concrete reaction pier (2). The drivers empty gas simultaneously through nozzles (3) into the expansion tunnel (5). The nozzles delay the emptying of the driver gas, producing longer flow durations. Liquid nitrogen, stored in a supply tank (15), is used as driver gas. It is evaporated and heated in pebble-bed superheaters (17) while it is pumped (14) into the drivers. The emptying of the driver gas is initiated by bursting diaphragms, or by opening fast acting valves (4), or both.

The expansion tunnel (5) is formed of prestressed concrete and has a semicircular cross-section with an area of 165m². The test section of steel construction (6) is located part way down the expansion tunnel. The thermal radiation sources (TRS) for simulating the thermal effects of nuclear explosions will be mounted in the floor of the test section just ahead of the target area. The TRS may be flanked by air curtains fed from a plenum in the floor (9). Jet pump ejectors (8) will be mounted overhead to evacuate the combustion products. The walls of the test section will be equipped with a large number of ports (10) for cameras, lighting and instrumentation. The test target (11) will be located in the test section on the downstream side of the thermal radiation sources (7). The soil tank (12) for testing shallow buried structures will be located in the floor of the test section. A rarefaction wave eliminator (13) will be located at the far end of the expansion tunnel.

In order for the Large Blast/Thermal Simulator to be useful for various system test requirements, it must be able to simulate several different types of shock wave parameters. Figure 3 shows a typical operational envelope of peak static pressure (associated with various yields of interest) and their respective positive phase durations. The variables of the shock waves which must be adjustable are the amplitude and duration. The amplitude of the shock wave can

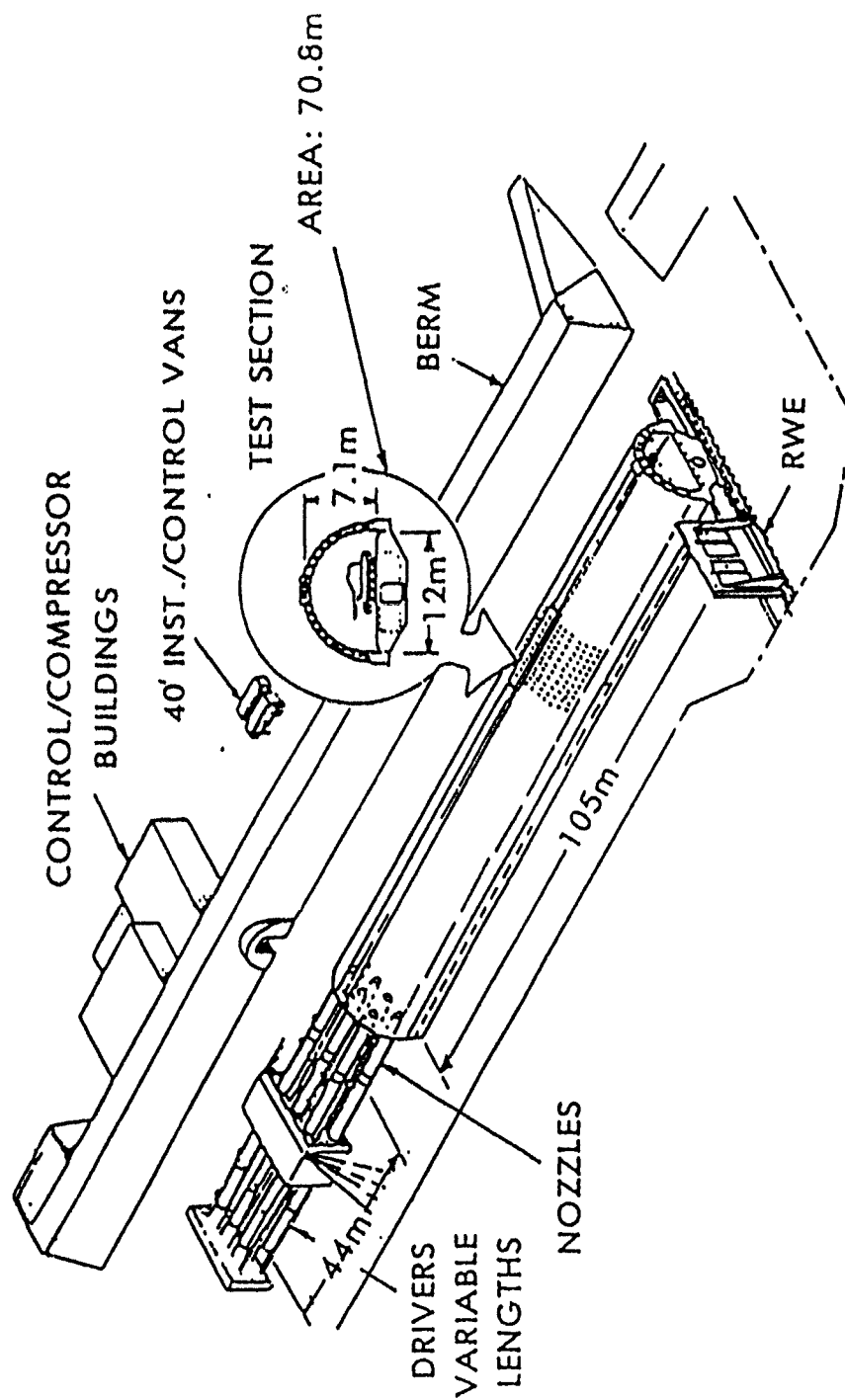
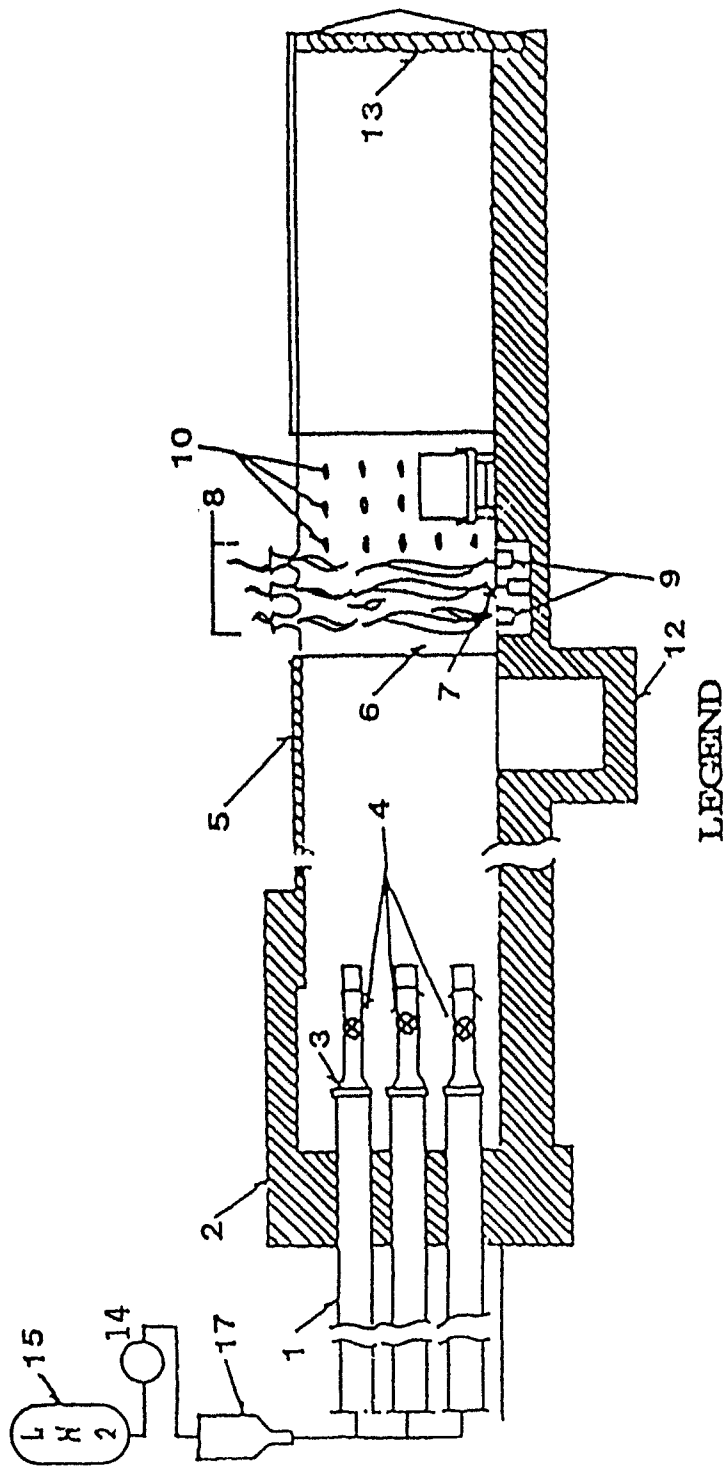


Figure 1. French (CEG) Large Blast Simulator (LBS) facility.



LEGEND

- | | | | |
|---|------------------------------|----|---------------------------------|
| 1 | Steel Driver Tubes | 9 | Air Curtain Plenum |
| 2 | Concrete Reaction Peer | 10 | Instrumentation and Light Ports |
| 3 | Converging Nozzles | 11 | Test Target |
| 4 | Throat Valves and Diaphragms | 12 | Soil Tank |
| 5 | Concrete Expansion Tunnel | 13 | Rarefaction Wave Eliminator |
| 6 | Steel Test Section | 14 | Cryogenic Pumps |
| 7 | Thermal Radiation Sources | 15 | Liquid Nitrogen Storage |
| 8 | Combustion Products Ejectors | 17 | Pebble-Bed Superheaters |

Figure 2. U.S. Large Blast and Thermal Simulator (LB/TS) facility concept.

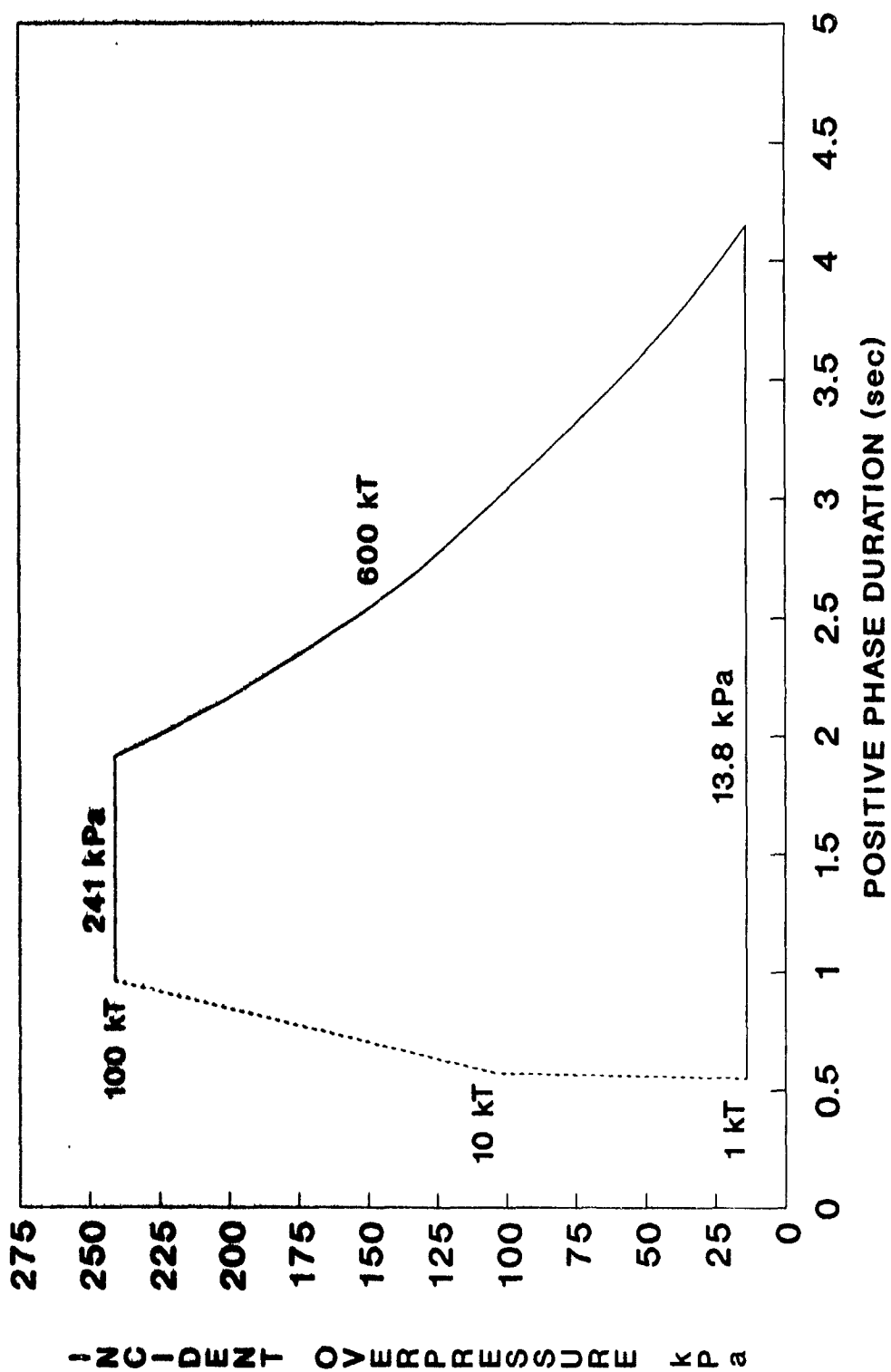


Figure 3. Operational envelope of the RME.

be adjusted by varying the initial driver conditions. The duration cannot be as easily adjusted. The major factors which affect the duration are the physical distances from the ends of the shock tube to the test section. The ends cause reflected, rarefaction, expansion and compression waves to travel across the test section in the shock tube (see Fig. 4). Depending on the location of the test section, with respect to the ends, these waves can alter the desired shock wave profile and produce an undesirable test environment (see Fig. 5). An open ended shock tube (downstream from the test section) probably creates the most detrimental wave disturbance problem. Referring to Figure 4, one can see the reflected expansion wave (R1) from the open end of the shock tube. In order to obtain the desired positive phase durations (and hence total impulses) shown in Figure 3, one can adjust the length of the shock tube (downstream from the test section) to delay the passing of the R1 wave across the test section.

The simple method of extending the duct beyond the test section to prevent the reflected wave from disturbing the desired test-section environment does not eliminate the reflected wave. Instead it delays the passage of this wave through the test section until after the test is complete. The required length of extra extension depends on the type and amplitude of the shock or blast wave. Longer duration waves obviously require longer tube extensions. The use of a sufficiently long tube extension will avoid all test-section disturbances during the testing time. Hence, this is the ideal approach from a performance viewpoint. For many small shock and blast tubes, the installation of additional duct length is not much of a financial or space burden. However, when the tube diameter is large, cost and space requirements can become exorbitant.

Another method of minimizing the disturbing effect of the reflected wave at the test section is to use a short length of duct terminated by a reflection or rarefaction wave eliminator (RWE). An RWE is a device that partially covers the open tube end, producing reflected shocks from the flow blockage segments and expansion waves from spaces open to the atmosphere. With the proper blockage to open area setting, these opposite types of waves cancel, and thereby minimize the reflected disturbance. If this disturbance is small, then the need for any long and costly tube extension for large facilities is simply alleviated. The degree of success of any RWE, however, depends partly on its design and mostly on whether it is passive, semi-active or fully active.

A passive RWE has a constant area opening (or blockage) that is preset for the type and amplitude of incident shock or blast wave, and a semi-active RWE has a pre-programmed open area variation with time for a certain expected shock or blast wave. Although a fully active RWE has never been used, its area variation with time would not be pre-programmed, but instead flow sensors and feedback would be used to automatically update the area opening with time to alleviate the reflected disturbance. A fully active RWE would need to be properly equipped with pre-programmed algorithms having the ability to quickly analyze sensor data and make good judgments as to the proper area setting to minimize the reflection. This appears to be a difficult task.

For larger shock tubes and blast simulators for which the cost of a tube extension becomes exorbitant in contrast to short extensions terminated by an RWE, a passive RWE is less costly than an active one, but an active RWE will perform better in alleviating the reflection from the tube end. Because the

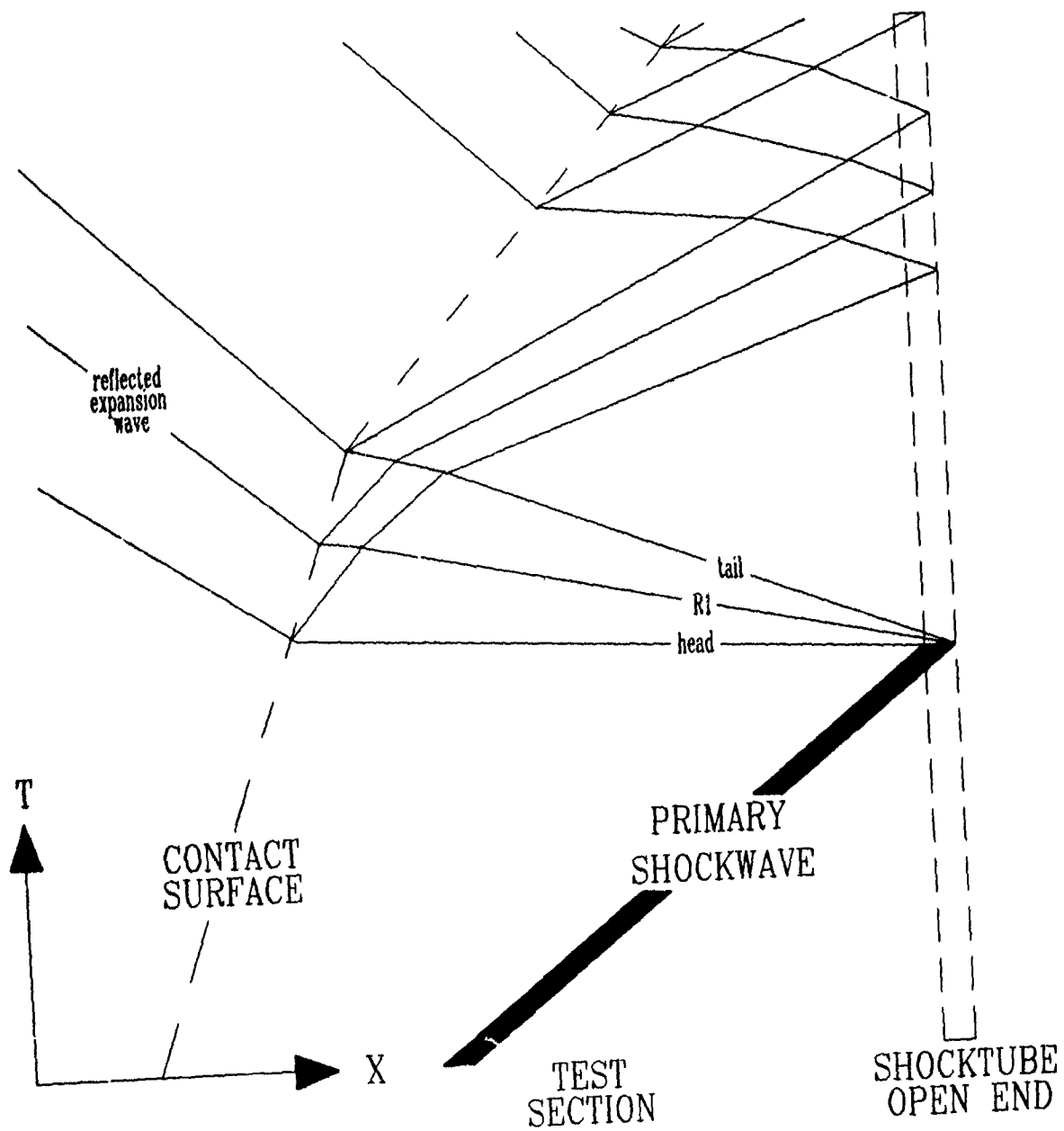
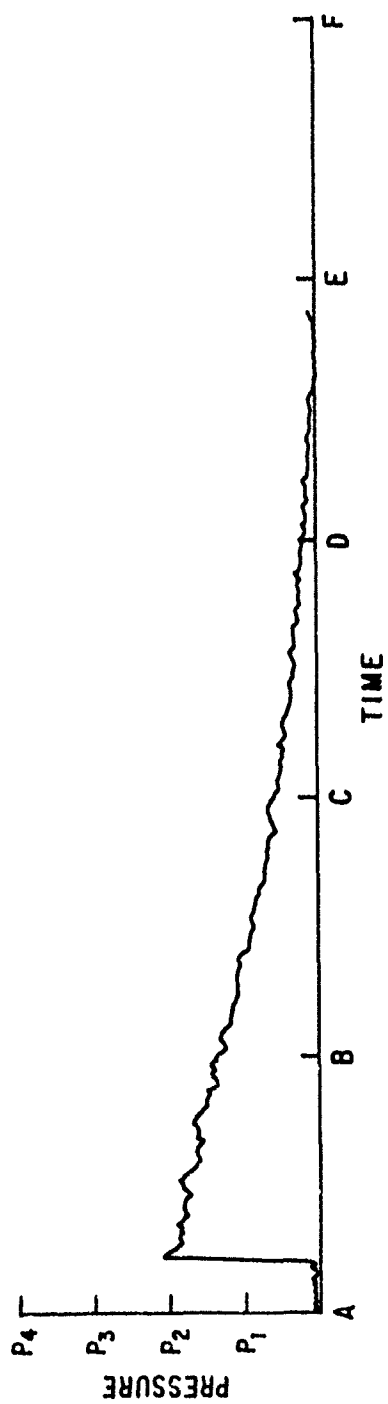
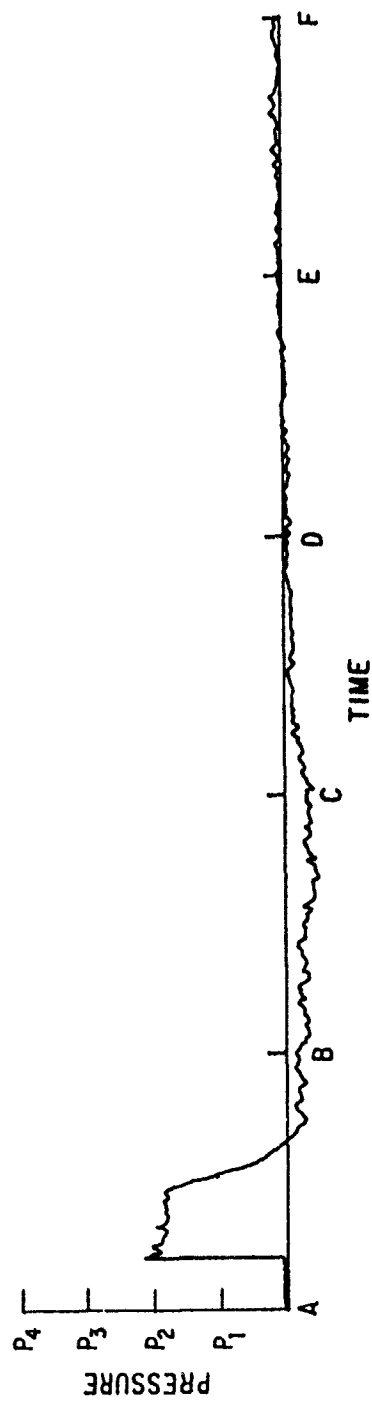


Figure 4. Typical wave diagram in an open ended shock tube.



a. Rarefaction Wave Eliminated



b. Effect of Rarefaction Wave

Figure 5. Waveform comparisons.

quality of blast simulation has become more important today, test-section disturbances from reflected waves are now less acceptable. Consequently, to conduct higher quality blast testing of military equipment, active reflection elimination is becoming a necessity for large blast simulators.

BACKGROUND

A recent concept study was conducted (Ref. 1) to examine various devices which could act as a Rarefaction Wave Eliminator (RWE) for the LB/TS. This study examined three different designs which were different in operation. The devices were: (1) a rotating louver concept, (2) a hinged louver concept, and (3) a stator-rotor concept. The stator-rotor concept was the most radical and although it would produce the proper environment, it became impractical due to the tremendous mass and polar moment-of-inertia that would have to be overcome to start its motion. The hinged louver concept is attractive because of its light weight but very large power requirements are dictated due to the aerodynamic forces that need to be overcome. Therefore, the rotating louver concept became the most attractive and was targeted for further investigations.

During this previous study it was also determined that a 100 percent open area (or absolutely no blockage) was required when simulated peak overpressures exceed 137 kPa. This creates a very difficult problem since the RWE cannot be placed at the open end of the LB/TS and then be required to operate within a window of only a few milliseconds. An alternative was to place side vents in the walls of the expansion tube as close to the RWE as possible. These side vents would also require a closure mechanism and be operated in tandem with the end section RWE. It was also estimated that 40 percent of the total cross section of the tube would be required for the side vents. This estimate was based on the fact that about 20 percent of the end of the tube is always blocked by the structure of the end section RWE in the most open position and that the side vents are only half as effective as the end vent section (due to the flow being nearly one dimensional). Therefore, the total amount of open area that is associated with an RWE is 120 percent of the cross sectional area of the shock tube.

Theoretical investigations which were also conducted during this study indicated that an active (or at least semi-active) RWE is required to achieve the proper simulation. A passive RWE does help to preserve some of the desired overpressure waveform, but it will always fail to preserve the entire waveform. Therefore, the impulses associated with the static and dynamic pressures will be less than required and systems will not be tested to the complete threat environment. Also, since a different amount of fixed blockage created by a passive RWE is unique to a given overpressure and yield simulation the passive RWE must be flexible to allow for easy modification. However, the penalty one pays for this is increased labor costs to modify the passive RWE between tests of varying conditions. Therefore, an active or semi-active RWE even becomes more cost effective when the cost is averaged over the life of the device.

The referenced study laid a good foundation for the further design and development of the LB/TS RWE. However, the designs to date were based heavily on theoretical considerations with little experimental data to substantiate the designs. The French government has operated an RWE on their large shock tube (the Simulateur de Souffle 'a Grand Gabarit or SSGG) located at the Centre d'Etudes de Gramat (CEG) but little data is available on the facility, much less the RWE. However, it is known that the RWE operates to their satisfaction (although limited to lower peak overpressures) and is based on a rotating plate type louver concept. Other RWEs exist at other shock tubes around the world but

these are some what of a pseudo-passive type. An example is the RWE at the Atomic Weapons Establishment located at Foulness, England. This RWE consists of a wall of aqueous foam at the end of the shock tube.

Due to these limitations, it was recommended that the most promising concept for the LB/TS RWE be demonstrated on a small scale. This demonstration would not be a truly scaled down version of the full scale concept but would be of sufficient similarity to prove that the concept was valid from a theoretical and shock physics viewpoint. In addition, the demonstration would prove the validity of the tools used in designing RWEs as well as providing input for the further improvement of these tools. A 1/57th scale was selected as the size of the RWE to be constructed since a shock tube existed at the BRL which was approximately this size and the costs for constructing an active RWE for this facility would not be extreme.

OBJECTIVES

The objectives for this effort can be roughly divided into two separate categories. One category is associated with the design, construction, and testing of the 1/57th scale RWE while the other is associated with the further evaluation of the LB/TS RWE design concept.

The overall objective of the 1/57th scale RWE development was to prove that the tools used to design a rotating louver RWE were valid. These tools included the RCM code and data developed during previous investigations (Refs. 2 through 4). The RCM code would be used to model the flow throughout the shock tube and then develop "closing functions" which determine the time dependent manner in which the RWE louvers operate. The previous design data was to be extended to account for theoretically based air flow over diamond shaped "airfoils" and determine the inertia of the RWE system, as well as determining the governing forces acting on the louvers.

The objectives of the large scale RWE for the LB/TS was to further the design of the rotating louver which was initially investigated during a previous study (Ref. 1). This investigation was to review the concept and develop more distinct operational and structural requirements. The study would include further examination of the forces both required and created and outline the requirements to meet the operational requirements. Finally, a cost estimate was to be prepared for the LB/TS RWE based on the data developed during this study.

A final objective of the study was to also examine the feasibility of developing a passive RWE for both the 1/57th scale and LB/TS RWE. If feasible, a design for both size shock tubes was to be developed.

INTENTIONALLY LEFT BLANK.

NUMERICAL PREDICTION OF BLAST-SIMULATOR FLOWS

The method of predicting unsteady flows in the 1/57-scale blast-wave simulator with an active reflection eliminator is a fairly challenging task if reasonably accurate predictions of the simulated blast wave are required. The task becomes even more challenging if the computational effort is kept reasonably small so that the numerical predictions can be done in a reasonable time with modern personal computers and workstations. The present method of predicting unsteady flows in an efficient manner for the 1/57-scale blast simulator is described in this section. This description includes the following:

- geometrical model of the blast simulator,
- equations governing blast-simulator flows,
- discharge coefficient for louvered RWEs,
- numerical solution of blast-simulator flows,

which are covered in individual sections.

INITIAL GEOMETRICAL MODEL OF BLAST SIMULATOR

The original 1/57th shock tube configuration and dimensions supplied by BRL are shown in Figure 6. The driver associated with this configuration is fixed in diameter and throat dimensions but, the length can be changed for any given test. Figure 7 shows a representation of the modeling of the driver and throat section of the shock tube as input into the RCM code. Table 1 shows the various combinations of driver length and driver to ambient pressure ratios which will produce a given peak overpressure and positive phase duration. The diaphragm used in this configuration self-bursts by slowly raising the driver pressure, thus allowing the high pressure driver air to progress down the remainder of the shock tube and create the simulated blast wave.

Six calculations were performed with the RCM code to obtain flow property histories at four locations along the tube. The six calculations performed are denoted by the asterisks in Table 1. The locations of the measurement stations are 1.218, 1.686, 2.205, and 5.53 meters downstream from the diaphragm. The results from these calculations are located in Appendix A. A brief discussion of one of these calculations (pressure ratio of 4.895 and driver length of 94.95 cm) will be presented to explain some of the phenomena occurring in this shock tube.

Figures 8 through 11 show time histories of the pressure, density, temperature, and velocity (all normalized to ambient conditions) at the four sampling locations. The long length of the driver produces a decaying blast wave that has a series of long, flat-topped decreasing steps produced by a wave traveling back and forth in the driver. Figure 12 shows x-t diagrams of the pressure, density, temperature, and velocity which helps to understand the variations in the time histories. One important item to note is that the contact surface moves downstream across the first three measurement locations and then back upstream across them once again. Also the rarefaction wave can be seen at late times moving upstream into the shock tube. This action is most readily

NOTES:

- 1) DIMENSIONS ARE IN CENTIMETERS
- 2) NOT TO SCALE
- 3) DIAPHRAGMS WERE AL
- 4) DIMENSIONS ARE FOR INSIDE DIAMETER
- 5) D_L VARIED FROM 6.03 TO 257.49
- 6) ST = 3, 5, 7, AND 20 DIAMETERS

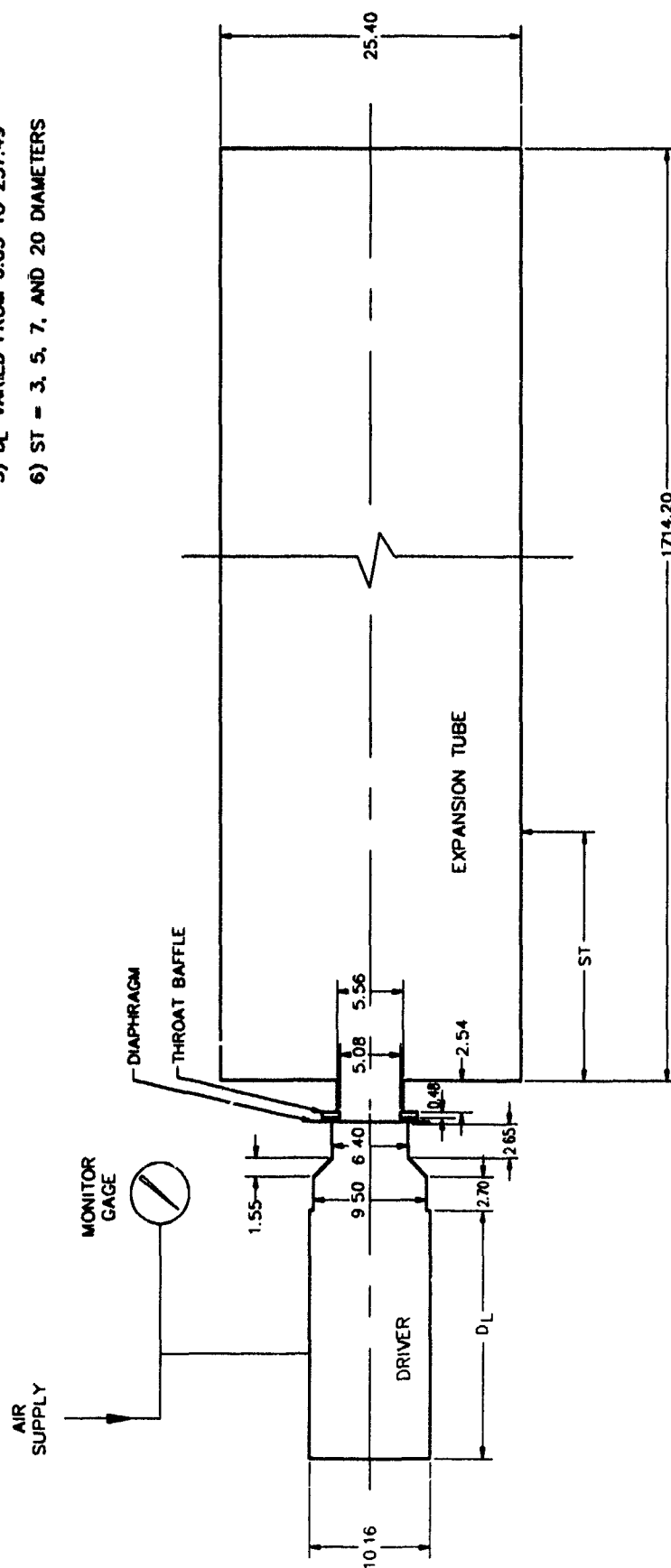


Figure 6. BRL 1/57th scale LB/TS geometry for unheated driver experiments.

Node densities in model

1	55.9 nodes per meter
2	74.1 nodes per meter
3	193.5 nodes per meter
4	170.1 nodes per meter
5	170.1 nodes per meter
6	144.4 nodes per meter
7	19.3 nodes per meter

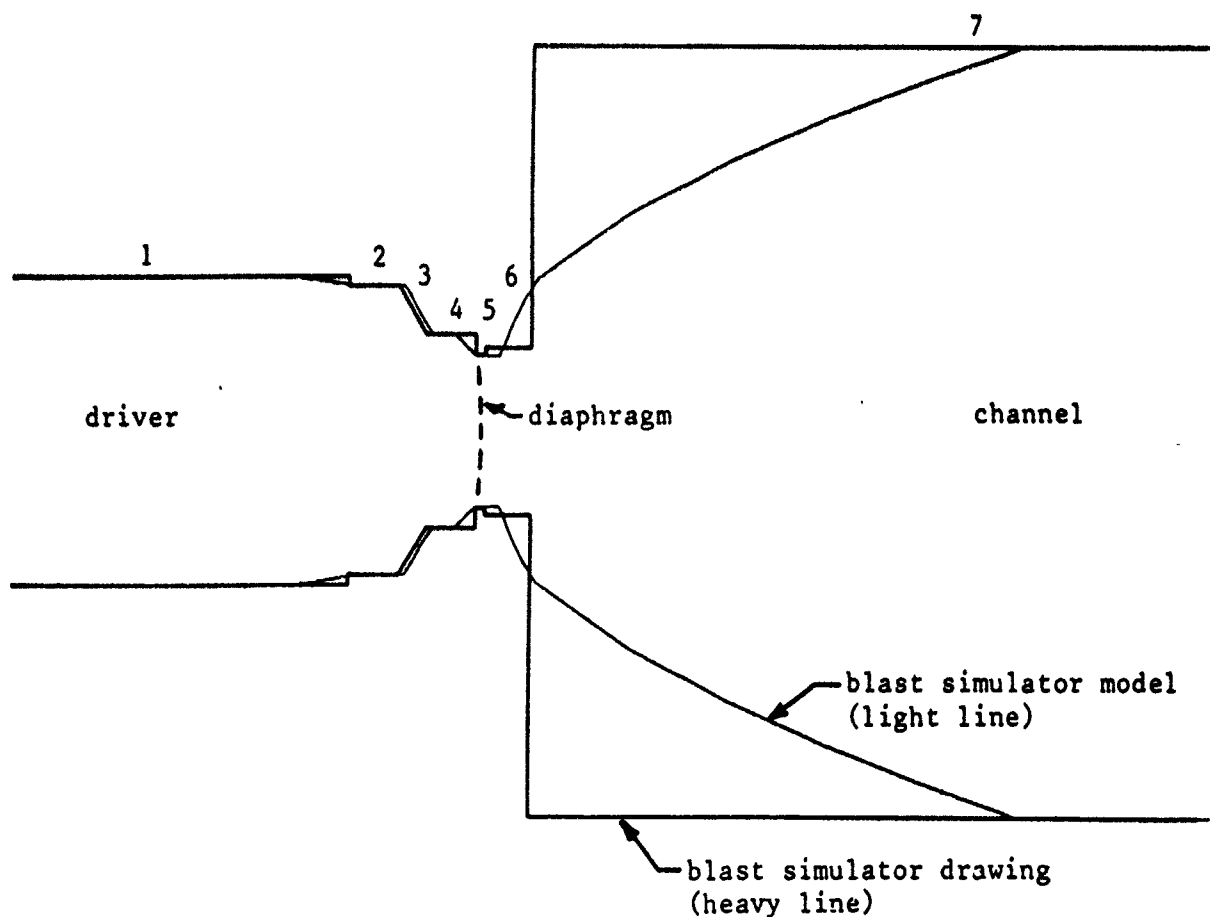


Figure 7. Expanded view of the throat section of the blast-wave simulator, showing the differences between the simulator drawing and model.

**Table 1. 1/57th Scale Shock Tube Driver Section Configurations
to Produce Various Blast Waves at the Test Section**

Driver Pressure		Driver Length, cm					
		11.12	33.98	67.00	94.95	145.74	294.15
kPa	P_{*1}						
483	4.767		X	X			
496	4.895				X		
545	5.379					X	X
1827	18.03		X	X			
1834	18.10				X	X	
2027	20.00	X					
5192	51.24	X		X			
5199	51.31		X		X		
5240	51.71	X		X			
14479	142.9	X					
14789	145.9		X				
14795	146.0	X		X			

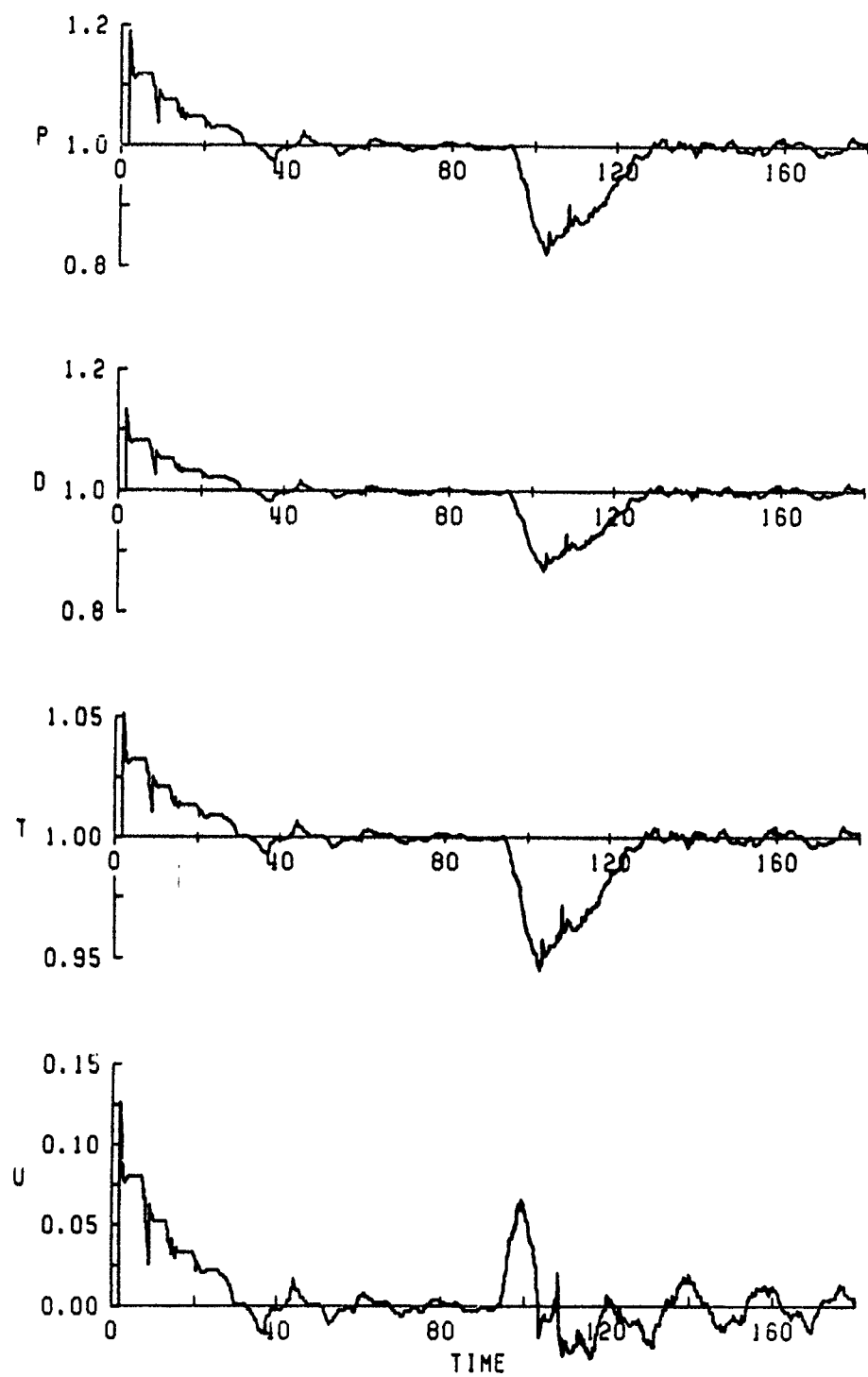


Figure 8. Time histories at location 1.828 m.

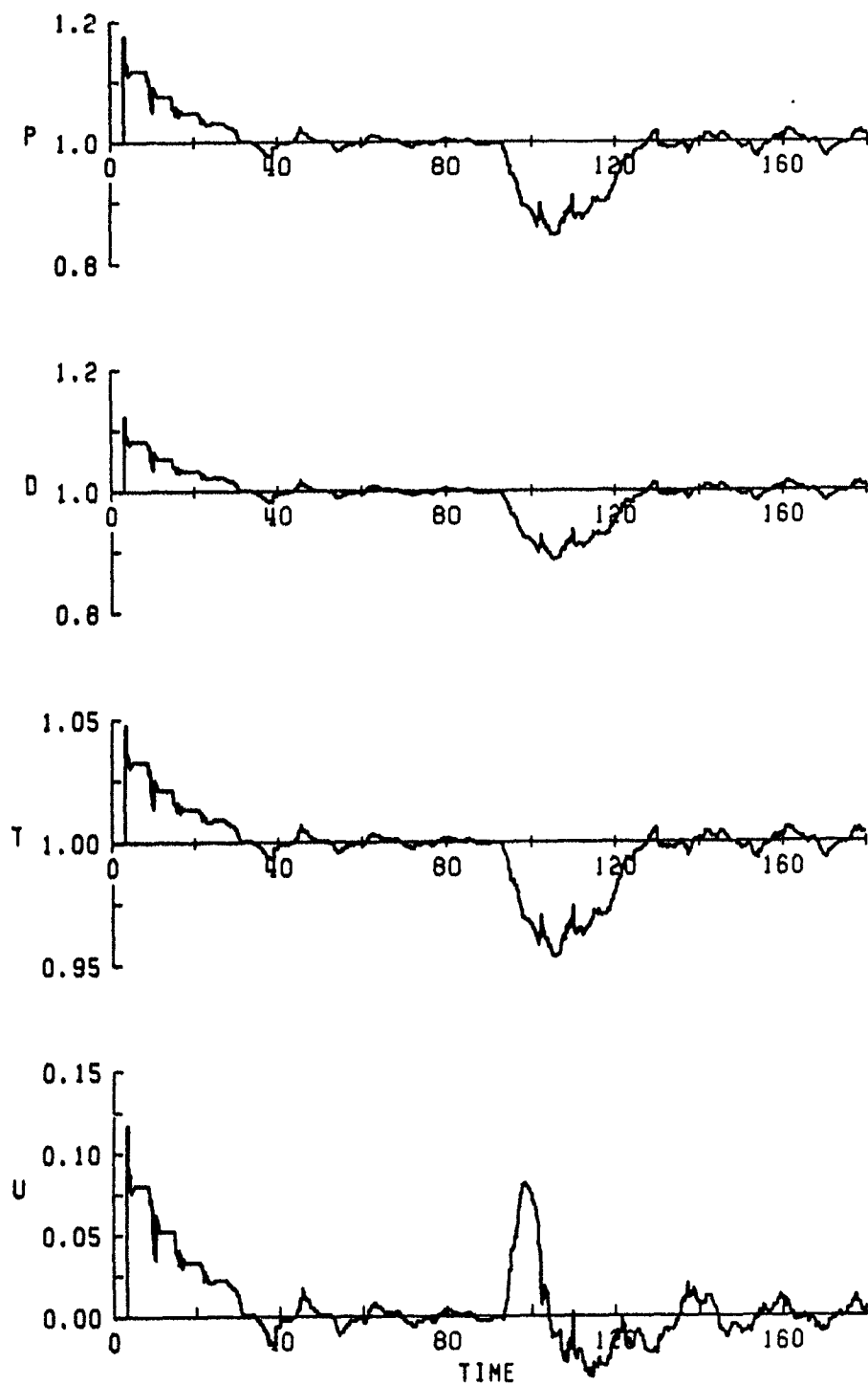


Figure 9. Time histories at location 2.295 m.

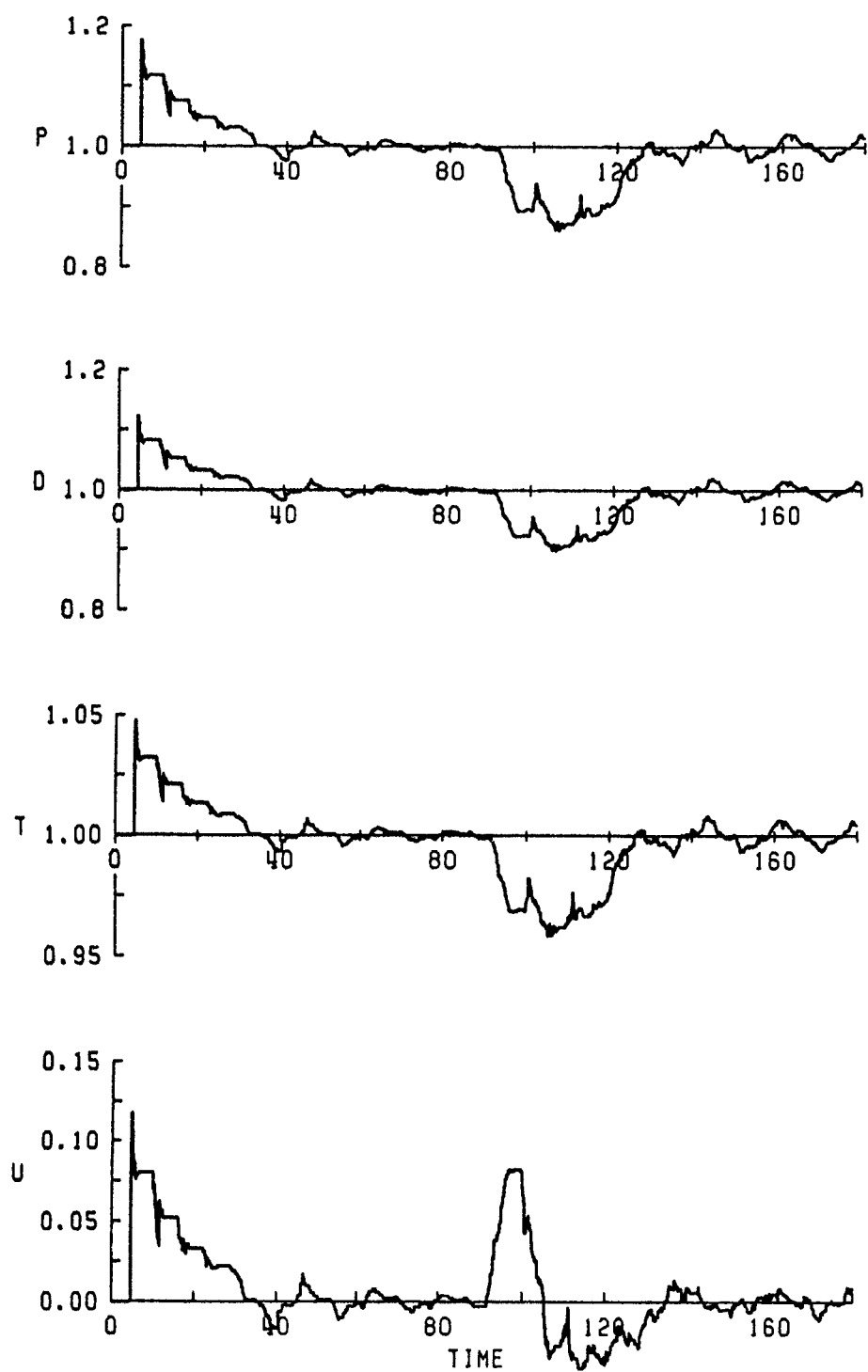


Figure 10. Time histories at location 2.815 m.

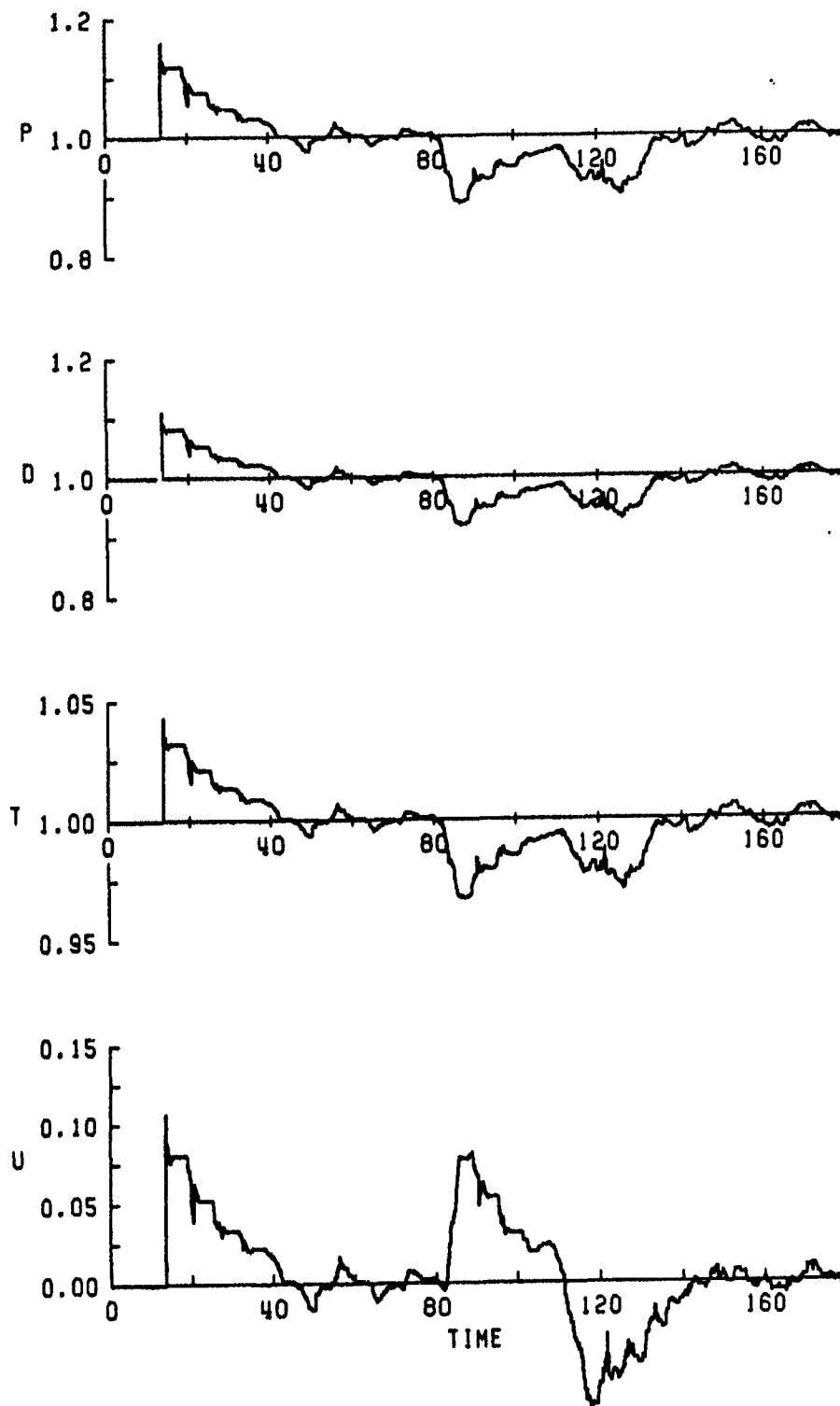


Figure 11. Time histories at location 6.139 m.

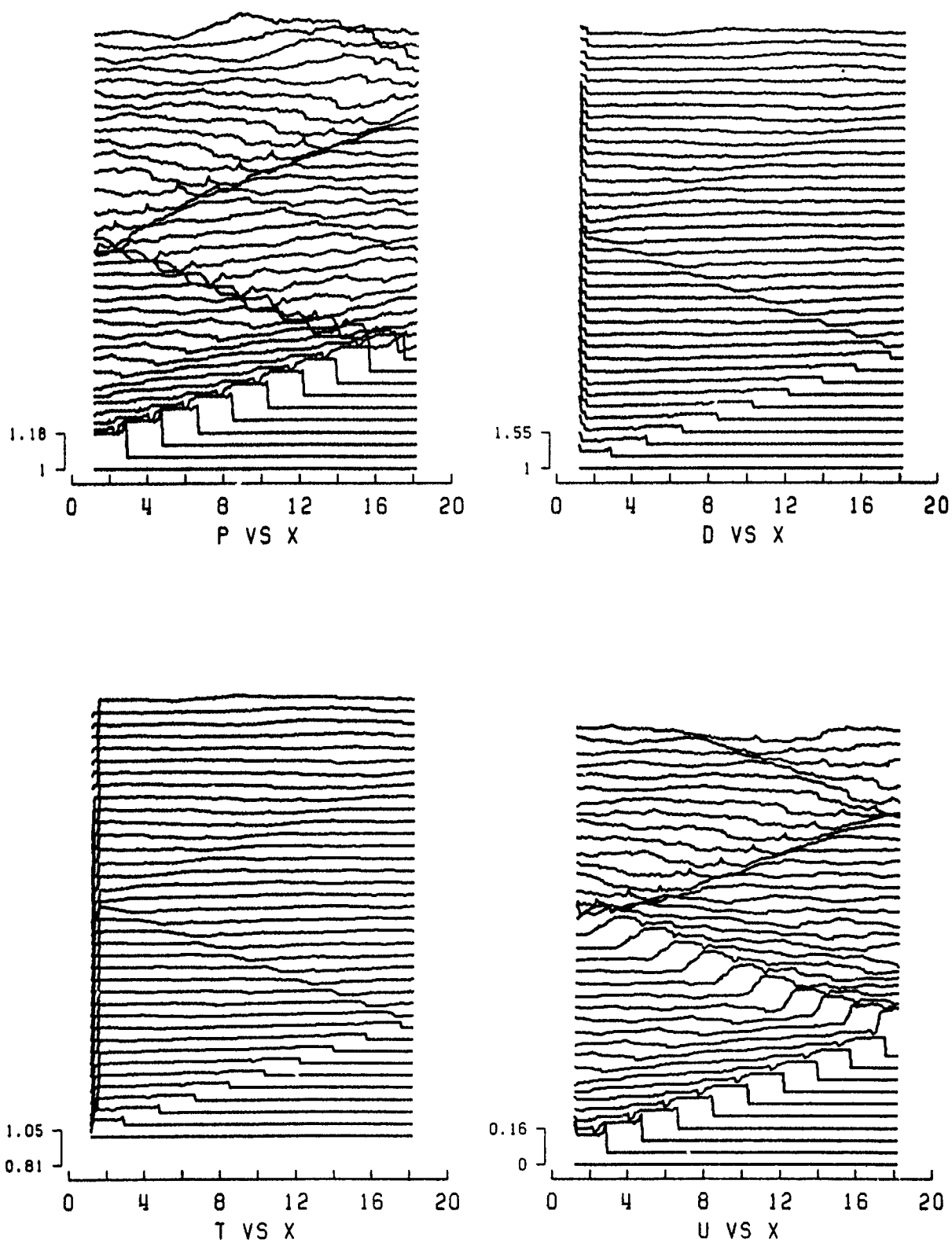


Figure 12. Spatial distributions at time 0.000 to 180.000.

apparent in the velocity time history at the 6.139 m sampling location. However, for this particular case the rarefaction wave does not influence the positive phase since the simulated tube is very long. Similar results and other features can be seen in the other calculations presented in the Appendix.

REVISED GEOMETRICAL MODEL OF THE BLAST SIMULATOR

The high-pressure driver of the 1/57-scale blast simulator is sketched in Figure 13a, where relevant dimensions are included. This driver has a fixed volume and consists essentially of: (a) a central cylindrical chamber with an internal piston or plug fixed in its rearmost position (as shown), (b) a converging duct segment with a short constant-area section to the diaphragm station, and (c) four relatively long pipes welded onto the central chamber at an angle of about 45° to the duct axis. These four pipes are spaced uniformly around the periphery of the central chamber (90° apart), and they contain more than half of the driver volume. After the diaphragm self-bursts by slowly raising the driver pressure, this initially high-pressure driver air escapes into the channel of the blast simulator, and this transient discharge process produces the simulated blast wave which moves along the channel to the test section.

The plug is an alternative to the diaphragm as a means of releasing the high-pressure air from the driver into the channel. In its forward most position, it initially seals the high-pressure driver air in the driver. However, when suitable electronic controls and hydraulic actuators are used to pull it backwards in a controlled manner, the area opening and air discharge rate can be controlled much better than the case of the diaphragm, to produce a simulated blast wave of better quality. This latter mode of operation with the plug valve was not used in this work, because the control system was not complete.

The cylindrical channel shown partly in Figure 13a is 25.4 cm (10 inches) in diameter and has a normal length of 17.13 m (56.2 feet). However, for some tests the channel length was extended by an additional 4.8 m (15.75 feet). The channel end opposite the driver terminates abruptly either with an end open to the atmosphere or with a reflection eliminator of the rotating louver type described earlier.

The driver, with its four pipe appendages, produces a fairly complicated multipipe and multibranched flow in the driver. For convenience in the following numerical computations, the driver's geometry is simplified such that only a single duct flow occurs. The four pipes are essentially rotated parallel to the driver axis and their areas and the area of the central chamber are then added together to obtain an equivalent single duct area distribution. The resulting area distribution with distance along this single duct is shown in Figure 13b. Note that the rotation of the four pipes parallel to the driver axis before summing the duct areas helps maintain the correct time sequence of wave motion in the driver, and this is much more reasonable than not rotating the pipes or rotating them to the perpendicular position. Figure 14 shows a typical result when using the RCM code with this driver geometry for one of the tests conducted at BRL. A full set of the calculational results are located in Appendix B with a comparison to the data shown in Appendix D.

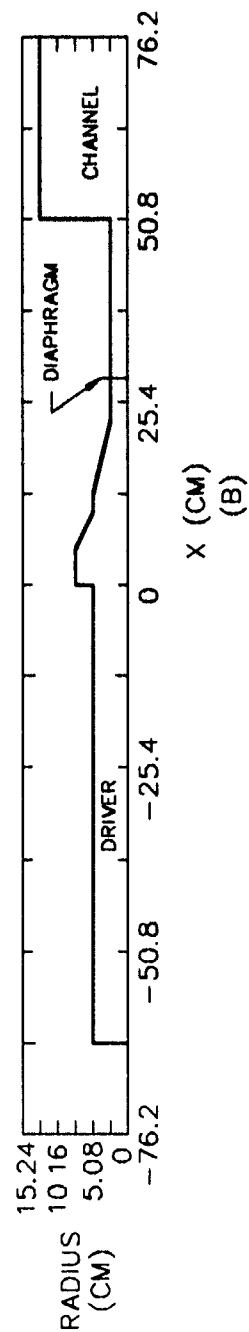
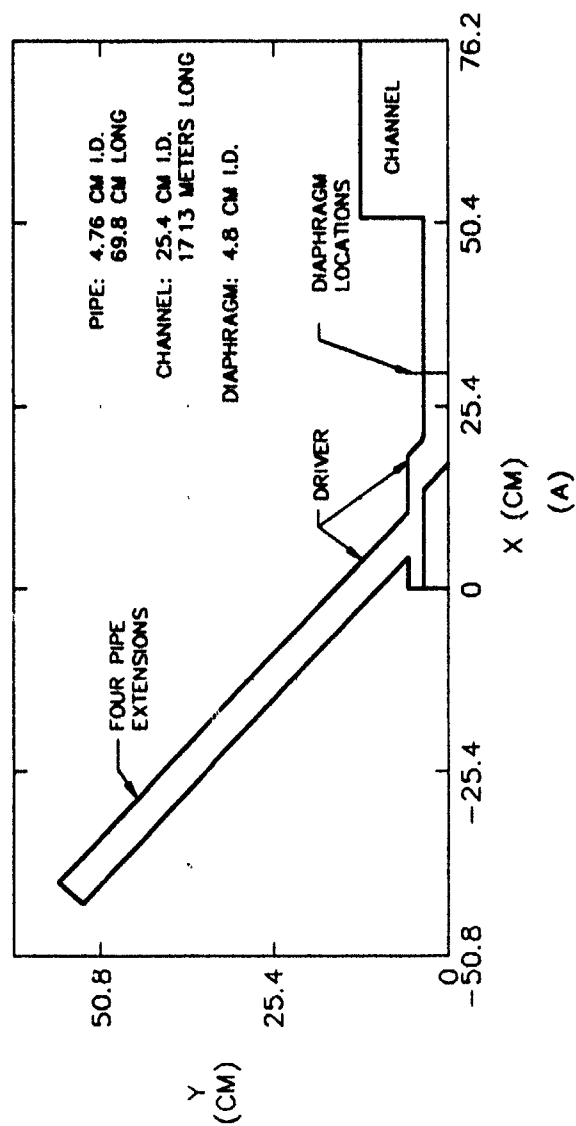


Figure 13. Driver of the BRL 1/57 scale blast-wave simulator.
 (a) scaled drawings,
 (b) one-dimensional representation for the numerical predictions

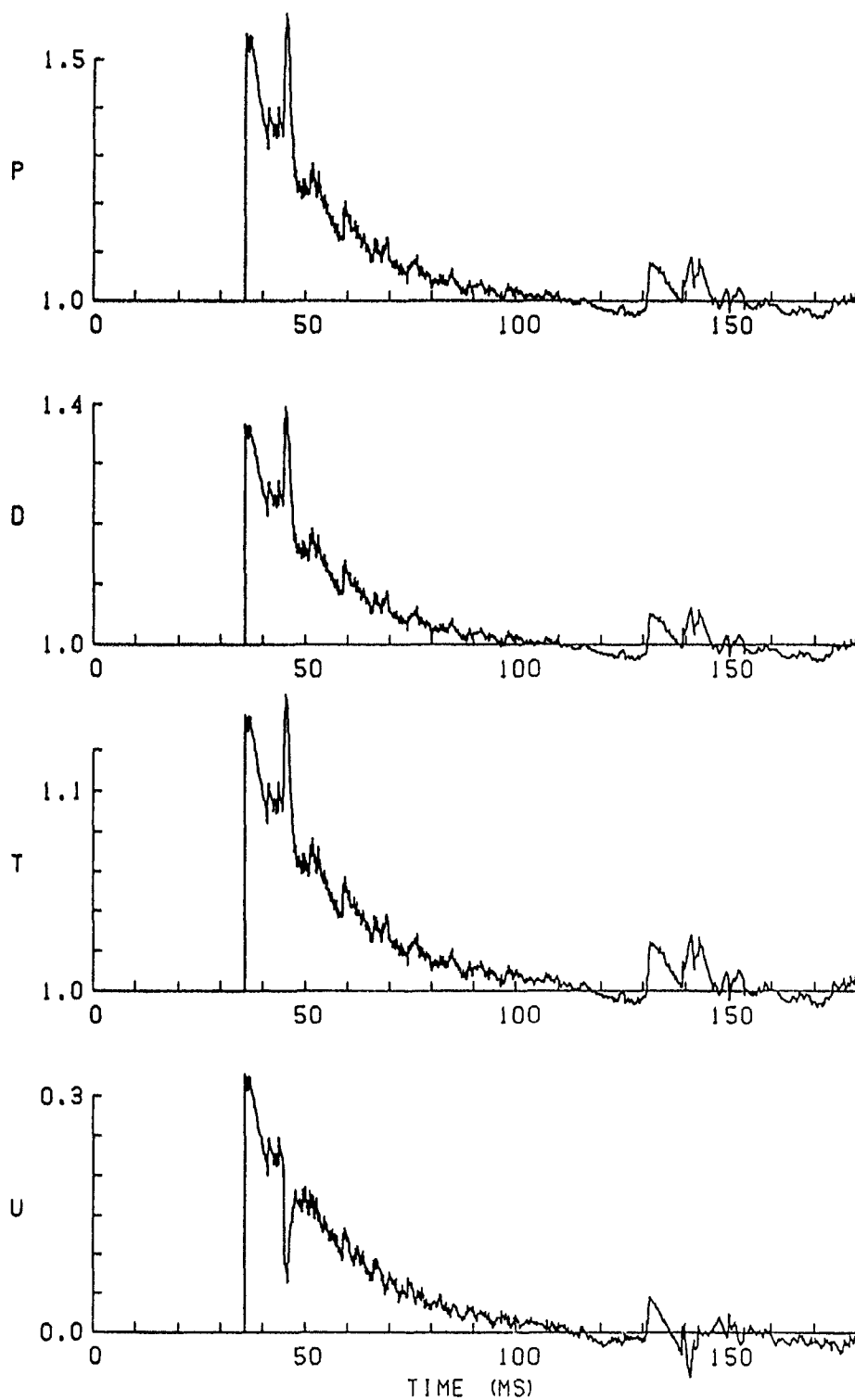


Figure 14. RCM calculational results from modeled driver.

EQUATIONS GOVERNING BLAST-SIMULATOR FLOWS

The flow in the blast simulator with the model geometry depicted in Figure 13b is treated as unsteady and one-dimensional. When the duct is long relative to its diameter, the computations will give reasonable results for the average flow properties across the duct. Many blast simulators satisfy this requirement because they are designed to produce essentially one-dimensional flows to achieve good simulations of blast waves.

The three equations of motion (continuity, momentum and energy), in partial differential form for describing fairly general one-dimensional unsteady flows of a compressible gas in pipes or ducts with area changes, can be expressed in weak conservation form as

$$\frac{\partial}{\partial t}[\rho] + \frac{\partial}{\partial x}[\rho u] = -[\rho u] \frac{1}{A} \frac{dA}{dx}, \quad (1)$$

$$\frac{\partial}{\partial t}[\rho u] + \frac{\partial}{\partial x}[\rho u^2 + p] = -[\rho u^2] \frac{1}{A} \frac{dA}{dx}, \quad (2)$$

$$\frac{\partial}{\partial t}[e] + \frac{\partial}{\partial x}[u(e + p)] = -[u(e + p)] \frac{1}{A} \frac{dA}{dx}, \quad (3)$$

where p , ρ , e , u , A , x and t denote the pressure, density, total energy per unit volume, flow velocity, duct area, distance and time, respectively. For a gas which is thermally perfect (i.e., $p = \rho RT$) and also calorically perfect (i.e., constant specific heats $C_v = \frac{1}{\gamma - 1} R$ and $C_p = \frac{\gamma}{\gamma - 1} R$), the energy can be expressed as $e = \rho C_v T + \frac{1}{2} \rho u^2 = \frac{1}{\gamma - 1} p + \frac{1}{2} \rho u^2$, where R , T and γ denote the gas constant, temperature and specific heat ratio, respectively.

Friction and heat transfer between the gas and duct walls have been neglected in this study because they are relatively small for flows in relatively large ducts. In addition, pressure losses due to flow turbulence generation and dissipation have been neglected (e.g., poor diaphragm breakage, flows passing over broken diaphragm remnants that protrude into the duct, flows passing through steep area reductions and enlargements).

The three previous partial differential equations and the state equation ($p = \rho RT$) become a closed set for the solution of the three dependent variables ρ , p and u , provided that the duct area is known or specified as a function of distance. In this study, all of the area changes in the blast simulator (Figure 13b), including the area reduction of the reflection eliminator, are taken as continuous and smooth, although some of these area transitions are very short. For each area change, the diameter, area, and spatial derivative of area are given by the following expressions

$$D(\hat{x}) = \sqrt{\frac{4}{\pi} A(\hat{x})}, \quad (4)$$

$$A(\hat{x}) = \sqrt{A_0 A_L} \exp \left[\ln \sqrt{\frac{A_0}{A_L}} \cos \left[\pi \frac{\hat{x}}{L} \right] \right], \quad (5)$$

$$\frac{dA(\hat{x})}{d\hat{x}} = \frac{\pi}{L} A(\hat{x}) \ln \sqrt{\frac{A_L}{A_0}} \sin \left[\pi \frac{\hat{x}}{L} \right], \quad (6)$$

where A_0 is the initial duct area at $\hat{x} = 0$, A_L is the final duct area at $\hat{x} = L$, $L = x_1 - x_0$ is the length of the area change, and \hat{x} is the local distance variable for the area change (i.e., $0 \leq \hat{x} = x - x_0 \leq L$). Note that this type of smooth area change starts and ends with the derivative $dA/d\hat{x}$ equal to zero, and $(1/A)dA/d\hat{x}$ is a symmetric function with its maximum or minimum value occurring at the center of the area change.

In the case of a rapid area change which ends abruptly with a sharp corner, like that of a sharp-edged orifice, sharp-edged slot, and the sharp edges of the slot between adjacent louvers of a reflection eliminator, the flowing gas separates from the duct surface and occupies a smaller flow area. In order to accurately predict contracting flows, the numerical solution for the flow must be obtained for the corresponding smaller flow area (in contrast to the larger geometrical duct area). To account for these flow contraction effects, which can be considerable (up to 50%), discharge coefficient C_d is introduced into the numerical flow model. This incorporation of C_d into equations 4-6 is done quite simply by replacing A_L with $C_d A_L$. Since $0 < C_d < 1$, the flow area reduction is always more severe than the geometrical reduction in duct area.

The discharge coefficient generally depends on both the duct geometry and flow conditions (e.g., area ratio, severity of the area change, specific heat ratio, flow Mach number), and its value changes as the flow conditions change. This introduces an additional time dependence of the flow area into the previous partial differential equations. However, this time-dependence effect is negligible in the solutions and therefore neglected. Consequently, the change in the value of C_d due to temporally changing flow conditions are the only important ingredient which should be included in the numerical model, and these theoretical and/or experimental results are required before the previous partial differential equations can be solved for the blast simulator flow. C_d values for reflection eliminators are the subject of the next section.

DISCHARGE COEFFICIENT FOR LOUVERED REFLECTION ELIMINATORS

The flow through a reflection eliminator consisting of a set of vertical louvers with counter rotating blades is rather complicated, and values of C_d are not known theoretically or experimentally. In order to simplify the process of

obtaining effective values of C_d for the case of louvers, a number of simplifying but reasonable approximations are made. Let the flow through the louvers be considered as two-dimensional, quasisteady, smooth, and isentropic for a given set of oncoming flow conditions and the louver geometry and angle. Then the flow approaching the louvers and the following contracting flows through the slots between adjacent louvers will appear much like those sketched in Figure 15. These flows are also compressible, have stagnation points (streamlines perpendicular to the louver surface), and separate at the sharp louver edges (top and bottom). The jet flows through the slots between adjacent louvers with their edges pointing downstream at angle β_1 and upstream at angle β_2 differ by having different values of the discharge coefficient (C_{d1} and C_{d2}). The stagnation pressure of the flow ahead of the louvers drives the jet flows into the atmosphere, and atmospheric pressure occurs behind the louvers and on the surface of the free jets.

For simplicity it will be assumed that each flow through a slot originates from the approximate geometrical upstream area between the pivot points of the corresponding adjacent louvers, with straight streamlines as sketched in Figure 16a. Then this type of upstream flow and corresponding flow through the slot has a simpler geometry and can be considered as independent. These simplified flows are then equivalent to the duct flows shown in Figure 16b and 16c. The flow in the duct leaves through a slot produced by the flap at angle β , where this angle lies in the range $0^\circ < \beta < 180^\circ$ (includes both β_1 and β_2). The solution for the discharge coefficient C_d for this type of duct flow is known (see the latter part of this section), and it can be used as a good approximation for the discharge coefficient for the louvers.

The jet flows through the slots with the louvers pointing downstream have a discharge coefficient C_{d1} , and those with the louvers pointing upstream have a different coefficient C_{d2} , even though their geometric open areas are the same. Since the mass flow rates for the jets from these opposite types of slots are given by $\rho_j u_j C_{d1} A_e$ and $\rho_j u_j C_{d2} A_e$, and the sum of these mass flow rates is equal to the total mass flow rate with an effective discharge coefficient in the form $\rho_j u_j C_d (2A_e)$, the effective discharge coefficient is given by

$$C_d = \frac{1}{2}(C_{d1} + C_{d2}). \quad (7)$$

One can also show that the upstream flow areas A_1 and A_2 , from which the mass flow rates for these two types of slots are obtained, are related according to the expression

$$\frac{A_1}{A_2} = \frac{C_{d1}}{C_{d2}}. \quad (8)$$

Hence, the flow upstream areas and mass flow rates for these two types of slots are not equal, but they are related through the discharge coefficients.

A relationship between the angle of the louvers, the open area of the reflection eliminator, and the channel area is often useful. If the total open area between the slots is denoted by A_{open} ($2A_e$) and the channel area is denoted

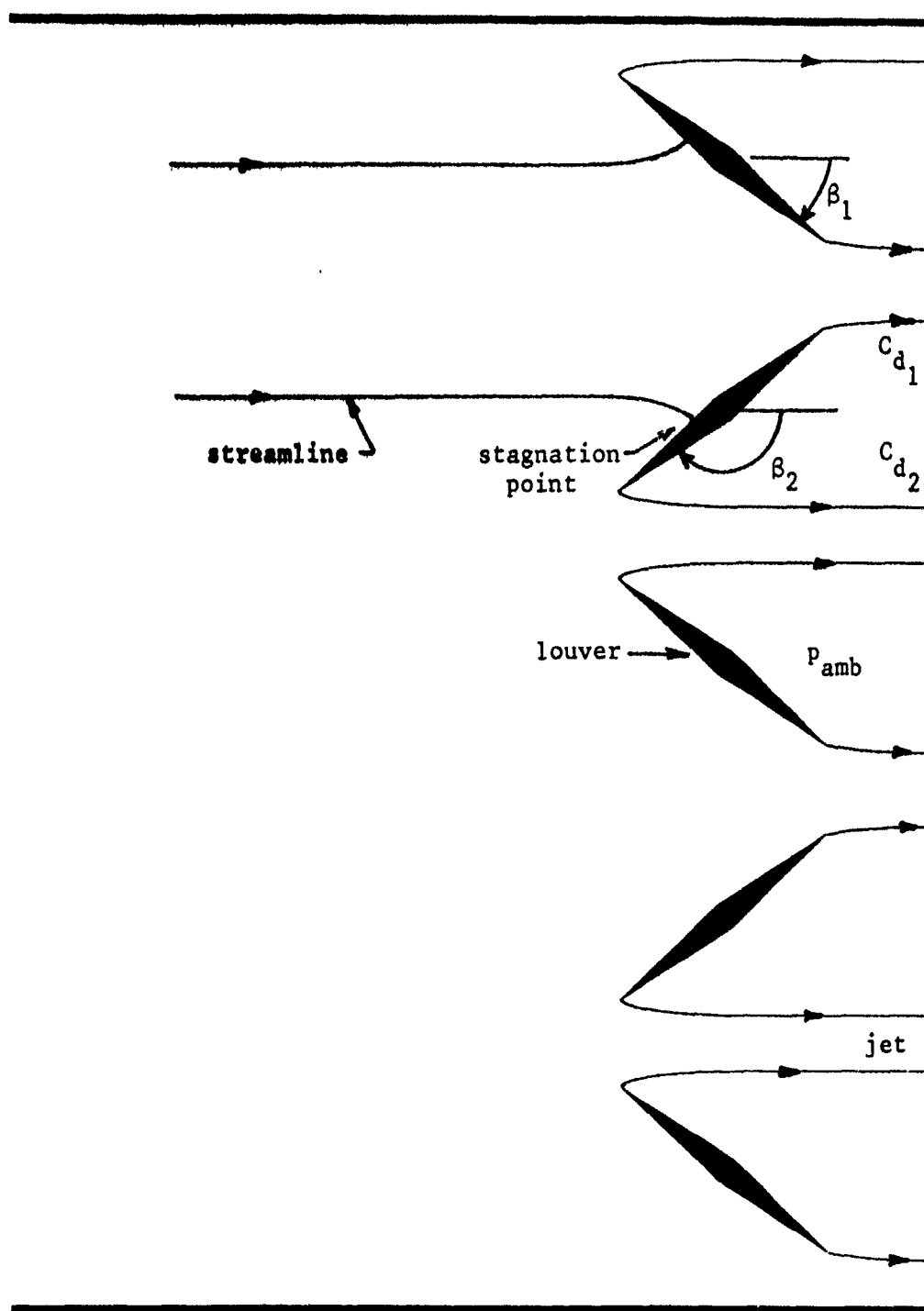


Figure 15. Illustration of quasisteady flow through the louvers of the reflection eliminator.

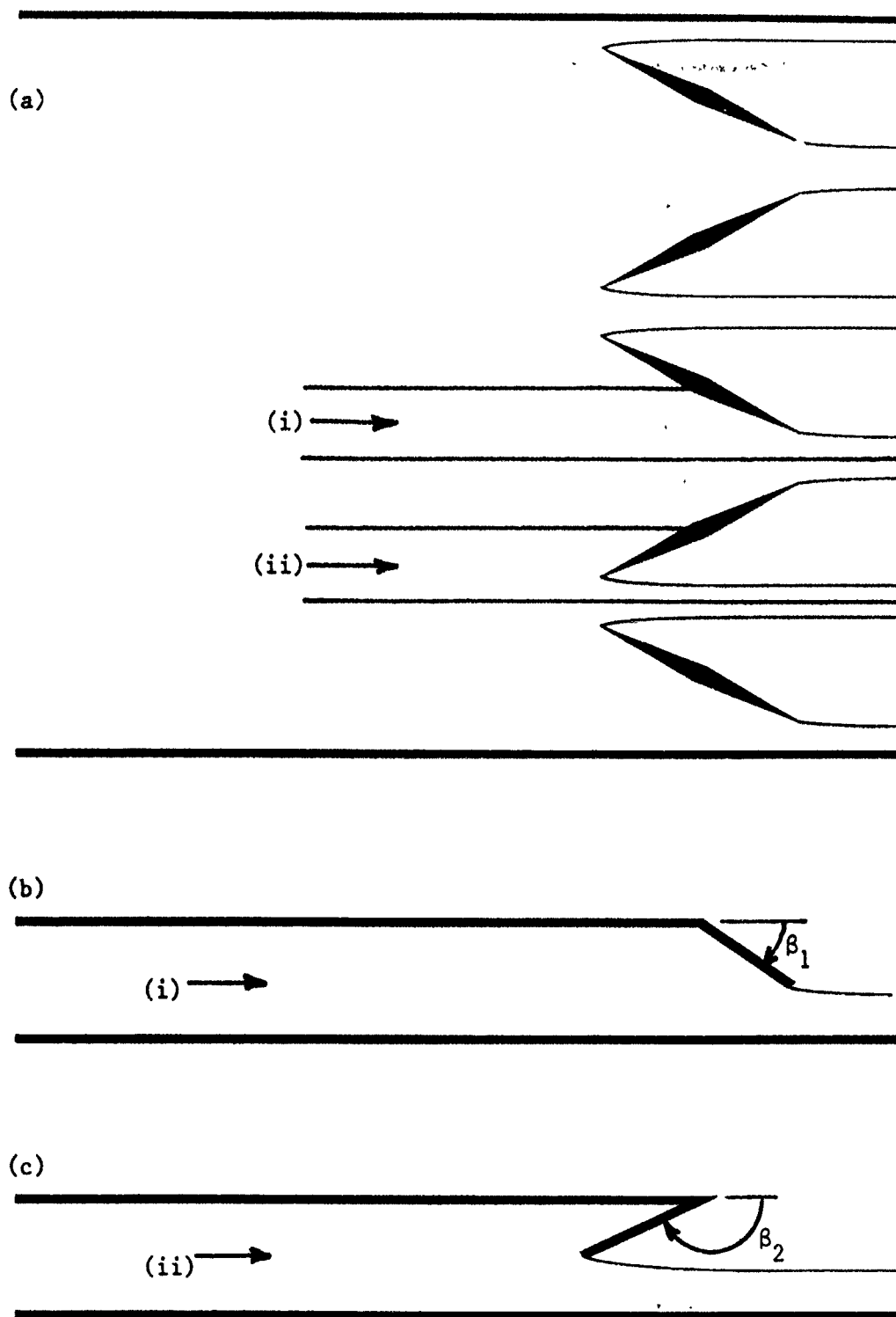


Figure 16. Illustration of the similarity between the flows through the louvers and the flows in ducts ending with a slot formed by an angled flap.

by A_{chan} ($A_1 + A_2$), then the angles β_1 and β_2 measured from the duct axis to the centerline of the louvers, as shown in Figures 16b and 16c, are given by

$$\beta_1 = \sin^{-1} \left[\frac{1}{s} \left[1 - \frac{A_{open}}{A_{chan}} \right] \right], \quad (9)$$

$$\beta_2 = \pi - \beta_1, \quad (10)$$

where l is the distance between adjacent louver pivot centers and s is the length of the louver blade. Since the louvers overlap slightly, the ratio l/s is not unity as might first be assumed, but it is slightly smaller at about 0.966. Hence, for this value the louvers are open for angles of $0^\circ < \beta_1 < 75^\circ$ and effectively closed for angles of $75^\circ < \beta_1 < 90^\circ$.

The method of obtaining values of C_{d1} and C_{d2} is now addressed, but the presentation begins with a description of jet flows from slots. A jet flow from a reservoir or duct to the atmosphere through a slot or an orifice is normally classified as subcritical, critical or supercritical, depending on the ratio of the flow stagnation pressure P_{atm} . An equivalent jet classification also in use is subsonic, sonic or supersonic. These three types of flows are illustrated in Figure 17, for the case of a duct ending with a central slot with the upper and lower flaps set at 90° . The critical pressure ratio is defined as

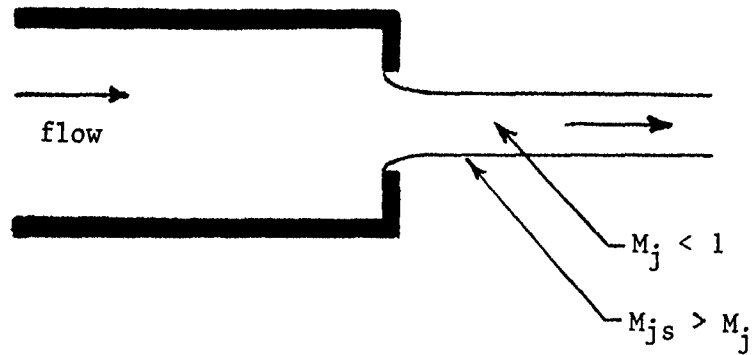
$$\eta_{crit} = \left[\frac{P_{atm}}{P_{stag}} \right]_{crit} = \left[\frac{2}{\gamma + 1} \right]^{\frac{\gamma}{\gamma - 1}}, \quad (11)$$

and it produces the sonic jet, which is the limiting case between subsonic and supersonic jet flows. This critical pressure ratio is equal to 0.52828 for $\gamma = 7/5$.

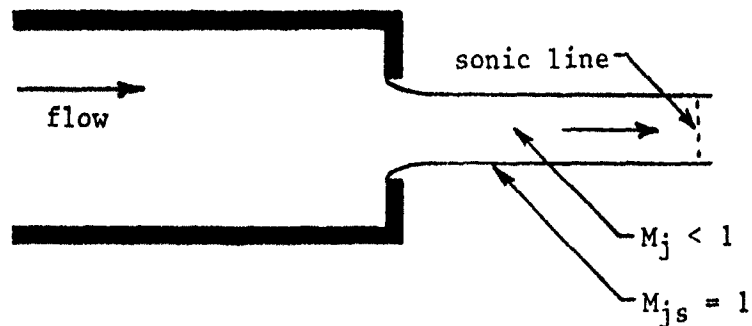
It is important to realize the significance of the classification of subcritical, critical and supercritical jets in regard to flows through reflection eliminators. The critical pressure ratio is produced by flat-topped shock waves having an absolute pressure ratio of only 1.7195 (72.8 kPa overpressure). In other words, the jet flows from reflection eliminators are subcritical or subsonic for shock pressure ratios below 1.7195 and supercritical or supersonic for larger pressure ratios. Since large blast simulators are normally designed to simulate blast waves with shock pressure ratios ranging from just above unity for weak blast waves (13.8 kPa overpressure) to as high as four for strong blast waves (310 kPa overpressure), the jet flows from reflection eliminators include all three classifications (subcritical, critical, and supercritical).

In the case of jet flows through well-rounded slots and orifices, or for jet flows that are ideally assumed as one-dimensional, the mass flow rate of the jet from conventional, steady, compressible, gasdynamic theory is given by

a) Subsonic free jet: $1 > \frac{P_{atm}}{P_s} > \eta_{crit}$



b) Sonic free jet: $\frac{P_{atm}}{P_s} = \eta_{crit}$



c) Supersonic free jet: $\eta_{crit} > \frac{P_{atm}}{P_s} > 0$

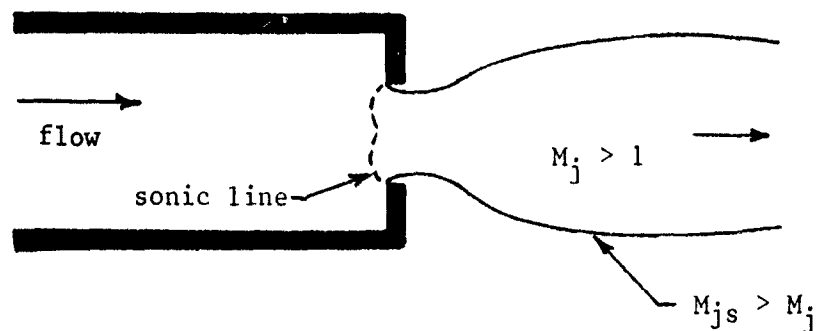


Figure 17. Sketches of a subsonic jet (a), sonic jet (b), supersonic jet (c) from a sharp-edged slot or orifice at the end of a duct, showing the jet contraction.

P_{atm}	atmospheric pressure outside duct
P_s	flow and jet stagnation pressure
M_j	flow Mach number inside jet
M_{js}	flow Mach number at jet surface
η_{crit}	$[2/(\gamma+1)]^{\gamma/(\gamma-1)}$ (0.528 for $\gamma=1.40$)

$$\dot{m} = A_e P_{stag} \sqrt{\frac{\gamma}{RT_{stag}}} M_j \left[1 + \frac{\gamma - 1}{2} M_j^2 \right]^{\frac{-(\gamma+1)}{2(\gamma-1)}}, \quad (12)$$

where A_e and M_j are the area and Mach number of the jet just as it emerges from the well rounded slot or orifice, P_{stag} and T_{stag} are the stagnation pressure and temperature of the flow, and R and γ are the gas constant and specific heat ratio of the gas. For subsonic flows, the pressure inside the jet is very nearly equal to atmospheric pressure and the Mach number M_j is then given quite accurately by

$$M_j = \sqrt{\frac{2}{\gamma - 1} \left[\left(\frac{P_{stag}}{P_{atm}} \right)^{\frac{\gamma-1}{\gamma}} - 1 \right]}, \quad (13)$$

$$1 < \frac{P_{atm}}{P_{stag}} < \left[\frac{2}{\gamma + 1} \right]^{\frac{\gamma}{\gamma-1}} = 0.52828, \quad (14)$$

where P_{atm} is atmospheric pressure and γ has been set equal to 7/5 for a perfect diatomic gas or perfect air to obtain the number 0.52828. Similar expressions can be written for the rates of flow of momentum and energy, but only the mass flow rate is required for illustration.

In the case of actual jet flows from a sharp-edged slot or orifice typical of those occurring in reflection eliminators, the previous mass flow rate equation should be considered as a simple one-dimensional or theoretical result. The actual mass flow rate from sharp-edged slots and orifices is lower than given by this equation because the flow cannot negotiate the sharp corners or edges of the slot or orifice. This results in a nonuniform distribution of pressure, density, velocity and Mach number across the emerging jet, and also a contraction of the emerging jet. A contraction or mass discharge coefficient C_d based on mass discharge can be defined as the ratio of the actual mass flow rate divided by the simple theoretical mass flow rate. In this standard approach, therefore, the previous equation for the mass flow rate is essentially modified by the addition of the jet contraction coefficient C_d , and the final result becomes

$$\dot{m} = C_d A_e P_{stag} \sqrt{\frac{\gamma}{RT_{stag}}} M_j \left[1 + \frac{\gamma - 1}{2} M_j^2 \right]^{\frac{-(\gamma+1)}{2(\gamma-1)}}. \quad (15)$$

A knowledge of the dependence of C_d on the flow upstream and through the slot is required before an accurate value of the mass flow rate can be obtained. Data for C_d can be either experimental or theoretical. If theoretical results are used, then these must correspond to the solution of the two-dimensional flow through the slot. This includes the flow approaching the slot, the flow through the slot with separation at the sharp edge, and the flow downstream in the contracting jet (which might be subsonic, sonic, or supersonic).

For subcritical or subsonic compressible jet flows from ducts through slots, Chaplygin's ideal gas jet theory [Ref. 2] has been well established to provide a possible means of solution of C_d for jet flows from slots. However, solutions in the final form of hypergeometric series are known only for certain simple duct geometries. Fortunately, some of these are fairly closely related to the geometry of reflection eliminators. Two such cases of end vents only with on-axis and off-axis jets are sketched in Figures 18a and 18b, and one case of a side vent only with an off-axis jet is sketched in Figure 18c. The solution for a reflection eliminator with a combined end and side vent can be approximated by combining the solutions for the end and side area openings and the discharge coefficients from the two cases shown in Figures 18a and 18c, although an obvious means of combining these solutions is not clear.

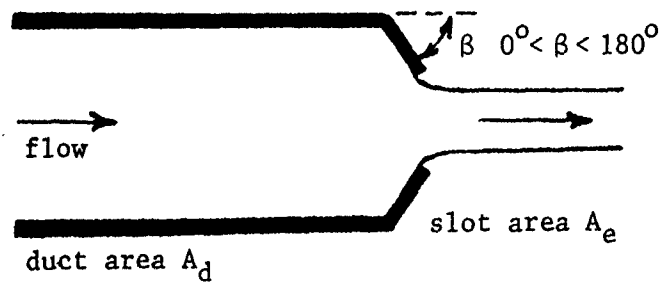
The solution for C_d for the geometry sketched in Figure 18a has now been well developed and embodied entirely in one subroutine for efficient use in computer codes for predicting unsteady flows in blast simulators. This took considerable effort and occurred in four stages. The first stage involved the generalization by Picket [Ref. 3] of Chaplygin's solutions to include the effects of the angle β from 0° to 180° , instead of just 90° as shown in Figure 18a. The second stage was studying and developing special methods of evaluating difficult hypergeometric series quickly and efficiently. The third stage was incorporating all of these results into a single computer program subroutine and making this subroutine robust (free of failure) for angles β ranging from 0° to 180° and specific heat ratios γ from 1.01 to 2. The final stage involved taking these solutions for subcritical flows and developing an extrapolation procedure to cover supercritical flows as well. This extrapolation was done partly on the basis of some available but very limited experimental data [Refs. 4-5], partly on the basis of some limited two-dimensional numerical results [Refs. 4-5], and partly on the basis of experience and intuition.

One set of results for C_d for the particular case of air flows ($\gamma = 7/5$) and an angle of $\beta = 90^\circ$ is presented in Figure 19 for illustration. However, results for different area ratios A_{chan}/A_{open} varying from 1 to ∞ are included. The experimental results in the form of "crosses" are for the particular case of $A_{chan}/A_{open} = 6$, which lies quite close to the line for $A_{chan}/A_{open} = \infty$. The theoretical solutions from Chaplygin's theory for subcritical flows are shown as solid lines, and the extrapolated results for supercritical flows are depicted with the dashed lines.

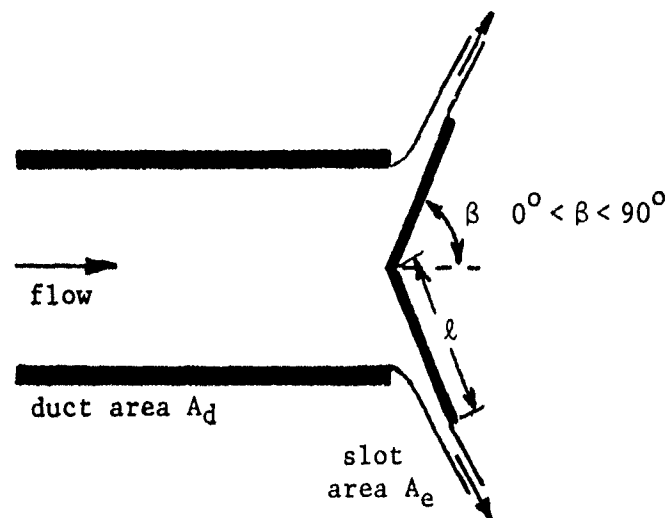
Some additional results in the same format, for the particular case of air flows through slots ($\gamma = 7/5$) and two other angles of β at 45° and 135° , are shown for interest in Figure 20. One can see that changes in the angle β produce significant changes in the discharge coefficient C_d . These results also illustrate the differences in C_d when the louver tips of a reflection eliminator are pointed outward ($\beta = 45^\circ$) and inward ($\beta = 135^\circ$).

Although the solution for the on-axis end jet (Figure 18a) is now well developed and in a convenient computer program subroutine to help in solving unsteady flows through reflection eliminators, there is still the important question of how accurate the results are in the supercritical region (extrapolated region). Some specially designed experiments would be very helpful in answering this

a) On-axis end jet



b) Off-axis end jet



c) Off-axis side jet

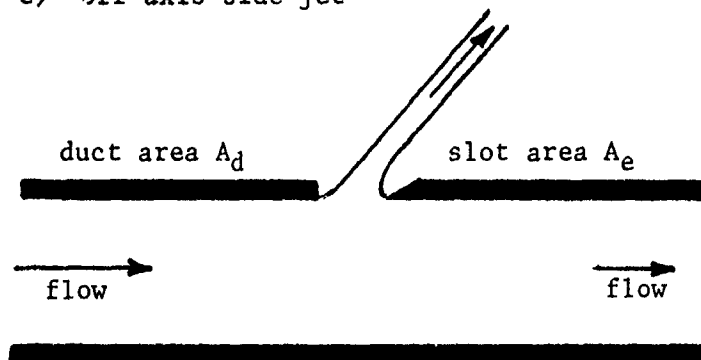


Figure 18. Sketches of an on-axis end jet (a), off-axis end jet (b), and off-axis side jet (c).

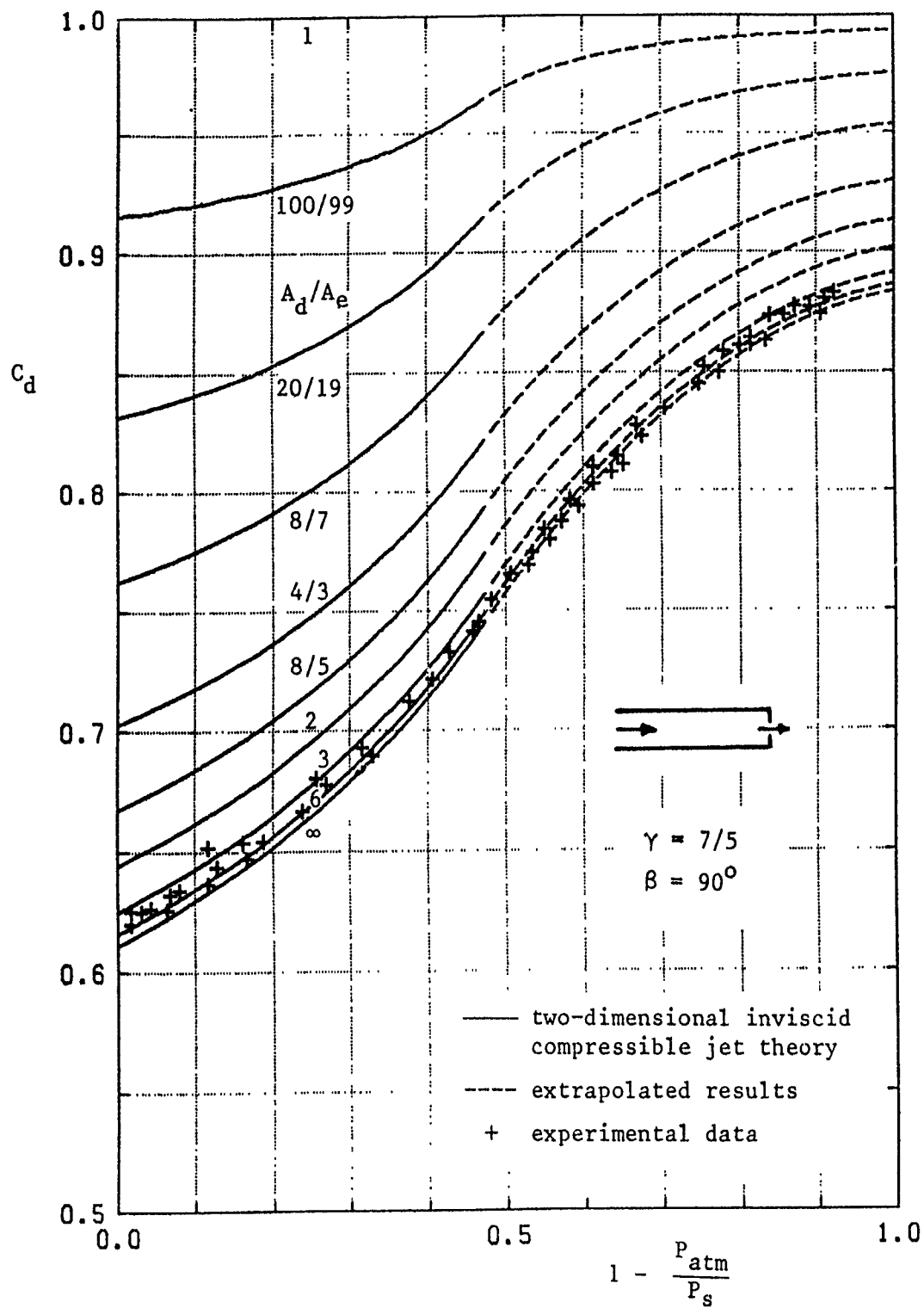


Figure 19. Contraction coefficient C_d as a function of the pressure ratio $1 - P_{atm}/P_s$ and the area ratio A_d/A_e .

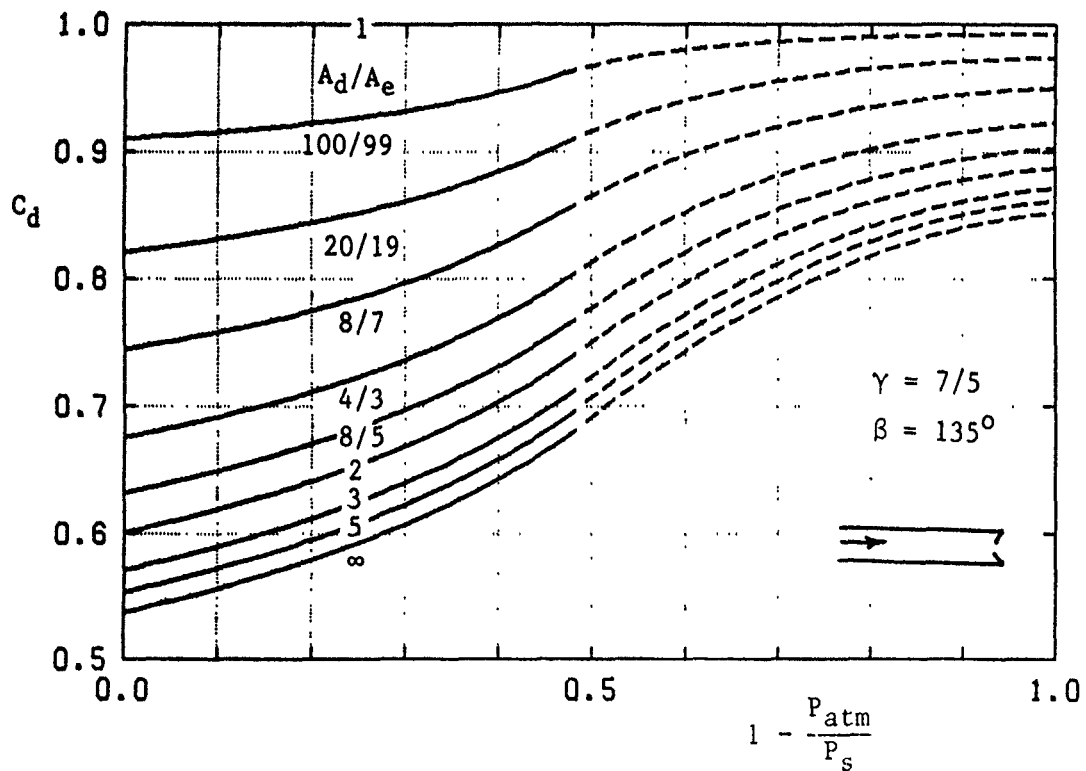
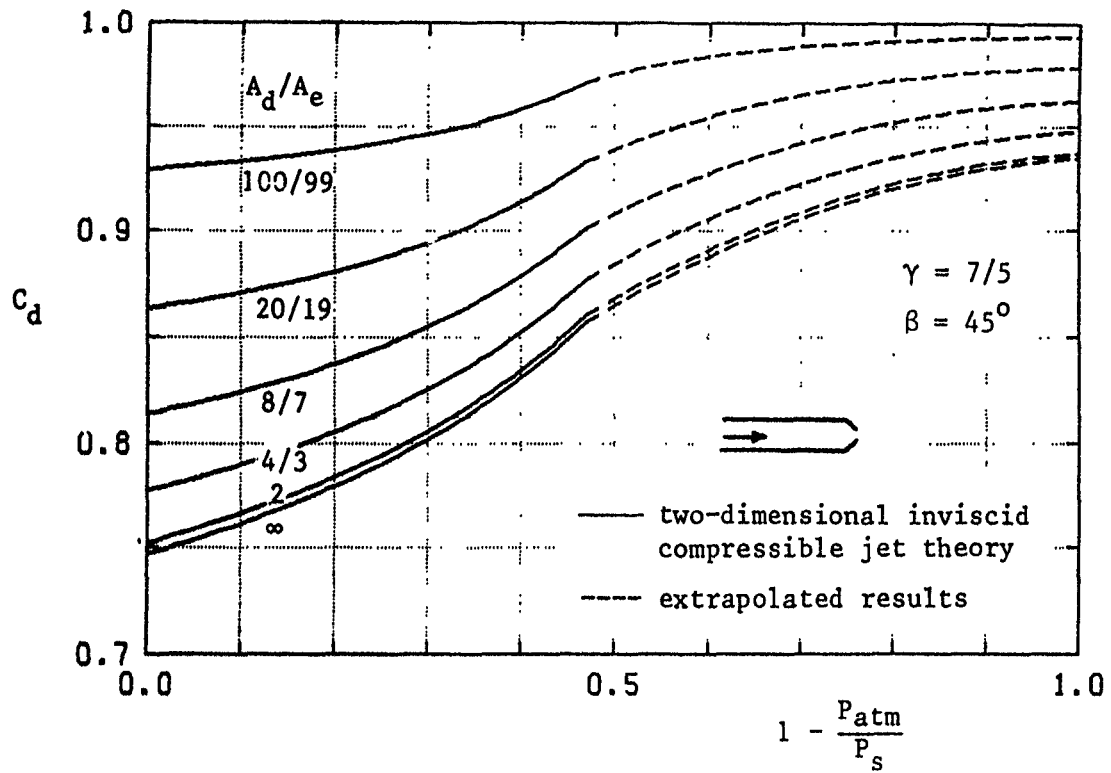


Figure 20. Contraction coefficient C_d as a function of the pressure ratio $1 - P_{atm}/P_s$ and the area ratio A_d/A_e , for two different end angles of 45° and 90° .

question and in providing data by which this extrapolation can be improved. However, time and effort were not available for doing such relevant experiments.

The solutions for the off-axis end jet (Figure 18b) and off-axis side jet (Figure 18c) are not at the same stage of development as that for the on-axis end jet (Figure 18a). The subcritical flows solutions based on Chaplygin's theory have been obtained with some important generalizations. The end plate for the geometry shown in Figure 18b can now be kinked (restricted to $\beta = 90^\circ$ previously) and also have any length l , and for the off-axis side jet (Figure 18c) the wall after the side slot does not have to be at the same vertical level as the wall ahead of the slot (as sketched in the figure). In addition to having these solutions well developed, the evaluation of the corresponding hypergeometric series has been studied and also reduced to convenient and efficient forms. However, the time and effort have not been available to embody these solutions into final computer program subroutines which can be used efficiently in the random-choice method for predicting unsteady flows in blast simulators. Furthermore, time and effort have not been available to extrapolate these subcritical solutions to cover the supercritical regime, which is an important step in obtaining accurate predictions of reflection eliminator area settings and unsteady flows in blast simulators.

In our early work on passive and active reflection eliminators, culminating in the paper in the proceedings of the Military Applications of Blast Symposium [Ref. 6], the contraction coefficient C_d was obtained for an end jet with an on-axis flow (Fig. 17a), for the case of a constant angle β of 90° . C_d was obtained for this restricted geometry from Chaplygin's theory for subcritical jet flows only, and C_d was simply held constant at the critical jet flow value for supercritical jet flows. This was the best procedure available then in view of our understanding of discharge coefficients at that time.

All of the previous presentation on the discharge coefficient pertains to the case when the flow leaves the channel (outflows). In the other case of inflows, the discharge coefficient is computed in the same manner as presented in the MABS paper [Ref. 6].

Additional information regarding the prediction of the discharge coefficient for flows through louvers, including the extrapolation procedure and a FORTRAN subroutine listing, are included in Appendix E.

NUMERICAL SOLUTIONS OF BLAST-SIMULATOR FLOWS

Euler's equations with inhomogeneous terms (Eqs. 1-3) are nonlinear and hyperbolic partial differential equations, and the solutions for blast simulators contains many discontinuities (shocks and contact surfaces). The method selected in this report to solve these equations is the random-choice method (RCM) which is based on the solution of Riemann problems with quasirandom sampling. The RCM uses an operator splitting technique to include inhomogeneous terms. The RCM is a rather unconventional finite-volume and explicit method of solution, which preserves the sharpness of discontinuities in a natural manner without smearing and Gibb's phenomena (numerical overshoots and undershoots at discontinuities). This is achieved with no extra effort, and no explicit artificial viscosity and implicit numerical viscosity are required.

The reasons for selecting the RCM for solving the blast-simulator flows in this study are: (a) simple method to apply to solve one-dimensional unsteady flows, (b) preserves discontinuities in a natural way, (c) has good accuracy, (d) boundary conditions are fairly easy to apply, and (e) uses variable node spacing and local time stepping which significantly reduces computational time. The RCM employed in this study incorporates all of the most recent improvements, including a very efficient Reimann solver with an effective quasirandom sampling procedure and a nonstaggered gridding system with variable node spacing and local time stepping. Some further details of this numerical method can be found in recent reports and papers [Refs. 7-11].

1/57TH SCALE SHOCK TUBE DESCRIPTION

The 1/57th scale shock tube located at the U.S. Army Ballistic Research Laboratory, Aberdeen, Maryland, is essentially a 25.4 cm (10 in.) diameter, air driven, circular steel shock tube. The tube is constructed in various lengths of flanged pipe which allow for rapid reconfigurations of total lengths of the tube. The majority of the expansion section of the tube is located outdoors with the driver and diaphragm sections located in a building. The normal length of the expansion section used in the RWE testing was 17.13m (56.2 feet).

During the calculation phase of the RWE development, it was assumed that the driver section would be similar to the "old" configuration. That is, the driver would have a constant interior diameter of 10.16 cm and a variable length of 11.12 to 204.15 cm. The driver would then neck down to the diaphragm section which was 6.4 cm in diameter. A sketch of the driver was shown in Figure 6. The selection of the desired peak over-pressure and durations to be created would be achieved by using various thickness and/or materials of diaphragms and varying the length of the driver section. Anticipated driver lengths and pressures were shown in Table 1. The actual breakage of the diaphragm would be achieved by increasing the driver pressure until the diaphragm ruptured on its own. This configuration of the shock tube was utilized in the RCM code calculations which were used as a basis for the design and operation of the 1/57th scale RWE.

During the interim period, after the shock tube characteristics were received and before the actual fielding and testing of the 1/57th RWE, the driver section changed dramatically. During the testing phase, the driver consisted of a completely new and unique configuration. This new design is based on a concept to provide quick closing valve(s) which can be used to shape the trailing edge of the pressure pulse. The actual diaphragm breakage is controlled by an externally controlled spear, once the driver section has come up to the desired pressure. The unique characteristic of this tube is that the storage of the majority of the high pressure gas is located in four of the driver closure tubes which are located at an approximate 45° angle off the central axis of the tube. The locations and interactions of the gasses flowing out of these tubes may cause a nonuniform flow which then may enter the expansion section causing other unknown characteristics in the pressure pulse. However, the configuration of the driver, during the RWE testing, involved only the use of the pressure fill sections and not the diaphragm spear feature (pressure only was used to burst the diaphragm). This configuration still leaves open the question of the uniformity of the flow leaving the driver section.

Finally, the existing tube had been fabricated to accept several types of pressure instrumentation at various locations on the different sections of tube. These locations can be fitted with either static or total pressure mounts/gages. The holes that are not used are filled with plugs to allow an undisturbed progression of the shock wave.

Further information of the specific configuration of the BRL 25.4 cm shock tube used for validation of the 1/57th RWE is presented in the section on "Operation of the RWE."

INTENTIONALLY LEFT BLANK.

1/57TH SCALE RWE DESIGN

APPROACH

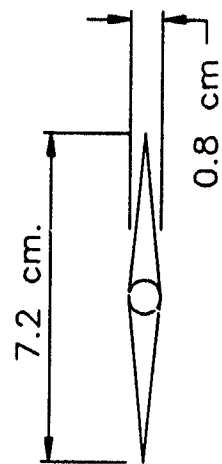
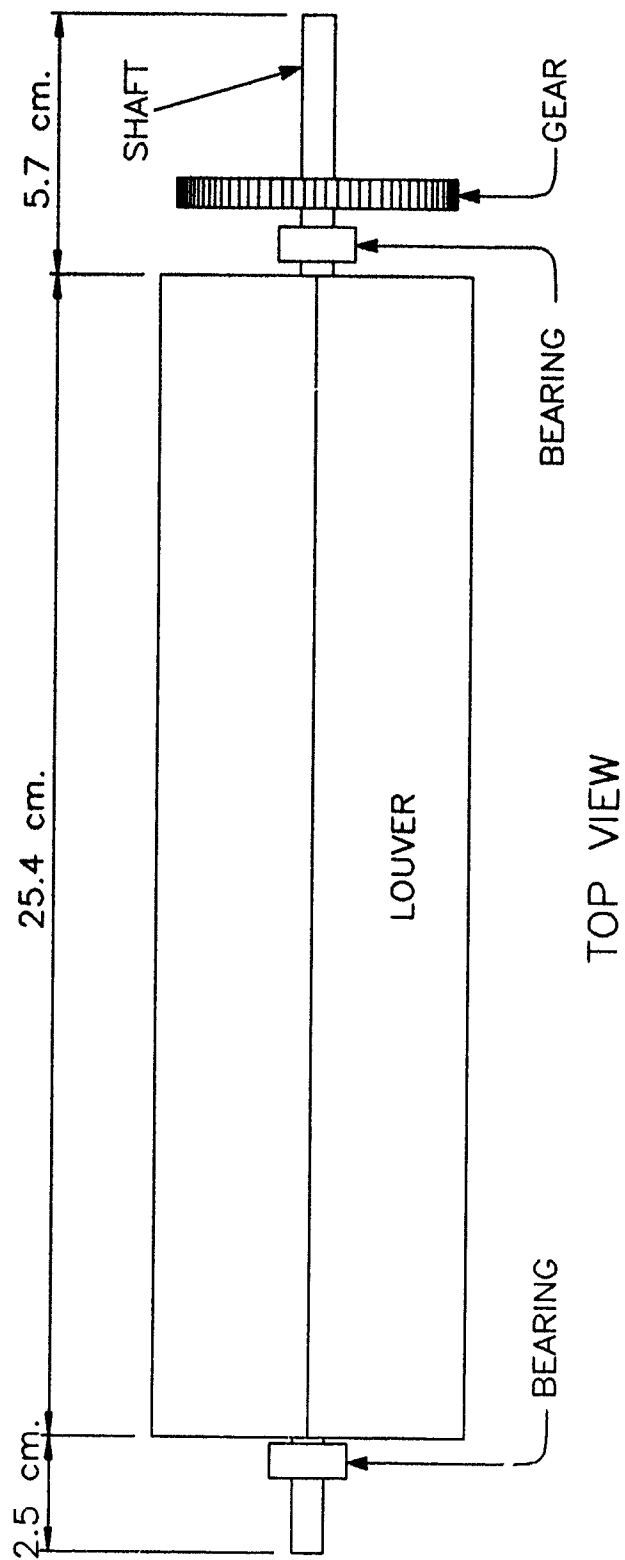
The purpose of the 1/57th scale RWE was to demonstrate the functionality of the LB/TS RWE concept of rotating louvers. The approach was to develop a design which was simple while remaining representative of the full scale LB/TS RWE system. From a practical perspective, this meant limiting the number of louvers in the system. The counter-rotating feature was seen as important and one that needed to be retained in the subscale RWE. This requires that an even number of louvers be used in the design. It was therefore decided that the 1/57th scale design would incorporate four or eight louvers.

A compromise was made in the time envelope over which the louvers were operated. On a strict scaling of the low yield case of the LB/TS, the positive phase duration of a 1/57th scale simulation would be about five milliseconds. As data on the candidate technologies for operation of the louvers was accumulated, it became obvious that execution of a specific motion profile over an interval that short was not practical. However, it is feasible to scale LB/TS high pressure, high yield conditions where the positive phase duration is two seconds. On a 1/57th scale, this would be about 35 milliseconds duration; this was found to be a typical positive phase duration for the driver on the 25.4 cm shock tube at BRL. Operation over a 40 millisecond time period was thus adopted as a design point for the 1/57th scale RWE system.

LOUVER DIMENSIONS

For a 25.4 cm diameter shock tube, four louvers would be spaced on 6.35 cm (2.5 in) centers; eight louvers would require 3.17 cm (1.25 in) spacing. This spacing corresponds to 75 cm center to center on the full scale LB/TS RWE, so that the dimensional scaling of the louvers would be 8.5% for the four louver case or 4.2% for the eight louver case. The other dimensions of the louver were to be scaled at the same proportions. Thus the louvers to be used in the 1/57th scale RWE would not be 1/57th of full scale, but would in fact be directly proportional in cross section to the latest proposed full scale design. The length of the 1/57th scale louvers was not scaled, since it was most practical to simply span the diameter of the 25.4 cm shock tube with the selected louvers. The four louver design was selected because of lower estimated machining costs for the fewer louvers and because the downscaled length of about 17 cm (6.8 in.) was close to the 25.4 cm span required for the small shock tube.

By retaining a cross section proportional to the full scale louver, the percentage of net area blocked by the louver will remain the same as in the full scale design. The closing function (open area ratio as a function of time) will therefore be similar to that required for the LB/TS RWE. This lends credibility to the 1/57th tests as representative of the effect of an RWE on the pressure decay profile of a simulated blast wave. The dimensions of the scaled louver cross section (see Fig. 21) are: chord length of 7.196 cm (2.833 in) and width of 0.79 cm (5/16 in.). The width is slightly over the 8.5% scale factor value of 0.75 cm; however, this dimension was selected to accommodate the tran-



END VIEW

Figure 21. 1/57th scale RWE louver geometry.

sition to mounting shafts at the ends of the louvers. Also, bearings used to mount the louvers to the housing are commonly available only with standard shaft sizes.

CALCULATION OF POWER REQUIREMENTS

A numerical model was developed to calculate louver position and power requirements for a single louver from the 1/57th scale RWE under loading from shock waves of different time durations. Two RWE configurations were used in the model, the first with four louvers spaced on 6.35 cm (2.5 in) centers and the second with eight louvers spaced on 3.17 cm (1.25 in) centers. Several louver cross sections were run in the model to obtain data on the impact of louver size on the power and torque requirement. The torque was specifically addressed in the model since one approach to the control of the 1/57th scale RWE is to use stepper motors which are usually torque-limited. A calculation of the bending stress and resulting displacement was also made for both louver configurations.

A solid cross section was assumed for the 1/57th scale louver design since it would be the simplest to machine. It offers the additional advantage of increased stiffness although the louver then has greater relative mass in comparison to the full scale design. For bending stress calculations, two materials were included: steel and brass. These were selected for their relative ease of machining and (in the case of steel) for the increased yield strength and modulus of elasticity. The deflection of the louver was calculated for the fully-open condition and for an arbitrary intermediate condition where a greater frontal area was exposed to the decaying static pressure during the passage of the shock wave. As expected, when including the effect of the reflection of the shock, the fully-open condition was less severe than the intermediate condition. The intermediate condition assumed an overpressure of 1.1 atm (16.1 psi), which occurs at a louver angular position of 15°. Maximum deflection for the four louver design was 0.018 mm (0.0007 in) for steel and 0.036 mm (0.0014 in) for brass. The eight louver design showed significantly greater deflections, 0.152 mm (0.006 in) for steel and 0.279 mm (0.011 in) for brass. All calculated deflections were judged to be small enough that they would not create a significant problem for the alignment and rotation of the louvers during operation of the RWE system.

Several assumptions were made to permit a calculation of the power and torque requirements for the 1/57th scale louver RWE. Perhaps the most significant was the duration of the positive phase of the shock wave in the 25.4 cm shock tube. If strict scaling is assumed for a 10 KT, 241 kPa blast wave, the time duration in the 25.4 cm shock tube is five milliseconds. This is unrealistic in several aspects: first, rotation of the louvers in an RWE from fully open to fully closed in such a short period of time imposes very large power requirements, and second, the event is not long enough to adequately demonstrate the effect of the RWE even if it could be made to operate in that time frame. Instead, the 600 KT condition was assumed, where the positive phase duration is about two seconds for the LB/TS. The 1/57th scale positive phase is then about 36 milliseconds.

The second assumption was that the rate of change in open area ratio for the RWE was constant over the positive phase duration of the scaled event. This is confirmed in a review of data from the ELIM computer model (Appendix F) for runs that used as input a computer generated pressure profile for a 241 kPa, 10 Kt blast wave. The ELIM output data, which describes the open area ratio as a function of time, is seen to be linear to a first approximation. This allows the use of a range of area ratio values of zero to one scaled inversely with the elapsed time over the positive phase duration (i.e., open area ratio of one at the start of the positive phase reduced to zero by the completion).

A simple numerical scheme was used to generate the values for the rotational velocity and acceleration terms in the calculation. The polar moment of inertia was computed from the dimensions of the scaled louvers and then used in the power calculation. The power calculation addressed the inertial requirements only and did not consider the aerodynamic forces generated by the motion of air over the louvers. This is in fact a conservative approach since the lift and drag forces act at a quarter-chord point, forward of the center of rotation. The lift and drag forces thus apply a moment in the direction of rotation of the louver and would reduce the requirement for torque from the louver prime mover.

Results from the model are shown in Table 2 below. Note that the power and torque data are for a single louver and are computed at the time in the positive phase duration where power and torque are maximum. It is quickly seen that the duration of the positive phase of the shock wave has a dramatic impact on the power and torque requirements; this is in agreement with results of full scale modeling and is due to the increase in both the angular velocity and angular acceleration when the RWE is forced to operate more quickly in the shorter time span. There is also a significant difference in the requirements for an eight louver configuration when compared to a four louver design. These advantages must be evaluated against the added complexity of the mechanical drive mechanism and controls for the system with the eight louver configuration.

Table 2. Power and Torque Requirements

No. of Louvers	Duration Pos. Phase T_{pp} (ms)	Chord Length (cm)	Louver Thickness (cm)	Power at 83% T_{pp} * (watts)	Torque at 83% T_{pp} * (m-kg)
4	36	7.19	0.757	4.4	0.0129
4	36	6.35	0.907	11.4	0.0246
8	36	3.60	0.378	0.28	0.0008
4	18	7.19	0.757	35.5	0.0519
4	72	7.19	0.757	0.56	0.0032
8	72	3.60	0.378	0.035	0.0002

* for a single louver

The chord length of the louver is also seen to be important in the results presented in the table. Again, this confirms full scale design results from other evaluations (Ref. 1). The louver with the 7.19 cm chord length is scaled from the 0.85 m chord length LB/TS louver and thus reflects the late time improvement in performance of the full scale unit (a discussion of the 7.19 cm chord length versus 6.35 cm spacing will be presented later).

A personal-computer version of the Random Choice Method became available later in the project and was used to predict the pressure profile for the 25.4 cm shock tube. The physical description of the driver was based on dimensions of the 25.4 cm shock tube initially provided by BRL. The model predicted positive phase durations of 70 milliseconds for a nominal 0.7 atm (10 psi) overpressure shock and 50 milliseconds for a nominal 1.4 atm (20 psi) overpressure shock. The positive phase duration of 36 milliseconds used in the power calculations is thus seen to be a conservative assumption.

LOUVER STRESS

There are three separate mechanisms that create stress in the 1/57th scale louvers. These mechanisms were analyzed individually to calculate maximum stresses, both axial and shear, that are imposed on the louvers. The first stress examined was the shear stress on the louver shafts from the overpressure load from the decaying shock wave. The worst case condition is one where the louver is fully closed at the arrival of the shock front and is exposed to the full overpressure over the entire cross section of the louver. Calculated shear on the shaft for this condition is 57 MPa (8,200 psi), assuming that the load is evenly distributed on the two shafts of a single louver. This calculation also included a factor of three to correct for the incident reflection of the shock as it impacted the closed portion of the louver.

Aerodynamic lift generated on the louver by the outflow from the shock tube resulted in additional shear on the shafts. The maximum lift load occurred when the louver was held at an angle of attack just under 15° during the passage of the shock front. The lift force generated was approximately 1200 N (270 lbf) and acted at the quarter cord length of the louver to produce 21 N m (185 in lbs) of torque at a 15° angle of attack. This torque on the shaft resulted in a shear stress of 210 MPa (30,400 psi) at the surface of the louver shaft. It should be noted that this analysis assumed the louver was held stationary as the shock front passed; in active operation of the louvers the aerodynamic torque was acting in the direction of rotation and thus reduced the shear stress on the shaft. However, this condition could prove catastrophic if the RWE is operated in the passive mode with an angle of attack near these positions.

At the location where the shaft merges into the louver there was a significant stress concentration due to the relatively large change in cross-sectional area. The ratio of the louver cross-sectional area to the shaft cross-sectional area was approximately 5.7:1. A review of available stress concentration literature suggested a factor of about three would be appropriate for such a condition. During the design, the fillet radius was maximized to reduce the chance of failure at this point.

The maximum bending stress on the 1/57th scale louver was due to aerodynamic lift and occurred at the midpoint of the louver when the louver was held at a 15° angle of attack during the passage of the shock front. The maximum bending stress generated was calculated at 62 MPa (9,000 psi) on the surface of the louver.

SYSTEM LAYOUT AND COMPONENT SELECTION

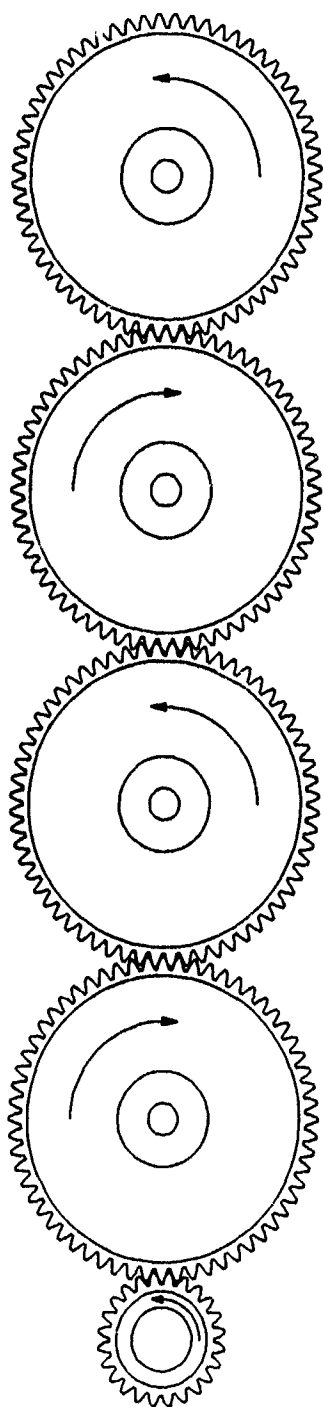
A four louver configuration was selected for the 1/57th scale RWE design based on data from the power and stress calculations. The louvers were operated via gears mounted to their shafts; the gears had a pitch diameter of 6.35 cm (2.5 in) so that each meshed directly with adjacent louver gears. This arrangement, shown in Figure 22, represented the simplest mechanism for rotation of the louvers.

One design change was investigated and subsequently adopted to further simplify operation of the louvers. Adjacent louvers were positioned with an angular offset with respect to one another. This modification was shown to allow the louvers to pass each other without interference even though the louver chord length was greater than the centerline distance between louvers. An angular offset of 5° was sufficient to avoid the collision of adjacent louvers during operation. The offset arrangement eliminated the need to decelerate the louvers near the point of contact between adjacent louver tips (near the fully closed condition).

Both stepper motors and servomotors were investigated for use as the power source in the 1/57th scale RWE. Units of both kinds which met performance requirements for the RWE were identified. Local manufacturer's representatives were visited for demonstrations of the candidate motors, and a motor selection computer program was acquired. The program was subsequently used to identify several configurations that could be used for the scale RWE.

Key parameters in the motor sizing analysis include the polar moments of inertia of the load (louvers) and the motor rotor, and the maximum torque available from the motor. The maximum torque is an inverse function of the angular velocity of the motor and drops off rapidly with increasing velocity. One way to diminish the impact of this condition is to gear the system such that the angular displacement of the stepper motor is less than that of the louvers. If the motor is geared 1:2, then it rotates 30° for the 60° of the louvers required for a full-open to full-closed cycle. However, in gearing the operation of the motor in this manner, the "reflected inertia" (effective inertia seen by the motor) is increased as the inverse square of the gear ratio (i.e., the effective inertia of the louver system is multiplied by four). The applicable design criterion for stepper motors is that the ratio of load inertia to rotor inertia should be less than ten; and for optimum response, it should be less than two.

Another criterion imposed on the search for a driver for the louvers is that the motor controls must permit the input of a variable motion profile over the time of the positive phase duration of the blast wave. The minimum acceptable resolution of the time step of the motor controller was about ten



LOUVER GEARS

MOTOR GEAR

Figure 22. Gear train showing direction of rotation.

milliseconds. This would allow the definition of at least three different motor speed/acceleration/ position coordinates over the nominal 40 millisecond duration of the baseline blast wave. The easiest means of providing such control to the motor is via a computer interface to an indexer/driver which actually generates the electrical pulses that drive the motor. The indexer/driver includes the power conversion and conditioning circuitry and a microprocessor that translates computer commands into voltages for the motor. Typically, a simple programming language has been developed by the manufacturer for operation of the stepper or servomotor.

The 1/57th scale RWE operation imposes a formidable motion profile because of the extremely short time duration of the blast wave positive phase. Typical angular velocity and angular acceleration profiles were calculated from available data, with the assumption that the worst condition would require the RWE louvers to move from a fully closed to a fully open condition in 40 milliseconds. Graphs of the results are shown in Figure 23. In an initial attempt to develop a program to control the stepper motor, the angular velocity was divided into three linear segments as indicated by the dashed lines on the plot. The control program consisted of the specification of an acceleration rate and final velocity for each segment, along with commands that initiate and stop the motion. Problems arose in that the program steps could not be transmitted to the indexer/driver fast enough to execute the program as written.

This led to the identification of an alternative computer control approach to the system. An upgraded computer control system was employed where a separate circuit board was installed in the personal computer which controlled the servomotor. The motor control boards in the computer communicated with the motor driver at much higher data rates and thus could be updated with position information more frequently. The computer could control the add-in board through most programming languages including PASCAL and BASIC with an update increment of two milliseconds. The net result of this approach was a much finer control of the motion profile of the louvers during their very short operating period.

In order to confirm that the prime mover would indeed provide a prescribed motion profile, a test was arranged to demonstrate the performance of the two candidate motors. A simulator was designed with a polar moment of inertia that was somewhat larger than that of the louver system so that if the test motor could rotate the simulator in a defined profile, it would clearly handle the actual 1/57th scale louver system.

The wheel was attached to a series of gears and shafts which were eventually connected to the shaft of the motor being tested. Table 3 shows a comparison of some of the simulator's inertia features and the corresponding 1/57th RWE features.

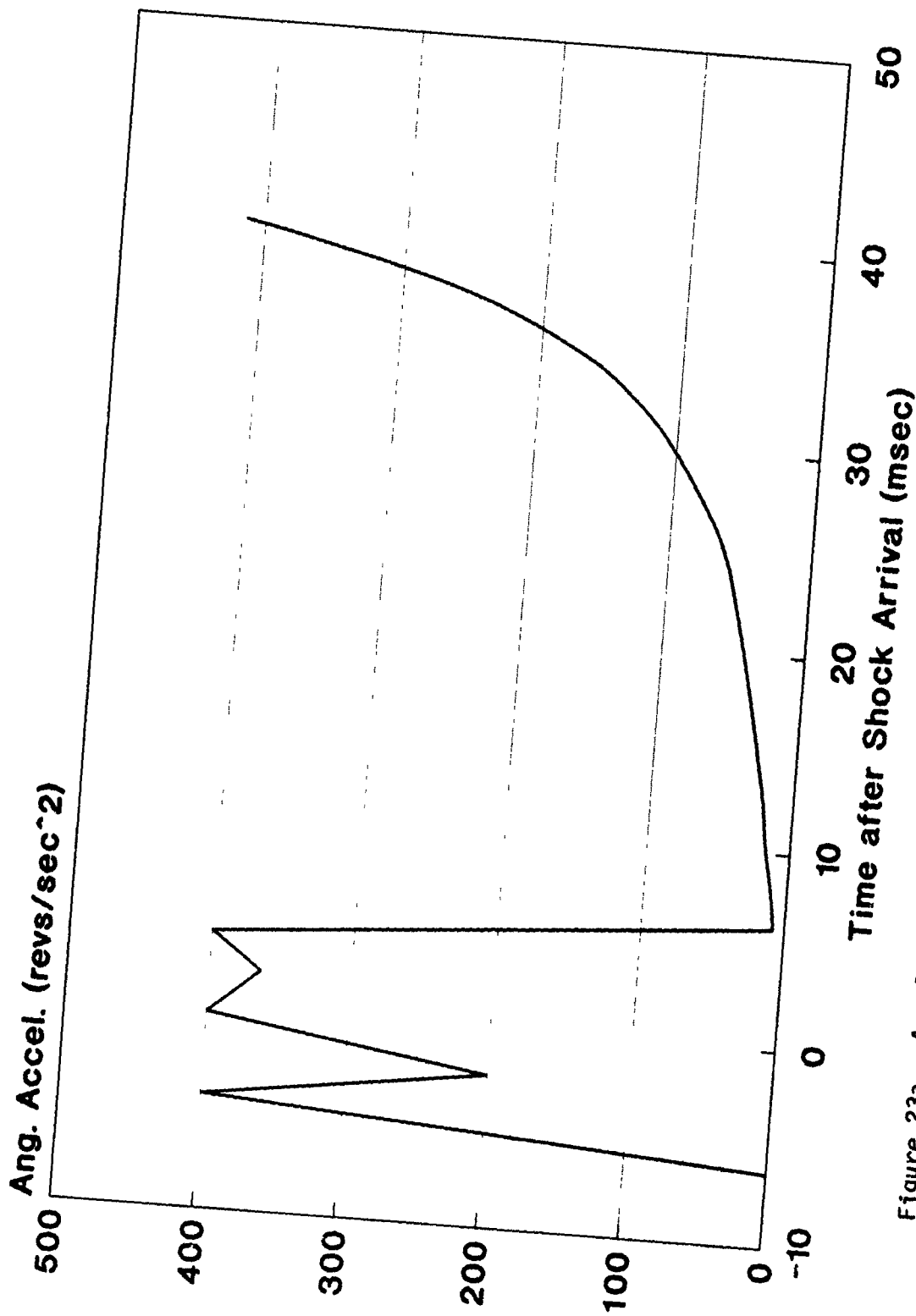


Figure 23a. Angular acceleration profile for 1/57th scale RWE.

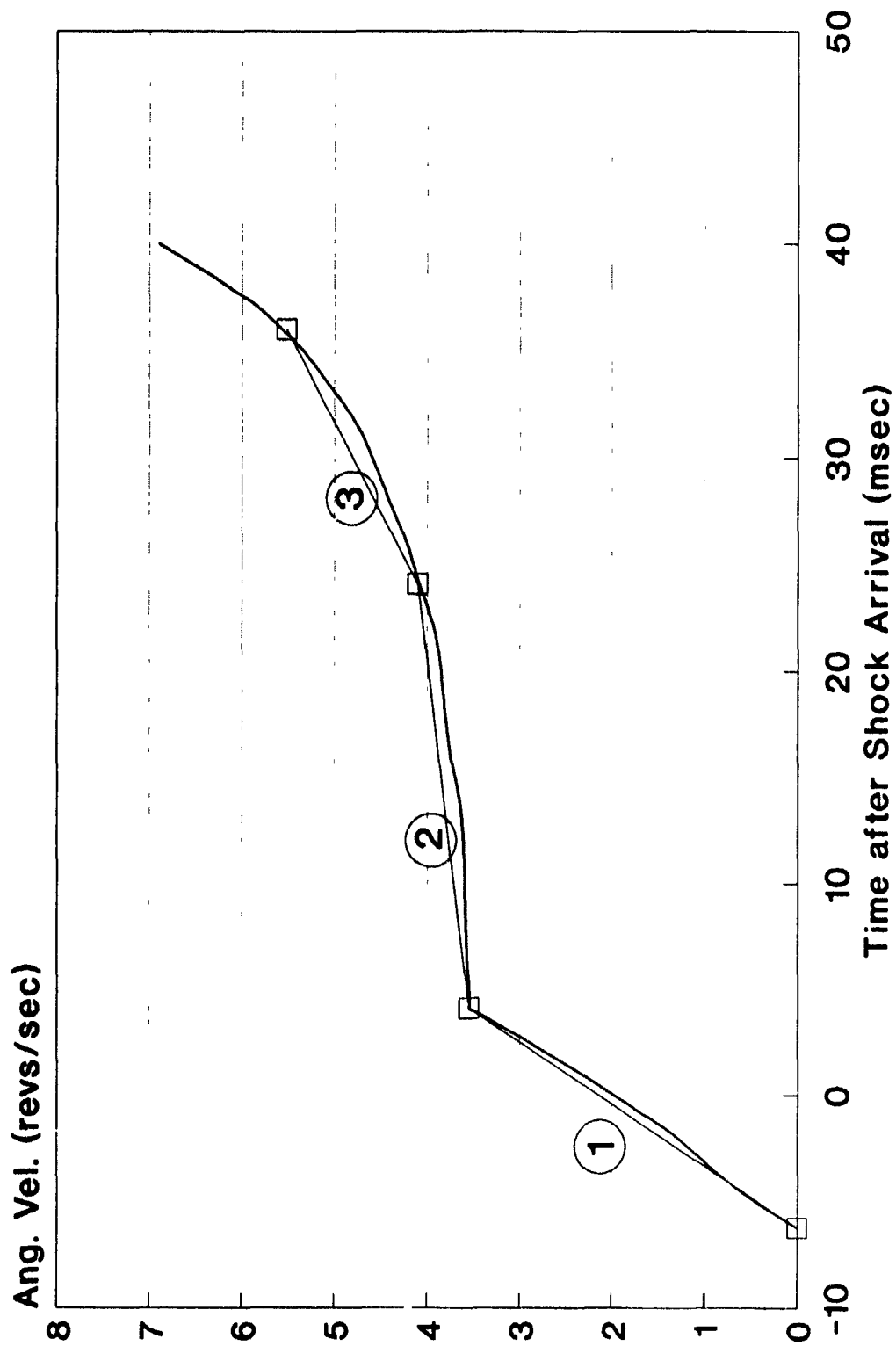


Figure 23b. Angular velocity profile for 1/57th scale RWE.

Table 3. Simulator and 1/57th RWE Inertia

<u>Feature</u>	<u>Simulator</u>	<u>1/57th RWE</u>	<u>Units</u>
A1 Disk	0.777		gm-cm ²
Brass Hub	0.009		gm-cm ²
7.62 cm Gear	0.031		gm-cm ²
A1 Louver		0.067	gm-cm ²
6.35 cm Gear		0.052	gm-cm ²
2.54 cm Gear		0.013	gm-cm ²
Bearing Friction		<u>720.0078</u>	<u>gm-cm²</u>
Subtotals	0.818	0.132	gm-cm ²
Gear Ratio	3:1	2.5:1	N/A
Reflected Inertial Load at Pinion	0.091	0.021	gm-cm ²
Drive Inertia			
2.54 cm Pinion	0.001	0.001	gm-cm ²
Shaft Coupling	<u>0.026</u>	<u>0.026</u>	gm-cm ²
TOTAL INERTIA	<u>0.119</u>	<u>0.049</u>	gm-cm ²

The simulator was scribed with series of fiduciary marks at a fixed radius, and four sets of light emitting diodes and photodetectors were positioned to detect motion of the simulator. Both candidate motors were tested, and the servomotor system was found to be superior in its ability to meet the defined profile and in its versatility in programming via the personal computer. The feedback feature of the servo system was found to be particularly valuable in the process of following the prescribed motion of the defined profile.

The brushless DC design of the servomotor has reduced rotor moment of inertia when compared to a motor that has conventional windings on the rotor. The brushless motor therefore features higher torque capacity for similar rotor inertia or, considerable reduction in rotor inertia for similar torque capacity. A further advantage of the servomotor is that the coefficients for the proportional, integral, and derivative (PID) gain equations that govern the feedback loop can be modified by the user. Thus the controller/motor system can be optimized to provide the tightest control for the angular velocity of the louvers, which results in greater tolerance on the position of the motor and louvers. This fine tuning is an interactive process and is best performed after the entire system is assembled.

The advantages and tradeoffs involved in using a gearing arrangement on the servomotor drive were investigated. The immediate advantage of a gear drive design is seen in the reduced required reflected moment of inertia of the load: the moment seen by the servomotor is reduced by the square of the gear ratio. The tradeoff is that the servomotor must run at higher velocity (i.e., for the one sixth turn that the louvers execute the servomotor must rotate through that angular displacement multiplied by the gear ratio). For example, if the gear ratio is 2.5:1, the servomotor would rotate 150° in the 40 millisecond positive

phase duration of the shock wave. This does not appear to be a constraint on the servomotor, since its top speed is above 3000 rpm (50 rps), compared to a maximum louver angular velocity of about 7 rps, which corresponds to a servo angular velocity of 17.5 rps for a 2.5:1 gear ratio. An added advantage in the geared design is that the torque required from the servomotor is reduced in direct proportion to the gear ratio. Since the velocity is *increased* by this same ratio, the motor power requirement (torque times velocity) remains the same regardless of the gearing arrangement.

Bearing loads for the 1/57th scale louvers were calculated so that bearings could be sized and selected. The load was assumed to be a 1.1 atm (16.1 psi) overpressure shock in the 25.4 cm shock tube. The load was calculated for a louver set at a 12° angle of attack and was multiplied by a factor of three to account for the initial reflection of the shock off the projected louver area. The load was found to be 1,265 N (285 lb) distributed over bearings on each end of the louver. A safety factor of two was used to determine bearing load so that each bearing was required to accept the entire load. Length of a bronze bearing for this application was found to 7 mm (0.3 in); during the initial tests, a self-aligning steel ball bearing was used to reduce friction and to ease the tolerance requirements on the louver mounts. The bearings had a shaft (inside) diameter of 7.9 mm (5/16 in) and were rated for a load capacity of 57,850 N (13,000 lb).

An analysis was done of candidate materials for gears to be used in the 1/57th scale RWE drive mechanism. Four materials were included with minimum yield stress as noted: carbon steel (137 MPa), brass (69 MPa), aluminum (83 MPa), and delrin, an acetal plastic (69 MPa). The maximum stress in each gear size was calculated based on maximum speed, torque, face width and pressure angle of the gear teeth. The minimum yield stress was then divided by the maximum gear stress to compute a "material factor of safety." The results, shown in Table 4, indicate that all of the materials checked provide a factor of safety of at least two for the louver gear regardless of pressure angle (labeled p.a. in the table). However, for the pinion, steel must be used in order to provide an adequate margin of safety in the stress generated in this gear.

Table 4. Material Factors of Safety for Gears

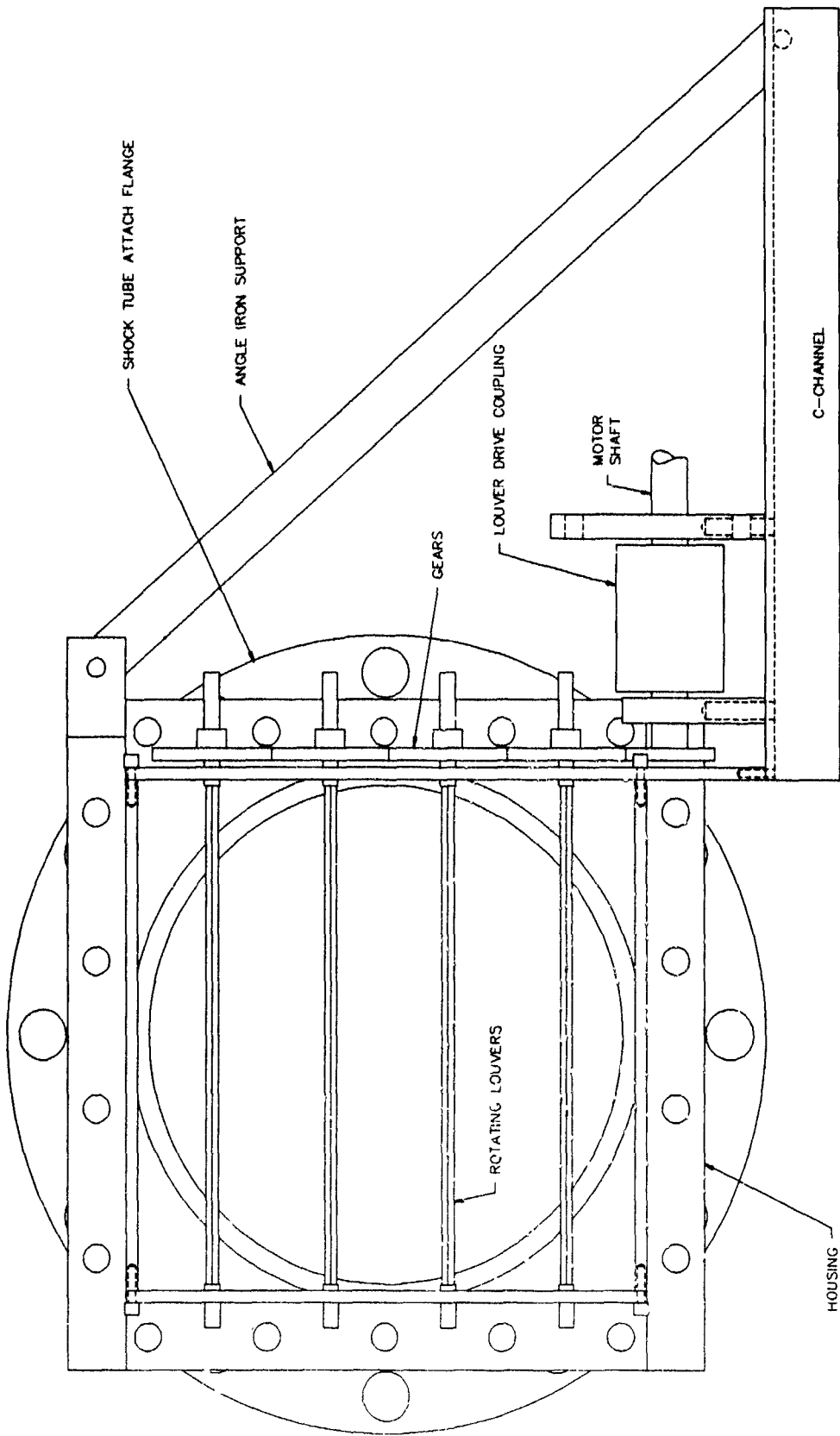
Description	Diam.(cm.)	Steel	Brass	Aluminum	Delrin
Drive Pinion	2.54	1.7	0.8	1.0	0.7
Drive Pinion	3.18	2.2	1.1	1.3	0.9
Louver (14.5° p.a.)	6.35	4.9	2.4	2.9	2.0
Louver (20° p.a.)	6.35	5.8	2.9	3.5	2.4

1/57th SCALE RWE CONSTRUCTION

Three primary features were considered during the construction of the RWE. The first being compatibility with the existing shock tube, the second, the RWE had to be easily maintained, and the third being that the RWE had to be fully self contained (i.e., not depend on any of the BRL facilities for support). In addition to these features, the RWE had to meet all of the design criteria to meet the operational requirements.

The compatibility issue was easily solved by constructing the mating end of the RWE to the shocktube out of the same size and weight of pipe and flange that the remainder of the tube was constructed. The pipe used was a 25.4 cm (10 in) inside diameter by 0.9525 cm (0.375 in) thick wall, schedule 40 steel pipe. The mating flange was a weld-on 68.04 kg (150 lb) with a raised face that matched the outer diameter of the steel pipe (see Figure 24). The length of the steel pipe was chosen based on the distance of the louver shafts (or the plane of the louvers in the closed position) to the free surface of the RWE flange being approximately one hydraulic diameter. On the end of the pipe opposite the flange, a 34.29 cm (13.5 in) by 34.29 cm by 0.9525 cm (0.375 in) steel plate with a circular hole, which matched the outer diameter of the pipe, was welded to the pipe. This plate had a series of holes along all four sides of its periphery to allow for attachment of other elements. The next element in the assembly was another steel plate with the same dimensions and bolt hole pattern as the previously describe plate, except that the interior circular hole matched the interior diameter of the steel pipe. The purpose of this plate was twofold. First, the elements holding and encasing the louvers required some type of rigid surface to be attached to and second, if one were in the correct operational conditions (i.e., high enough overpressure) washers could be placed on the bolts between the plate welded onto the pipe and this intermediate plate to provide a passive side vent.

The next portion of the RWE assembly is the actual housing of the louvers (see Figure 25). For maintainability purposes, this housing is actually made up of four parts. Each part is a piece of 0.9525 cm (0.375 in) thick angle iron which has been modified with one side being 6.985 cm (2.75 in) wide and the other 3.175 cm (1.25 in) wide (the length for each part varied, see Figure 25). The faces of the sides were milled smooth to provide intimate contact to other surfaces. Each part of angle is unique and must be in a specific place for the unit to be assembled. The shorter of the two widths of each angle were drilled with holes to match the bolt hole patterns in the two plates discussed previously. When observing the RWE from a front view, the top and bottom angles were free from holes or other protuberances. However, the ends of each short width side had three holes drilled and tapped to accept a 0.635 cm (0.25 in x 20) diameter bolt. Again referring to the RWE from the front view, the left and right angles were of different lengths and drilled in four places each, to hold the bearings for the four louvers. As seen in Figure 25, the center to center spacing between the louvers is 6.35 cm (2.5 in) starting 3.968 cm (1.5625 in) below the interior surface of the top angle. The holes drilled for the mounting of the bearings were 1.905 cm (0.75 in) in diameter. These holes were not drilled through, but a small lip with a slightly smaller diameter was left remaining on the exterior side. The purpose of this lip was to insure the bear-



RAREFACTION WAVE ELIMINATOR

1/57 SCALE
FRONT VIEW (OPEN)

Figure 24. End view of 1/57th scale RWE.

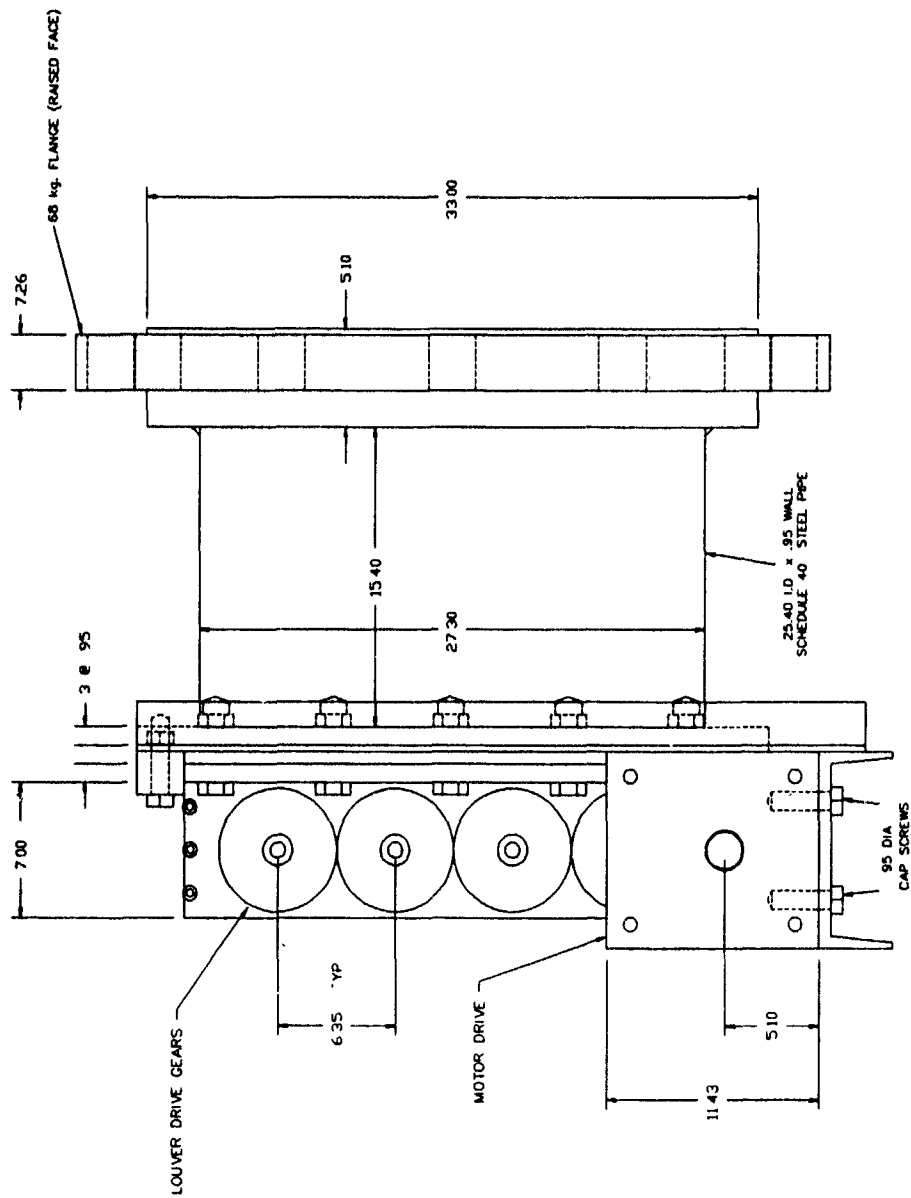


Figure 25. Side view of 1/57th scale RWE.

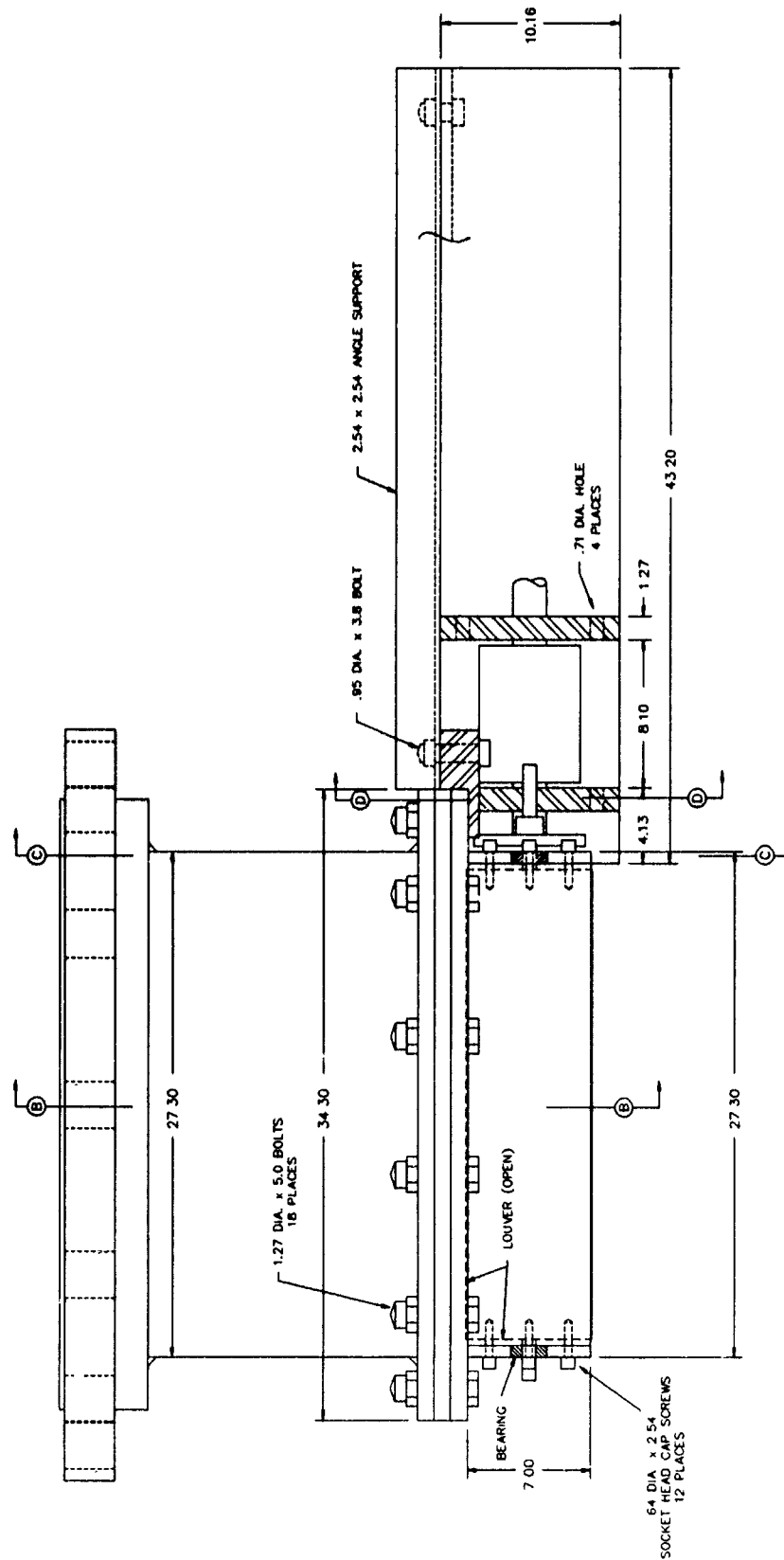
ing would not slip out of its mounting hole. Both of these pieces of angle had clear through holes 0.7937 cm (0.3125 in) in diameter drilled into them at six locations each (see Figure 26). These holes would be used along with 0.635 cm x 20 x 2.54 cm (0.25 in x 20 x 1.0 in) bolts to connect the angles. The angle on the right side extended below the bottom angle to allow for attachment of a section of 10.16 x 3.968 x 39.37 cm (4 x 1.562 x 15.5 in) "C" channel which would be used to position and support the servo stepper motor.

The "C" channel had clear through holes drilled into it at various locations to allow mounting to the right side enclosure angle, to allow attachment of motor mounting and shaft alignment plates, and to allow attachment of an angle iron support. These items are depicted in Figure 25. The plate for the motor mounting is the furthestmost right plate in Figure 25. This plate has a 2.222 cm (0.875 in) hole drilled through its center to allow passage of the motor shaft. The plate also has four smaller holes drilled through near each corner to allow for mounting of the motor. The vertical plate to the left of the motor mounting plate contains a hole through the center to allow mounting of a bearing for the 1.27 cm (0.5 in) shaft from the coupler to the drive gear or pinion. The purpose of this bearing is to assure that the drive gear is in the correct position to mate to the bottom louver gear. The final hole in this channel is at the rightmost side and located on the back face of the channel. This hole is used to bolt a 2.54 x 2.54 cm (1 x 1 in) piece of angle iron which extends up to the right hand side of the RWE enclosure. The purpose of this element is to act as a brace to prevent the motor support channel from acting as a cantilever beam only attached by two bolts. All of the elements thus far discussed are constructed of steel materials.

The remaining elements of the RWE assembly consist of the louvers and off-the-shelf components such as bearings, gears, a coupler, and bolts and nuts. The louvers constructed are shown in Figure 27. Each of the four louvers were machined from one piece of bar stock. The primary louver shape is an elongated diamond with a major to minor chord ratio of approximately 9:1. The diamond shaped portion of the louver was 25.4 cm (10 in) in length with a 0.793 cm (0.3125 in) shaft on both ends. One shaft was 2.54 cm (1.0 in) long and fit through the bearing on the left side of the RWE housing. The shaft on the other end was 5.715 cm (2.25 in) long and fit through the bearing on the right side. This longer shaft also had two flat surfaces ground onto two sides, perpendicular to each other to provide a bearing surface for set screws in the louver gear. The louvers were made of 7074 aluminum and had very sharp edges.

The gears on the louvers had a 0.635 cm (0.25 in) bore, 60 teeth, a pitch diameter of 6.35 cm (2.5 in), and an outside diameter of 6.56 cm (2.58 in) which results in a pressure angle of 20 degrees. The drive gear, which was connected to the shaft via the coupler to the motor, had a 1.27 cm (0.5 in) bore, 24 teeth, a pitch diameter of 2.54 cm (1.0 in), and an outside diameter of 2.75 cm (1.08 in) also resulting in a pressure angle of 20 degrees. All of the gears were made of 2024 anodized aluminum. As mentioned previously, two set screws were installed in the hub of each gear 90 degrees apart.

Two types of bearings were used in the RWE assembly. The bearings on the shafts on the ends of each louver were a spherical ball bearing. This bearing is essentially a portion of a single ball with a central bore that fits into a



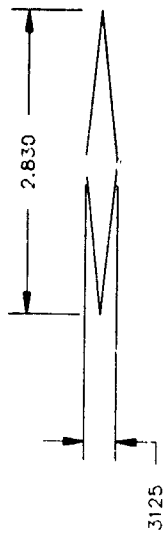
NOTES

1 DIMENSIONS ARE IN CENTIMETERS

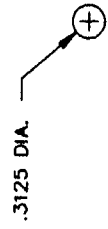
R.W.E

1/57 SCALE - TOP VIEW

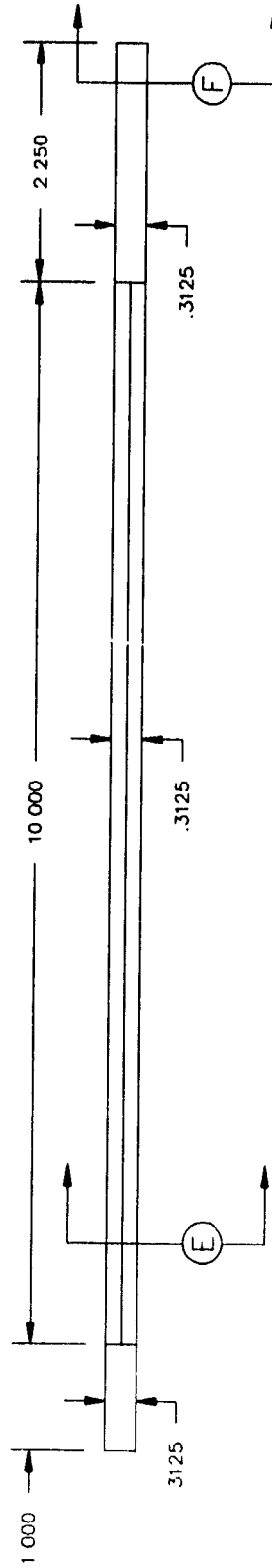
Figure 26. Top view of 1/57th scale RWE.



SECTION E



SECTION F



LOUVER DETAIL

NOTES :

1. DIMENSIONS ARE IN INCHES

Figure 27. 1/57th scale RWE Louver.

hollow cylindrical housing. There are two main advantages with this type of bearing. The first is the bearing can take tremendous unidirectional loads due to the large surface contact area and the second is that these bearings are self-aligning which allows for ease of alignment and will allow some movement if the shaft slightly bends elastically. The only other bearing used was a standard type roller ball bearing located on the drive gear shaft. The purpose of this bearing was to maintain the position of the drive gear to ensure proper alignment with the gear on the bottom most louver.

One three jaw coupler was used to connect the motor shaft to the drive gear shaft. In addition to the flexibility of the three jaw coupler to account for shaft to shaft misalignment, the coupler also allows for coupling two different size shafts together. In the case of the RWE, the motor shaft was 1.905 cm (0.75 in) in diameter, while the drive gear shaft was 1.27 cm (0.5 in) in diameter (this was due to the maximum allowable bore in the drive gear). Additionally, the three jaw coupler allows for the use of an insert between the two three jaw coupler elements. Various materials may be chosen for these inserts which operate in various performance environments. The insert chosen for the RWE coupler was made of brass since it provides optimum performance at high torque loads.

The final element constructed for the 1/57th scale RWE was a housing that covered the gear drive train. This housing is shown in Figure 28 and simply consists of formed sheet metal to help protect the gear train from the natural elements. The housing also served as a mounting surface for some of the electronic components used to try to determine the actual position of the louvers during a test.

All metal, non-moving parts of the RWE were painted with a rust deterring paint prior to shipping to the BRL. Bearings were also lubricated to minimize the amount of corrosion that would take place. However, this is a formidable task in the brakish atmosphere at BRL, and several signs of rust were noted after the first day of exposure.

A series of construction drawings and photographs of the completed RWE are located in Appendix G.

The construction of the RWE was straight-forward and built with simplicity in mind. Many features are present which can cause the RWE to be reconfigured in different operational geometries. All of the connections which require high maintenance and interchange of parts are bolted connections which only require a few hours of time to maintain. The device is fully capable of being self supporting and no other interfaces with the hardware are required other than nominal upgrades or modifications.

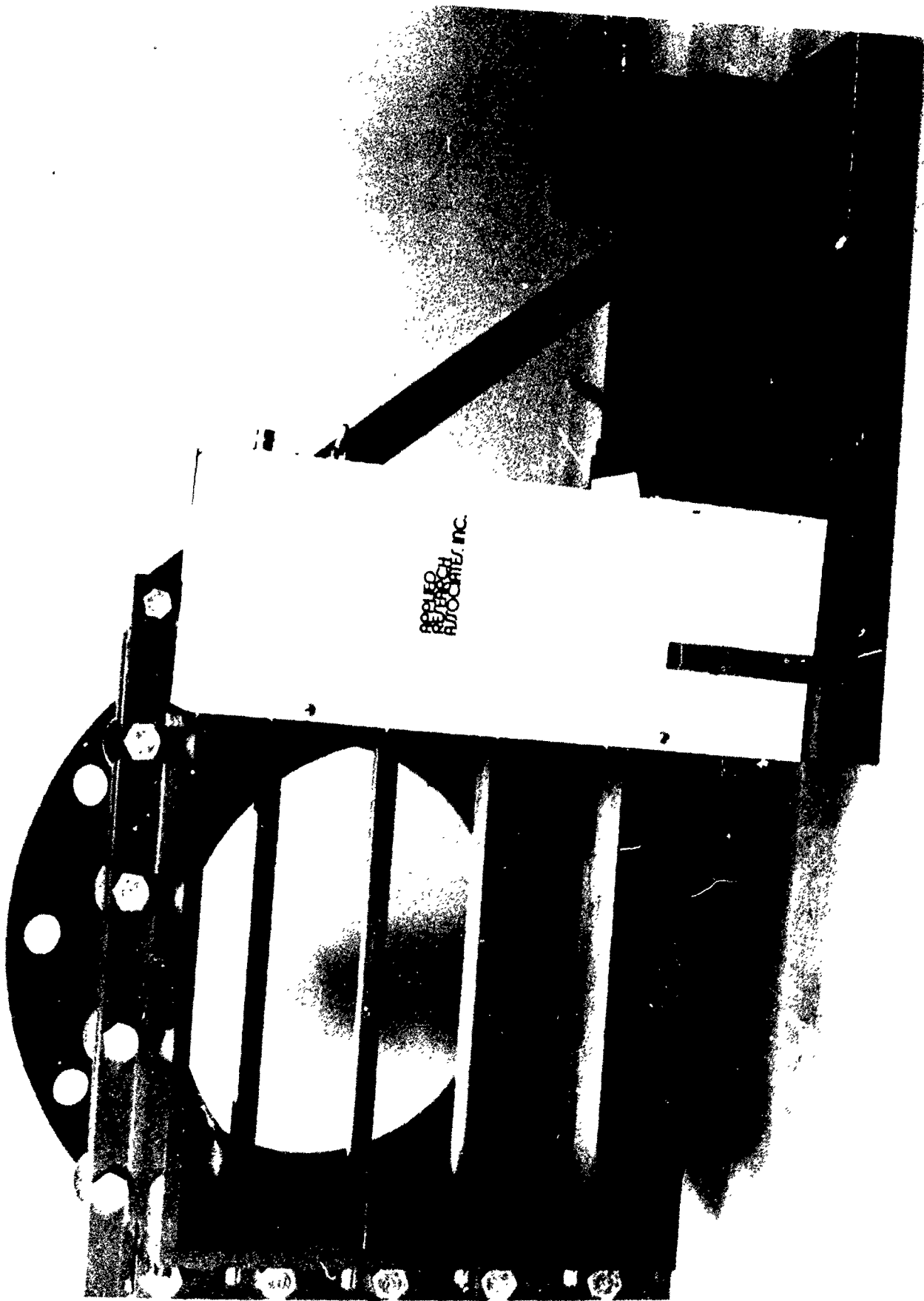


Figure 28. Environmental housing of gear train.

1/57TH SCALE RWE OPERATION

MOTION CONTROL ALGORITHMS

The servomotor that drives the 1/57th scale RWE is controlled by a personal computer (PC). An indexer circuit board supplied by the motor manufacturer which is installed in the PC converts the control commands into "step" pulses at rates as high as 500,000 per second. These pulses are used by the motor driver to control position, velocity and acceleration of the servo. An external adapter box houses the connections to drive the motor which is controlled by the PC indexer. The external adapter also has connectors for auxiliary inputs and outputs as well as for optional rotary position encoders for the motor. Auxiliary inputs are used for such functions as limit switches and external triggers which can be incorporated in algorithms for control of the servomotor. The external adapter box requires a five volt DC external power supply to operate its optically isolated interface.

The motion profile to be executed by the louvers is very short in duration and requires fine control of the louver position as a function of time. Thus the update interval of the motion control device must be as small as practically possible with maximum resolution of angular position. Two aspects of the drive train design contributed to the precision of the positioning that could be achieved. The first was that the gear ratio of 2.5:1 of the drive train. This meant that the servomotor rotated two and one half times as far as the louvers during the start to finish motion of the louvers. The second was that a resolution of 5,000 steps per revolution was implemented on the servomotor selected to power the louvers, allowing very precise control of the rotor position of the servomotor.

The personal computer indexer features an operating mode that considerably eases the programming of the motion profile for the 1/57th scale louvers. The mode, termed "timed data streaming," allows any positioning or velocity profile to be followed by the servomotor by dividing the profile into small straight line segments. A series of commands is required to operate the servomotor system in this mode. The first command sets the mode and is followed by commands in a time update interval (in milliseconds). The smallest update interval allowed in the system is two milliseconds. Succeeding commands are a series of values that designate the number of steps (calculated from a resolution of 5000 steps per revolution) that the servomotor is required to move in each update interval. One additional command is utilized in the operation of the 1/57th scale RWE: a triggered hold command. This delays execution of the motion profile until a specified trigger condition is satisfied. This would allow a pressure transducer in the shock tube to activate the motion profile of the RWE. A schematic of the entire command train is shown in Figure 29.

PREPARATION OF MOTION PROFILE DATA SETS

The motion profile to which the servomotor is driven is based on the pressure decay profile expected for an infinitely long shock tube; that is, one in which no rarefaction wave is present. This profile can be obtained in several

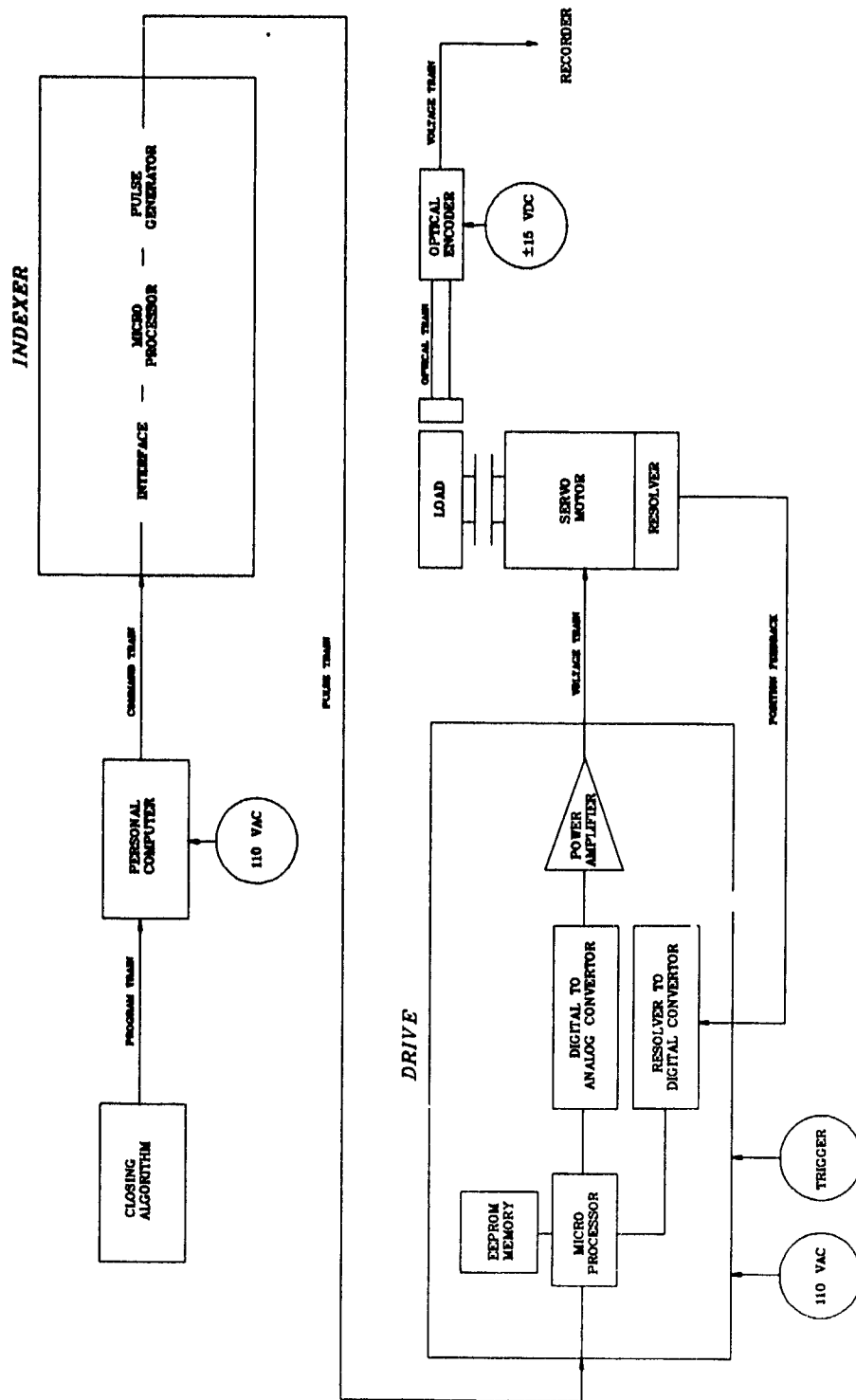


Figure 29. 1/57th scale RWE control schematic.

ways. The first is to add an extension to the shock tube on which the RWE is to be installed and make a measurement at the planned RWE station for driver conditions for which the RWE will be operated. A concern for this approach is to make certain that the measured profile is properly interpreted so that the contact surface and/or flow disturbances are correctly identified. An alternative is to model the performance of the shock tube with a computer program. The concern for this option is that the configuration of the shock tube can significantly impact the shape of the pressure decay so all details of the shock tube must be included in the model. Of course, the greater the detail, the more computer time required to run the model. One other alternative is to scale the profile from one measured upstream in a short shock tube for an initial condition of interest. This is perhaps the least accurate, but simplest method of acquiring a pressure decay profile.

The next step in the generation of a motion profile for the servomotor is to create an array of data of open area ratios that corresponds to the pressure decay profile values at specified time steps. This step can be accomplished with the computer program ELIM (see Appendix F). The program uses a quasi-steady state approach to the calculation of open area ratios and requires as input an overpressure ratio and radius of rounding for the RWE outlet (in order to compute a jet contraction coefficient for the flow). The output area ratios are between zero and one, representing the fraction of the shock tube cross section that must be open for the specified overpressure.

The final step in the process is the calculation of incremental steps to be moved by the servomotor in each time step of the controlling computer program. A simple program is required to produce this data. Key parameters for the calculation are the resolution of the servomotor, the gear ratio of the drive train, and the data set of time from shock arrival and the corresponding RWE open area ratio. The output of the program is a series of values for the incremental steps for each time interval of the servomotor controlled. This data series is written as an ASCII file that is subsequently read and used as input by the servomotor control software.

The computer program for the prediction of the open area ratios for the RWE runs only for overpressure ratios greater than one (i.e., during the positive phase of the pressure decay). The louvers are effectively closed at the end of the positive phase because of the clearance between adjacent louvers of about a millimeter. This minimal clearance condition is maintained as the louvers continue to rotate for approximately 60°. Then the louvers begin to move apart and the open area ratio starts to increase. This is a condition that is calculated as necessary to use an active RWE during the negative phase of the pressure decay.

There is no simple means to predict the open area requirements for the negative phase as a function of time; however, calculations with the RCM code performed at the University of Toronto indicate that the rate of increase in the open area ratio during the negative phase is greater than the rate of decrease at the completion of the positive phase. With this in mind, a motion profile was developed for the negative phase of the 25.4 cm shock tube tests. The rate of rotation of the louvers was increased rapidly immediately after a closed condition was achieved and was then decreased to a value above the final increment

at the end of the positive phase. After an additional 20 milliseconds, the louvers were brought to rest. This negative phase motion profile was strictly an estimate and the results will merit further examination.

SERVOMOTOR CONTROL SOFTWARE DEVELOPMENT

Software for basic operational checkout of the servomotor indexer control board, driver and motor unit was included with the servomotor system. Specific applications software was not included although there were a series of modules from which a control program could be constructed. The modules included communications to and from the indexer circuit board via the personal computer bus as well as reset and timing functions. The vendor had prepared a simple control program that was used in the demonstration of the ability of the servomotor to execute a motion profile with a two millisecond time interval. The demonstration program did not include the implementation of a trigger function although it was known to be available in the system.

In order to use the indexer to operate the servomotor, it was necessary to incorporate a trigger. The actual motion profile of the servomotor had to be initiated by the passage of the shock front upstream from the end of the shock tube where the RWE was mounted. The operational program was modified to add the trigger function, but the execution was found to be intermittent, and the time between trigger initiation and the start of motion in the servomotor was measured to be about 30 milliseconds. This was borderline in terms of the possible locations for a transducer from which to trigger the motion (due to shock tube length), but more importantly, the time lag was found to be variable between 22 and 40 milliseconds. The standard deviation of the variation was 4 msec., which presented a condition where there was too much uncertainty over the exact time at which the RWE would be triggered. This variation could create a significant mismatch between the actual RWE open area and the needed RWE open area, which would alter the effect of the RWE on the pressure profile of the shock decay from the desired correction.

A program was written in Turbo C 4.0, and the modifications to add the trigger function were also included. Several algorithms to reduce the execution time of program with the trigger function implemented were written and tested but never functioned properly. As an alternative, a BASIC program was written which employed modules supplied by the servomotor vendor. The program execution was much slower than the Turbo C version, but execution time became irrelevant since the motion profile was loaded into the indexer but was not initiated until the trigger signal was activated.

The BASIC program was written and proven with a series of tests where the time between trigger and the start of motion of the 1/57th scale louvers was measured. For this new program, the average time from trigger to the start of motion was 11.7 ms with a standard deviation of 0.6 ms. These figures represented a condition that is more easily accommodated in the location of the trigger pressure transducer upstream of the RWE.

Several features were added to the software during its initial operation on the BRL 25.4 cm shock tube. A function to preset the louvers to the initially required position for peak pressures below the 2.4 atm (35 psi) was programmed. The user simply enters a figure which is the number of servomotor steps that the louvers are to be rotated and hits the ENTER key on the personal computer; the servomotor will then position the louvers at this position. Another function resets the louvers to the fully open position after the completion of the programmed motion profile (i.e., rotates the louvers 180° so the optical tracker is in the proper position).

INTENTIONALLY LEFT BLANK.

EXPERIMENTAL PROGRAM

SHOCK TUBE CALIBRATION

Prior to installation and testing of the RWE, several tests were conducted to "calibrate" the BRL shock tube. These tests consisted of operating the tube at the three nominal test conditions: 34.5, 68.9, and 103.3 kPa. Several tests were conducted at each pressure level with the tube configured with 17.13 m of expansion section to an open end condition (i.e., the tube was open to the atmosphere at the location where the RWE would be later attached). After these tests were complete, an additional set of tests were conducted at the same pressure levels with a tube extension (4.28 m) on the end of the previous open end (Fig. 30). Results from both sets of these tests were used as a comparison for the results obtained when the RWE was operating. The open tube results would show the immediate effect of the rarefaction wave in the test section, while the extended tube results would show more of the positive phase duration (approximately an additional 25 ms) until the delayed arrival of the rarefaction wave. Therefore, the RWE results should follow the extended tube results and then keep the pressure up through a gradual decay to ambient pressure in the proper time frame. Table 5 denotes the tests used for the "calibration" and their respective peak pressures and the shock tube configuration.

Table 5. Shock Tube Calibration Configuration

<u>Test Identifier</u>	<u>Peak Pressure (kPa)</u>	<u>End Configuration</u>
BLINE*6	34.9	Open
BLINE 7	34.0	Open
BLINE 8	71.4	Open
BLINE 9	76.3	Open
BLINE 10	94.6	Open
BLINE 11	92.9	Open
BLINE 12	40.0	Extended
BLINE 13	40.2	Extended
BLINE 14	82.9	Extended
BLINE 15	83.7	Extended
BLINE 16	115.4	Extended
BLINE 17	100.9	Extended

* abbreviation for baseline

Static and total piezoelectric pressure gages were located at various distances along the shock tube to measure the environment. Of primary interest were two specific locations. The first location was immediately downstream of the diaphragm. The output of this gage would be utilized to trigger the RWE system. Previous tests that were conducted indicated that the transit time of the shock wave from this location to a location just upstream of the RWE loca-

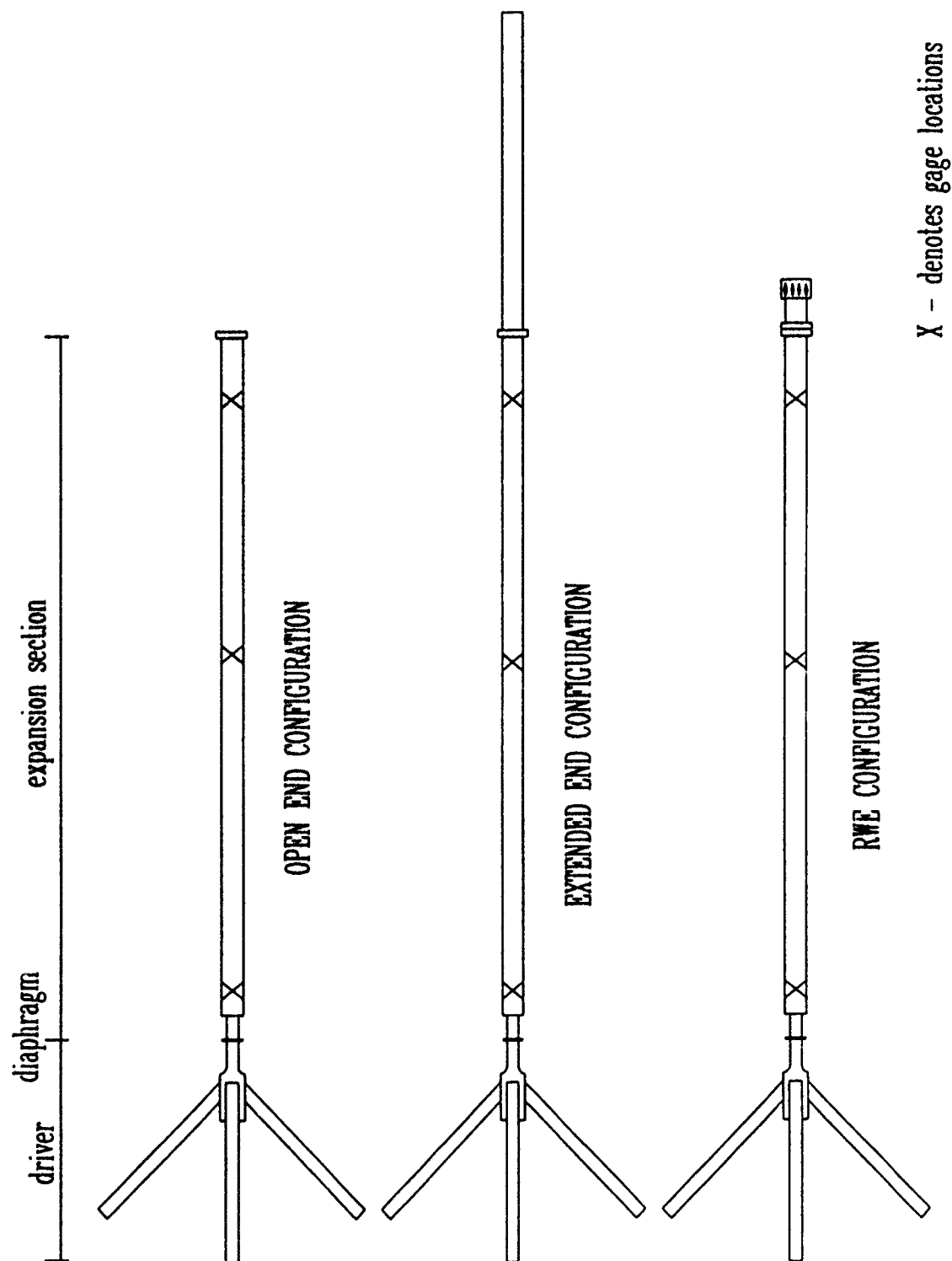


Figure 30. Various shock tube configurations for 1/57th scale RWE tests.

tion was on the order of 12 ms. The second location of interest was at a position approximately three hydraulic diameters upstream from the end of the tube. This location was termed the "test section." The gage results from this position would be used to evaluate the performance of the RWE. Table 6 gives the location and type of instrumentation used in the calibration tests.

Table 6. Pressure Gage Locations

<u>Test Identifier</u>	<u>Distance from Diaphragm (m) (type of pressure measurement)</u>			
	<u>Gage 1</u>	<u>Gage 2</u>	<u>Gage 3</u>	<u>Gage 4</u>
BLINE 6 through 17	0.42-Static	1.94-Static	13.47-Static	13.47-Total*

* Note: Total pressure port is facing upstream

When the calibration and RWE tests were conducted, the shock tube valve system was not working so the operation of the tube consisted of retracting the plug/valve and then filling the driver reservoir until the pressure exceeded the burst pressure of the diaphragm. No effort was made to actuate the plug/valve. Nitrogen gas was used to fill the driver section, and various thicknesses of diaphragm materials were used to allow for variations in driver pressures and shock amplitudes. Table 7 presents the driver conditions for the calibration tests.

Results from the calibration tests are shown in Appendix C.

Table 7. Shock Tube Calibration Driver Conditions

<u>Test Identifier</u>	<u>Driver Pressure (MPa)</u>	<u>Diaphragm</u>		<u>Peak Pressure Obtained (kPa)</u>
		<u>Material</u>	<u>Thickness (mm)</u>	
BLINE 6	1.826	Mylar	.254	34.9
BLINE 7	1.895	Mylar	.254	34.0
BLINE 8	6.271	Aluminum	1.016	71.4
BLINE 9	6.685	Aluminum	1.016	76.3
BLINE 10	10.062	Aluminum	1.549	94.6
BLINE 11	9.958	Aluminum	1.549	92.9
BLINE 12	not recorded	Mylar	.254	40.0
BLINE 13	not recorded	Mylar	.254	40.2
BLINE 14	6.133	Aluminum	1.016	82.9
BLINE 15	6.271	Aluminum	1.016	83.7
BLINE 16	10.406	Aluminum	1.575	115.4
BLINE 17	10.268	Aluminum	1.575	100.9

OPTICAL TRACKER

An "optical tracker" was designed and developed in an attempt to measure the true position of the louvers versus the desired position (see Figure 29). The device was fairly simple and consisted of a commercially available light emitting diode/photodiode (LED/PD) unit and a scribed surface. The LED/PD required only a power source (9 volt battery) and a few resistors to condition the signal to operate. The surface of one of the gears on one of the louvers was painted black and then scribed at every 6 degrees. The scribe marks were made deep enough to ensure that the aluminum material of the gear was observable. This method was adopted since a high contrast ratio was desired between the scribe marks.

The theory behind the optical tracker is that as the gear rotates and a light source is directed at the scribed gear a reflection of the light will occur. This reflected light will be more intense if a reflective surface is present (the scribe marks) than a darker (less reflective) surface. The photodetector will pick up the reflected light and convert the signal into an analog output. The difference between the amplitudes of the signal from the reflected light will indicate when a scribe mark passed by the photodetector and hence the position of the louver.

The optical tracker was installed on the gear on the upper most louver of the RWE. This location was chosen since this gear/louver combination would experience the most deviation from the desired position due to the additive effects of the gear to gear connections and backlash. The electronics for the optical tracker were installed on a small circuit board attached to the gear train housing. A simple on/off switch was mounted on the gear housing to supply power to the LED/PD unit and a coaxial port was also installed to provide a pick-up of the resultant signal.

RWE TESTS

Upon completion of the calibration tests, the 1/57th scale active RWE was installed on the open end of the shock tube. Control cables were routed back to the enclosure housing the driver section of the tube. The RWE stepper motor controller was connected to an isolated power supply since it creates high voltage and noise which could contaminate the instrumentation for the shock tube operation and data recording. The PC controller and indexer were also set up in this building. A terminal strip was installed next to the computer to allow for connection of the external trigger. The external trigger was obtained by splitting the output from the first gage downstream from the diaphragm and taking one of these outputs and inputting it into an amplifier. The amplifier was then set with a gain that would be sufficient enough to trigger the RWE command train.

In an attempt to monitor the operating mechanical performance of the RWE, the output from the optical tracker was fed back to the recording unit. The output from the tracker would be recorded, along with pressure transducers, during a test. All recording and reduction of the data was performed by BRL personnel.

Prior to testing, several dry runs were conducted with the RWE to ensure that it was functional. Arbitrary, as well as actual closing functions, were programmed into the stepper motor controller. These command trains were then given a manual trigger by applying 5 volts across the appropriate terminal strip locations.

Since the actual operation conditions of the shock tube were different than was initially assumed due to the change in driver geometry, the closing functions developed using the RCM code were useless. Fortunately, new closing functions could be developed on site using the actual results from the calibration tests. The only problem in using the calibration data was that the influence of the rarefaction waves was present in the data. To overcome this deficiency, experienced judgment was used to extend the pressure profile to an estimated true positive-phase duration. An example of this estimation is shown in Figure 31. This scenario is for a high-pressure case and shown are the actual data from an open-end and extended calibration test. The dash-dot line shows the estimated pressure profile upon which the closing function was developed.

Figure 32 shows the closing functions used for all three different pressure amplitude tests. There were two different closing functions used for the high-pressure tests: RWE7 and RWE8, since less than encouraging results were obtained from test RWE7. An interesting feature noted in Figure 33 is that the RWE appears to be in the completely closed configuration for a long period of time (approaching 40 msec duration). However, this is not actually the case. Since the louvers overlap and are offset by a small angle relative to the neighboring louvers, the RWE appears to be completely closed when the louvers are at 59 degrees above or below a horizontal plane instead of 90 degrees to this plane. Then, as the louvers rotate through the 90 degree position, the RWE does not appear to be opening until the louvers have rotated to 121 degrees. This aspect of the RWE was determined during the design process and taken into account. Figure 34 provides more insight into how this problem is overcome. The figure shows the closing rate at which the louvers must move for each different pressure amplitude. Between 40 and 80 msec there is a dramatic change in the rate at which the louvers are rotating. This period is the same as when the RWE appears to be closed. Essentially, the RWE motor is operating at its maximum speed (without creating a stall condition) to transverse the 62 degree "closed" region as quickly as possible. During later times, the RWE is essentially coasting and stopping at the fully open position.

When comparing the theoretical RWE closing functions and the functions actually used in the testing, a difference will be noted in the initial area ratios. The theoretical ratios are slightly below those used in the tests. The rationale for this discrepancy is due to the actual physical geometry of the RWE. In the area of transition from a circular tube to the location of the louvers, the RWE expands into a square geometry. This transition space appears to the shock wave as an immediate area expansion, hence creating rarefaction waves. Therefore, the actual initial louver settings were adjusted to make the RWE more closed, thus creating stronger reflected waves which would balance the rarefaction waves.

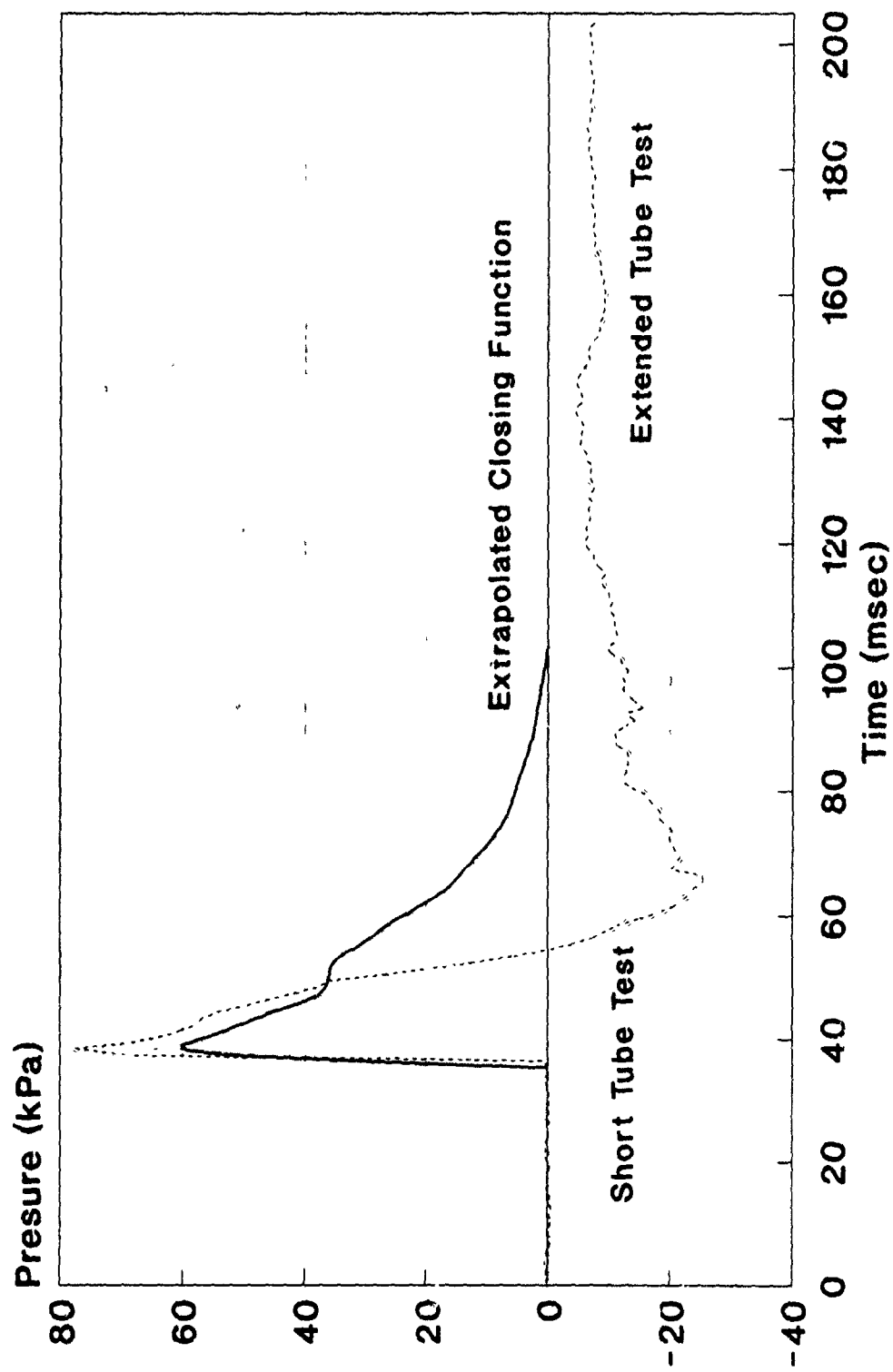


Figure 31. Estimation of closing function based on test data.

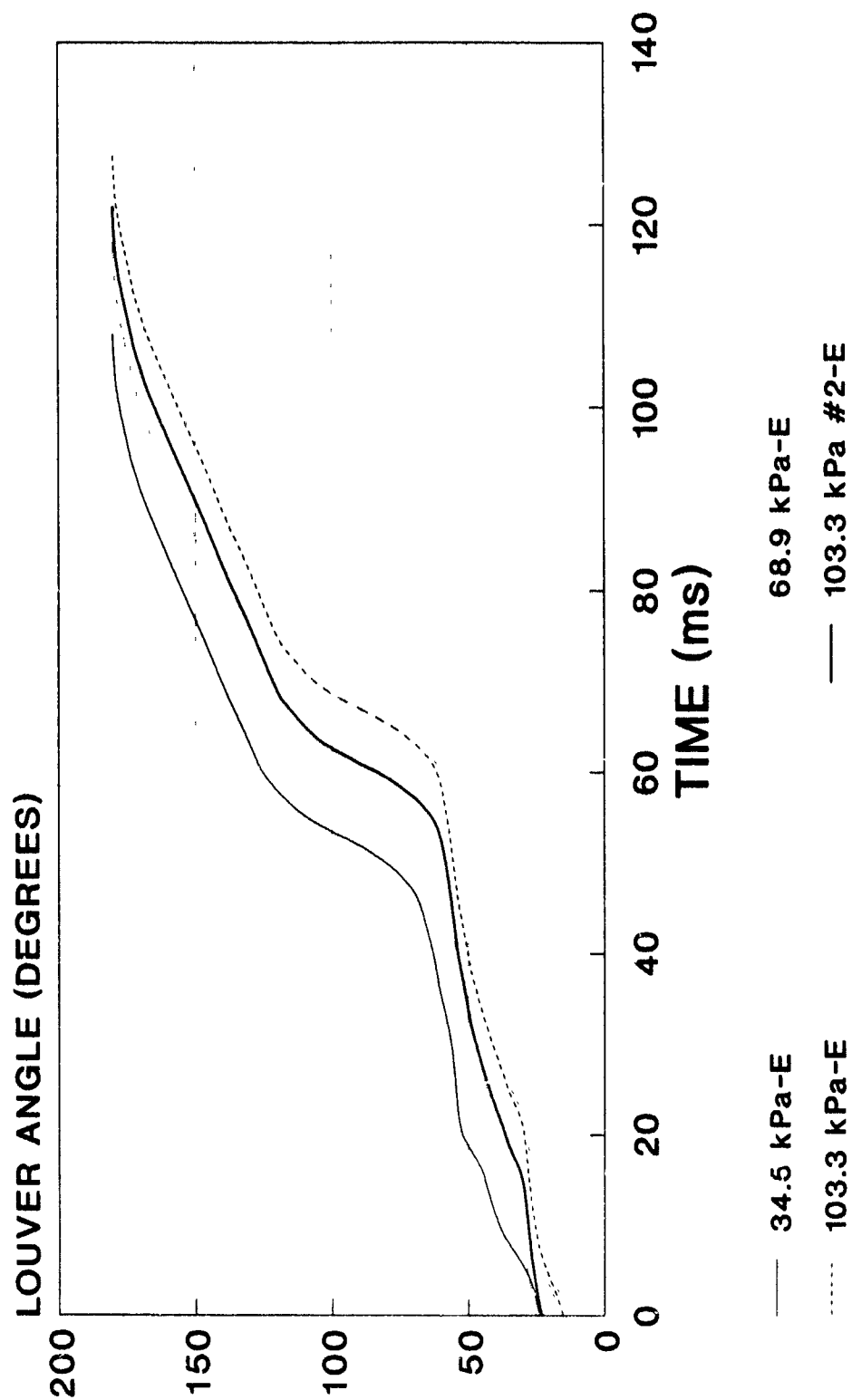


Figure 32. Experimental closure rate comparisons at 3 pressures.

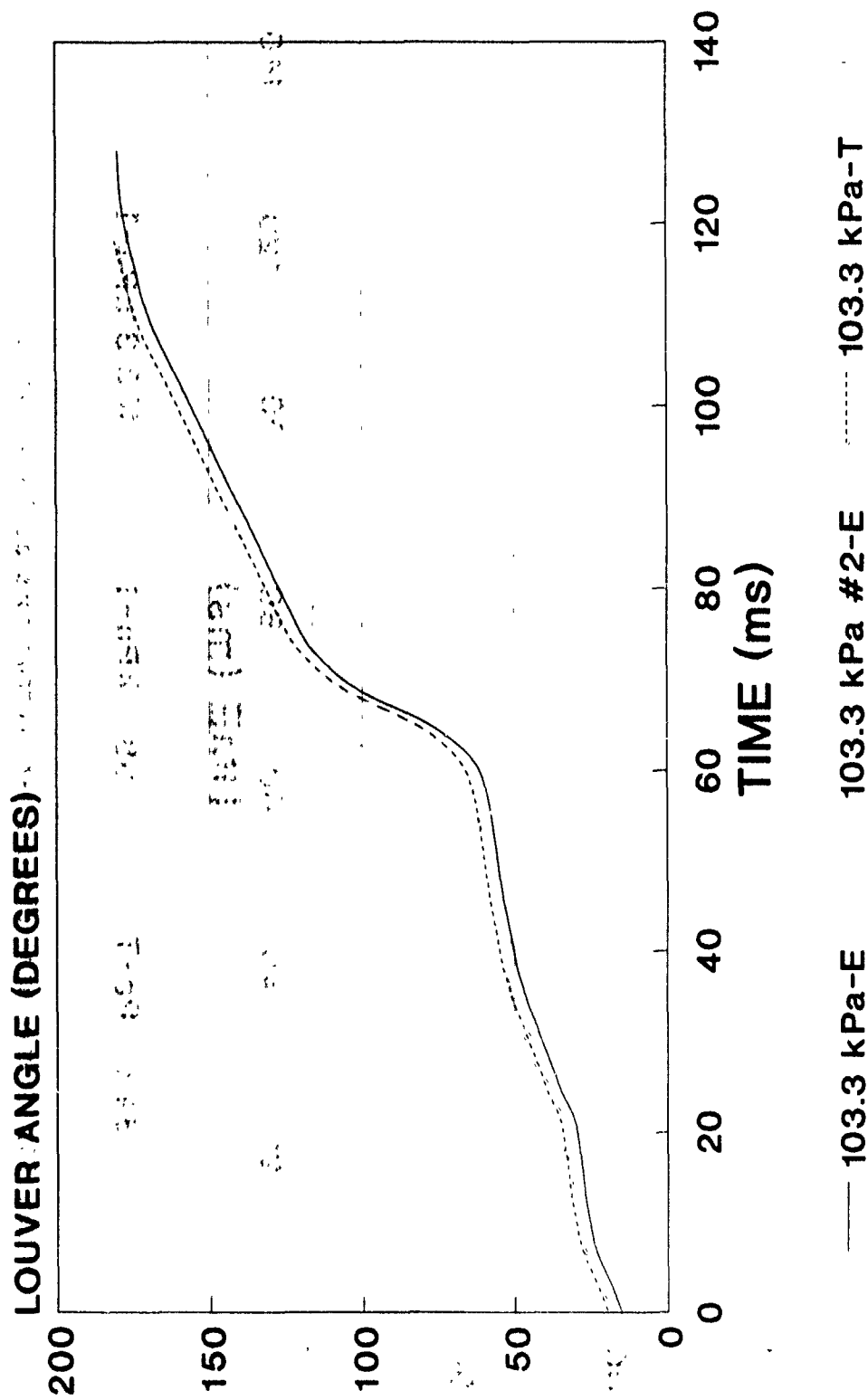


Figure 33. Closure rate comparisons at 103.3 kPa.

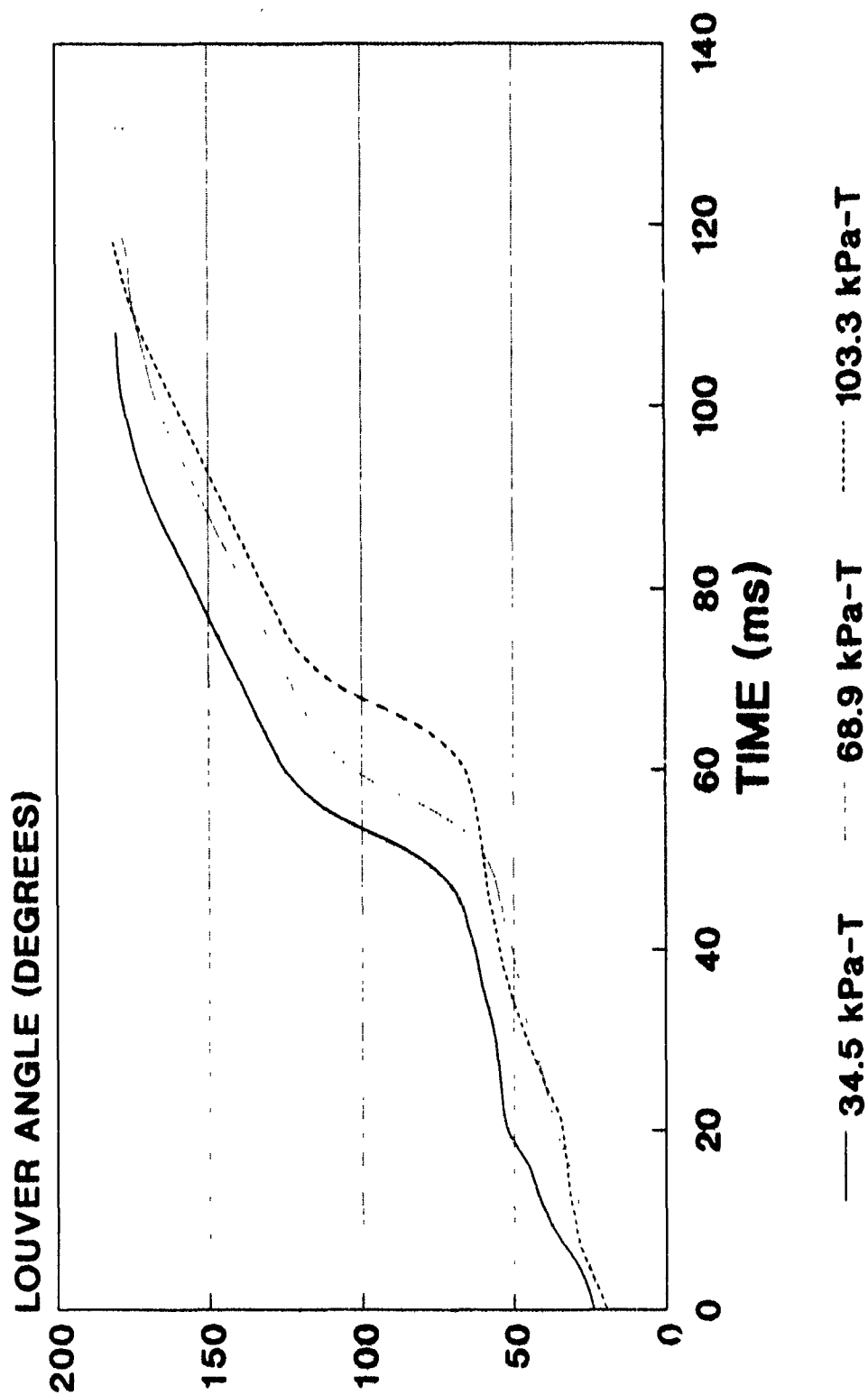


Figure 34. Theoretical closure rate comparisons at 3 pressures.

The optical tracker provided less than desired results during the testing. One of the major drawbacks was the effort required to reduce the data. The data obtained by the tracker is a series of spikes which are related to the passage of the scribed marks under the photo detector. The time difference between the spikes must be derived and then divided by the distance between the scribe marks to obtain the velocity and later position of the louvers. This is a time consuming effort and not convenient for rapid turn around of tests. An alternative method of obtaining this measurement was developed on site by attaching a rotary potentiometer to the shaft of the upper most louver. After calibration of the potentiometer and louver, a curve was developed to define the relative position as a function of voltage. This method was employed on several of the latter tests and reasonable results were obtained.

Specific results from each test series (low, moderate, and high pressures) are discussed in a following section.

1/57th SCALE RESULTS

The results from the initial series of 1/57th scale tests (RWE numbers 1 through 8) were met with mixed emotions. The closings functions anticipated for the RWE via the RCM code would be incorrect since the predicted overpressure waveforms differed so much from the overpressure time histories obtained on the short and extended tube tests. New closing functions had to be developed, on site, which took into account the actual driver geometry and were based on the data obtained during the open and extended tube tests. Fortunately, a routine was available in the ELIM computer subroutine which allowed this transformation to take place, along with some educated judgment, as to when the positive phase would be complete (an extension of the extended tube results). With the use of this subroutine, closing functions were developed which worked well.

Three tests each were conducted with the RWE in place for the low and moderate overpressure tests, nominally 37 and 78 kPa (5 and 11.3 psi). Two RWE tests were conducted at higher overpressure levels of nominally 107 kPa (15.5 psi). The results for the test series are presented in comparison form in Appendix C. This appendix also shows comparisons between similar configuration tests to demonstrate repeatability of the facility.

The test data was obtained at two locations along the tube. However, three pressure records are shown. The first measurement location is 177.8 cm (70 in) downstream from the diaphragm. The second and third measurement locations are 1539.24 cm (606 in) downstream from the diaphragm location. This later location holds both a static and total pressure measurement gage, however the total measurement gage is oriented upstream which gives little information on any velocity dependent flow properties generated by a rarefaction wave.

The first series of RWE tests started with low overpressure conditions (approximately 37 kPa). Figure 35 shows the results from the static overpressure data acquired during several of these tests at the location closest to the RWE. (Additional test data may be found in Appendix C). The data obtained from the short tube test clearly shows the rarefaction wave at 14 to 15 msec after the arrival of the incident wave. When the tube is extended, the presence of the

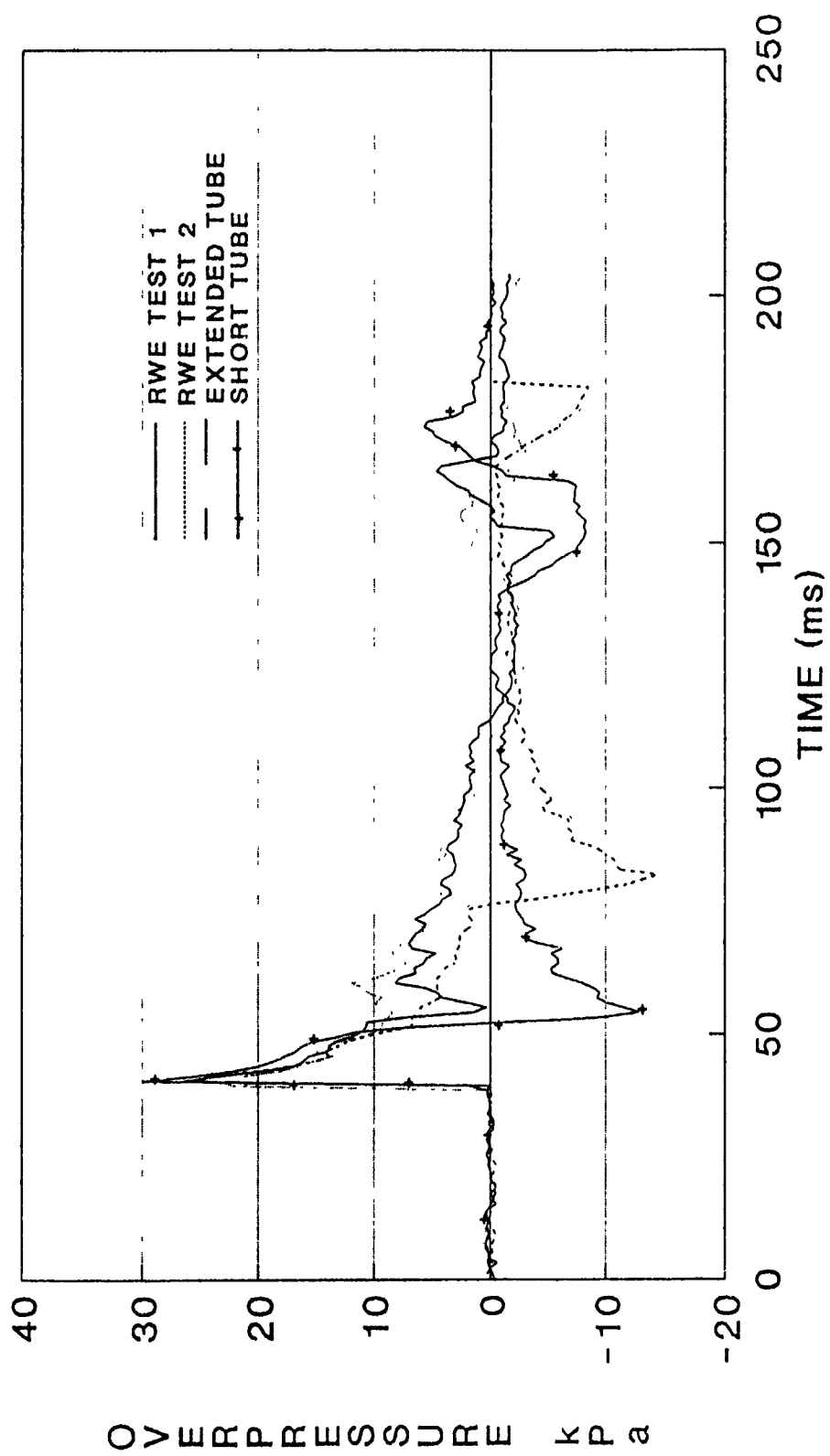


Figure 35. Results from 34.5 kPa pressure tests.

rarefaction wave is not seen by the gages until nearly 35 msec after primary shockwave time-of-arrival. The other two data traces in the figure show the overpressure histories obtained when using the RWE. The data from RWE Test 1 shows a large drop in pressure at approximately the same time as the onset of the rarefaction wave from the short tube test. This indicates that the RWE was not closed enough at the time of shock arrival (TOA) at the RWE. The pressure then starts to recover but is higher than the extended tube test data. The other RWE data (Test 2) had the closing function modified by shifting the closing function up by 2 msec (the minimum time step of the servo motor). This action results in the elimination of the large drop in pressure seen on RWE Test 1, but again the remaining pressure history is higher than the extended tube results. Since both of the RWE test data show this higher pressure level at the later times one can conclude that the RWE is closed too much during this portion of the shock wave passage. However, the RWE is effective in maintaining the positive phase with the durations being 75 and 73 msec for RWE Tests 1 and 2, respectively. Most of the data traces, short and extended tube tests included, show significant pressure bumps at 20 and 30 msec after shock arrival. Since these bumps are present in all of the test data (see the total pressure and tests data at the 177.8 cm gage results in Appendix C), they are probably real and could be caused by the driver geometry.

The next series of tests was conducted at a moderate overpressure of approximately 78 kPa. Figure 36 shows the comparison of a short, extended and two RWE tests. As observed in the low pressure tests the rarefaction wave is very distinguishable on the short tube test occurring at 12 msec after shock time of arrival. The extended tube test shows more of the positive phase with the delayed rarefaction wave arriving at 40 msec. The closing function used for both of the RWE tests shown was the same. The results are interesting in that the pressure from RWE Test 5 unexpectedly drops off at 52 msec after TOA. This drop off in pressure may be attributed to the plug in the driver accidentally moving forward and sealing off the flow of the gas in the driver section. (Note that the plug was never physically restrained from being able to move.) The positive phase duration obtained on RWE Test 4 appears reasonable with a total duration of 82 msec. The excessive closure of the RWE, as seen in the low pressure tests, was accounted for in these tests and the matching of the pressure profile to the extended tube results is much better. Also, note that the pressure bumps located at various times are also seen in these tests which further confirms the suspicion that they are products of the driver geometry.

The final series of tests was conducted at the higher overpressure of 107 kPa. Figure 37 shows a comparison between a short, extended, and two RWE tests. The rarefaction wave is present on the short tube test occurring 15 msec after TOA. The extended tube test did provide some information, but the delayed rarefaction wave arrived at 37 msec after TOA which limited the amount of useful information for comparison of the RWE results. The data obtained on RWE Test 7 show a significant drop in pressure about 17 msec after shock TOA. Initially this drop was thought to be caused by a mismatch of the timing of the closing function similar to the situation in RWE Test 1. Therefore, for RWE Test 8, the closing function was moved earlier in time by 4 msec. This correction seemed to work as the significant drop in pressure was eliminated. However, an actual rise in pressure was obtained at about 20 msec and then there appears a tremendous drop in pressure. In fact, the RWE was damaged on this test. The second

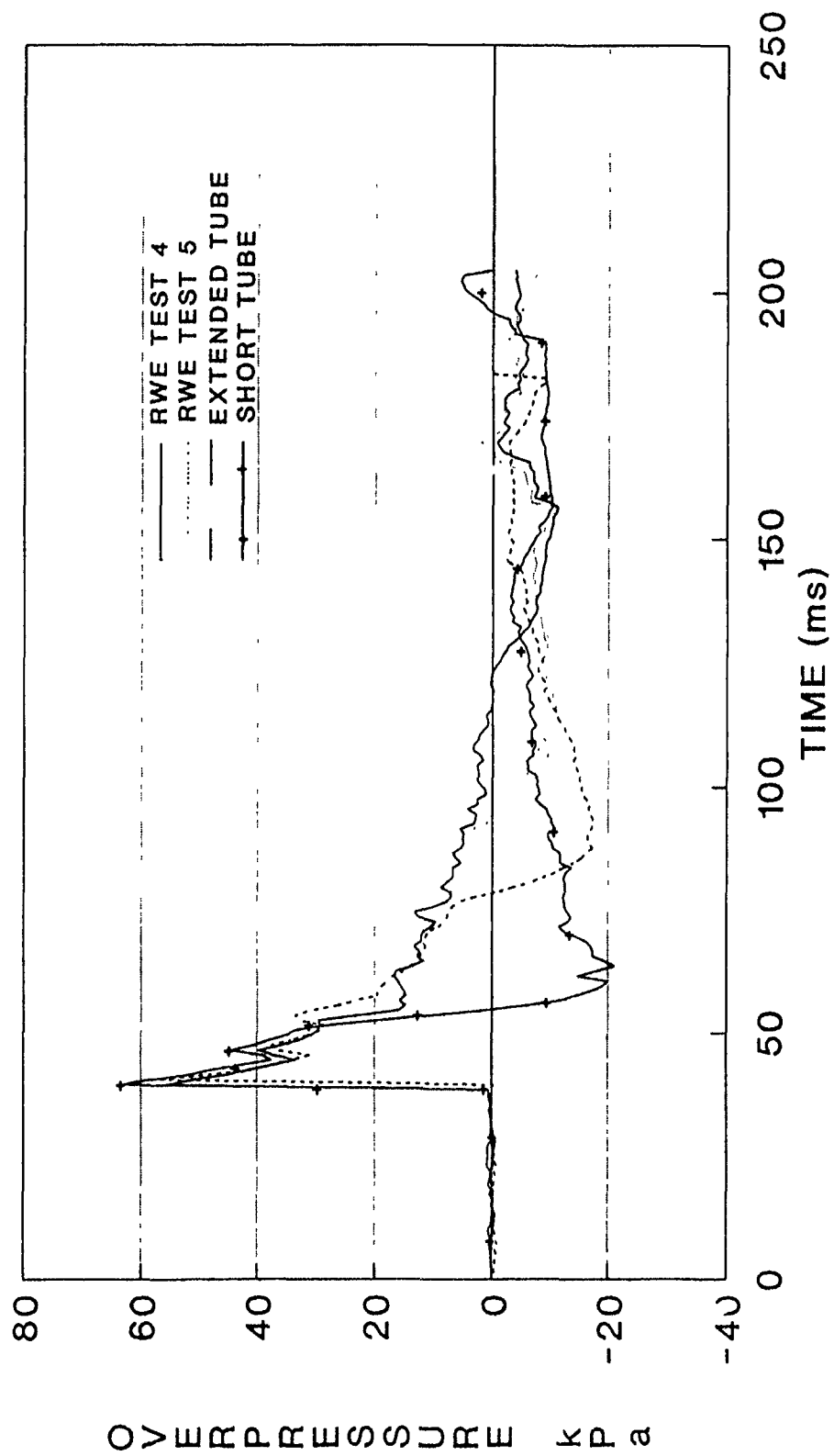


Figure 36. Results from 68.9 kPa pressure tests.

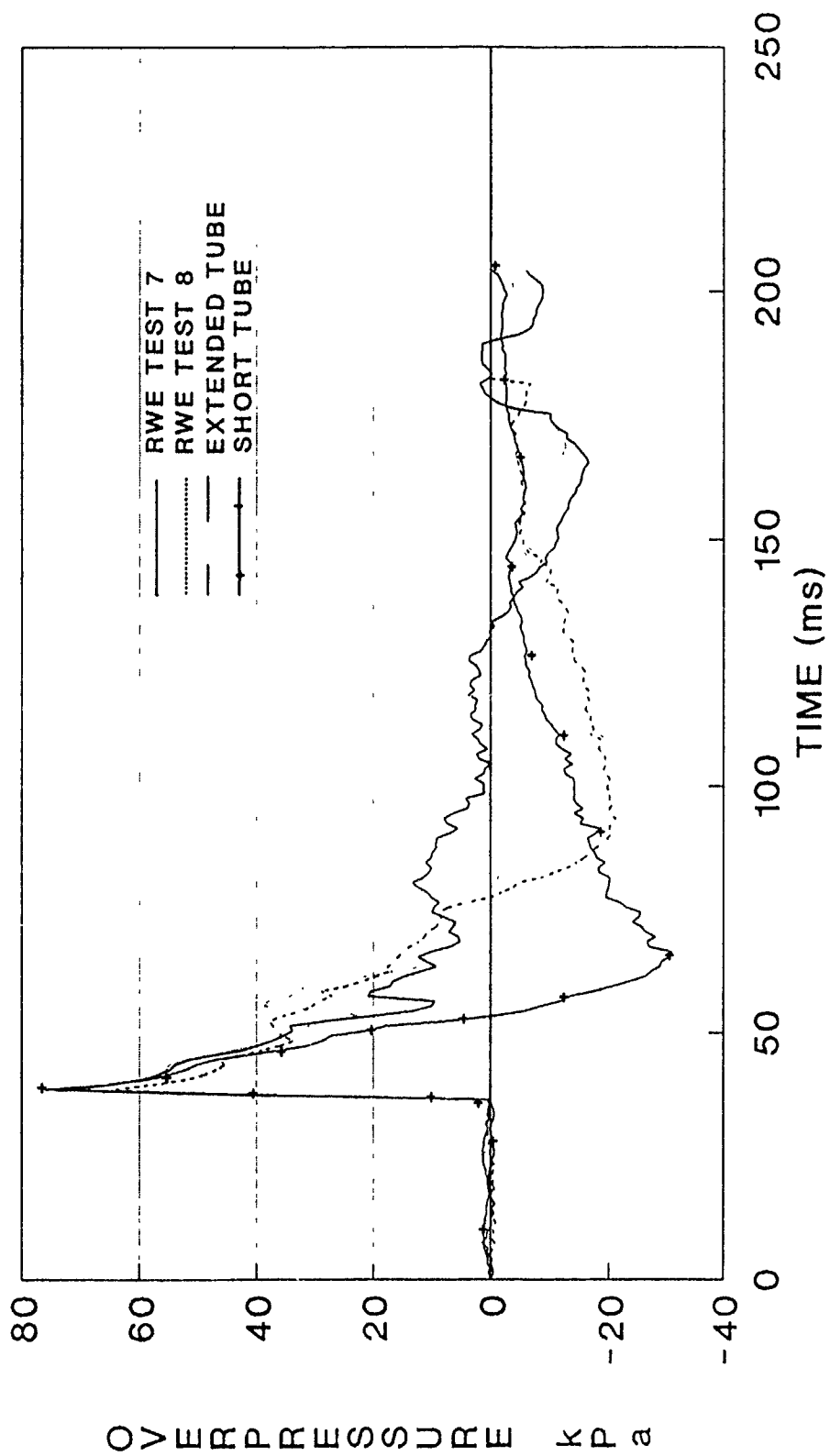


Figure 37. Results from 103.3 kPa pressure tests.

louver from the top sheared off at the diamond shape/shaft interface on the side closest to the gear. This failure caused the RWE to be inoperative, and thus the large drop in pressure. Looking closely at the data from the extended tube test, a slight rise in pressure is seen at approximately 10 msec after TOA. This rise was not felt as a significant feature after looking at the field plots and was essentially ignored when developing the closing function for these high pressure tests. Therefore, the RWE was told to close too much too soon and hence a higher reflected wave (the rise in pressure at 20 msec on RWE Test 8) and load on the RWE louvers were created. Even with this problem the later time history of RWE Test 7 does not match the extended tube results and does not appear to be very accurate.

As indicated earlier, a full set of the data obtained from these test series is presented in Appendix C. All of the data appear consistent with the discussions presented above and further substantiation of some of the theories presented is apparent.

DESIGN MODIFICATIONS

As mentioned in the results section, the RWE suffered a major failure during Test 8. An analysis of this failure revealed that three factors were found to have contributed to the failure. The first factor was that the RWE was programmed to close through a hump in the extended tube pressure trace that was thought to be an error. In fact, this hump was real and the RWE louvers experienced a higher loading than they were designed for. The second factor was the use of spherical bearings. The loads which were produced on the louvers were high enough to cause a higher than expected deflection of the mid-section of the louver. These deflections then allowed the ends of the louver shafts to deflect further than anticipated (due to the "self aligning" feature of the bearings) and resulted in binding of the gears, thus preventing a free rotation. The third factor was the material chosen for the louvers. 7074 aluminum was selected for the louver material due to ease of machining and low moment-of-inertia. However, the penalty paid was a lower material yield strength which resulted in the shearing-off of the shaft of one end of the louvers.

With this information, the louvers and mounting bearings were redesigned. The louvers remained the same geometry with the aluminum material being replaced by "stressproof" steel. This steel, while having high machining factors, has an ultimate tensile strength of 861 MPa (125,000 psi). Thus, since the material strength goes up, the deflections at the mid-louver location go down. Additionally the louver support bearings were changed to a roller pin bearing which still accepts the high unidirectional forces but does not have the ability to allow the shaft to vary at such large angles. The increase in inertia due to the change in material does not affect the performance of the system since the system was designed for steel louvers. These modifications were made and the new elements shipped to BRL for further testing.

1. The first part of the document
2. describes the general situation
3. and the objectives of the project.
4. It also outlines the scope of the
5. study and the methods used to
6. collect and analyze the data.
7. The second part of the document
8. presents the results of the study
9. and discusses the implications of
10. the findings. It also includes
11. a conclusion and recommendations for
12. further research.

13. The third part of the document
14. contains a list of references
15. and a list of figures and tables.

INTENTIONALLY LEFT BLANK.

FULL SCALE RWE DESIGN

OPERATIONAL DESCRIPTION OF THE LB/TS

In a combined blast and thermal test simulation, the firing sequence would be initiated after the driver tubes had been filled with heated nitrogen to the specified pressure. First, the thermal radiation at the test target would be generated by burning an aluminum-powder/oxygen mixture. The hot aluminum oxide produced by the combustion would irradiate the target and move upwards toward the ceiling where it would be removed from the LB/TS by ejectors. Secondly, the blast wave would be initiated by bursting the diaphragms or opening the throat valves. After the incident shock is established, the throat valves, if used, would be closed gradually to meter the flow in such a manner as to shape the pressure decay to match a free-field blast wave. The simulated blast wave moves down the expansion tunnel and commences loading the target. At the end of the expansion tunnel, the blast wave interacts with the RWE which partially reflects the incident shock. After the incident shock has passed, the RWE acts as a convergent nozzle producing a local acceleration of the flow to match the exit pressure to the ambient conditions. When the RWE is properly set, neither a rarefaction nor a recompression wave is reflected into the expansion tunnel.

The flow patterns encountered in an LB/TS are much more complex than those encountered in a straight shock tube. Figure 38 shows a schematic comparison of the flow patterns in a straight shock tube and in a blast/wave simulator based on a quasi-one-dimensional analysis (Ref. 17). The initial flow pattern in a straight shock tube is made up of a primary shock (2) moving into ambient air (1), followed by a contact surface (3) which separates the hot gas processed by the shock from the cold gas initially in the driver (4). A rearward facing rarefaction wave in the driver (5) accelerates and cools the driver gas. For low shock overpressures, the flow in an LB/TS is similar to that in a straight shock tube in that it is subsonic everywhere with a steady expansion in the convergent nozzle and a steady compression in the divergent nozzle.

Generally, the flow in an LB/TS is distinguished from the flow in a conventional shock tube by the occurrence of choked flow in the throat of the nozzle (7) and by a recompression shock (1) compensating for the supersonic expansion of the flow in the divergent nozzle (8). As the driver empties, the subsonic flow expands isentropically in the convergent nozzle (6) such that it becomes sonic in the throat. The flow then becomes supersonic as it continues to expand in the divergent nozzle; but because the flow behind the primary shock (2) is subsonic, a recompression shock (10) must form to decelerate the supersonic flow to match the velocity across the contact surface (3). For moderate shock overpressures, the flow forms a standing shock part way through the divergent nozzle. The subsonic flow behind it goes through a steady compression in the remaining part of the nozzle.

For high shock overpressures, the recompression shock is swept out of the nozzle and down the expansion tube. It is followed by a region of supersonic flow at extremely low pressure. In extreme cases, the recompression shock may be swept past the test section. The passage of either the contact surface or the recompression shock through the test section will destroy the blast simula-

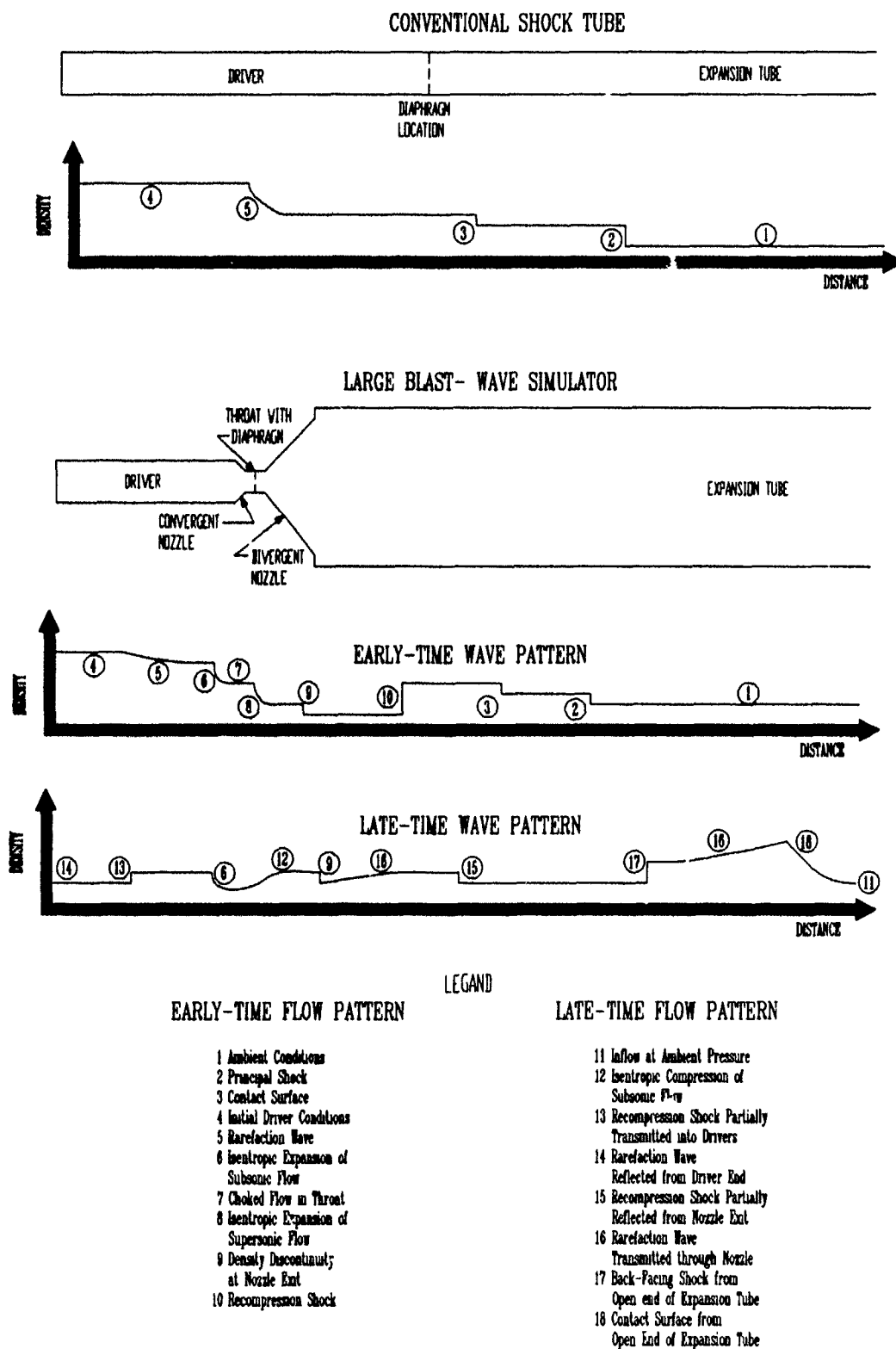


Figure 38. Illustration of physical flow phenomena.

tion for most test conditions because the low static and the high dynamic pressure following the recompression shock do not properly simulate the desired blast wave. The high dynamic pressure due to the density increase across the contact surface also does not properly simulate a blast wave. At later times, the recompression shock returns to the nozzle exit where it is partially reflected (16) and partially transmitted (13) moving upstream into the drivers.

Late-time wave patterns are also illustrated in Figure 38. The decay of static and dynamic pressure necessary for the simulation of a blast wave is produced by rarefaction waves which, in the absence of closing valves, are reflected from the closed ends of the drivers (4). Moving forward, the rarefactions interact with the convergent nozzle and are partially transmitted and partially reflected. The transmitted parts of the rarefactions (15) overtake the recompression shock, the contact surface and the incident shock, each at different times because the drivers are of different lengths. This overtaking by the rarefaction waves causes a decrease in flow (particle) velocity, locally. The drop in the flow velocity causes a decrease in the forward velocity of the contact surface and of the recompression shock and limits the distance both waves move down the expansion tunnel. The rarefaction waves overtaking the incident shock decrease its strength. The parts of the rarefactions which are reflected from the convergent nozzles move back into the drivers but cause a secondary shock to move forward through the nozzle into the expansion tunnel.

The end of the expansion tunnel is open to let the driver gas escape during and after the test period. However, in the absence of an RWE, rarefactions (16) will proceed upstream from the open end of the expansion tunnel after the incident shock (3) has exited. A back-facing shock from the open end (17) brings the overexpanded driver gas back to ambient pressure and ambient air (18) moves back into the expansion tunnel. Thus, series of rarefaction waves and shocks move up and down the expansion tube restoring the tube to ambient conditions. The upstream traveling disturbances from the open end will alter the flow pattern in the test section during the test period if they are not prevented from doing so. The simple method of extending the duct behind the test section far enough so that the disturbances arrive only after the test period is completed is too costly on the large scale of the proposed LB/TS.

Another method for eliminating, or at least minimizing, the effects of rarefaction waves on the blast wave simulation consists in utilizing a RWE.

SELECTED DESIGN

The configuration recommended for use as the Rarefaction Wave Eliminator (RWE) on the Large Blast and Thermal Simulator (LB/TS) now under design features rotating louvers mounted horizontally in eight columns, each about two meters wide. The louvers are positioned on 0.75 m vertical centers, with a total of 100 louvers in the RWE structure which can be attached to the open end of the LB/TS. An additional 34 louvers are installed in 17 side vents cut into the wall of the LB/TS near the RWE. The louvers feature an elongated diamond cross section, with a span of 2.029 meters, a chord of 0.85 m and a depth of 0.0889 m.

The louvers are supported on a series of structural beams that are secured to a movable carriage mounted on rail tracks. The beams have a deep web, up to

36 inches, where bearings and operational hardware for each louver are located. The structural members have been sized to easily withstand the total load imposed on the louvers from the maximum LB/TS blast wave.

The louvers are rotated by a series of hydraulic servo-actuators that supply torque via a rack and gear mechanism. The hydraulic system is designed to be modular so that off-the-shelf hardware can be used and that failure of a single component will not cause failure of the entire RWE system.

The RWE structure is mounted on a platform supported on crane rails so that the RWE can be moved into position and secured to the end of the LB/TS, or moved to the side to allow access to the interior of the LB/TS. The rail transport will easily support the 49,900 kg total static load of the RWE. An additional structure needs to be built along side the rail line to provide support to the top of the RWE, which extends over 10 meters above the track level, and consequently has a very high center of gravity.

ROTATING LOUVER JUSTIFICATION

Three major pieces of data were used to support the selection of rotating louvers as the best concept for the RWE for the full scale LB/TS. The first is that a similar large design has proven successful in the shock tube facility at the Centre d'Etudes de Gramat, France; secondly, rotating louvers were found to be the most efficient approach in an earlier design evaluation (Ref. 1); and finally, this effort produced a scale model of a rotating louver RWE that demonstrated effective performance in the reduction of rarefaction waves in tests of a 25.4 cm diameter shock tube at the U.S. Army Ballistic Research Laboratory at Aberdeen Proving Ground, Maryland.

The rotating louvers on the large shock tube in Gramat are preprogrammed to operate at a linear closing rate that is roughly designed to match the particular pressure profile to be generated. The shock tube is very large, a hemicylinder about seven meters in radius. Nonetheless, the device has been shown to have a significant impact on the shape of the positive phase duration of the blast waves simulated in the facility.

The earlier efficiency study was conducted by the authors of this report while at the Denver Research Institute, and addressed the development and technical evaluation of three alternative design concepts for an active rarefaction wave eliminator for the LB/TS (Ref. 1). Three ideas were put forth for assessment: a rotor-stator (expanding fan) design, a hinged bi-fold louver, and a louver that rotated about its center of mass. In terms of operating power and total mass of the system, the rotating louver concept had by far the lowest requirements. Fine tuning has been done on the details of the design in this project, but the overall concept remains as developed in the previous work.

As part of the current effort, a 1/57th operational scale model of a rotating louver RWE was designed, constructed and tested on the 25.4 cm shock tube at BRL. Test results present conclusive evidence that the RWE reduced the effect of rarefaction waves on the overall shape of the positive phase of the pressure profile at different peak pressures. There was also some non-required influence

by the RWE on the creation of a proper negative phase in some of the tests. The overall conclusion was that the use of RWEs can improve the performance of shock tubes where simulations of overpressure histories are impacted by rarefaction waves.

SIDE VENT CONFIGURATION

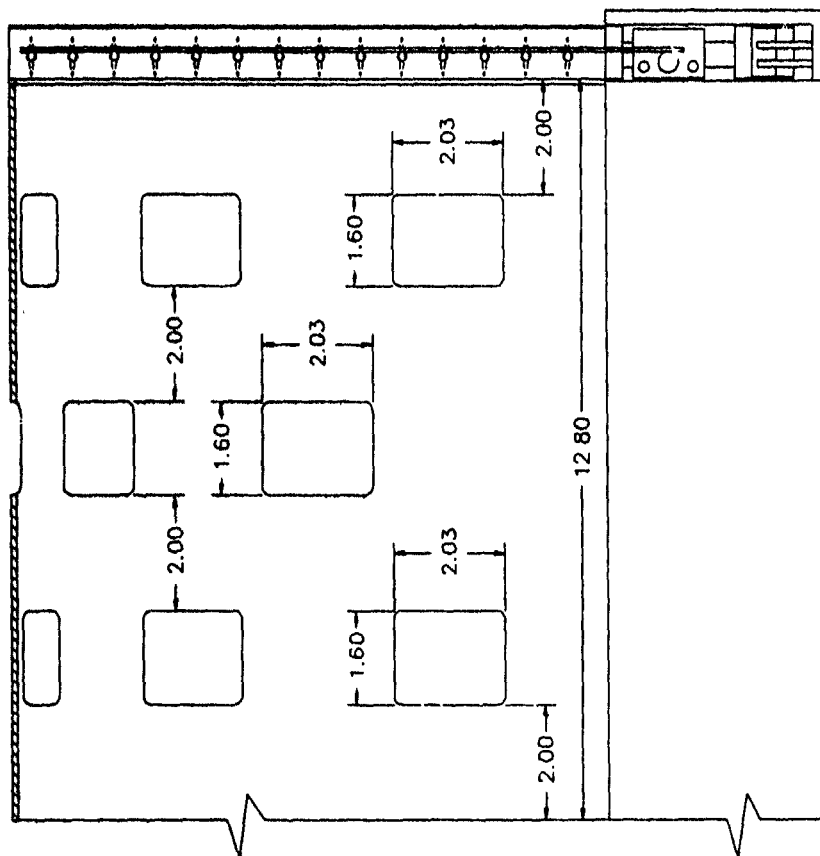
The side vent configuration for the full scale RWE is presented in Figure 39. The shape of the individual vents has been specified so that each will accommodate two of the louvers to be used in the end mounted RWE section. The vents are thus 2.03 meters long by 1.5 meters wide. The vents are arranged in two arc rows of six separated by an arc row of five for a total of 17 side vents; their positions are staggered in order to maintain maximum strength in the LB/TS side wall. In a fully-open position, about 11% of the vent area is blocked by the louver so that the 17 vents provide a maximum net area of 45.6 m^2 , or about 28% of the end cross section of the LB/TS.

The side vents are operated by a hydraulic system similar to the mechanism used on the end-mounted RWE louvers. A hydraulic servo-actuator will be located on the shell of the LB/TS and will drive a toothed rack positioned to operate the louvers in three vents, one in each arc row. An additional mechanism on each vent will reverse the direction of rotation for the other louver in the pair so that they rotate towards each other as do adjacent louvers in the end-mounted RWE. Since the side vent servo-actuator is driving six louvers, it can be the same size as the one used to operate seven louvers on the end-mounted RWE. This commonality will reduce fabrication and design costs, and should simplify maintenance requirements as well.

A calculation of the power requirement showed that sequential operation of the side vents was very costly in terms of power. This is an operating mode where the side vents are moved from the full open to the full closed position in the time period where the total open area ratio requirement for the blast wave is above the 80% maximum available from the end-mounted RWE system. The end vents then take over and operate to satisfy the changing open area ratio. This approach requires that the louvers in both systems rotate at high rates; it was realized that there would be significant advantage to simultaneous operation of the louvers since the resulting rate of rotation would be much slower, particularly for the side vent louvers. The power for louver rotation is a function of both the rate of rotation (angular velocity) and the rate of change in the rate of rotation (angular acceleration) so that any reduction in the angular velocity (and angular acceleration needed to reach that velocity) would be reflected in a proportionally greater reduction in the power requirement. The side vents are thus operated over the entire positive phase duration of the blast wave with a power requirement that is identical to that of the end-mounted RWE louvers.

POWER CALCULATIONS AND IMPACT ON DESIGN

An investigation was conducted to assess the impact of louver dimensions on the power requirements for operation of the rotating louvers during the positive phase of the passage of a blast wave. The objective of this work was to opti-



NOTE: ALL DIMENSIONS ARE IN METERS

Figure 39. LB/TS RWE cross section showing side and end vents.

mize the performance of the RWE while minimizing the amount of power needed to operate the louvers. As a "worst case" scenario, a positive phase duration of 289 milliseconds was chosen, which is associated with a 10 kT yield. The louvers were required to move from a fully open to fully closed position in this time, and the inertial power required to meet the motion profile was calculated. A simplified (quasi-steady state) version of the UTIAS computer model for the prediction of open area ratios was used to construct a closing profile for the RWE.

Performance of louver design alternatives was evaluated with a computer model assembled as a spreadsheet. Data for alternative designs were graphed for comparison and are presented later in this report. This approach permitted a quick, yet thorough, investigation that resulted in an improved louver design and predicted power requirements for the RWE.

HYDRAULIC DESIGN PARAMETERS

A design of the hydraulic system for operation of the rotating louver RWE was performed. A primary concern of the design effort was the identification of a concept that could accommodate the need for very rapid motion of the louvers, while at the same time maintaining fine control of the motion. The key to the solution of this problem is in the use of servo feedback to verify that the motion is being executed as programmed. Again, the 1/57th scale working model provided some guidance as to the feasibility of this approach. An electric servomotor was used as the power supply for the 1/57th scale louver system, and was found to track the programmed motion profile quite well. The use of a larger shock tube with an RWE would allow a hydraulic servo-mechanism to be tested to demonstrate the full scale LB/TS RWE design.

A modular approach to the specification and design of an RWE hydraulic operator was followed and is discussed in detail later in this report.

STRUCTURAL DESIGN

Three specific aspects of the structural design of the RWE for the LB/TS were examined in this study. These included a stress analysis of the louver configuration as modified in early design optimization activities; a review of the stresses on the main support beams for the RWE structure; and a preliminary design of a carriage to move the RWE into position on the end of the LB/TS and away when not needed.

The louver stress analysis addressed several loading modes and presents data on the reaction of the configuration to the maximum expected overpressure blast wave. The conclusion is that the current design is structurally sound and should easily survive all but the most blatant abuse (i.e., setting of the louvers in a more closed than required condition).

The support members of the RWE structure were confirmed as sound with an adequate margin of safety (1.5, based on a reflection coefficient of 3) for the most severe blast environment expected in the LB/TS.

The preliminary design of a carriage for positioning of the RWE employs as a base of support a standard railway flatcar with simple modifications to support the extreme height of the RWE and the limited travel to which it will be subjected. Details of the design are also included in later sections of this report.

OPTIMIZATION OF THE LOUVER CROSS SECTION

An analysis was conducted on the power requirements for motion of the louvers and of the impact of louver dimensions on required power. The baseline assumption was a 241 kPa (35 psi) overpressure blast wave with a positive phase duration of 289 ms which represents a 10 kT nuclear yield simulation. This short positive phase duration yields the maximum power requirement since it forces the most rapid rotation of the louvers. A spreadsheet model was programmed for the calculation of polar-moment-of-inertia of a single louver and a table was created to compute the power requirements every 15 milliseconds over the given positive phase duration. The calculations assumed that the louvers operated simultaneously in the end and side vent sections of the RWE, instead of sequentially (side vents first, followed by end vents). Dimensions of the optional louver design from Reference 1 were used in the determination of the polar-moment-of-inertia for the baseline case. The chord length of the cross-section of the louver and the outside diameter of the central bar on which the louver pivots were treated as variables in the evaluation of design alternatives to minimize power consumption.

The angular position of the louvers was computed for various time intervals and the finite difference scheme was then used to calculate both angular velocity and angular acceleration from the time interval. The power requirement was computed as the product of the applied torque and the angular velocity.

Results from the model are shown in Figure 40. In reference to this figure, the case labeled "baseline" presents the power requirements as shown in the final report of the initial design, (Ref. 1). This reference reported that the end louvers did not begin to move until the overall open area ratio requirement dropped below the maximum amount available from the additional use of end vents. This is the "sequential" mode of operation noted previously. The other cases shown all represent louvers which start to move as soon as there is a need for a change in area ratio. For these cases it is assumed that there are side vents that supplement the end vents in order to provide the capacity to meet requirements for total open area ratios greater than 0.8 times the cross section of the LB/TS (20% of the actual open area is taken up by blockage of the flow by static presence of the RWE). The side vent louvers operate simultaneously with the end vent louvers and, in fact, the power requirements are identical for both, equal to the values plotted on the figure.

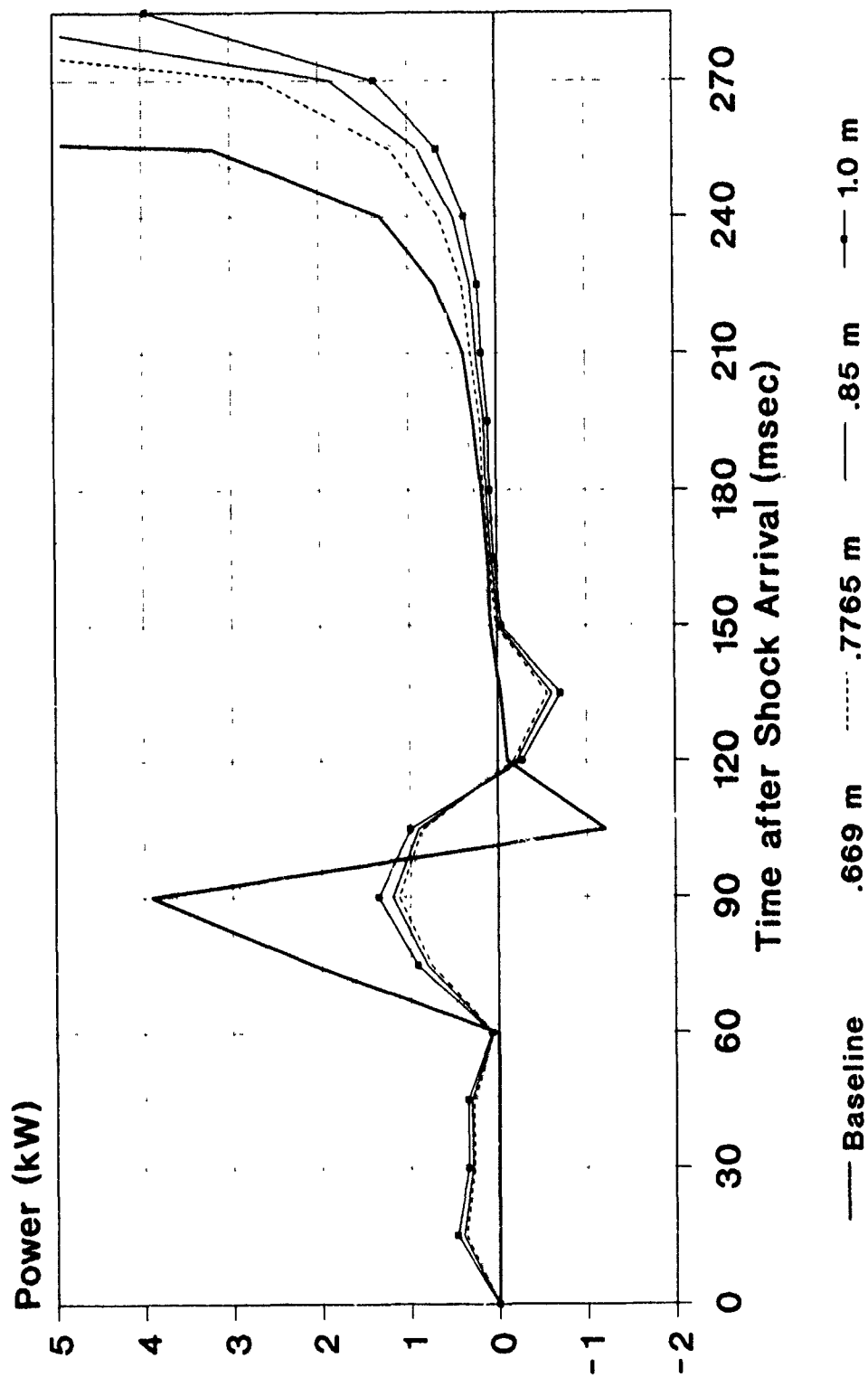


Figure 40. Rotating louver power comparison of alternate designs.

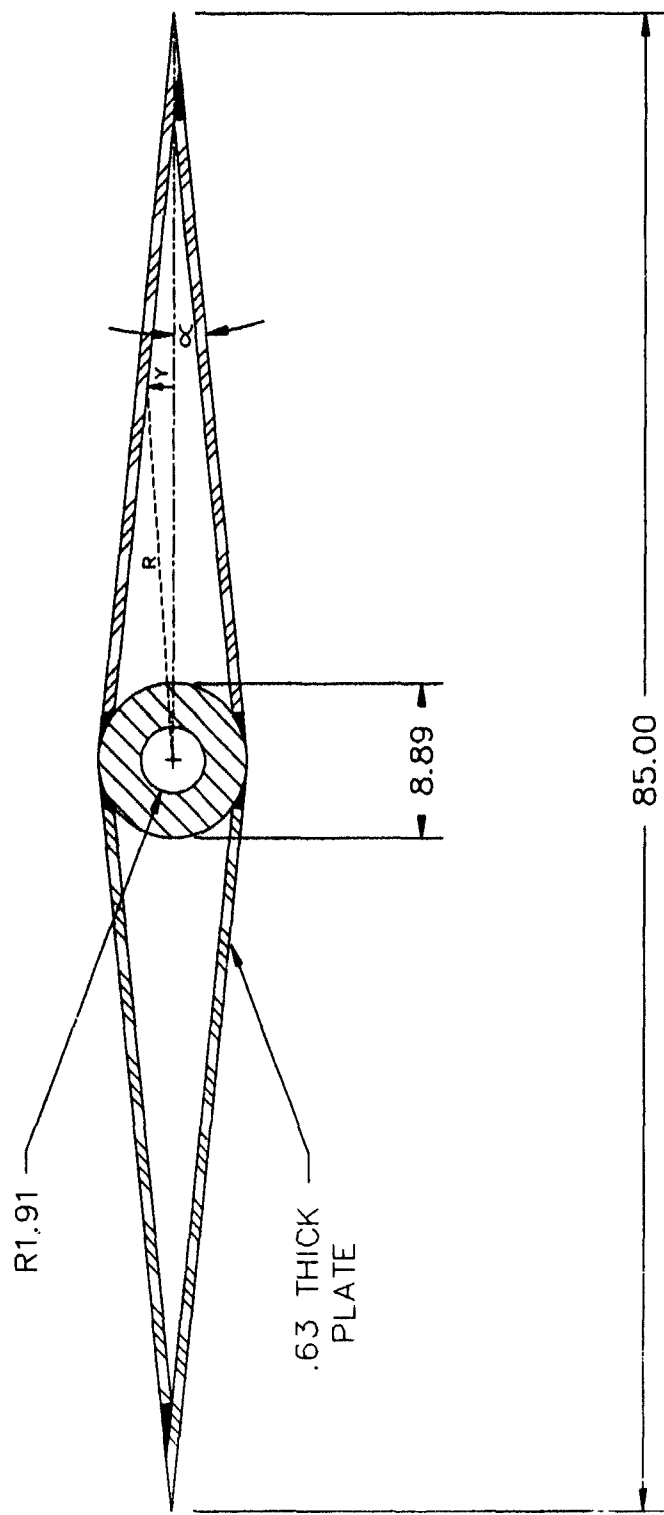
The advantage of simultaneous operation is seen at two different times in the time-history shown on Figure 40. The first is at 90 milliseconds, where there is a sharp peak in the baseline case. This occurs because the louver starts from rest and must generate a rapid change in open area to follow the rapid decay of the simulated blast wave. In fact, because of this exponential decay rate the low yield simulation requires the greatest rate of change in open area ratio and thus demands the greatest power. The second power peak is seen near the end of the simulated blast wave. At this time, the power requirement rises because the louver is nearly perpendicular to the flow, and a large change in angular position is needed to generate a small change in open area ratio.

The relationship between angular position and open area is a function of the sine of the angle between the chord of the louver and the direction of flow; as the angle approaches 90° , the sine function changes little for incremental changes in angle when compared with the change for similar increments at smaller angles. One obvious solution to this problem is to lengthen the chord of the louver cross-section such that the tips of adjacent louvers meet (producing a totally blocked cross-section) at an angle to the direction of flow of less than 90° .

The additional data on Figure 40 show the results of lengthening the louver chord. The trade-off is the increased polar moment-of-inertia of a wider louver for the reduced rotation that is required to create a given open area ratio. The benefit of the widened louver design is seen at overpressure duration times greater than 240 ms, where power requirements are lowest for the longest chord configuration. The penalty for the increased polar moment-of-inertia is seen earlier at the 90 ms time where power for the longest chord design is perhaps 20% greater than for the optional louver design. One other penalty that would be paid for a longer chord louver design (not reflected in the power calculation) would be an increase in the amount of material and therefore in the cost of fabrication.

However, the power savings near the end of the simulation are considerable, and make the consideration of a wider louver design preferable. The approach to the specification of peak power supply for the RWE would involve cutting off the power requirement at the end of the simulation at some value below the peak shown on the figure. This would be acceptable because the slower motion of the louver near the end of its travel would cause only small deviation from the simulated pressure history since the overpressure at this point is well under 6.9 Kpa. Based on the data presented in Figure 39, a peak power of 1.5 kw per louver would seem to be adequate for the RWE; thus the total power for 134 louvers would be about 201 kw. This compares to a previous requirement of 400 kw for the end louvers and over 3000 kw for the louvers in the side vents. The side vent requirement is very large because of the very fast operating times (full open to full closed in 75 ms) needed in the sequential operating mode.

The power analysis shown in this report led to the selection of 0.85 m as the chord length for the louver cross section. In addition, the central bar on which the louver pivots was reduced in size to 0.0889 m (3.5 in) diameter. The net result is a lower power requirement for operation of the louver and a greater maximum open area available for the end-mounted section of the RWE. The new cross section is shown in Figure 41.



NOTE: DIMENSIONS ARE IN CENTIMETERS

Figure 41. LB/TS RWE rotating louver cross section.

OFFSET OF ADJACENT LOUVERS

One concern with the full scale louver configuration developed in the design activity described above, was the blast loading that would be incurred on adjacent louvers as their edges touched in the fully closed position. This was of considerable interest since the louvers would be rotating at their greatest velocity at the time of this impact. The blast loading could cause significant damage to the louvers, and was a distinct disadvantage to the long chord length configuration. A potential solution to this problem was discovered and its feasibility was subsequently investigated.

The way to avoid the collision of adjacent louvers was to install them with a permanent rotary offset; that is, one louver would be positioned with its chord at a small angle to the chords of its neighbors rather than parallel in the fully opened position. Of course, adjacent louvers rotate in opposite directions, so that once motion is initiated they are no longer parallel, but the original concept was to move the louvers such that at any instant in time, the positions of adjacent louvers would be mirror images of each other. This new idea was to have one of the pair of louvers start at a slightly greater angle to the direction of flow so that as the tips of adjacent louvers neared each other, the one at a greater angle would move behind the other and contact would be avoided.

A computer program was written to plot the locations of adjacent louvers as they rotated through angular positions that would bring them near contact. This effort was undertaken to determine the minimum offset angle required at which there was no contact between adjacent louvers. The vertical spacing between louver pivot shafts is 0.75 m (29.5 in); while the chord length of the new louver design is 0.85 m (33.5 in). Thus, a rotation of two adjacent louvers toward each other without the offset would normally result in an interference before both louvers reached a fully closed (vertical) position. The plots generated by the program are shown in Figure 42. One louver was offset 5° relative to the other; e.g., when the upper louver was at an angle of 0° relative to the direction of flow, the lower louver was at +5°. The louvers are then rotated toward each other in five degree increments. In the configuration under study there would be contact of the ends of the louvers at an angle of about 62° if there was no offset; the figure demonstrates that contact can be avoided if an offset is used. In the figure, identical line weights are used to outline the positions of adjacent louvers at the same instant in time.

The tips of the louvers are seen to pass within about a centimeter or so (when scaled to full size) at 70° angular displacement of the upper louver, but no interference occurs. The later time conditions indicate that the gap has increased a little at 75° and continues to grow up through 90°. This result is significant in that it allows the use of the longer chord louver design for the full scale RWE with its lower power requirement without imposing a problem with sudden contact of the louver tips while still moving at considerable velocities (i.e., the louvers don't "slam shut").

If there is a desire to shape the blastwave in the negative phase, which can be accomplished to some extent, then the louvers would have to be programmed to move faster through the fully closed position. This requirement is due to the

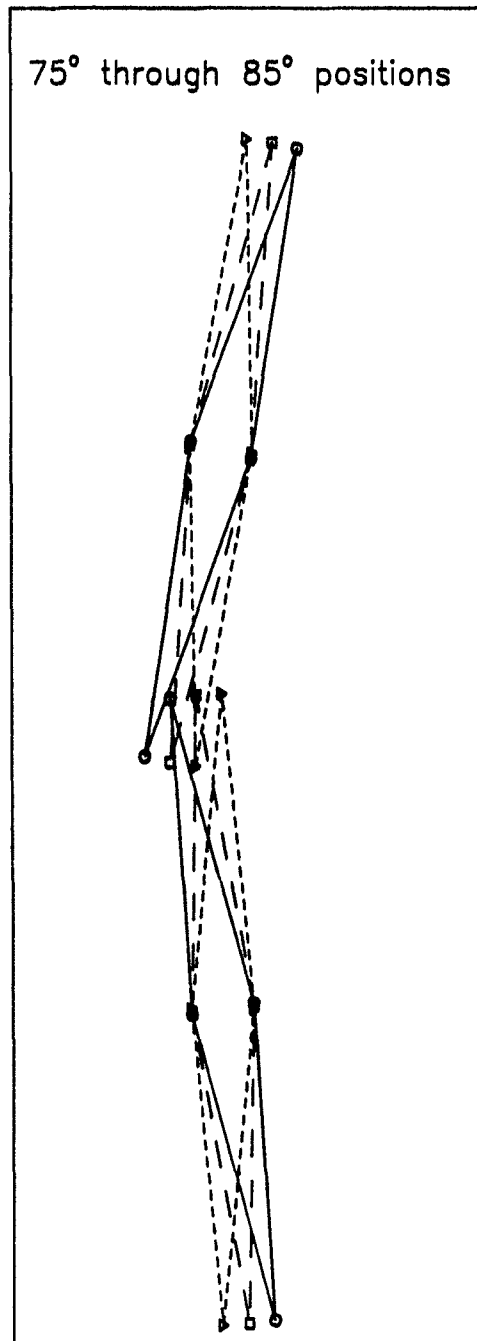
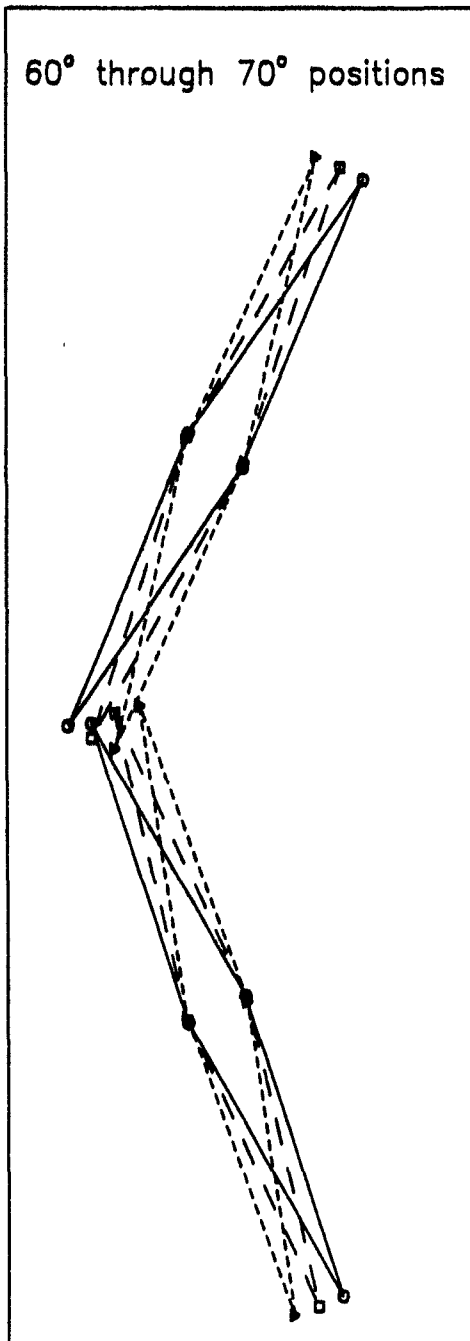


Figure 42. Louver offset position projections.

longer chord length which means a fully closed condition is encountered before the louvers are perfectly vertical and the first opening occurs at a like angle. Therefore, the closed condition is maintained through a large angle of rotation and hence some finite amount of time.

OPERATING MECHANISM

The rotating louvers are positioned in eight columns to cover the open end of the LB/TS. Bearings in which the louvers rotate are mounted in large beams at the ends of the louvers. The beams are the primary load bearing members, and also provide a framework to attach the mechanisms for application of torque to the louvers. All of the interior beams are "I" beams while the RWE end members are "T" sections. The louvers are rotated about the central bar that forms a shaft on which a gear is mounted at the supporting beam. The gear is driven by a rack to generate torque for the rotation of the louver. A servo-hydraulic actuator provides the force that moves the rack vertically during passage of the blast wave. Adjacent louvers are driven from alternate ends to rotate in opposite directions. This is accomplished by locating the rack on opposite sides of the driven gear. Thus, one rack is always moving downward, and the mass of the rack aids in the motion, rather than contributing to the load on the servo-actuator.

In order to keep the actuator power requirements within the scale of available off-the-shelf hardware, the operating mechanism is designed to be modular. Parallel systems are installed on each of the support beams to operate groups of louvers simultaneously. This offers redundancy that avoids the potential problem of a major failure that would incapacitate the entire RWE system, and should also result in reduced costs in design, installation and maintenance of the RWE.

STRUCTURAL ANALYSIS

A stress analysis of the full scale louver configuration presented above was completed using pressure profile data for a 241 kPa, 10 KT simulation. Three different stresses were considered in the analysis.

In the first condition, the louver is treated as a simply-supported beam with a uniform load applied along the length of its shaft as shown in Figure 43. This loading produces a bending stress in the louver that reaches a maximum value of 250 MPa on the outer skin at a location one half the shaft length of the louver. The loading changes as a function of louver position for two reasons: first, the overpressure from the blast decays over the positive phase of the blast simulation; and second, the projected louver area increases as the louver orientation with respect to the flow axis changes. The moment-of-inertia of the louver section decreases as a function of time during the passage of the blast wave because of the decrease in section depth as the louver chord rotates with respect to the flow axis. In this loading condition the louver's maximum moment-of-inertia, $6.5 \times 10^4 \text{ cm}^4$, occurs for the fully open position where its section depth is equal to its chord length, as seen in Figure 43. The minimum moment-of-inertia, 1011 cm^4 , value occurs in the fully closed position where its section depth is equal to the outside diameter of the louver shaft.

STAGNATION PRESSURE
APPLIED AS DISTRIBUTED LOAD

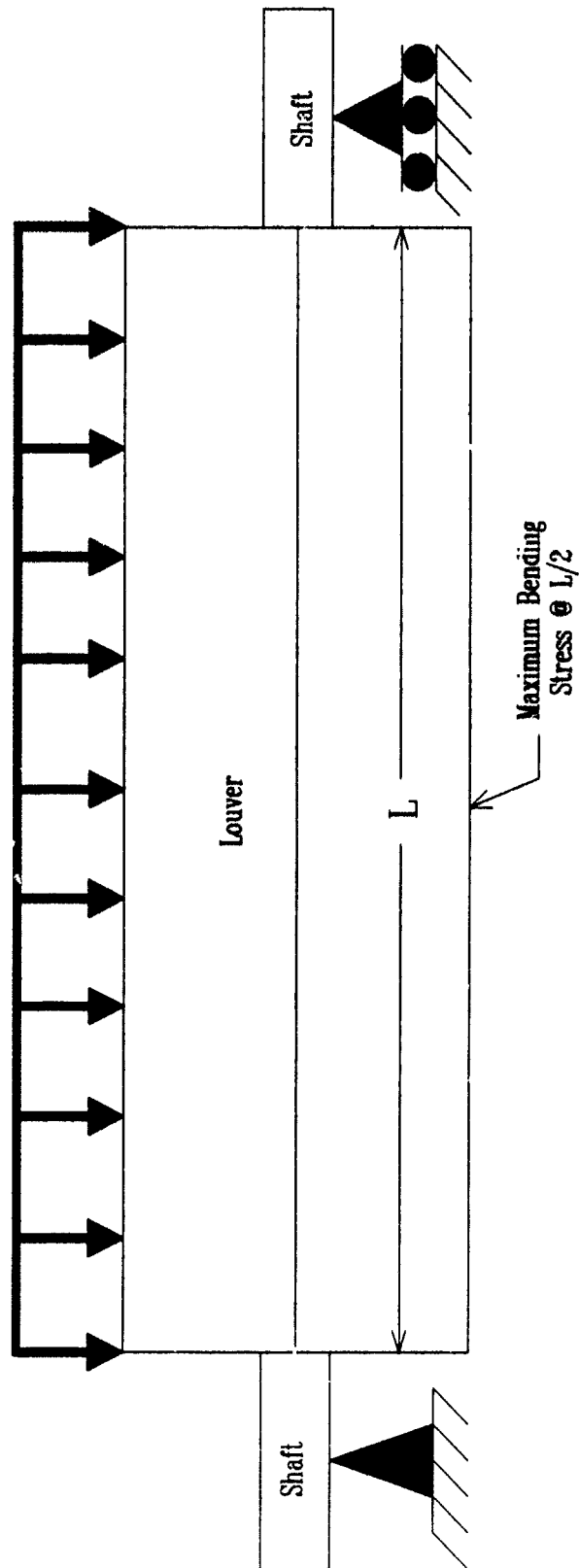


Figure 43. Bending along axis of a typical louver.

The second loading condition considered the cross section of the louver as shown in Figure 44. In this case, half of the louver section is treated as a cantilever beam to determine the magnitude of the stresses generated along the chord length. The maximum stress generated by this load condition again occurs at the outer skin at half the chord length. The maximum value of the stress due to this loading configuration is less than 6.9 kPa when the louver rotation follows the specified RWE profile.

The third loading condition considered in the analysis was the shear stress on the louver shafts. Calculations were based on the total loading due to stagnation pressure with a contribution from the reflection of the oncoming blast as it interacts with the louver cross section. A reflection coefficient of 3 was used to account for the additional loading from the shock, as described in the Air Force Manual for Design and Analysis of Hardened Structures (Ref. 12). This reflection coefficient is actually a function of the angle of incidence between the blast front and the surface upon which the blast impacts and the peak amplitude of the blast wave; the factor of three used in the calculation is for a 0° angle of incidence. In fact the louver in the proper position for arrival of a 241 kPa overpressure blast would be closer to a 90° angle of incidence, and would thus have a lower reflection coefficient. The calculation therefore represents a conservative approach. It is important to note that this blast reflected pressure is instantaneous and is immediately relieved upon passage of the blast; it must nonetheless be included in the load analysis. The shear stress generated in the shafts was found to be less than 15.85 MPa for the reflected shock loading so that the most severe stresses on the louver are those generated in the first load condition (bending stress).

Figure 45 presents a plot of bending stress in the louver as a function of the angular position of the louver with respect to the flow in the LB/TS. Bending stress was calculated for the first load condition with the addition of a term for the increased load due to reflection of the blast upon arrival as noted above and separately for aerodynamic-generated lift on the louver. The analysis considered the RWE as both an active system and a fixed or passive system. The data shown in Figure 45 is for the active system only.

For the active system the louver angular position is assumed to change as a function of time to generate the open area ratio needed for proper RWE operation. The stress generated by overpressure on the louver is thus a product of decaying static pressure and an increasing projected area of the louver as it rotates toward a closed position. The stress generated due to aerodynamic lift was determined as function of the lift coefficient (i.e., attack angle), dynamic pressure, and moment-of-inertia of the louver. The equations used to calculate the lift coefficient generated by the louver at angles of attack less than 16° was based upon symmetric plan forms in steady state, subsonic flows (Ref. 13).

For angles of attack greater than 16°, an equation $C_l = \left[\frac{1}{0.222 + 0.283/\sin\theta} \right] \cos\theta$, for the lift coefficients for thin flat plates inclined to a flow at angles up to 90°, was employed (Ref. 13).

In the analysis of the passive system, the louvers were assumed to be held at a fixed position or angle with respect to the flow axis for the entire positive phase duration of the simulation. For the overpressure stress, the passive

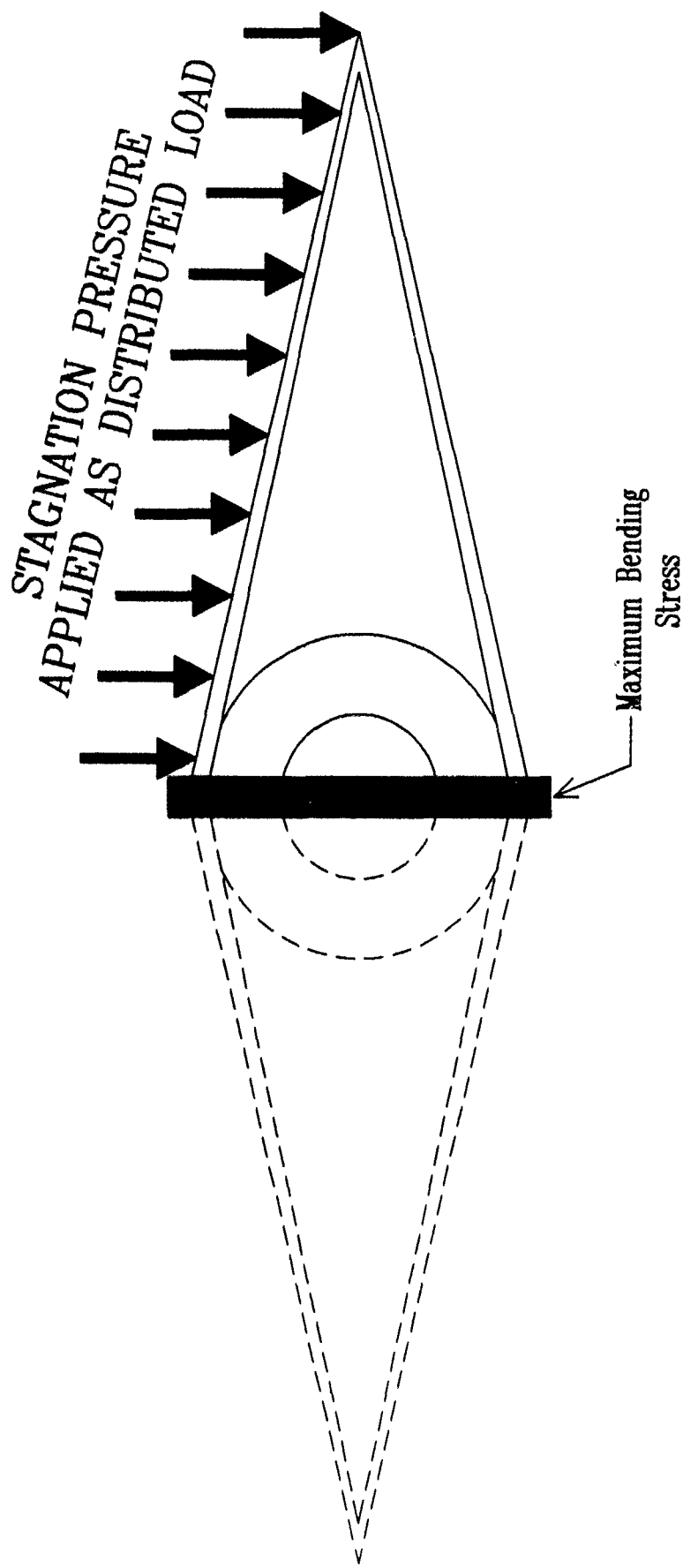


Figure 44. Bending on cross section of typical louver.

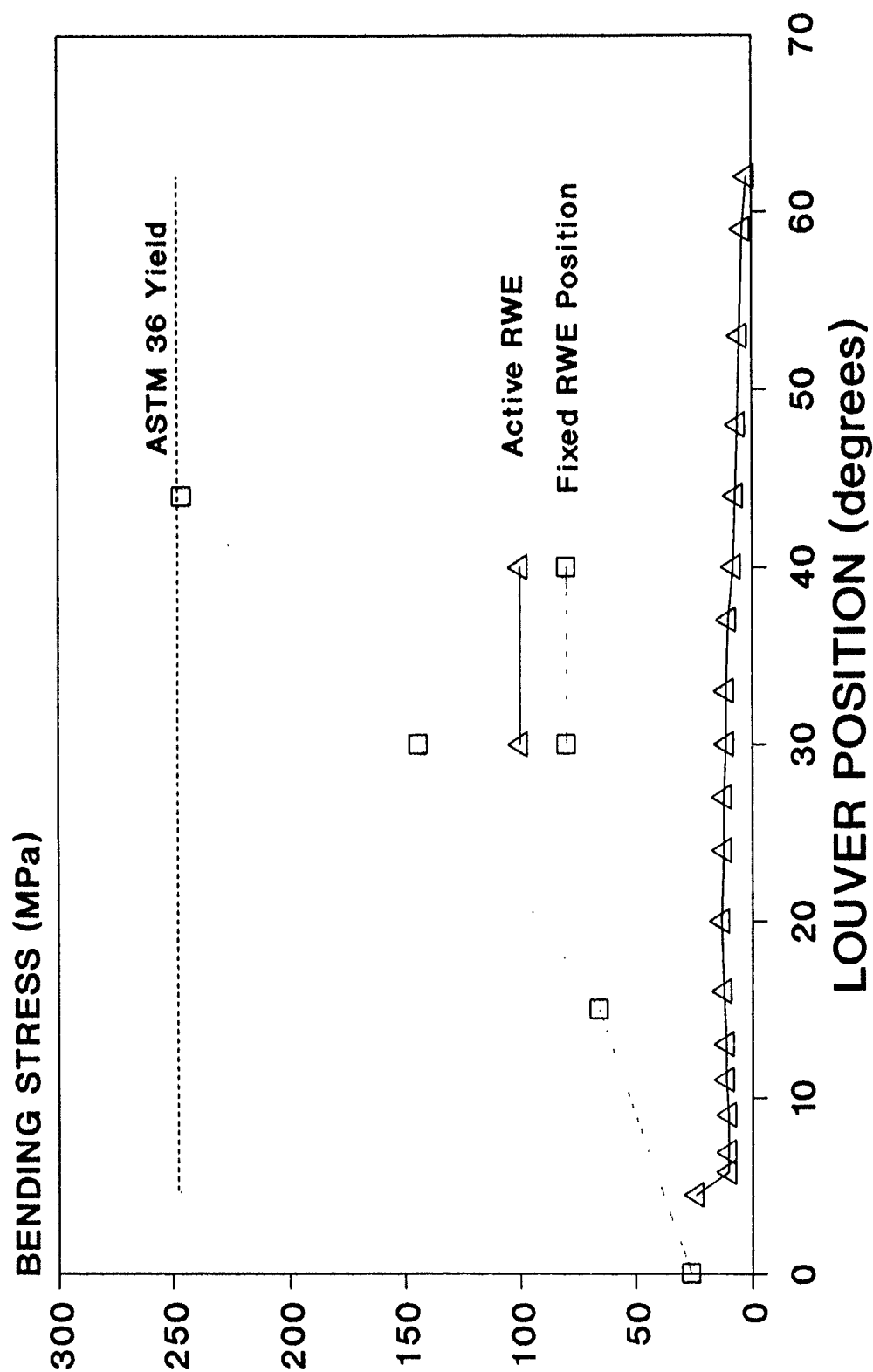


Figure 45. Bending stress for fixed and active RWEs.

case data shows that at an angle greater than 45° during the passage of the initial shock through the RWE, the louver would exceed 250 MPa stress in the louver. The lift generated stress peaks at 250 MPa which occurs at an angle of attack of $7-9^\circ$. The lift stress reaches its maximum at this angle due to the relatively high flow velocity, large lift coefficient, and small moment of inertia of the louver in the direction normal to the flow. This condition could occur if the RWE were operated as a passive device.

RWE CARRIAGE

The entire structure of the RWE and its hydraulic driver system are mounted on a mobile carriage to permit installation and removal of the system at the open end of the LB/TS. The mobile carriage will use conventional railway components combined with a steel guidance and support structure as seen in Figure 46.

The total weight of the RWE louvers, support beams, and hydraulic system is calculated at 49,900 kg. A conventional railway flat car with a carrying capacity of 63,500 kg and a length of 15.2 meters will form the chassis of the RWE carriage. The rail carriage will be propelled by the use of electric motors geared to the axles of the flat car. The carriage will be traversed into position at the end of the LB/TS and secured. The distance between the end of the LB/TS and RWE structures can be made variable or fixed dependent on the decision of active or passive side venting. Via a second set of rails imbedded on the deck of the carriage parallel to the direction of gas flow, the RWE structure can be advanced laterally across the carriage assembly toward the end of the LB/TS structure. The RWE will then be secured to the pre-stressed steel cables on the end of the LB/TS.

When the RWE is uncoupled from the end of the LB/TS, the steel guidance and support structure will assure the vertical stability of the RWE and carriage assembly. The steel structure will act as a guide during the traversing process and provide access to the upper louvers and drive system components when the RWE system is stored adjacent to the LB/TS. During the traverse process and while the RWE is stored clear of the LB/TS end, it is susceptible to wind loading. The steel guidance and support structure will prevent the possibility of toppling of the RWE system due to excessive wind loading and a relatively high center of gravity.

RWE SUPPORT BEAMS

A structural analysis of the RWE vertical support beams was performed to determine approximate beam sizes. Calculations were based on the predicted conditions and louver positions for a 35 psi, 10 KT case. Total loading on the beam was determined by superimposing the load due to the louvers and the loading on the face of the beam due to stagnation pressure. The load due to the louvers was assumed to be the force component acting in the direction of flow down the LB/TS. The louver force in this plane was taken as the product of the aerodynamic drag and the overpressure times the projected frontal area of the louvers. The loading was assumed to be uniform along the length of the beam and the beam was considered to be simply supported. A reflection coefficient of 3 was

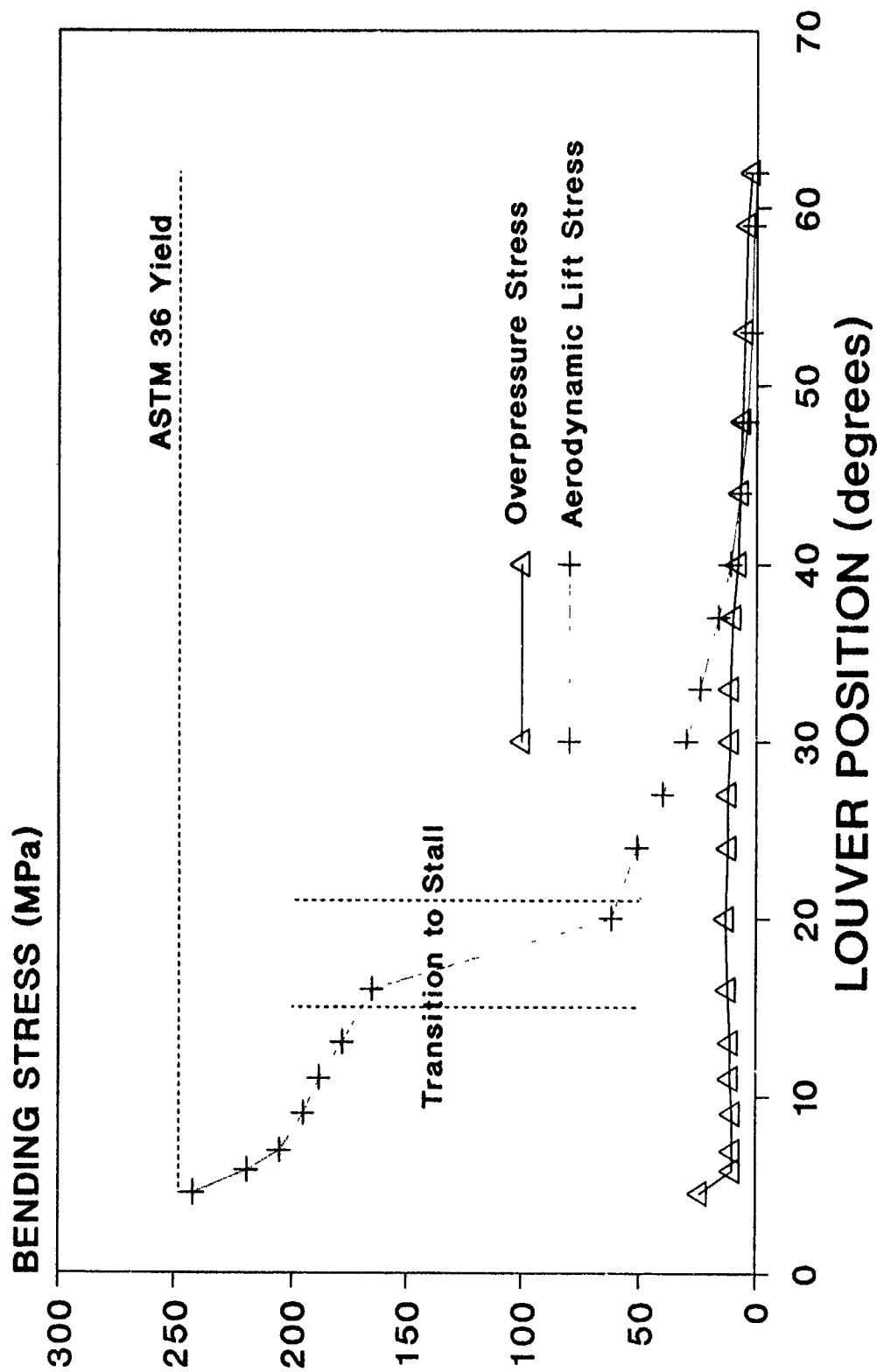


Figure 46. Bending stress versus louver position.

applied to account for the additional loading of the shock on the beam face. The reflection coefficient was not applied on the louvers because the angle of incidence between the shock front and the louver surfaces was less than 10°.

To accommodate the optimized louver geometry and driver system components, wide flanged steel I-beams of the W36-135 to W36-194 sizes are the preferable shapes for the support structure fabrication. These beams have sufficient web depth to allow full louver rotation inside the flanges and can provide the best trade off between flange width (i.e., blockage) and maximum moment of inertia. Analysis of the loading on the majority of the support beams shows that there is an inadequate margin of safety using single beams and conventional grades of steel. The most practical alternative is to physically stack two beams flange to flange to achieve the necessary strength. Using this approach, the center support beams would be fabricated out of two W36 x 194 sections bolted together at the flanges to provide a sufficient margin of safety for shock loading. Table 8 summarizes the recommended beam sizes, calculated loads, stresses, and safety factors. The loading on beams 8 and 9 is dramatically reduced as the beams themselves are out of the flow. Total loading is due only to the overpressure on the projected frontal area of the louvers and to the aerodynamic drag of the louvers. The W36 x 135 beam size is recommended only to maintain uniformity in the interface between the louver bearings and drive assemblies and the support beam geometry.

Table 8. Support Beams for the LB/TS Reflected Wave Eliminator

Beam No.	Steel Shapes	Moment of Inertia (cm ⁴)	Effective Length (m)	Load ¹ Force (tons)	Maximum Stress (MPa)	Safety ² Factor
1	Doubled W36x194	2.57x10 ⁶	10.75	340	161.8	1.5 (2.6)
2 & 3	Doubled W36x194	2.57x10 ⁶	10.50	337	156.7	1.5 (2.7)
4 & 5	Doubled W36x194	2.57x10 ⁶	9.50	331	139.4	1.7 (3.0)
6 & 7	W36x194 & W24x120	1.47x10 ⁶	7.75	275	142.0	1.7 (2.6)
8 & 9	Single W36x135	3.25x10 ⁵	4.00	30	39.6	6.2

¹ The component of the load forces generated on the face of the support beam incorporate reflection coefficient of 3.

² Figures in parenthesis are safety factors without the reflection coefficient. Safety factor calculated based ASTM 36 steel.

DESIGN OF THE HYDRAULIC POWER SYSTEM FOR THE FULL SCALE RWE

Guidelines

The prime requirement for the hydraulic power system for the operation of the louvers in the full scale RWE is that relatively high power output be provided for a very short period of time. The approach to meeting this requirement in the most cost effective manner is through the use of hydraulic accumulators. A small system power supply (pump) can be operated over long periods of time, on the order of minutes, to charge the accumulator(s), which can then supply hydraulic fluid at high flow rates in a "burst" mode. This relieves the system of the requirement of large pump size and flow capacity that is only used for very short time spans. The system power output becomes effectively divorced from the supply pump power input.

Another guideline for the design of the hydraulic system is the use of a modular approach for the selection of components. The most logical size breakpoint is by sections in which the louvers are arranged in the support frame. In the current design there are eight sections with 10 to 14 louvers per section. A layout has been developed that allows all actuators to be powered downward so that the weight of the drive rack need not be supported by the hydraulic actuator and summed into the load.

This approach permits the use of smaller components and keeps even the instantaneous power requirement for a single actuator at a manageable level, around 15 kw (20 HP), which is the power required for the operation of seven louvers simultaneously. Multi-member linkages or sophisticated mechanical transmission devices make simultaneous operation of multiple sections of louvers more prone to problems; therefore the modular arrangement is favored.

A novel concept for control of the hydraulic actuator that couples a mechanical servo feedback with the hydraulic control valve/actuator is now commercially available and appears ideal for the RWE system. The control valve in this device is operated by a stepper motor which is programmed to provide a defined motion profile for the actuator. The feedback loop then assures that the imposition of the load on the system does not alter the motion profile of the actuator. This is an ideal approach for the operation of the full scale RWE, as the motion profile executed by the louvers will be a function of the blast wave parameters in the LB/TS. Several limitations on the performance of the actuators are imposed when specific models are selected from the vendor. These include a maximum linear extension rate of 1.5 m/s (five feet per second) and a maximum fluid flow rate through the control valve of 115 liters per minute (30 gallons per minute). Both of these criteria impact the design of the means by which the hydraulic servos drive the louvers, particularly in the diameter of the drive gear that is mounted to the louver shaft. There are upper and lower limits to the gear size based on the actuator extension velocity and fluid flow rate.

Hydraulic Component Selection

A preliminary layout and design for the hydraulic system has been completed. A schematic is presented in Figure 47. System components considered in this activity include selection and sizing of a linear servo actuator for control of a section of louvers and sizing of accumulators, pumps, and hydraulic transfer lines. Details such as relief valves, servo actuator control system, filters, supply tanks and component mounting have not been included.

Servo Actuator

The hydraulic servo actuator is sized to the power requirement to operate a bank of five to seven louvers in a section of the RWE. The power requirement is determined by the geometry of the louver design and the rate of change in louver position as a function of time. For the most severe case in the LB/TS, the positive phase duration of the simulated blast wave is about 0.3 seconds, during which the louver must rotate from a full open to a fully closed position, a total of about 55° . The maximum power needed is 1.5 kw per louver for a total of 10.5 kw (14 HP). The delivery mechanism for this power is a gear mounted on the end of the louver that is driven by a vertically translating rack (see Figure 39). The rack is connected to the hydraulic actuator and is positioned via bearings to operate in the vertical direction. The maximum velocity at which the rack must travel is a function of the rate of rotation of the louver and the drive gear diameter; the force applied to the rack by the actuator is determined by dividing the power requirement by the velocity. Once the force is known, the actuator can be sized for a given operating hydraulic pressure or range of pressures. The actuator size is therefore a function of the gear size, required power and system hydraulic pressure.

The candidate servo actuators have three fundamental limitations: a maximum extension velocity of 1.5 meters per second, a maximum fluid flow rate of 115 liters per minute, and a maximum system pressure of 15.5 MPa. For gear sizes to 30 cm (12 in), the velocity requirements for the actuator are well within the limitation; however, depending on the specific actuator selected, the flow rate may be exceeded for short periods of time.

Operation of the actuator in an excess flow mode results in an increased pressure drop through the control valve and the reduction of available power at the actuator. Hydraulic design literature notes that the pressure differential for a control valve is approximately 344 kPa at the rated flow rate, with a 1.9 cm ($3/4$ in.) valve rated at 134 kpm, somewhat above the values presented in the data for the servo actuators. A 20.3 cm (8 in.) diameter driven gear (mounted on the shaft of each louver) has been selected for the baseline design. The servo actuator that drives the gear employs a 60 mm (2.362 in.) diameter hydraulic cylinder. When operated at 10.3 MPa (1,500 psig), the maximum linear velocity reached to meet the required torque for the louvers is 0.82 m/s (2.7 ft/s). This servo actuator is commercially available off-the-shelf, Model SVIZ-60 from Stauff Corp., Walldwick, NJ.

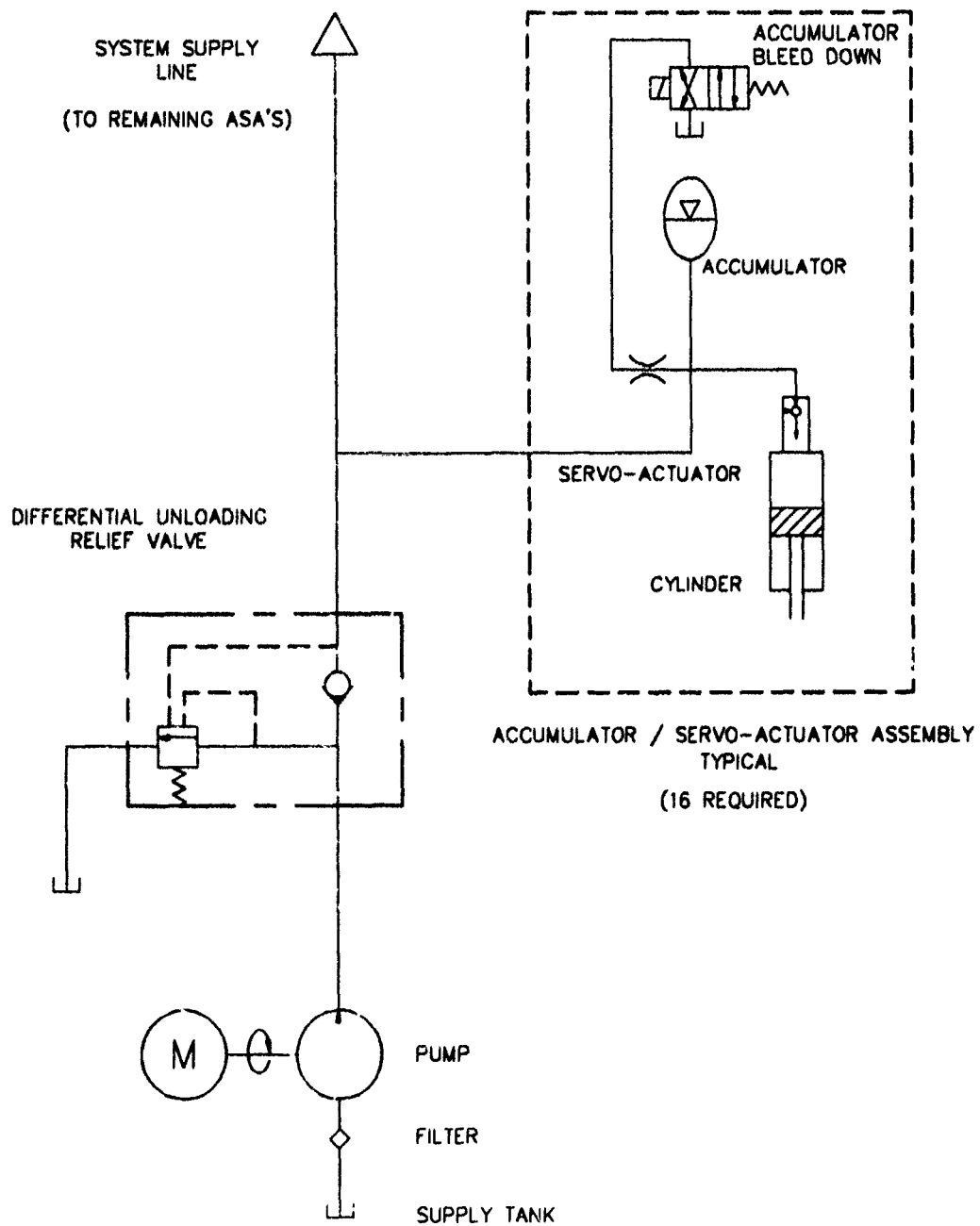


Figure 47. Hydraulic system concept schematic.

Accumulator

The RWE total operating time is less than a few seconds, which means that the accumulator would be discharged in a condition where the expansion of the compressed gas would be adiabatic--this was the assumption used in the sizing calculation. The accumulator was sized per the method described in the Parker Fluidpower Design Engineer's Handbook (Ref. 14) and was found to be 57 liters (15 gallons) for 13.78 MPa to 10.3 MPa (2000 to 1500 psig) operating condition. The suggested configuration is to use a four liter (one gallon) accumulator for each actuator, with a relatively short length of large diameter (3.81 cm) hydraulic tubing to minimize pressure drop between the accumulator and the actuator. In addition, a control valve will be installed on the accumulator which provides a safety vent at shutdown. This valve relieves pressure from the accumulator, and thus prevents accidental operation of the hydraulic actuators when the hydraulic system is not powered up.

Pump

A 20 liter per minute (5 gpm) pump system has been selected that will recharge the accumulators in under a minute, since total flow requirement to the actuators is less than four gallons. Total power requirement for such a system (201 pm at 13.78 MP) would be about 7.9 kw (10 horsepower).

Hydraulic Tubing

Maximum flow conditions in the individual hydraulic circuits will occur near the end of the positive phase duration of the simulated blast wave, and will be somewhere between 115 and 150 lpm (30 and 40 gpm). Standard design practice is to keep the maximum fluid velocity in the tubing below 4.6 m/s (15 fps) to minimize the potential for damage to the system from water hammer when valves are quickly closed. To maintain flow velocity below this value, minimum fluid tubing size is 3.81 cm (1-1/2 in.). There are several tubing material/wall thickness combinations that will satisfy Class B safety requirements. Both 304 stainless steel and mild steel tubing can be specified, with appropriate wall thicknesses. The 3.81 cm diameter tubing will be needed only on the accumulator to servo/actuator legs of the system. The overall flow loop that feeds the individual circuits from the pump/return tank can be in the 1.27 to 1.9 cm diameter range, since its peak flow rate is much lower.

INTENTIONALLY LEFT BLANK.

FULL SCALE RWE OPERATION

The first activity of the operation of the RWE must start several hours prior to the actual test. During this time the hydraulic fluid is circulated through the filtration system. This activity is necessary to insure that the fluid is as clean as possible so the servo valves will not become clogged and inoperable. This process will also bring the fluid up to operating temperature. The total time duration and when it should begin is dependent on the volume of the hydraulic fluid that is required by the entire system.

The next activity is to program the proper closing function into the RWE controller (probably a Personal computer 386 type machine). The closing function can be developed with either a subroutine such as the ELIM code or by looking up a function that had been previously developed for a particular test condition and programming it into the RWE controller. Inputting the proper closing function is important since the controller will check the status of various parameters of the tube, such as the driver pressure, to insure that the proper closing function has been programmed for the specific test being conducted. If an error is detected and not manually corrected in a soon enough time frame, the the RWE louvers will be instructed to remain in a fully open position during the entire test. The rationale for providing this check is for safety purposes. If this situation occurs, the test may have other than the desired results since a rarefaction wave will cross the test section but the facility will not be damaged.

The next activity is to move the RWE from the retracted position to the end of the expansion tube. This activity should take place after the test target is in place and all supporting equipment is removed from the simulator. However, this activity should be completed prior to the installation of any detonators on the diaphragms since it is anticipated that personnel will be at the RWE location during the transport. The next activity is to activate the attachment mechanisms which couple the RWE to the expansion tube. Proximity sensors installed on these mechanisms will signal the RWE controller that all of the mechanism are in place.

Once the RWE is in place and properly attached, the hydraulic accumulators will be pressurized. This pressurization will be monitored by the RWE controller. The RWE will then be exercised by the RWE controller. This exercise will consist of slowly rotating the RWE louvers back and forth. During this activity, diagnostic information will be fed back to the RWE controller to ensure that all of the RWE elements are operating as desired. This exercise also helps to maintain the lubrication of the mechanical joints such as bearings. With all conditions in a positive attitude, the RWE will then manually be given the command to execute the closing function for the upcoming test. Again diagnostic measurements will be made and analyzed to insure that the RWE operated properly.

The next activity would then be in a closer time sequence to the fire pulse which starts the diaphragm rupture. Approximately 30 minutes prior to diaphragm rupture the RWE would be slowly exercised to maintain lubrication. After this activity is finished the louvers would be positioned at the proper initial

angle of attack for the particular test being conducted. The accumulators would then be filled and checked. The closing function would be installed and the RWE controller, in conjunction with the LB/TS facility controller would have complete control (unless a manual override was forced). The RWE controller would observe the pressures in the drivers as well as the RWE hydraulic pressures. Once the driver pressures have reached their maximum level a check would be made to ensure that the closing function programmed matches the driver pressure. As the fire pulse is sent to the detonators on the diaphragms, a split of this signal is sent to the RWE controller. The RWE closing function is then initialized and an internal countdown clock is started. The countdown time is based on the pre-derived expectation of how long it takes the blast wave to reach the RWE for a specific test condition. Three to four pressure transducers, at different locations along the test section, near the test section are then sampled to determine blast wave time of arrival. Quick calculations are performed to determine the blast wave velocity and check the expected velocities for the particular test being conducted. If every item is agreeable and all the systems report ready conditions, the RWE is set into motion with the side louvers closing first (if required) and the end section louvers finishing the closure. If any system condition is negative then the RWE is instructed to move to the most open position and remain there for the duration of the test.

During the test, diagnostic measurements are made and stored in memory for future analysis. The RWE is then inspected for any damage that may have occurred due to test target pieces impacting the RWE. If the inspection proves positive the RWE is retracted from the end of the expansion tube and moved into the retracted position.

ESTIMATED FULL SCALE RWE COSTS

Based on the current level of design described in the previous sections, a rough costs estimate has been developed. The basis for the costs was derived from adding together all of the similar items and determining the unit price from various vendors. If an item requires fabrication, estimates were received from various fabricators pertaining to that item. Therefore, the costs presented in Table 9 are constructed costs. Also, the costs have been broken into categories of similar materials.

Table 9. Estimated Costs

<u>Category</u>	<u>Quantity</u>	<u>Cost</u>
Steel (plates, bar, beams, etc.)	911,000 lbs	\$2,290,000
Mechanical Components (bearings, gears, etc.)	Various	480,000
Hydraulic Components	Various	580,000
Instrumentation and Controls	Various	<u>550,000</u>
TOTAL		<u>\$3,900,000</u> *****

INTENTIONALLY LEFT BLANK.

PASSIVE RWE DEVELOPMENT

Passive RWEs are attractive since they are lower in capital costs than an active RWE. Many passive RWE designs are used in various blast simulators around the world with one of the most notable at AWE, Foulness, England (Ref. 15).

However any passive RWE has its limitations. During the study of active RWEs, it became apparent that a passive RWE is only partially effective. An examination of the experimental data obtained by Coulter and Kingery (Ref. 16) shows that a properly tuned passive RWE can provide some useful waveforms. However, these passive devices are set (amount of blocked area versus open area) for the entire passage of the blast wave and therefore cannot be as effective as an active RWE. Also, since each blocked area ratio is different for each overpressure, tests being conducted on a large number of various geometries would have to be available to meet the full range of operational requirements for the LB/TS. This scenario becomes less desirable since an extremely large amount of manpower would be required to set up the passive RWE and less than desirable results would be obtained.

However, if a passive RWE were really desired one could study its effectiveness using an active RWE. The active RWE would be used, however the louvers would be locked into a specific place for a given test. These results could then be studied to actually determine the overall effectiveness (both static and dynamic impulses) of a passive RWE. In fact, the RWE which was to be developed for the 1/57th scale shock tube would be a perfect level to try this idea since the operational cost for testing at this scale are very small in comparison to larger scale tubes. This approach was discussed with the project sponsor and it was agreed to abandon any further development of a passive RWE.

INTENTIONALLY LEFT BLANK.

CONCLUSIONS

An extensive amount of effort was applied toward developing the design tools for RWEs, updating the RCM code, developing, constructing, testing, and analyzing the 1/57th scale RWE, and furthering the design of the LB/TS RWE. The initial conclusion was that the objectives of this effort were met. Several design requirements which needed detailed input were identified as well as problem areas in the design approach. However, the design methodology proved to be sound and with the inclusion of the lessons learned, other RWE designs should improve.

The 1/57th RWE that was designed, constructed, and tested showed promise in the concept of a rotating louver design. Some modifications were necessary to improve the design, but this was anticipated since this was essentially a prototype. The device seems to produce the desired results and is easily adaptable to changing environments. One of the biggest drawbacks of this system was the limited resolution of the servo stepper motor of 2 msec. When the entire positive phase durations are on the order of 20 msec, not many of the details of the flow can be influenced by the RWE. However, positive results were still observed and the RWE was characterized as a "forgiving" device (i.e., it does not have to be exactly set). The other valuable piece of information obtained from these tests was that an RWE must be tuned to the facility it is operating upon. Each facility has its own unique set of characteristics which can vary from the ideal scenario (which the design tools are based). This fact was evident in the RCM calculations, completed with the two different drivers. However, the fact remains that the 1/57th scale RWE was effective in eliminating the rarefaction wave when properly instructed to do so.

The modified design tools were applied toward the further design of a rotating louver RWE for the LB/TS. During this design effort loads were estimated, structural members sized from the results of stress analyses, hydraulic parameters defined and component sizes estimated. This design allowed for a rough estimate of the cost for the LB/TS RWE to be generated. One of the important facts that was further defined during this study was the need for side vents when operating at high overpressures. The amount of side venting required is also a function of the minimum amount of blockage that the end section of the RWE produces. If this later number is kept to a minimum, then the amount of side vent area required is also kept to a minimum. An additional feature which was found to be very important is the operational sequence of the side and end vent louvers. If both systems are operated together for the entire blast wave passage, then the hydraulic power requirements are reduced. However, some small magnitude of rarefaction waves will be allowed to proceed back towards the test section. On the other hand, if these waves are not allowable, then the side vents must close first and then the end vents close which increases the hydraulic power requirements. The decision on which method to choose is based on costs versus fidelity.

INTENTIONALLY LEFT BLANK.

RECOMMENDATIONS

The 1/57th scale RWE should be tested at higher overpressures to obtain a better representation of the range over which it is effective. If the overpressures are high enough, spacers should be used between the support plates to create a passive side vent. Test data from these tests would be very interesting in attempting to understand the physics of the flow through these areas.

A better representation of the modeling of the flow in shock tubes should be developed. This may include modifications to the current version of the RCM code or by developing some other tool. The primary problem is that the flow in shock tubes and blast simulators is at least two-dimensional and it currently is not treated properly in a one-dimensional approximation. However, two-dimensional codes are fairly expensive to exercise and may not be well suited for defining the many various closing functions that the RWE requires for different test scenarios. However, some method must be developed and validated soon since it will be impossible to attach an extension onto the LB/TS to obtain "near-ideal" conditions.

The final recommendation is to pursue a program to construct a larger scale model of the LB/TS RWE. This device could be placed on a tube such as the 2.44 m shock tube at BRL. On this scale, actual hydraulic actuation could be achieved such as on the LB/TS RWE design. Also, the operational aspects of the RWE system could be debugged. Diagnostic data could be obtained from this device which would verify assumptions, provide critical experimental flow data, and improve the design process further. This exercise would probably provide valuable input to the LB/TS RWE design and could minimize final costs.

INTENTIONALLY LEFT BLANK.

REFERENCES

1. Guice, R. L., et al, 1990, *Large Blast and Thermal Simulator Reflected Wave Eliminator Study*, BRL Contractor Report BRL-CR-628, Ballistic Research Laboratory.
2. Chaplygin, S. A., 1902, *On Gas Jets*, in Russian, translated in 1944 as NACA TM 1063.
3. Picket, J. S., 1989, *The Generalization and Evaluation of Solutions Occurring in Chaplygin's Ideal Jet Theory*, M.A.Sc. Thesis, Institute for Aerospace Studies, University of Toronto.
4. Benson, R. E. and D. E. Pool, 1965, *Compressible Flow Through a Two-Dimensional Slit*, International Journal of Mechanical Science, 7, pp. 315-336.
5. Benson, R. E. and D. E. Pool, 1965, *The Compressible Flow Discharge Coefficients for a Two-Dimensional Slit*, International Journal of Mechanical Science, 7, pp. 337-353.
6. Guice, R. L. and J. J. Gottlieb, 1987, *Passive and Active Reflection Eliminators*, Tenth International Symposium on Military Applications of Blast Simulators, I, pp. 114-141.
7. Gottlieb, J. J., 1988, *Staggered and Nonstaggered Grids with Variable Node Spacing and Local Time Stepping for the Random-Choice Method*, Journal of Computational Physics, 78(1), pp. 160-177.
8. Gottlieb, J. J. and C. P. T. Goth, 1988, *Assessment of Reimann Solvers for Unsteady One-Dimensional Inviscid Flows of Perfect Gases*, Journal of Computational Physics, 78(2), pp. 437-458.
9. Gottlieb, J. J. and D. S. Anderson, 1987, *On Random Numbers for the Random Choice Method*, University of Toronto Institute for Aerospace Studies, UTIAS Technical Note No. 258.
10. Groth, C. P. T. and J. J. Gottlieb, 1988, *Numerical Study of Two-Stage Light-Gas Hypervelocity Projectile Launchers*, University of Toronto Institute for Aerospace Studies, UTIAS Report No. 327.
11. Zhang, K. Y. and J. J. Gottlieb, 1986, *Simulation of a Blast Wave in a Shock Tube by Using Perforated Plates in the Driver*, Institute for Aerospace Studies, University of Toronto, University of Toronto Institute for Aerospace Studies, UTIAS Report No. 304.
12. Crawford, R. E., et al, 1974, *Air Force Manual for Design and Analysis of Hardened Structures*, AFWL-TR-74-102, Air Force Weapons Laboratory.

13. Blevins, R. D., 1984, *Applied Fluid Dynamics Handbook*, Van Nostrand Reinhold Co., New York.
14. *Design Engineers Handbook*, 1979, Bulletin 0224-B1, Parker Hannifin Corp.
15. Borgartz, B., 1987, *AWE Foulness Nuclear Blast and Thermal Simulators*, Tenth International Symposium on Military Applications of Blast Simulation, II, pp. 34-55.
16. Kingery, C. N. and G. A. Coulter, 1985, *Rarefaction Wave Eliminator Concepts for a Large Blast/Thermal Simulator*, BRL-TR-2634, Ballistic Research Laboratory.
17. Opalka, K. O., 1987, *Large Blast-Wave Simulators (LBS) with Cold-Gas Drivers: Computational Design Studies*, BRL-TR-2786, Ballistic Research Laboratory.

APPENDIX A
INITIAL RCM CALCULATIONAL RESULTS

INTENTIONALLY LEFT BLANK.

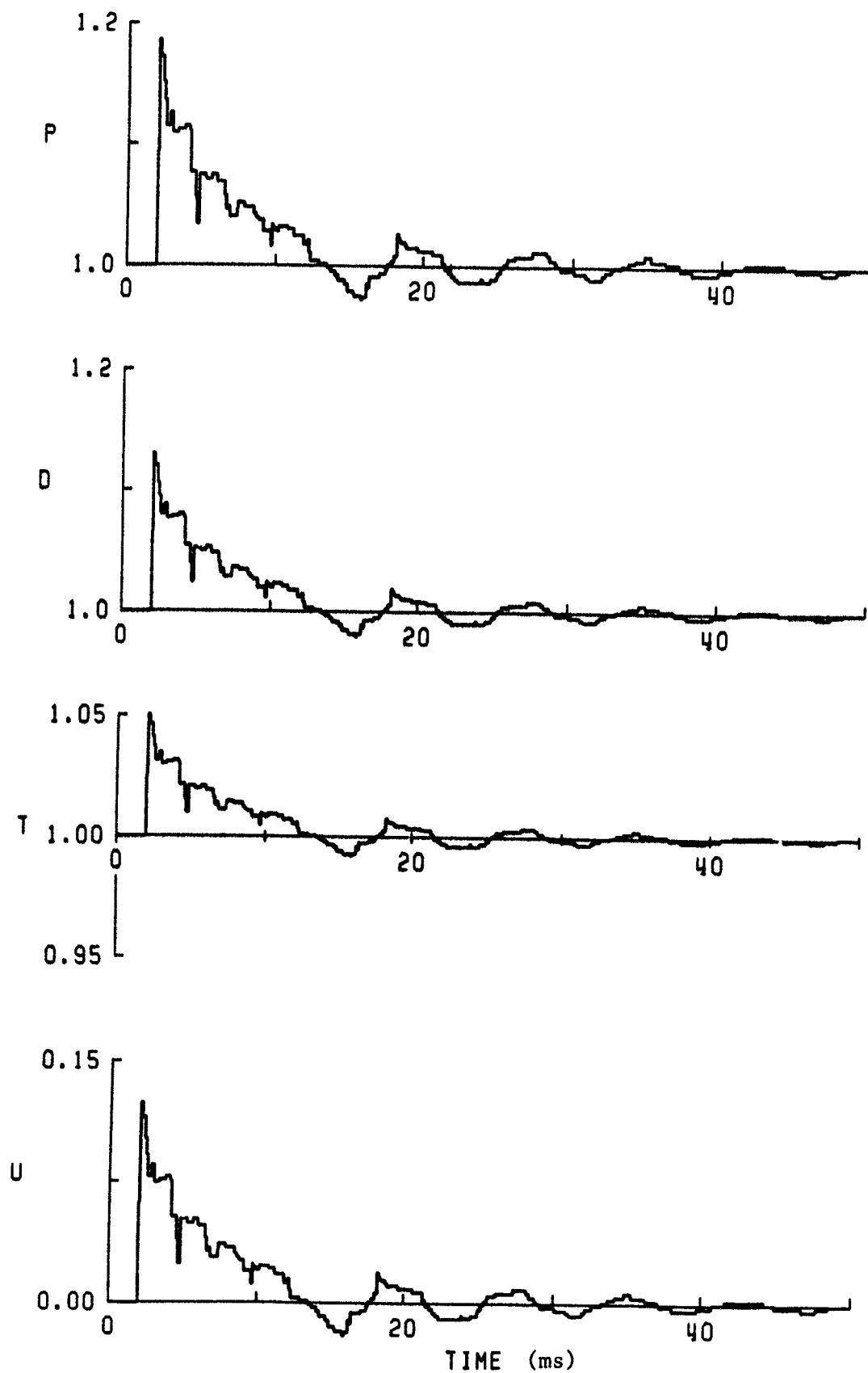
CASE # 1.

$$P_{41} = 4.767$$

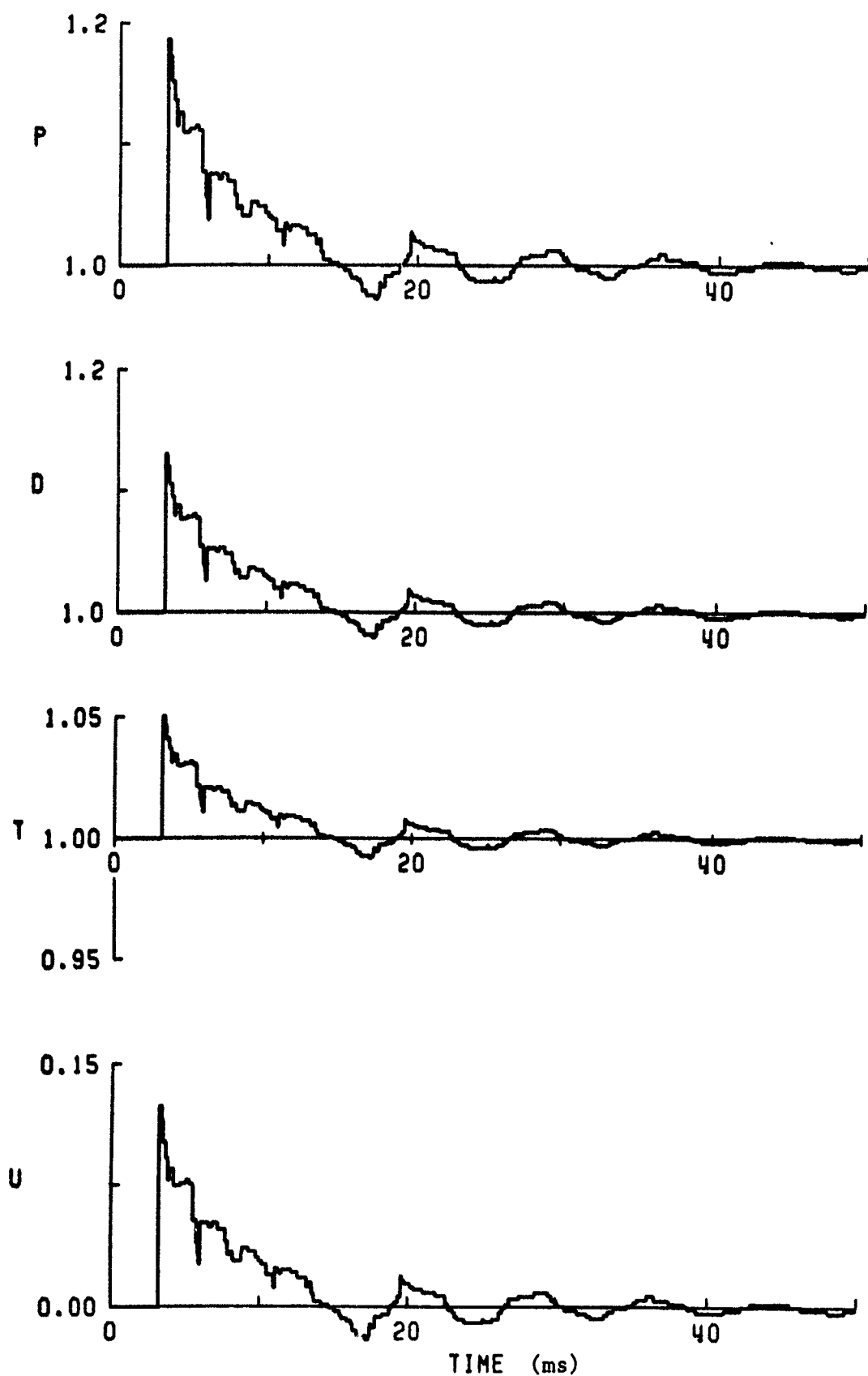
$$L_{\text{driver}} = 33.98 \text{ cm}$$

Comments:

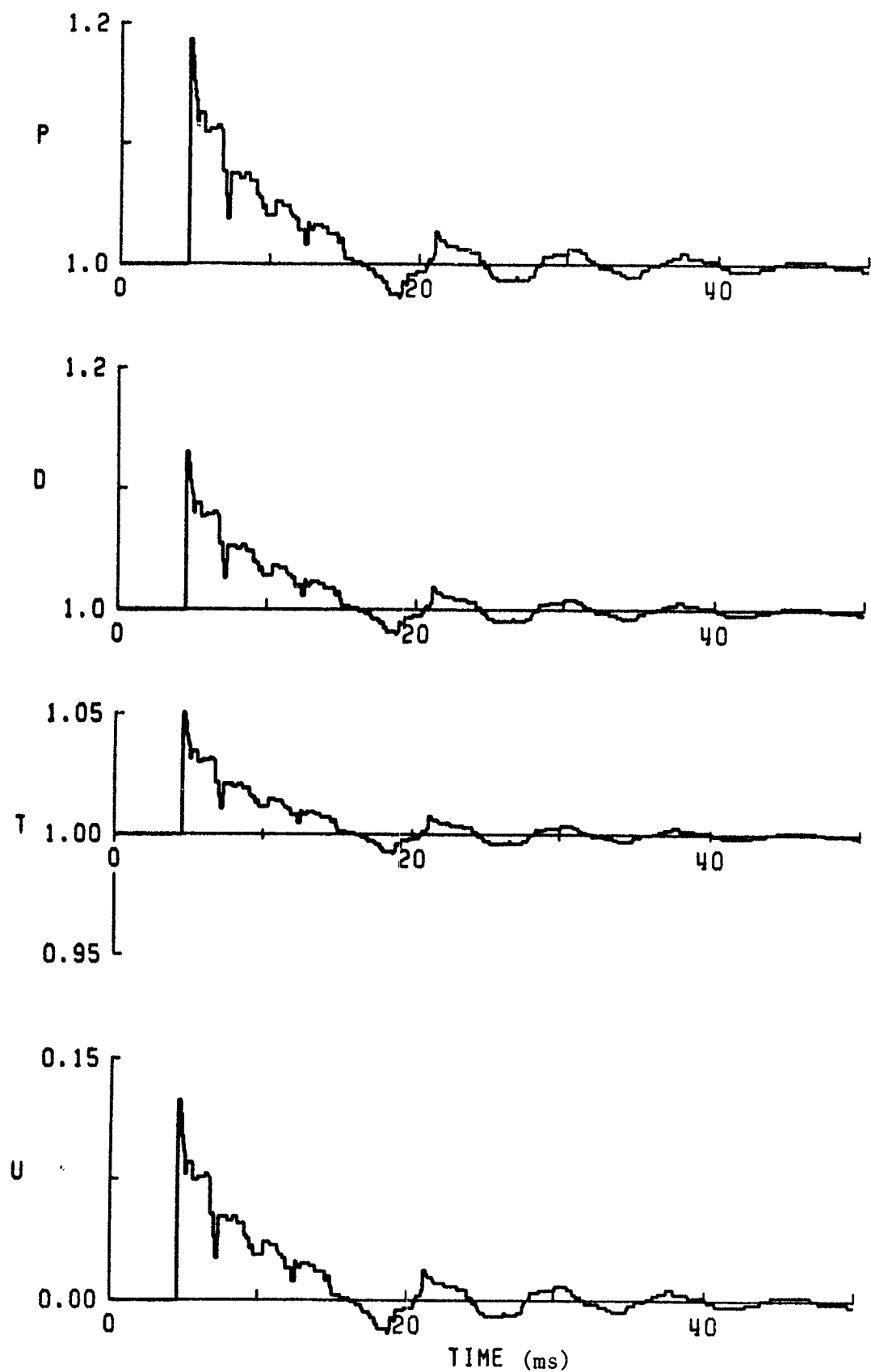
- 1) We get a decaying blast wave with oscillations. These cyclical oscillations are due to the reverberation of the wave in the driver (criss-crossing wave that drops the driver pressure in steps with time).
- 2) Open end effects are absent, because the wave from the end does not reach the test stations in the time scales shown (extension is really long).
- 3) Contact surface does not reach the test stations in the time scales shown, because the wave decays away too quickly.
- 4) Friction, heat transfer, and head losses would, if included, smooth the profiles somewhat and reduce the amplitudes of the peaks (both positive and negative peaks).
- 5) Four temporal signatures at each of the four test stations are shown.
- 6) Spatial distributions are shown for two distance ranges:
 - a) 0 to 1 m - essentially the driver portion with nozzle
 - see deep drop in pressure at throat and large increase in velocity at throat
 - later times shows flow reversals in throat with pressure rises and velocity drops
 - b) 1 to 12 m - essentially the channel
 - shows wave motion spatially with the cyclical components



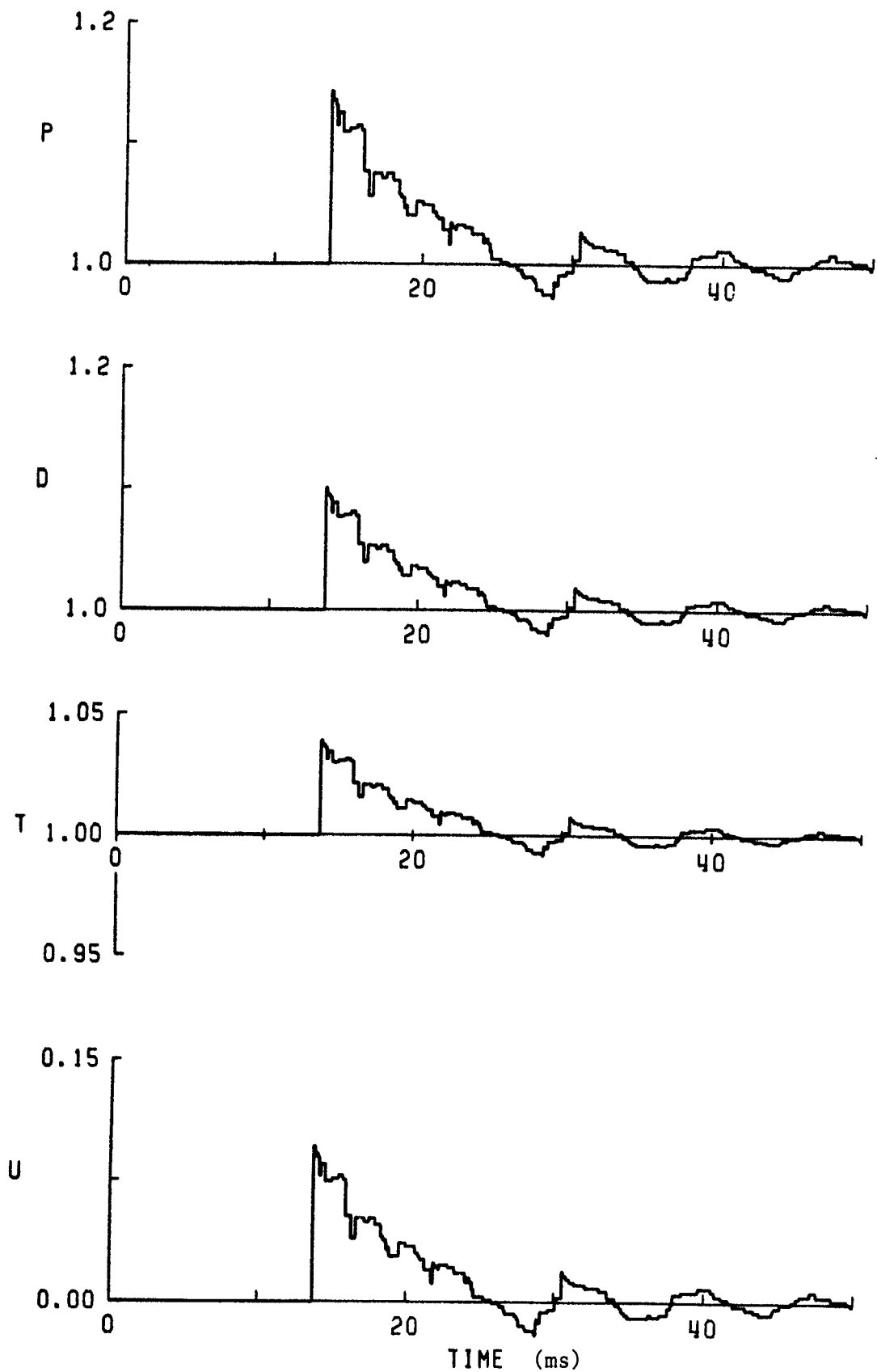
TIME HISTORIES
LOCATION: 1.218 m (3 diameters)



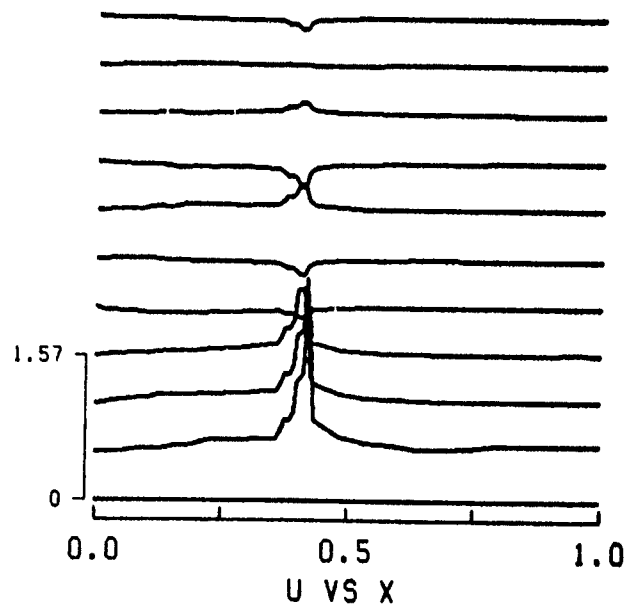
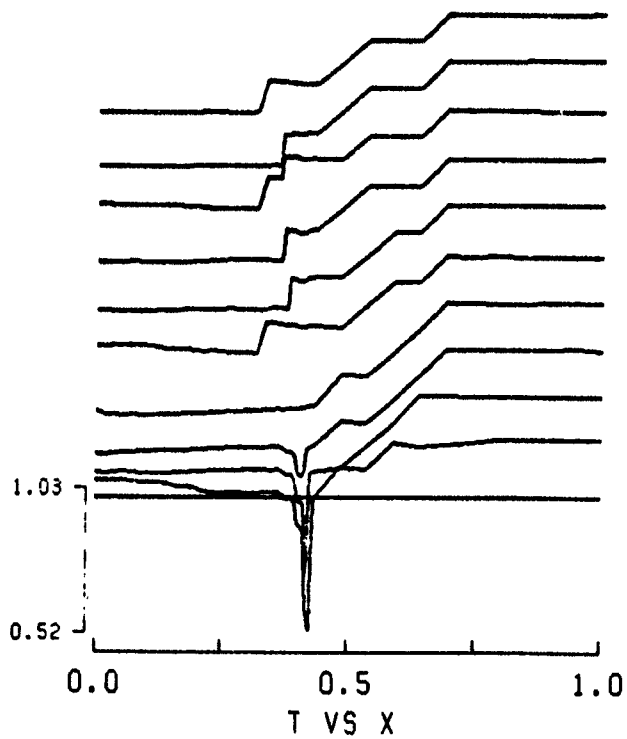
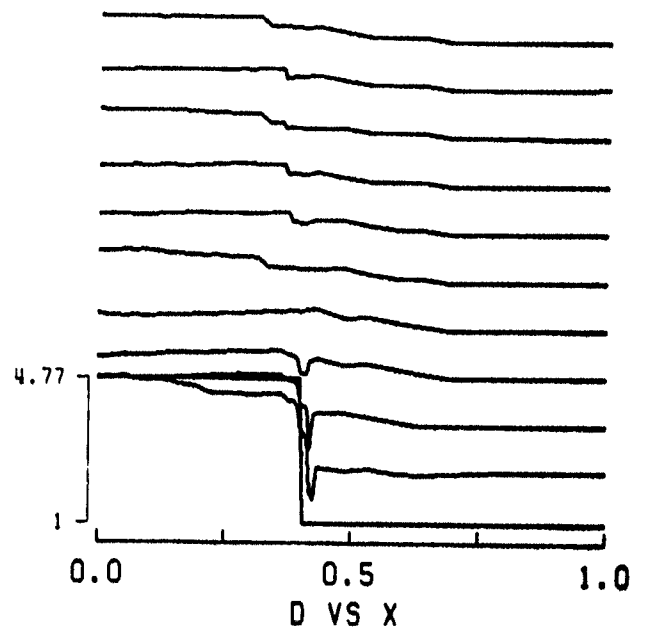
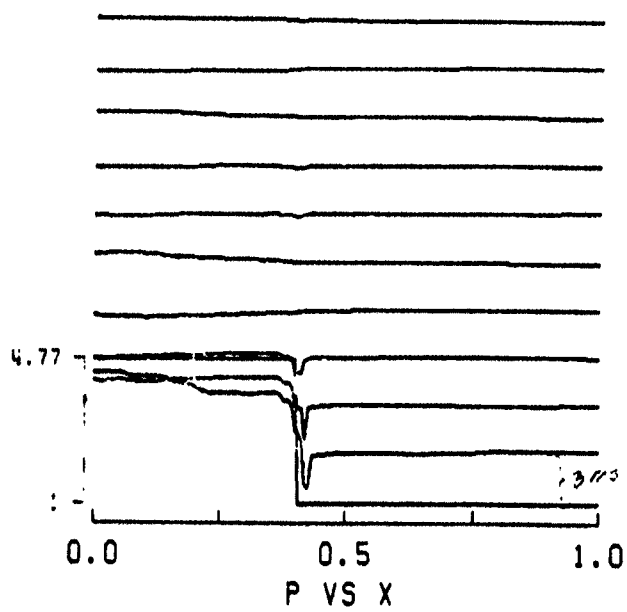
TIME HISTORIES
LOCATION: 1.686 m (5 diameters)



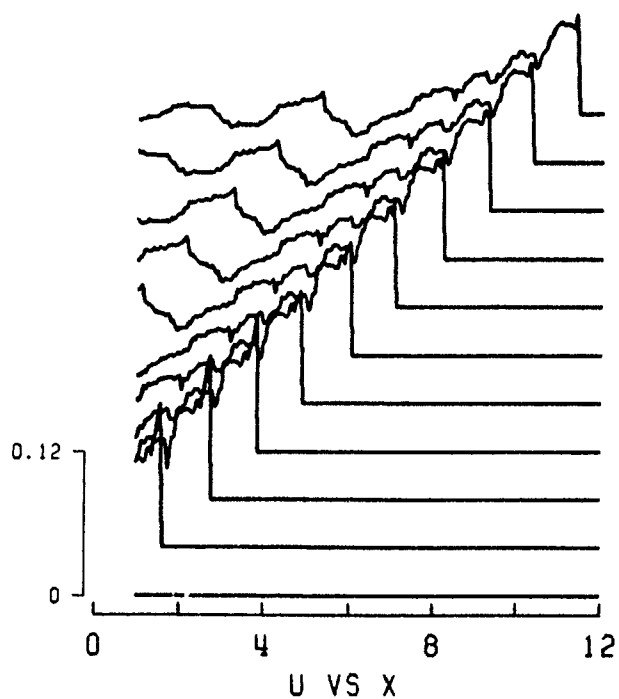
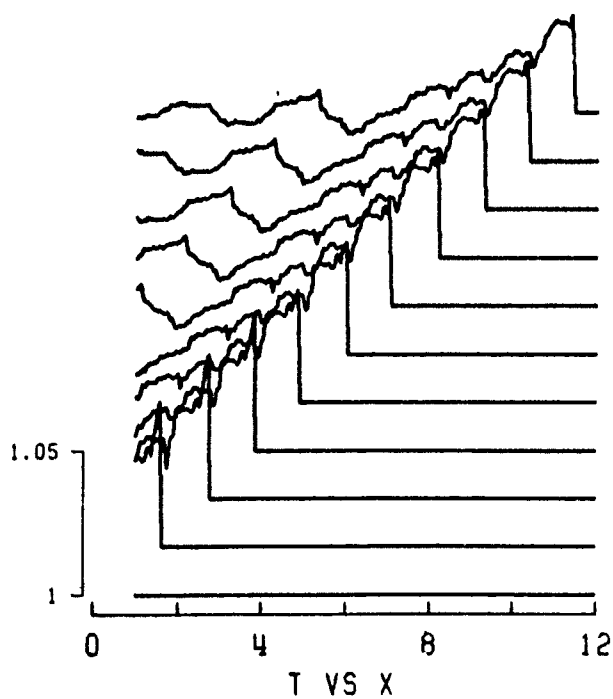
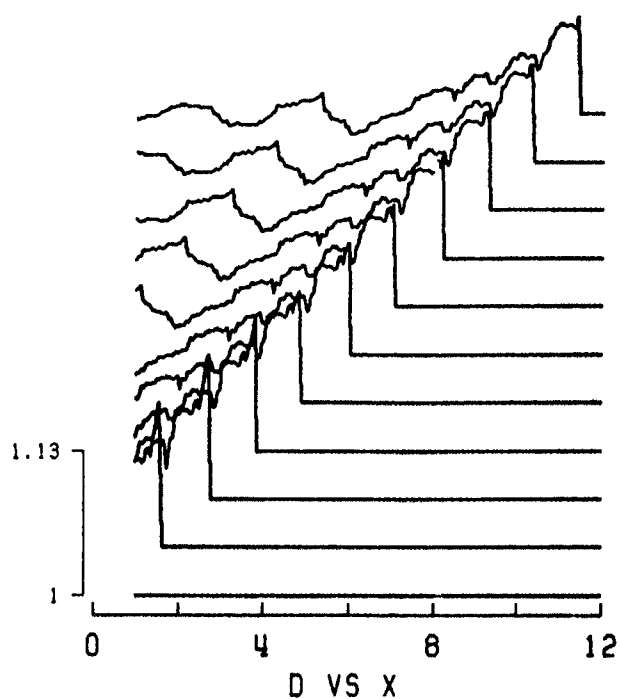
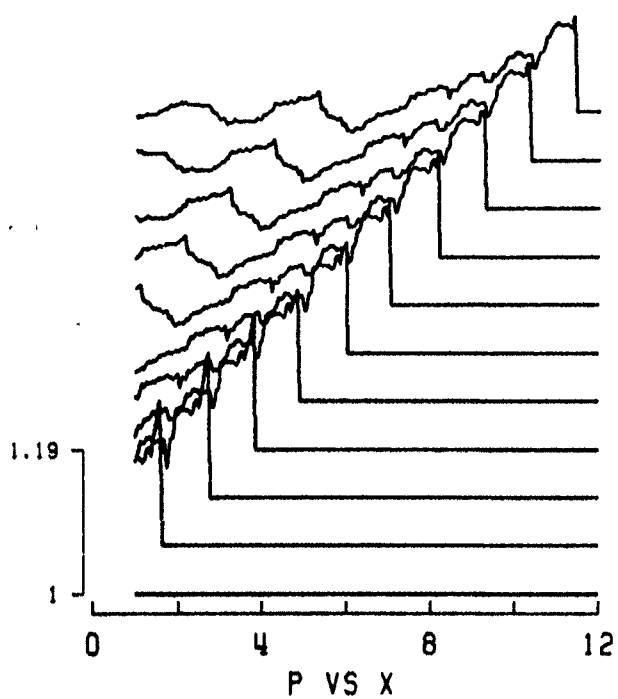
TIME HISTORIES
LOCATION: 2.205 m (7 diameters)



TIME HISTORIES
LOCATION: 5.530 m (20 diameters)



SPATIAL DISTRIBUTIONS
TIME: 0.000 10 30.002 ms



SPATIAL DISTRIBUTIONS
TIME: 0.000 TO 30.002 ms

CASE # 2.

$P_{41} = 145.9$ (much higher than case #1)

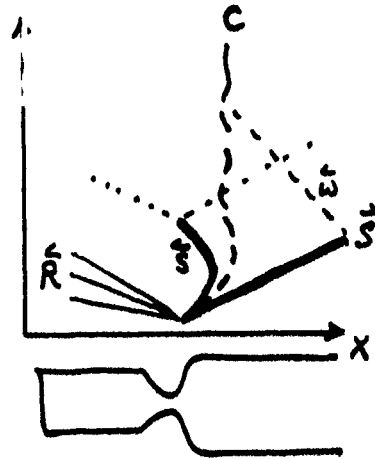
$L_{\text{driver}} = 33.98$ (same as case #1)

Comments:

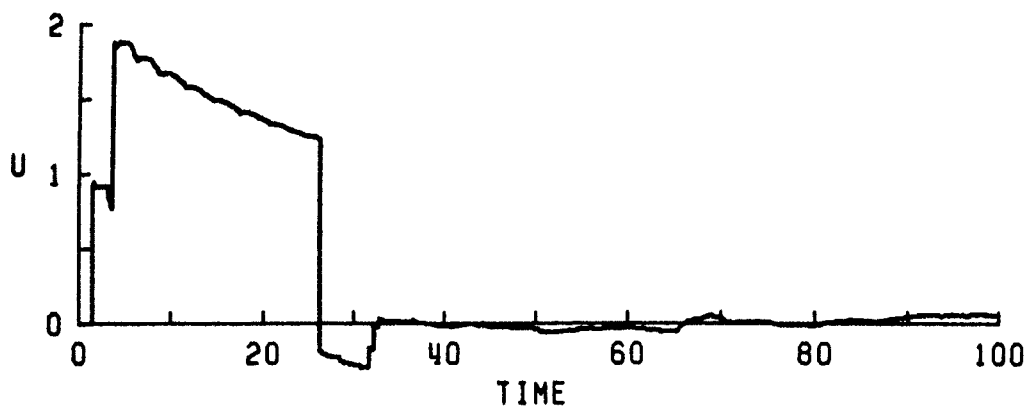
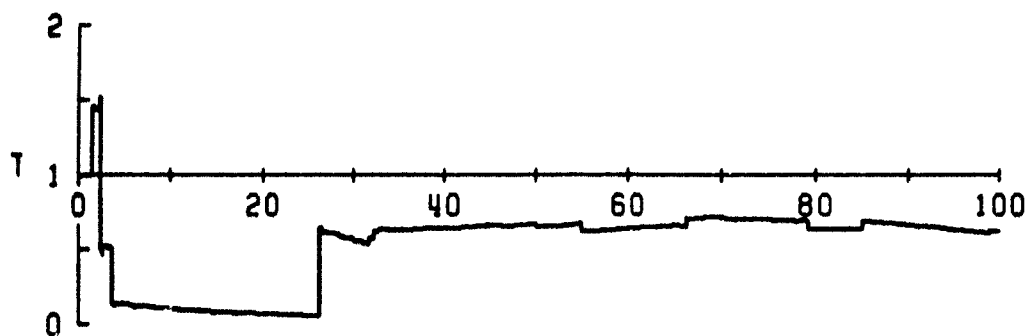
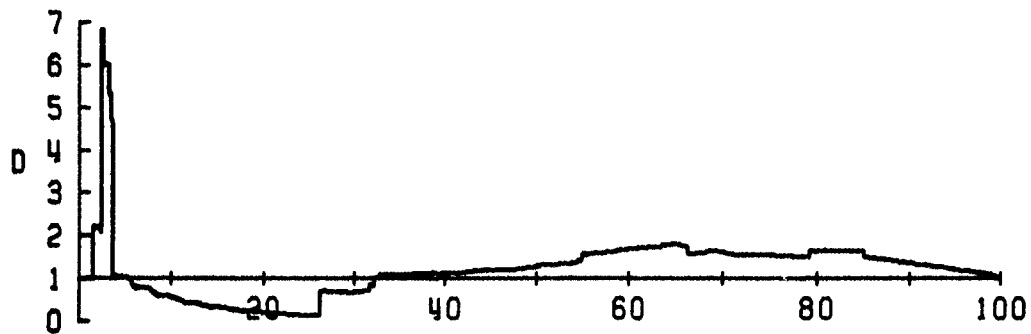
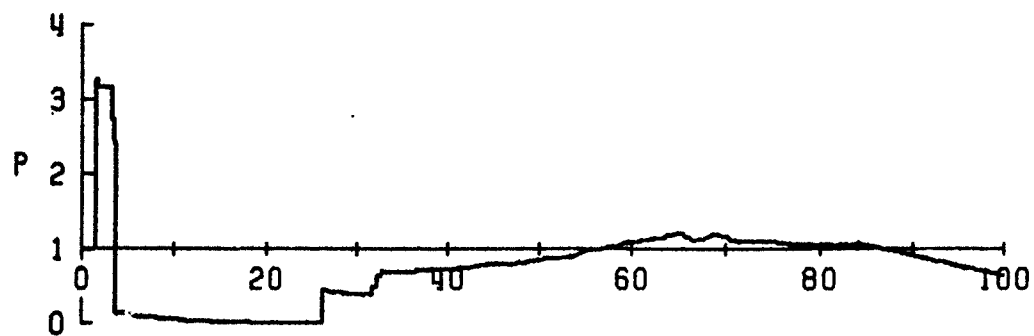
1. These results are easy to understand if you know about contact surface movements and swept-back shocks.

The primary shock \hat{S} goes to duct end and reflects as the reflected wave \hat{W} . Contact surface C moves out and in, out and in (oscillates).

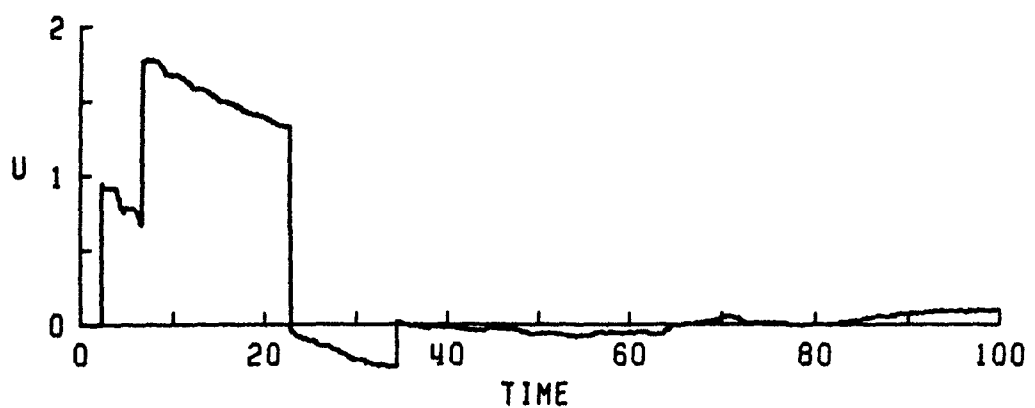
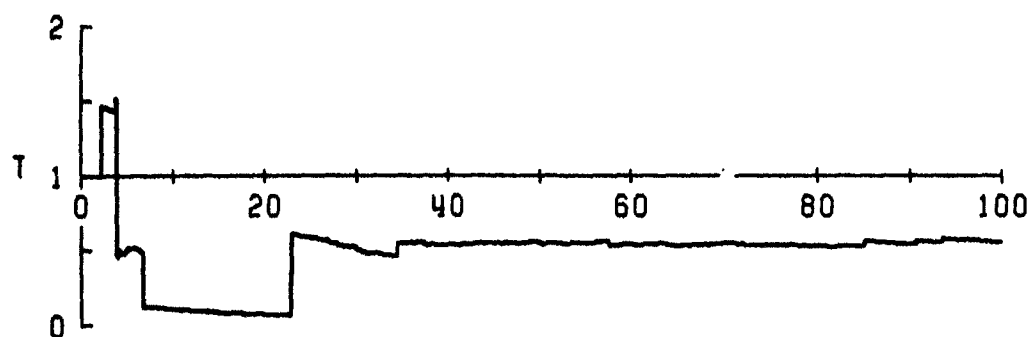
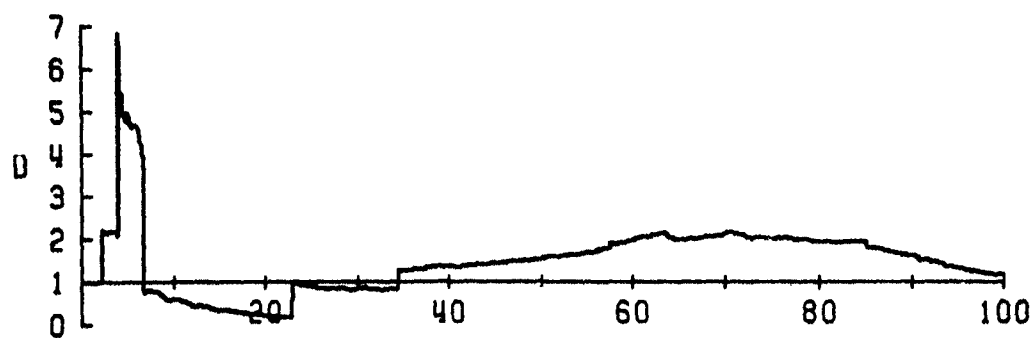
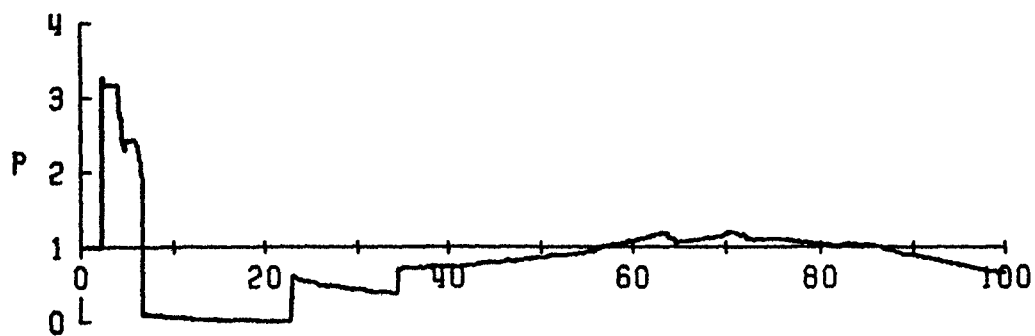
The choked flow creates a supersonic flow in expansion, which is made supersonic by the upstream-facing but swept-back shock \hat{S} . It is swept downstream first, then makes its way upstream and into the area change, producing a transmitted wave into the driver (sometimes) and always a reflected shock that moves out along the channel.



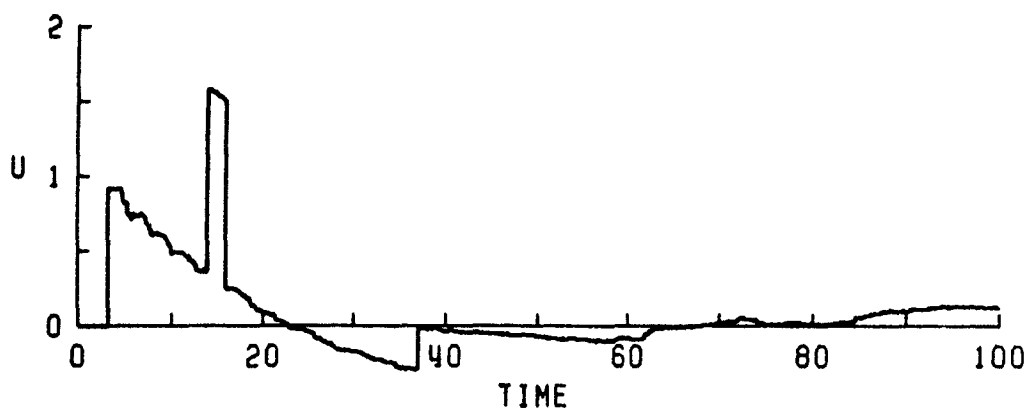
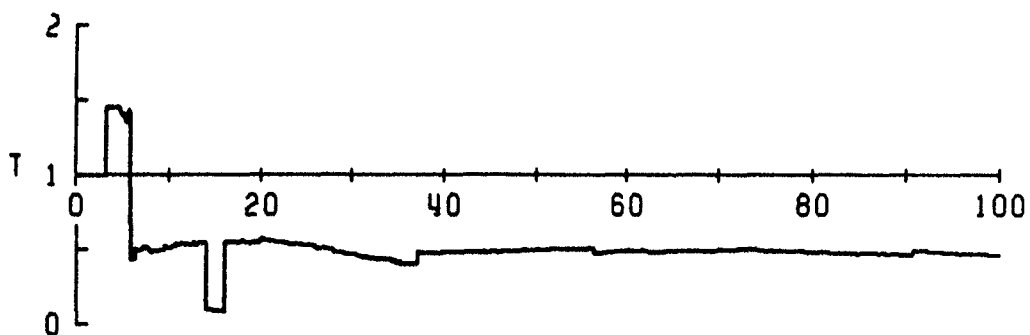
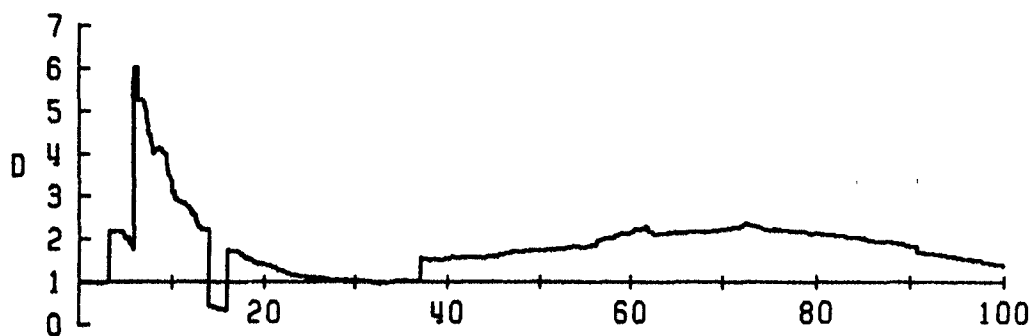
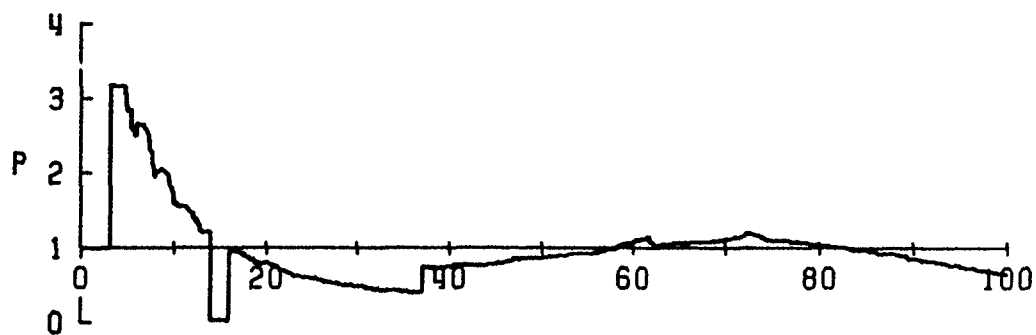
2. At the first test station (3 diameters) the primary shock arrives first (increases in P, D, T, and U). Then the contact surface is swept by (can be seen in D and T only), followed almost immediately by the swept-back shock (seen in P, D, T, and U). Later the swept-back shock passes by again, as it goes upstream (smaller amplitude). This is followed by the reflected shock of the upstream-facing wave. Then the traces settle down with oscillation of long duration.
3. The second and third stations (5 and 7 diameters) show similar effects, but the third station only catches a small view of the upstream-facing shock reversing at times of 16 and 17 ms.
4. The fourth station sees only a glimpse of the contact surface moving downstream and then upstream past the test station (can only be seen in D and T). The shock at a time of 58 ms is due to the upstream-facing shock reflecting from the area change. The shock at 97 ms is coming as a reflection of the primary shock from the open end. Eventually it would appear at the other test stations, if the computations were continued. It basically restores near ambient conditions in the shock tube ($P \approx 1$ and $U \approx 0$).



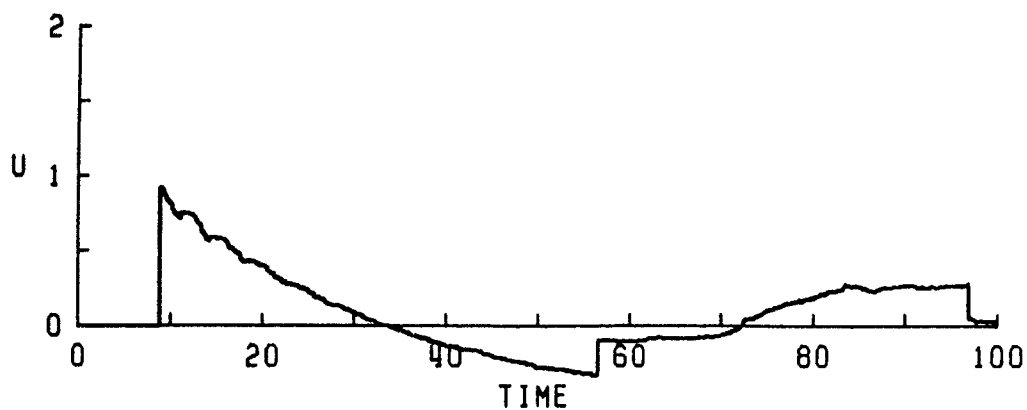
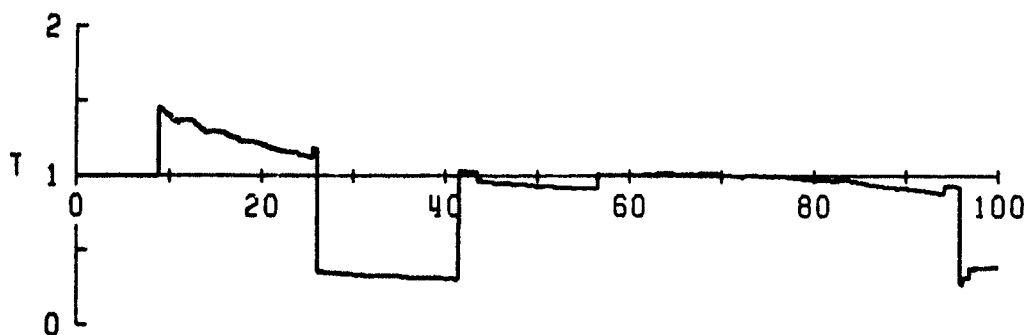
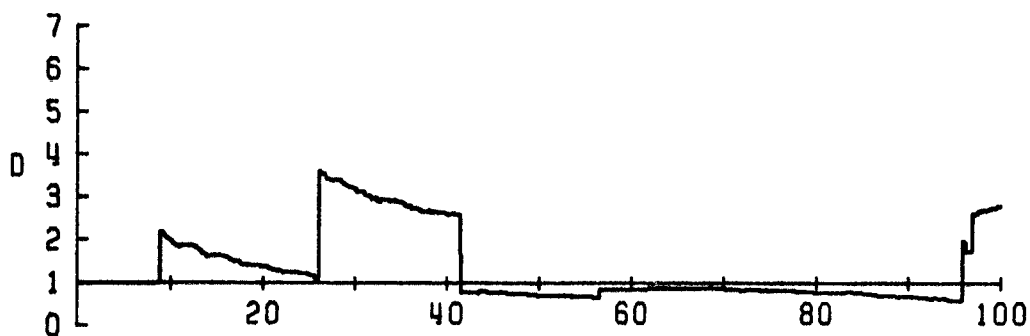
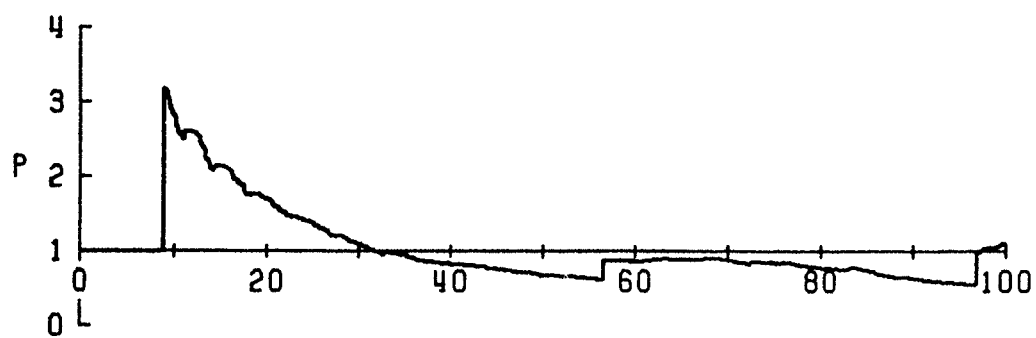
TIME HISTORIES
LOCATION: 1.218 m (3 diam)



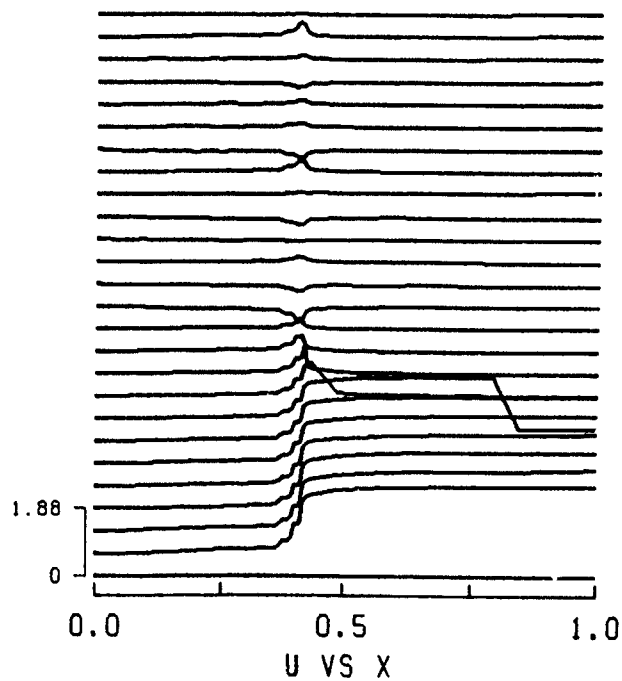
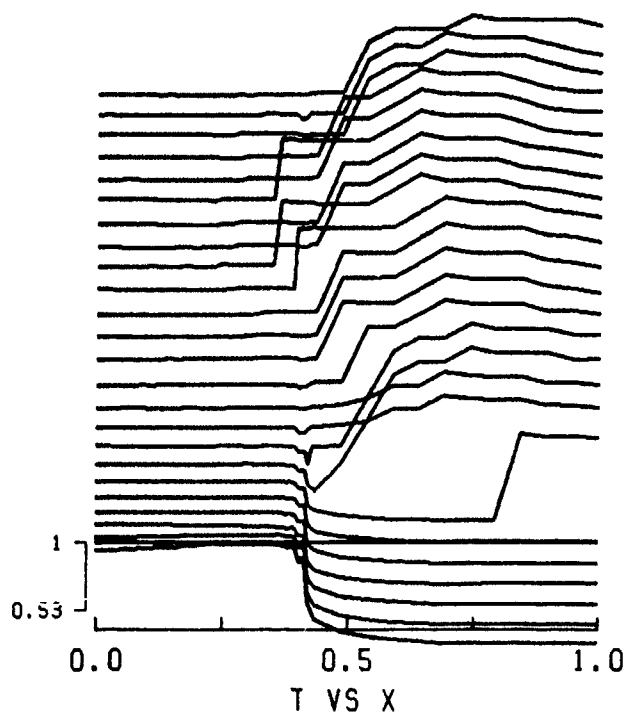
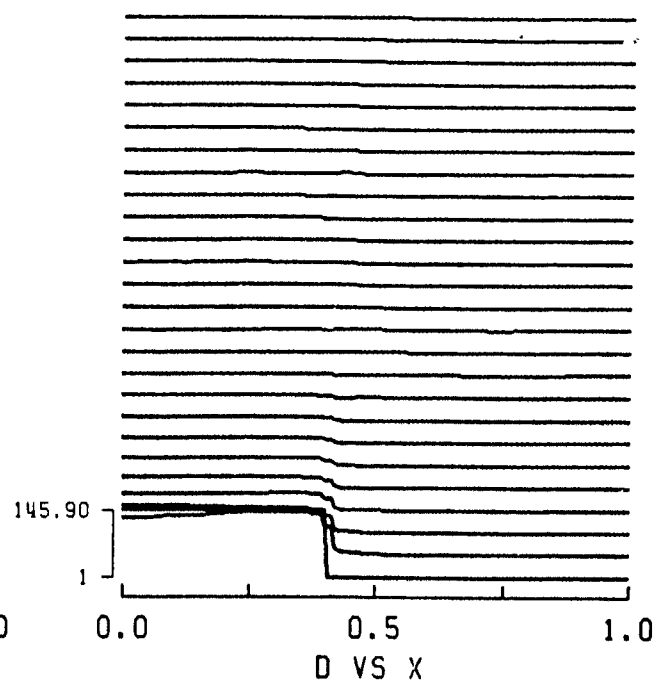
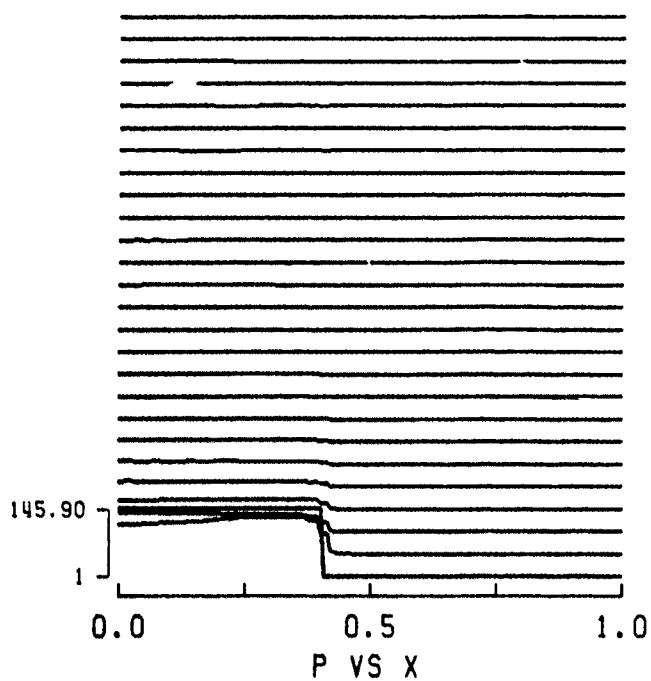
TIME HISTORIES
LOCATION: 1.686 m (5 diam)



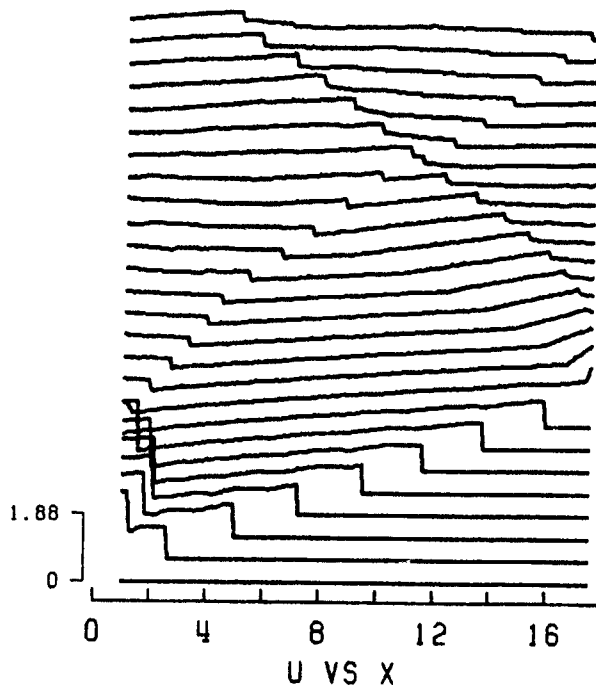
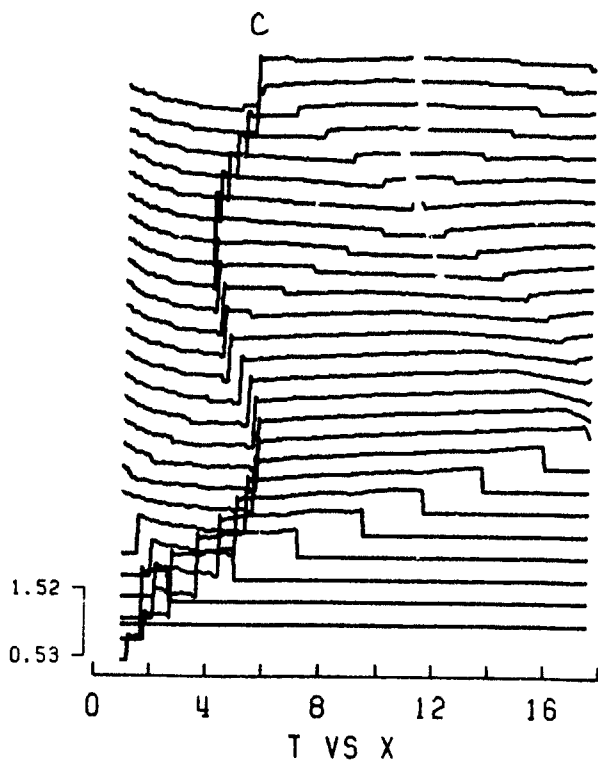
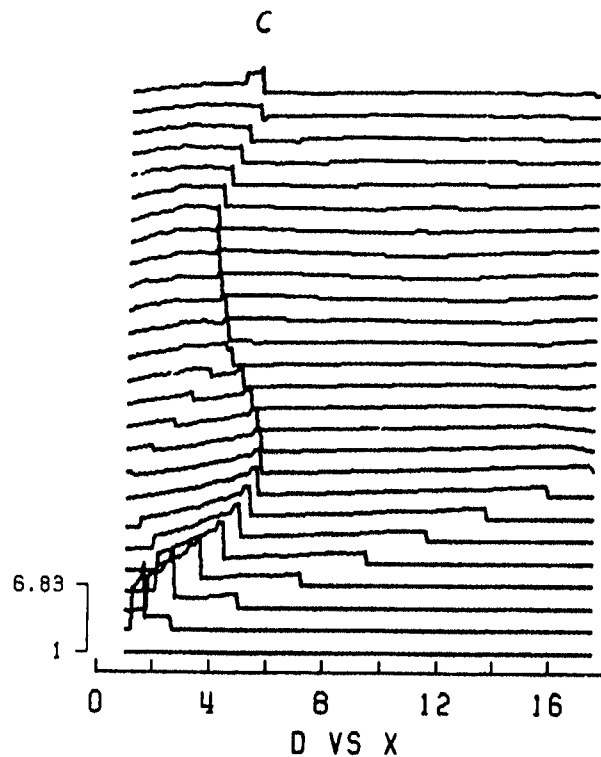
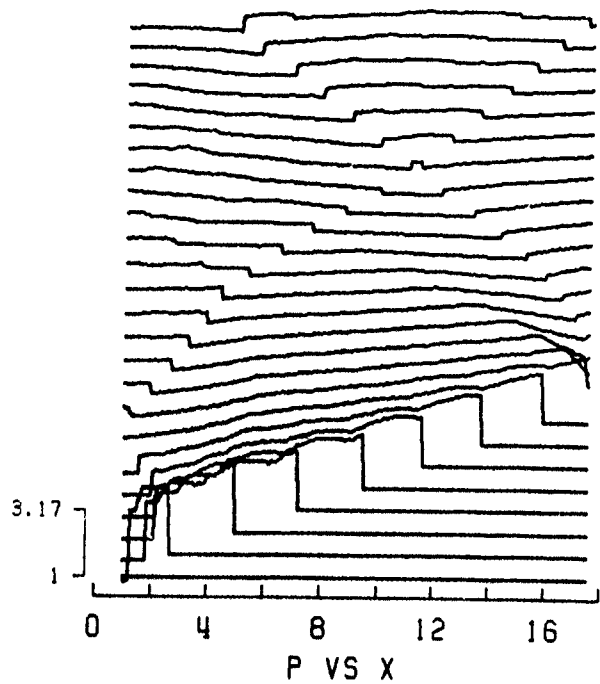
TIME HISTORIES
LOCATION: 2.205 m (7 diam)



TIME HISTORIES
LOCATION: 5.530 m (20 diam)



SPATIAL DISTRIBUTIONS
TIME: 0.000 TO 100.000 ms



SPATIAL DISTRIBUTIONS
TIME: 0.000 TO 100.000 ms

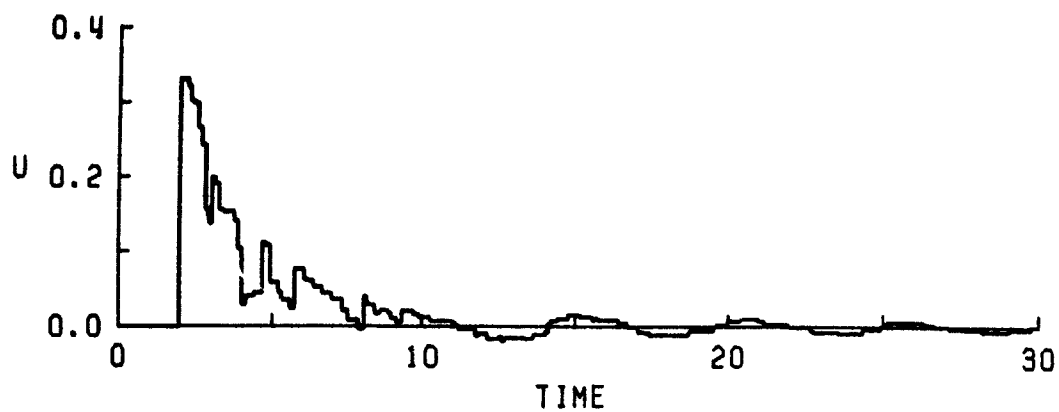
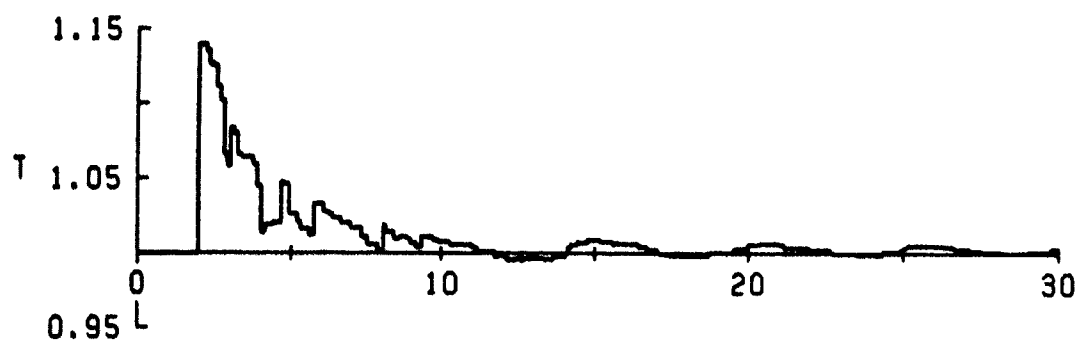
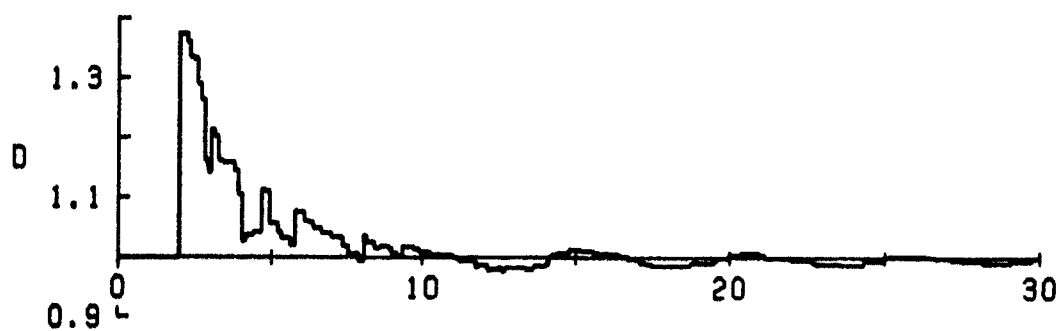
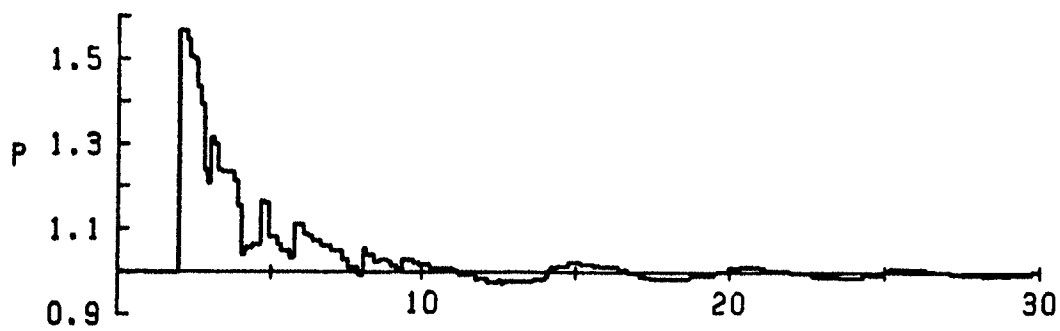
CASE # 3.

$P_{41} = 20$ (intermediate between cases # 1 and 2)

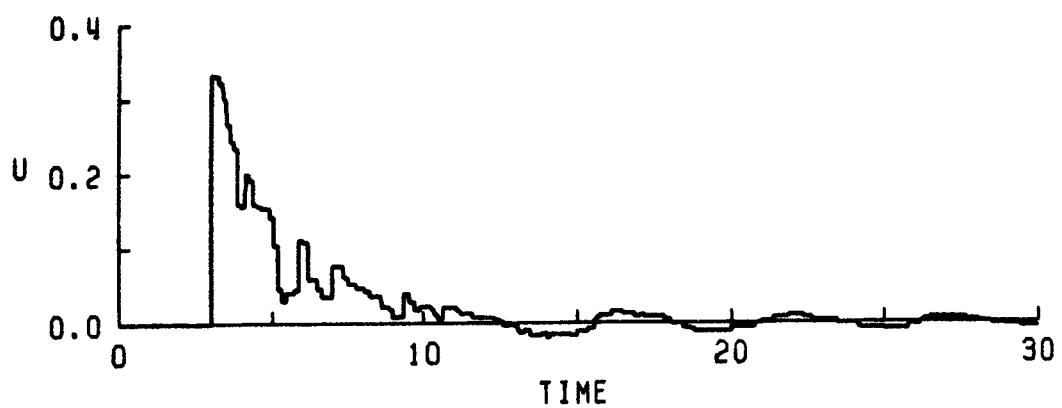
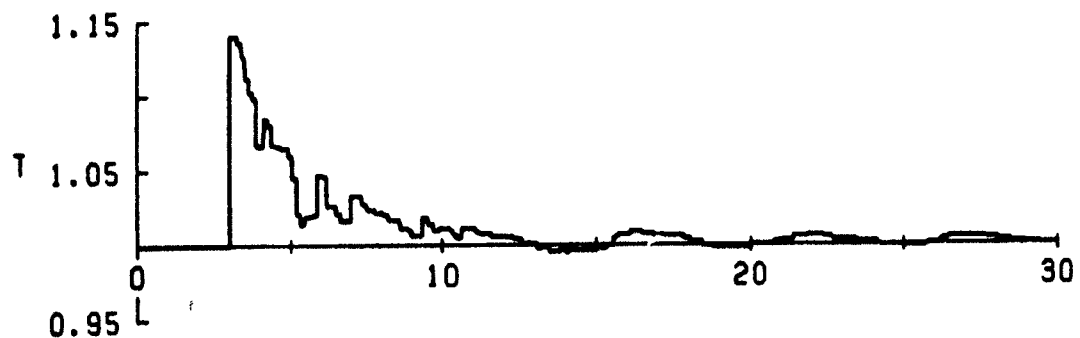
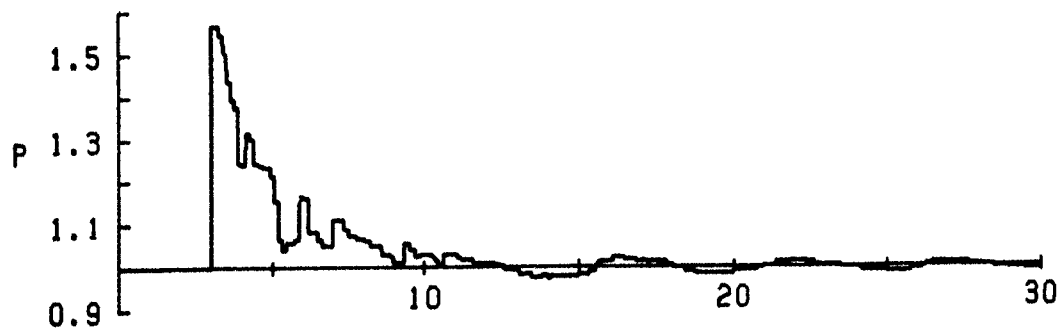
$L_{\text{driver}} = 11.12 \text{ cm}$ (very short driver)

Comments:

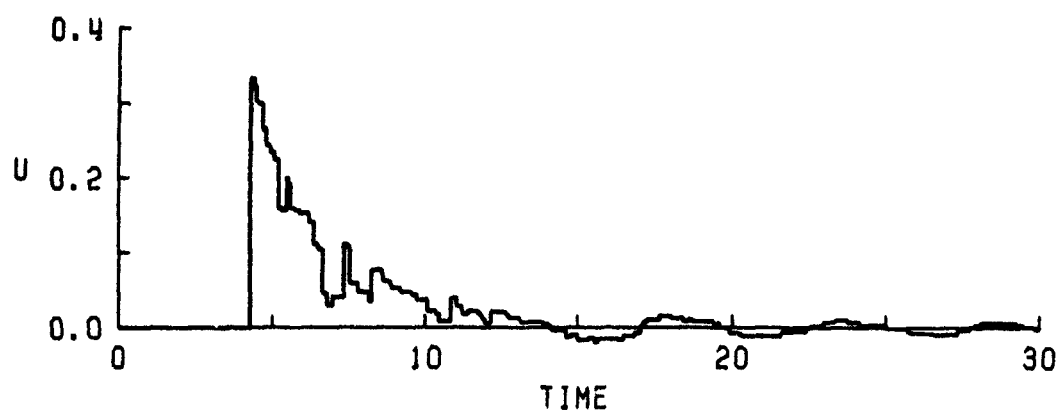
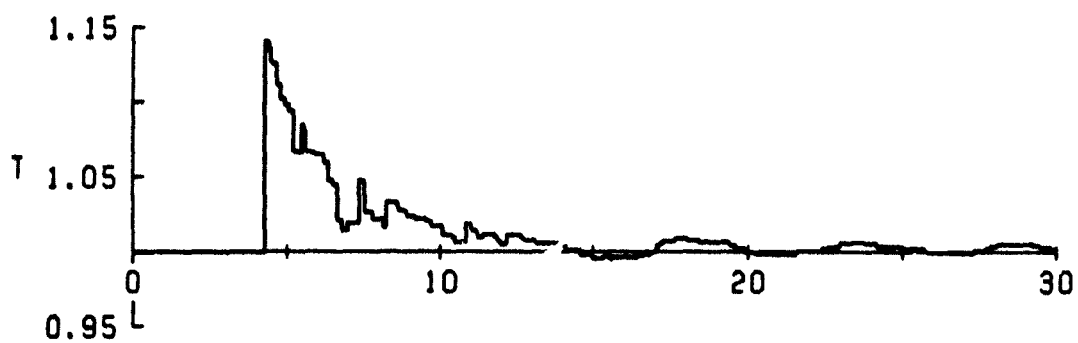
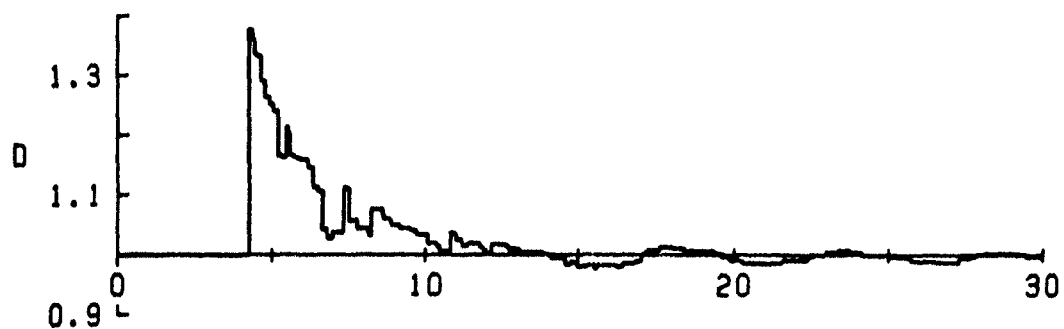
- 1) The short driver length means that the wave that criss-crosses the driver does this more frequently and discharges the driver more quickly. Hence, we have a shorter duration blast wave simulated in the channel.
- 2) The shorter driver and more rapid criss-crossing frequency shows up in higher frequency oscillations in the blast wave in the channel.
- 3) The open end does not produce a reflected wave that returns in time to affect these results.
- 4) The swept-back shock exists for only a short while, and it doesn't affect the results.
- 5) The contact surface doesn't reach the test stations; so it does not appear in the temporal profiles.



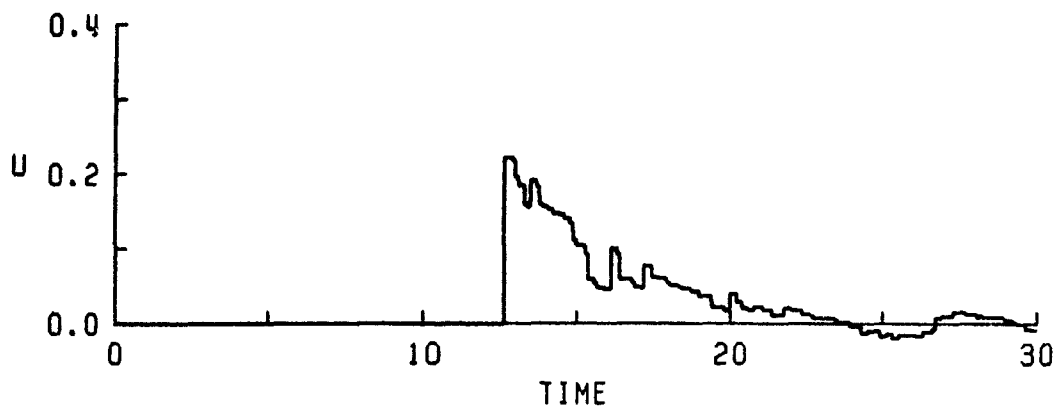
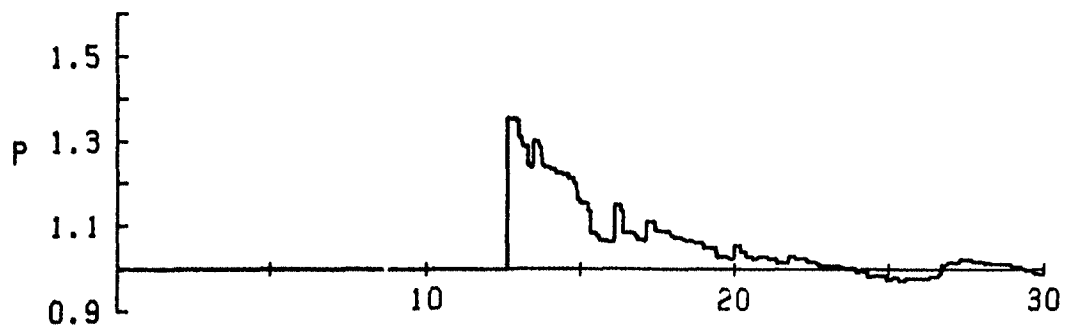
TIME HISTORIES
LOCATION: 0.990 m (3 diam)



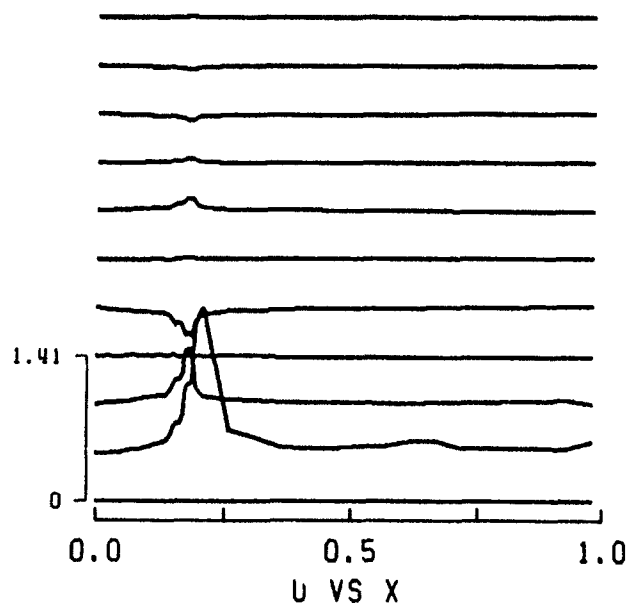
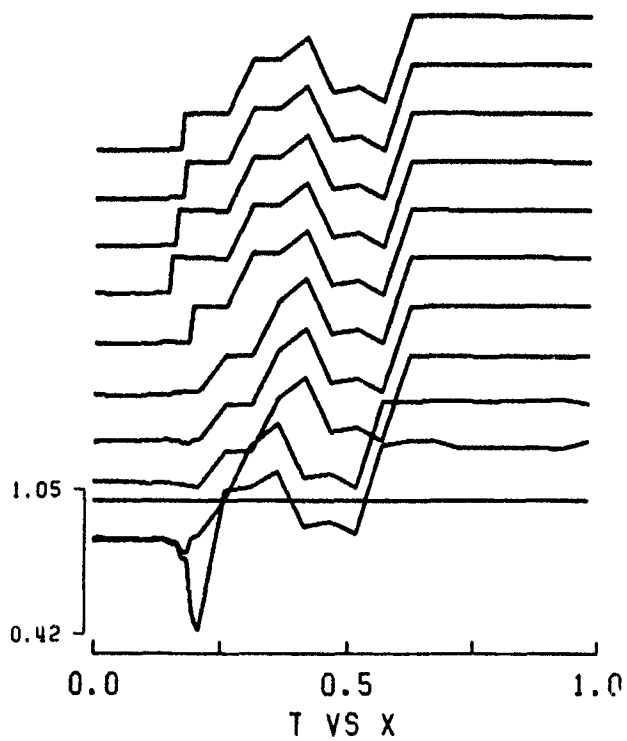
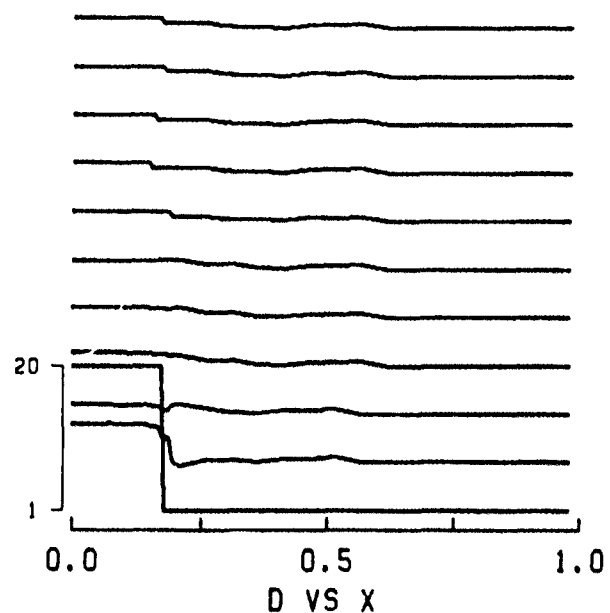
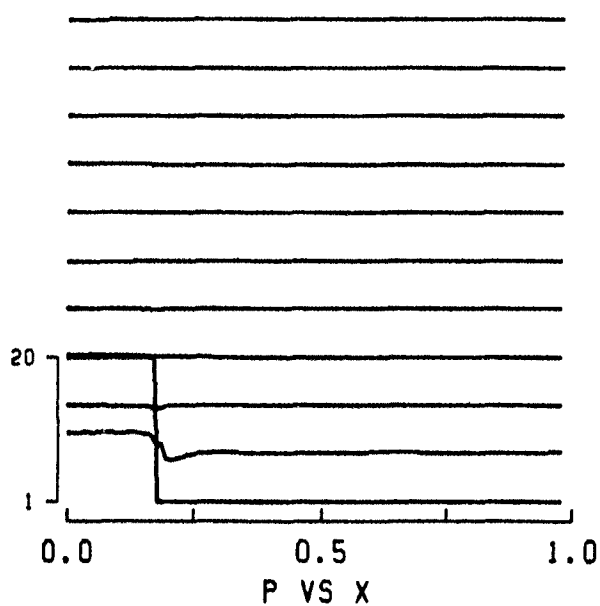
TIME HISTORIES
LOCATION: 1.457 m (5 diam)



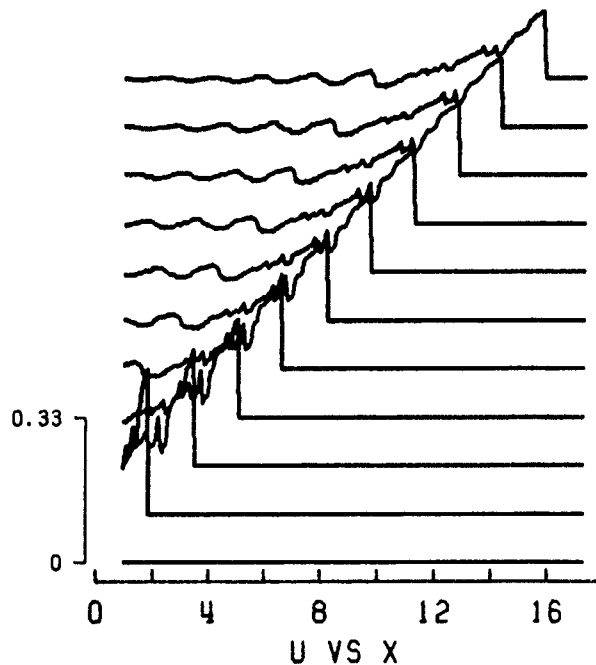
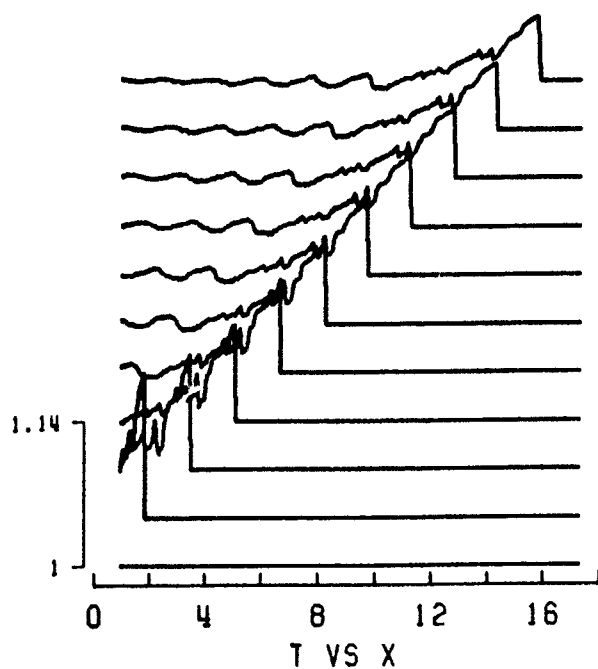
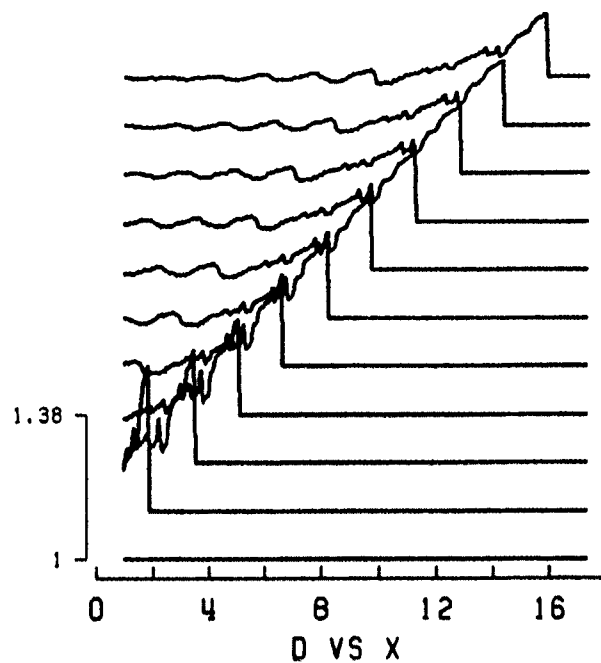
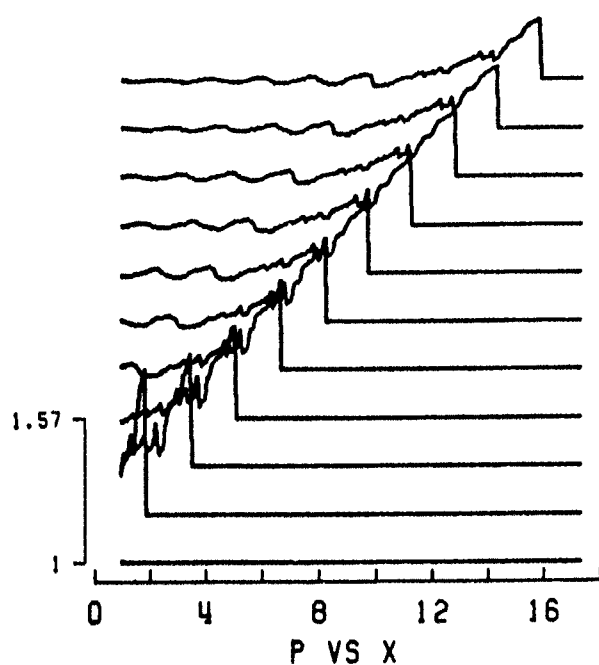
TIME HISTORIES
LOCATION: 1.976 m (7 diam)



TIME HISTORIES
LOCATION: 5.301 m (20 diam)



SPATIAL DISTRIBUTIONS
TIME: 0.000 TO 40.006 ms



SPATIAL DISTRIBUTIONS
TIME: 0.000 TO 40.006 ms

CASE # 4.

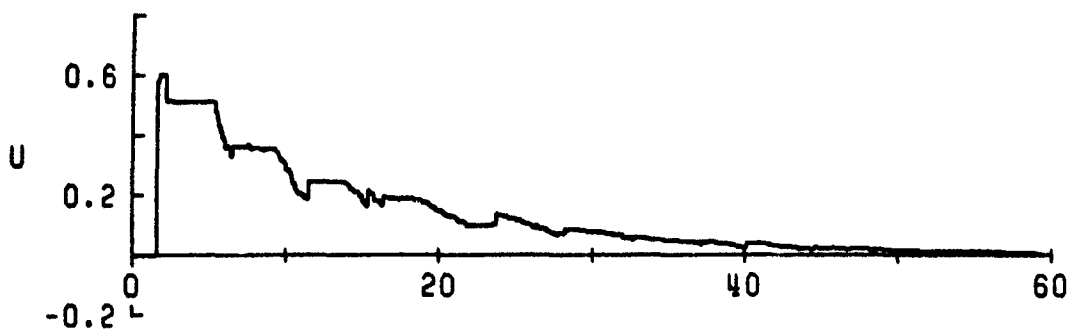
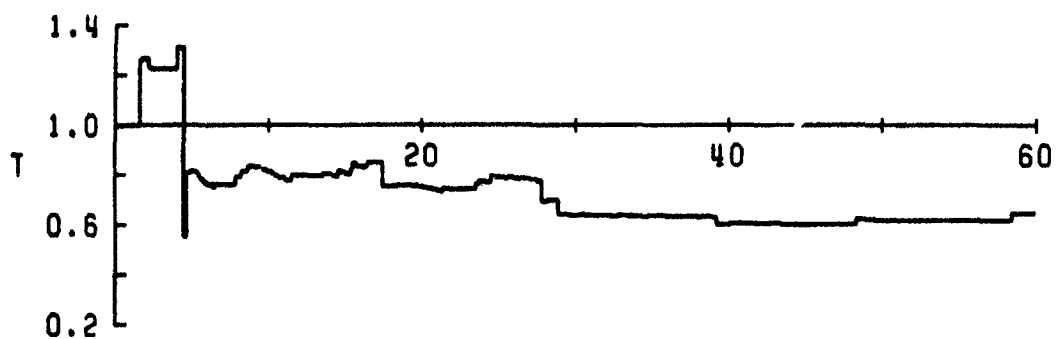
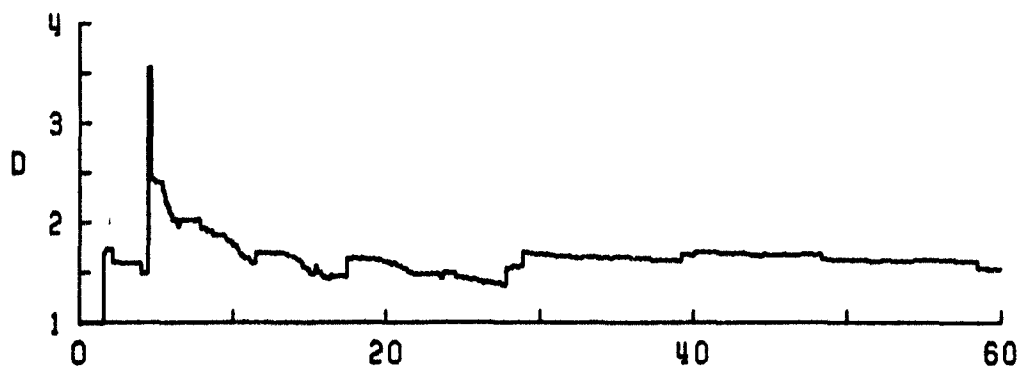
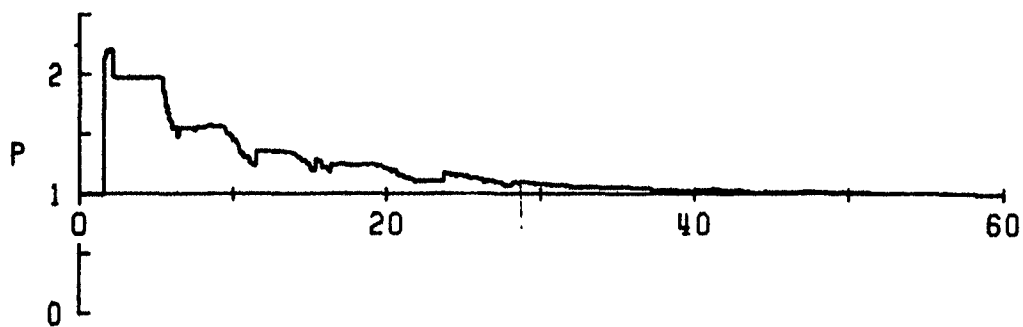
$$P_{41} = 51 \frac{1}{4}$$

$$L_{\text{driver}} = 67.0 \text{ cm}$$

Comments:

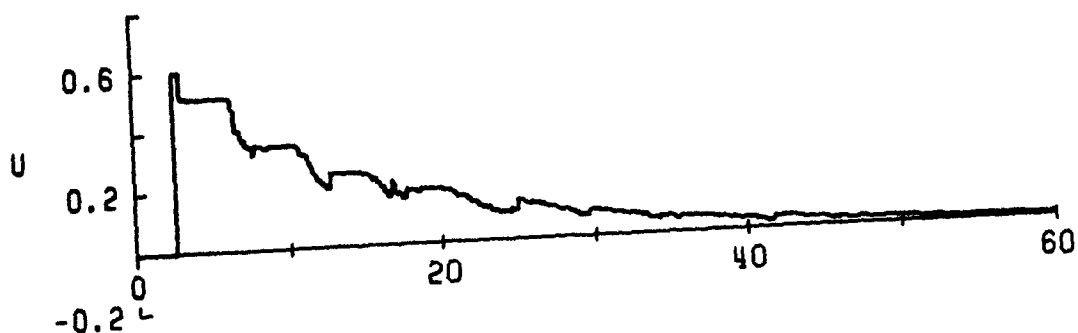
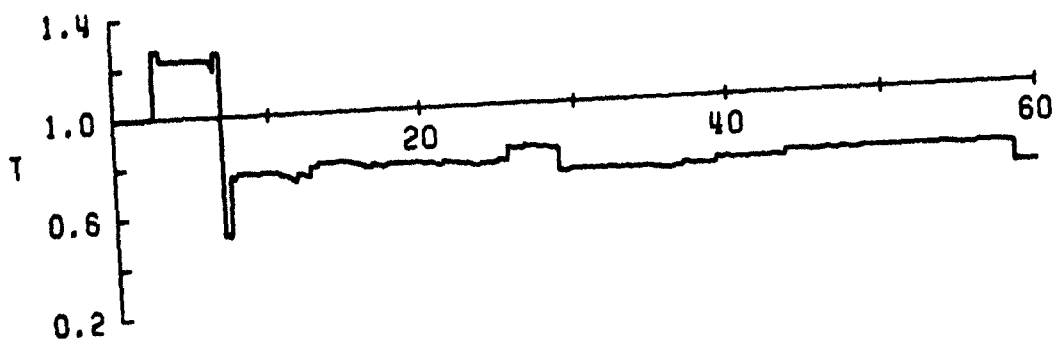
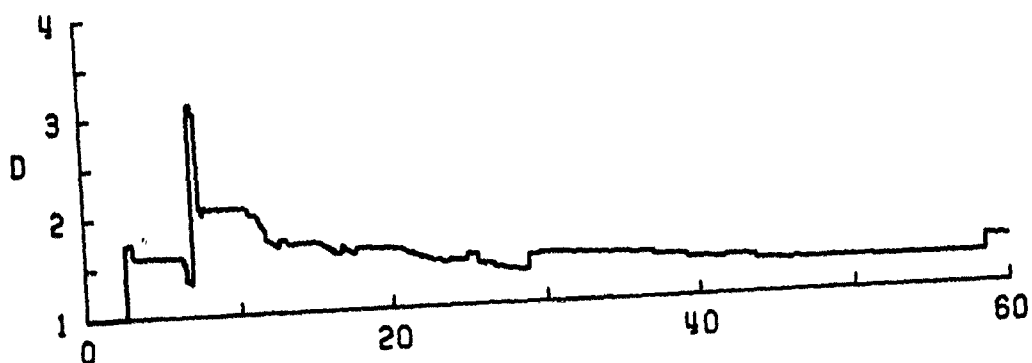
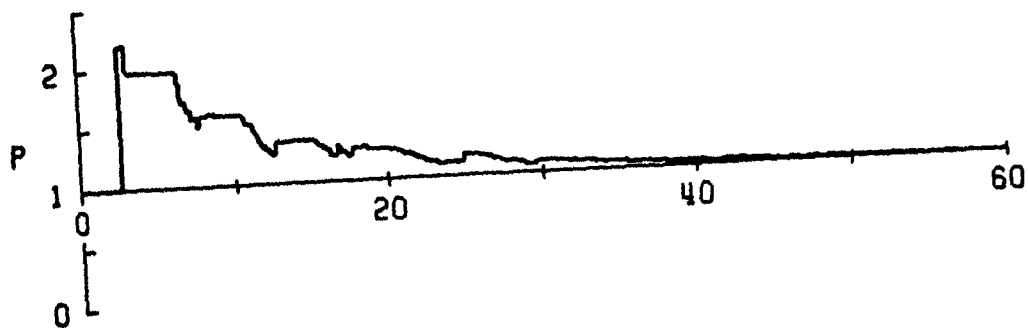
- 1) This longer driver produces a decaying blast wave that has a series of decreasing amplitude steps, as the wave in the driver criss-crosses it.
- 2) The contact surface moves out past stations 1, 2 and 3 and back past them.
- 3) The swept-back shock does not reach any of the test stations.
- 4) Two sets of time histories are presented:
 - a) Time scale of 0 to 60 ms
 - b) Time scale of 0 to 150 ms

The short time scale shows the main wave moving outwards. The longer one shows the reflected wave from the open end moving into the duct.



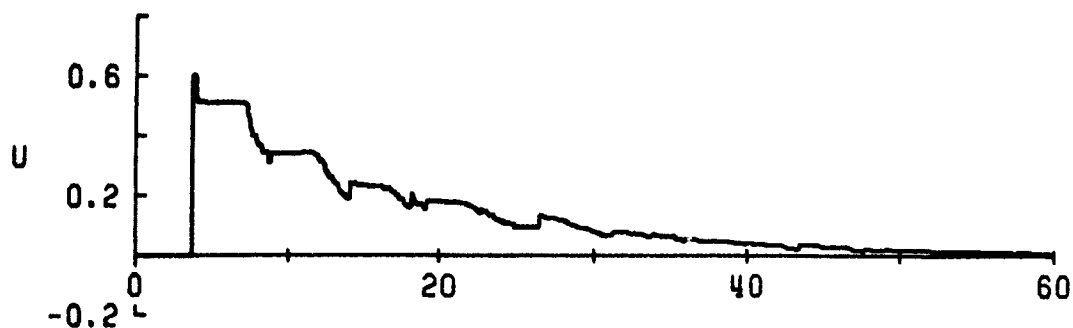
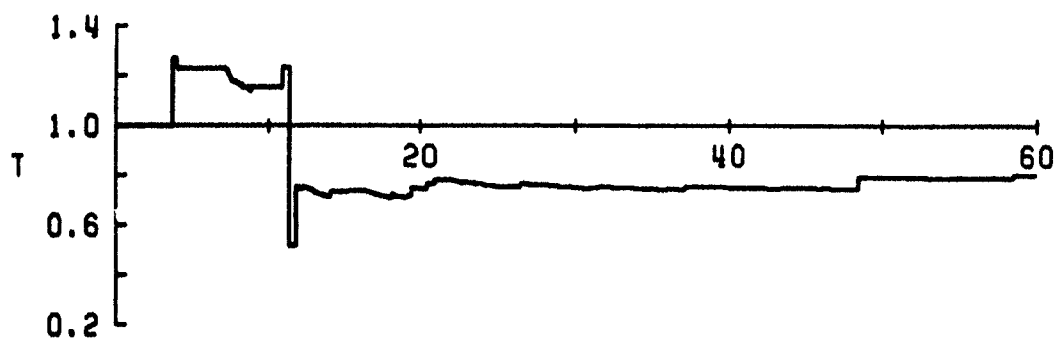
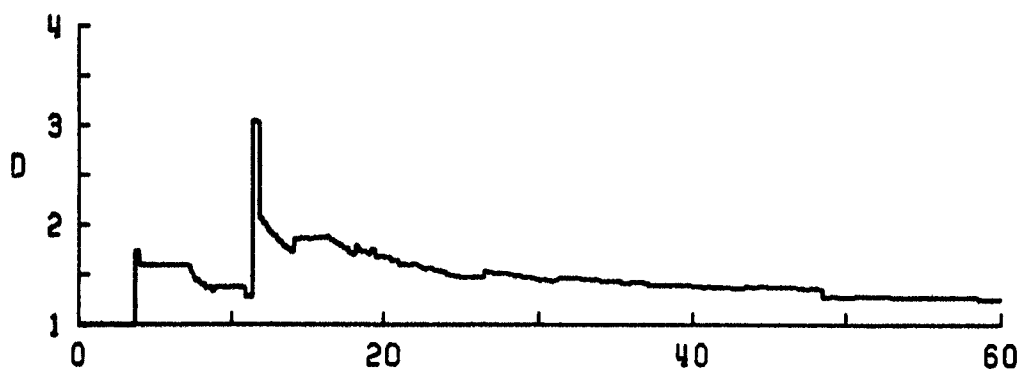
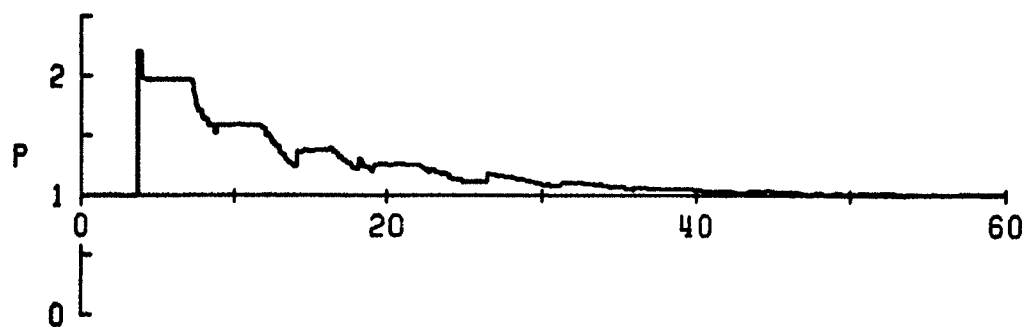
TIME

TIME HISTORIES
LOCATION: 1.548



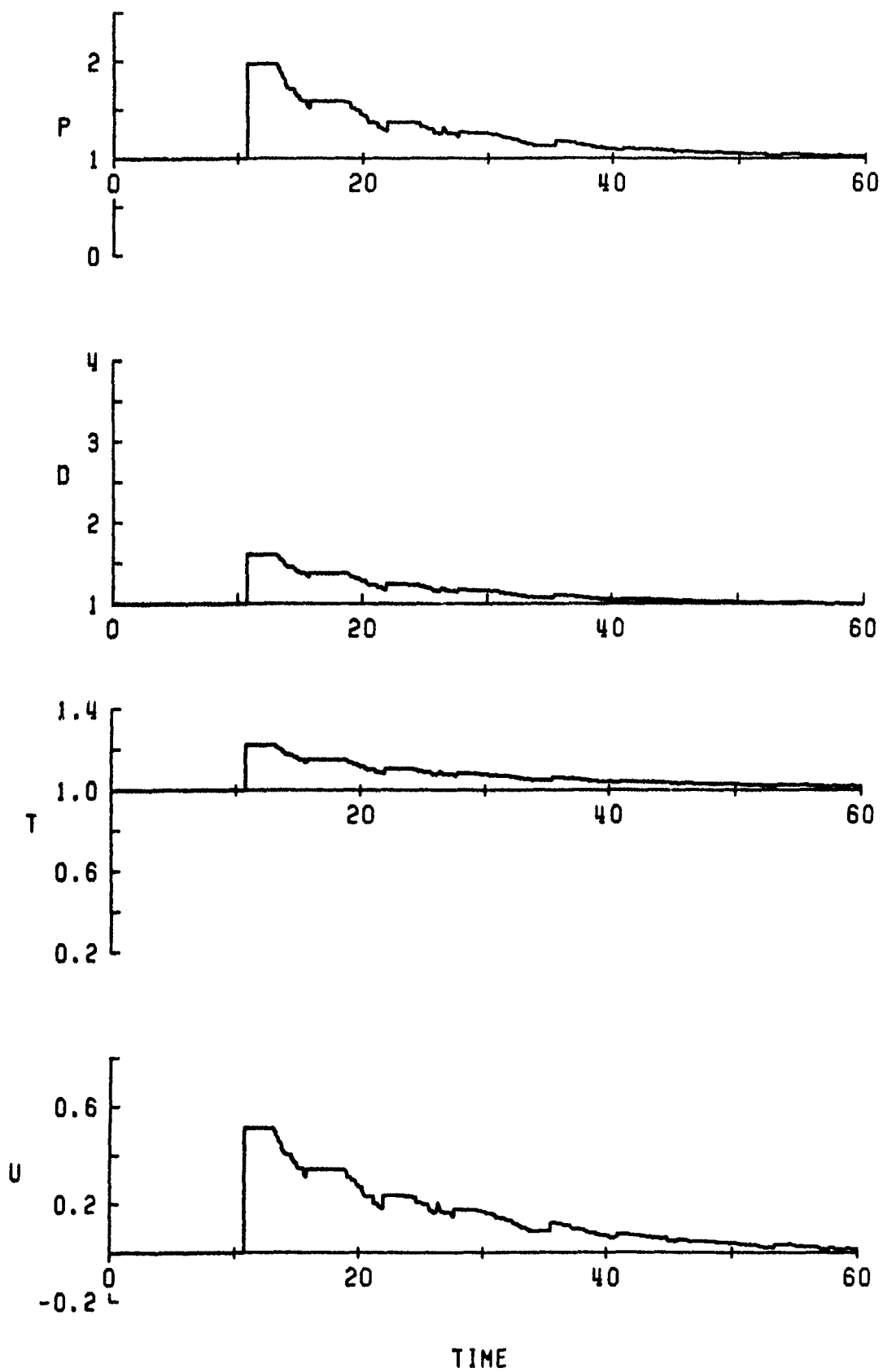
TIME

TIME HISTORIES
LOCATION: 2.016

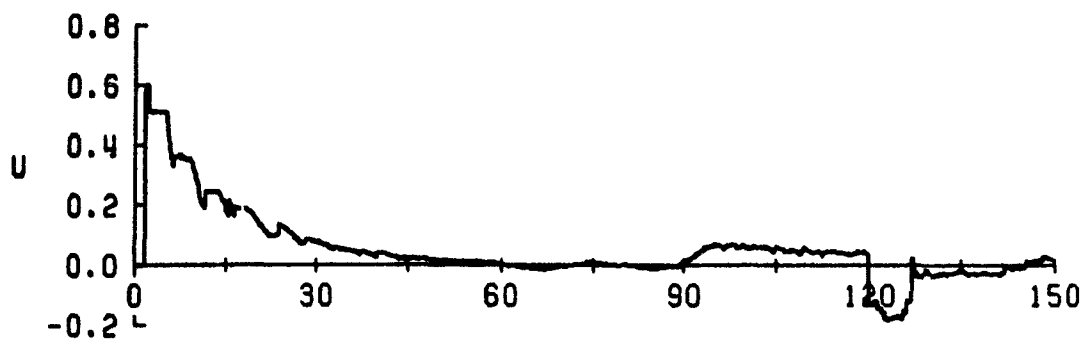
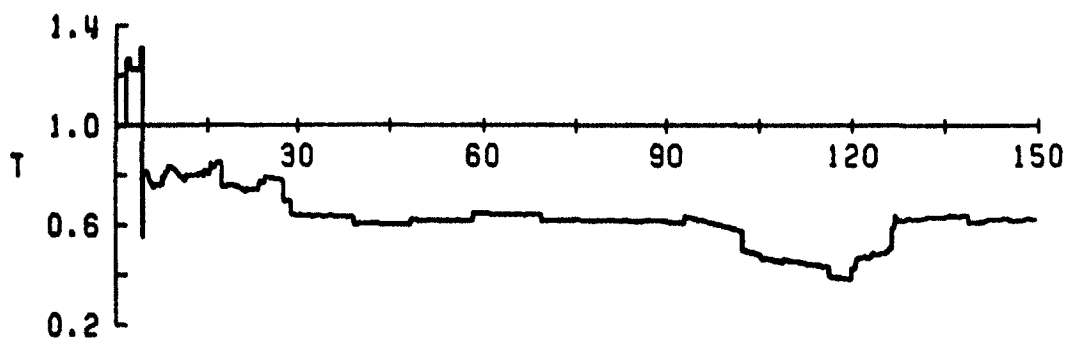
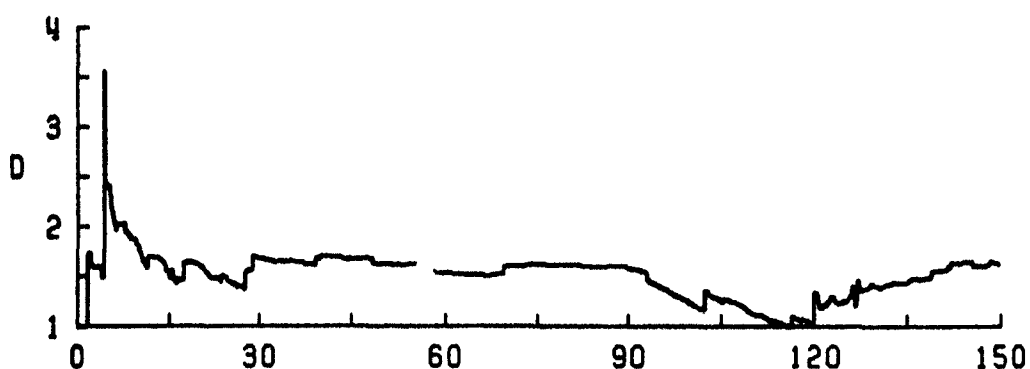
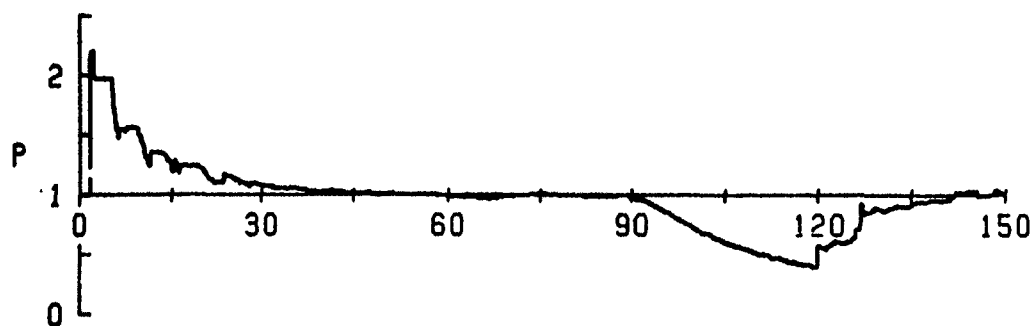


TIME

TIME HISTORIES
LOCATION: 2.535

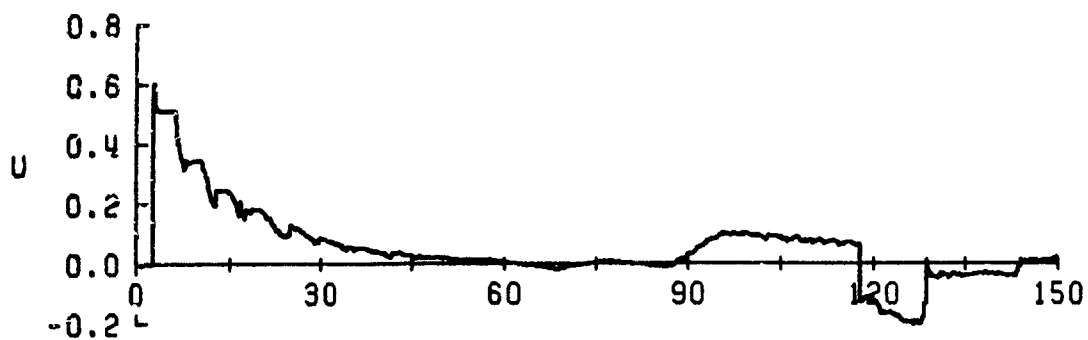
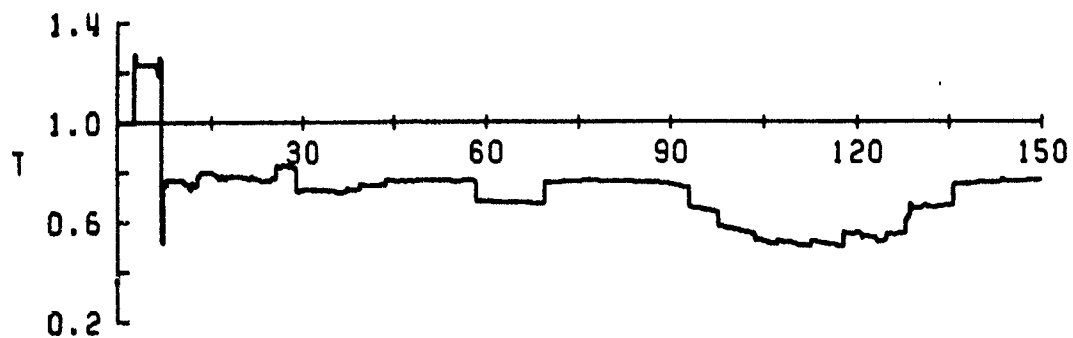
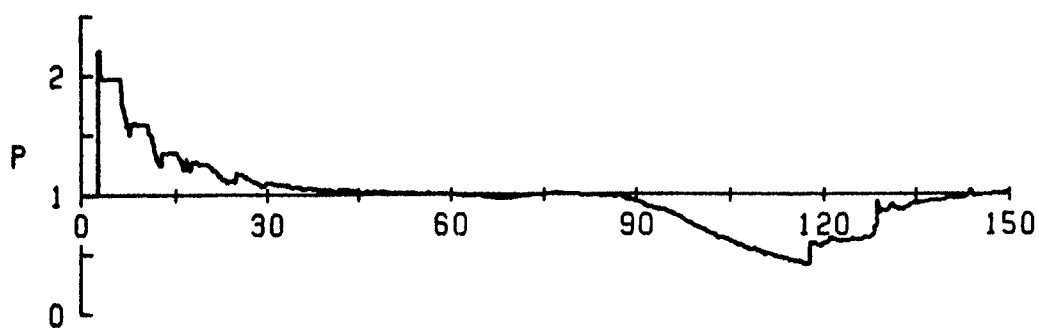


TIME HISTORIES
LOCATION: 5.860



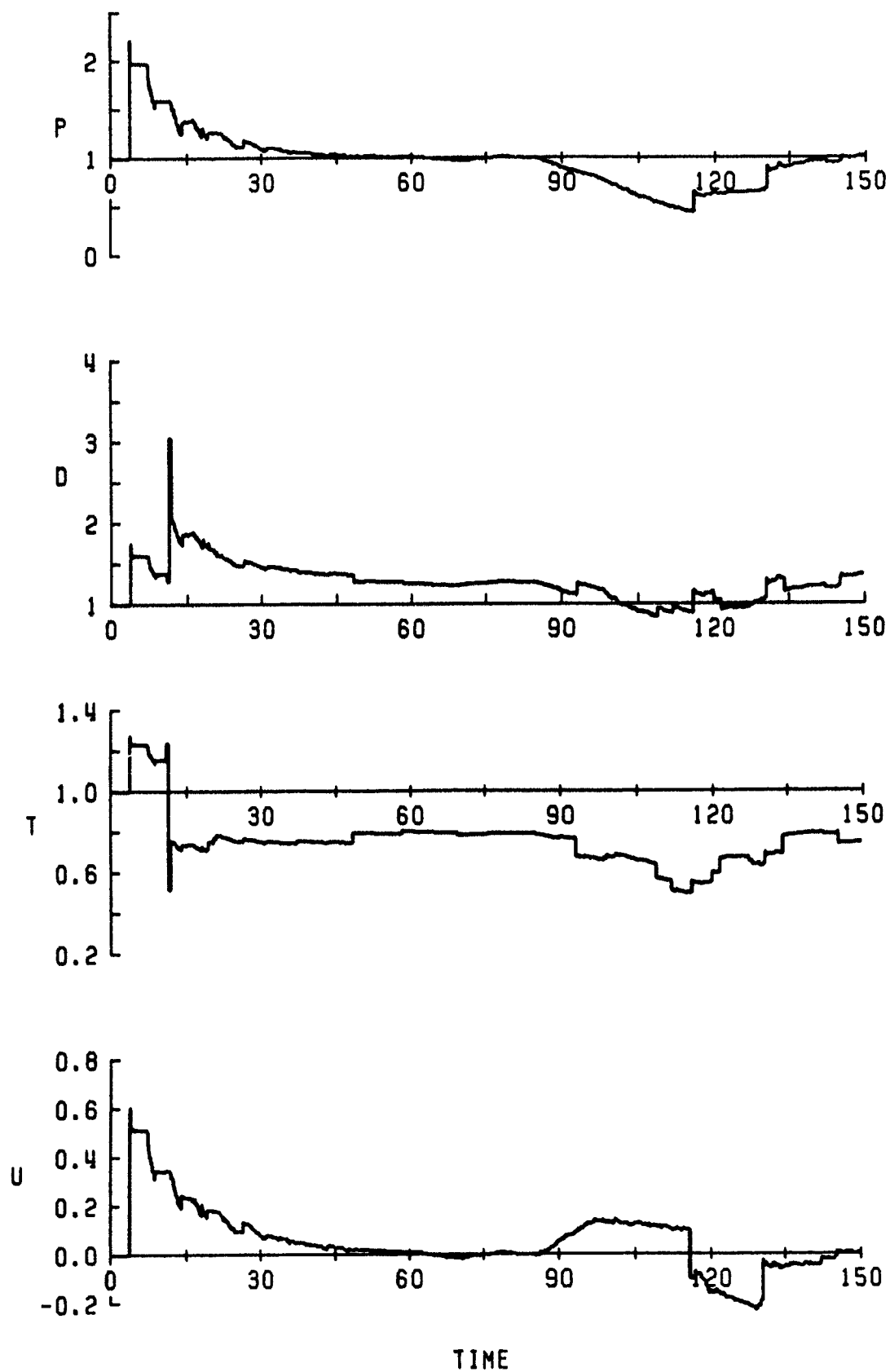
TIME

TIME HISTORIES
LOCATION: 1.548

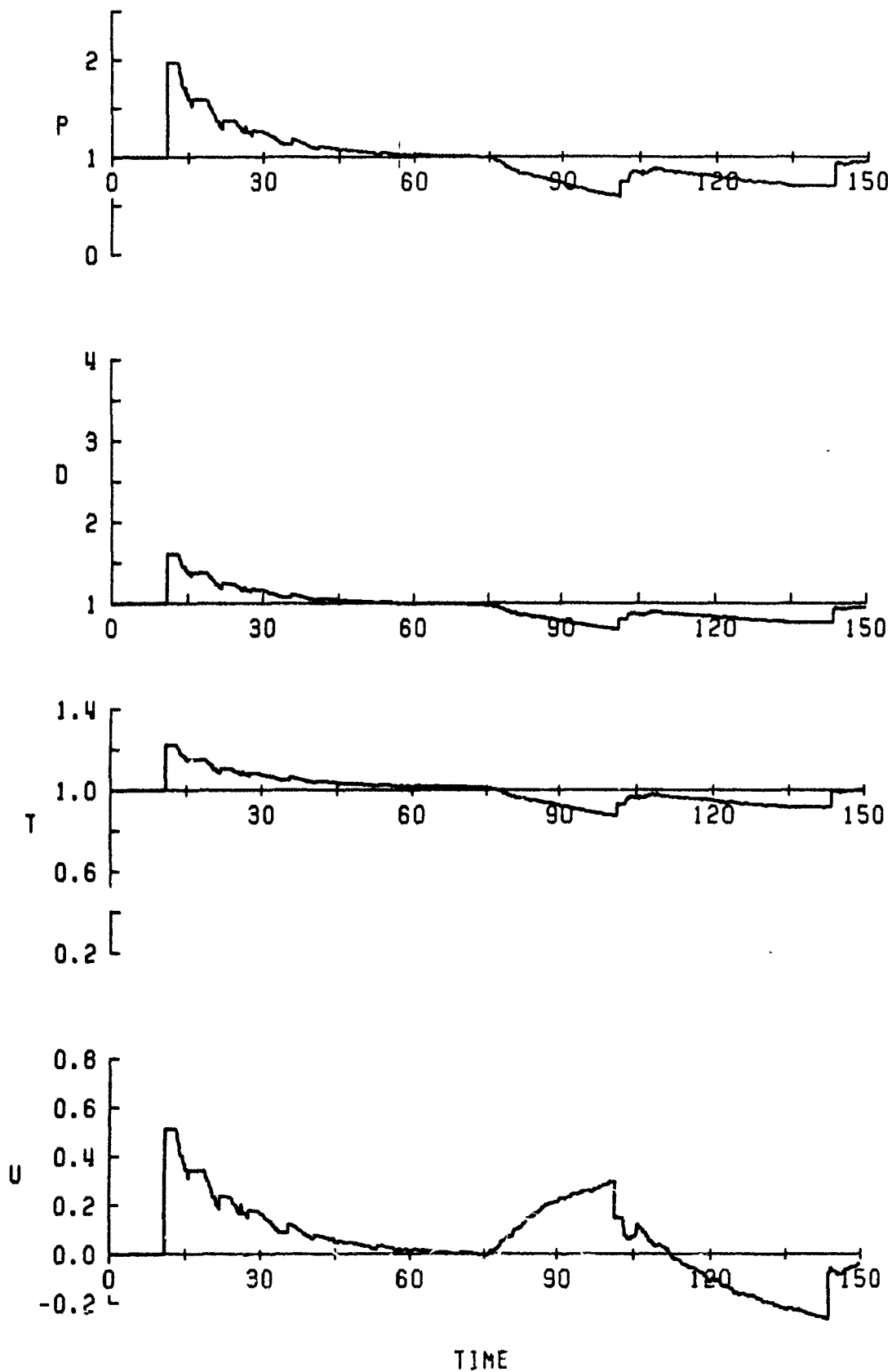


TIME

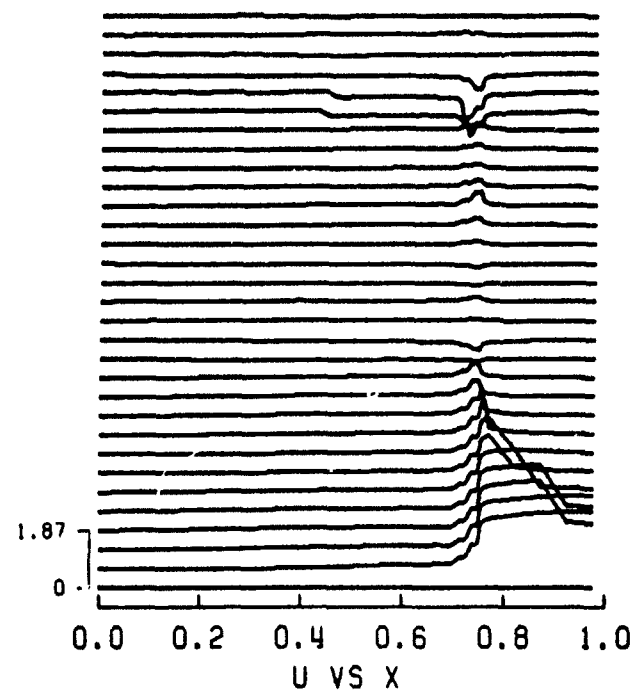
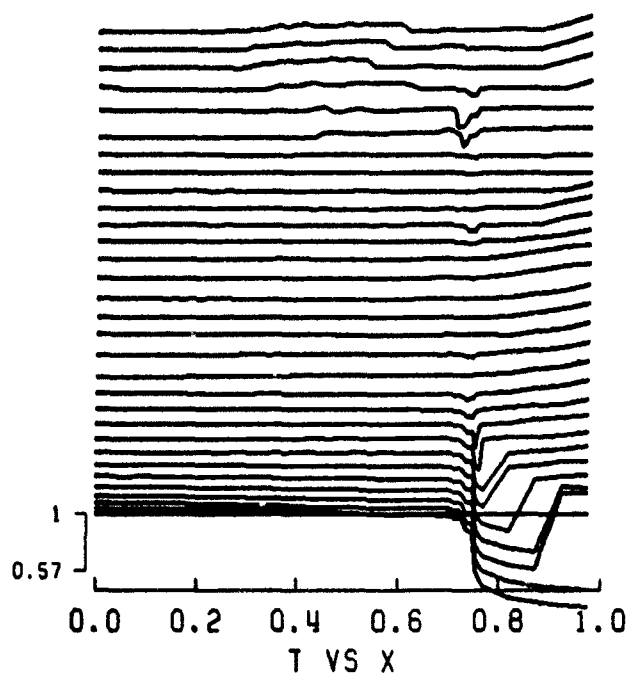
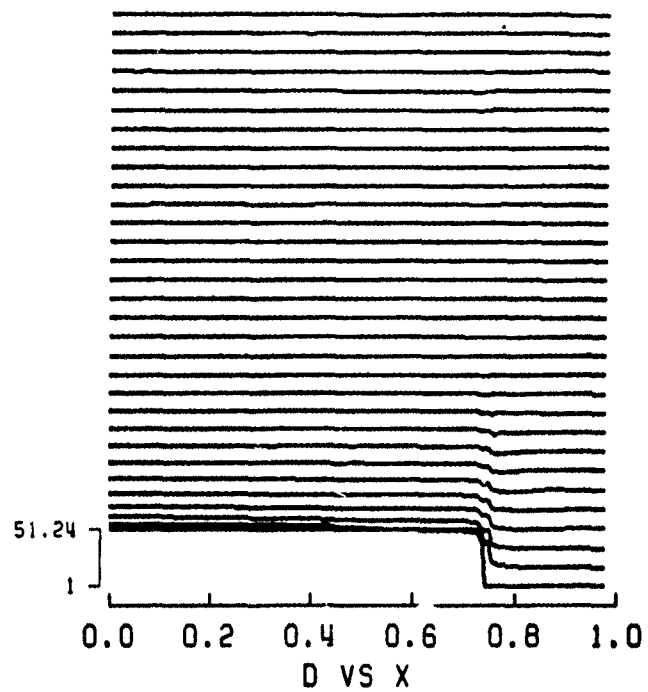
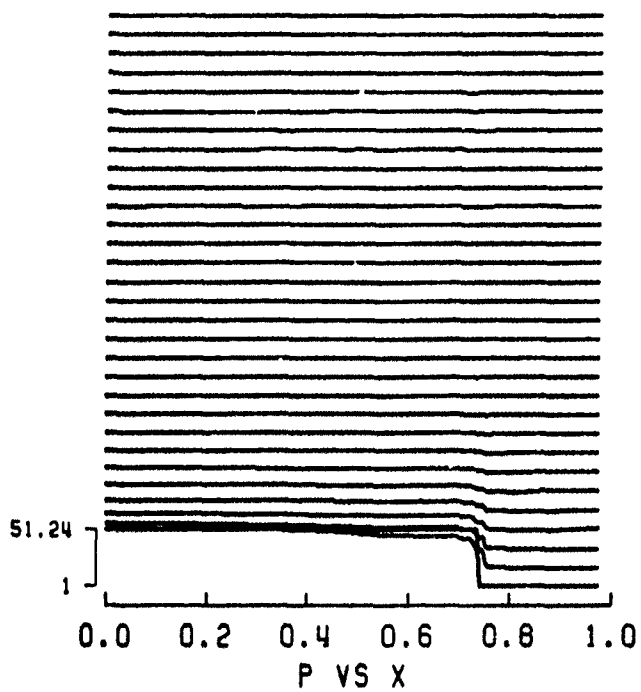
TIME HISTORIES
LOCATION: 2.016



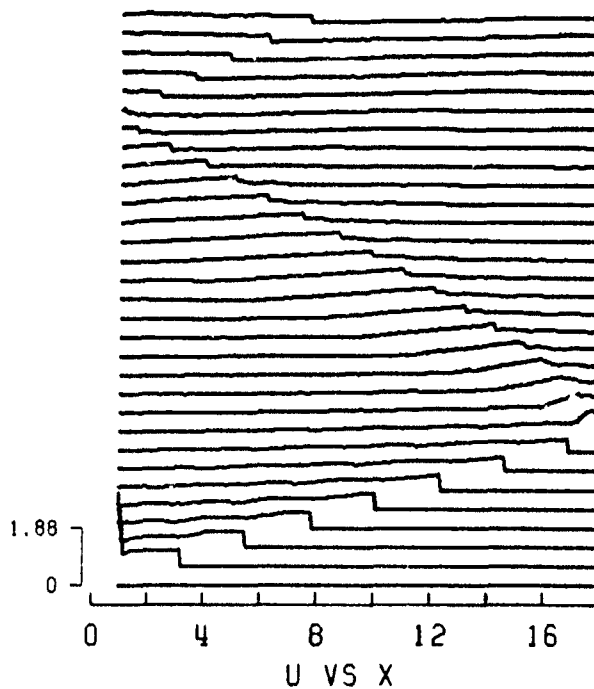
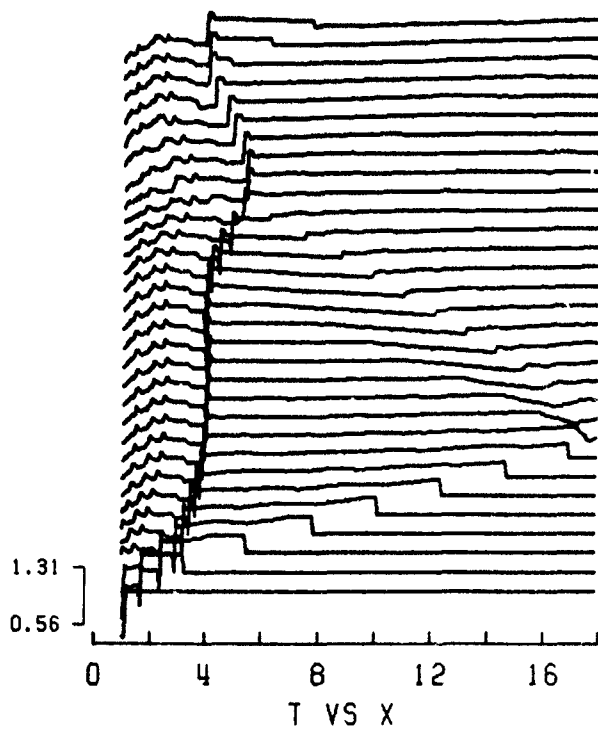
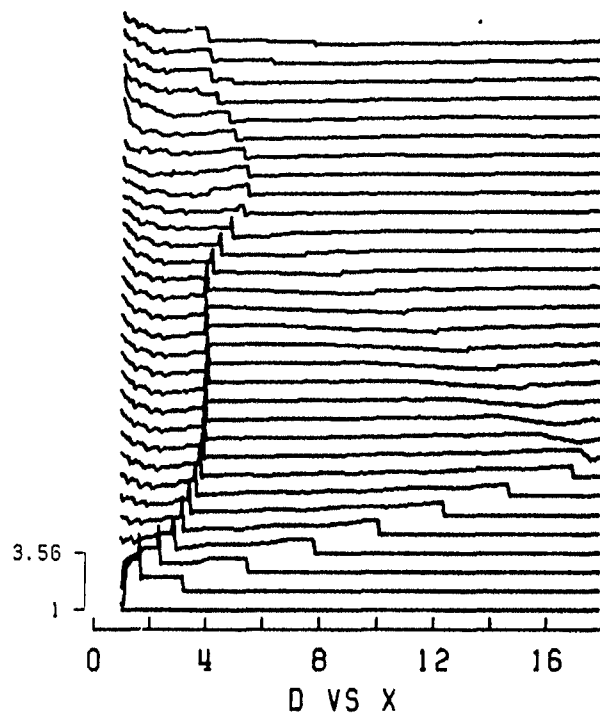
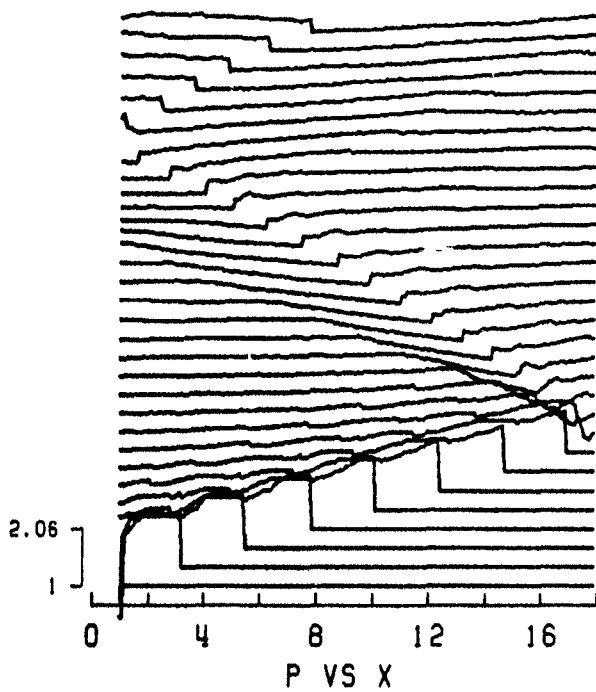
TIME HISTORIES
LOCATION: 2.535



TIME HISTORIES
LOCATION: 5.860



SPATIAL DISTRIBUTIONS
TIME: 0.000 TO 150.010



SPATIAL DISTRIBUTIONS
TIME: 0.000 TO 150.010

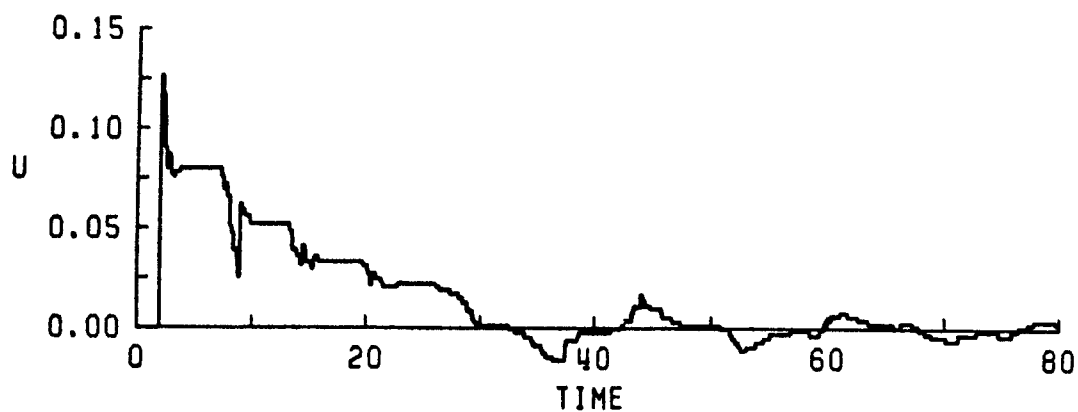
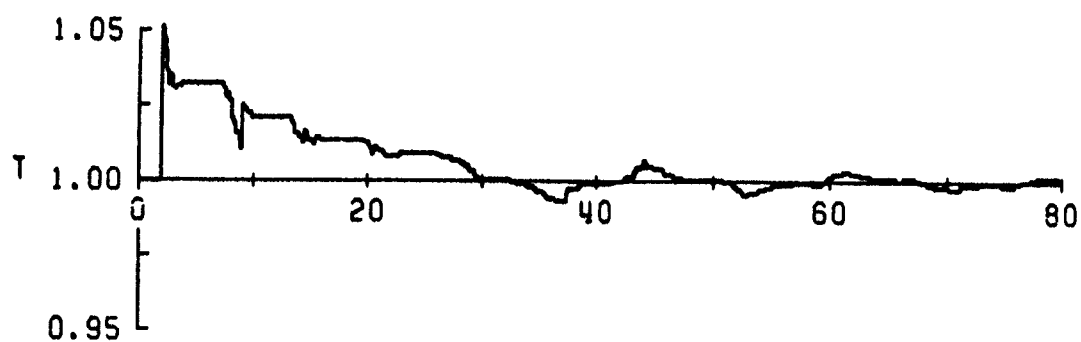
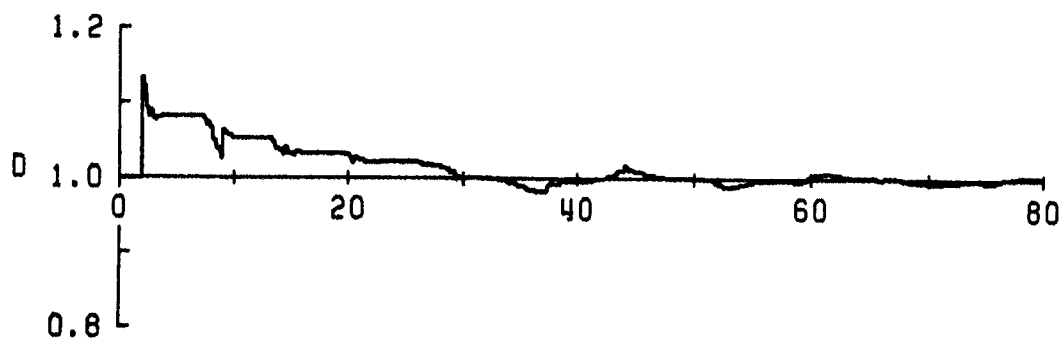
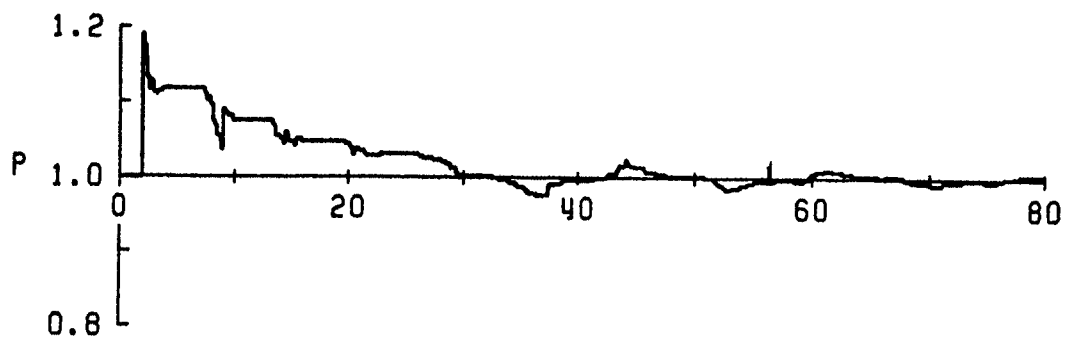
CASE # 5.

$$P_{41} = 4.895$$

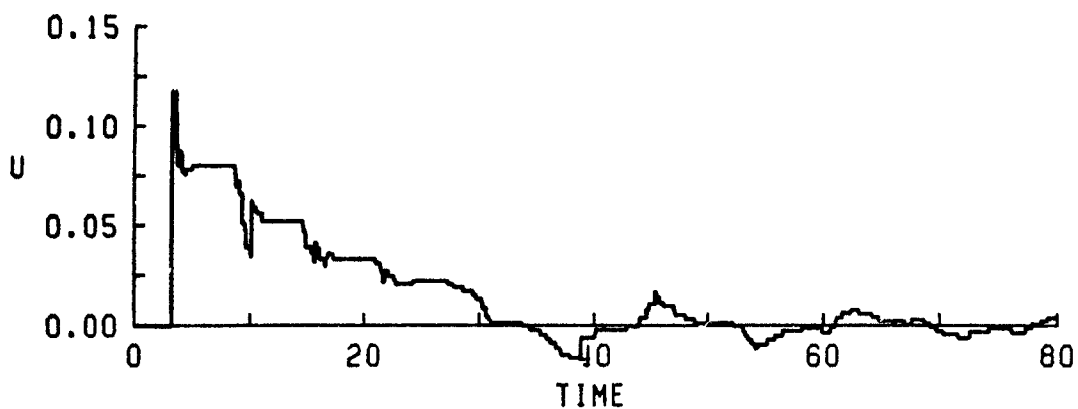
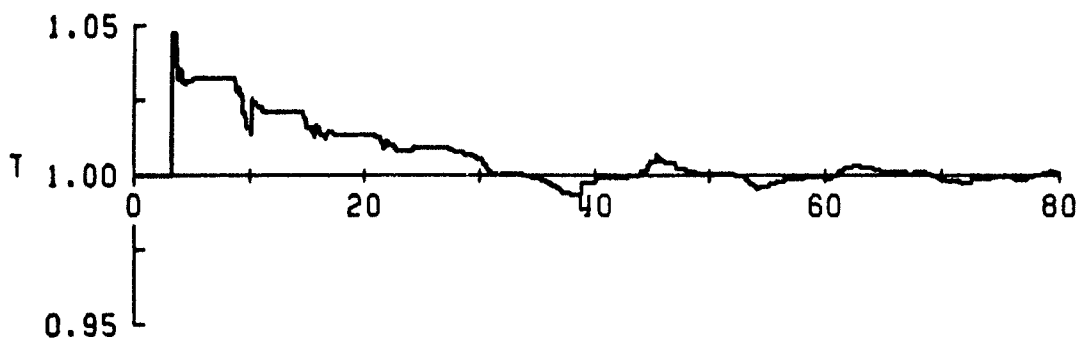
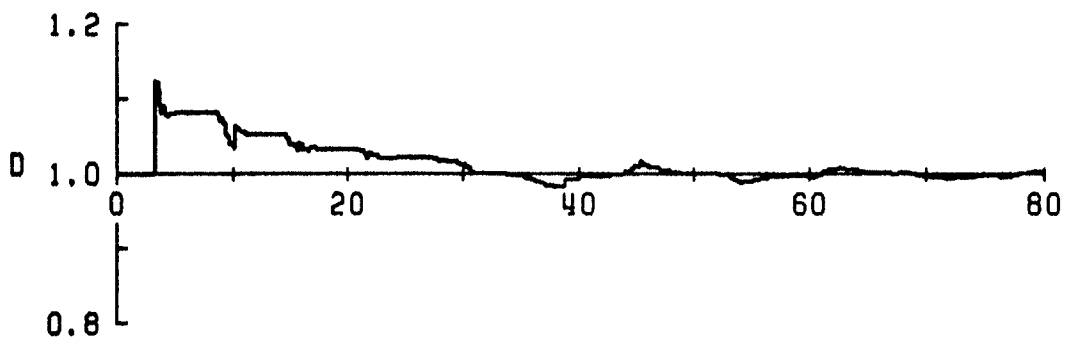
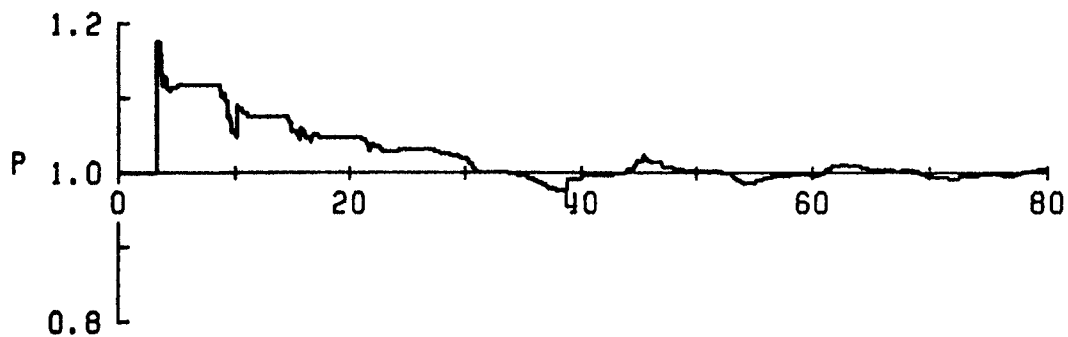
$$L_{\text{driver}} = 94.95 \text{ cm}$$

Comments:

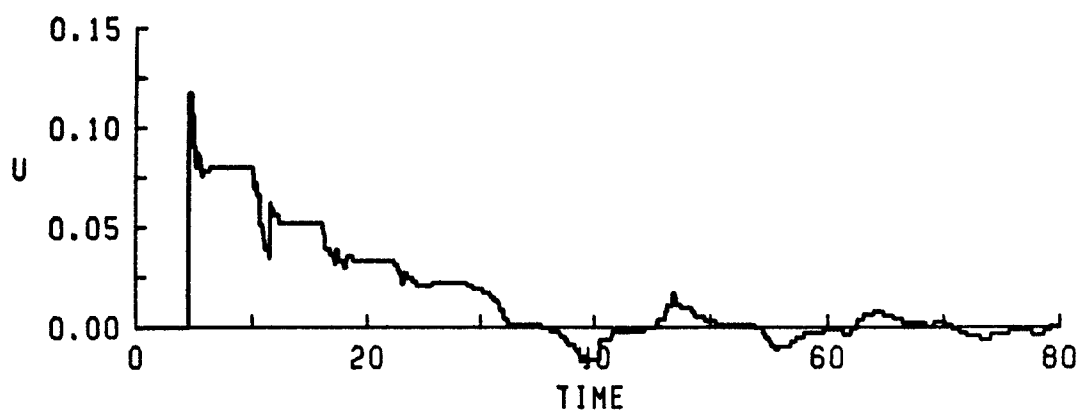
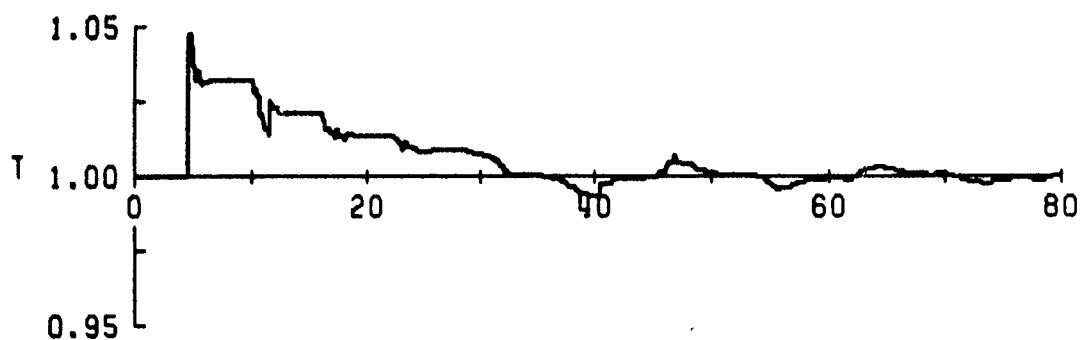
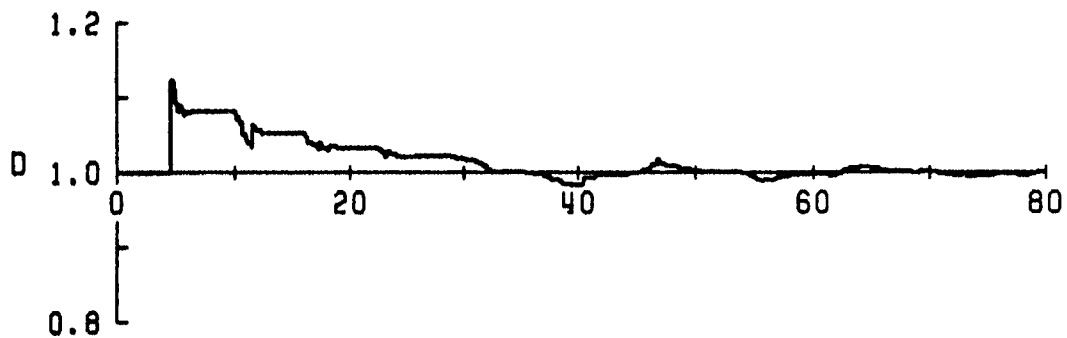
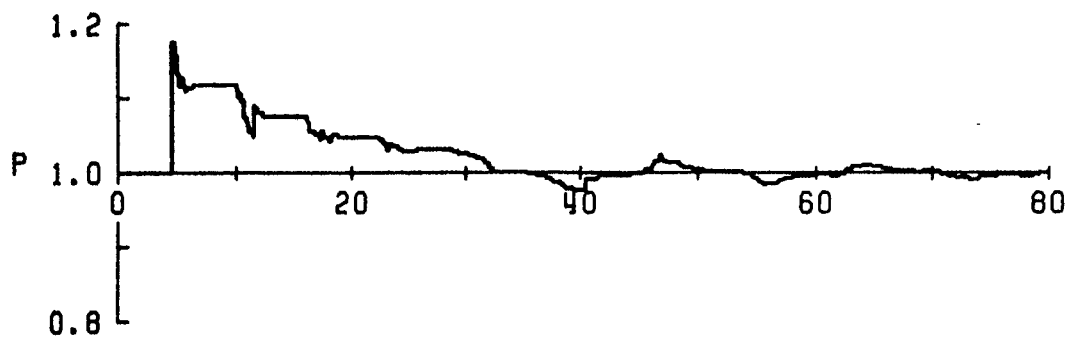
- 1) These results are very similar to case #4, except we now have longer flat-topped decreasing steps from the longer driver, and the blast amplitude is weaker.
- 2) The weaker blast front makes the reflected wave from the open end appear larger. When P_{21} goes to unity, the reflected wave strength is equal to the incident shock amplitude.
- 3) Two sets of results with different time scales is given to highlight the reflected wave from the open end, which arrives at late times.
- 4) This is a 3-hour run on our minicomputer (main one at UTIAS).



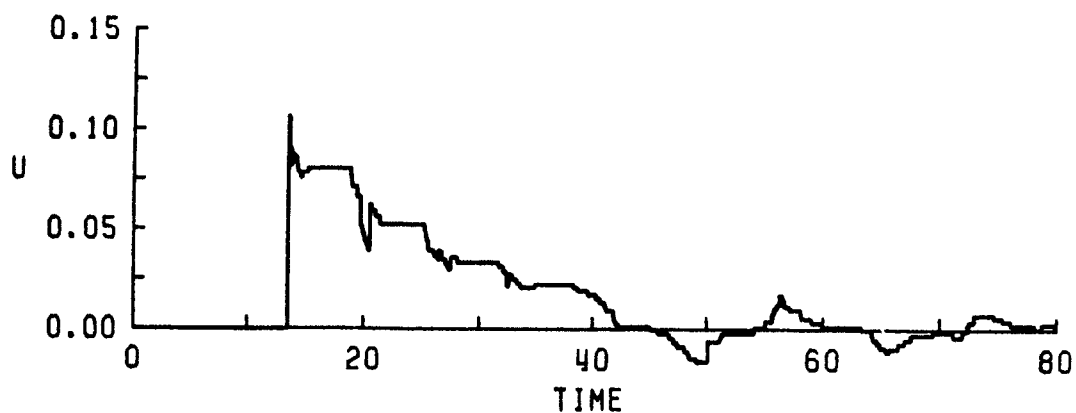
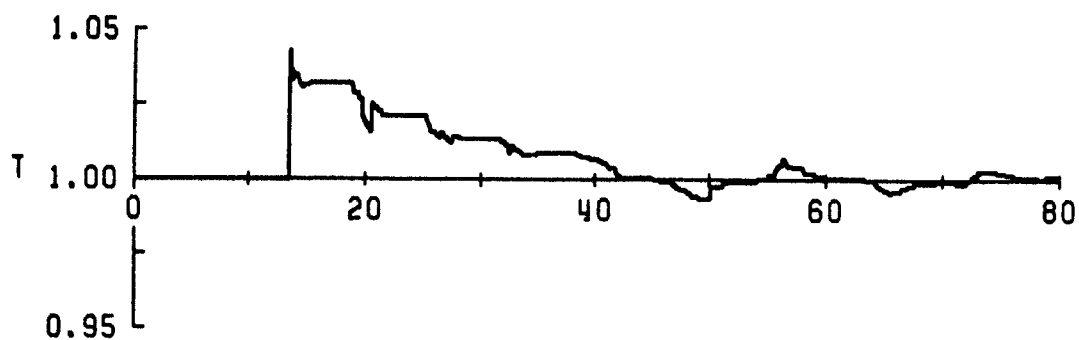
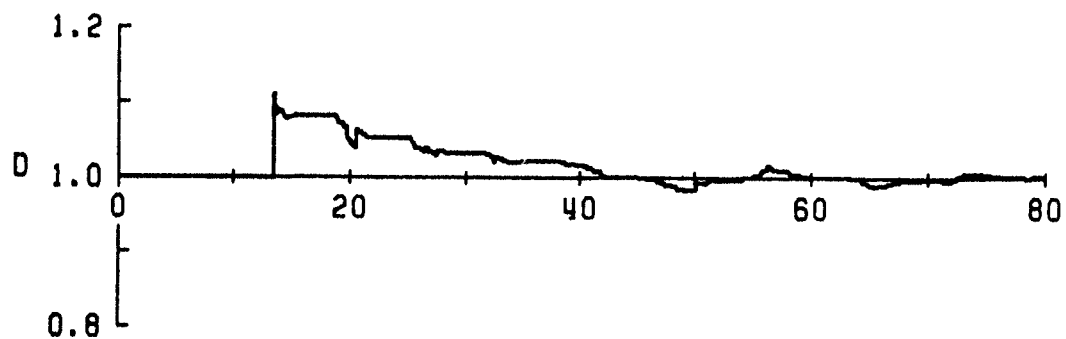
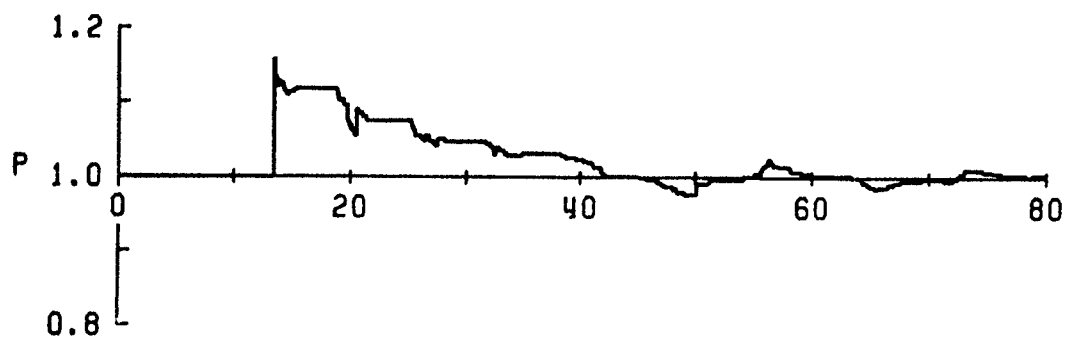
TIME HISTORIES
LOCATION: 1.828



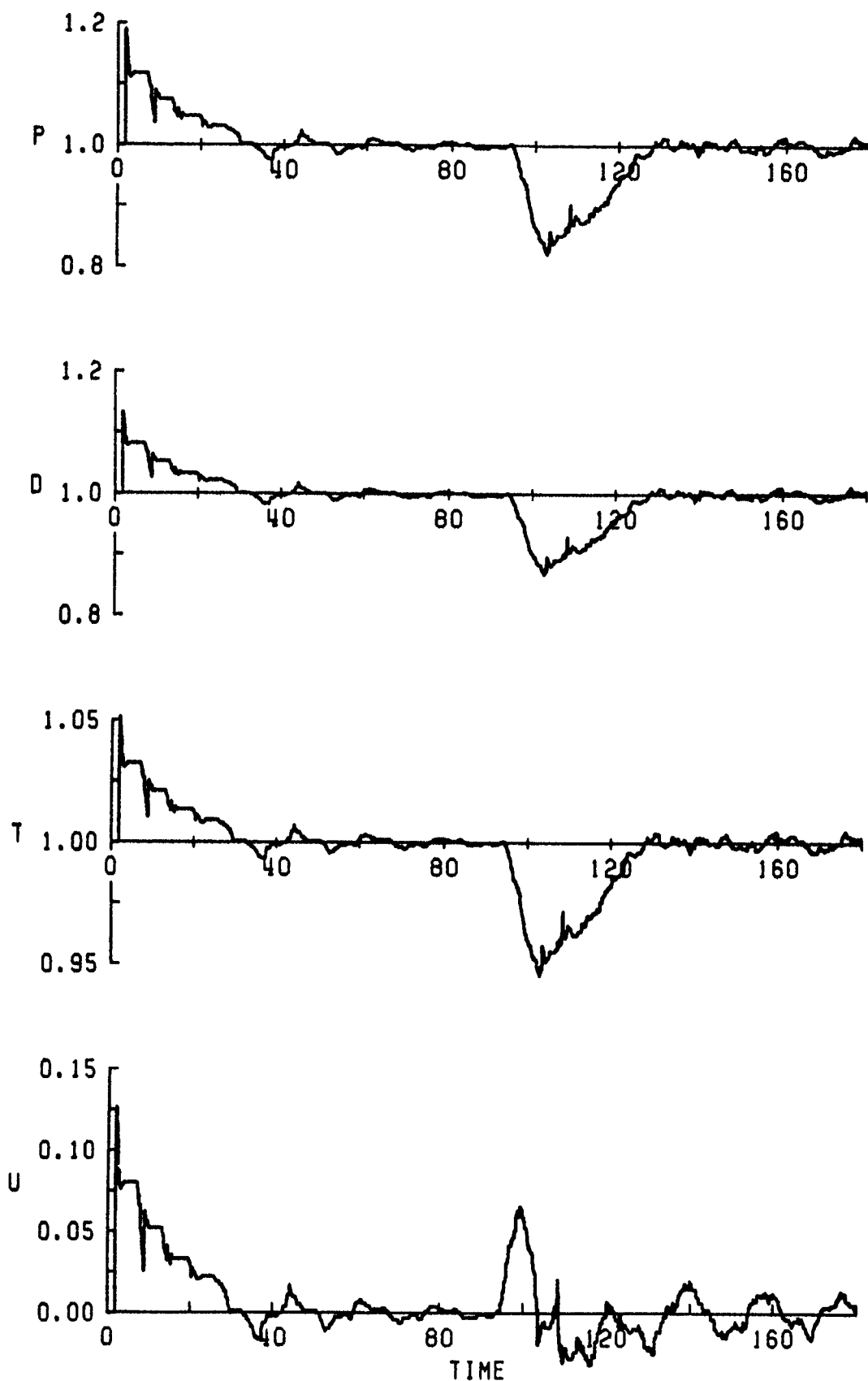
TIME HISTORIES
LOCATION: 2.295



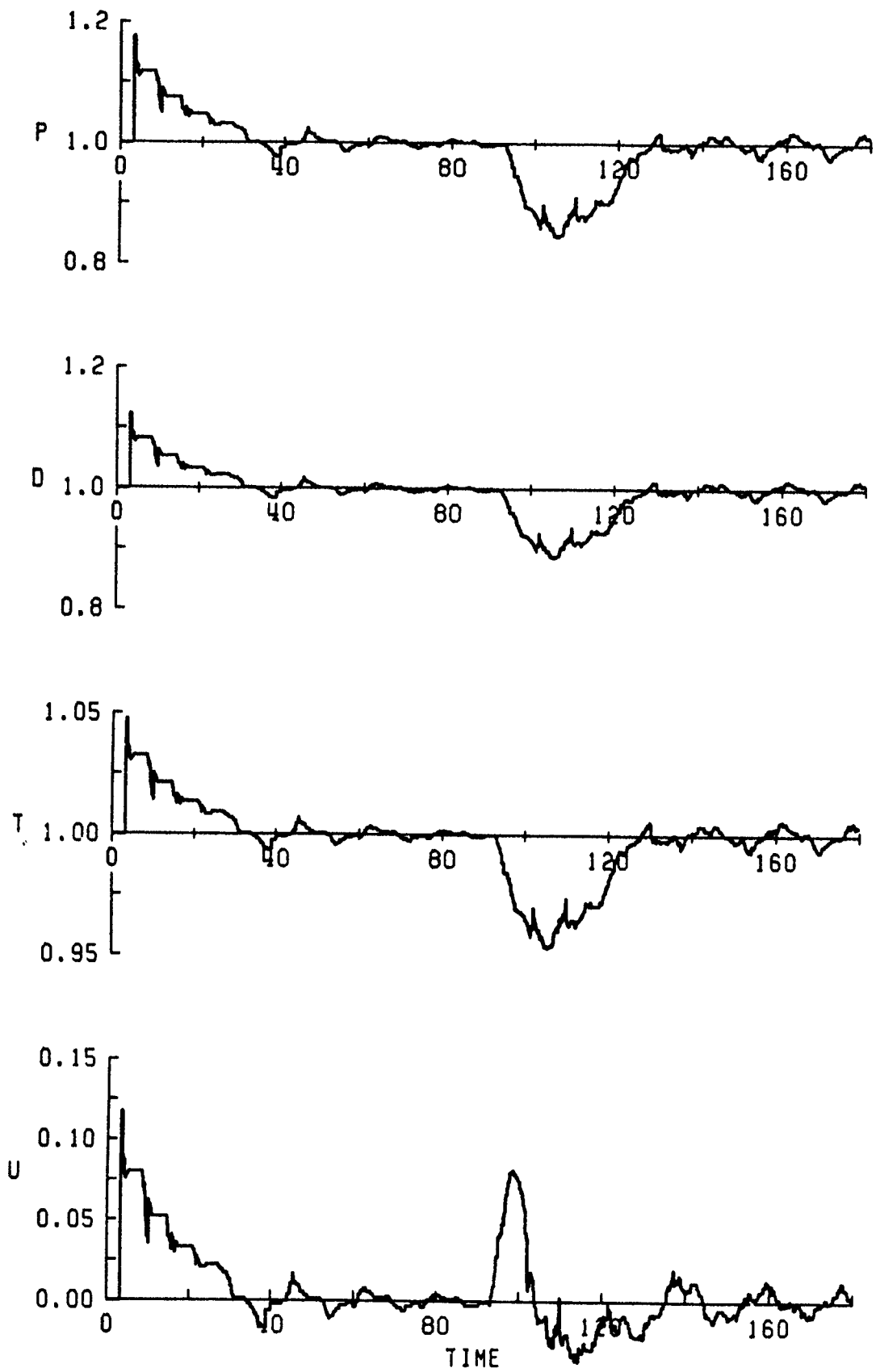
TIME HISTORIES
LOCATION: 2.815



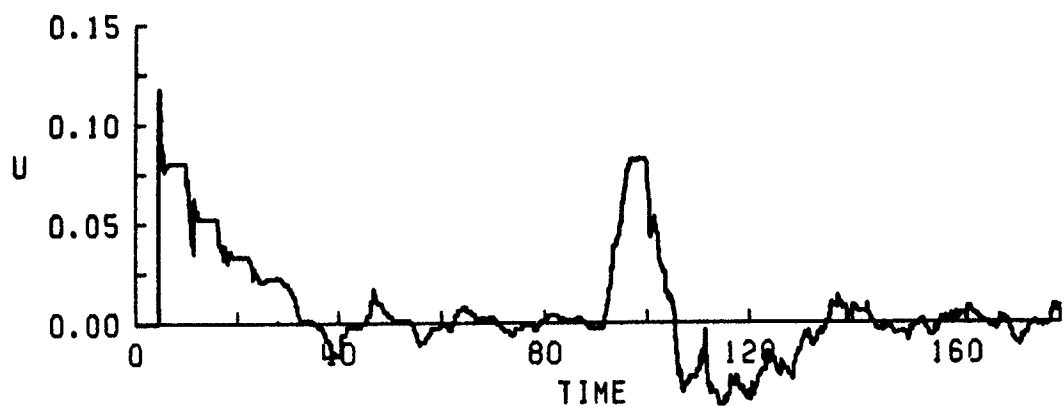
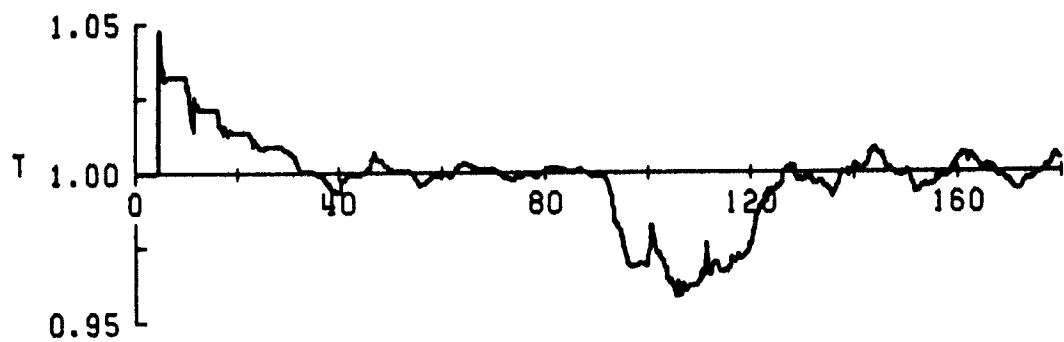
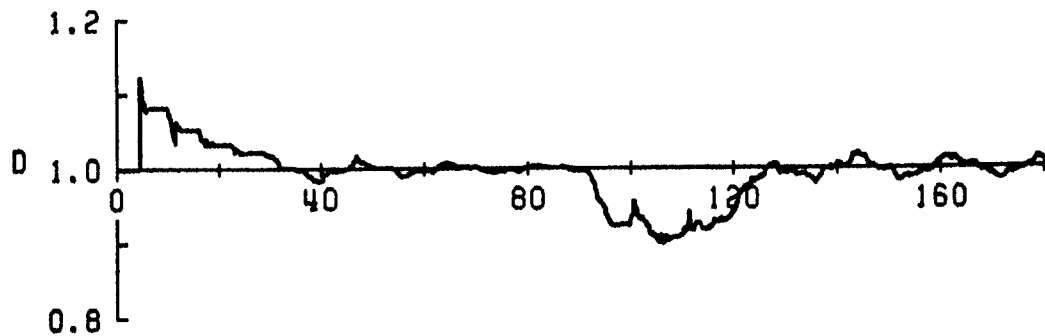
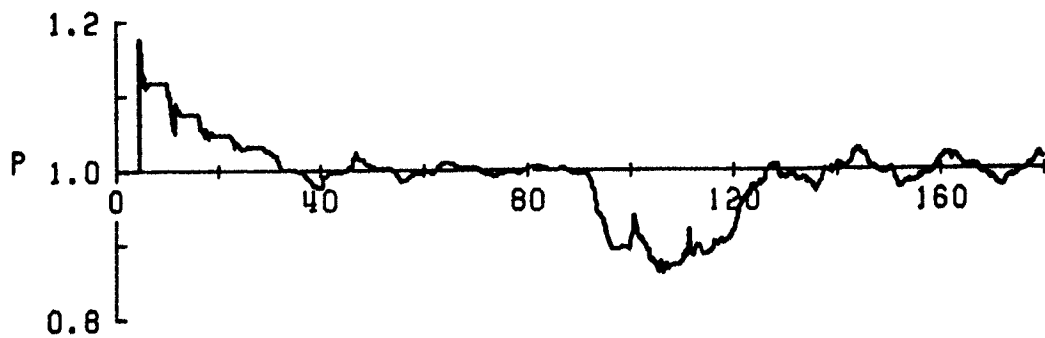
TIME HISTORIES
LOCATION: 6.139



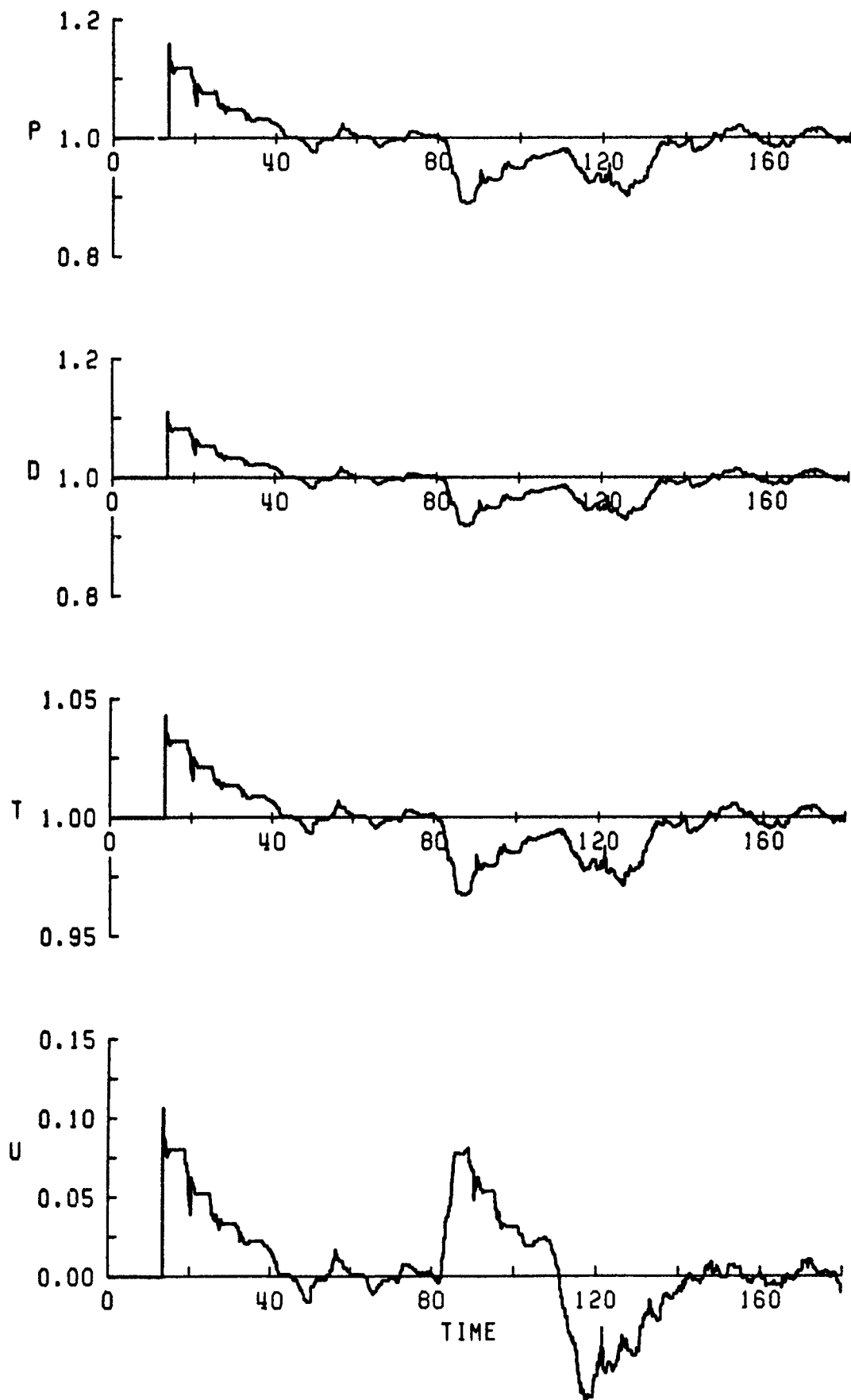
TIME HISTORIES
LOCATION: 1.828



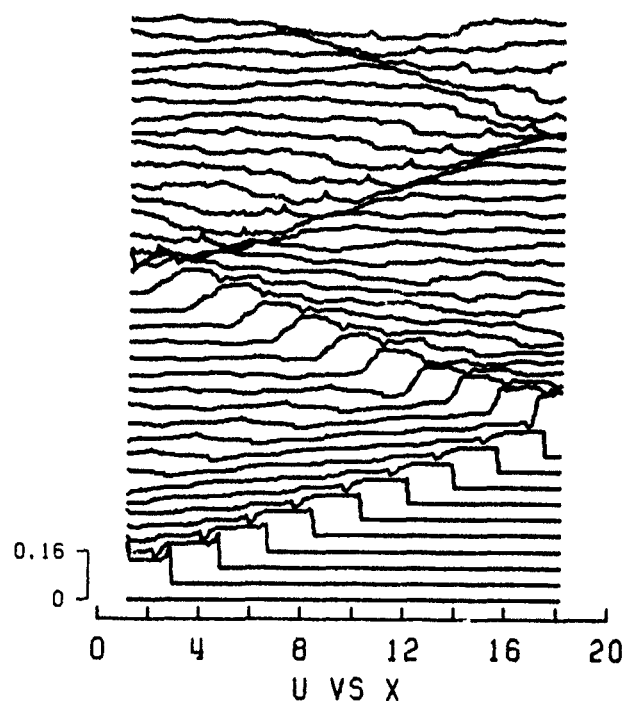
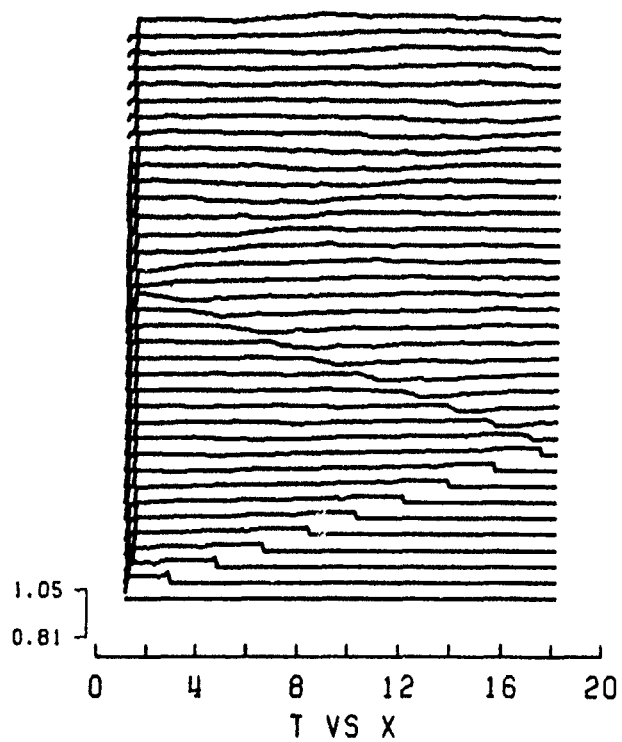
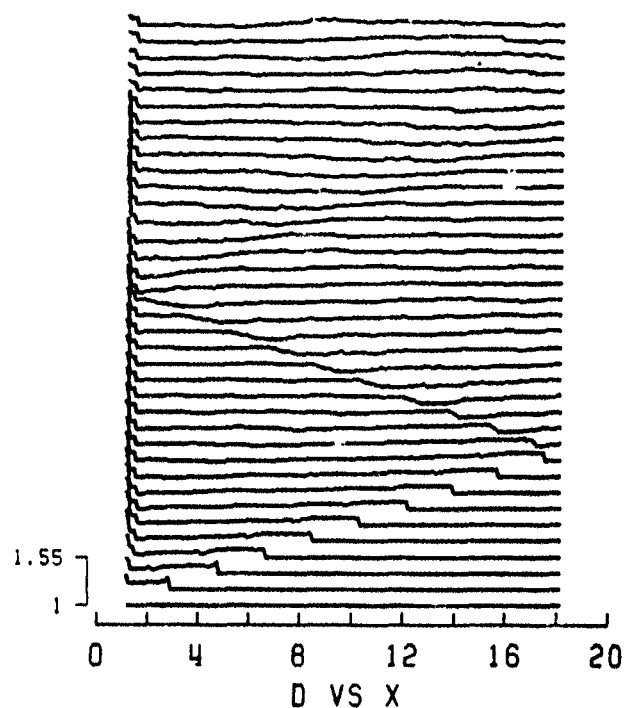
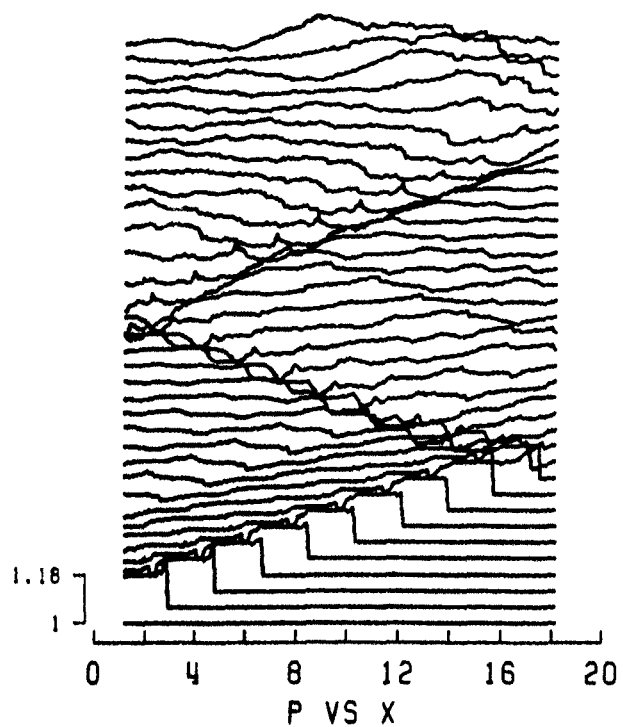
TIME HISTORIES
LOCATION: 2.295



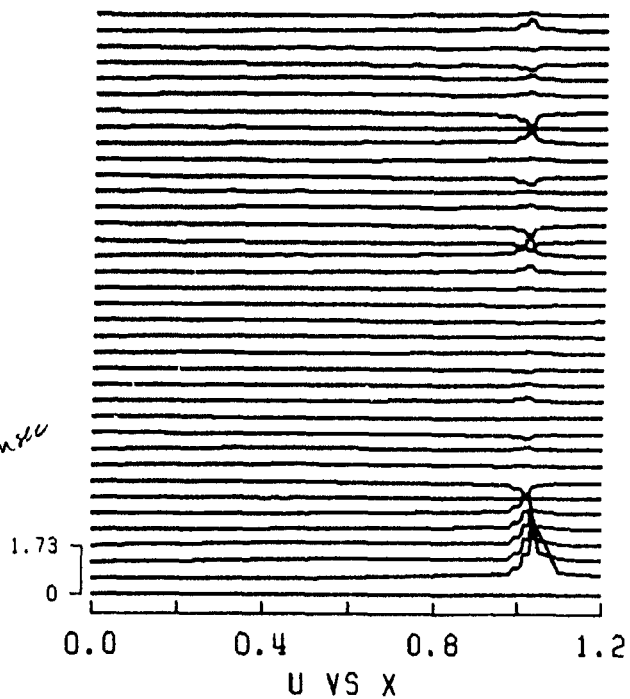
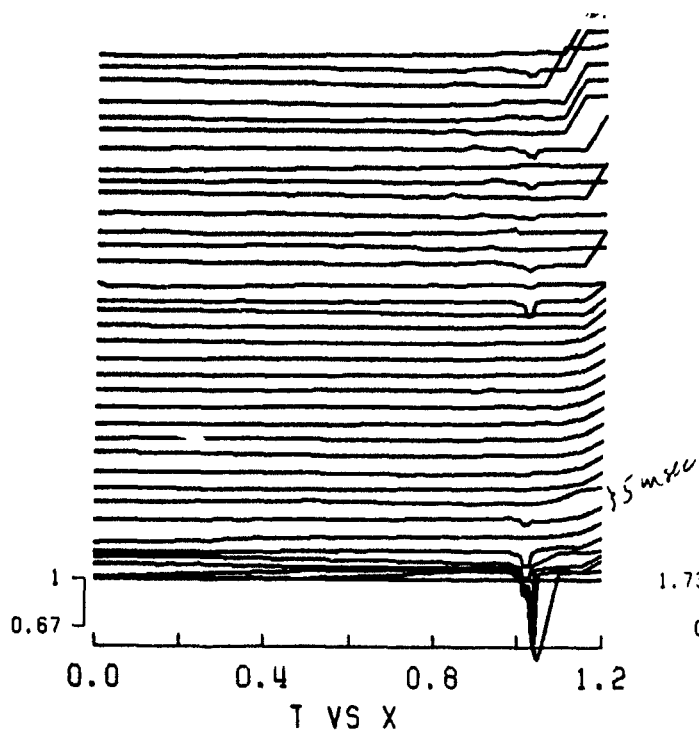
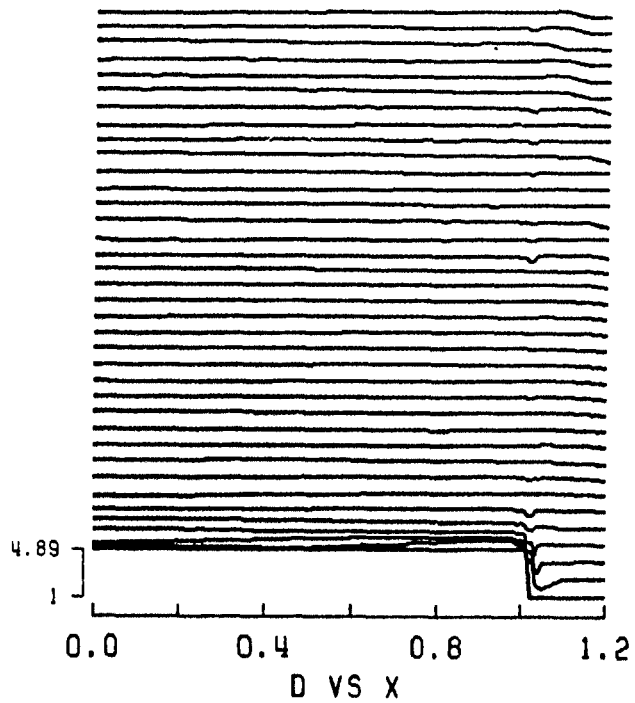
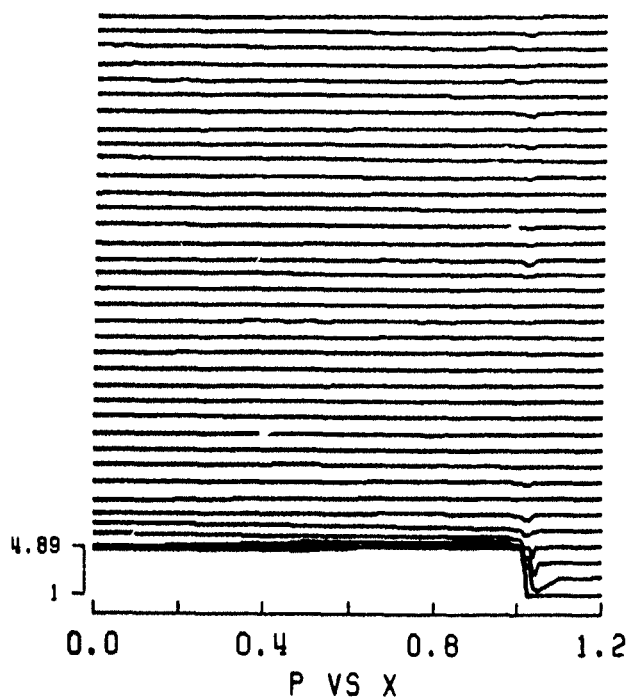
TIME HISTORIES
LOCATION: 2.815



TIME HISTORIES
LOCATION: 6.139



SPATIAL DISTRIBUTIONS
TIME: 0.000 TO 180.000



SPATIAL DISTRIBUTIONS
TIME: 0.000 TO 180.000

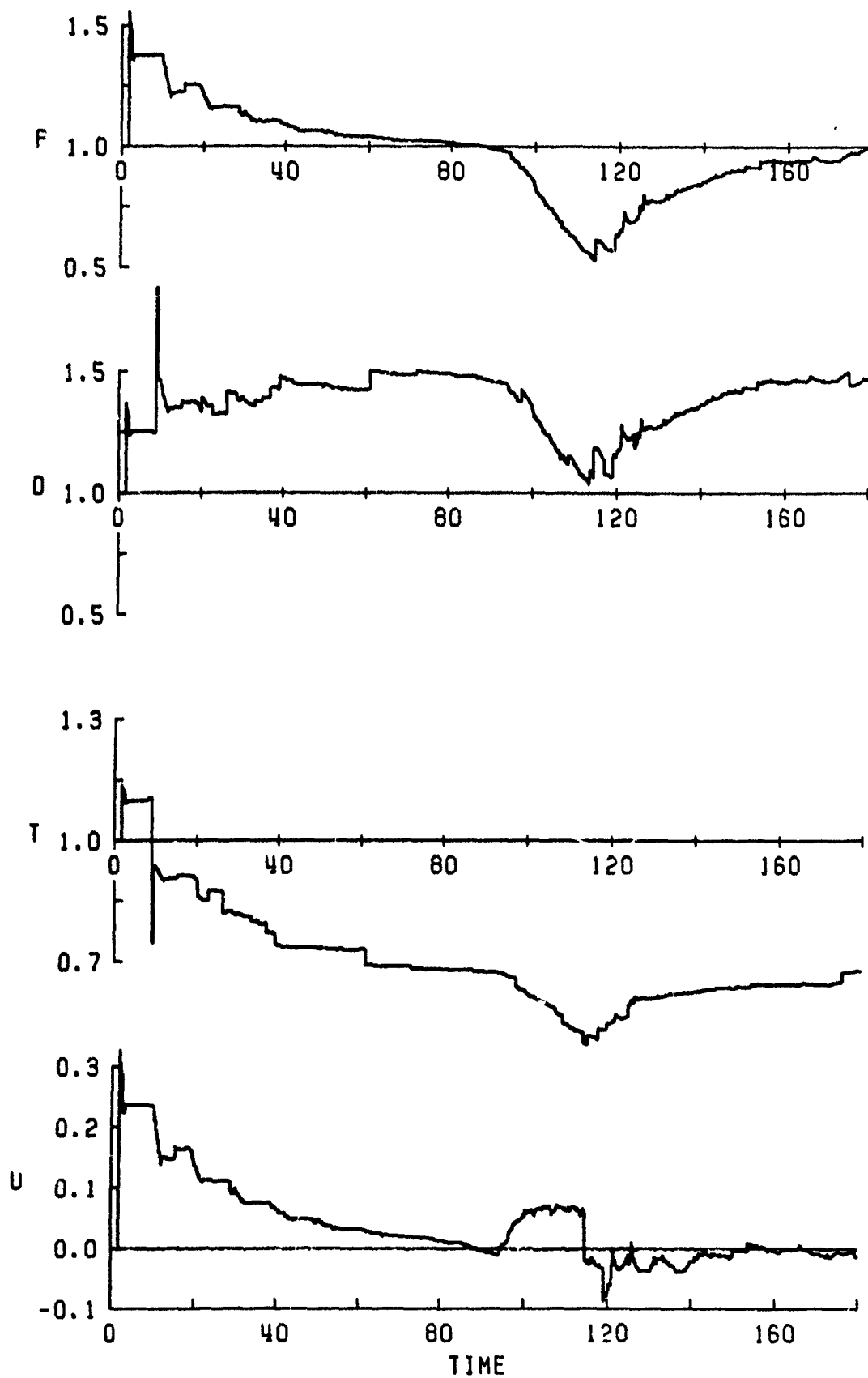
CASE # 6.

$$P_{41} = 18.03$$

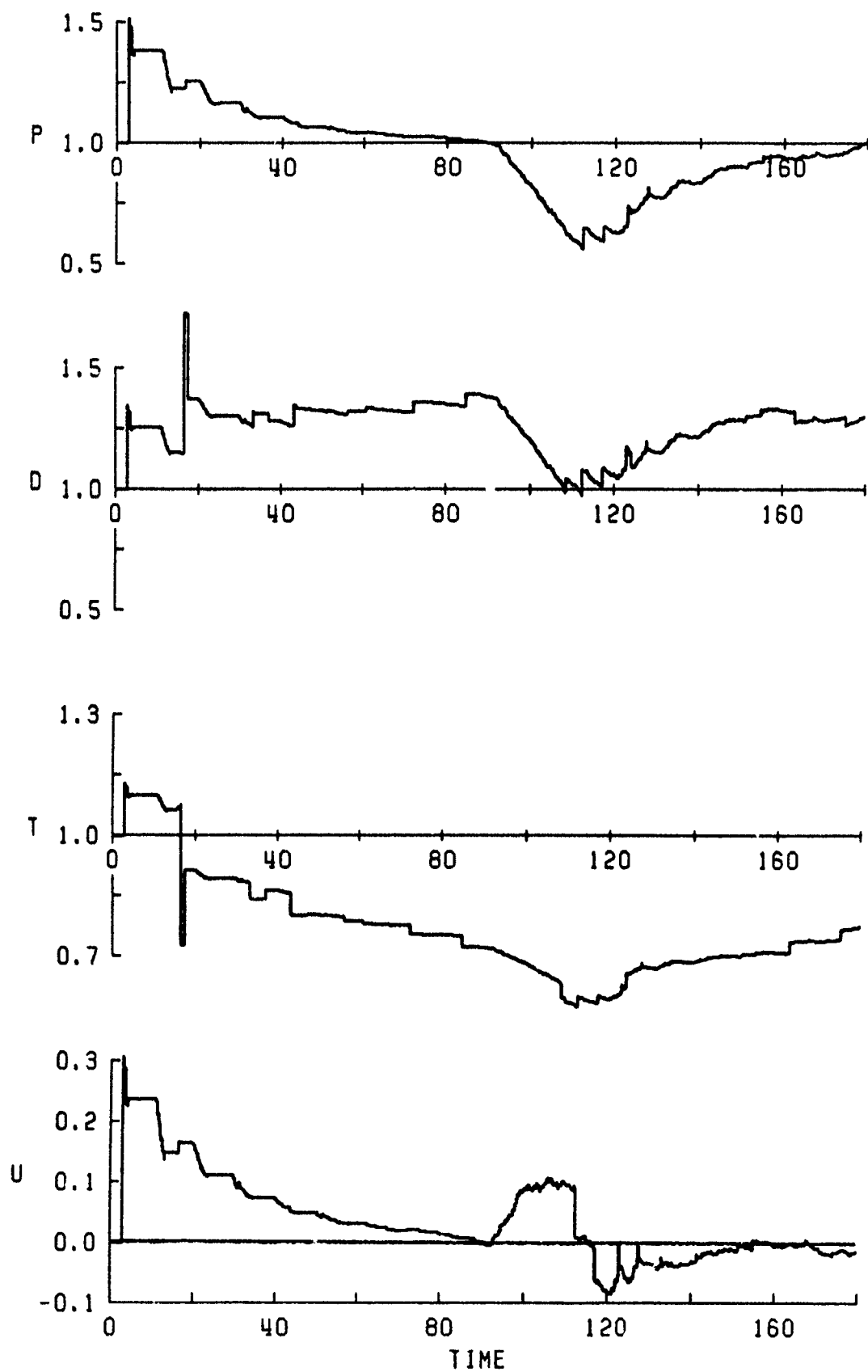
$$L_{\text{driver}} = 145.74 \text{ cm}$$

Comments:

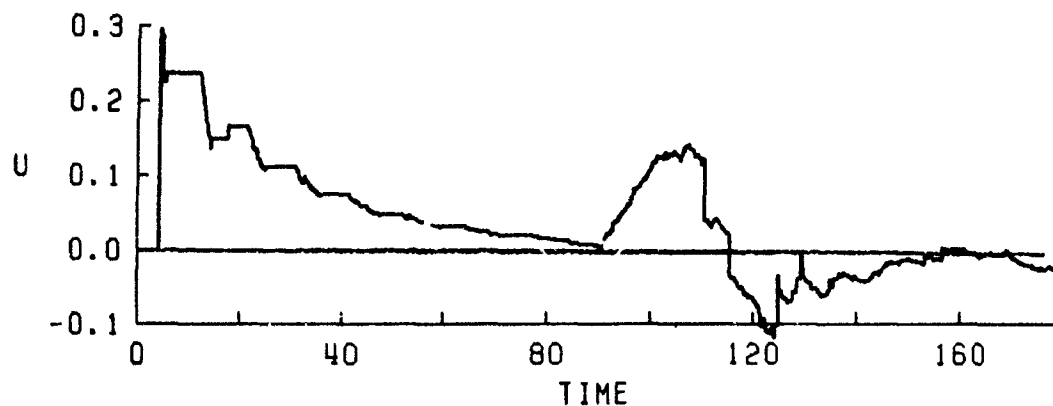
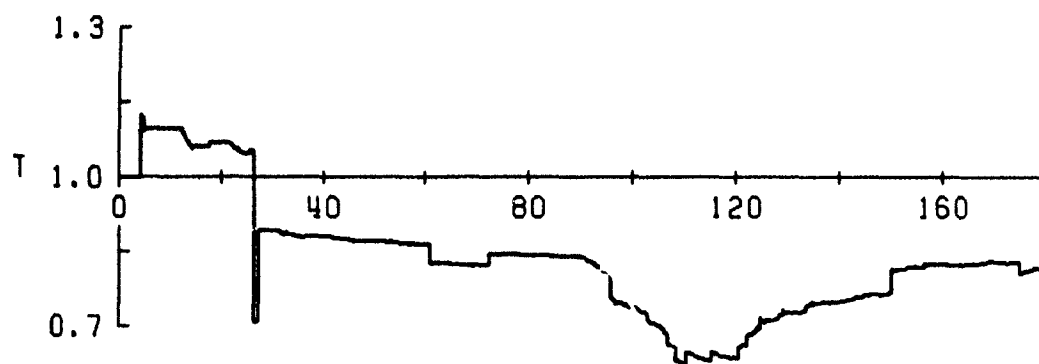
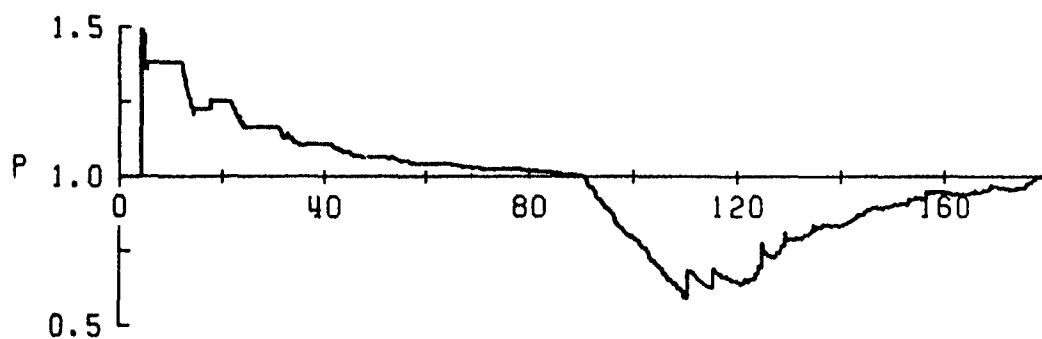
- 1) These results have very long duration steps in the decaying blast profile, because of the long driver length.
- 2) Contact surface almost reaches the four test station, and disrupts the initial three test station results for density and temperature.
- 3) Open end effects are seen. The reflected wave would be smaller in amplitude in real life due to friction, heat transfer, head losses and entrance effects.



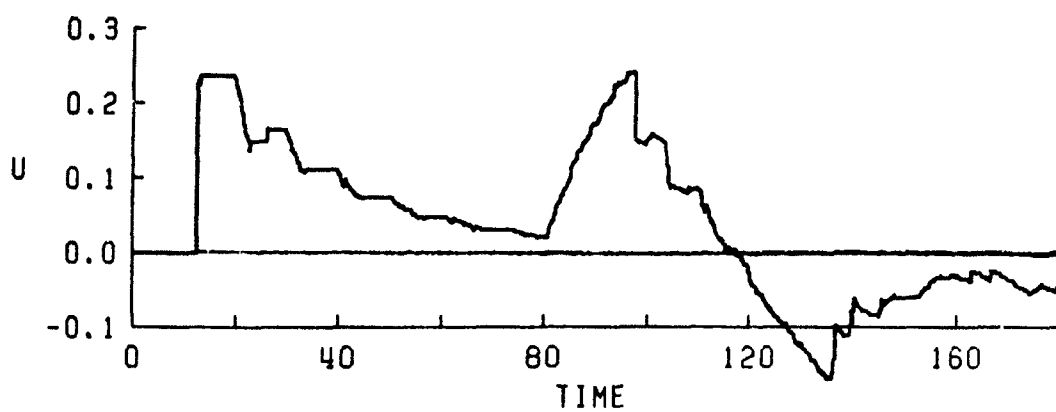
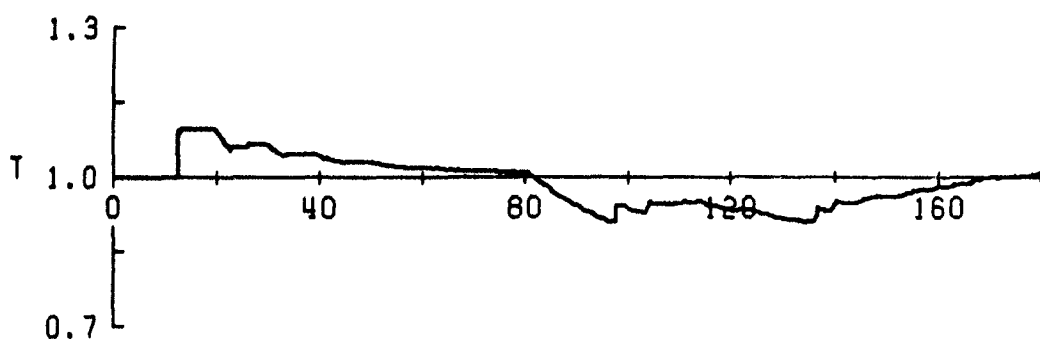
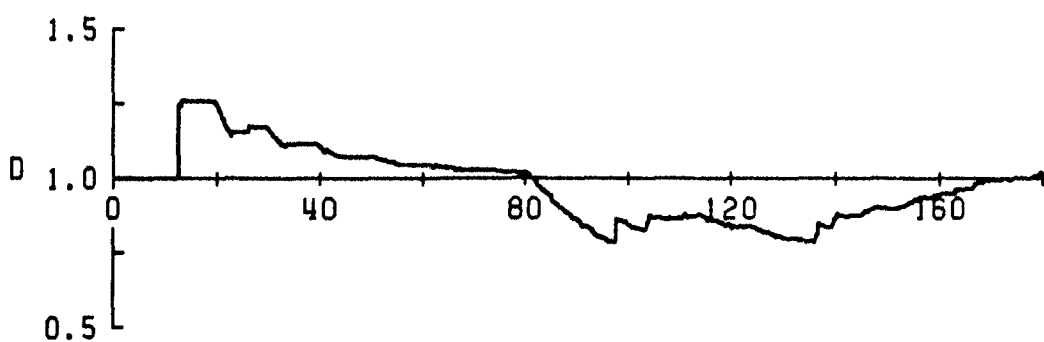
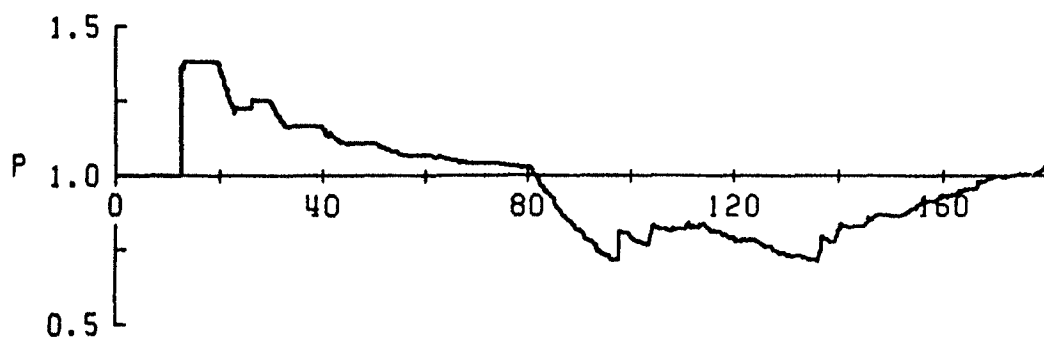
TIME HISTORIES
LOCATION: 2.336



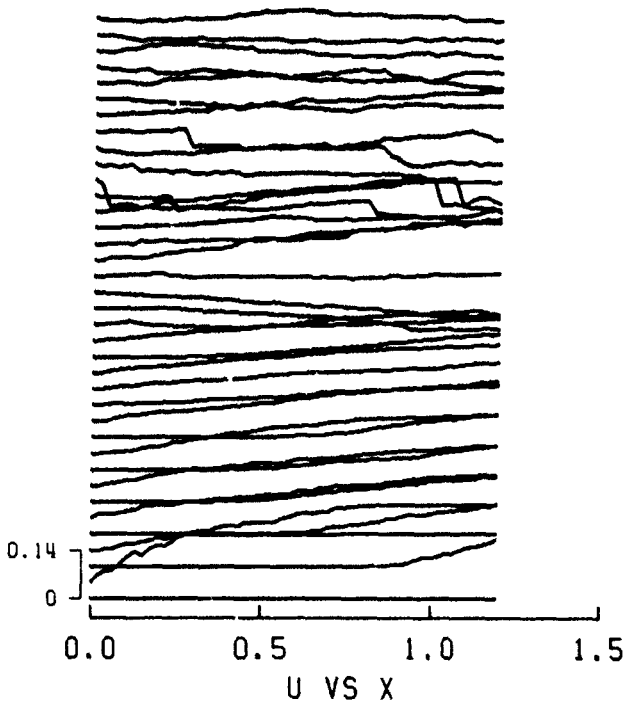
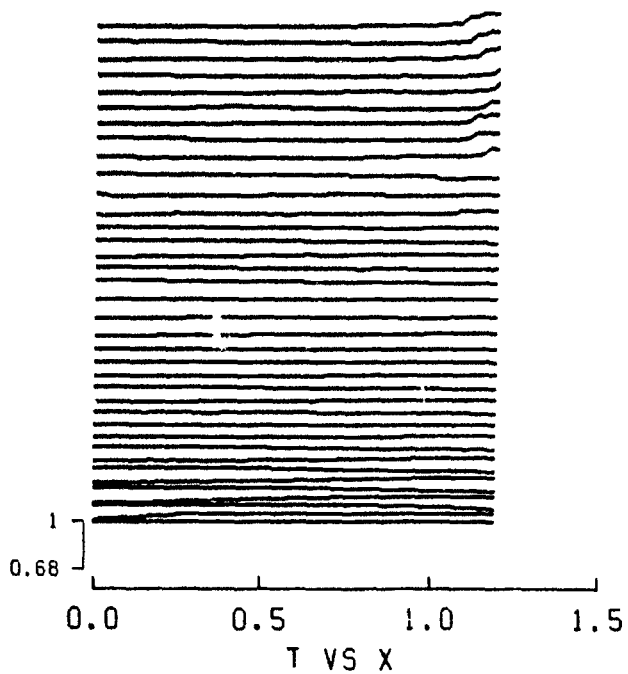
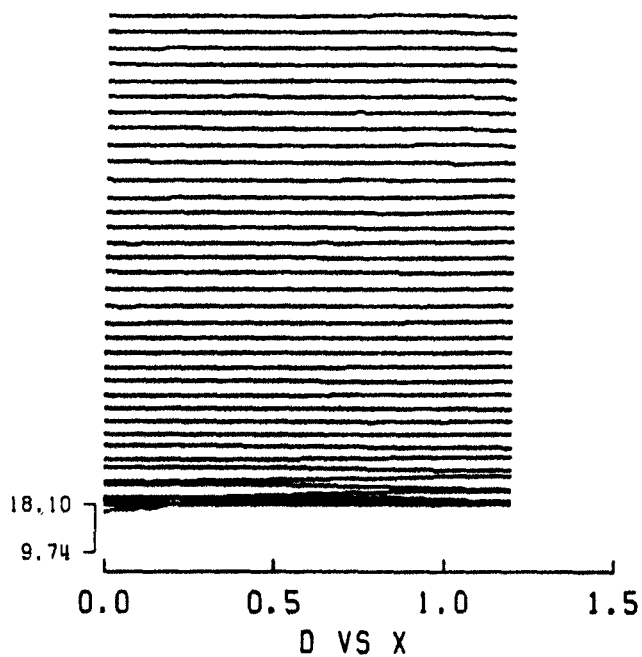
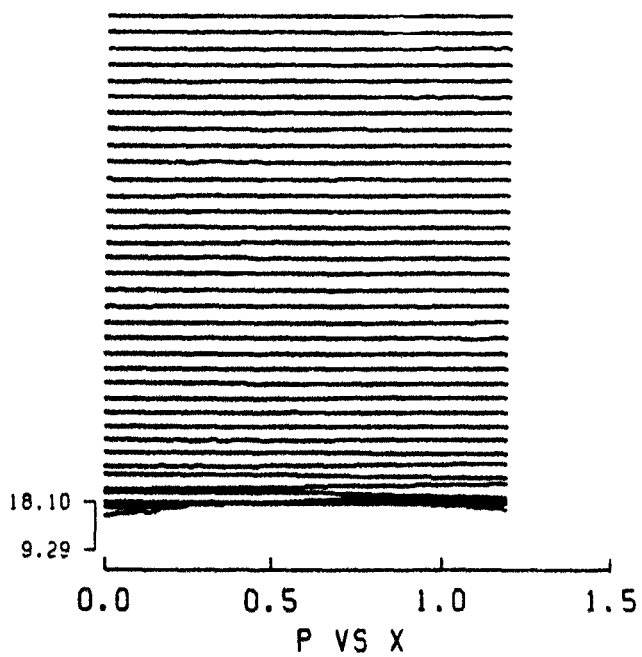
TIME HISTORIES
LOCATION: 2.803



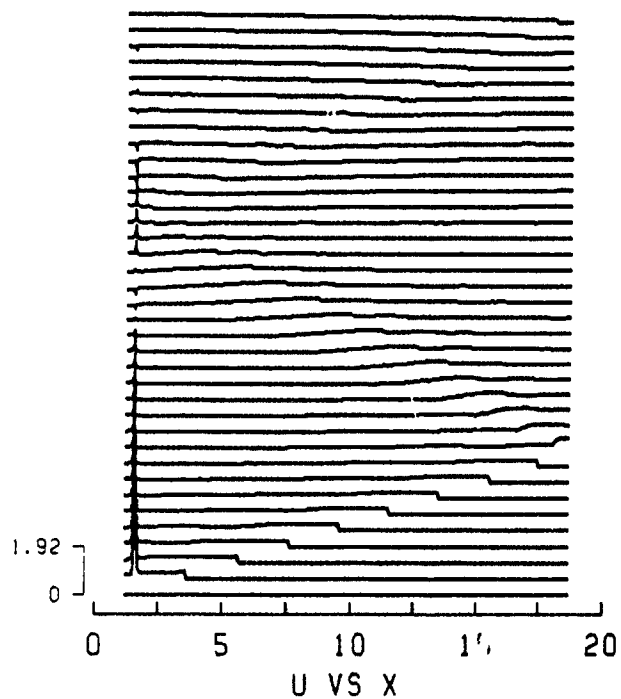
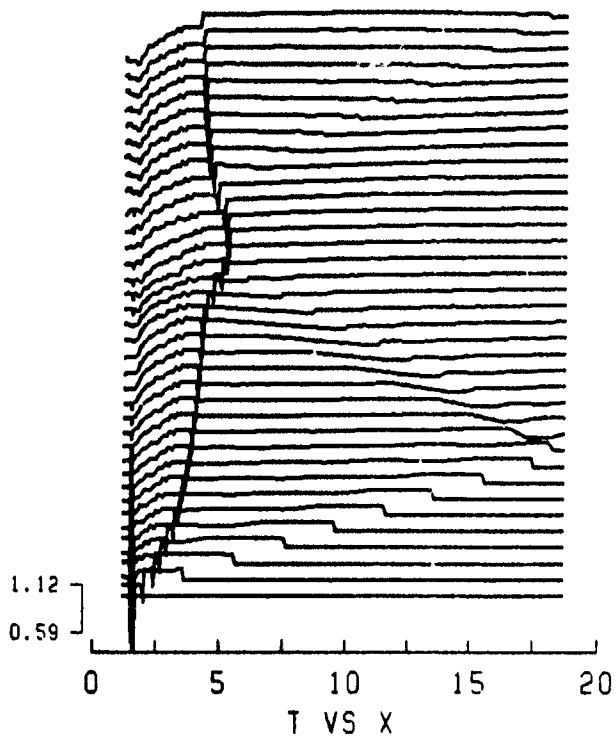
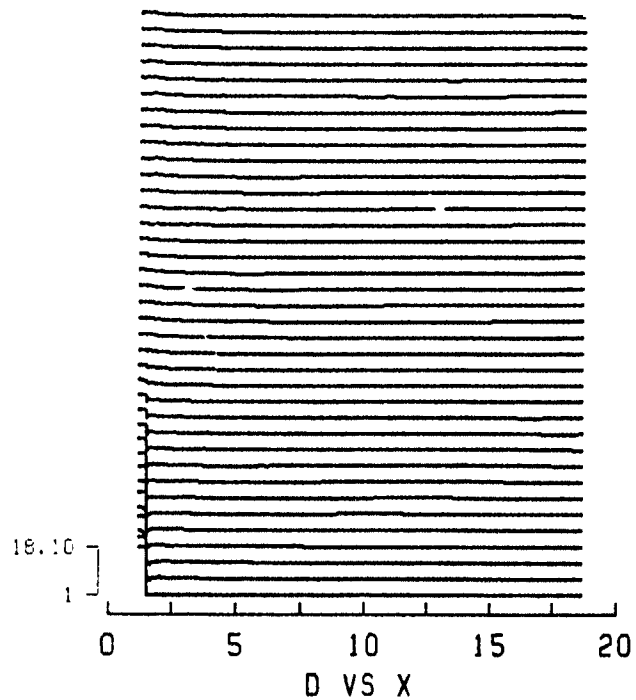
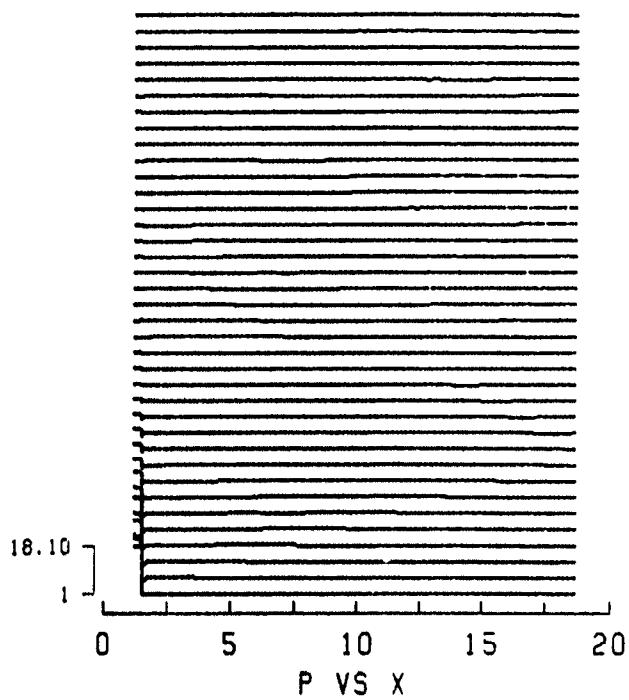
TIME HISTORIES
LOCATION: 3.323



TIME HISTORIES
LOCATION: 6.647



SPATIAL DISTRIBUTIONS
TIME: 0.000 TO 180.000

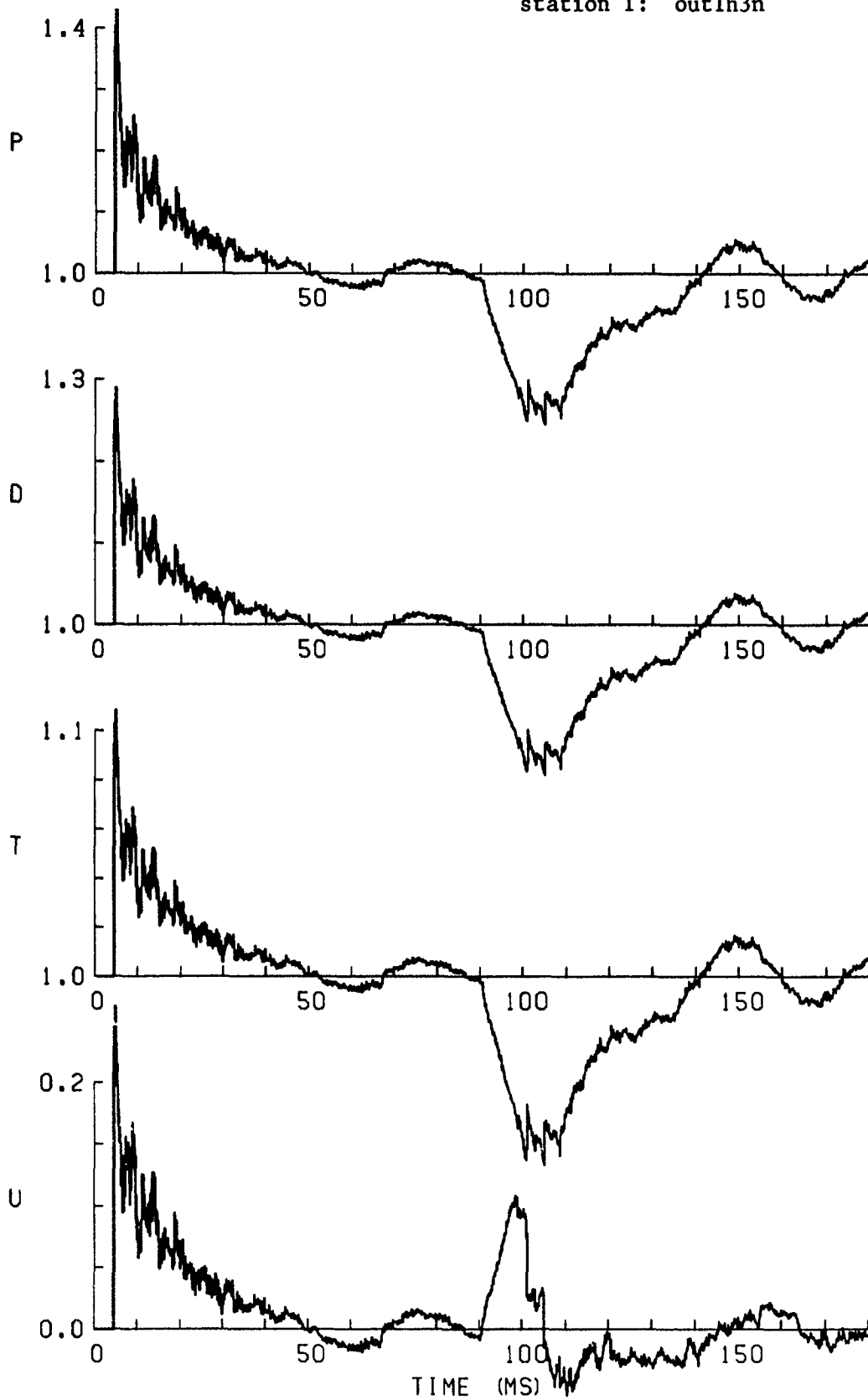


SPATIAL DISTRIBUTIONS
TIME: 0.000 TO 180.000

APPENDIX B
IMPROVED DRIVER RCM CALCULATIONAL RESULTS

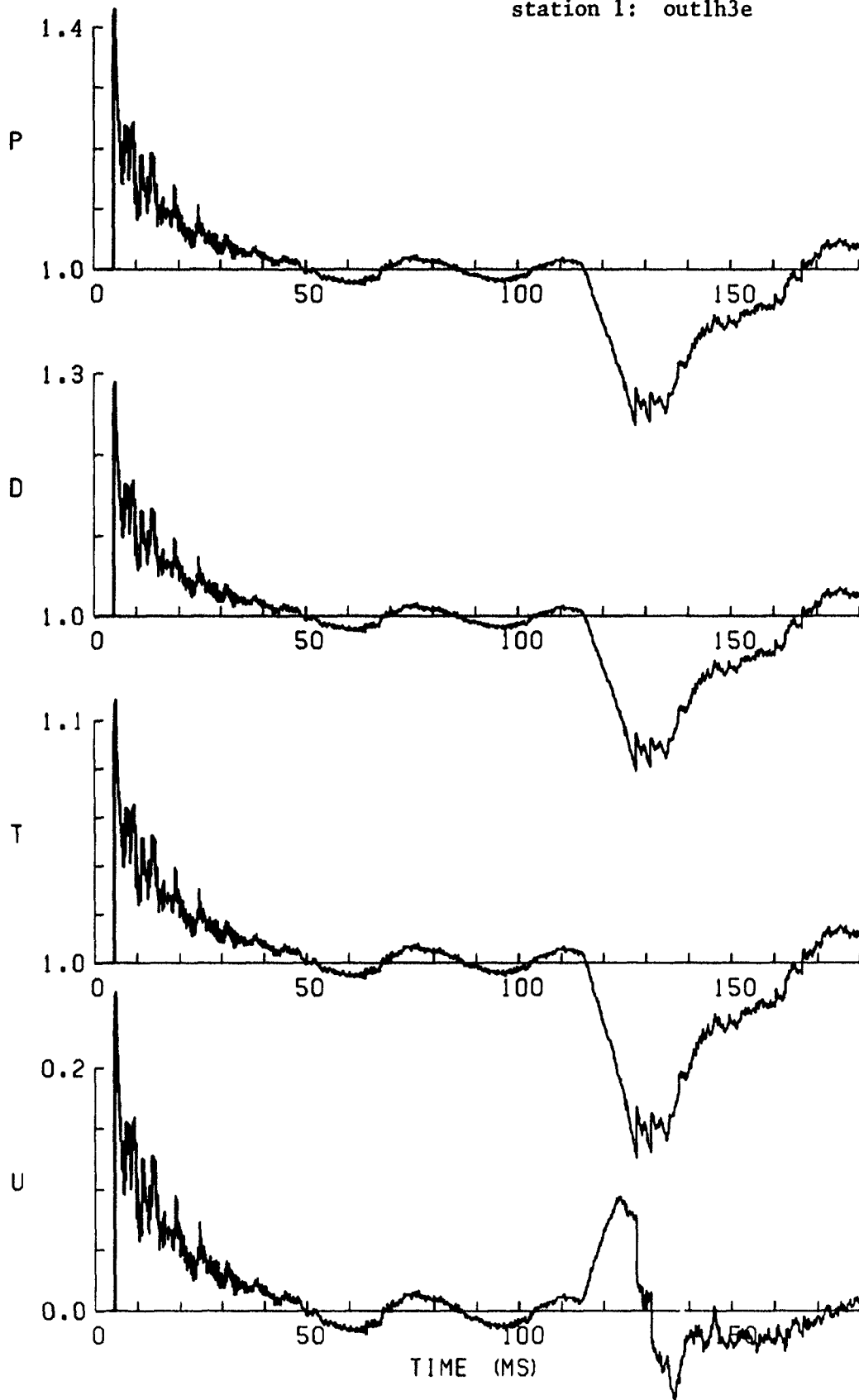
INTENTIONALLY LEFT BLANK.

3 psig overpressure blast wave
normal length channel
no RWE
station 1: outlh3n



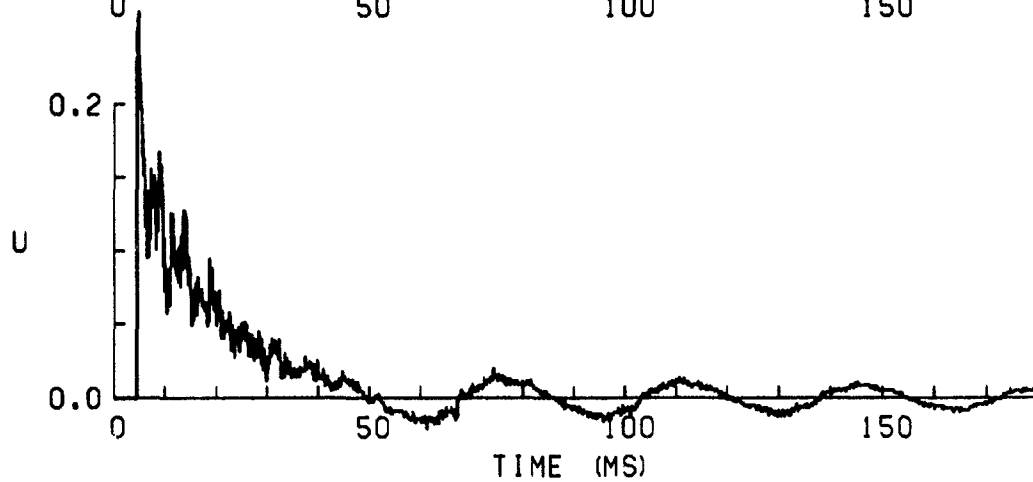
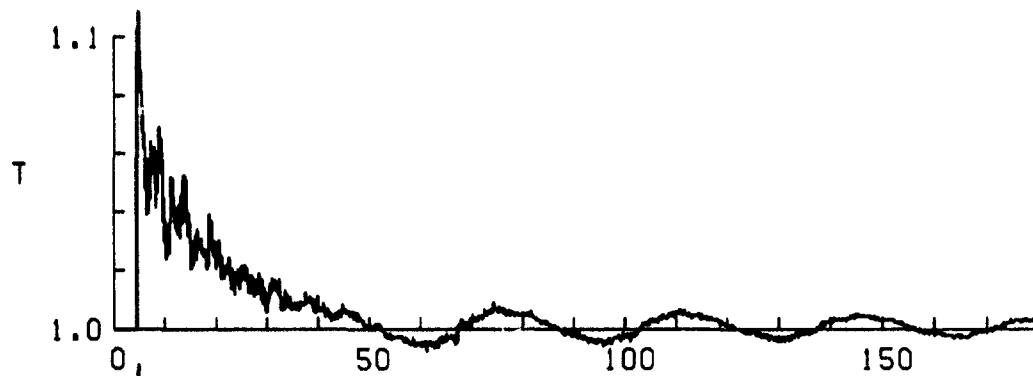
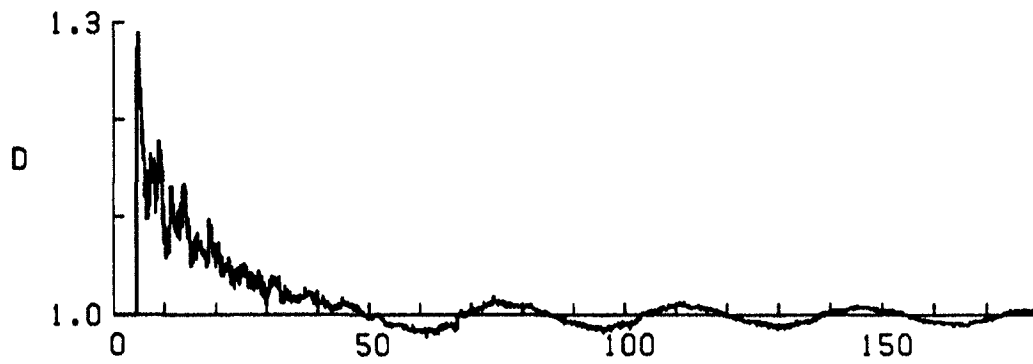
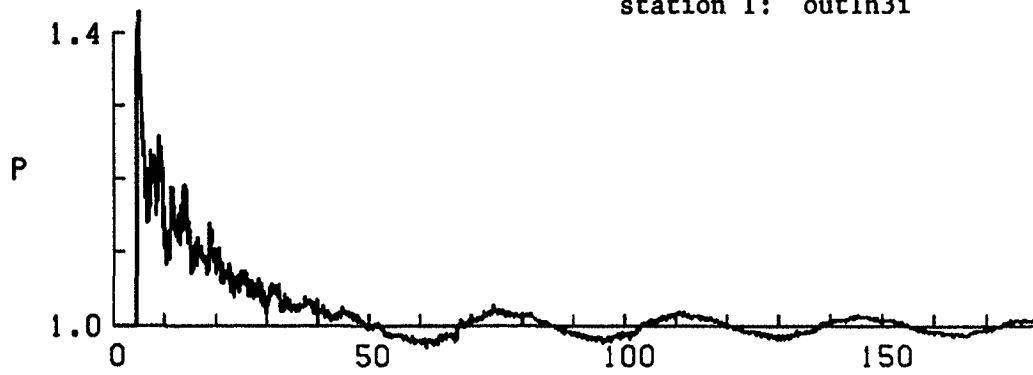
TIME HISTORIES
LOCATION: 2.302

3 psig overpressure blast wave
extended length channel
no RWE
station 1: outlh3e



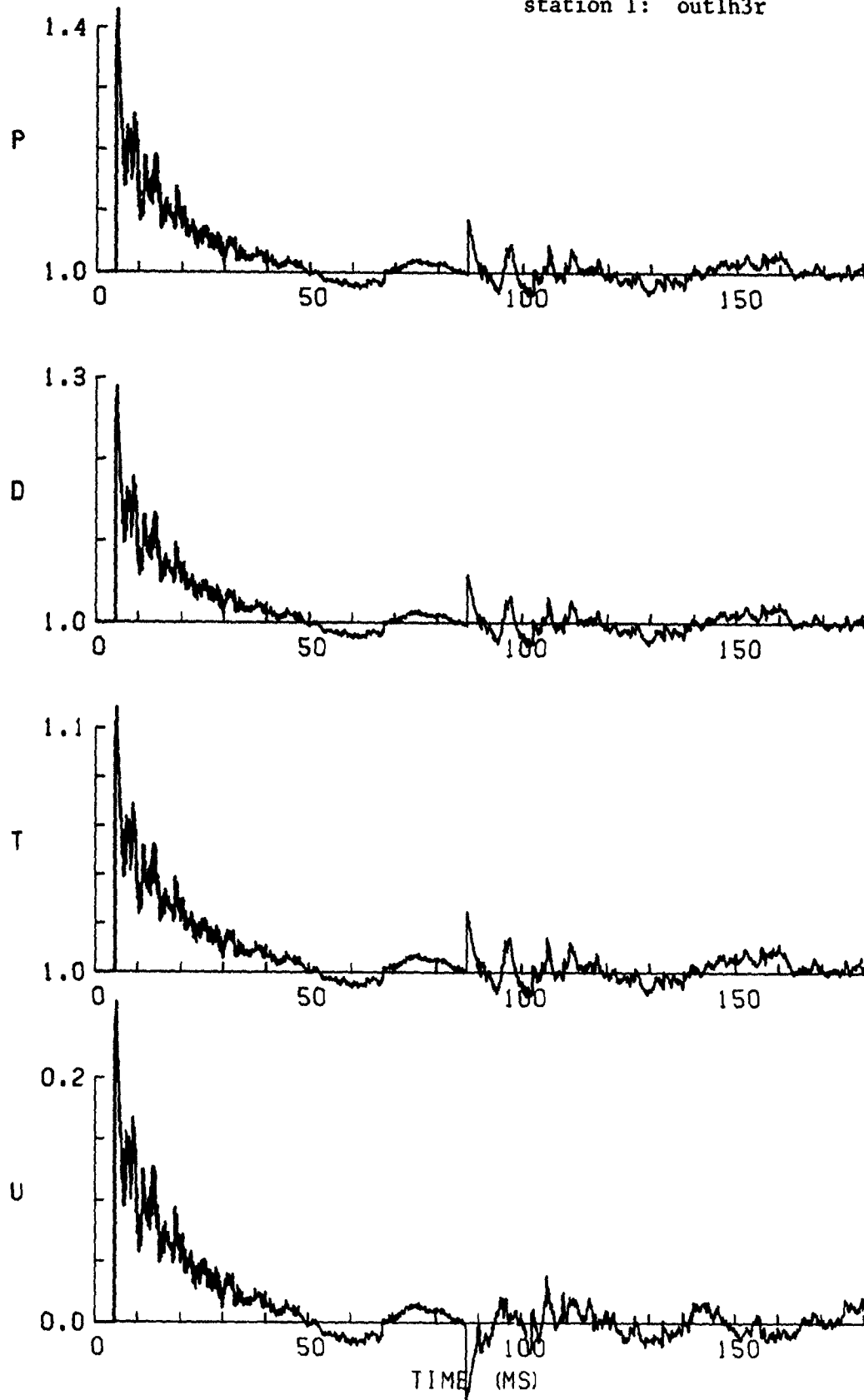
TIME HISTORIES
LOCATION: 2.289

3 psig overpressure blast wave
infinite length channel
no RWE
station 1: outlh3i



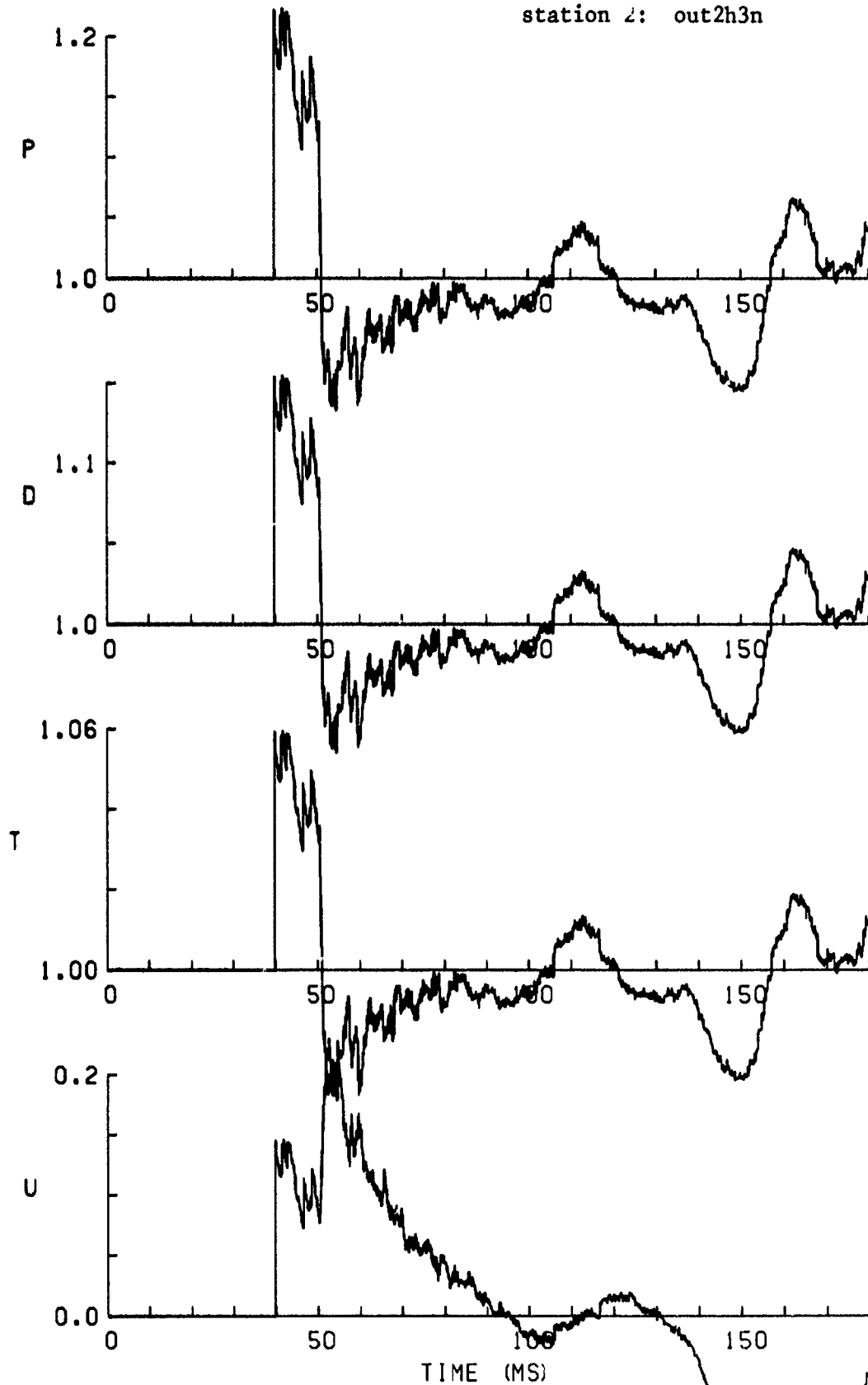
TIME HISTORIES
LOCATION: 2.302

3 psig overpressure blast wave
normal length channel
active RWE
station 1: outlh3r



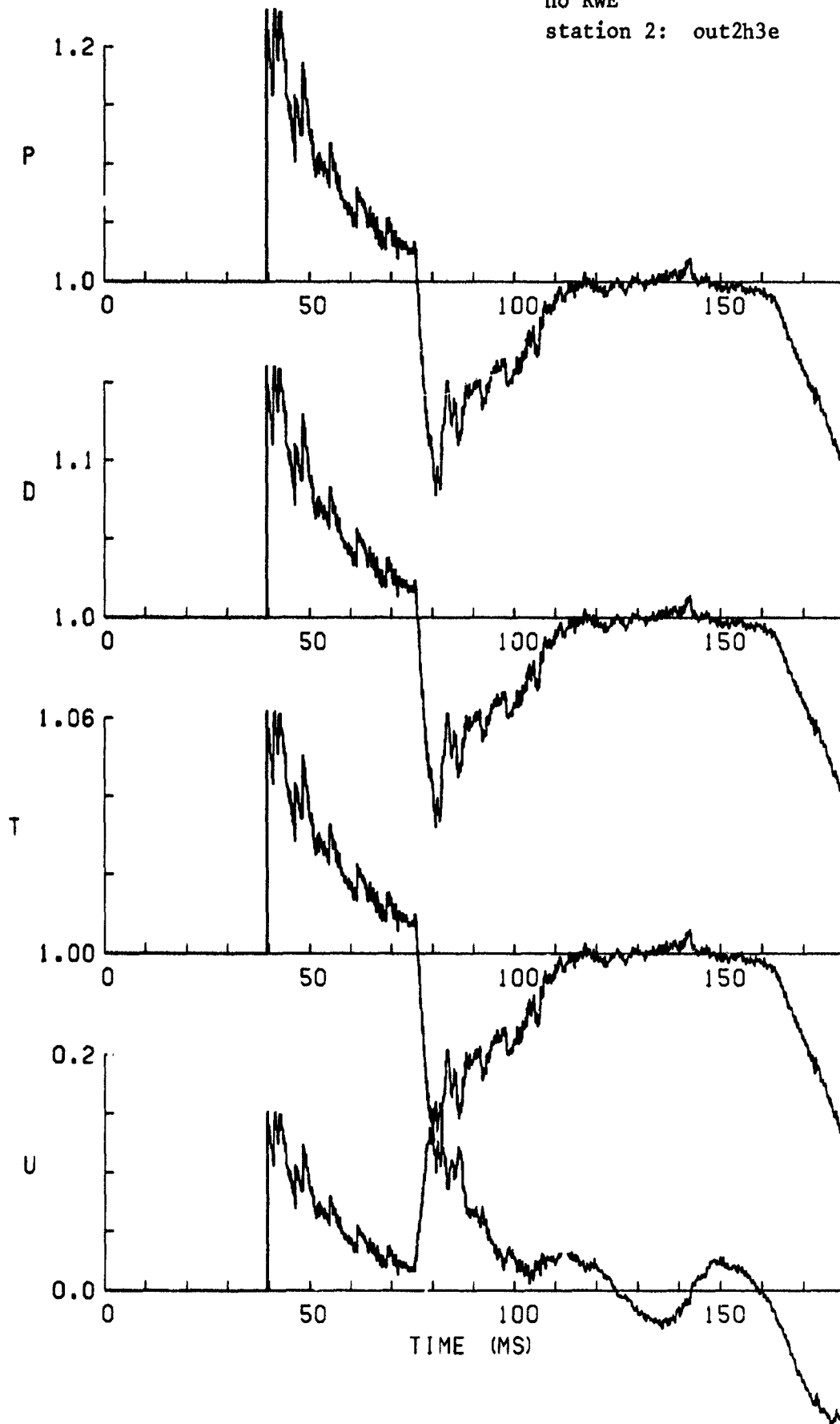
TIME HISTORIES
LOCATION: 2.302

3 psig overpressure blast wave
normal length channel
no RWE
station 2: out2h3n



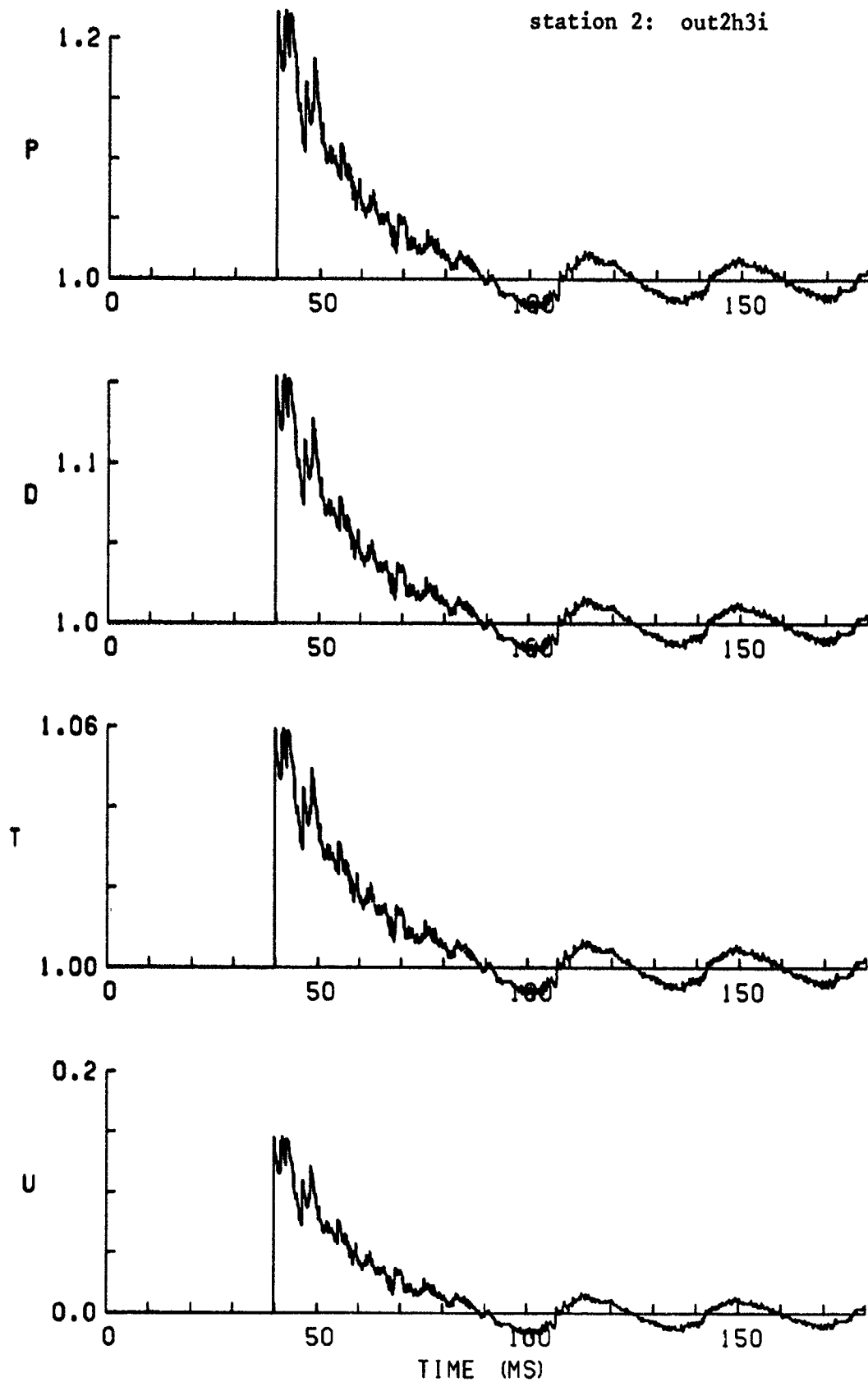
TIME HISTORIES
LOCATION: 15.916

3 psig overpressure blast wave
extended length channel
no RWE
station 2: out2h3e



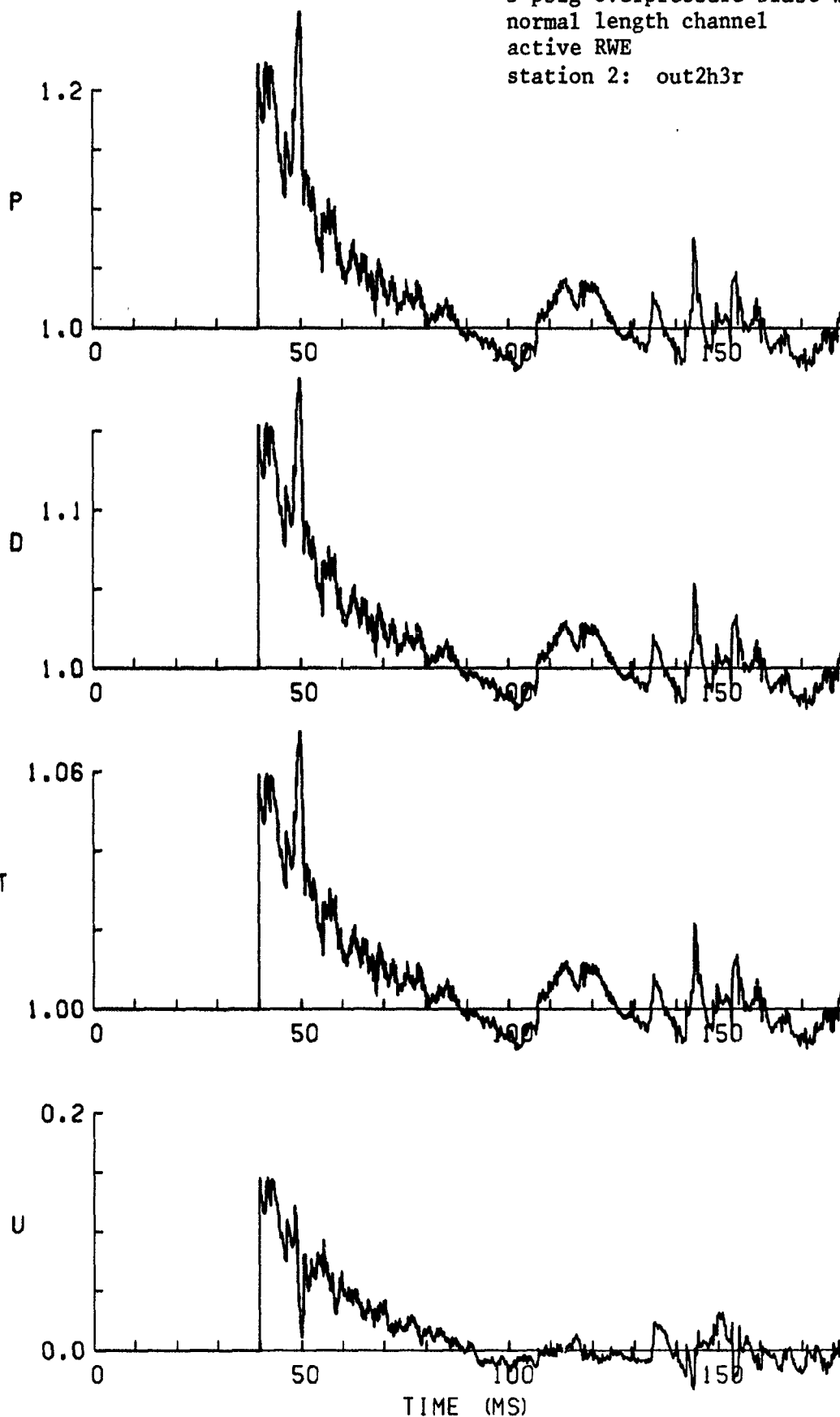
TIME HISTORIES
LOCATION: 15.904

3 psig overpressure blast wave
infinite length channel
no RWE
station 2: out2h3i



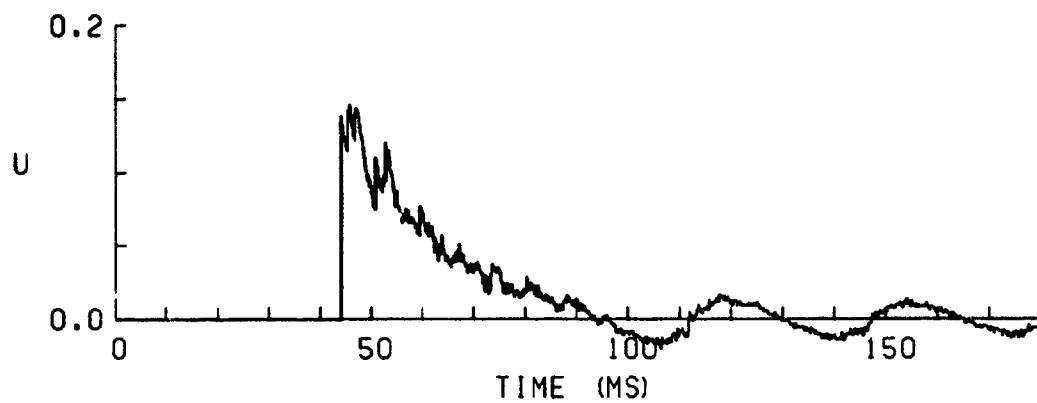
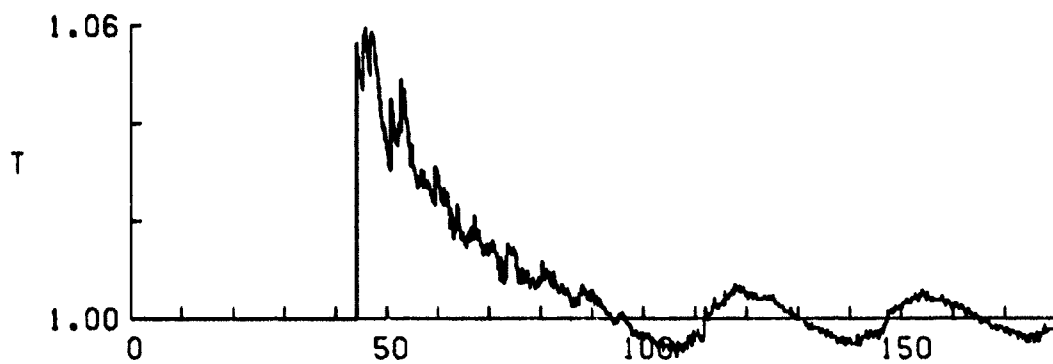
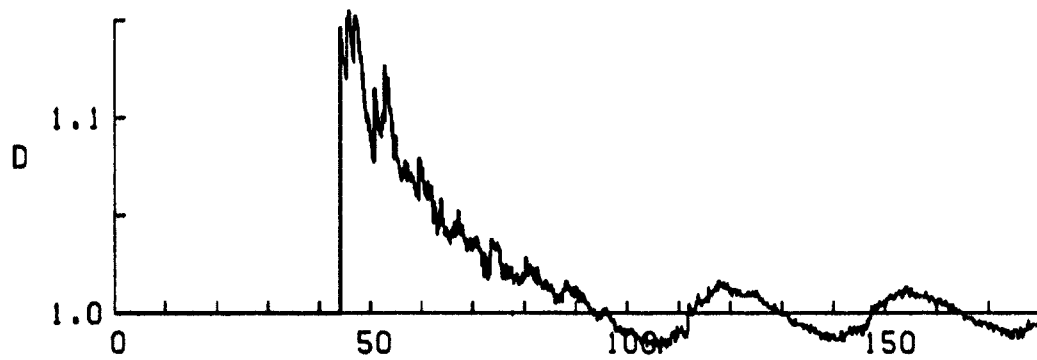
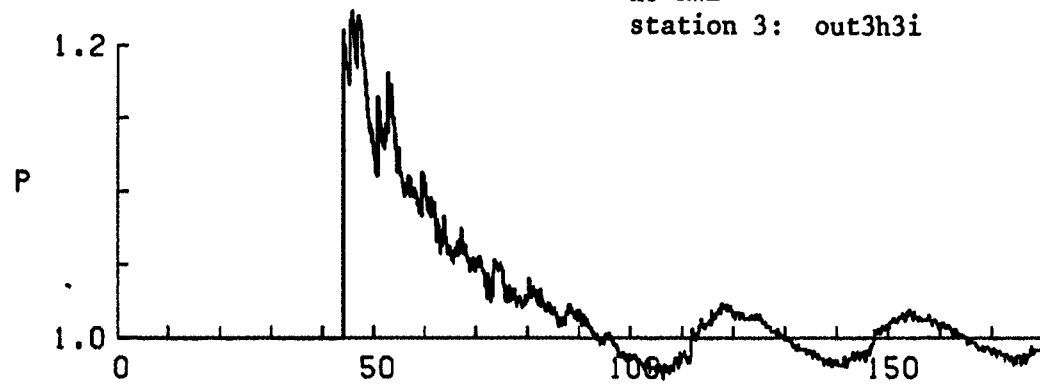
TIME HISTORIES
LOCATION: 15.916

3 psig overpressure blast wave
normal length channel
active RWE
station 2: out2h3r



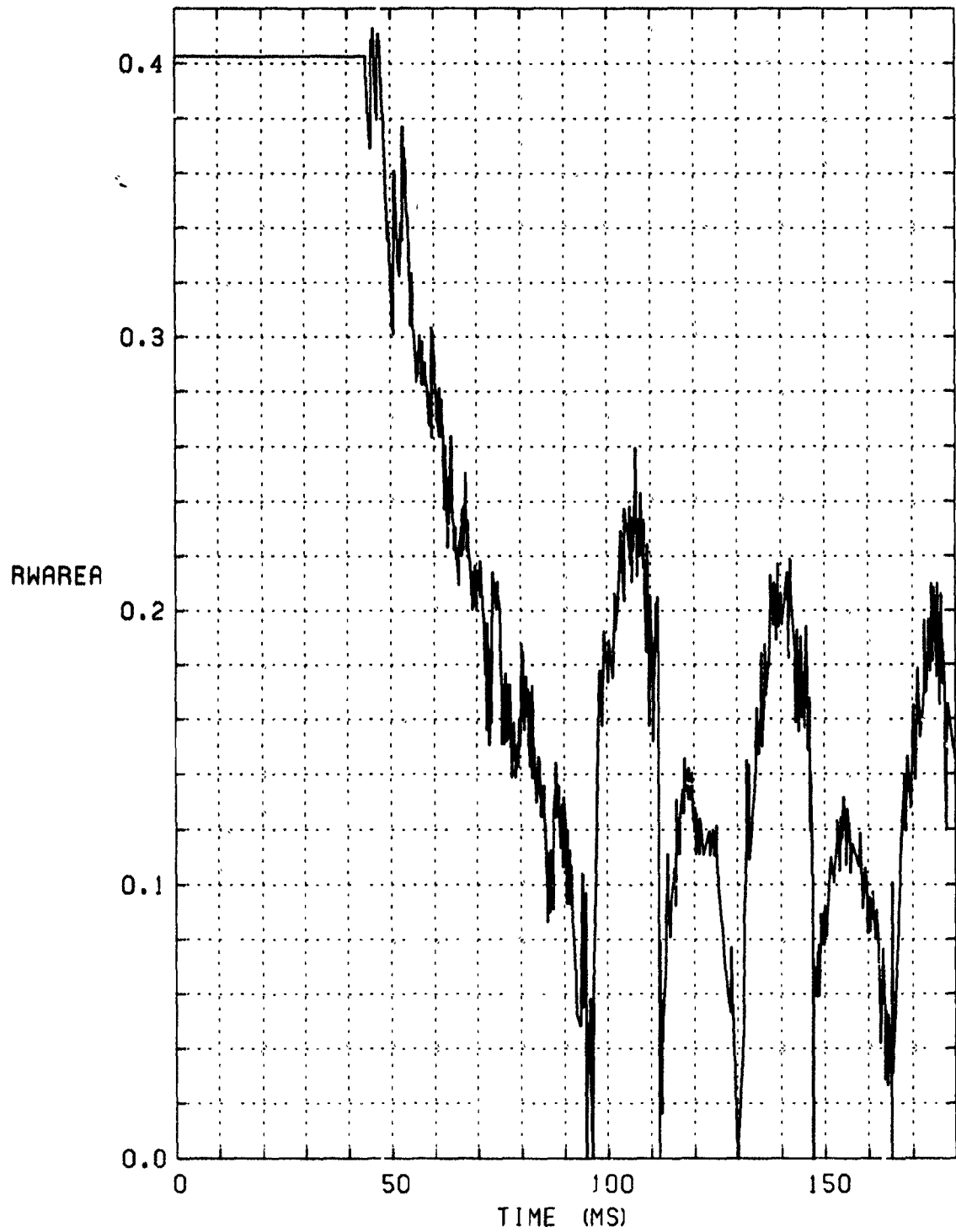
TIME HISTORIES
LOCATION: 15.916

3 psig overpressure blast wave
infinite length channel
no RWE
station 3: out3h3i

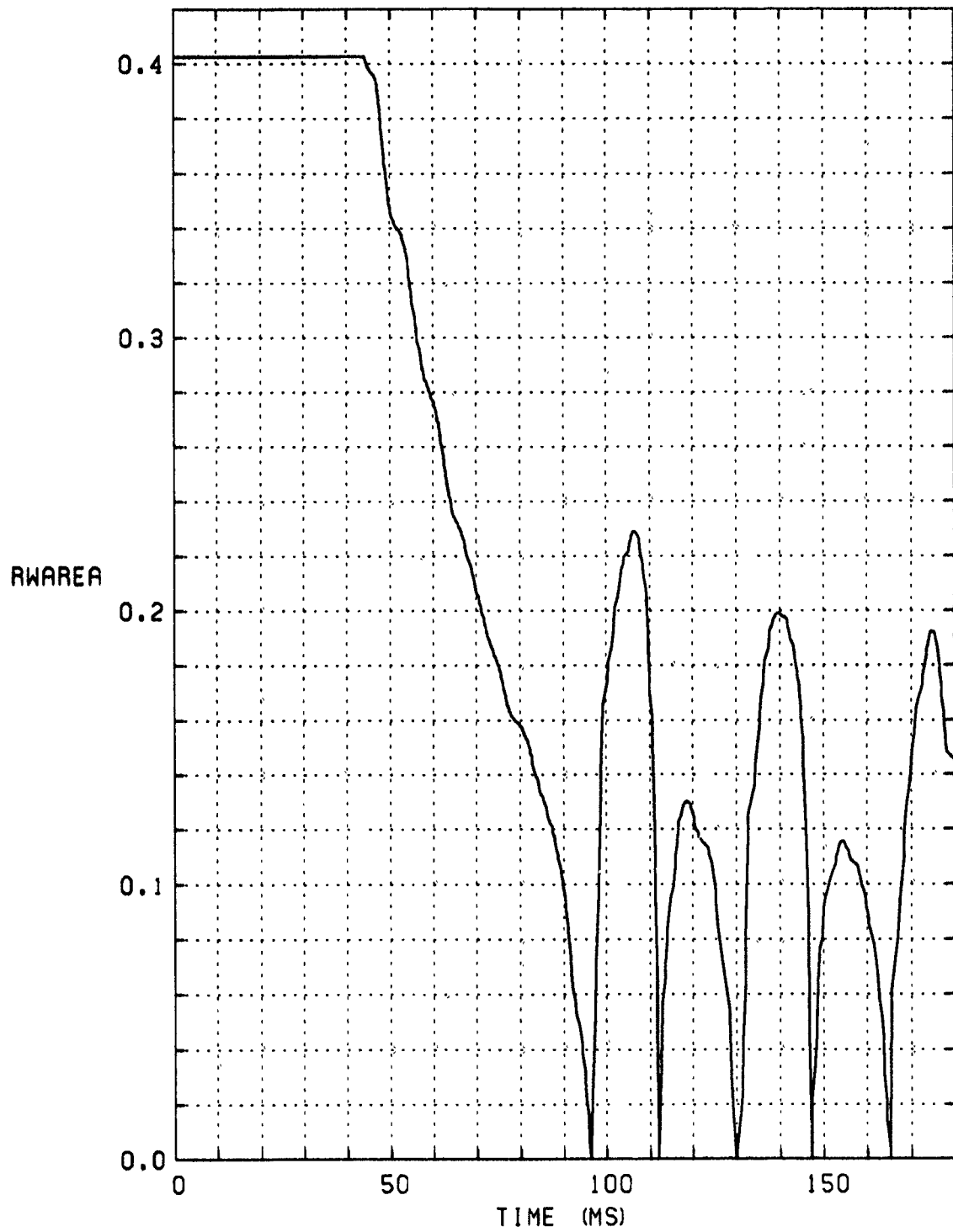


TIME HISTORIES
LOCATION: 17.599

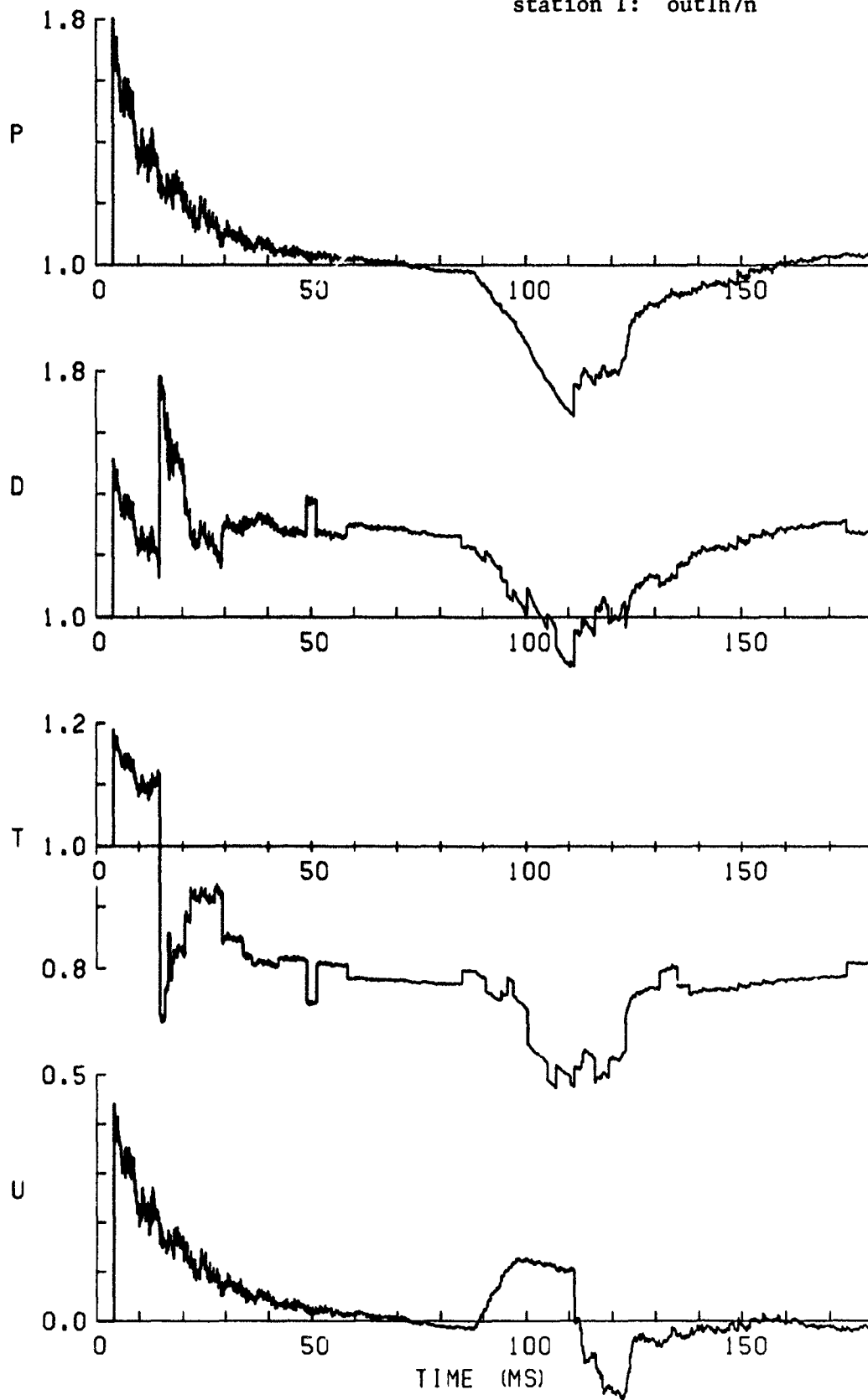
3 psig overpressure blast wave
RWE open-area-ratio setting
unfiltered
station 3: RWE3U



3 psig overpressure blast wave
RWE open-area-ratio setting
filtered
station 3: RWE3F

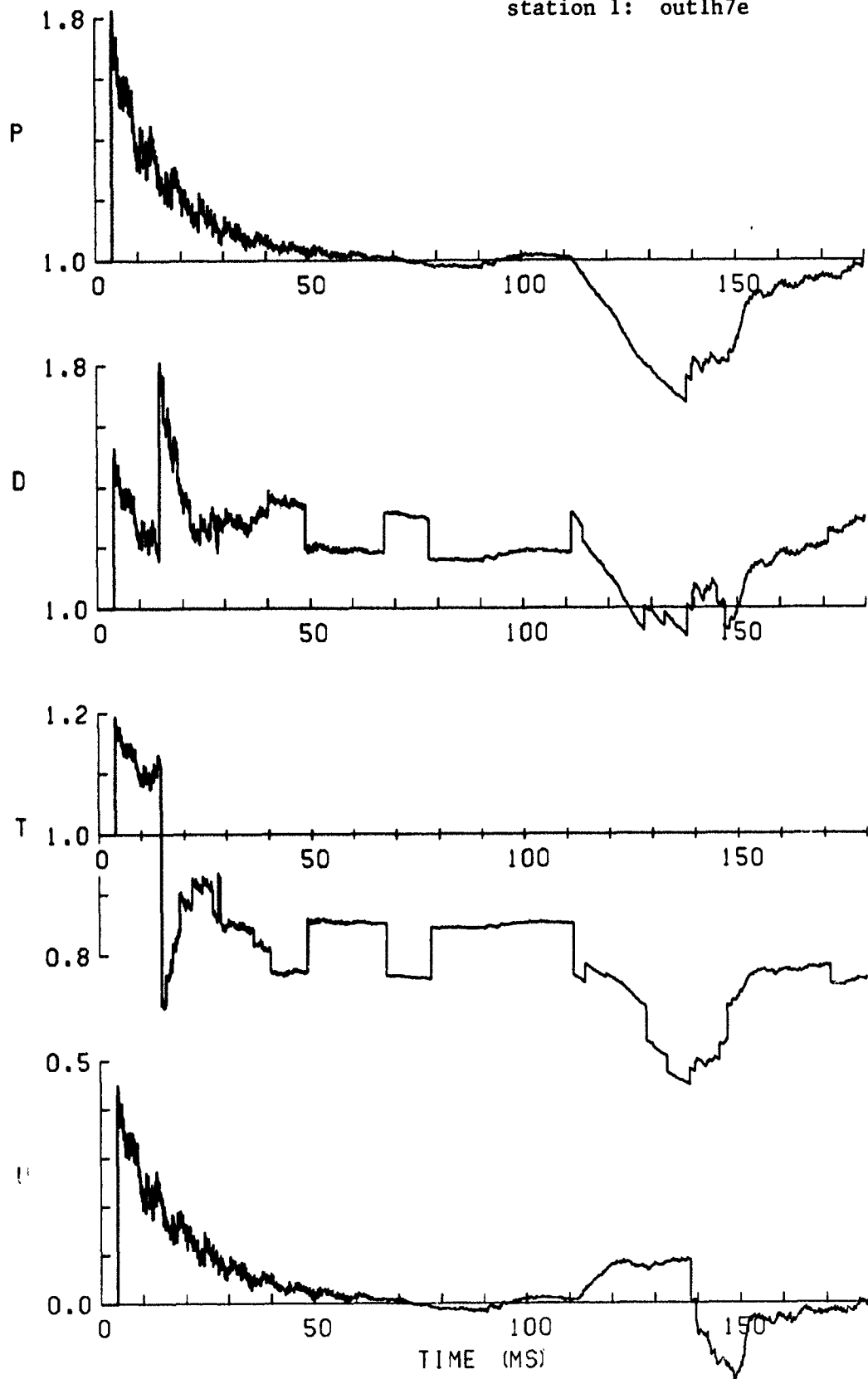


7 psig overpressure blast wave
normal length channel
no RWE
station 1: outlh7n



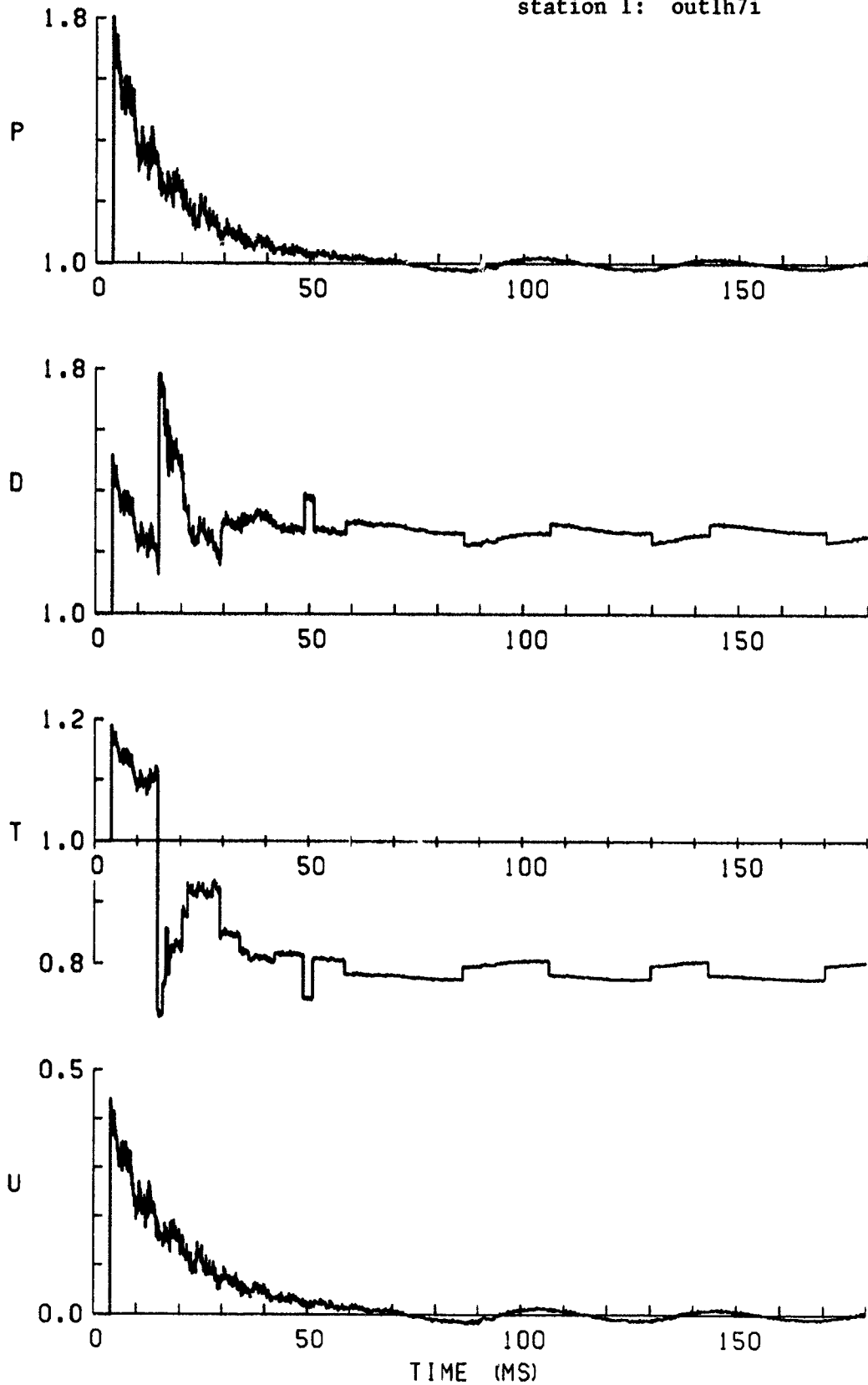
TIME HISTORIES
LOCATION: 2.302

7 psig overpressure blast wave
extended length channel
no RWE
station 1: outlh7e



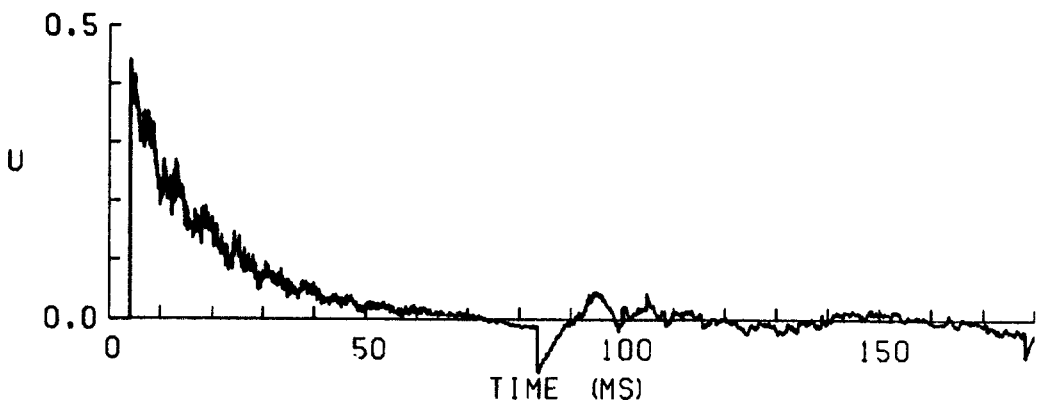
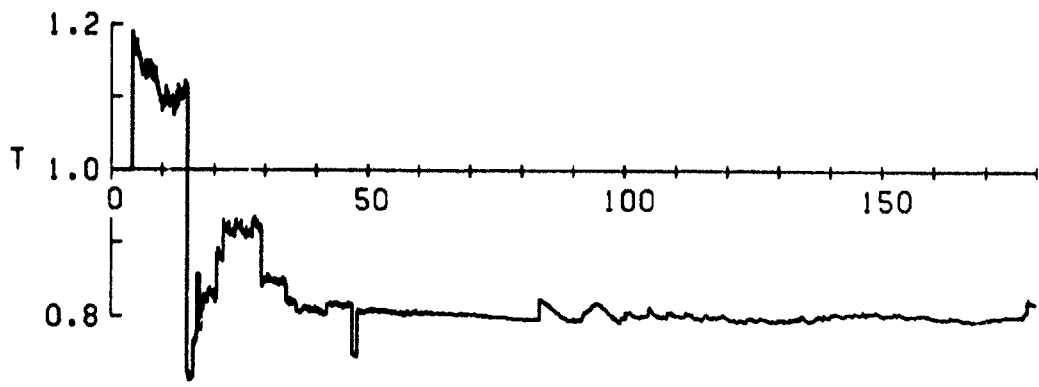
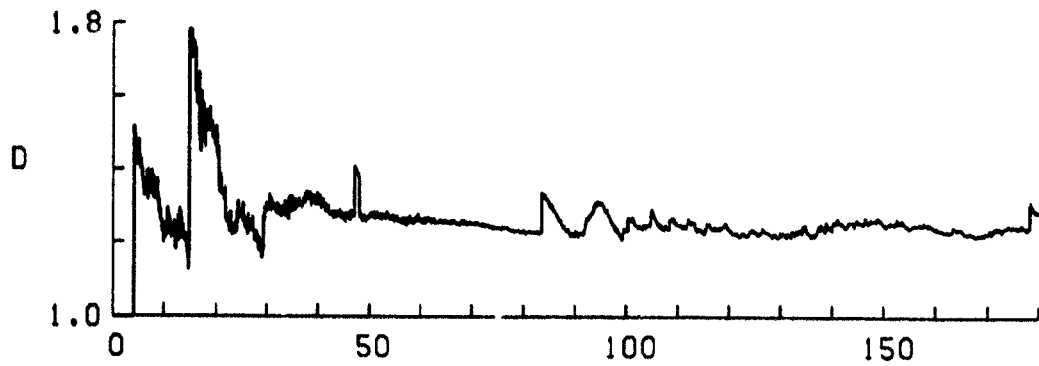
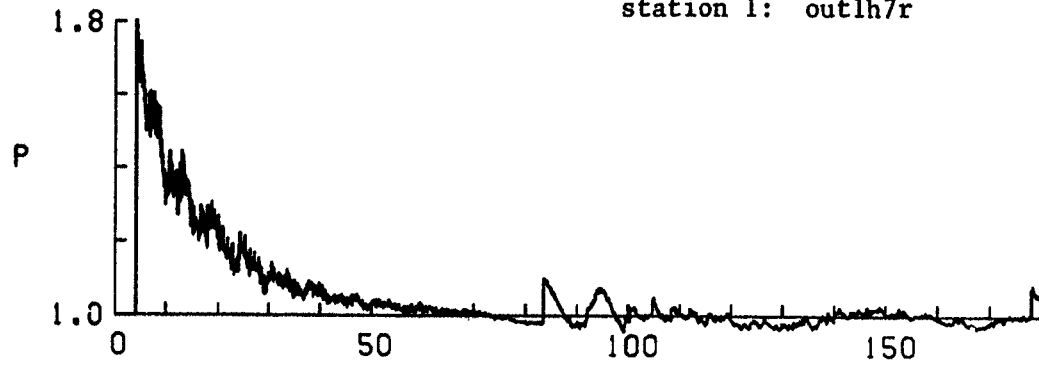
TIME HISTORIES
LOCATION: 2.289

7 psig overpressure blast wave
infinite length channel
no RWE
station 1: outlh7i



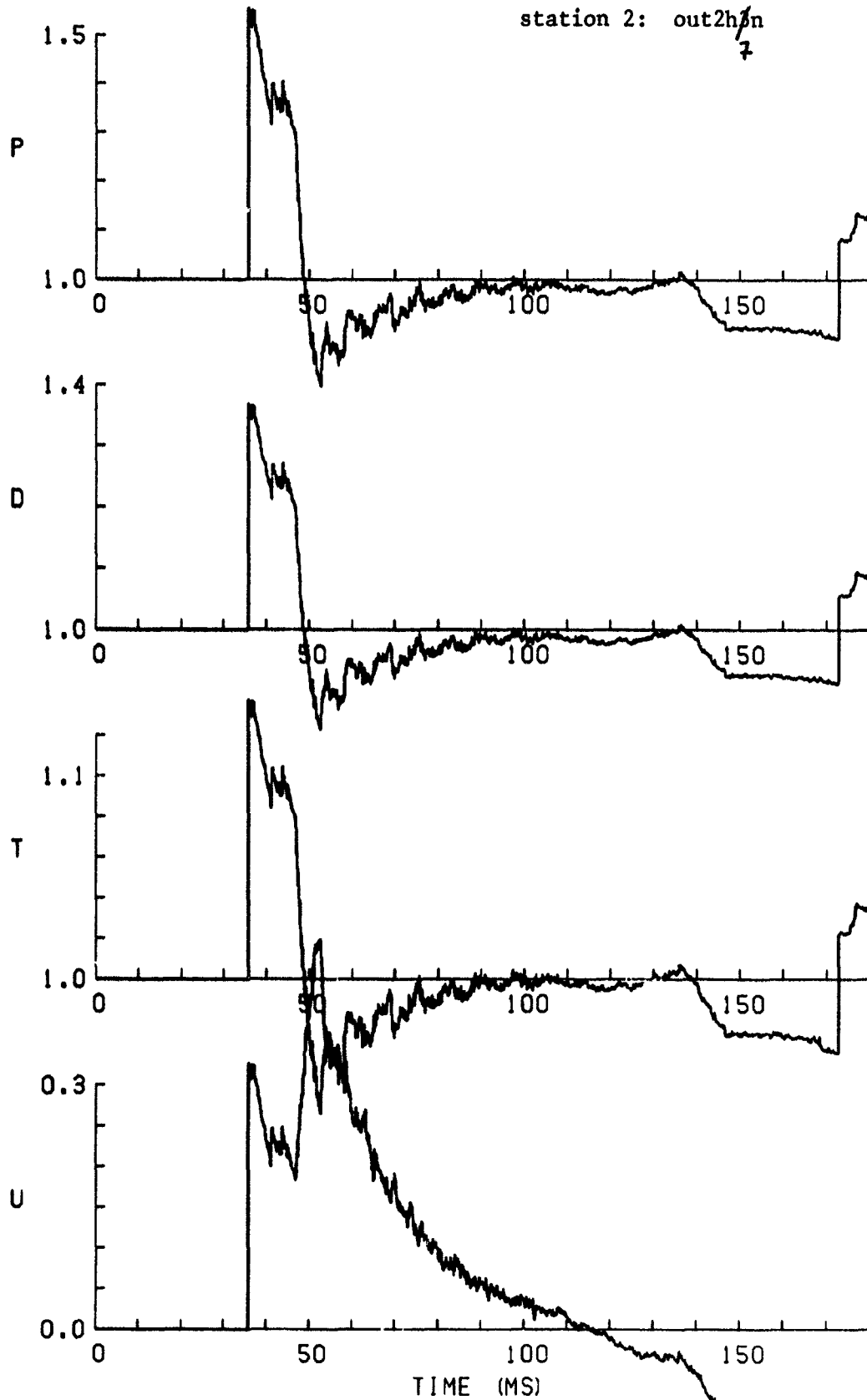
TIME HISTORIES
LOCATION: 2.302

7 psig overpressure blast wave
normal length channel
active RWE
station 1: outlh7r



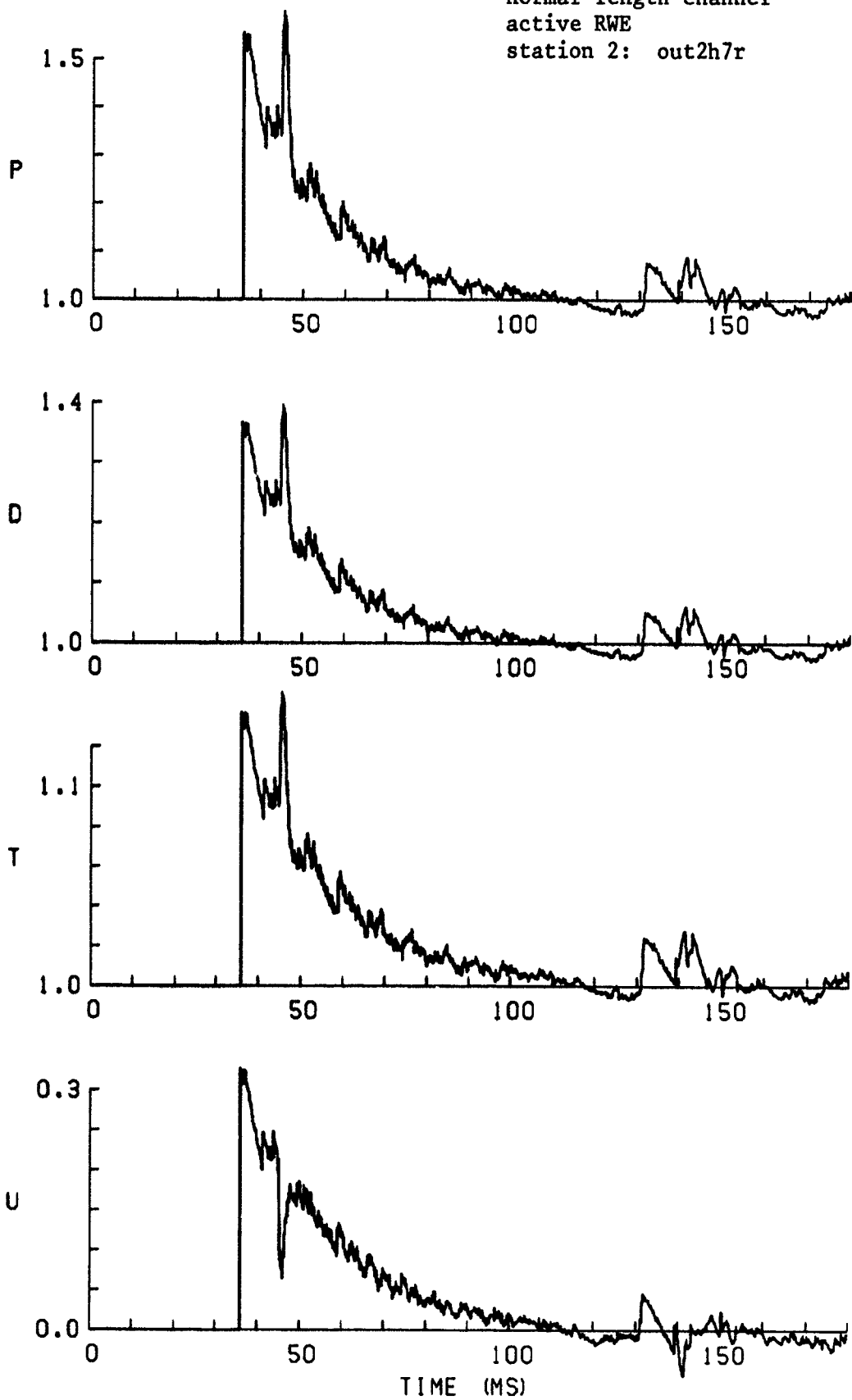
TIME HISTORIES
LOCATION: 2.302

7 psig overpressure blast wave
normal length channel
no RWE
station 2: out2h/n
7



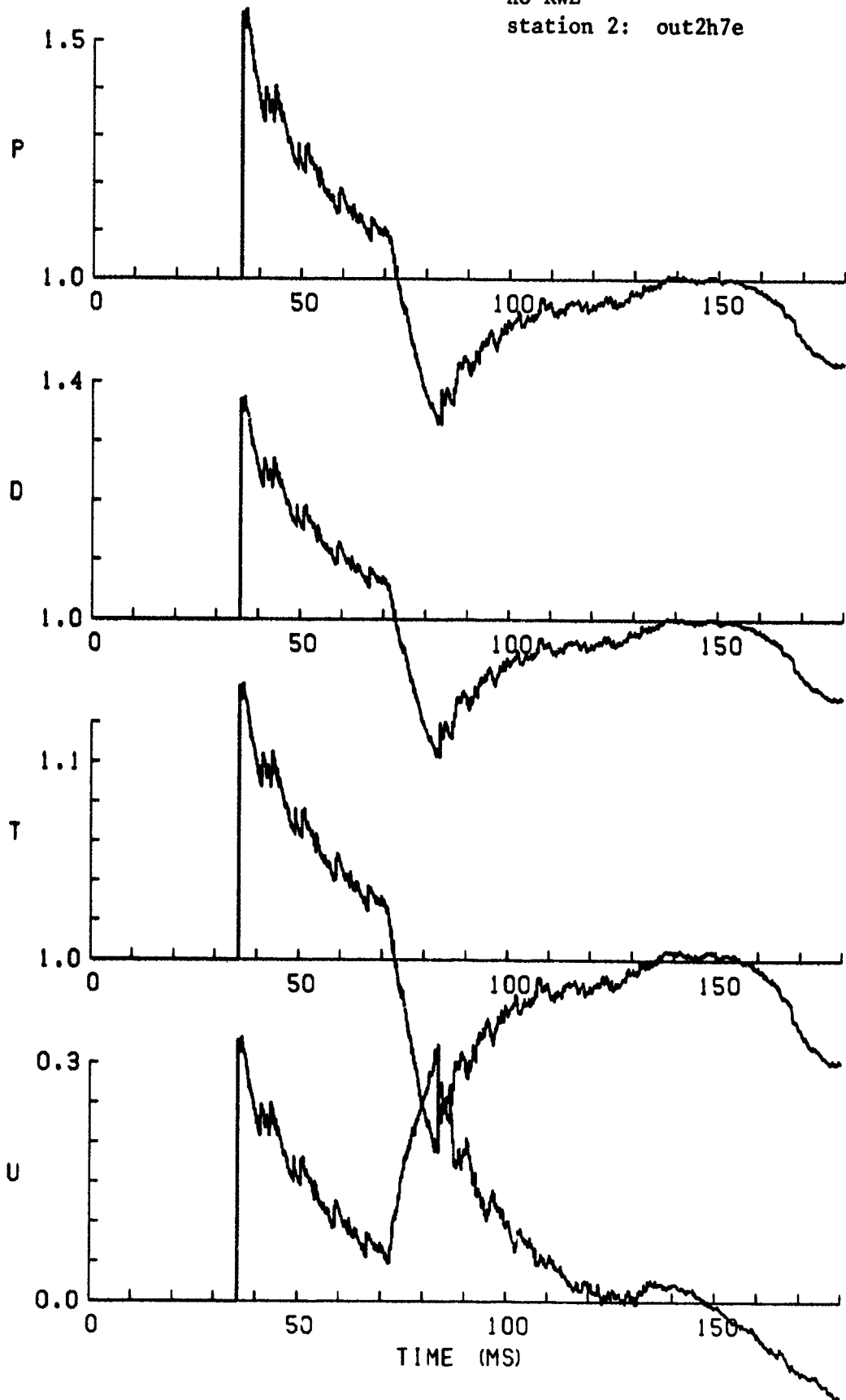
TIME HISTORIES
LOCATION: 15.916

7 psig overpressure blast wave
normal length channel
active RWE
station 2: out2h7r



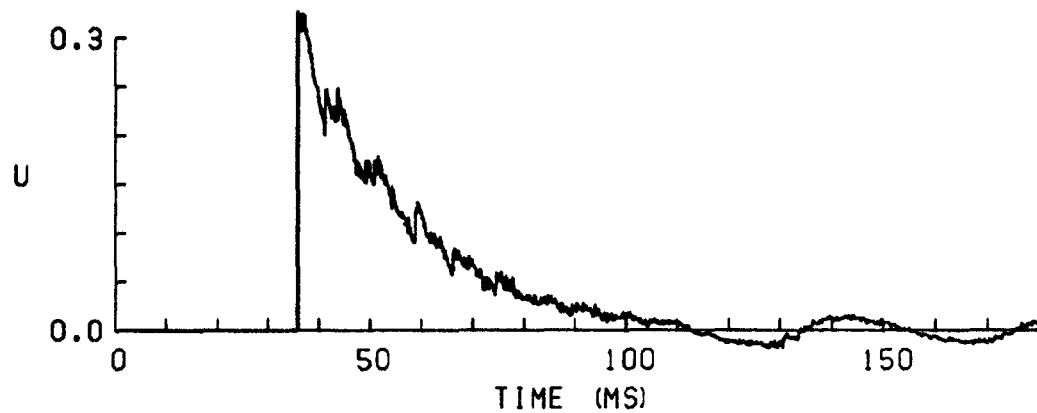
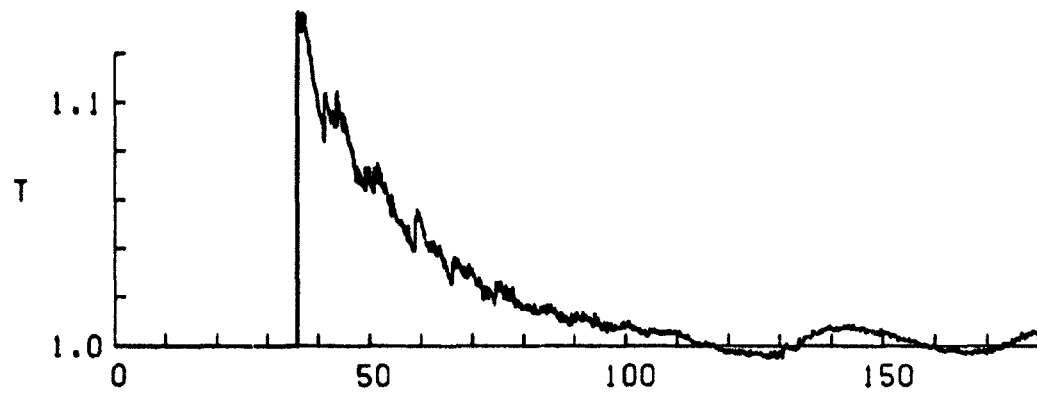
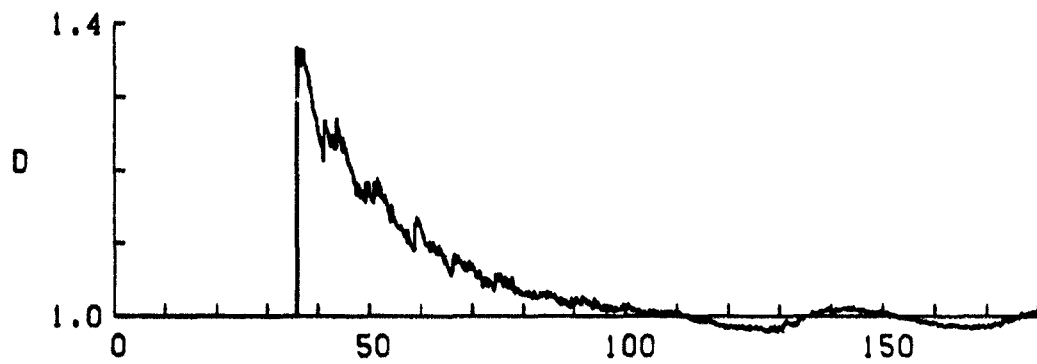
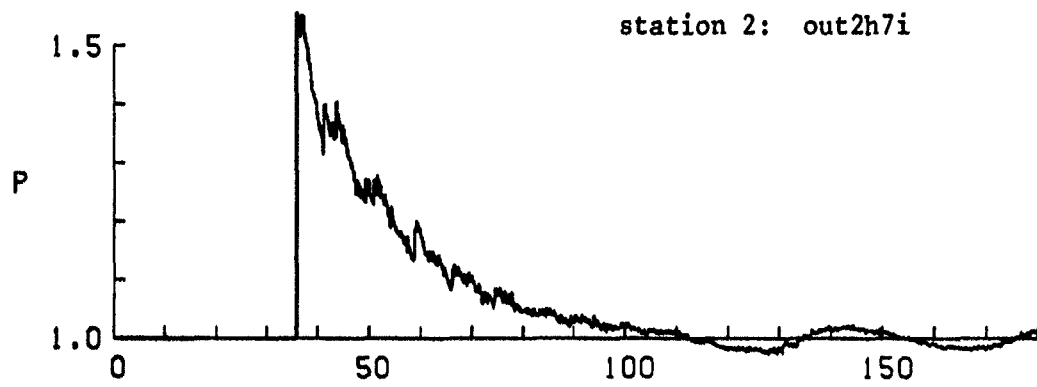
TIME HISTORIES
LOCATION: 15.916

7 psig overpressure blast wave
extended length channel
no RWE
station 2: out2h7e



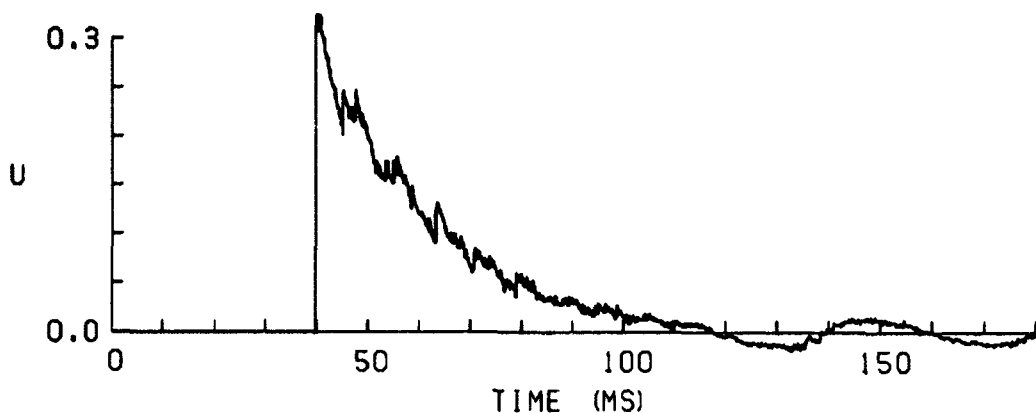
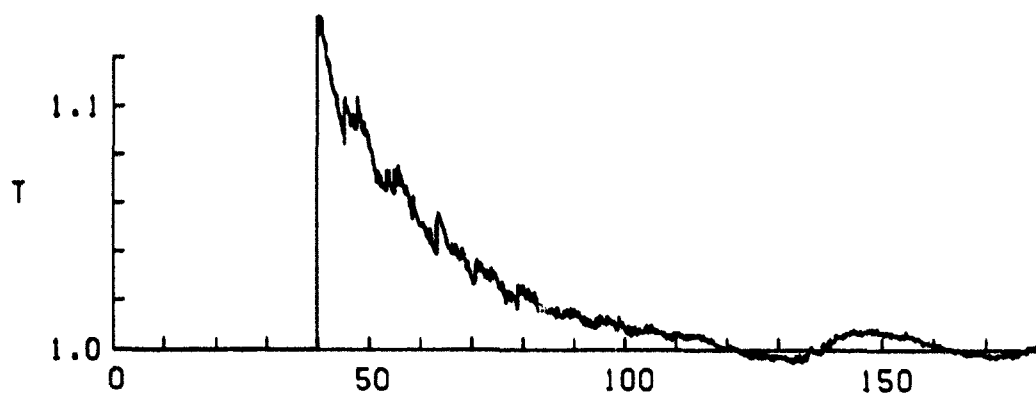
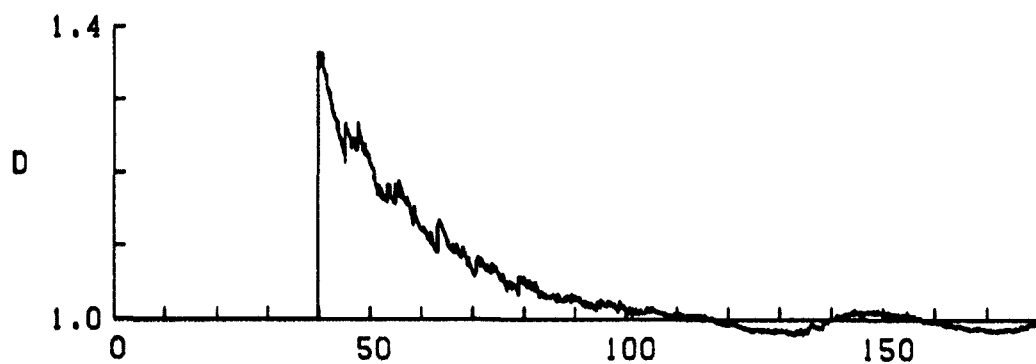
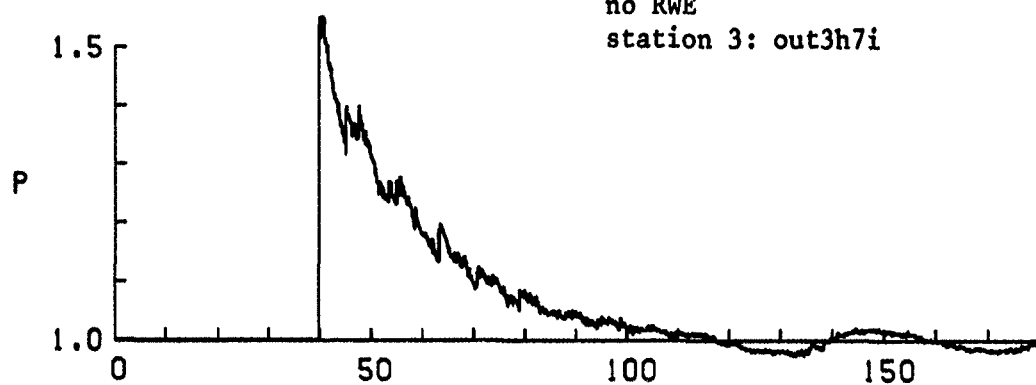
TIME HISTORIES
LOCATION: 15.904

7 psig overpressure blast wave
infinite length channel
no RWE
station 2: out2h7i



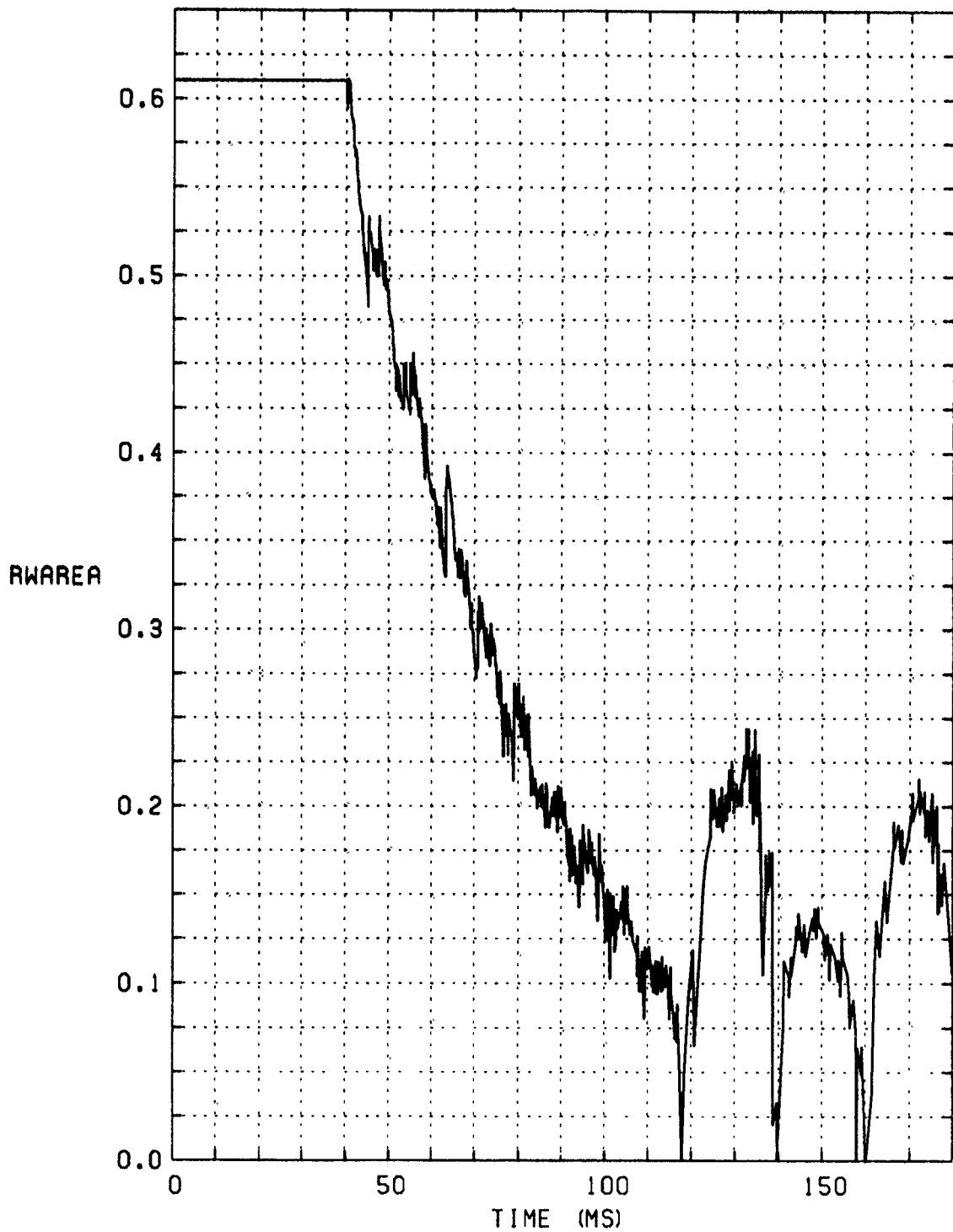
TIME HISTORIES
LOCATION: 15.916

7 psig overpressure blast wave
infinite length channel
no RWE
station 3: out3h7i

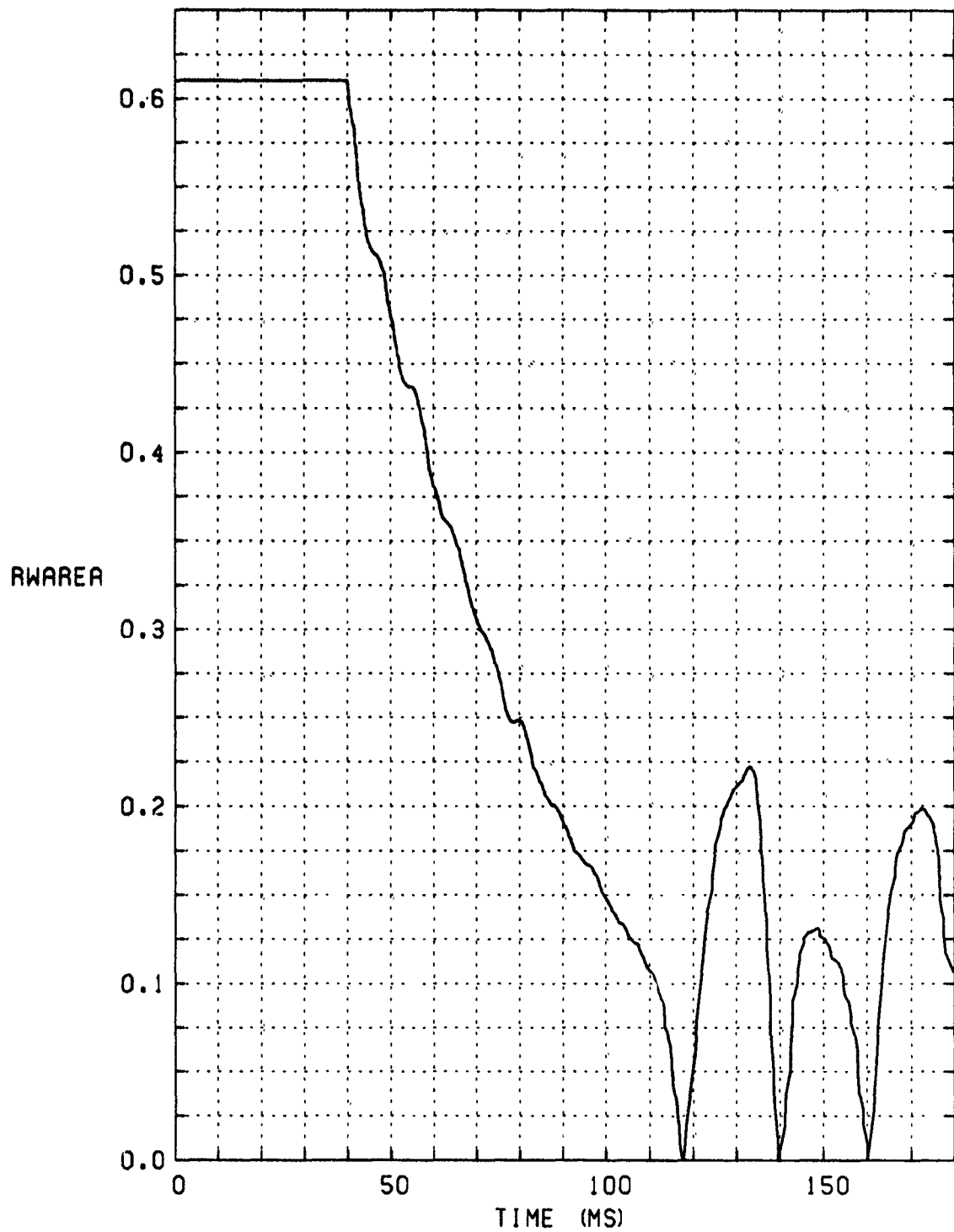


TIME HISTORIES
LOCATION: 17.599

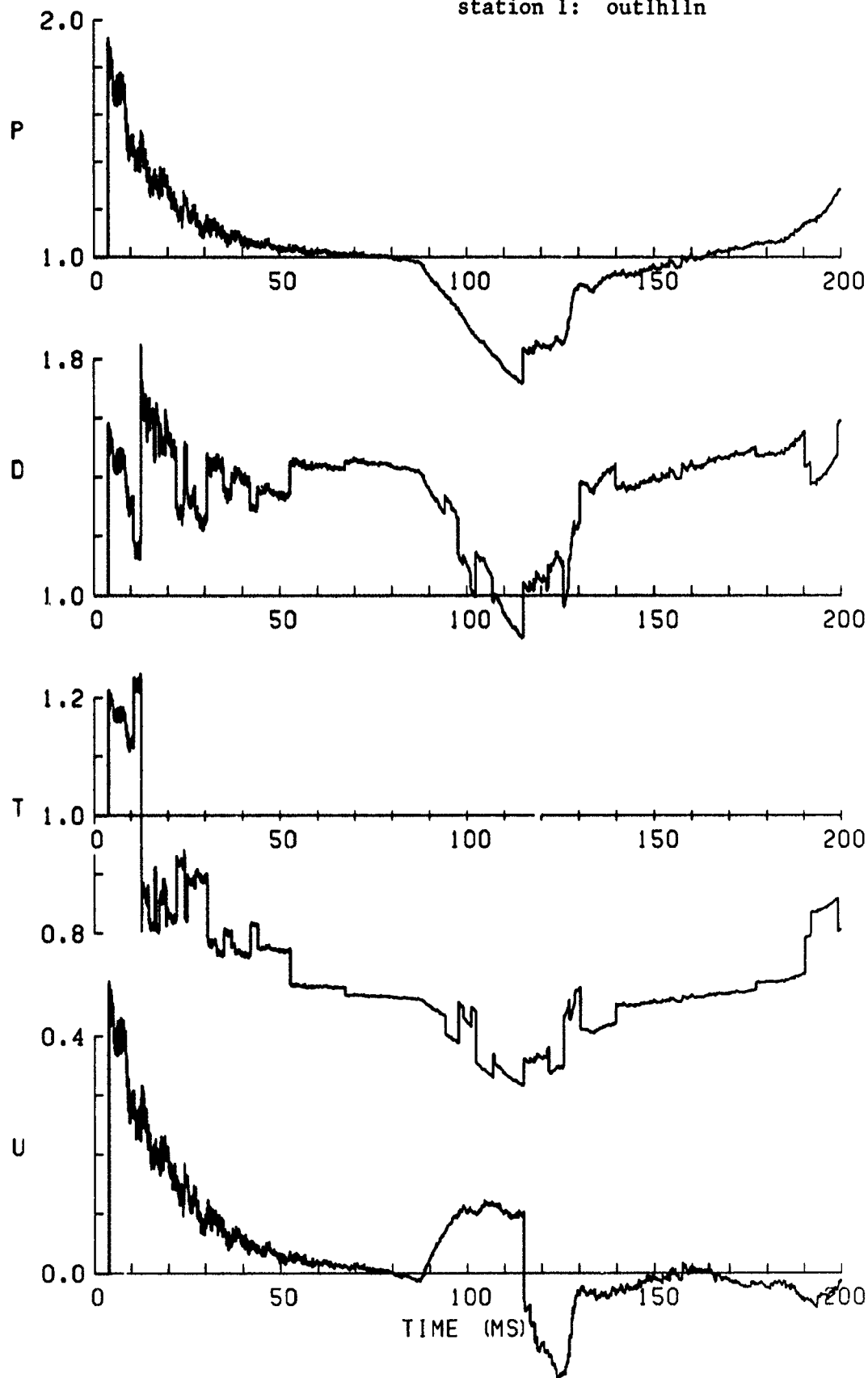
7 psig overpressure blast wave
RWE open-area-ratio setting
unfiltered
station 3: RWE7U



7 psig overpressure blast wave
RWE open-area-ratio setting
filtered
station 3: RWE7F

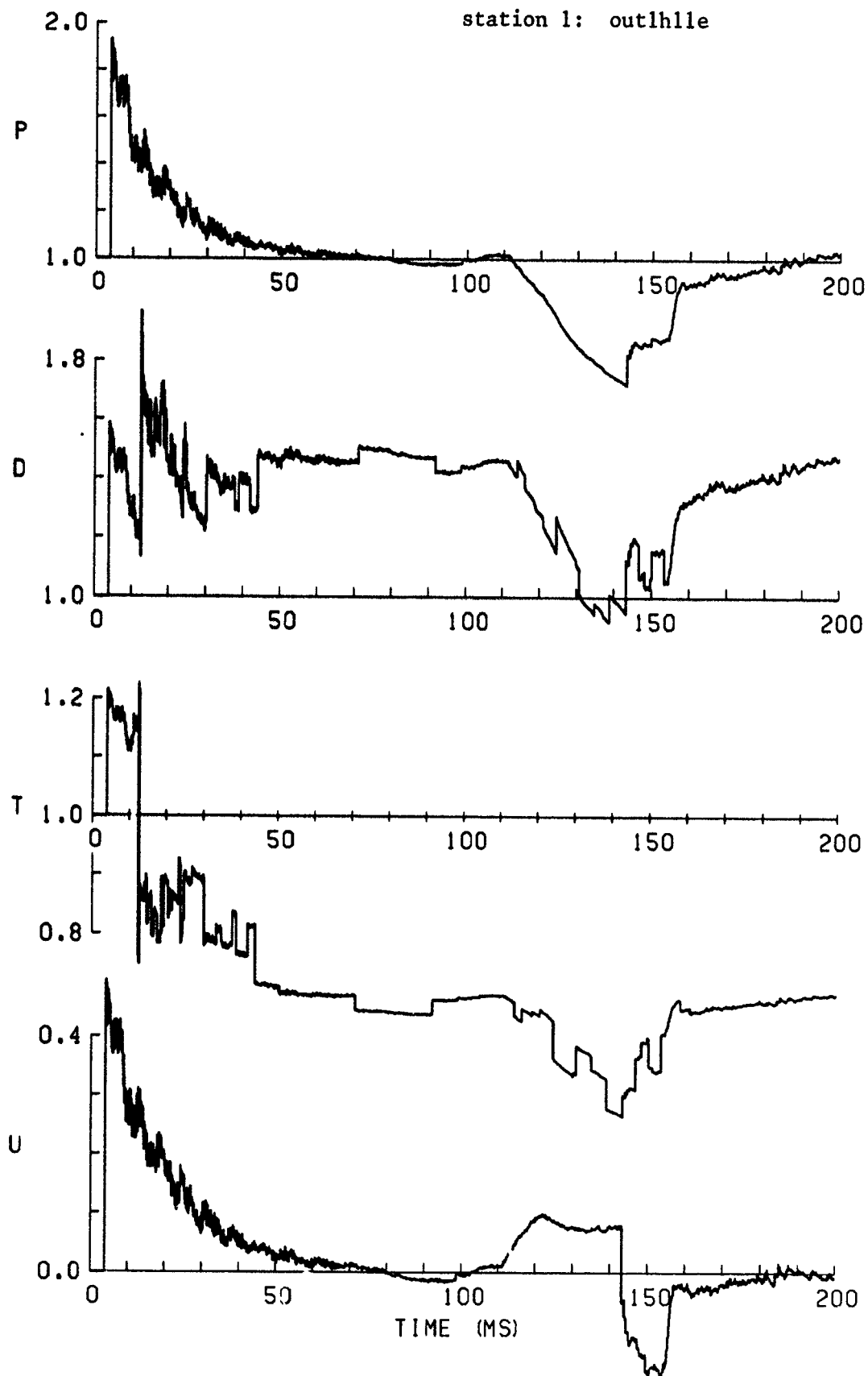


11 psig overpressure blast wave
normal length channel
no RWE
station 1: outlh1ln



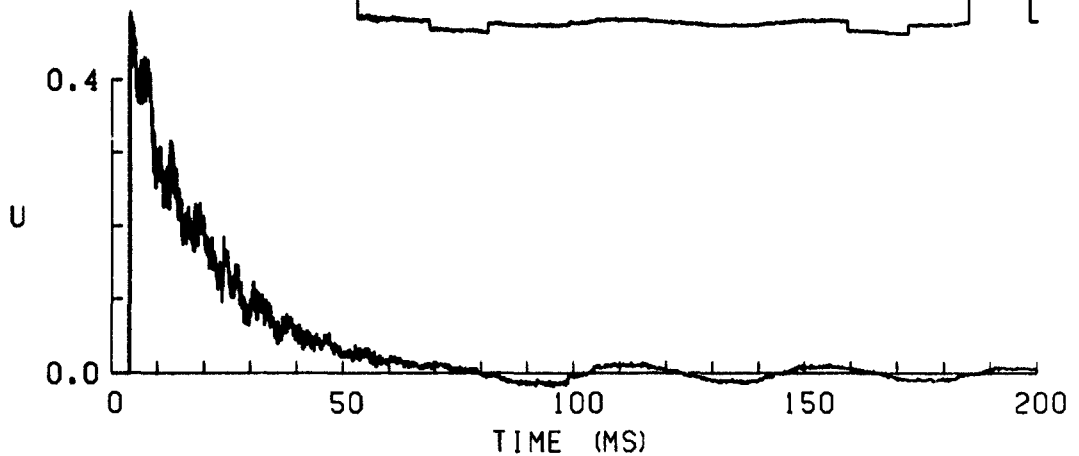
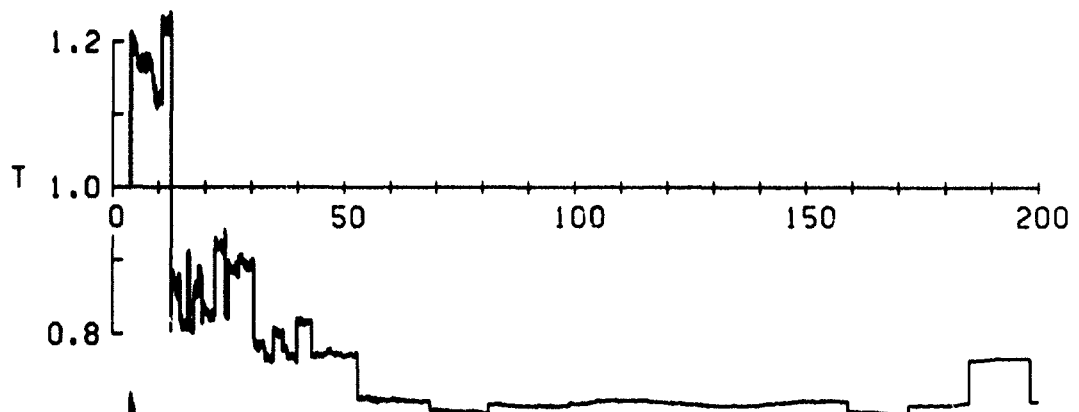
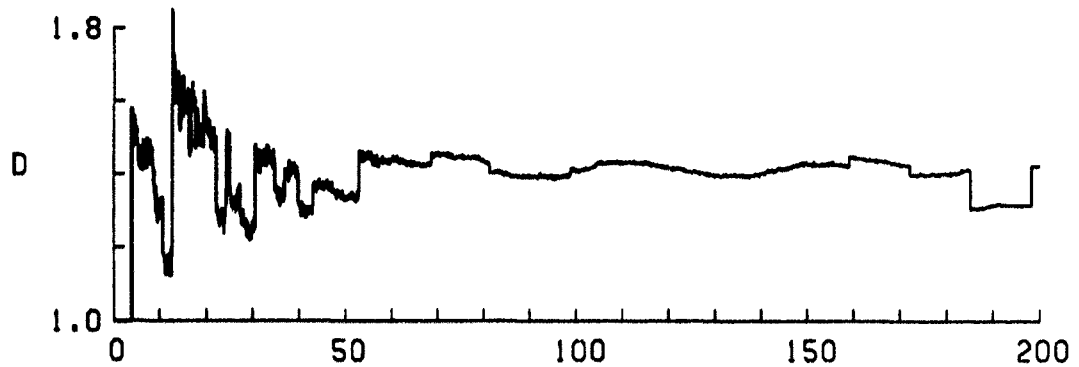
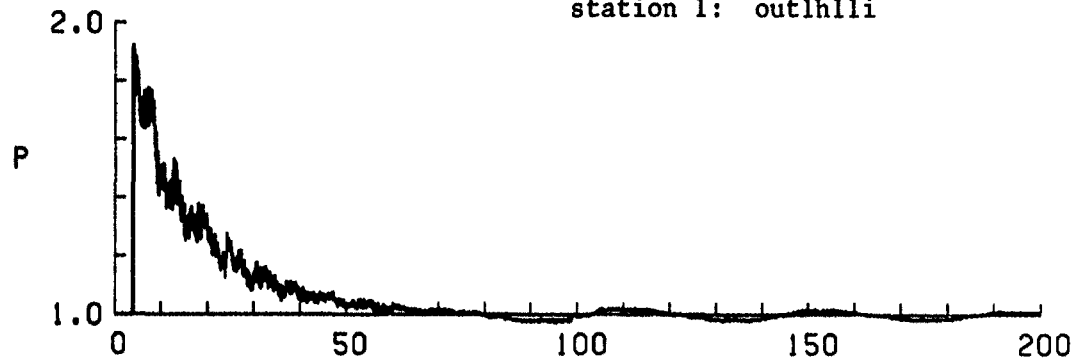
TIME HISTORIES
LOCATION: 2.302

11 psig overpressure blast wave
extended length channel
no RWE
station 1: outlhile



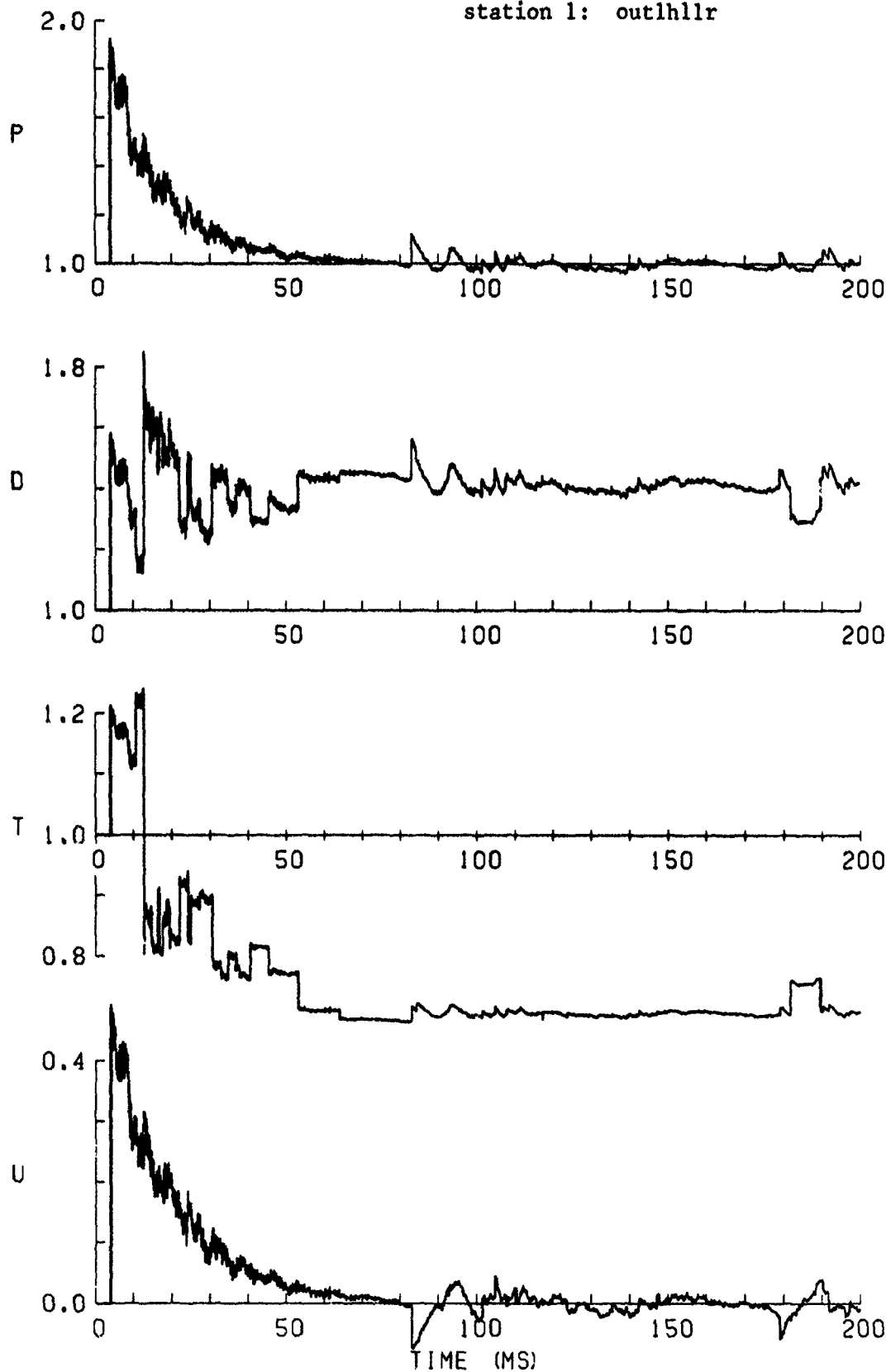
TIME HISTORIES
LOCATION: 2.289

11 psig overpressure blast wave
infinite length channel
no RWE
station 1: outlhlii



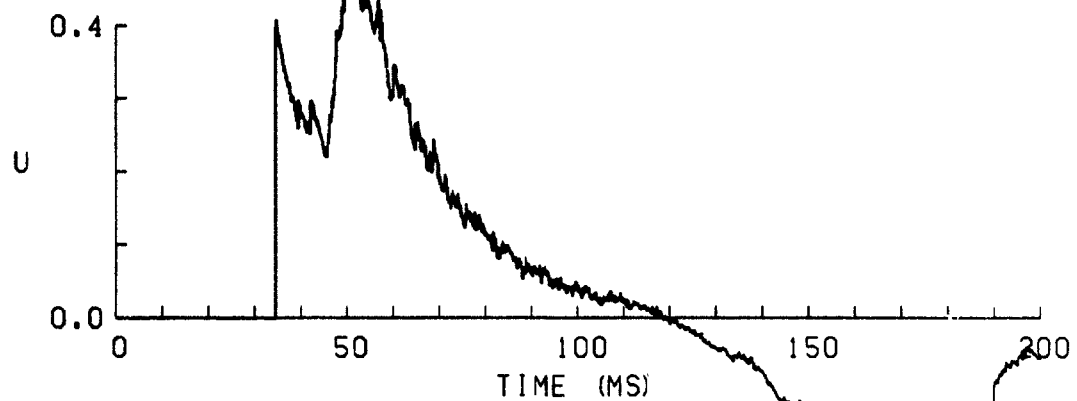
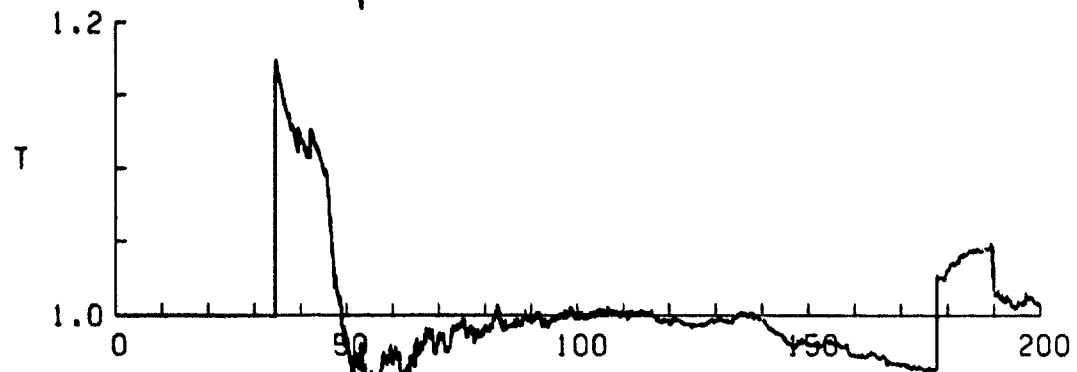
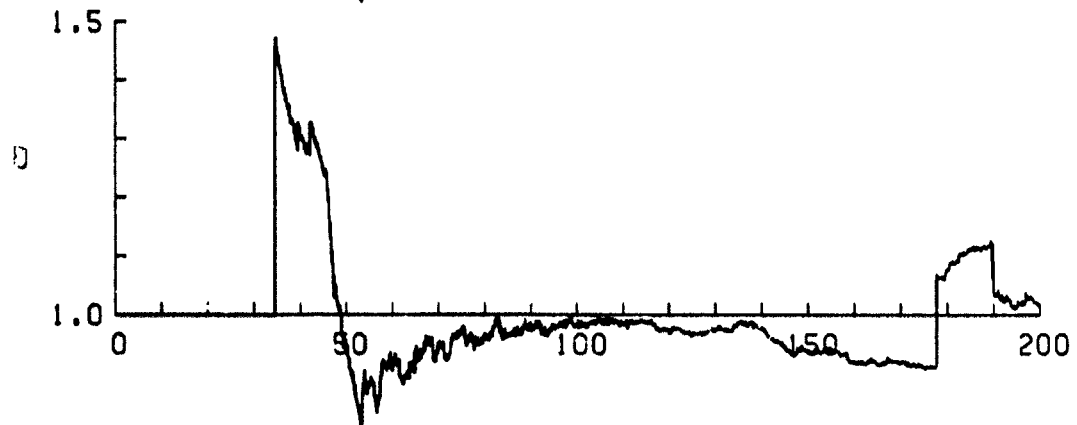
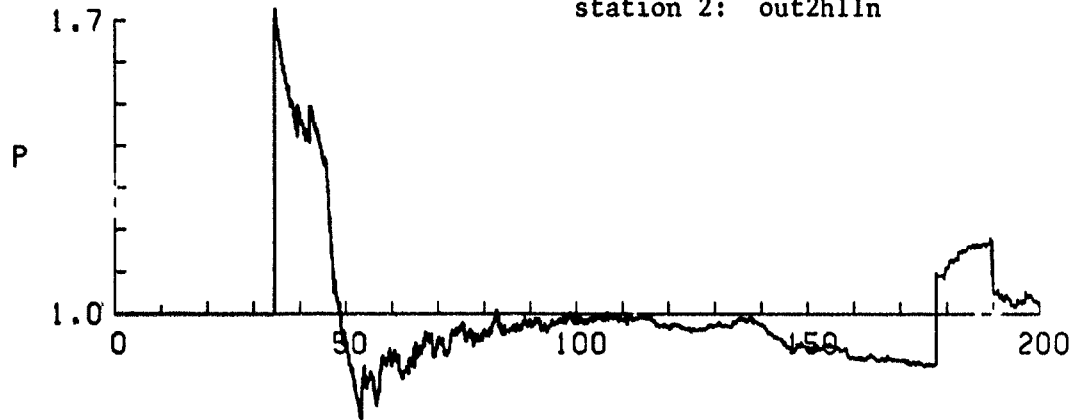
TIME HISTORIES
LOCATION: 2.302

11 psig overpressure blast wave
normal length channel
active RWE
station 1: out1hl1r



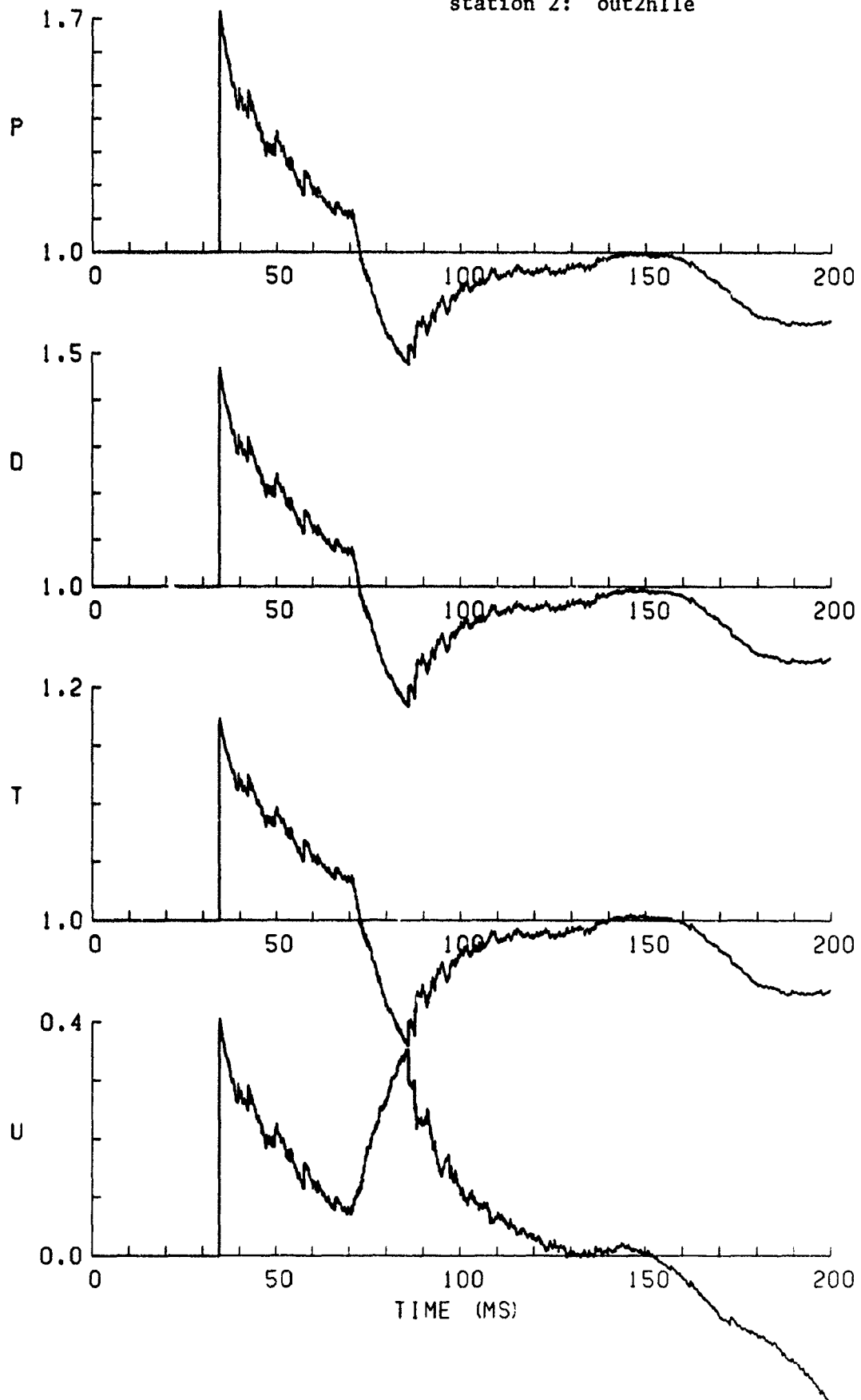
TIME HISTORIES
LOCATION: 2.302

11 psig overpressure blast wave
normal length channel
RWE
station 2: out2h11n



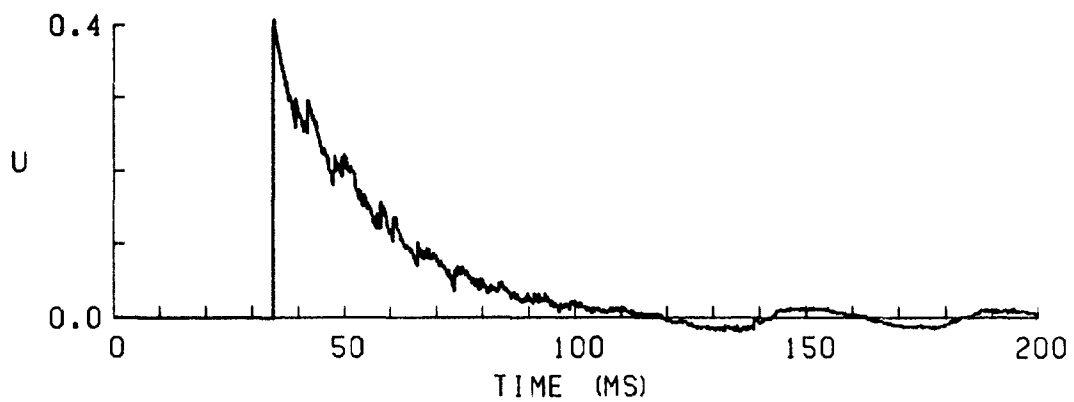
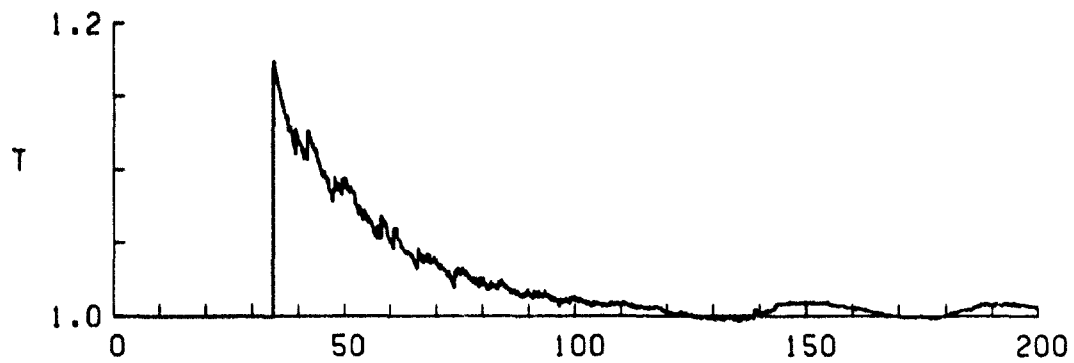
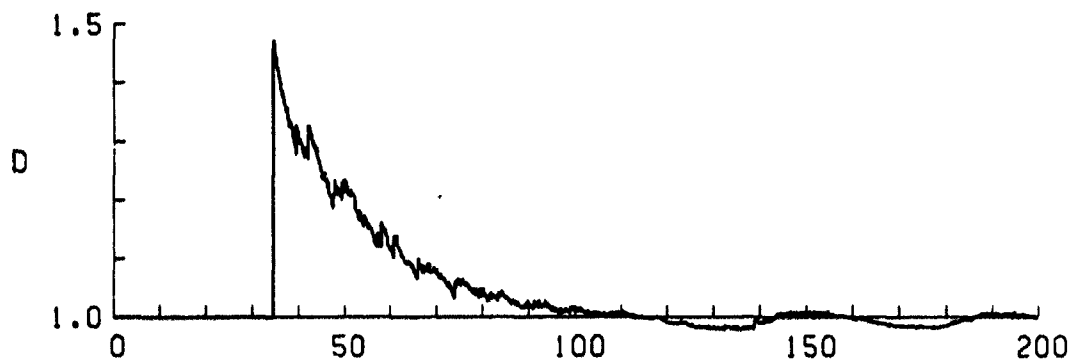
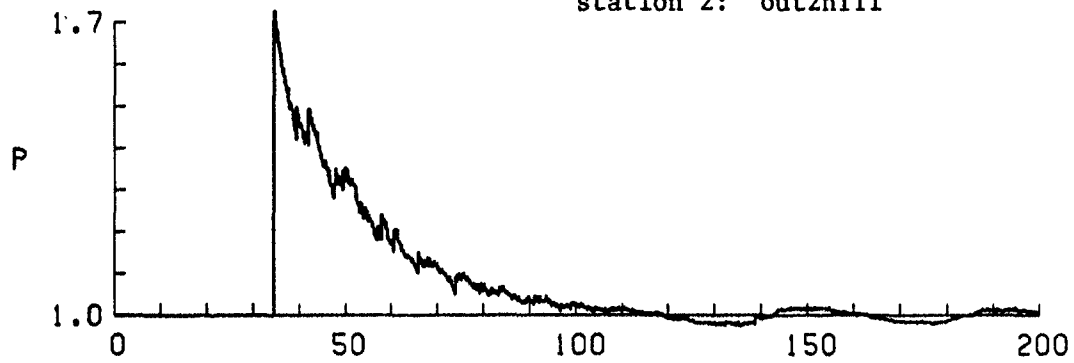
TIME HISTORIES
LOCATION: 15.916

11 psig overpressure blast wave
extended length channel
no RWE
station 2: out2h1le



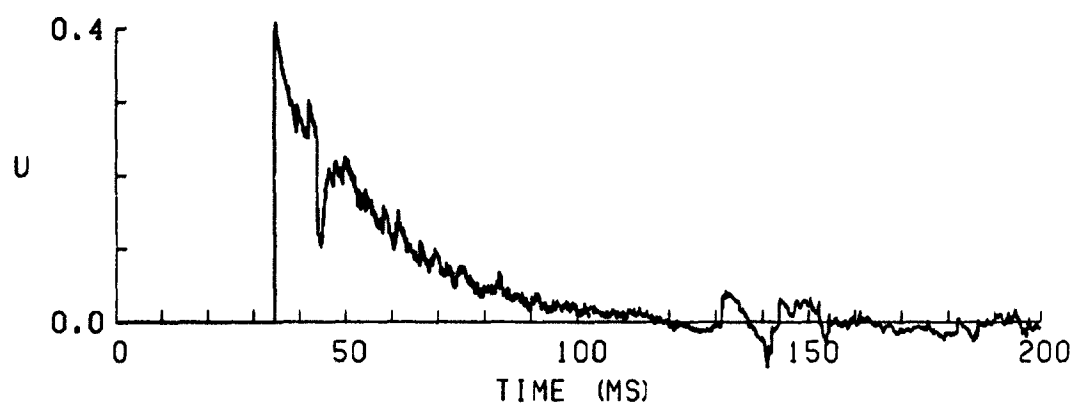
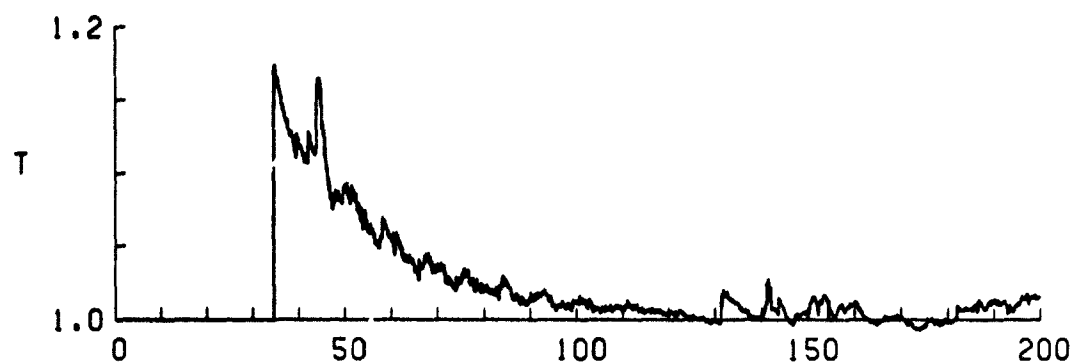
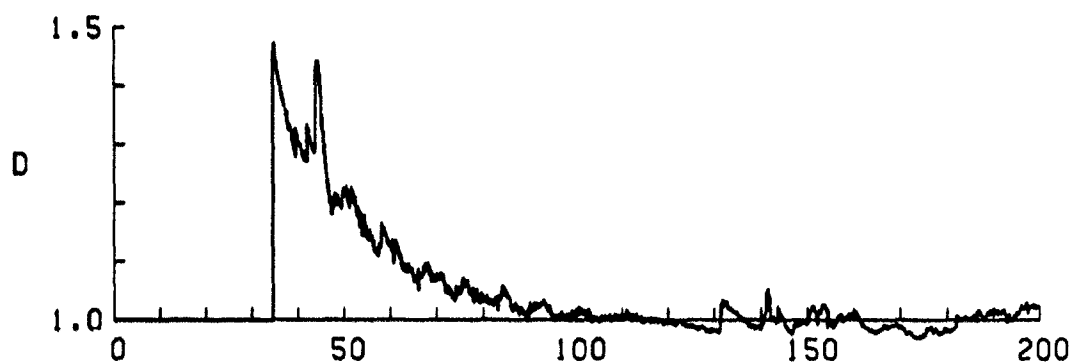
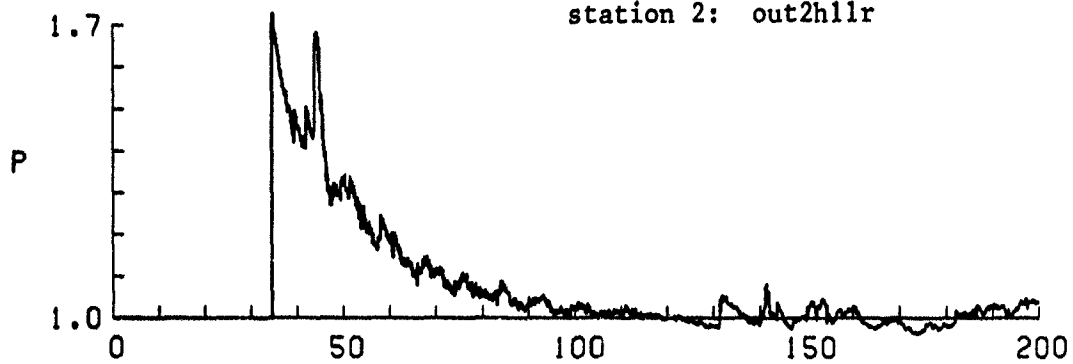
TIME HISTORIES
LOCATION: 15.904

11 psig overpressure blast wave
infinite length channel
no RWE
station 2: out2h1li



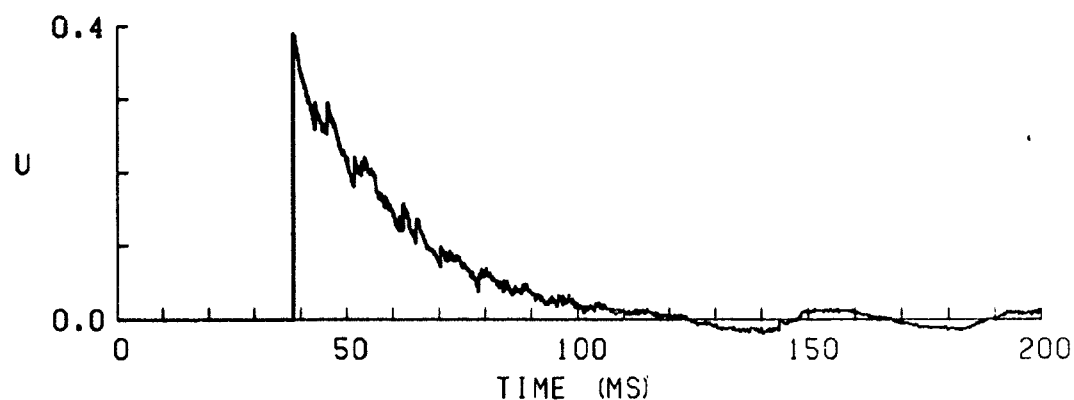
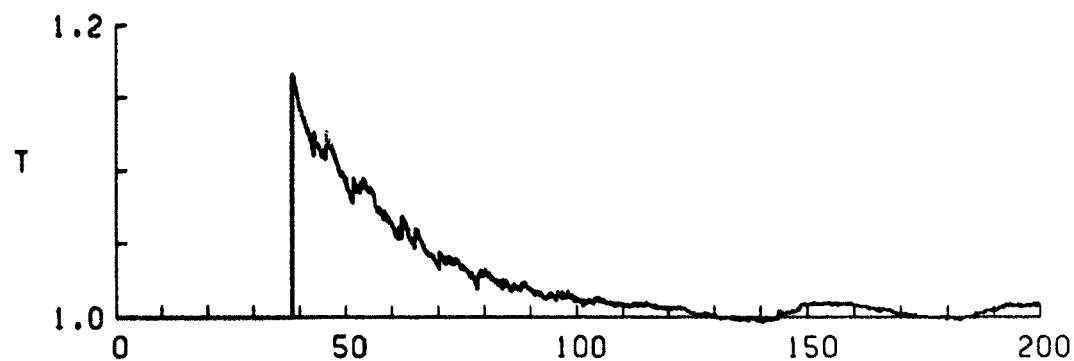
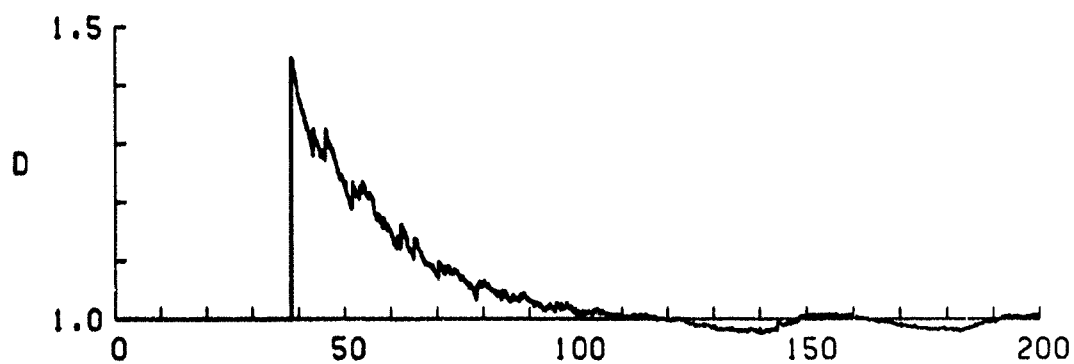
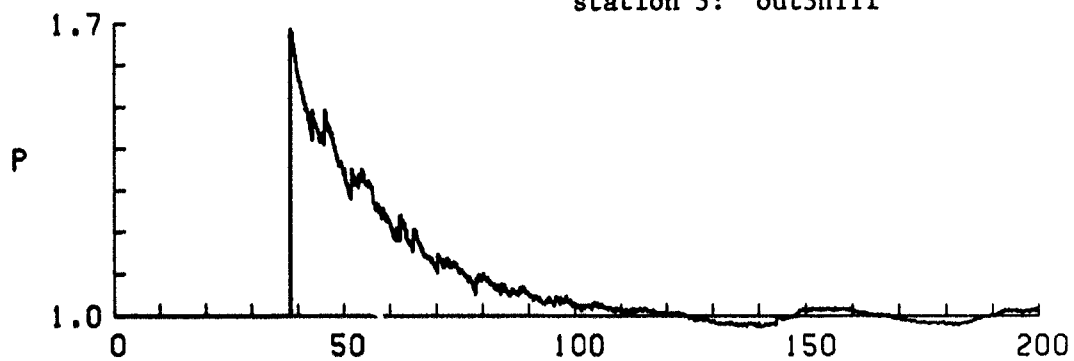
TIME HISTORIES
LOCATION: 15.916

11 psig overpressure blast wave
normal length driver
active RWE
station 2: out2h1lr



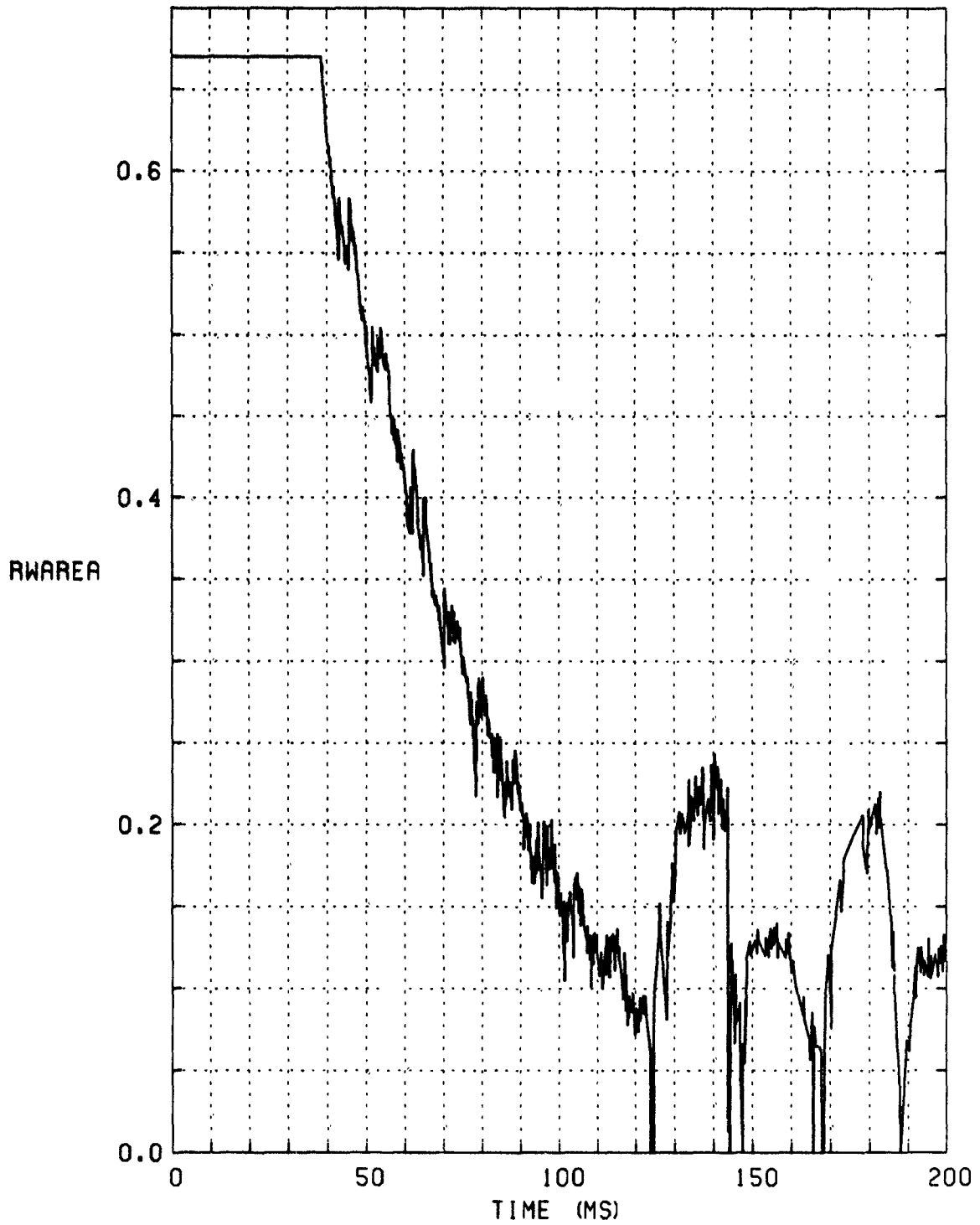
TIME HISTORIES
LOCATION: 15.916

11 psig overpressure blast wave
infinite length channel
no RWE
station 3: out3h11i

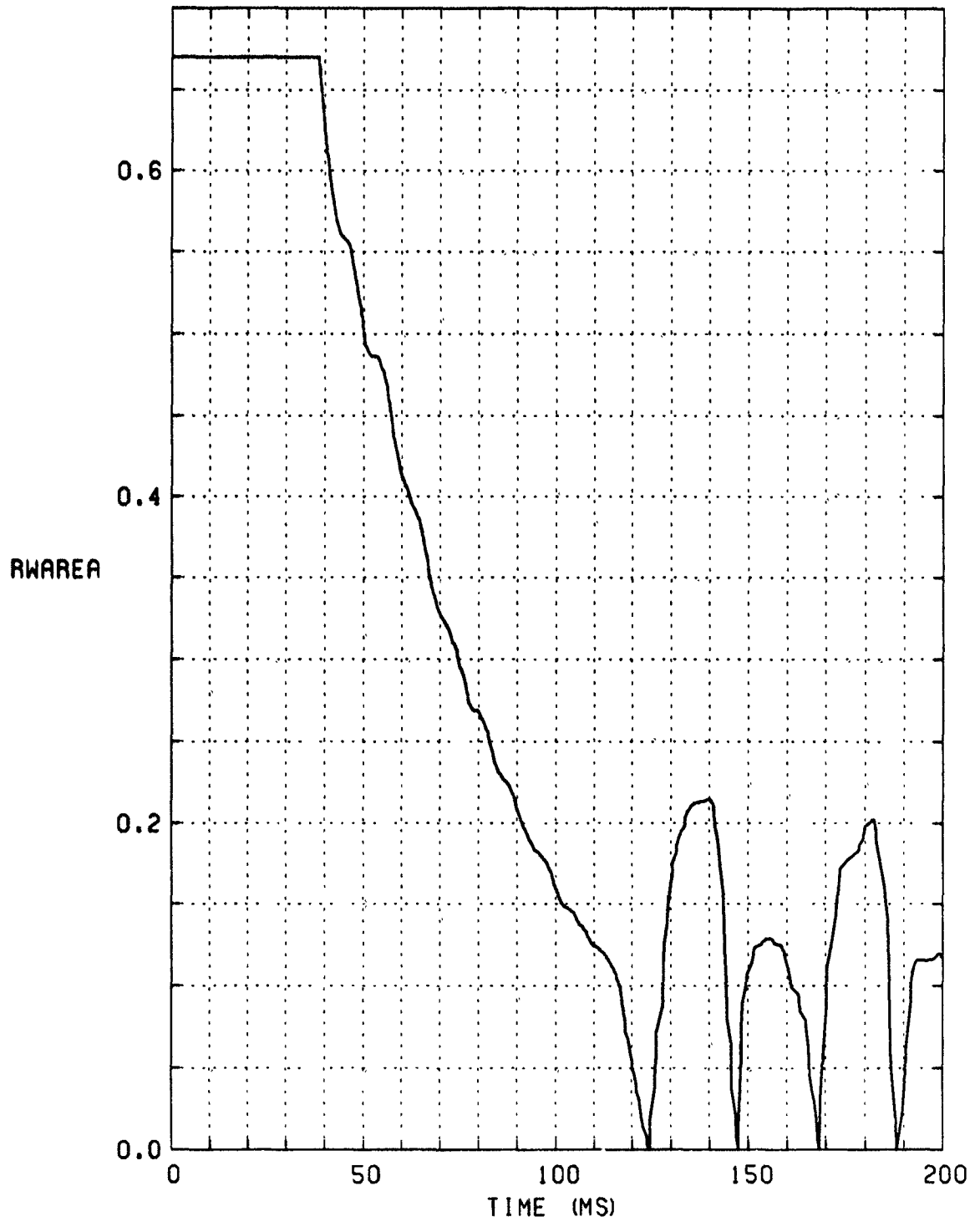


TIME HISTORIES
LOCATION: 17.599

11 psig overpressure blast wave
RWE open-area-ratio setting
unfiltered
station 3: RWE11U



11 psig overpressure blast wave
RWE open-area-ratio setting
filtered
station 3: RWE11F



INTENTIONALLY LEFT BLANK.

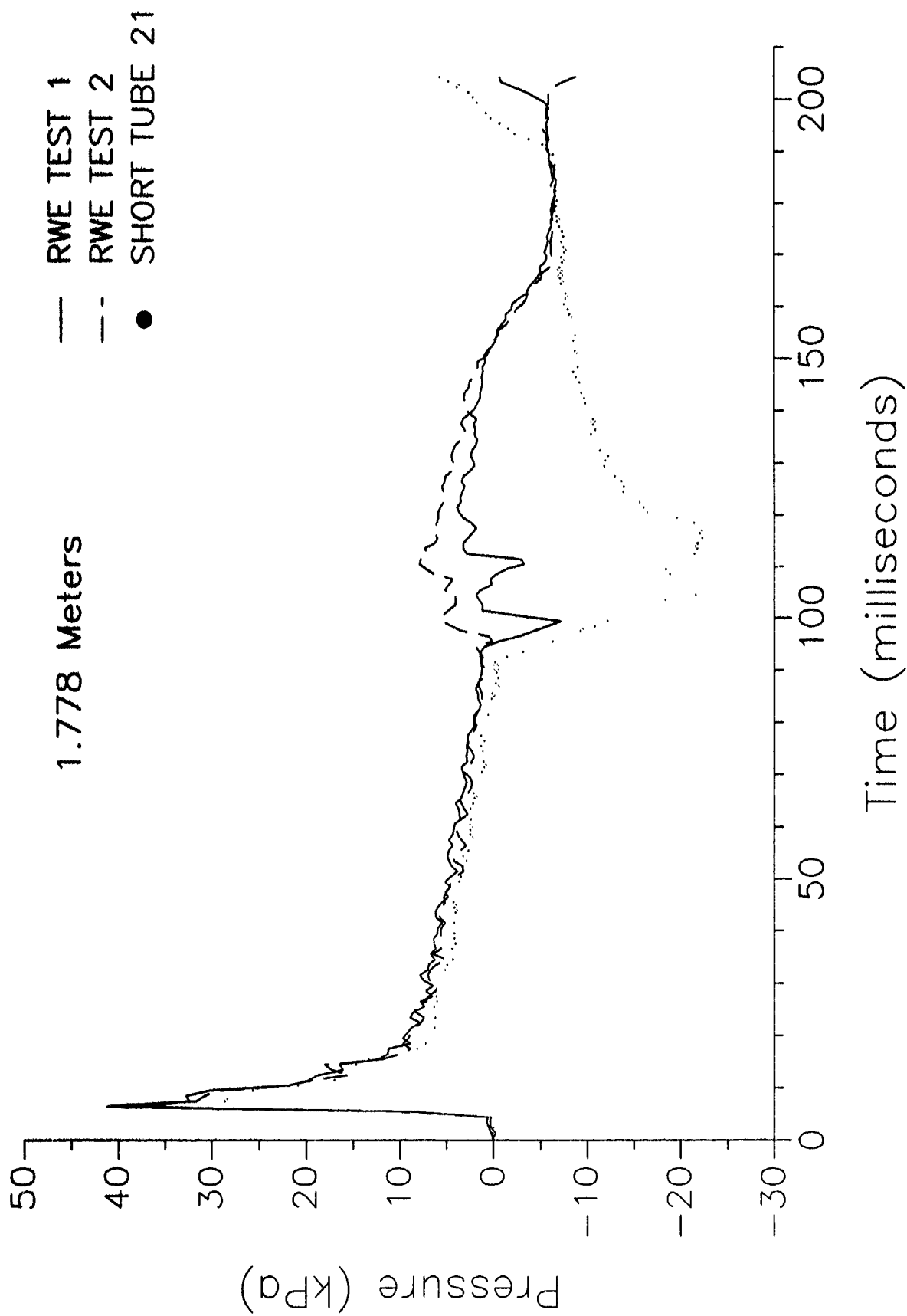
APPENDIX C

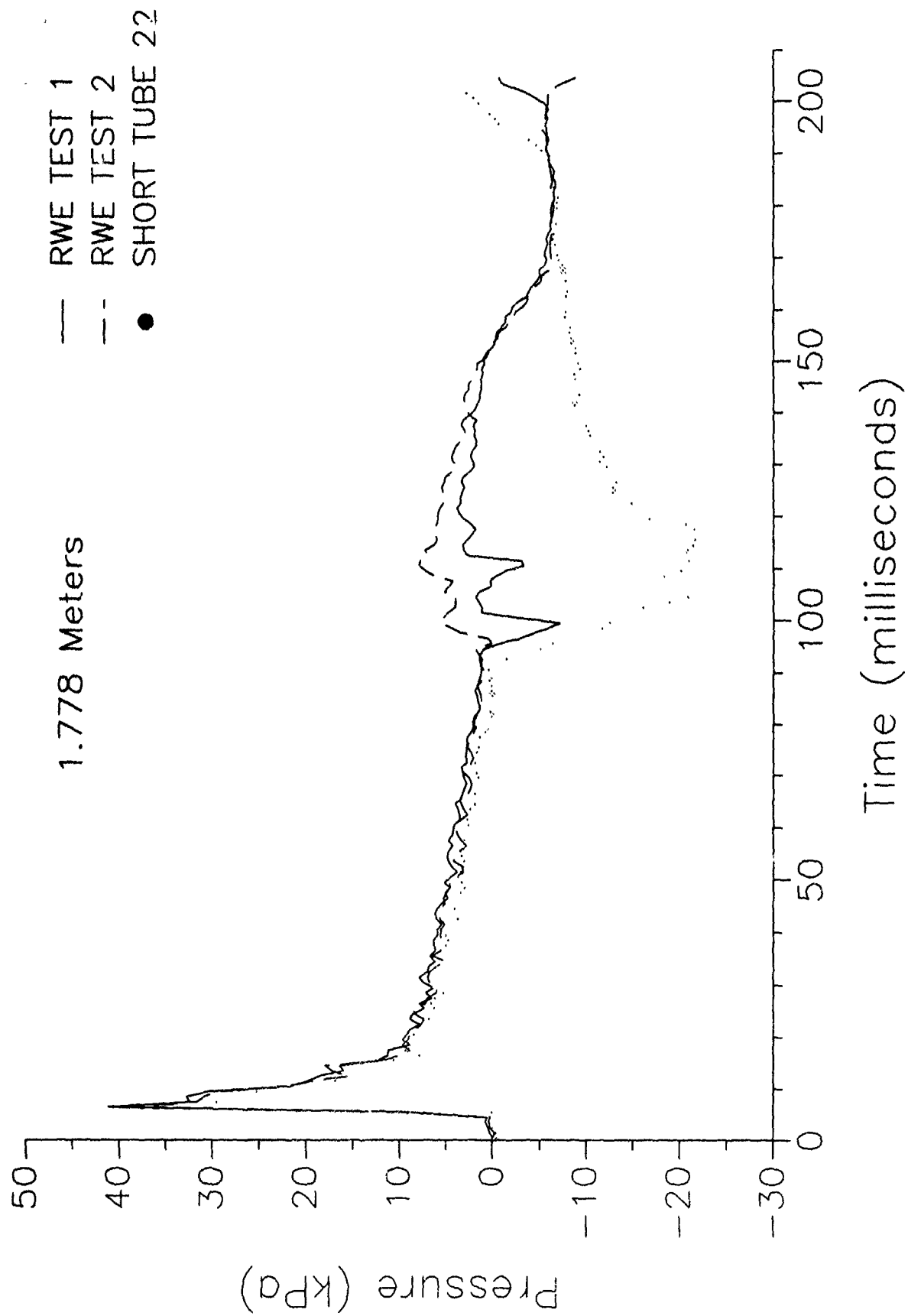
COMPARATIVE TEST RESULTS FROM SHOCK TUBE CALIBRATION AND RWE TESTS

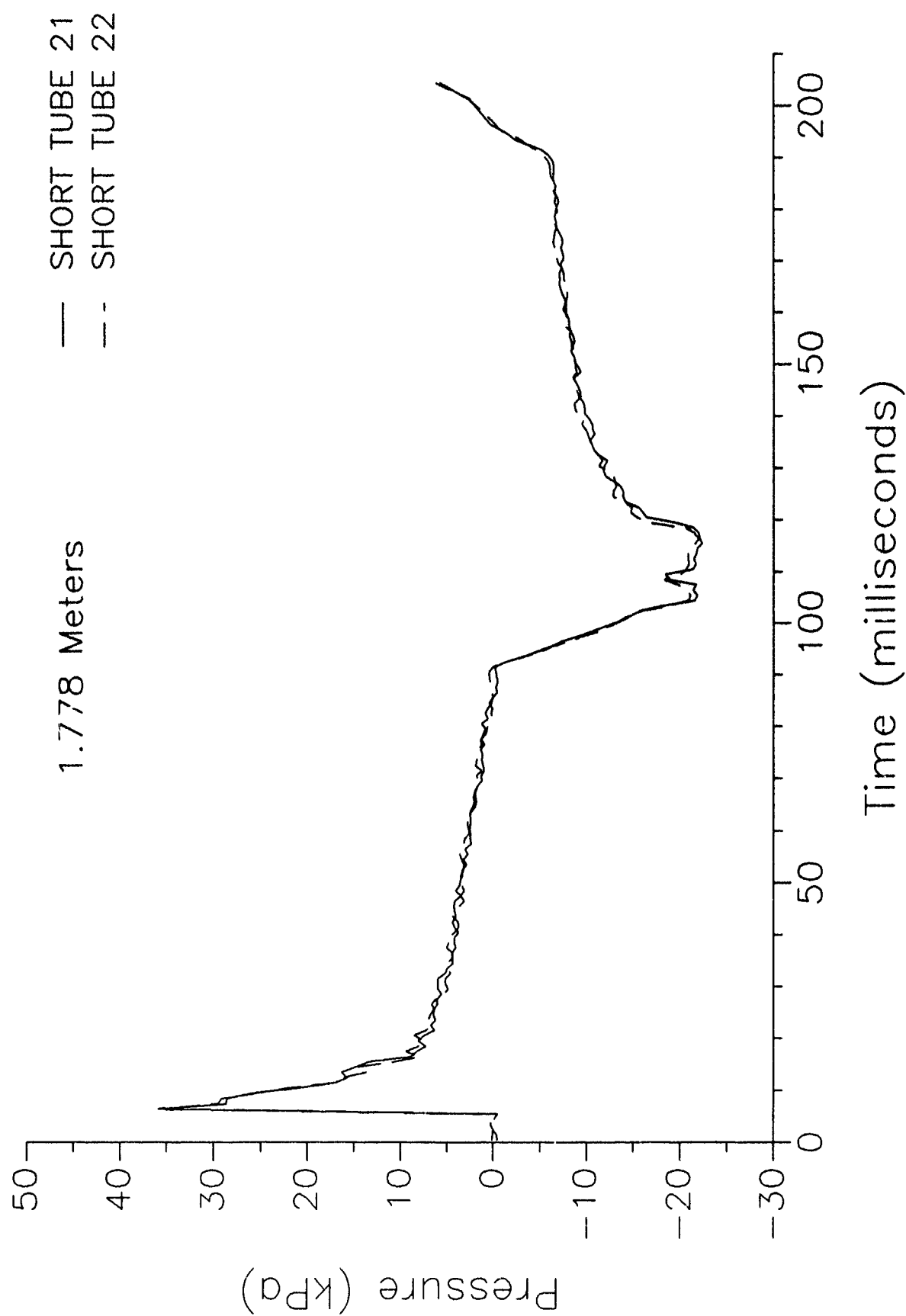
INTENTIONALLY LEFT BLANK.

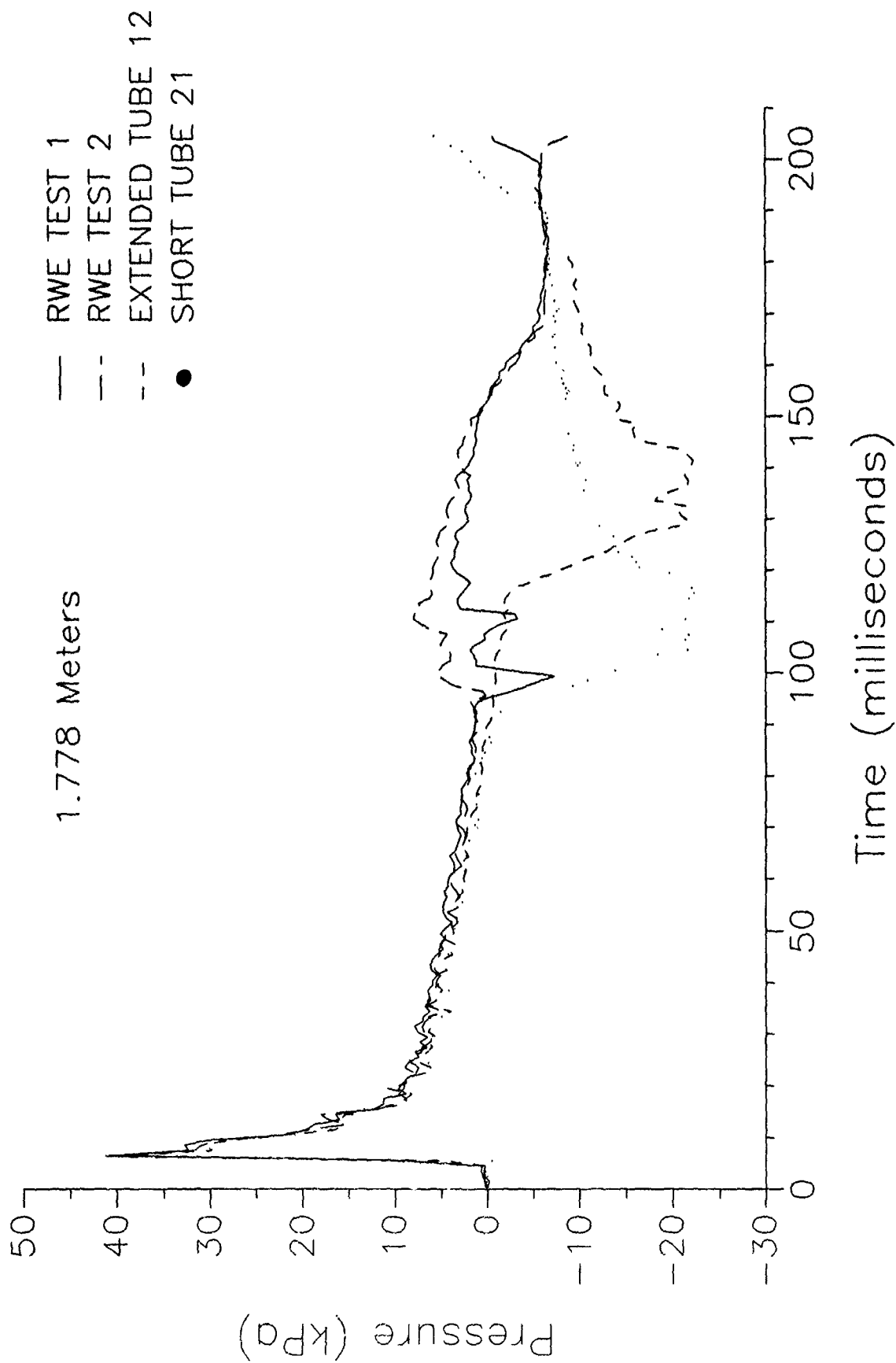
RESULTS FROM 34.5 kPa TESTS

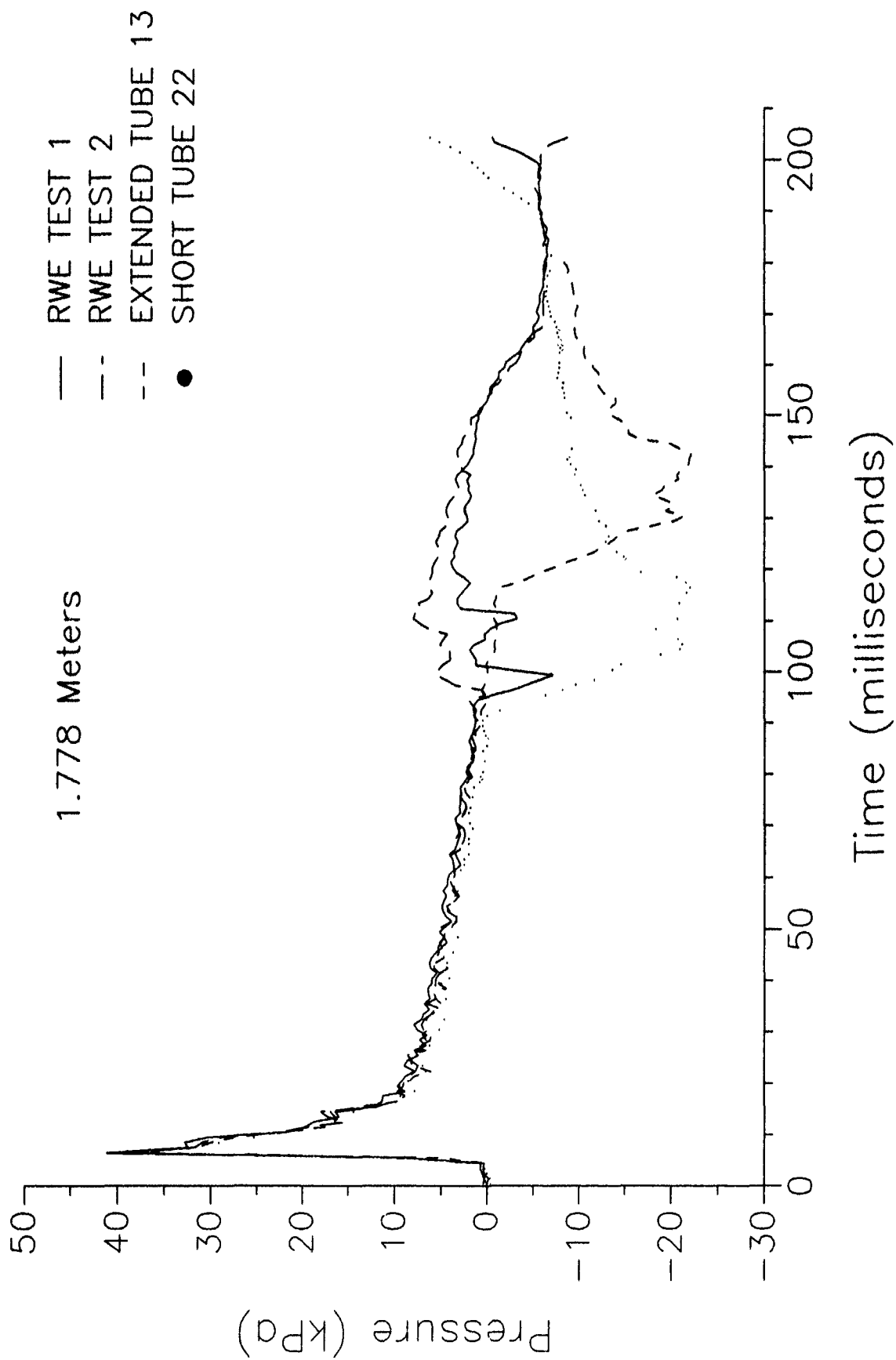
INTENTIONALLY LEFT BLANK.

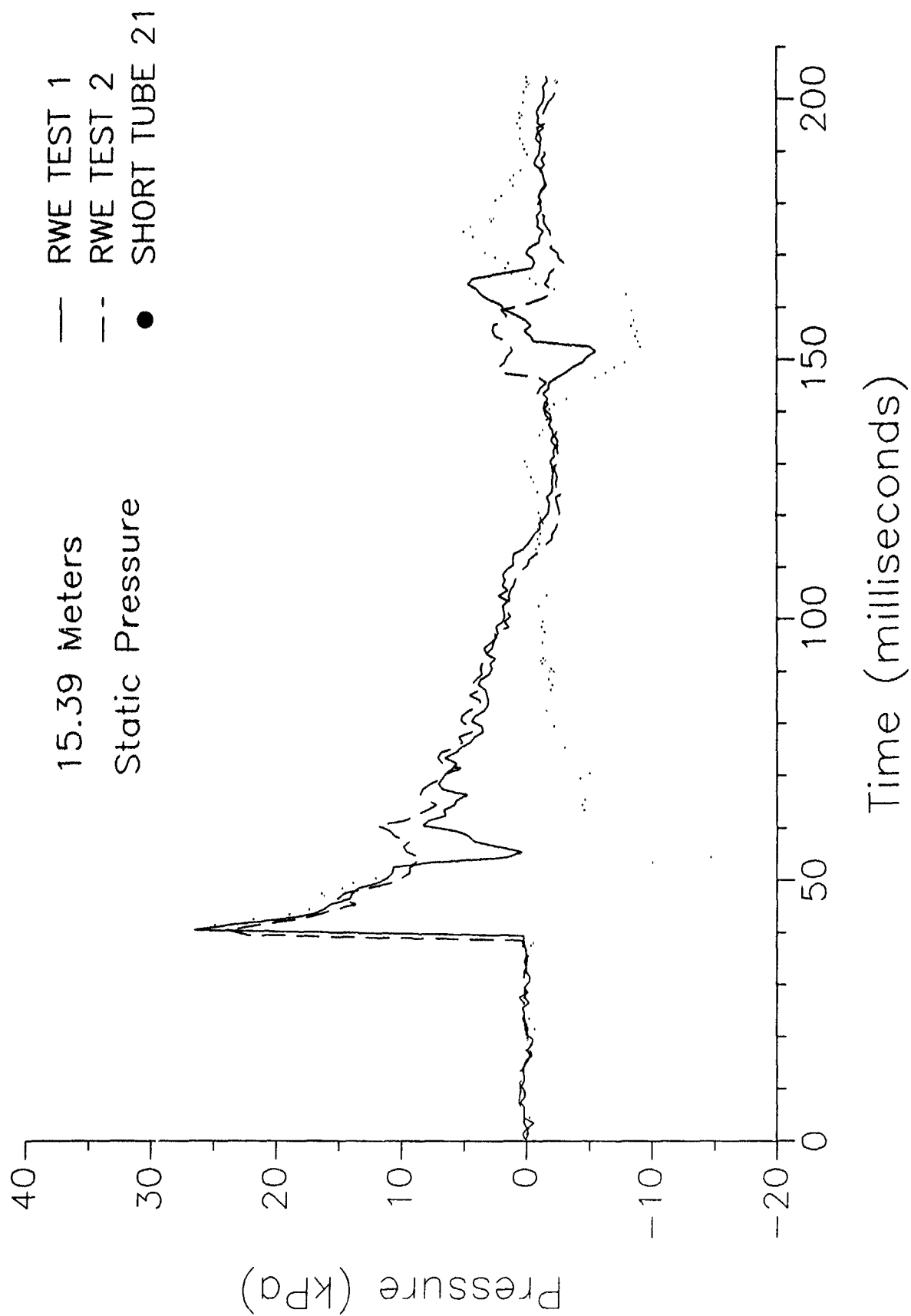


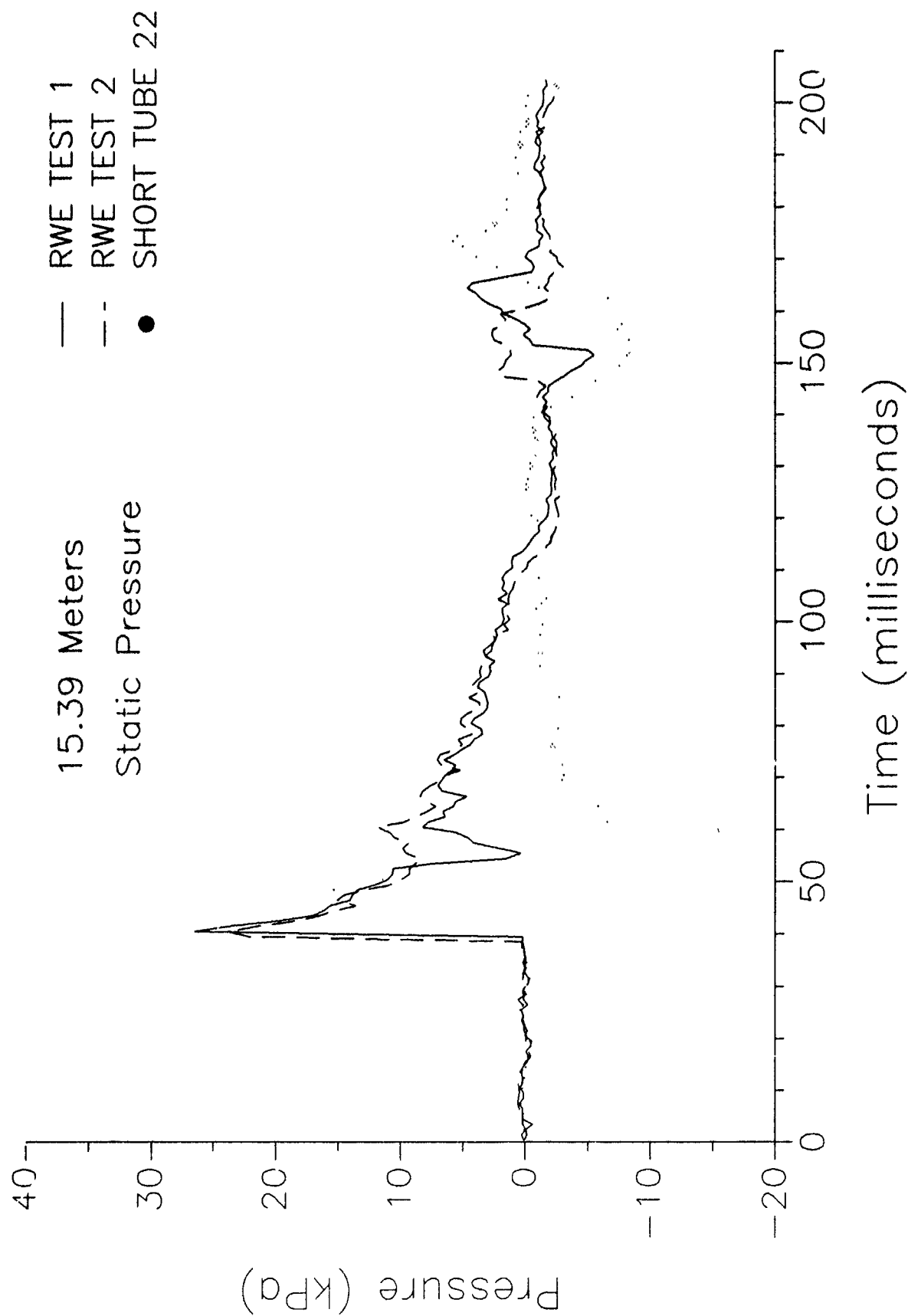


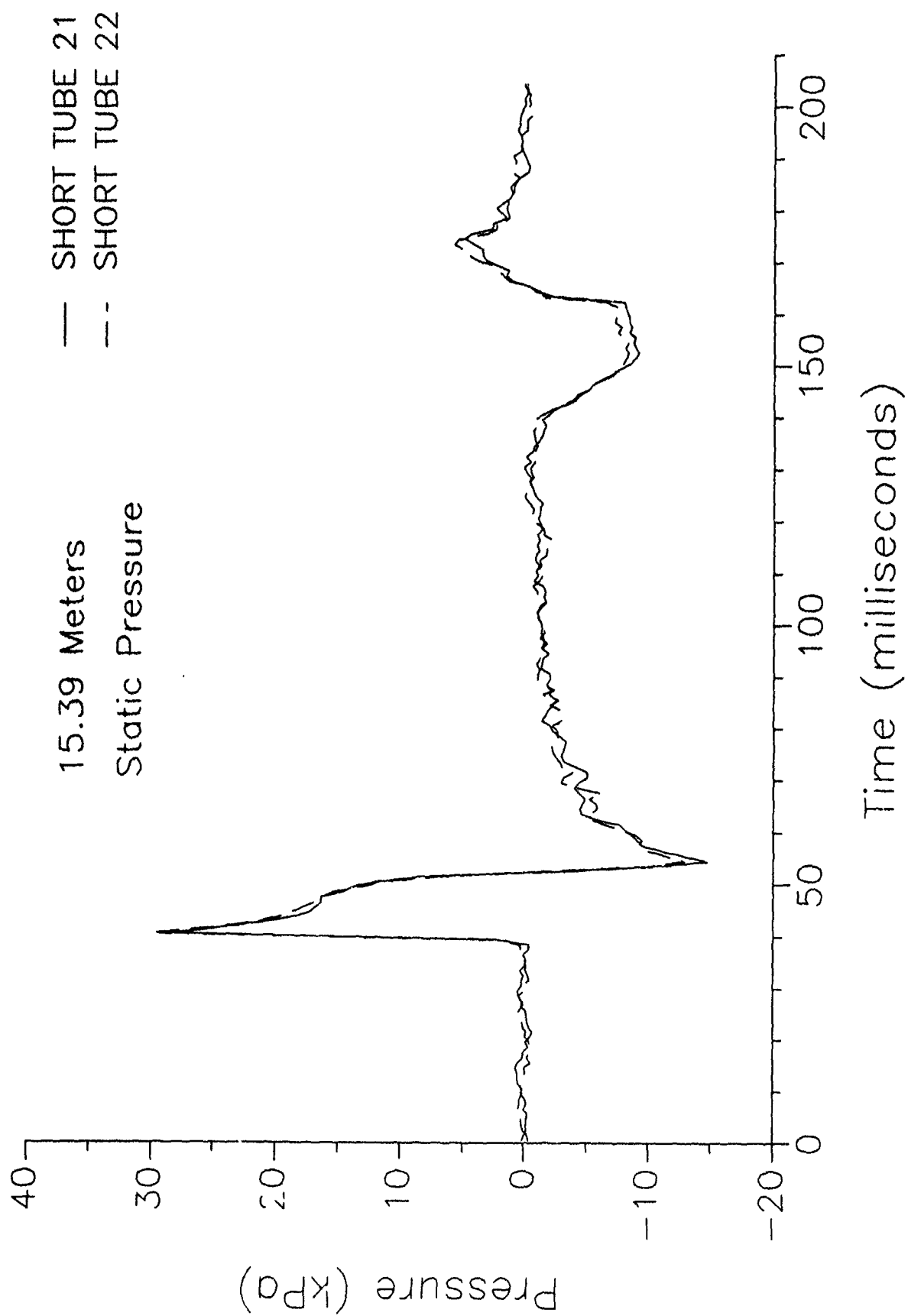


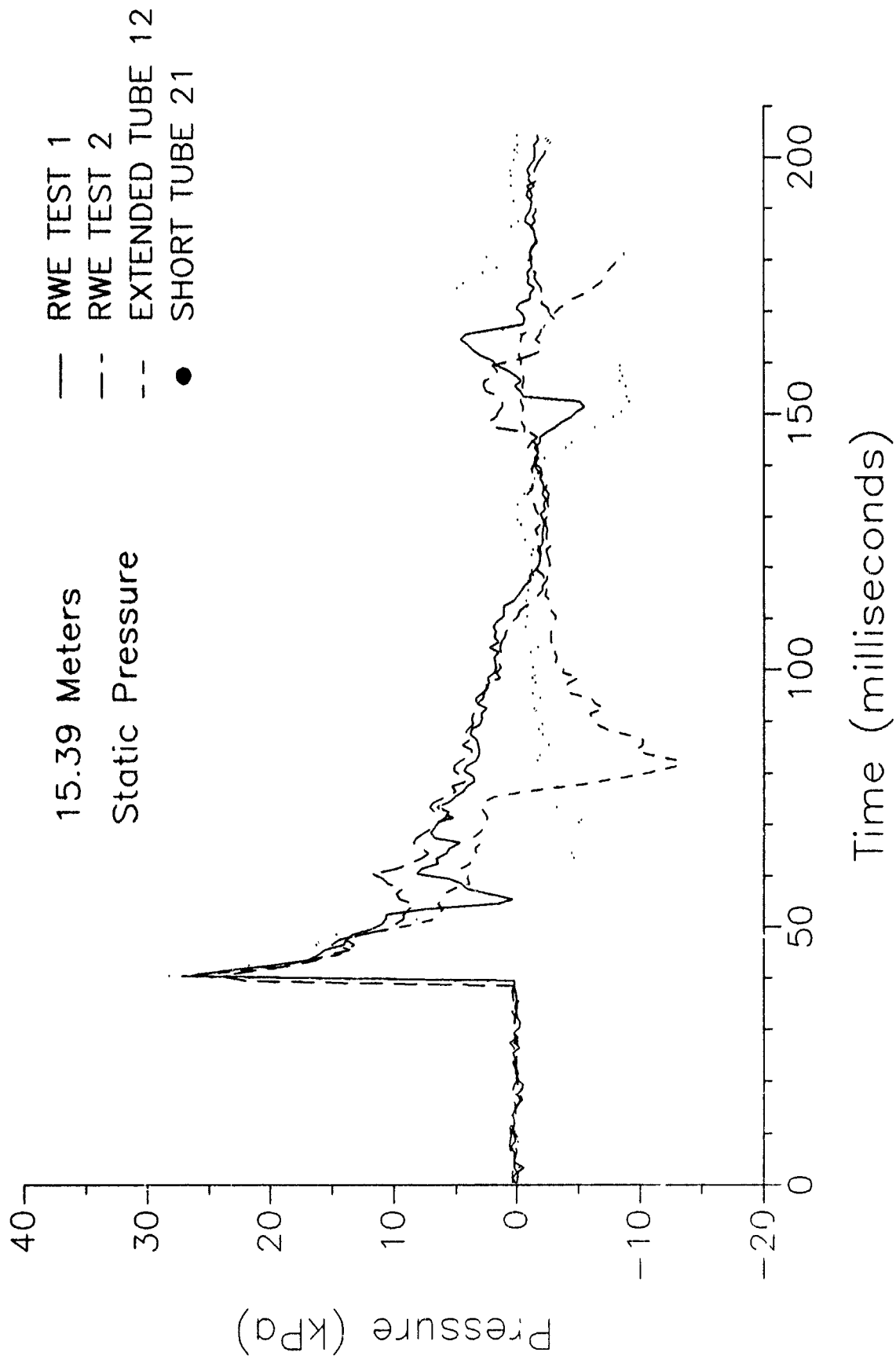


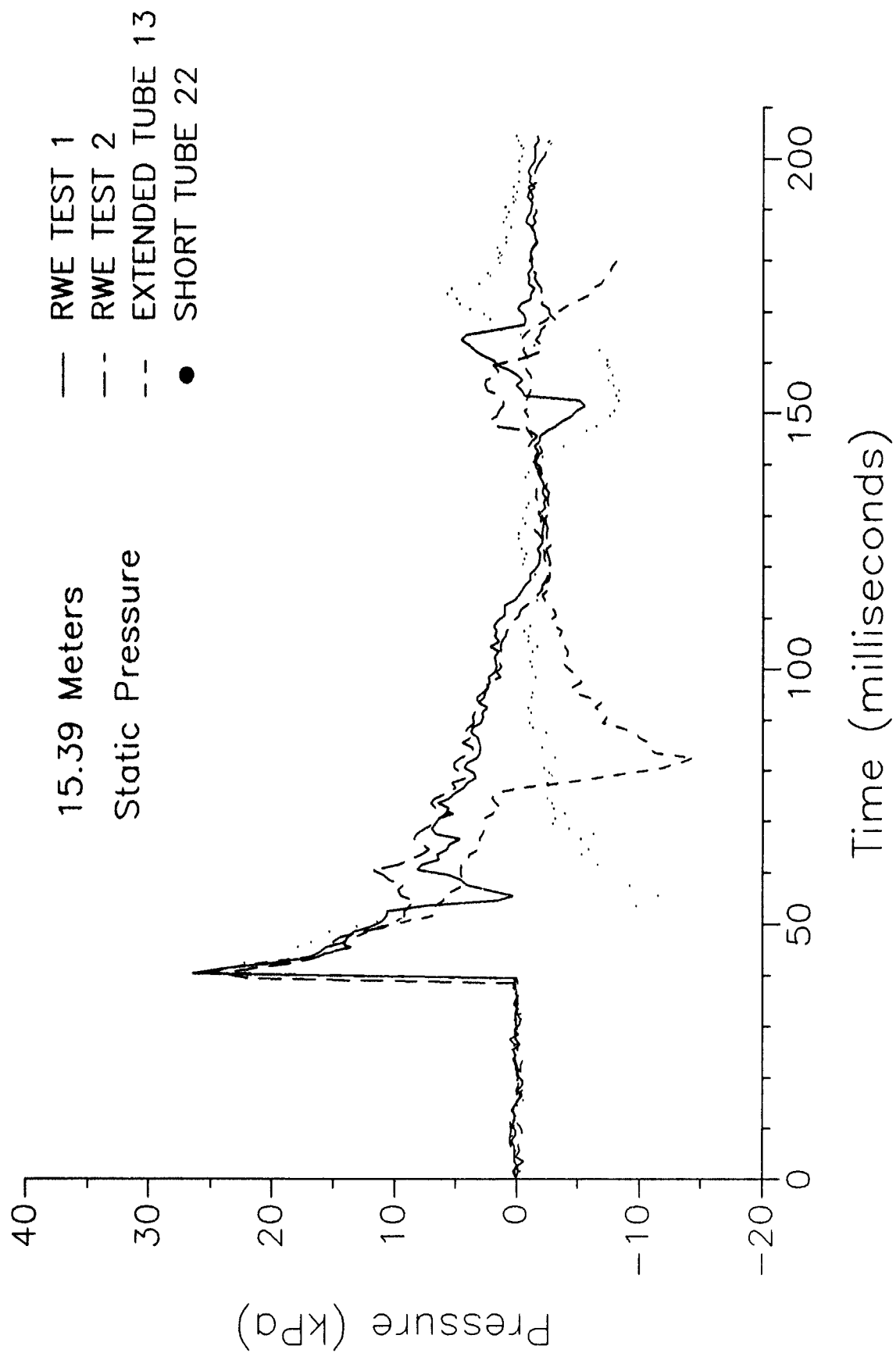


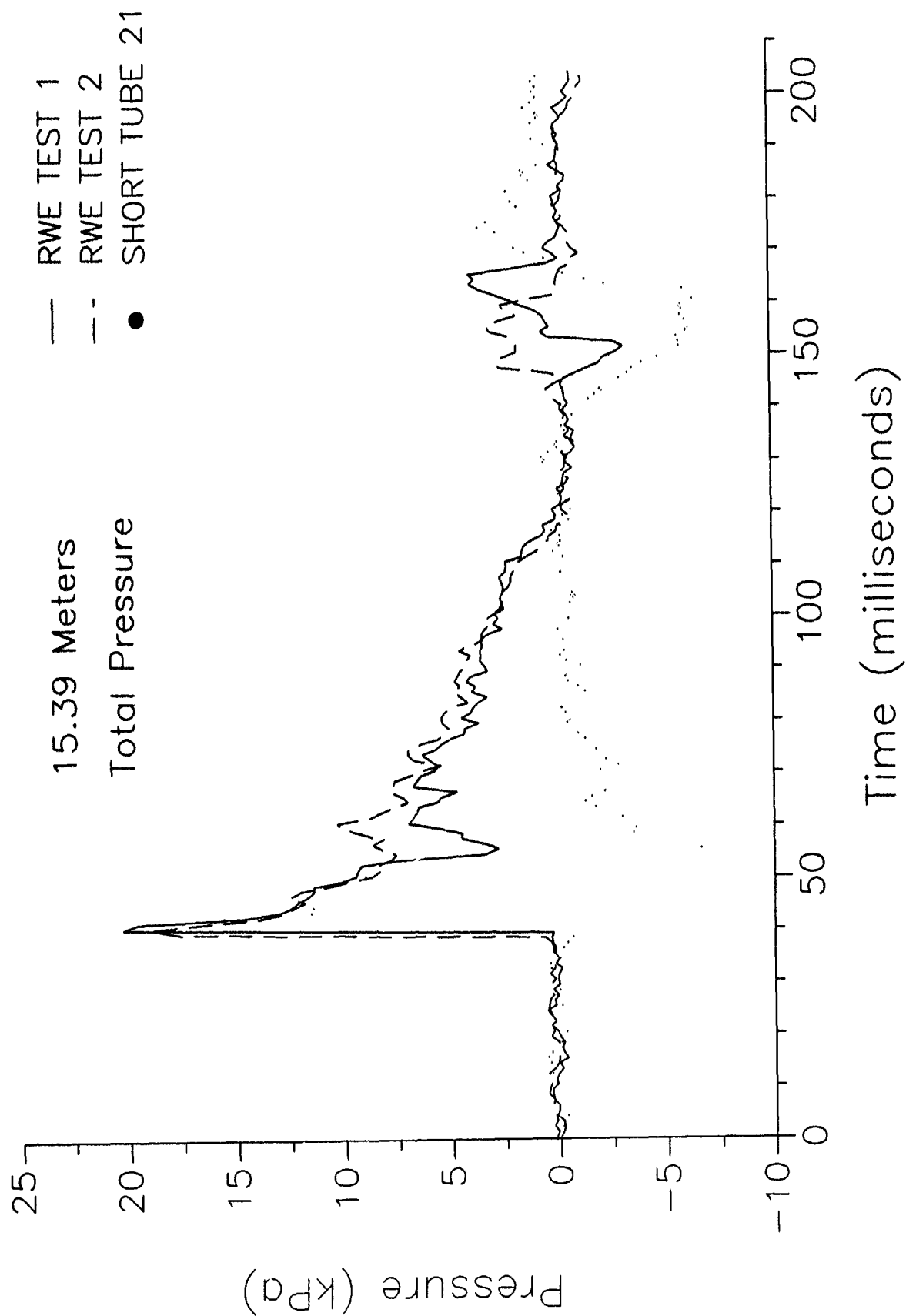


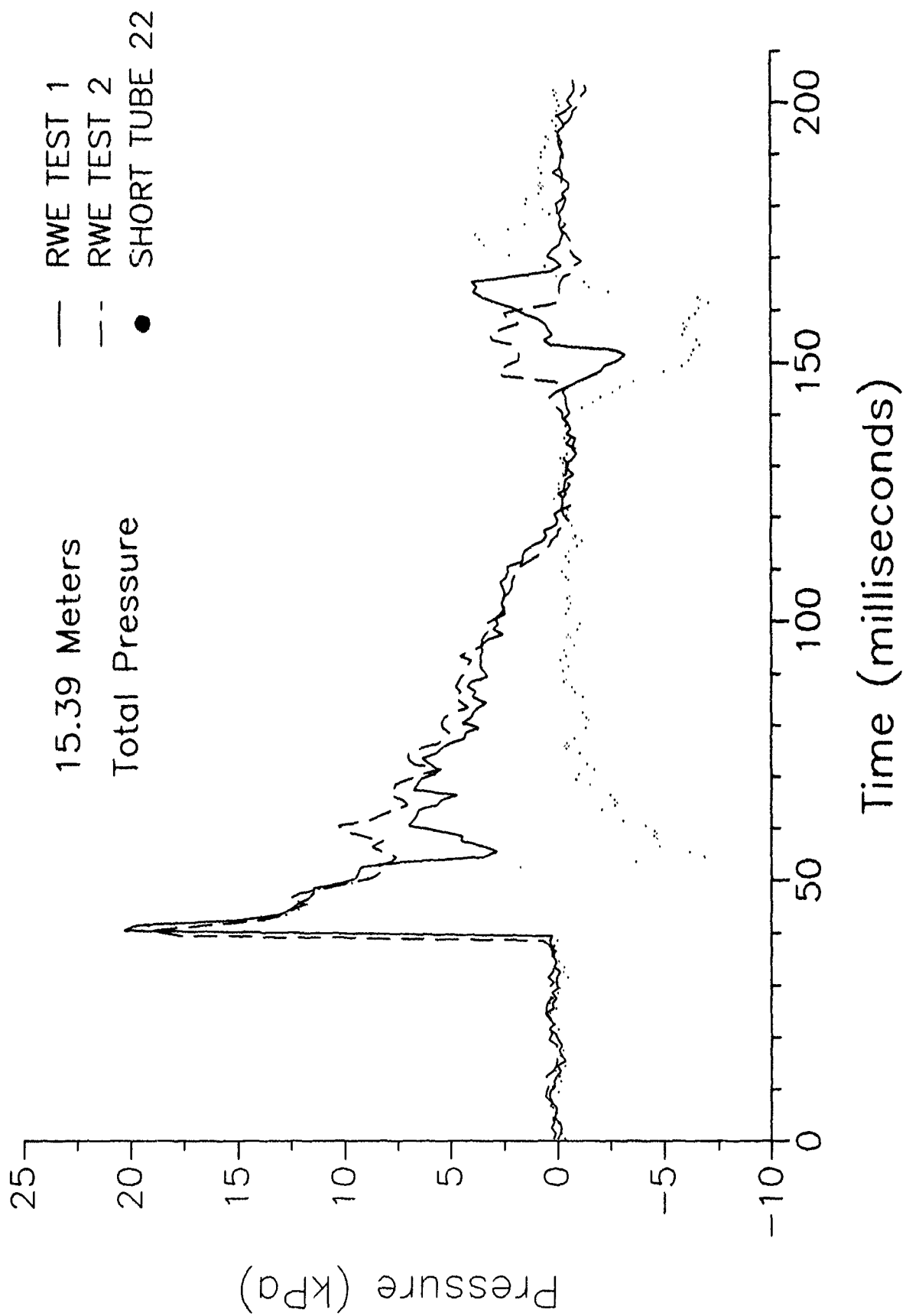


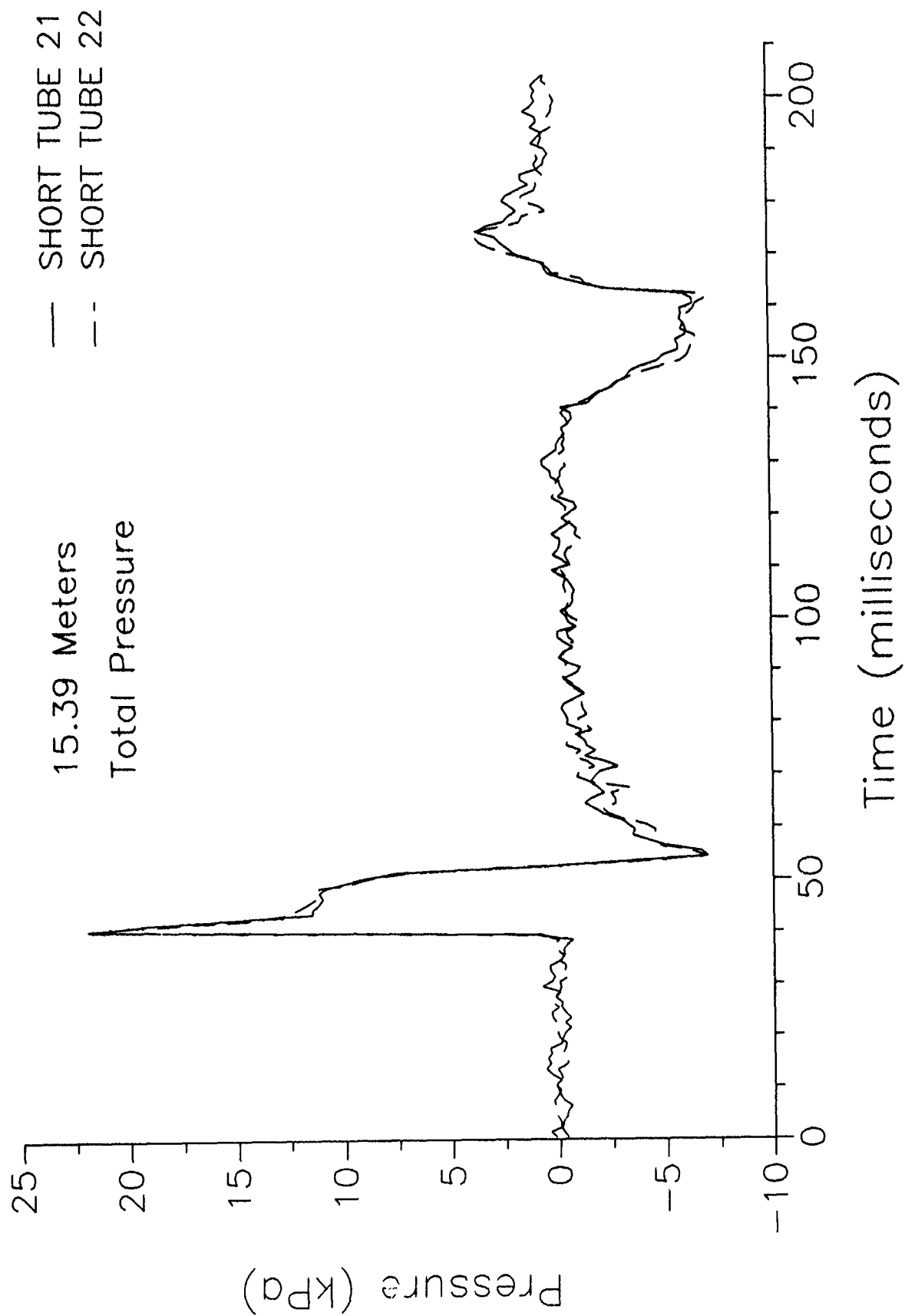


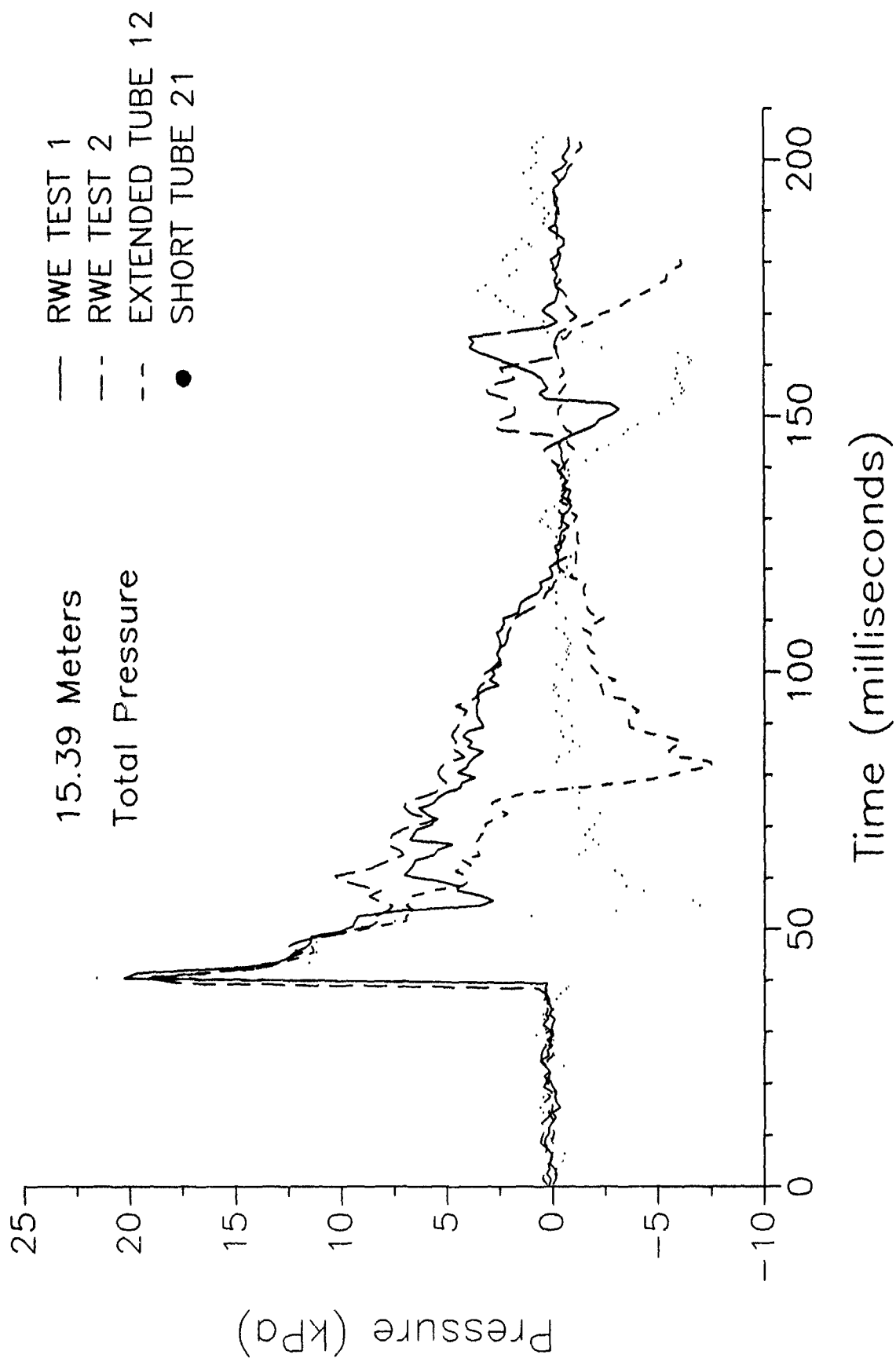


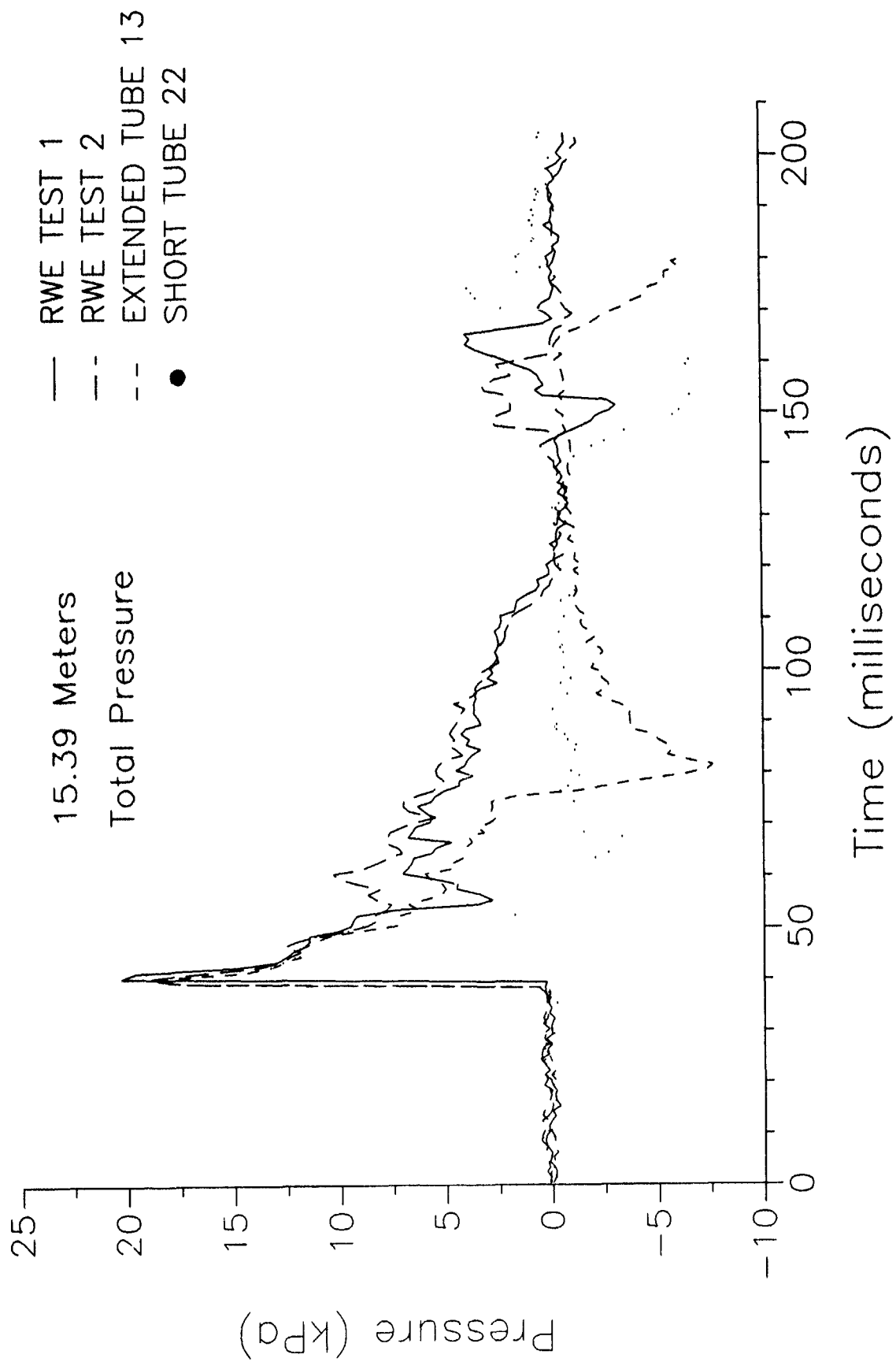








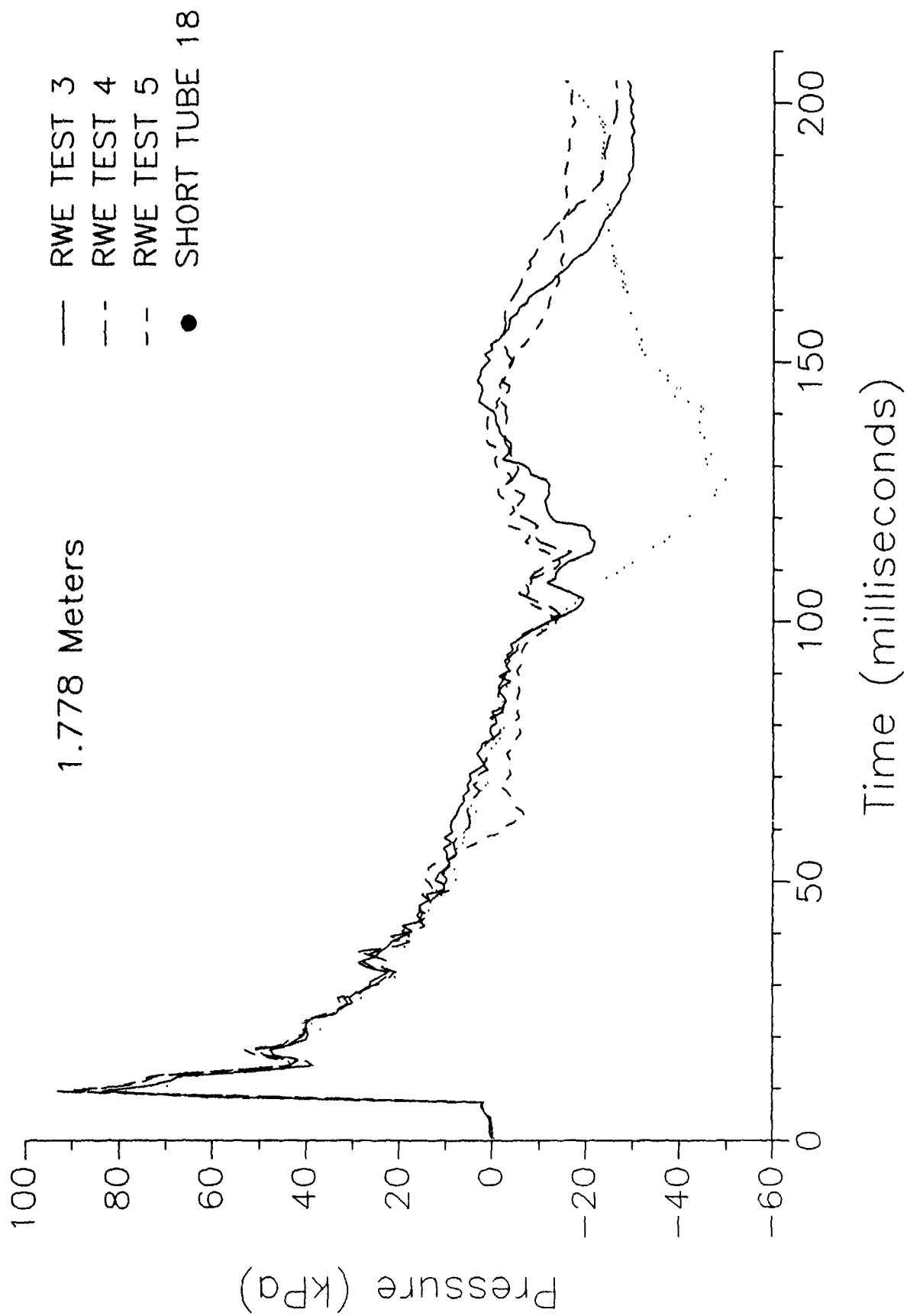


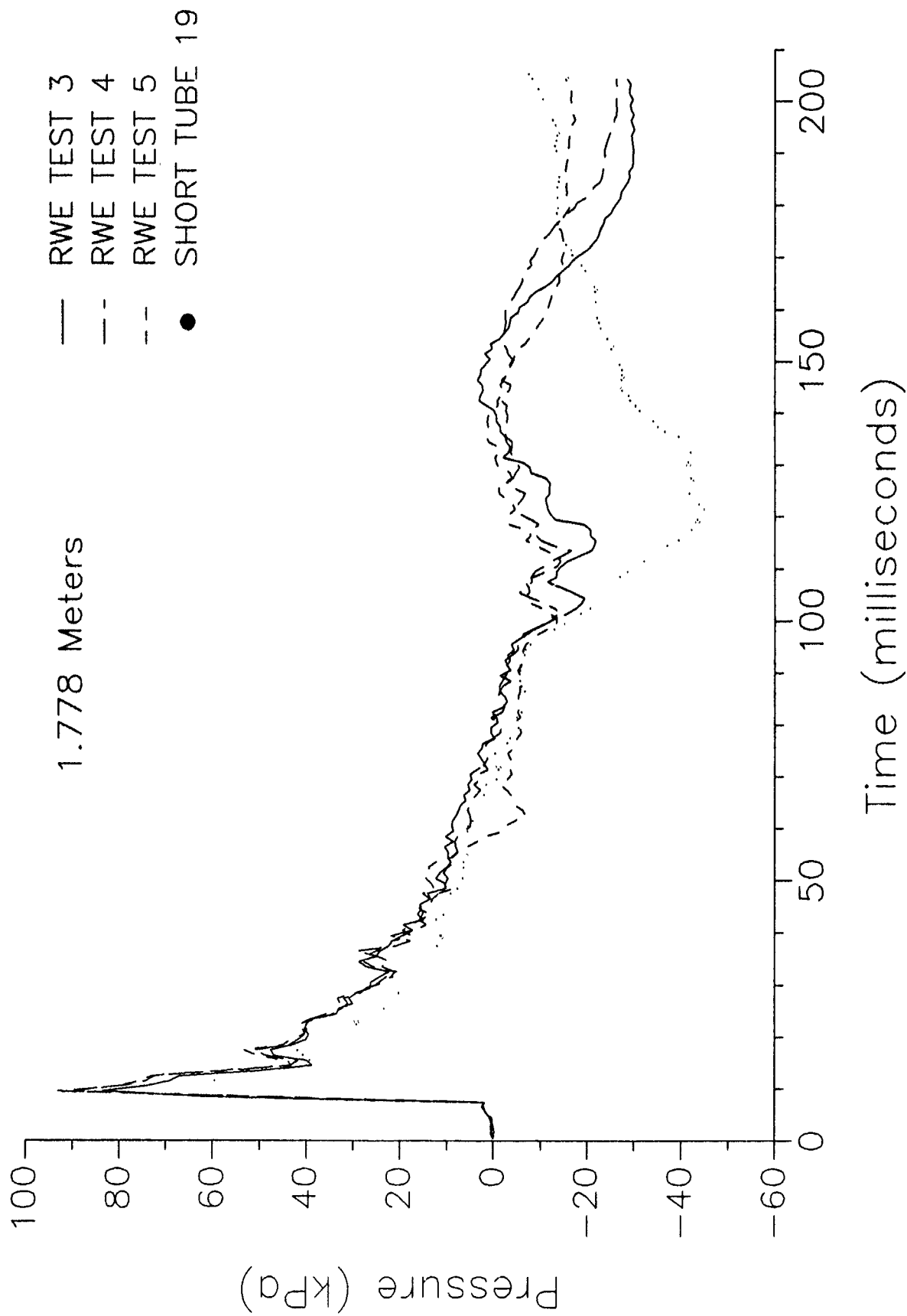


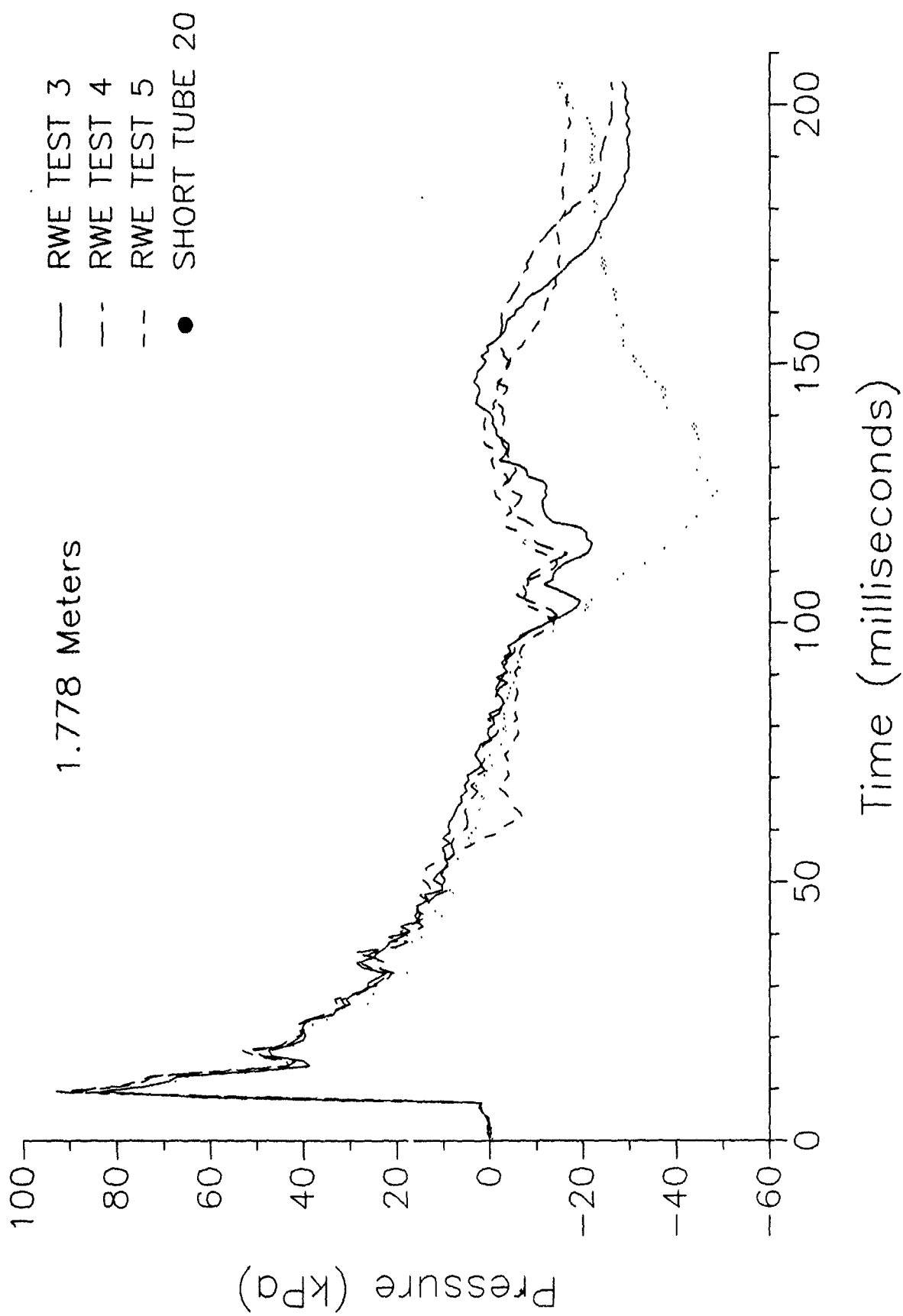
INTENTIONALLY LEFT BLANK.

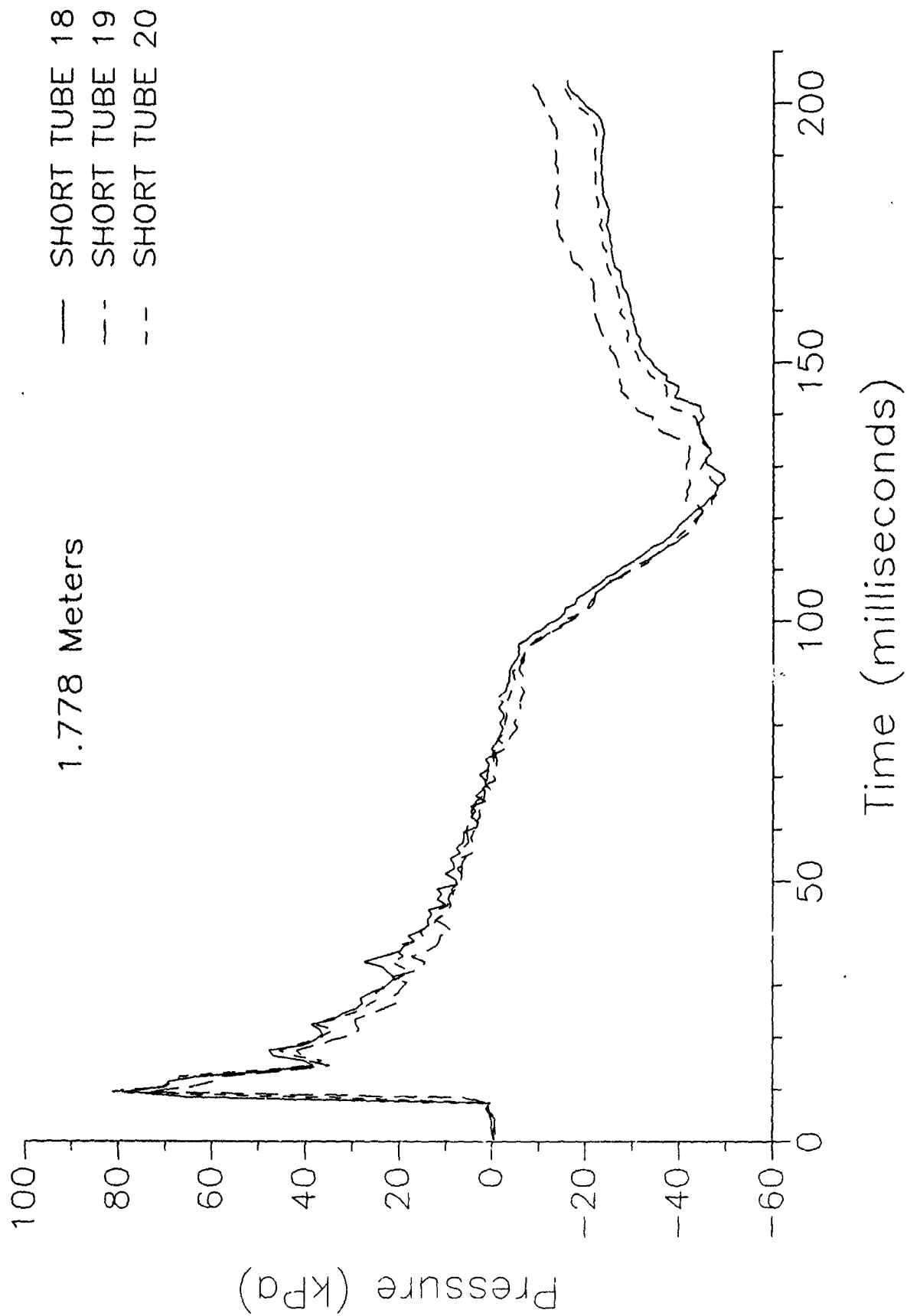
RESULTS FROM 68.9 kPa TESTS

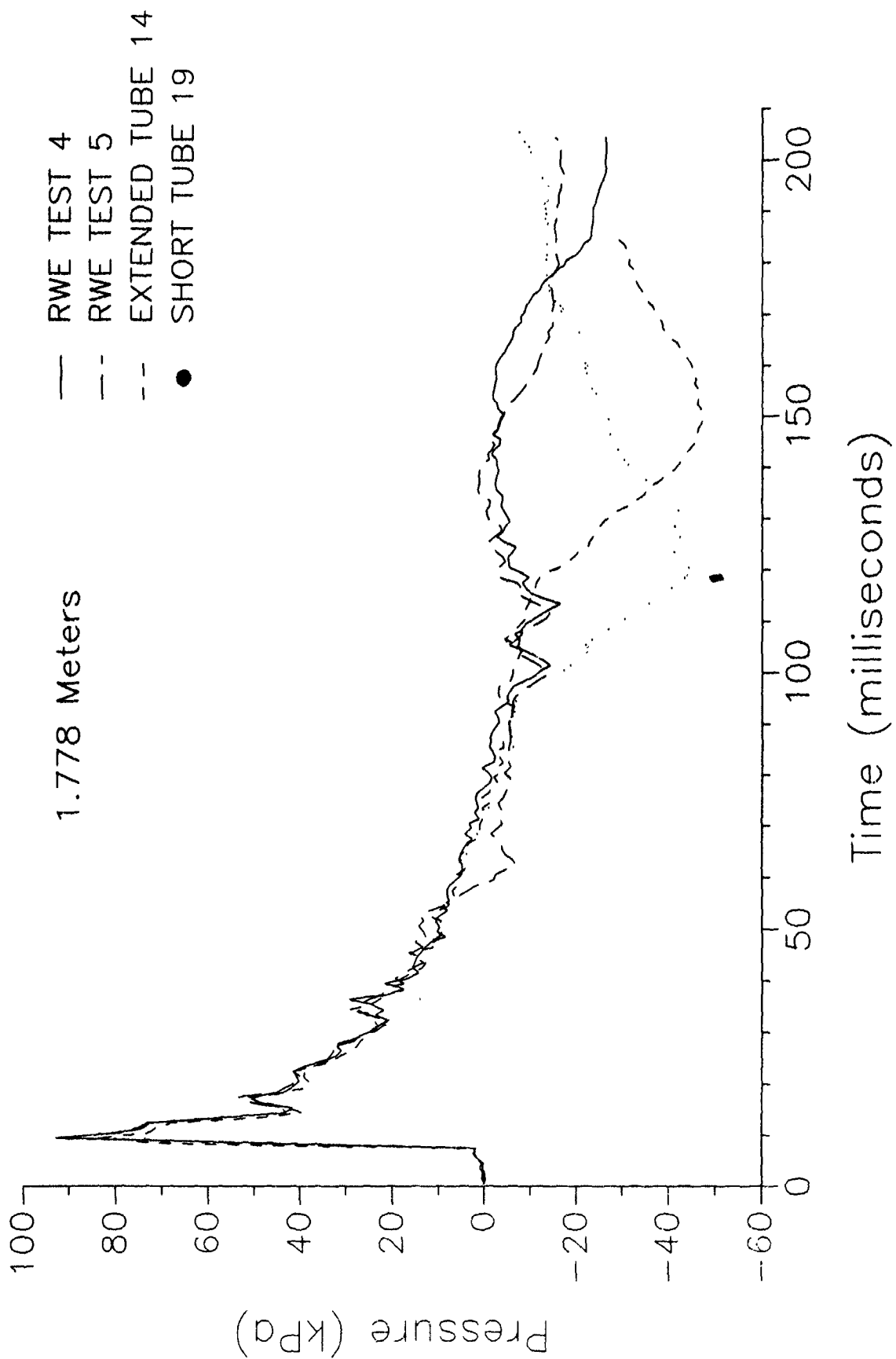
INTENTIONALLY LEFT BLANK.

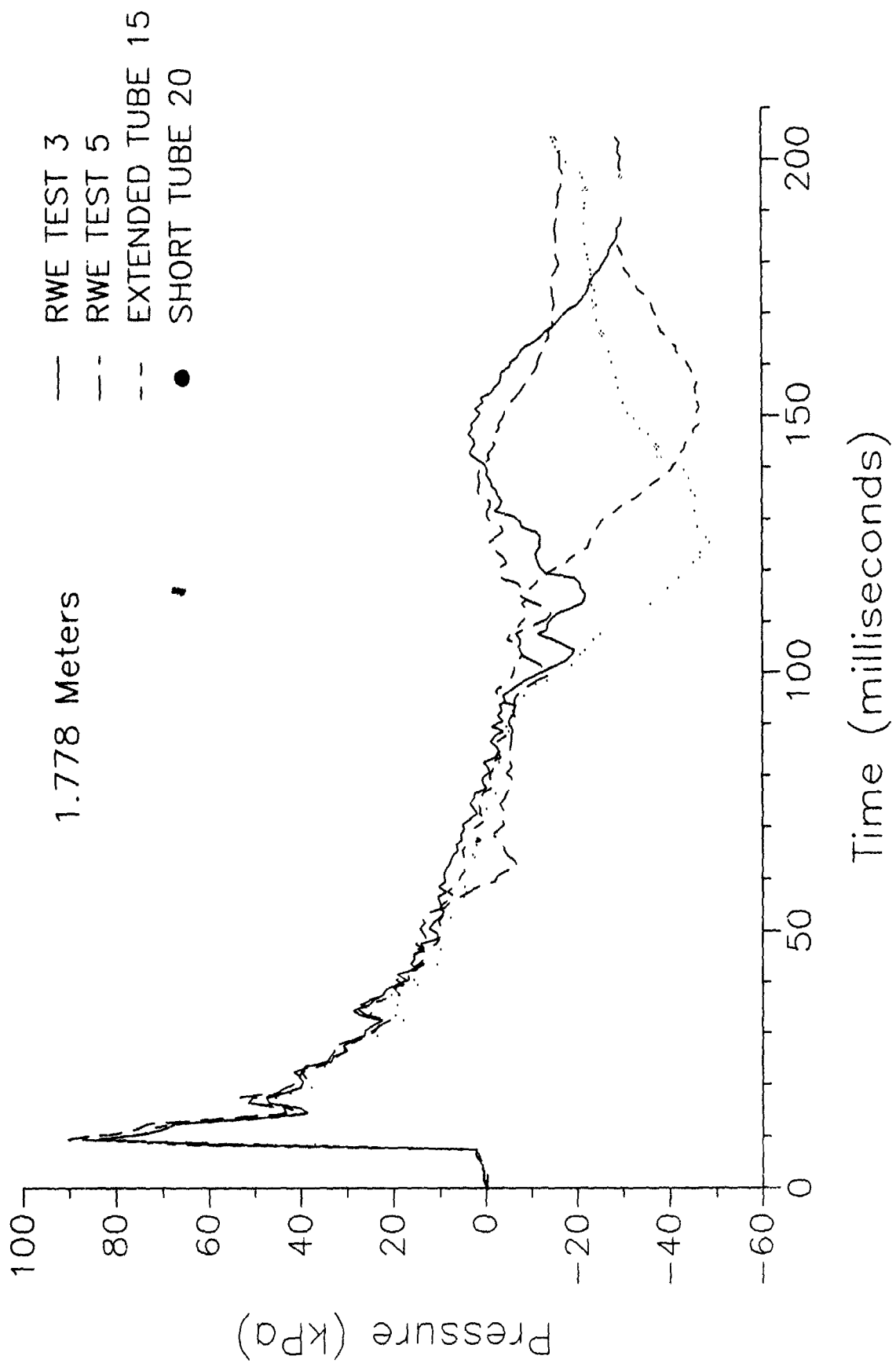


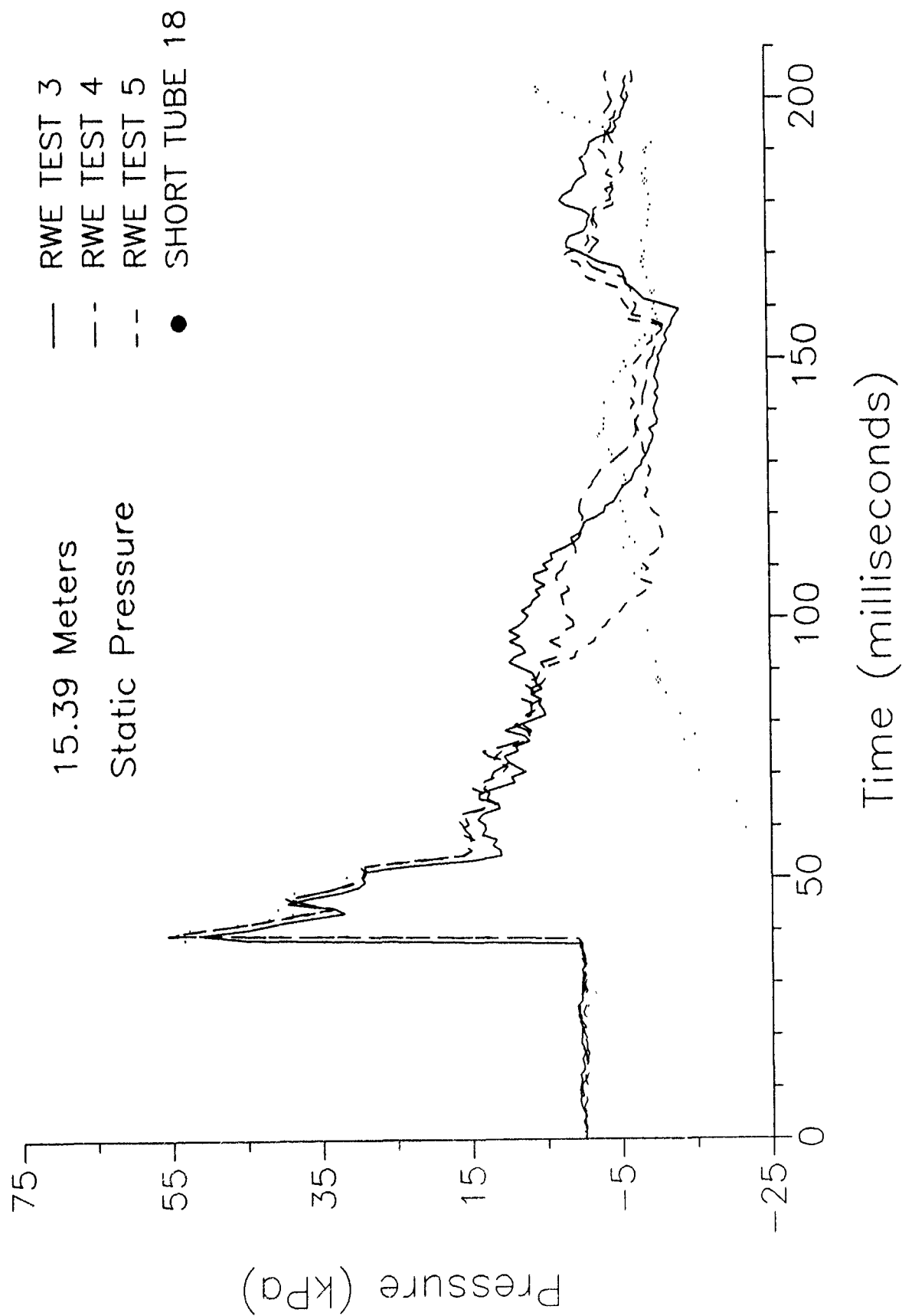


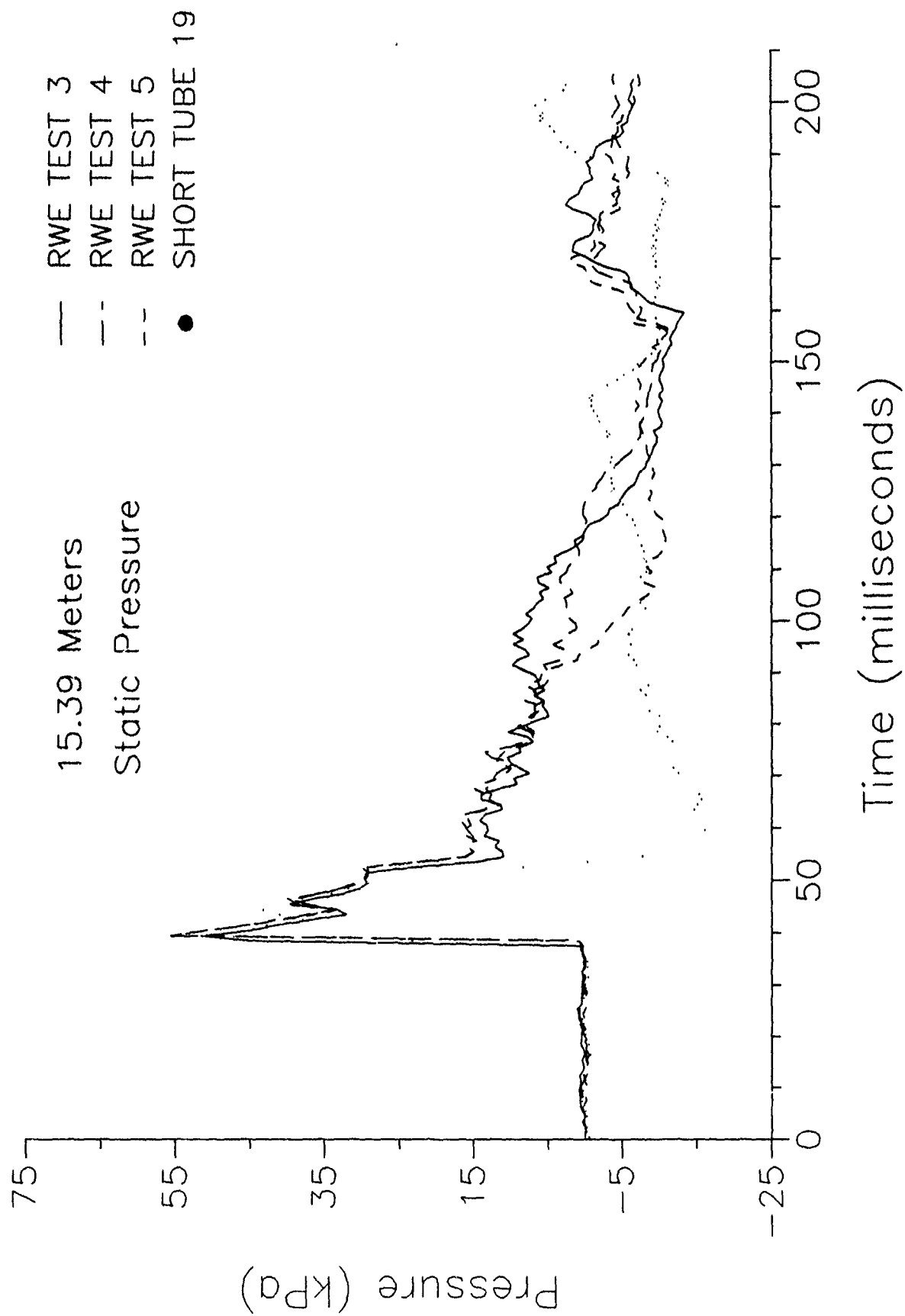


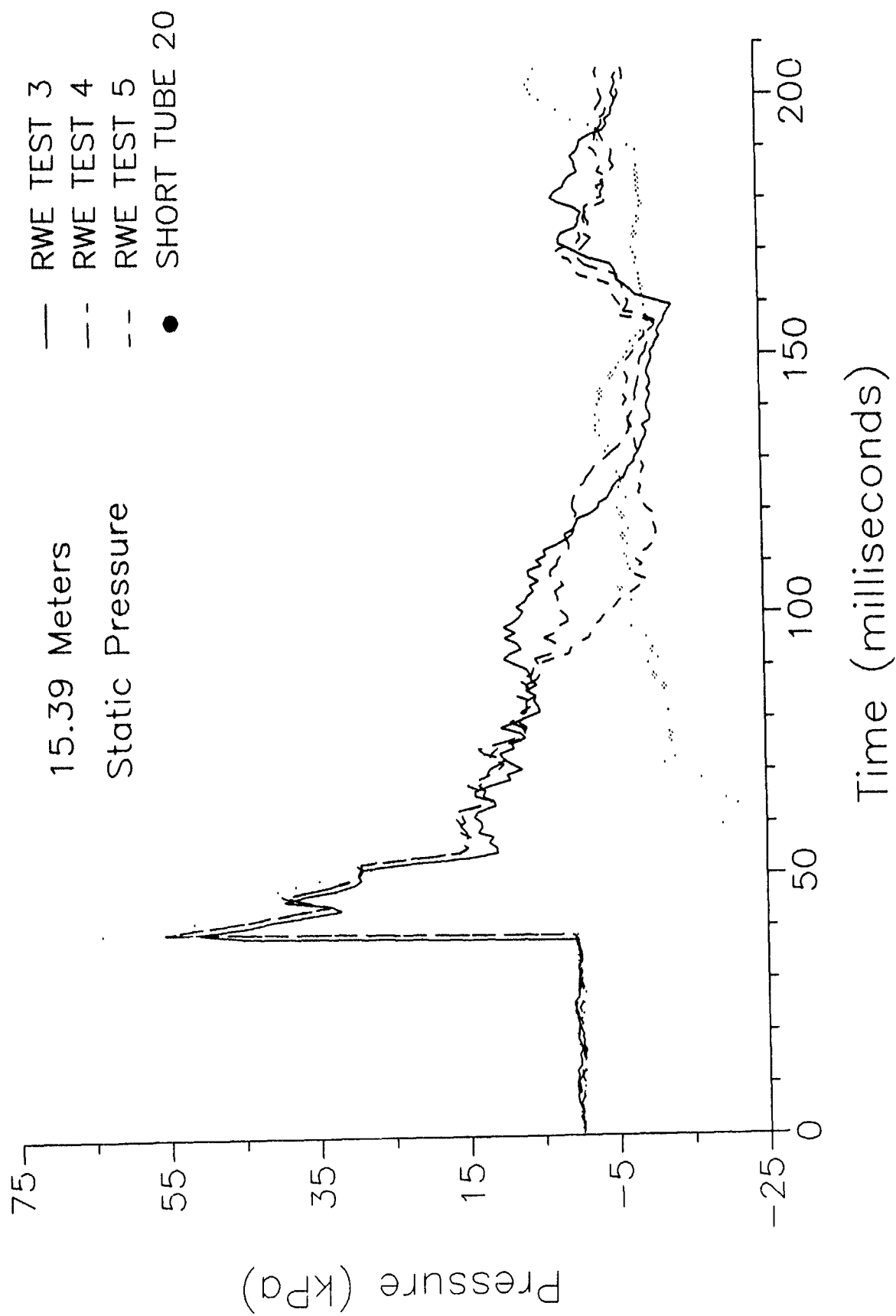


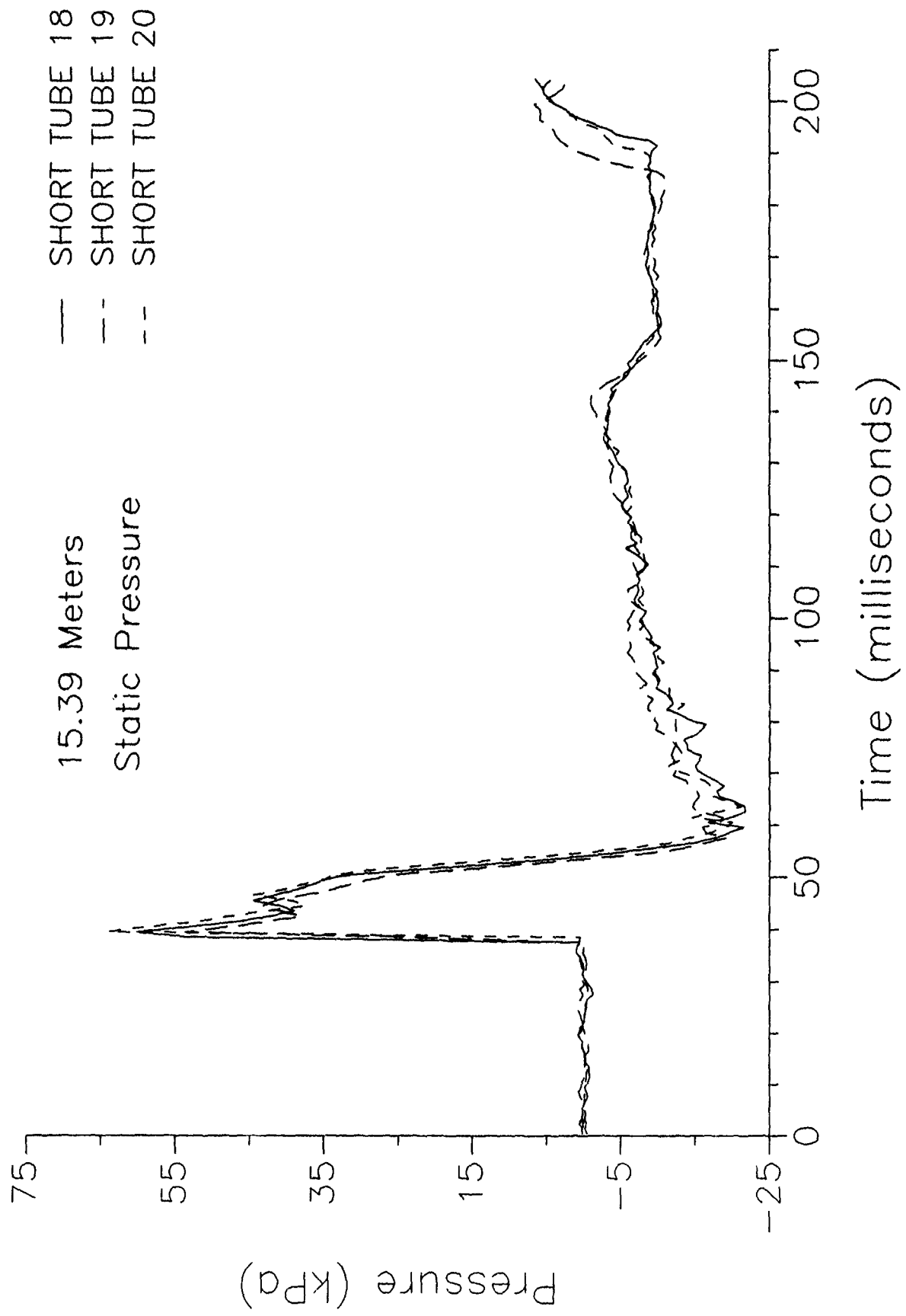


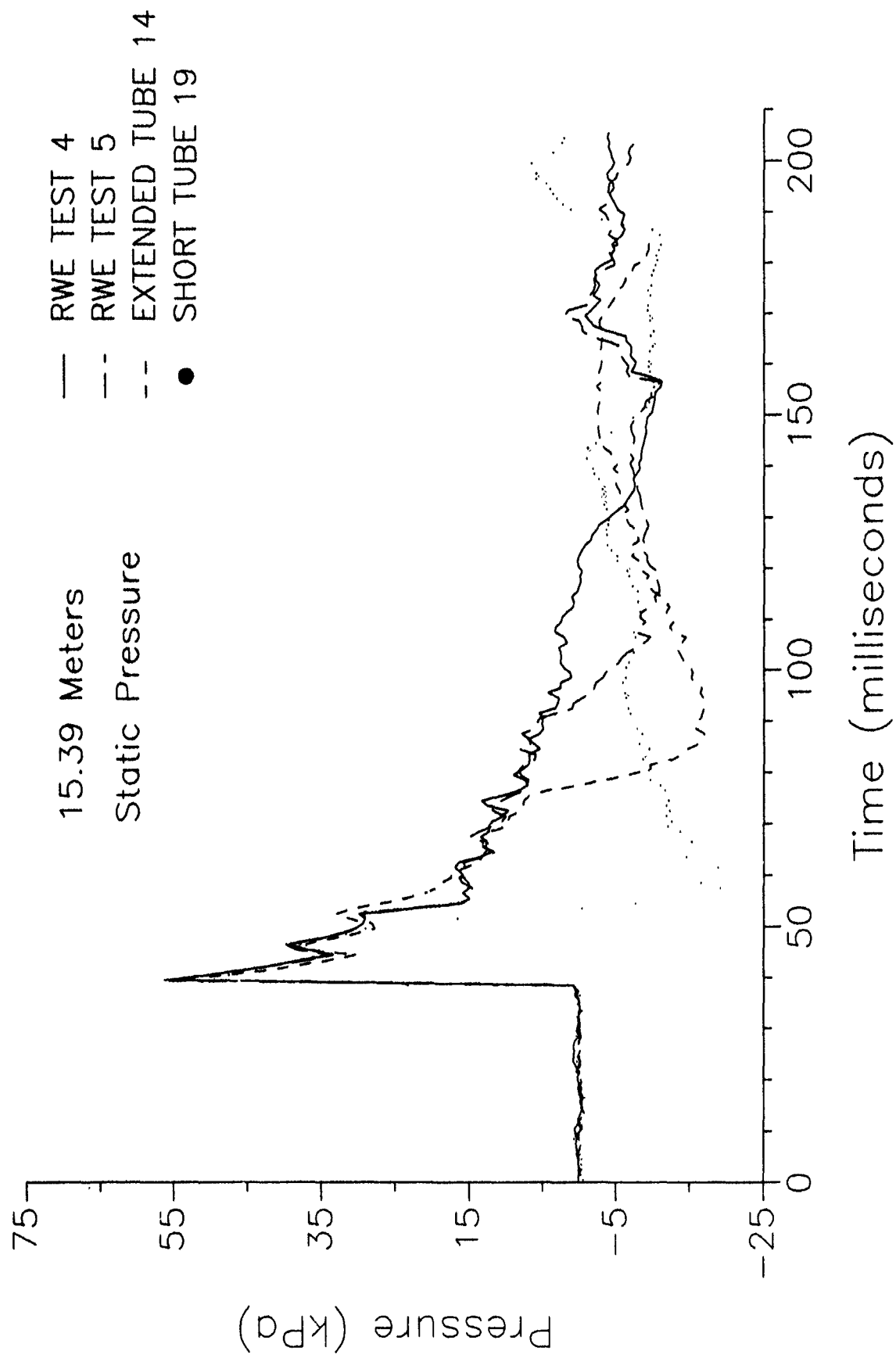


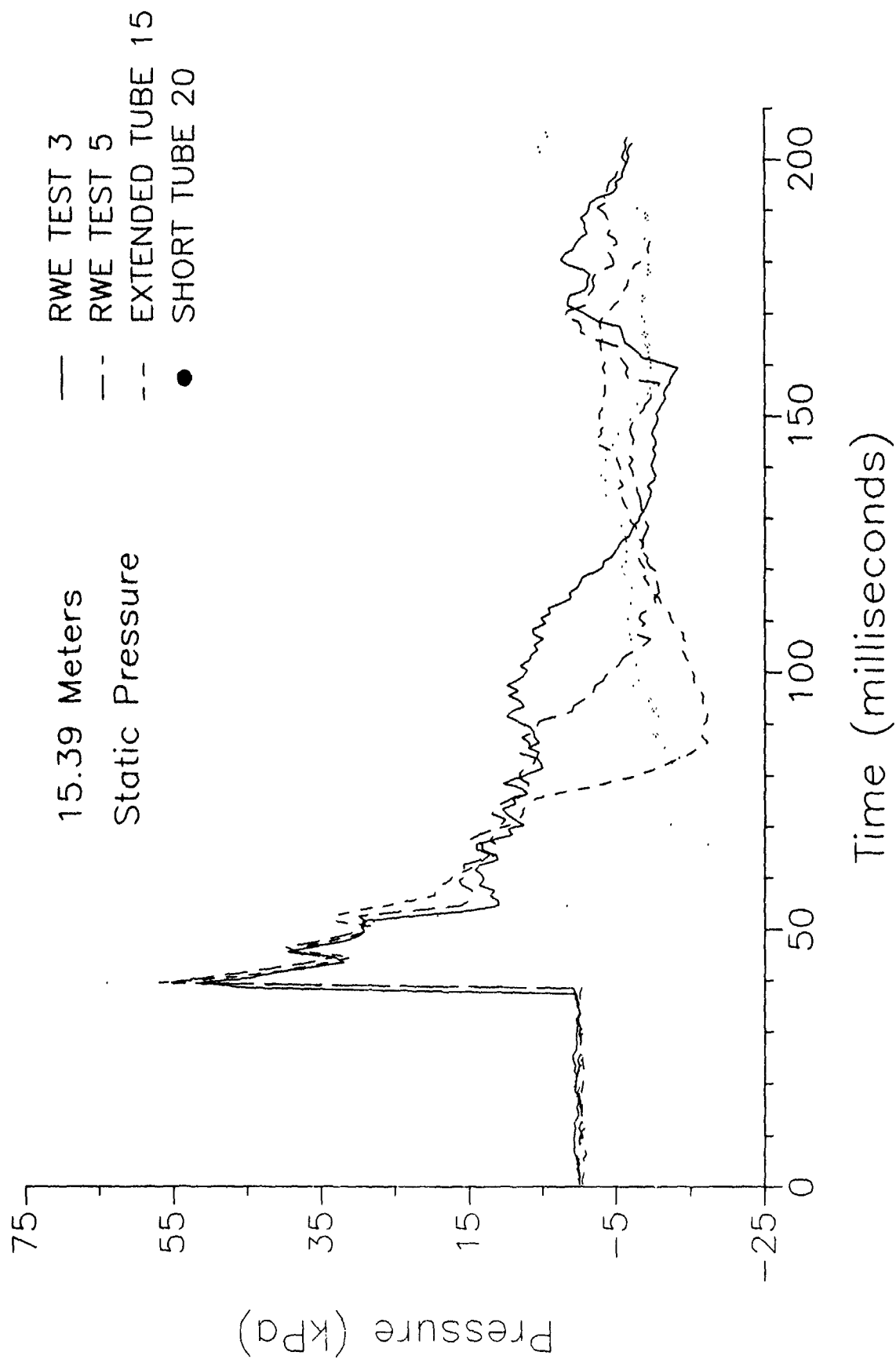


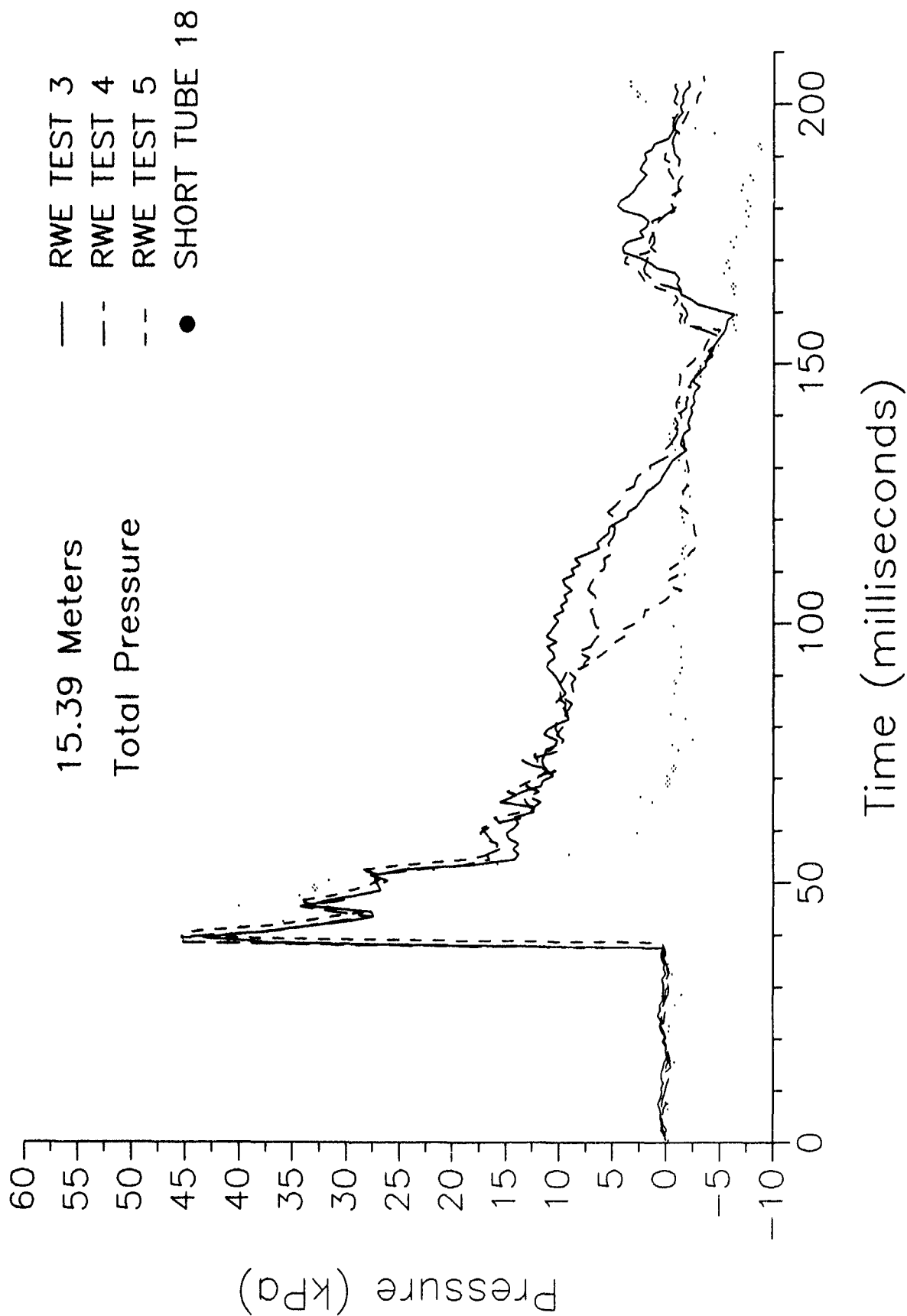


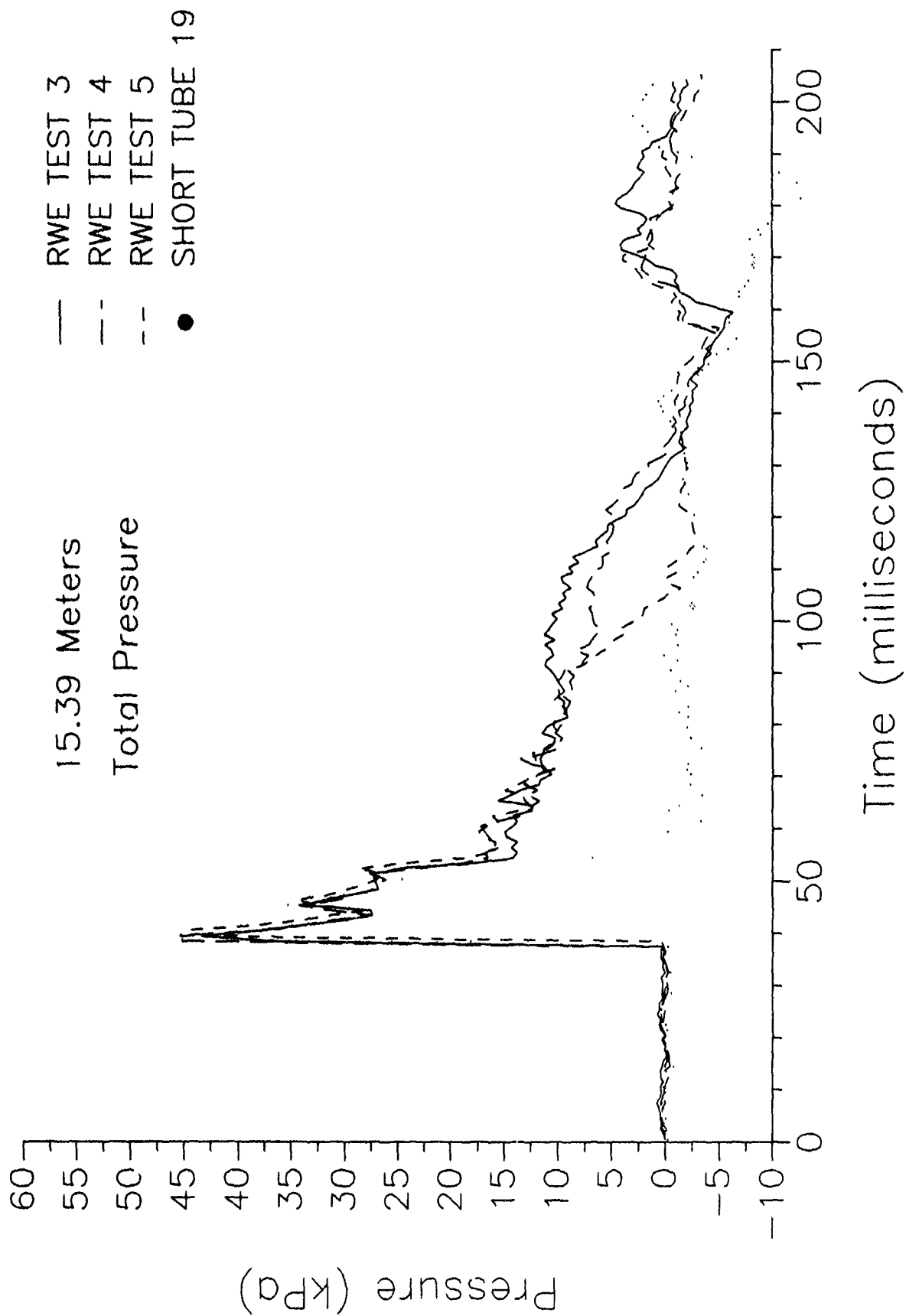


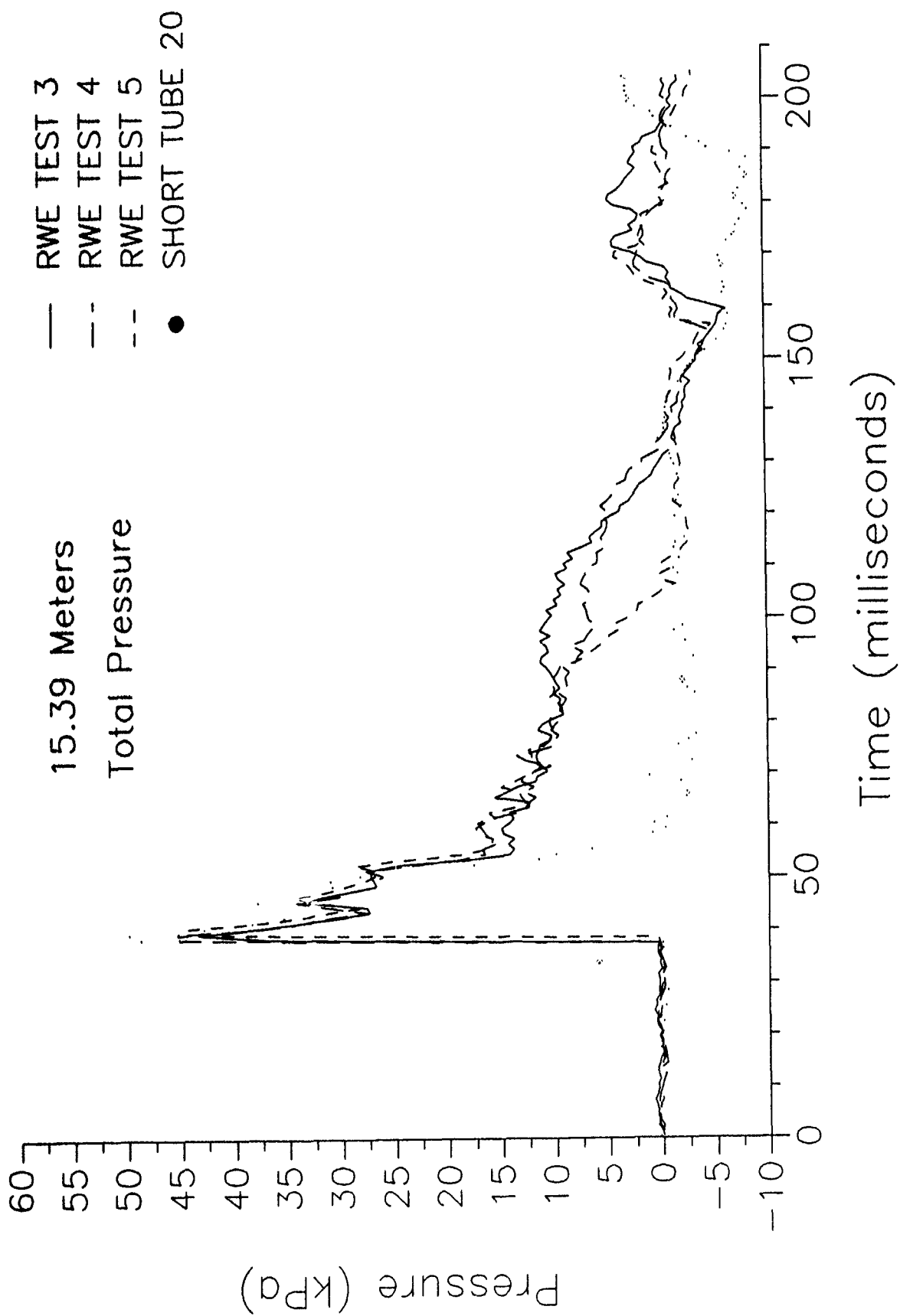


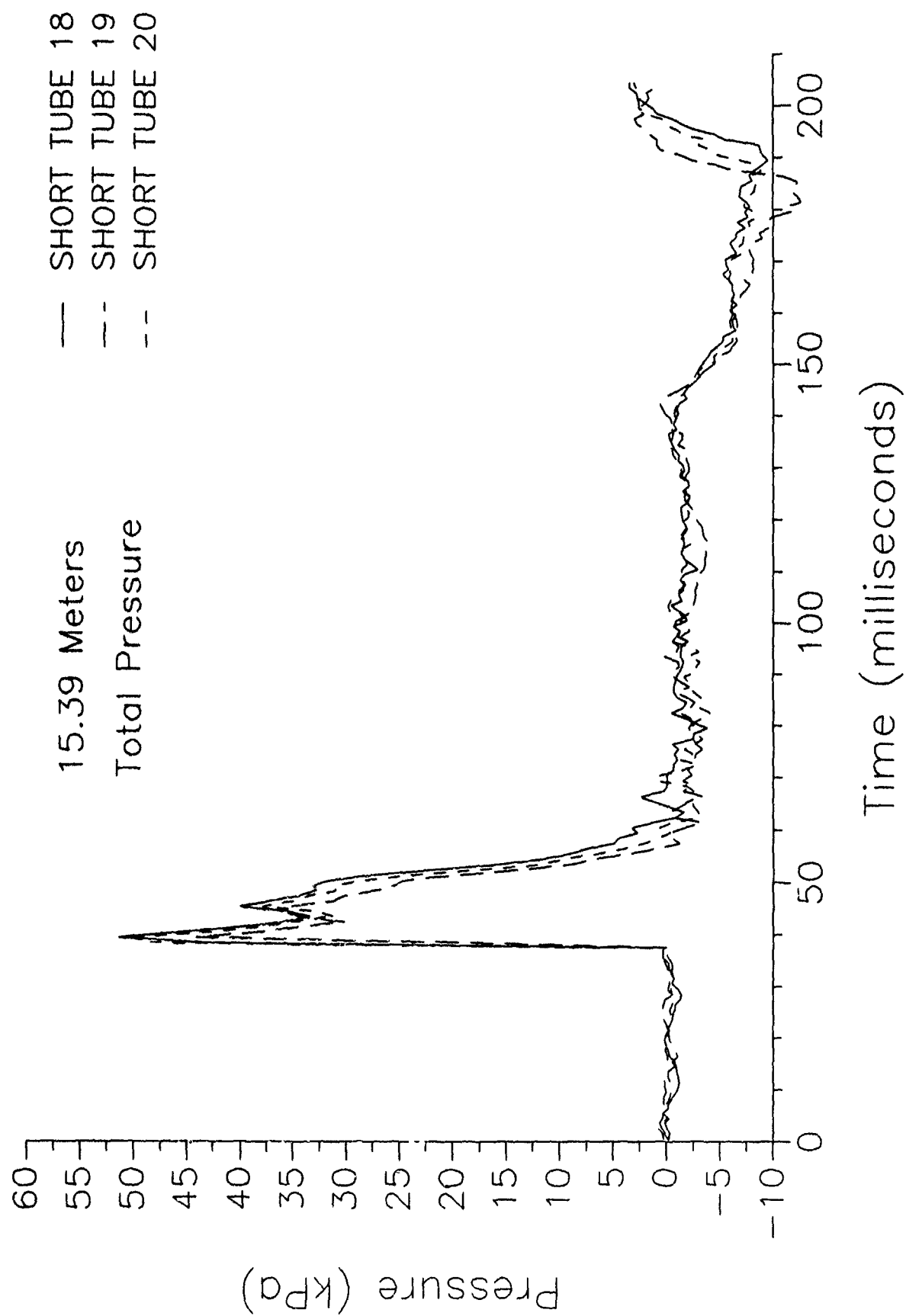


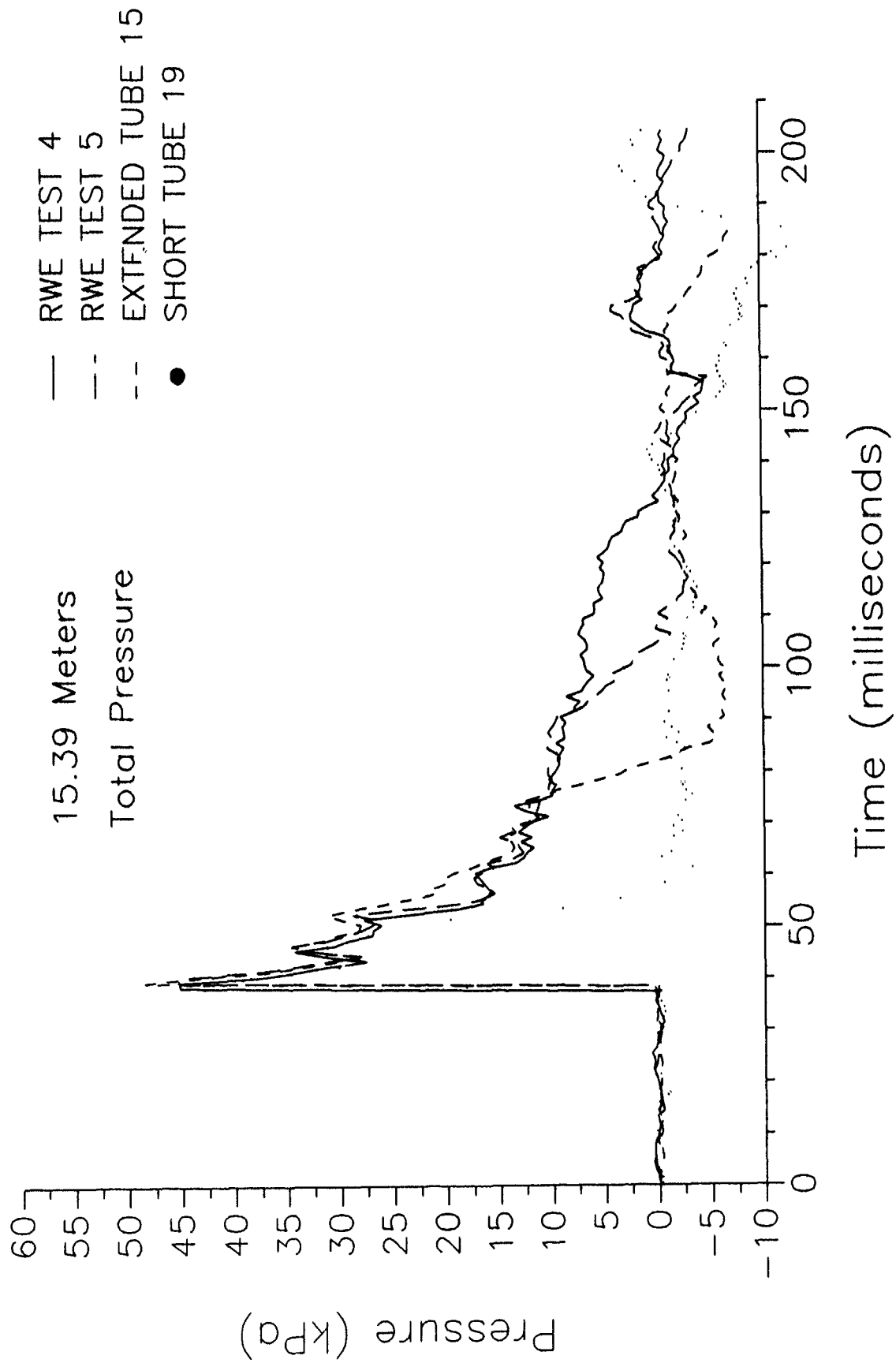


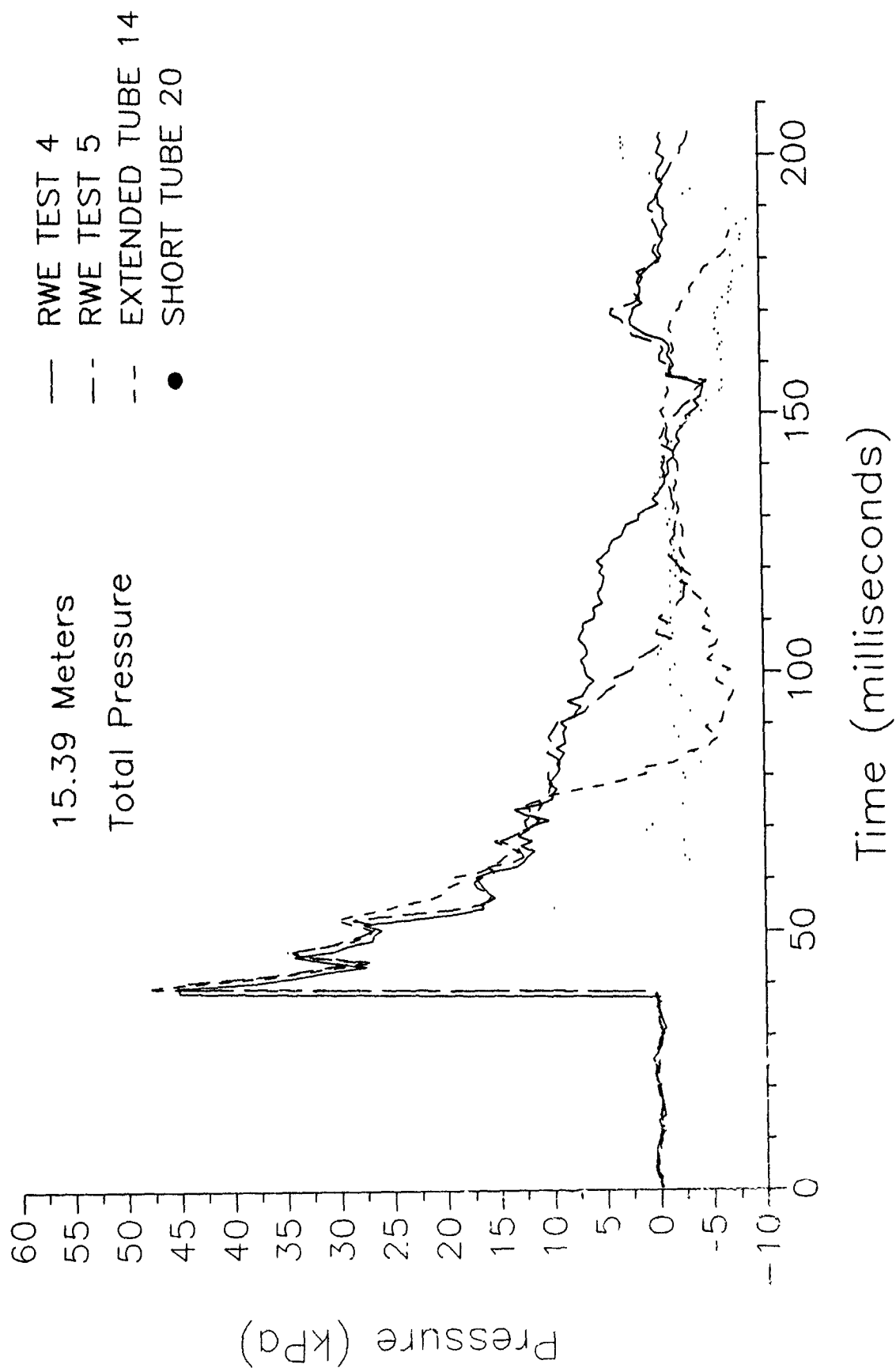






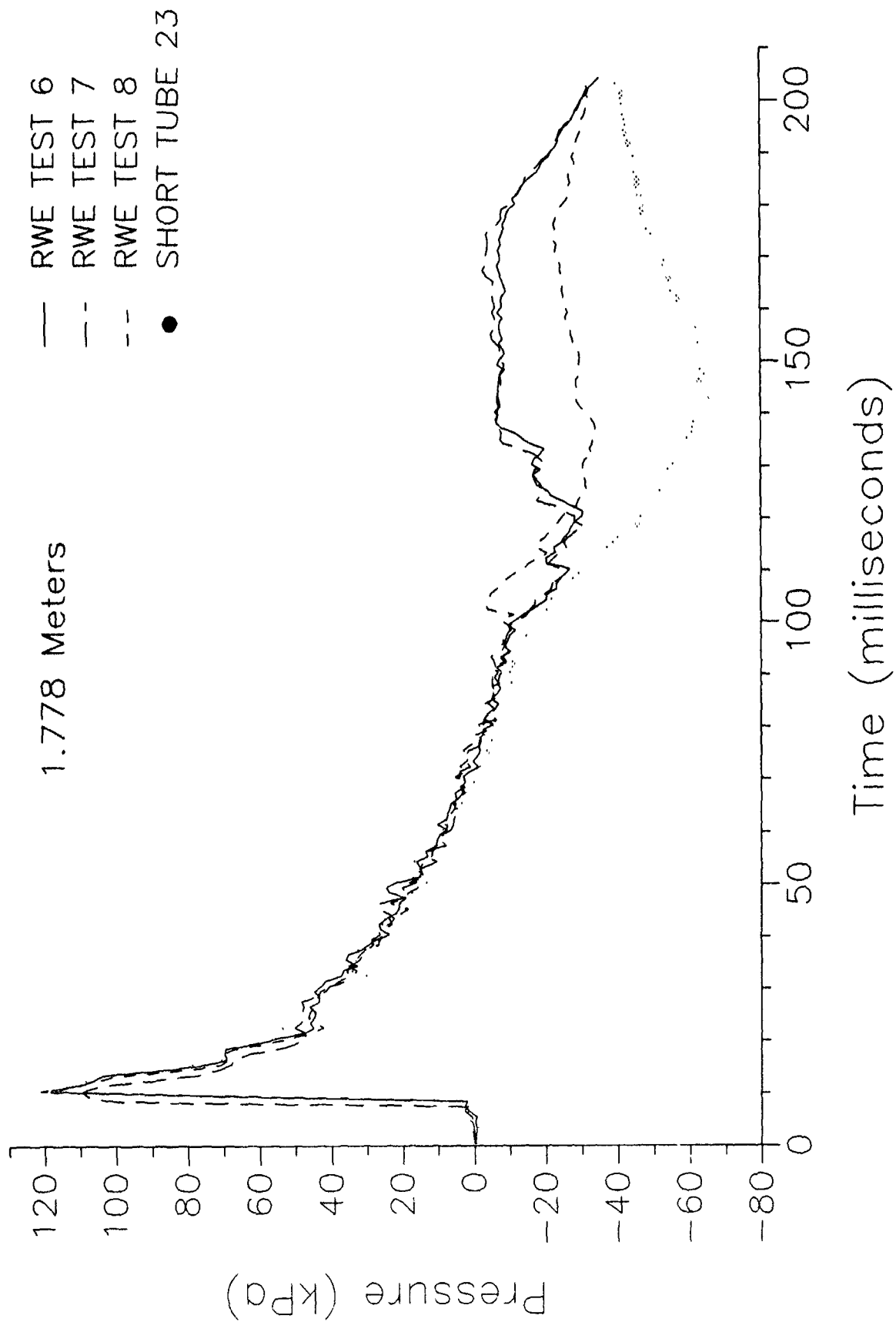


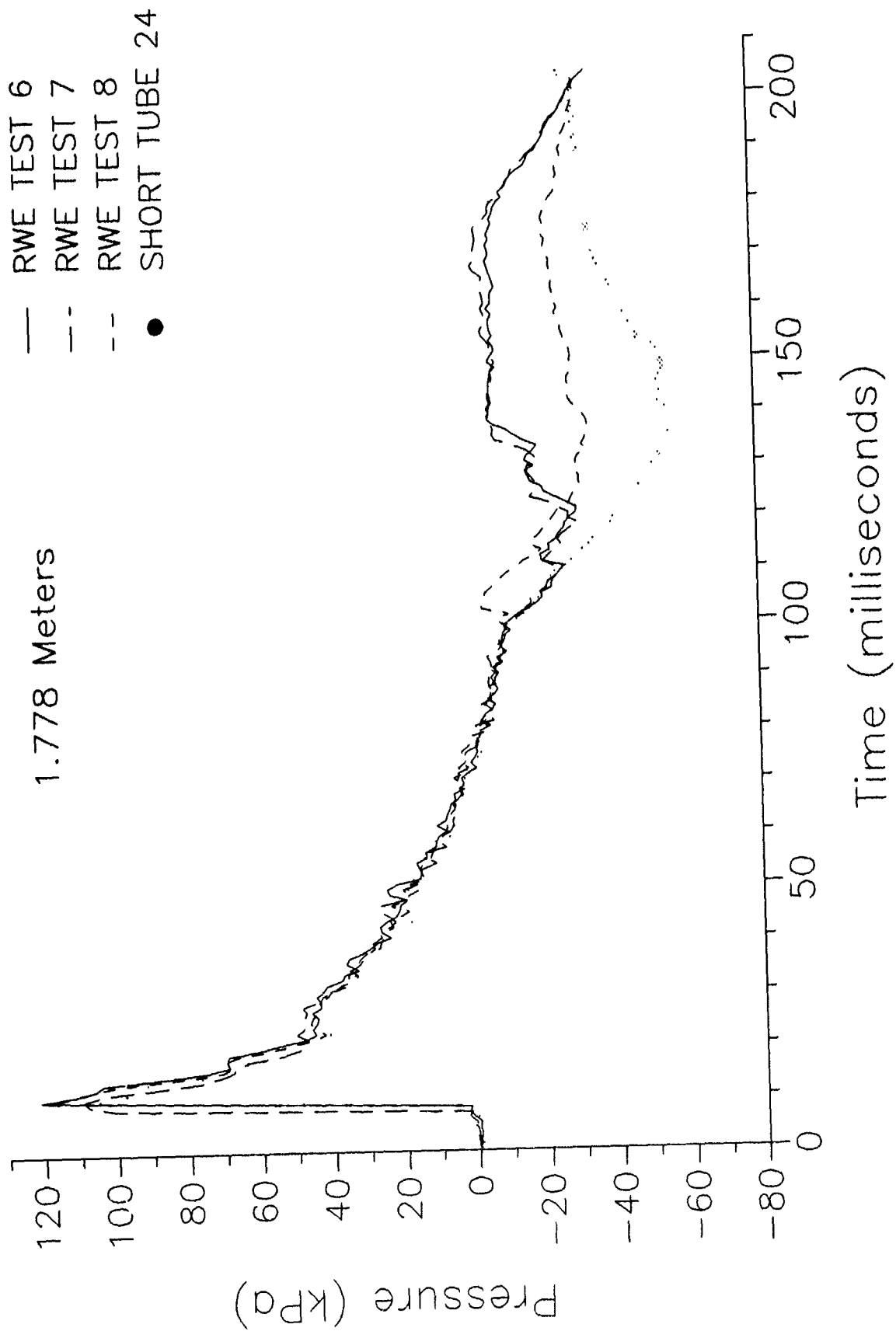


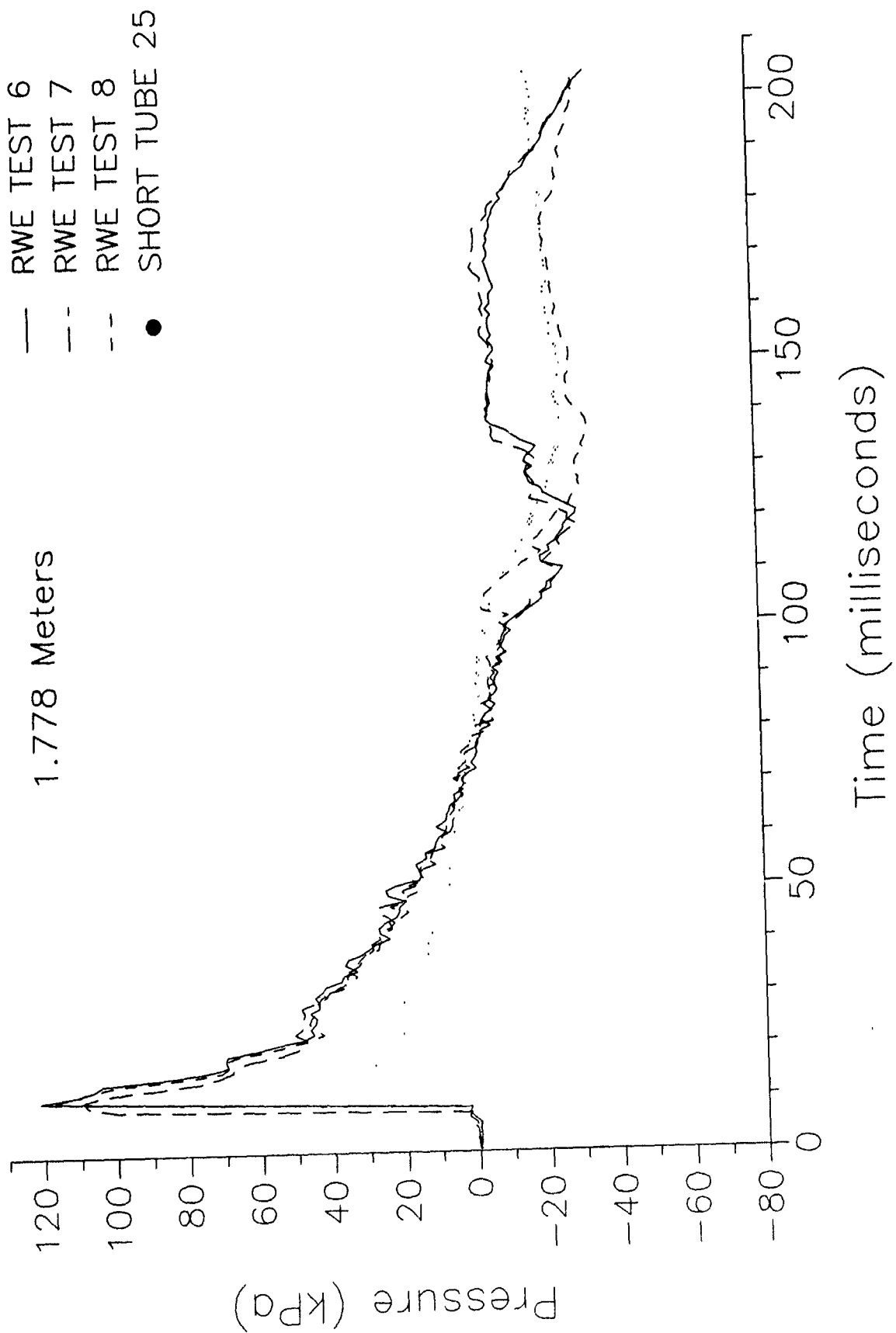


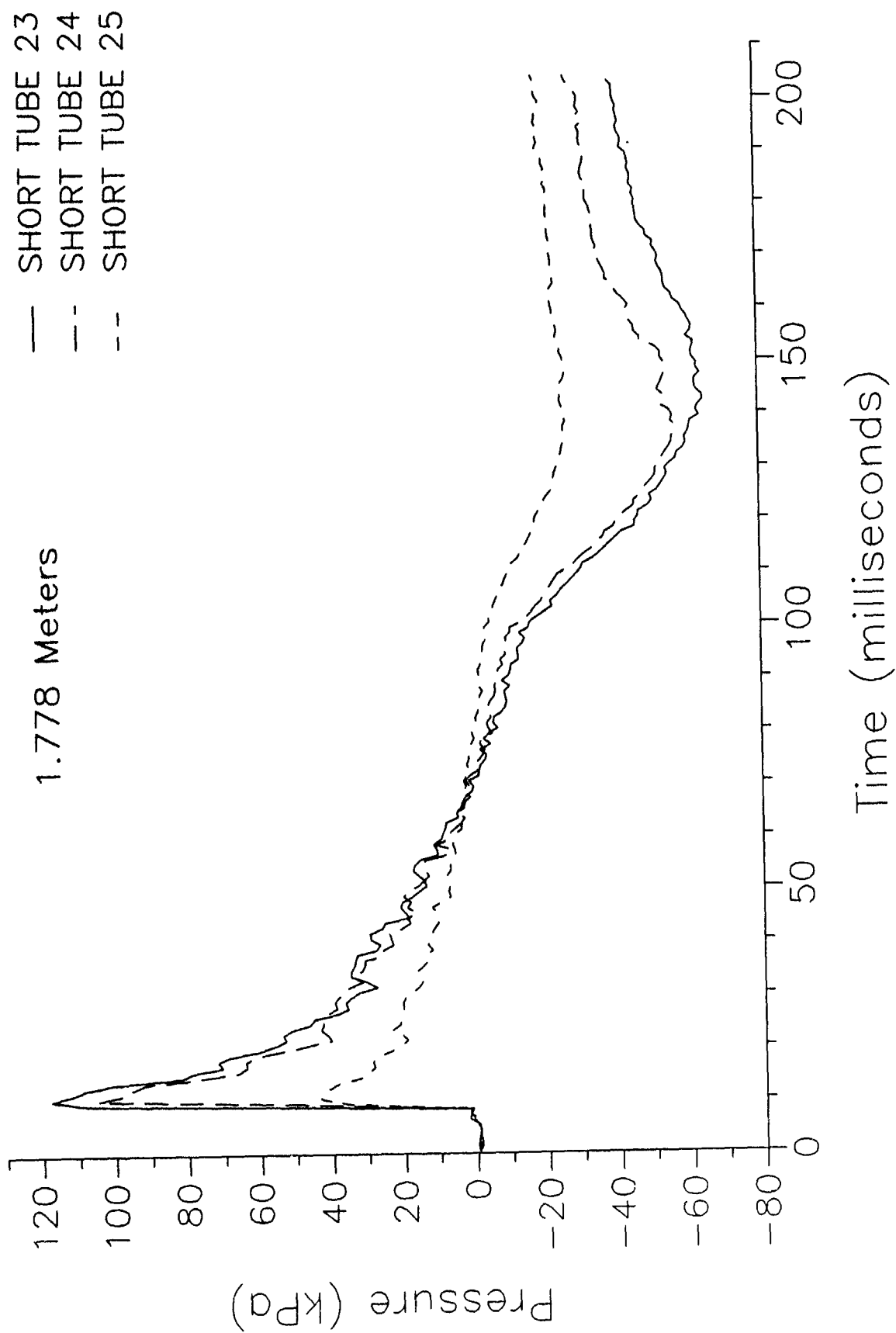
RESULTS FROM 103.3 kPa TESTS

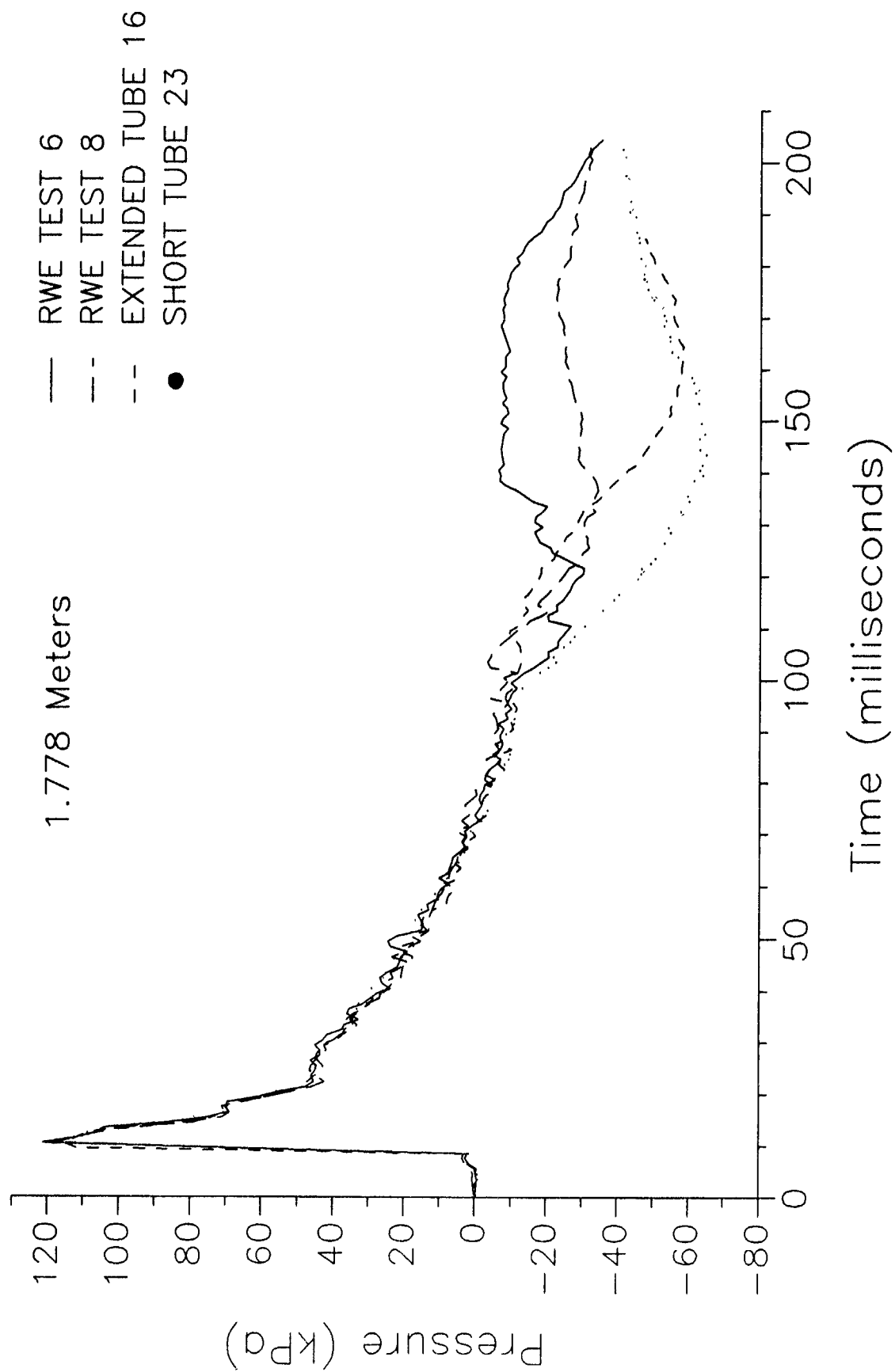
INTENTIONALLY LEFT BLANK.

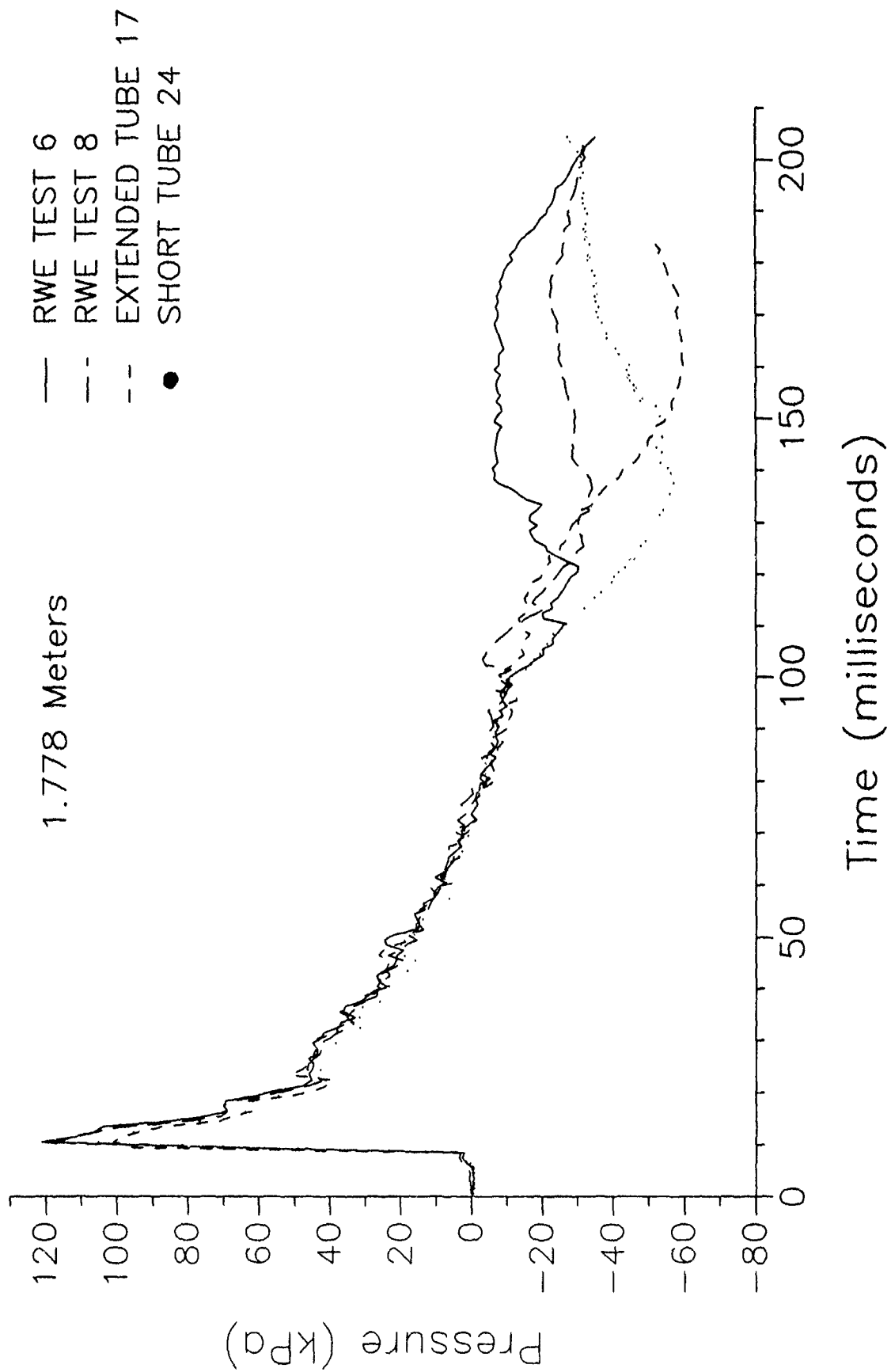


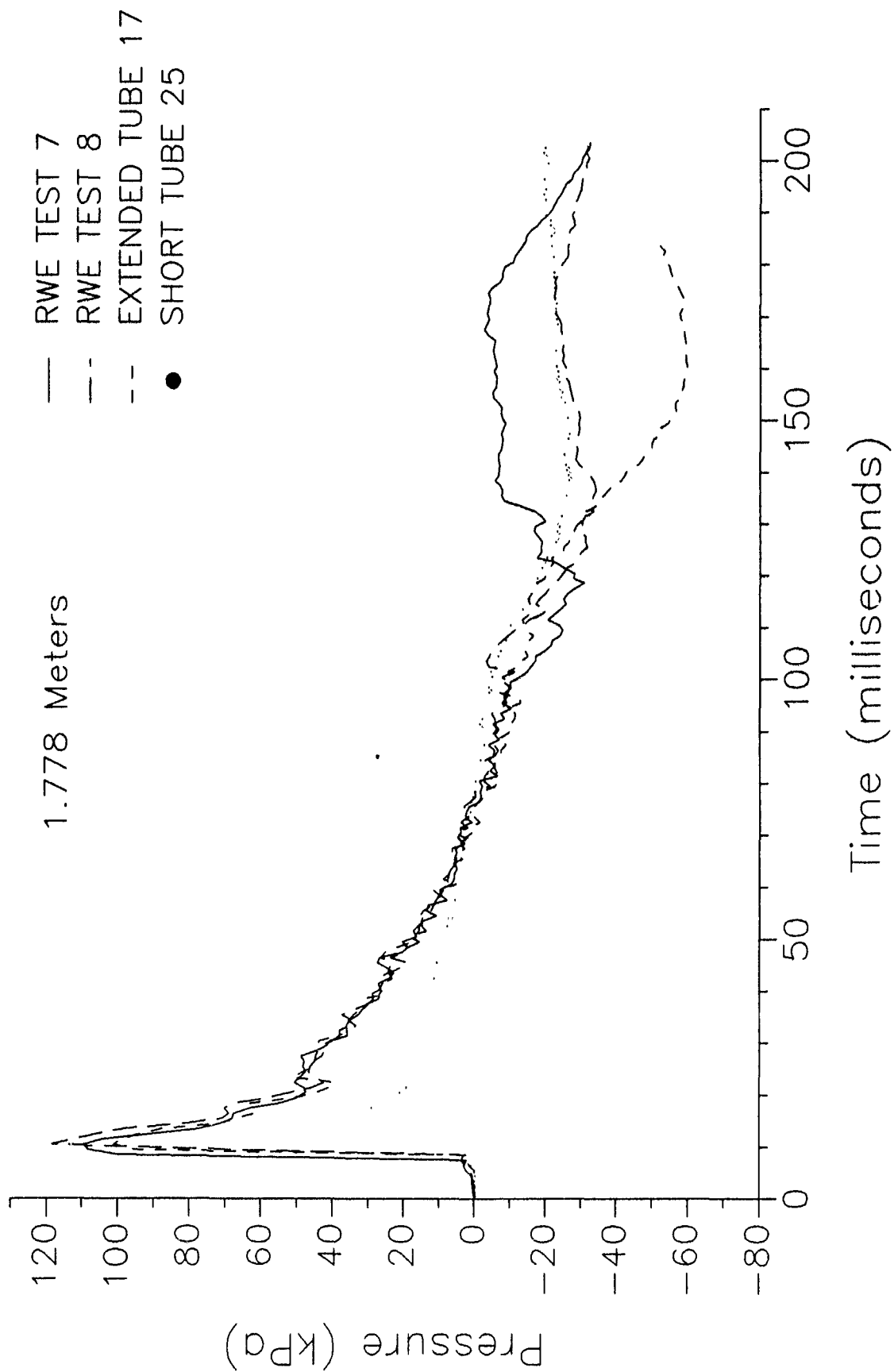


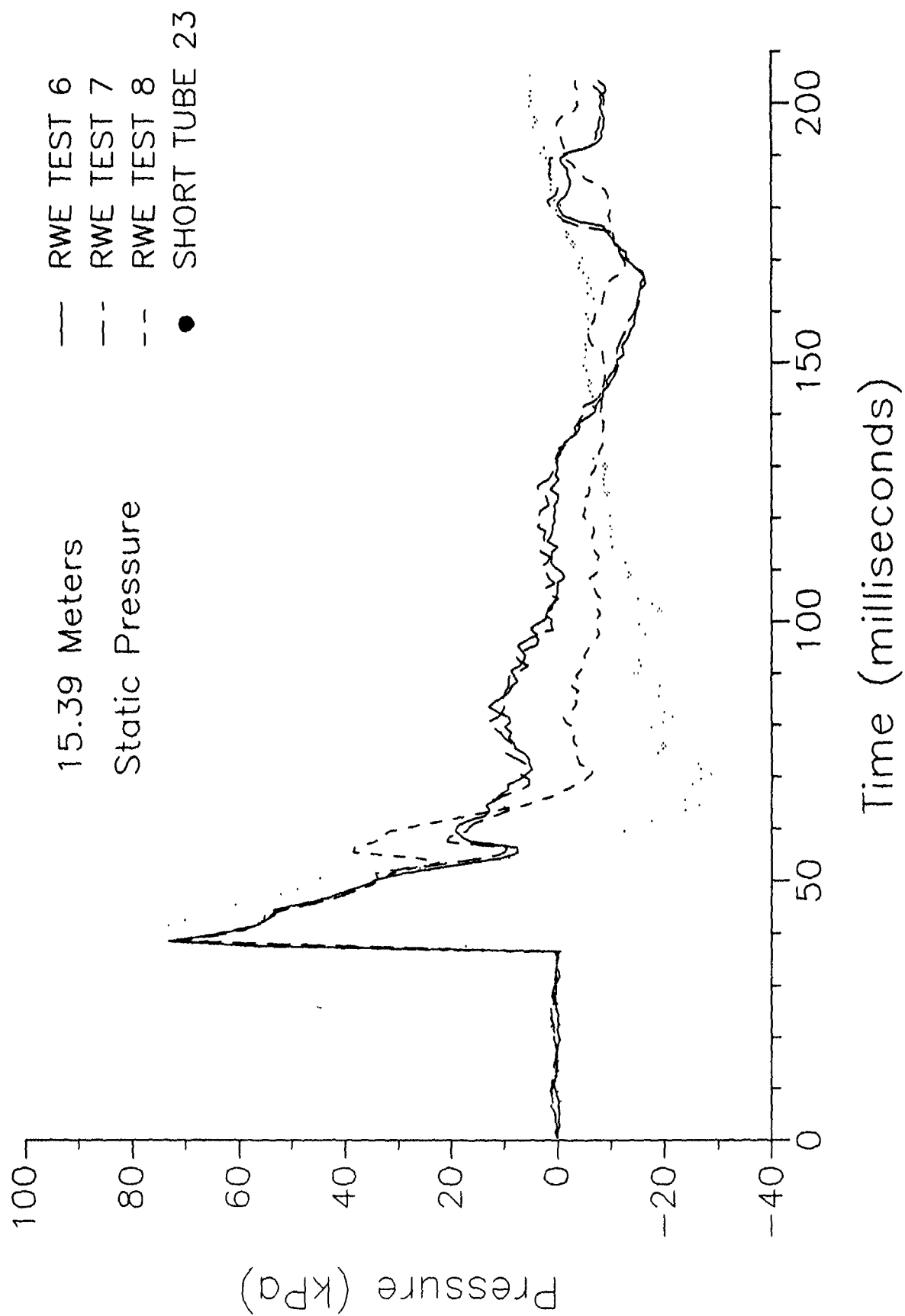


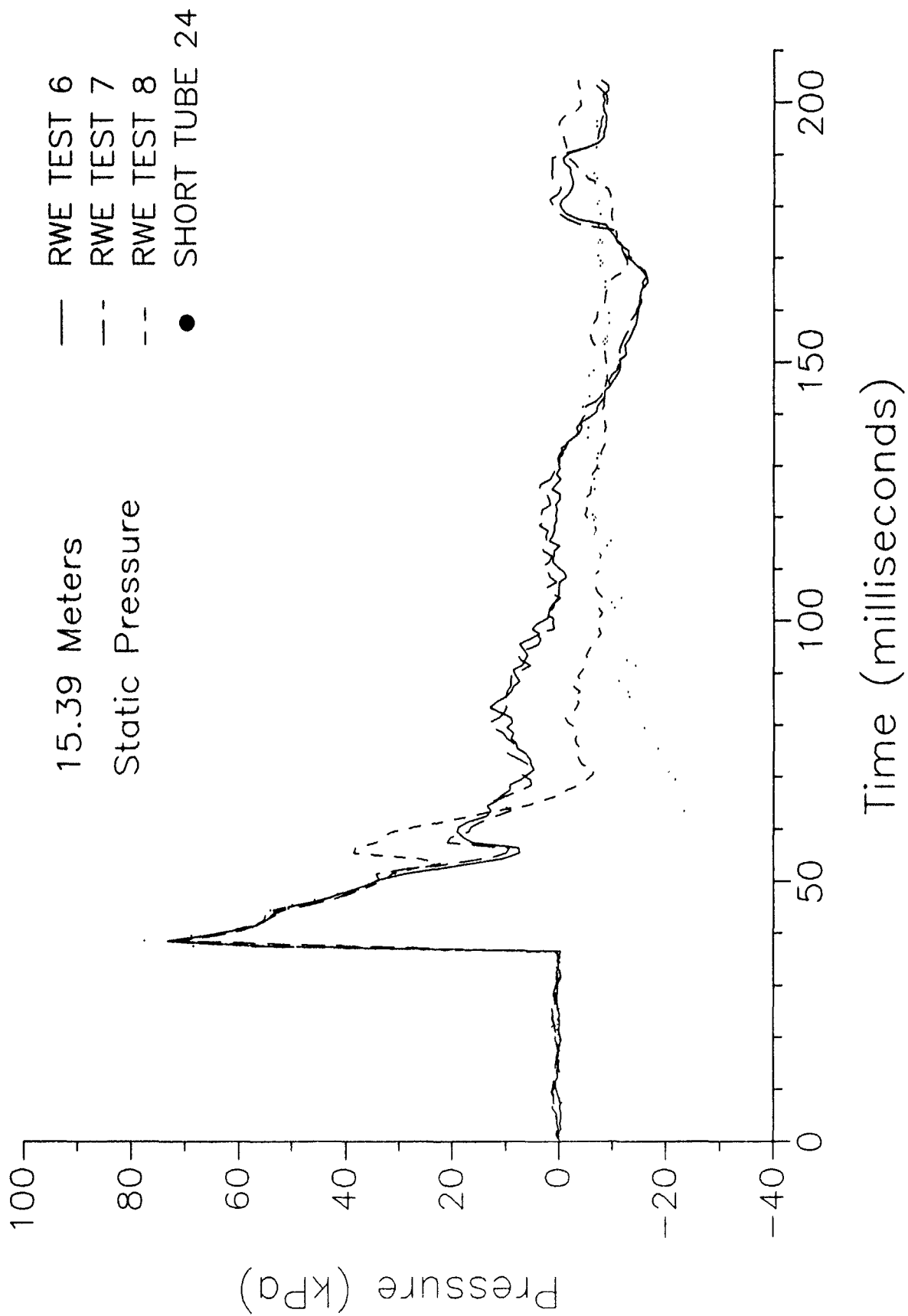


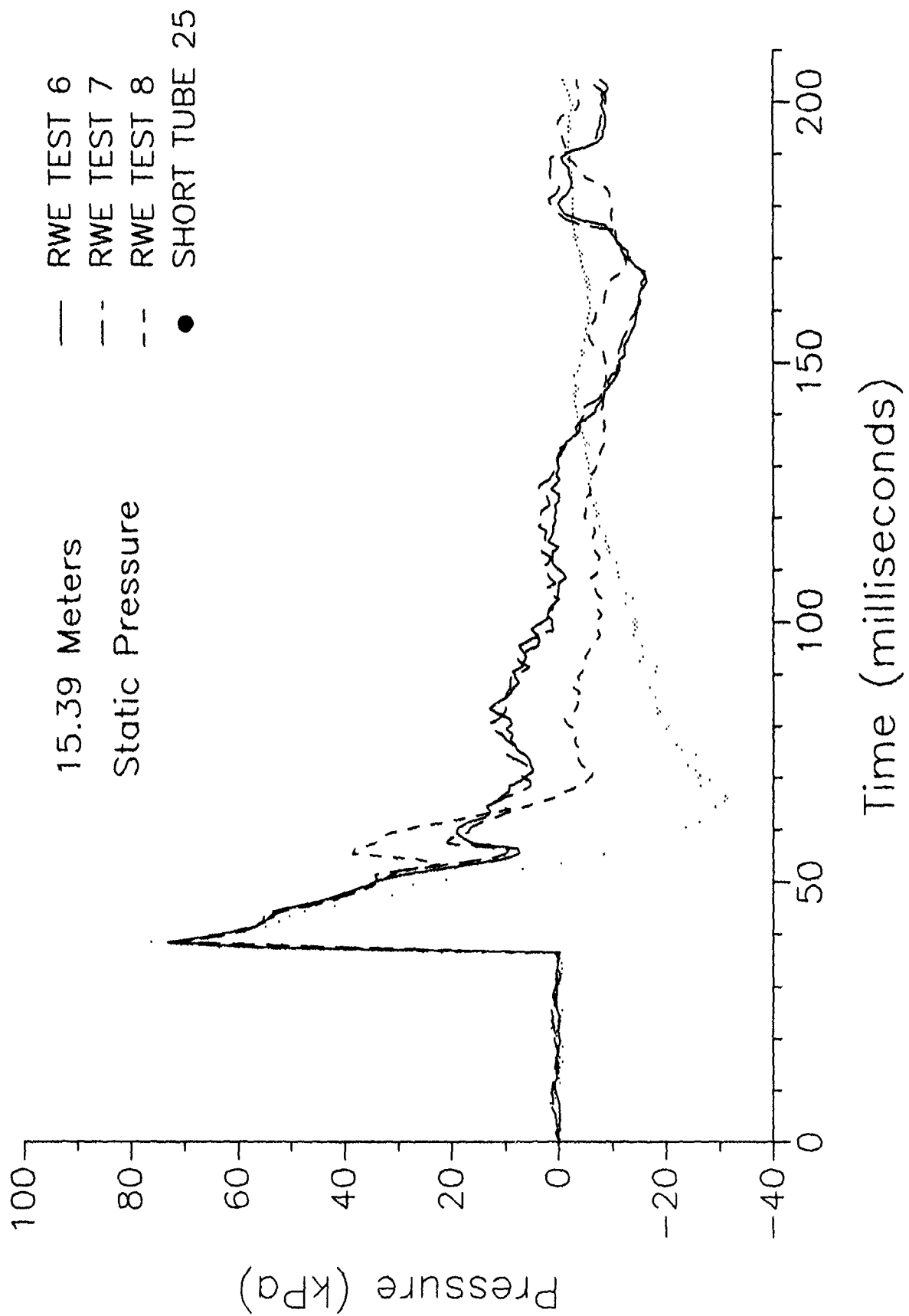


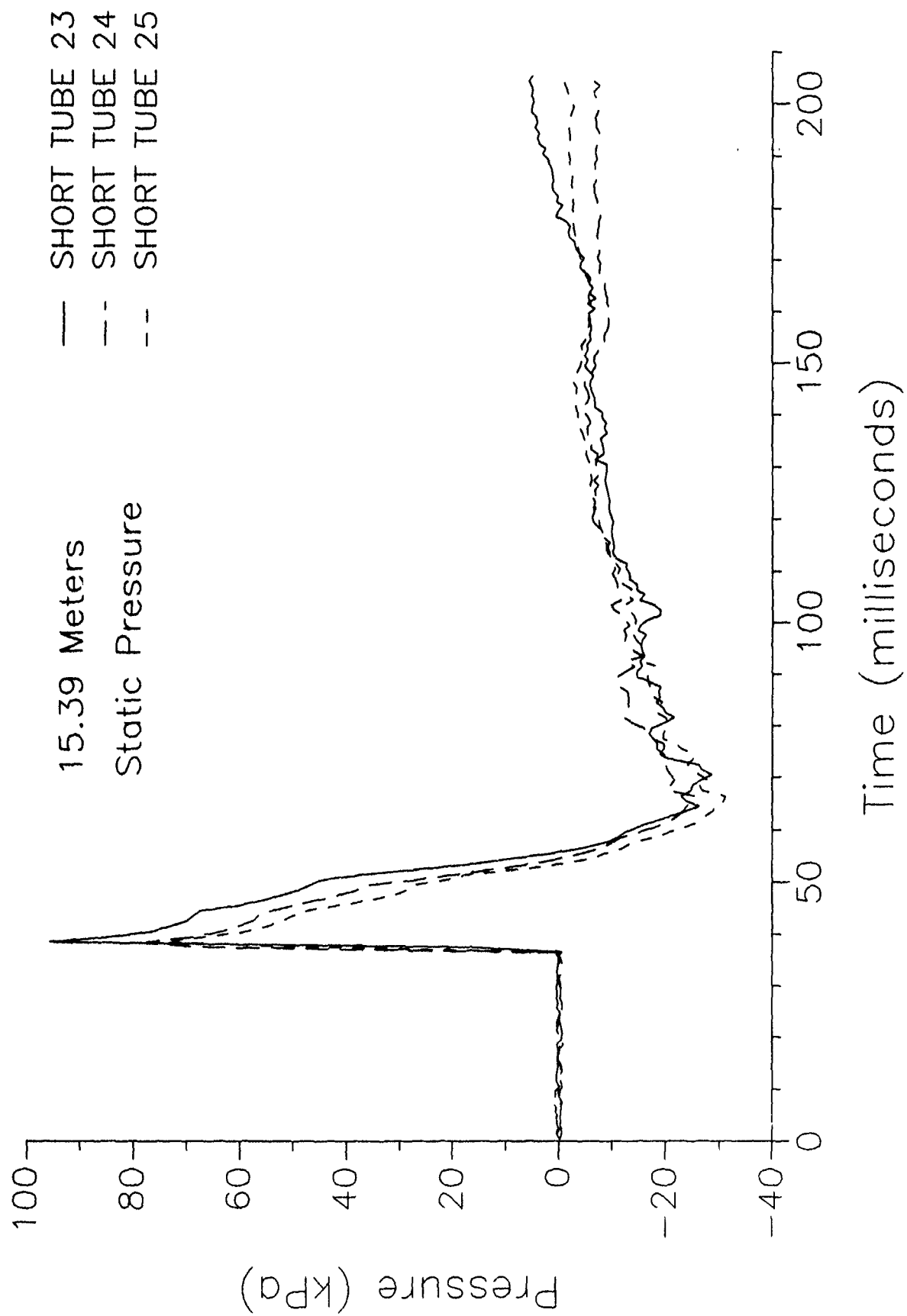


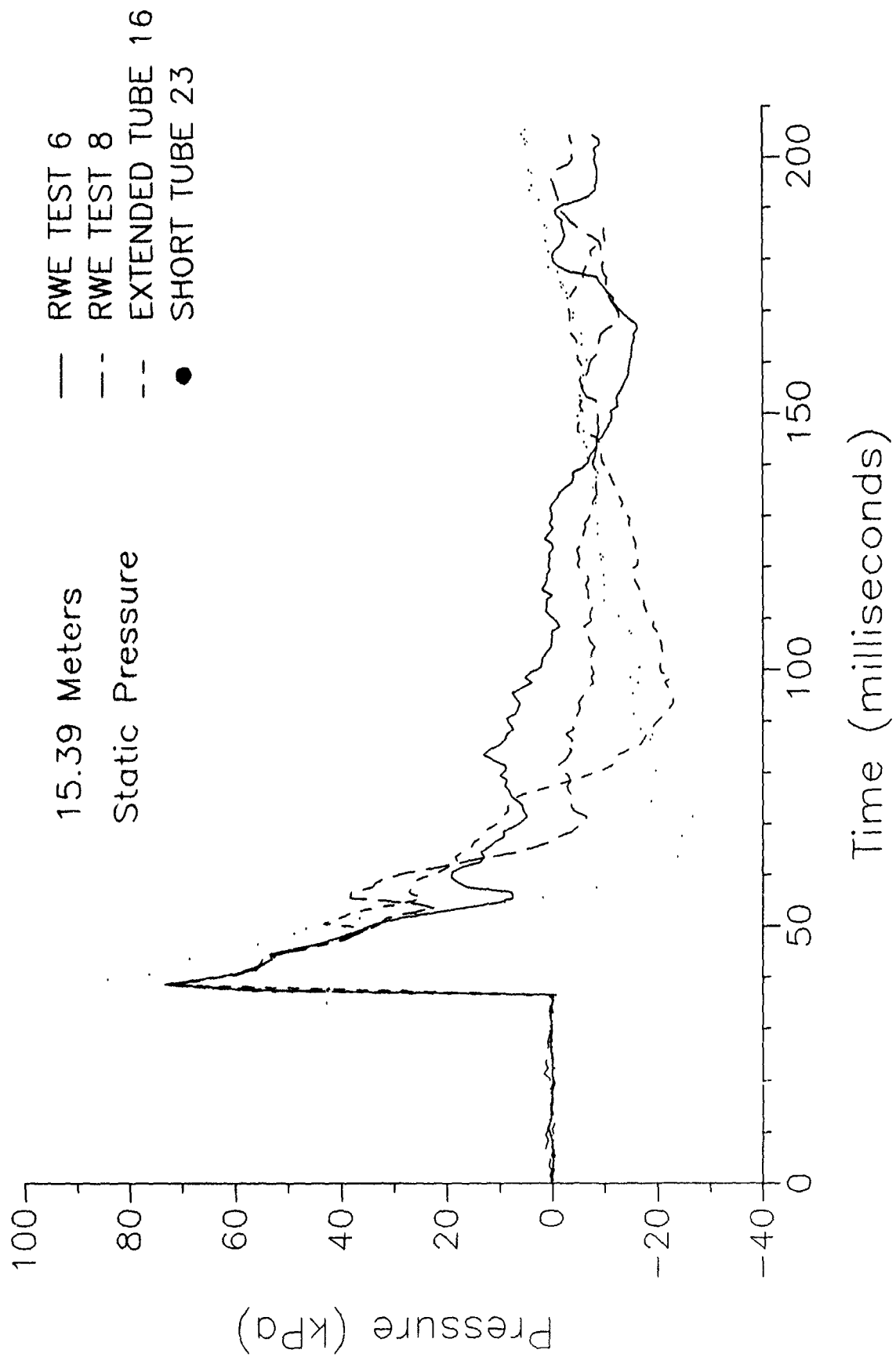


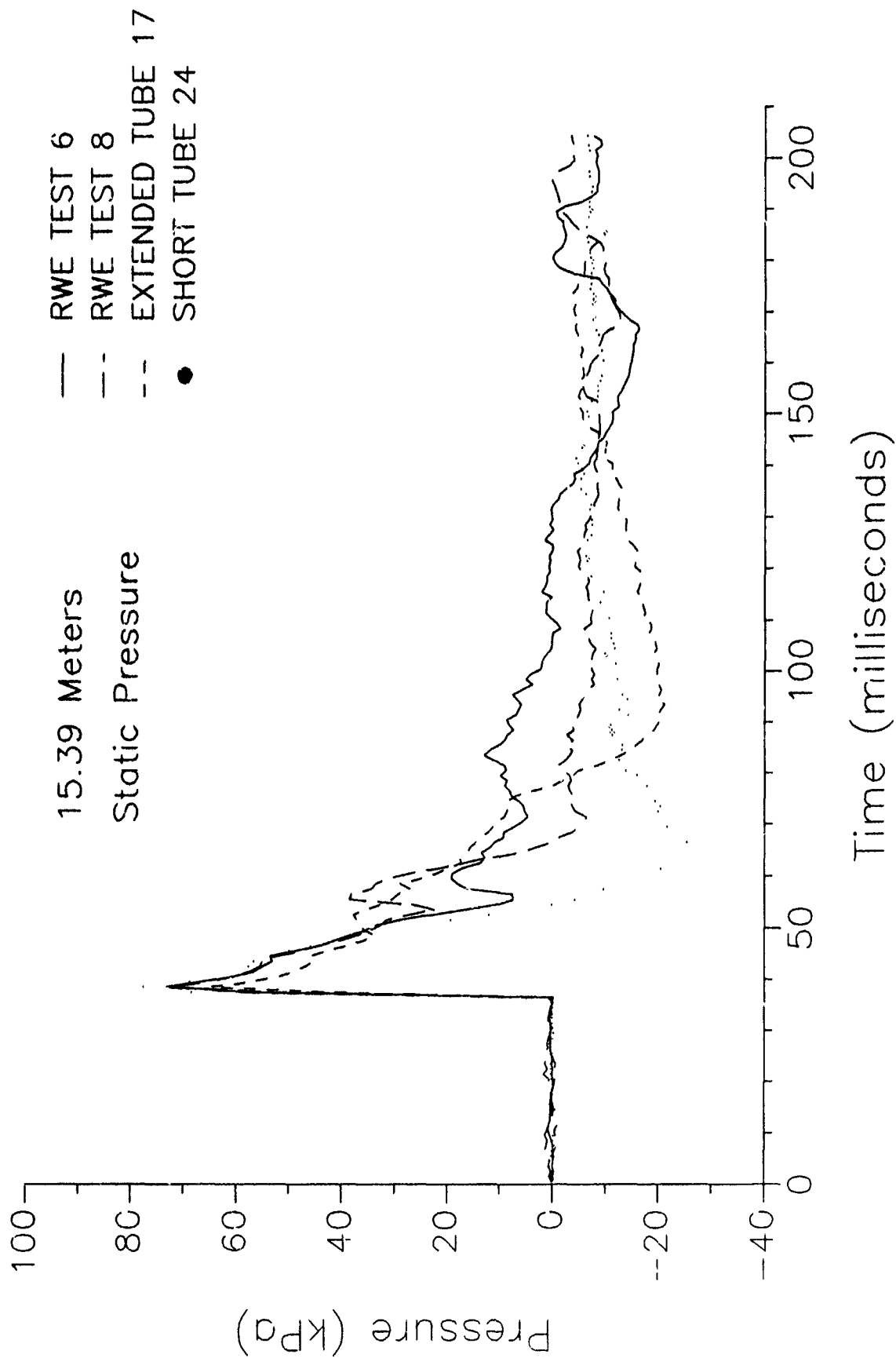


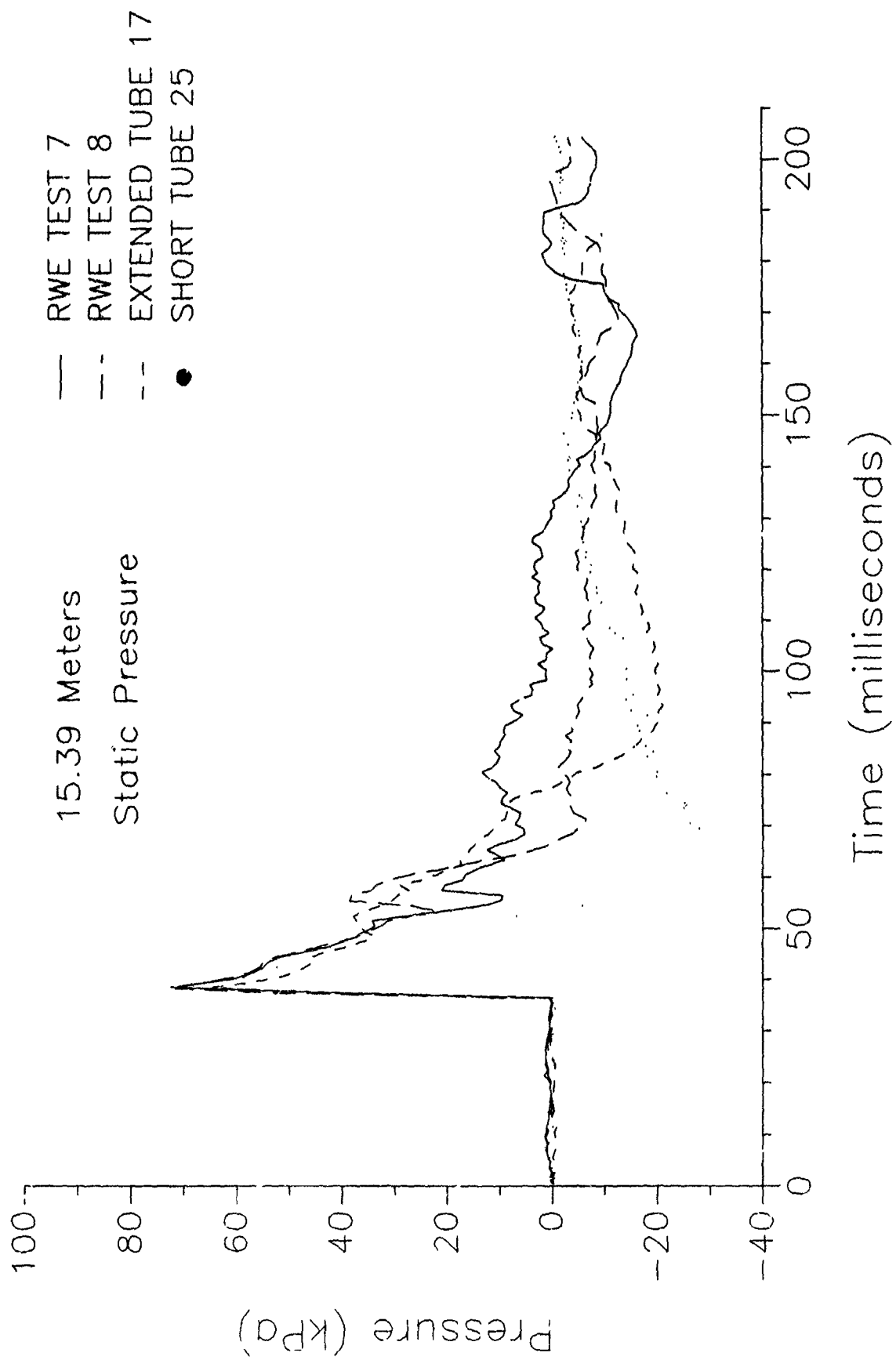


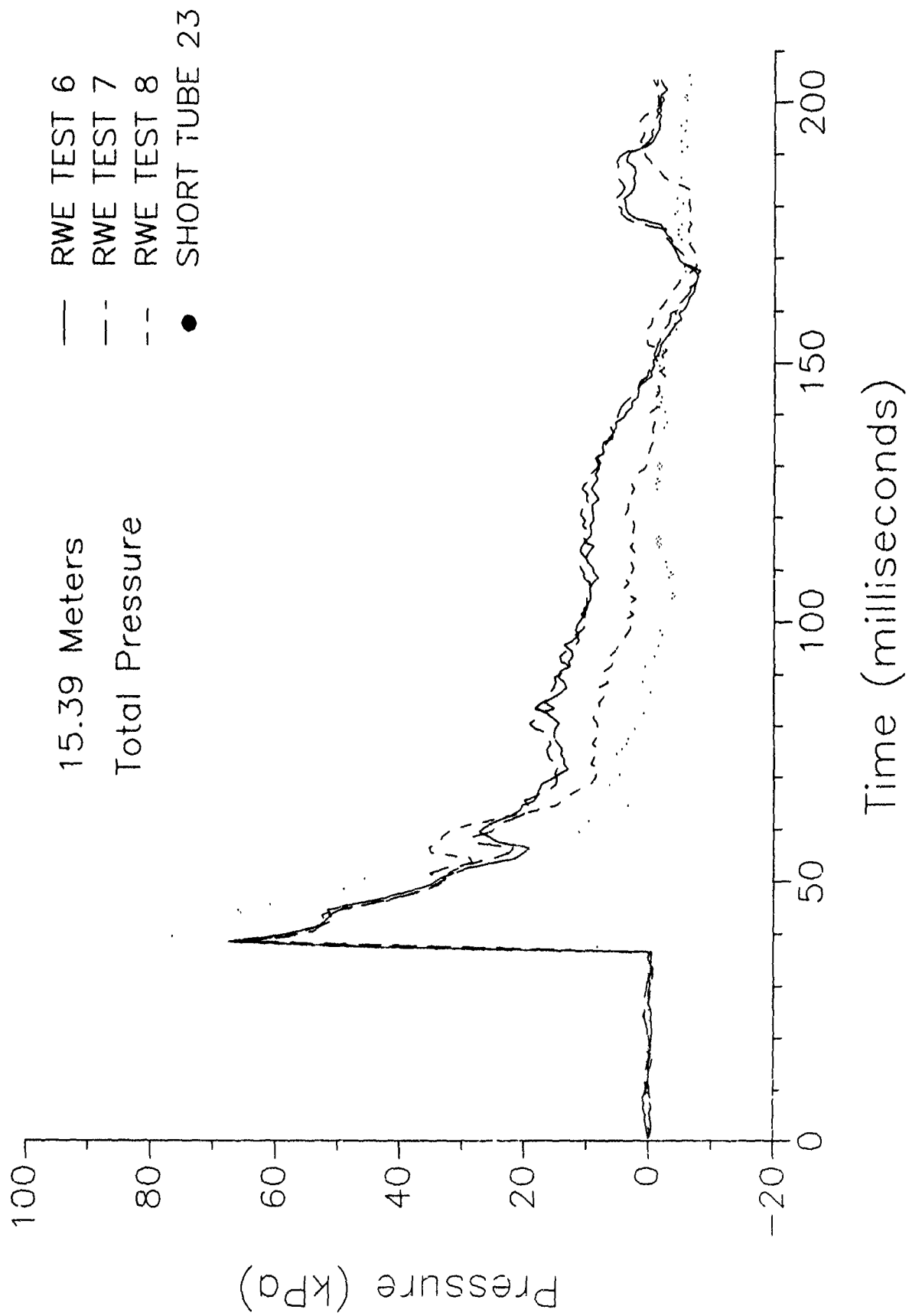


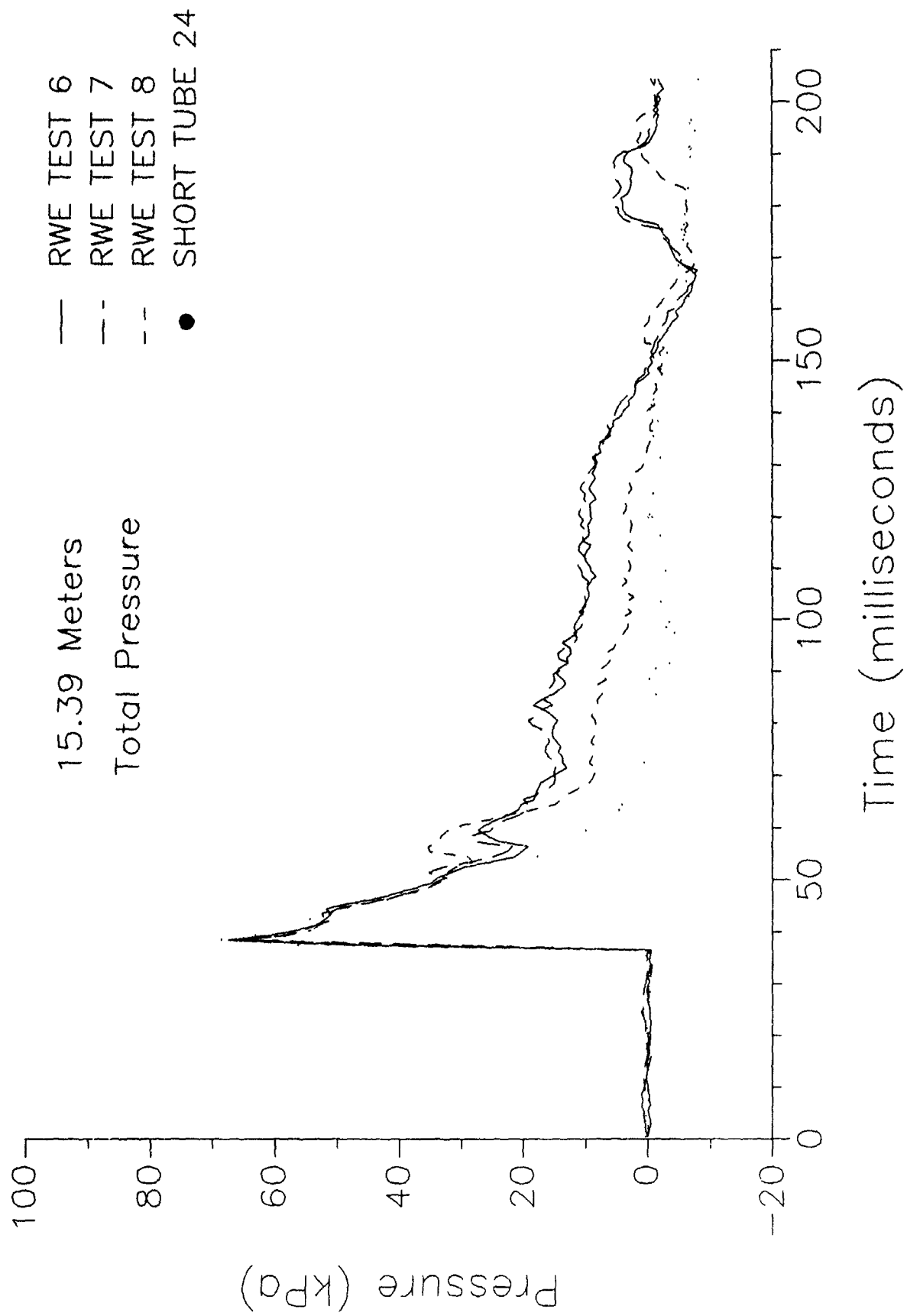


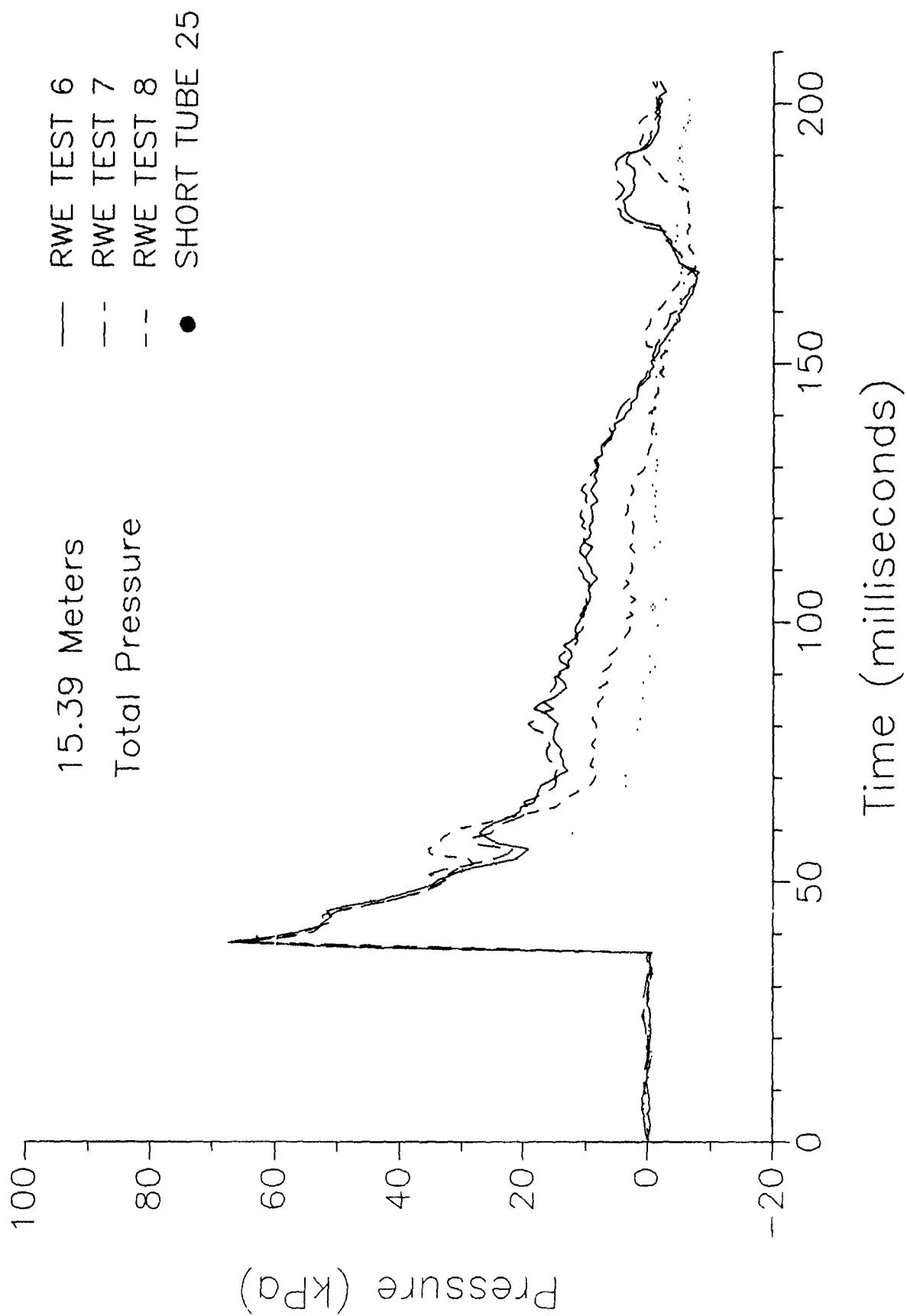


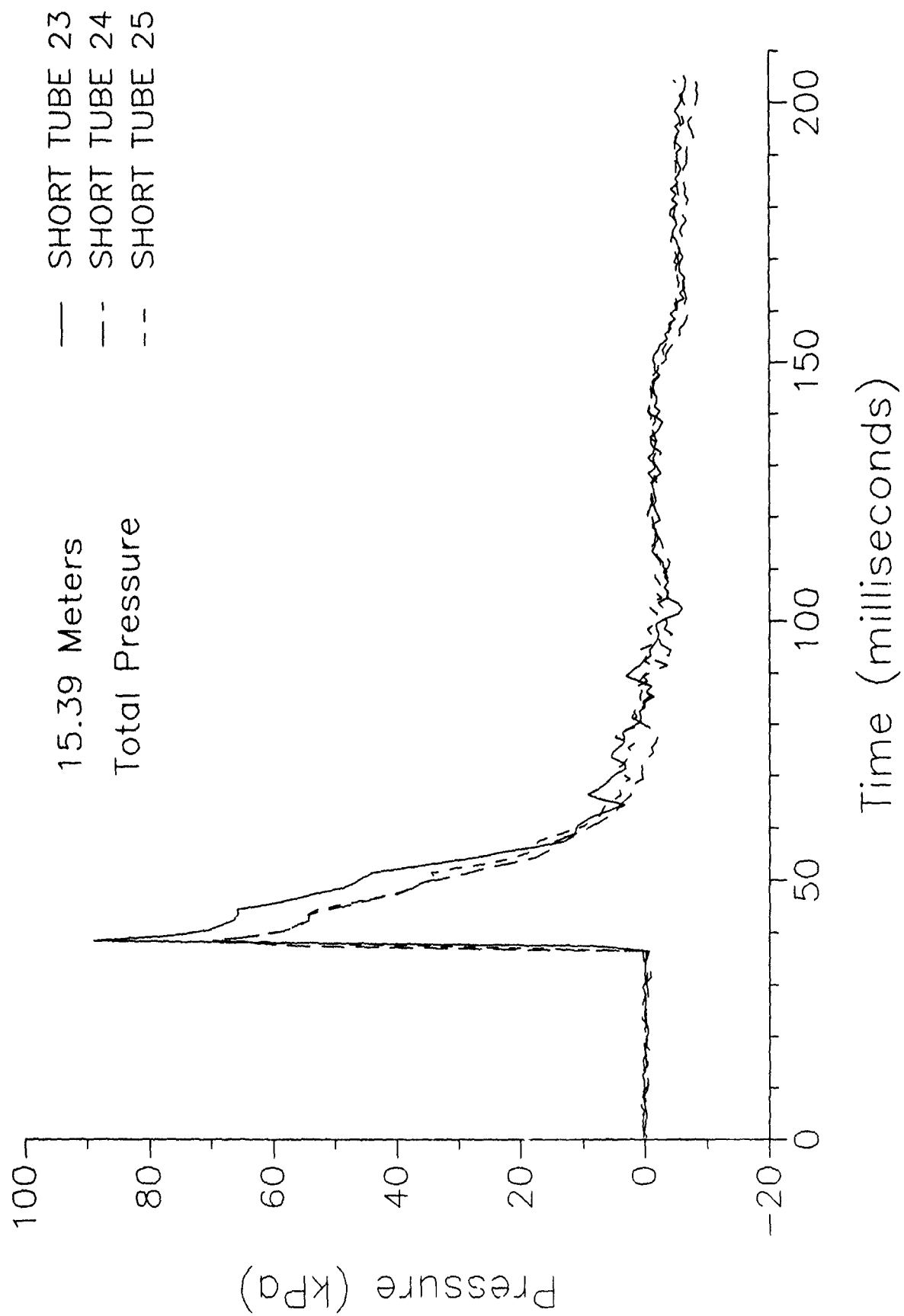


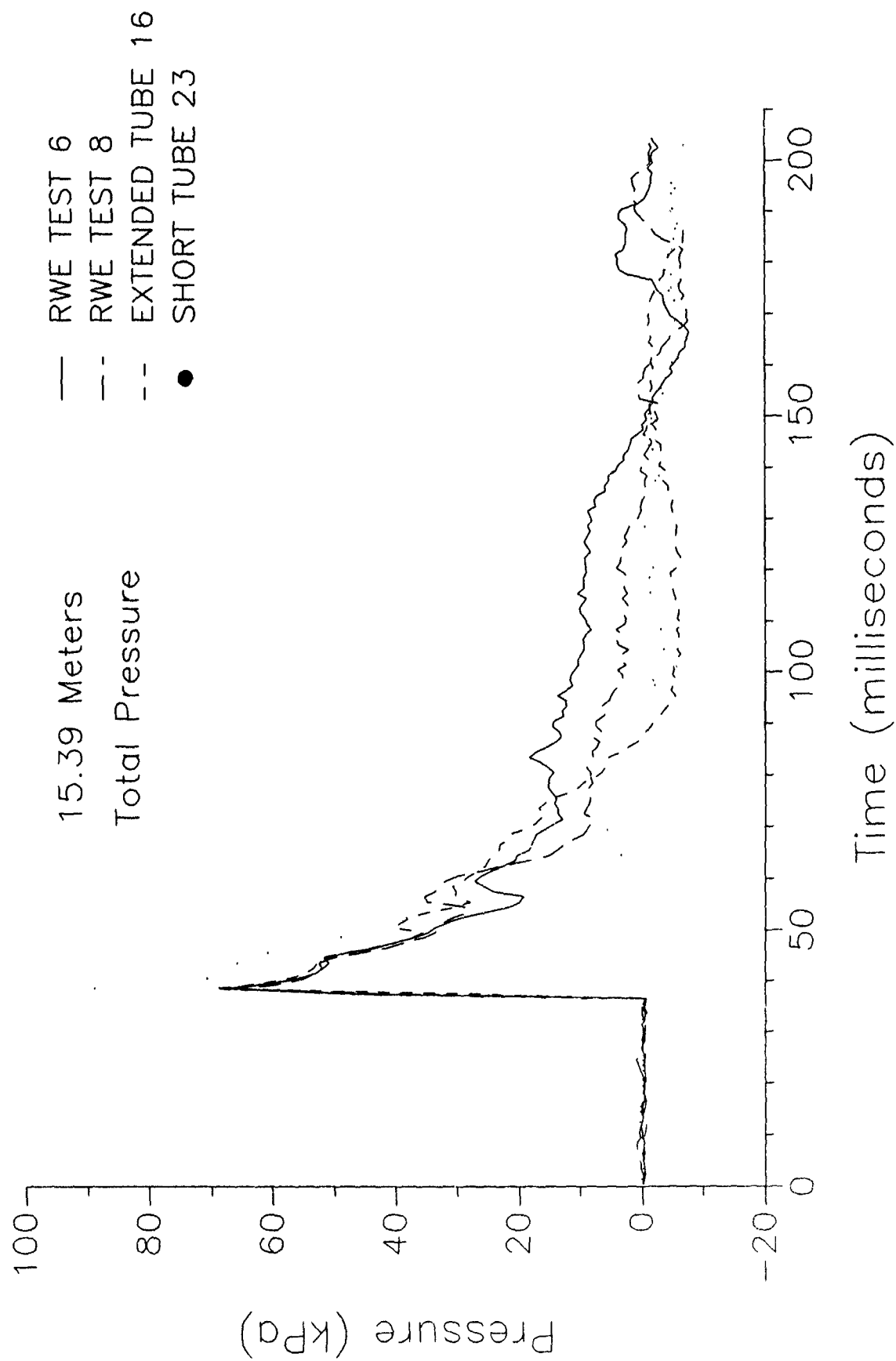


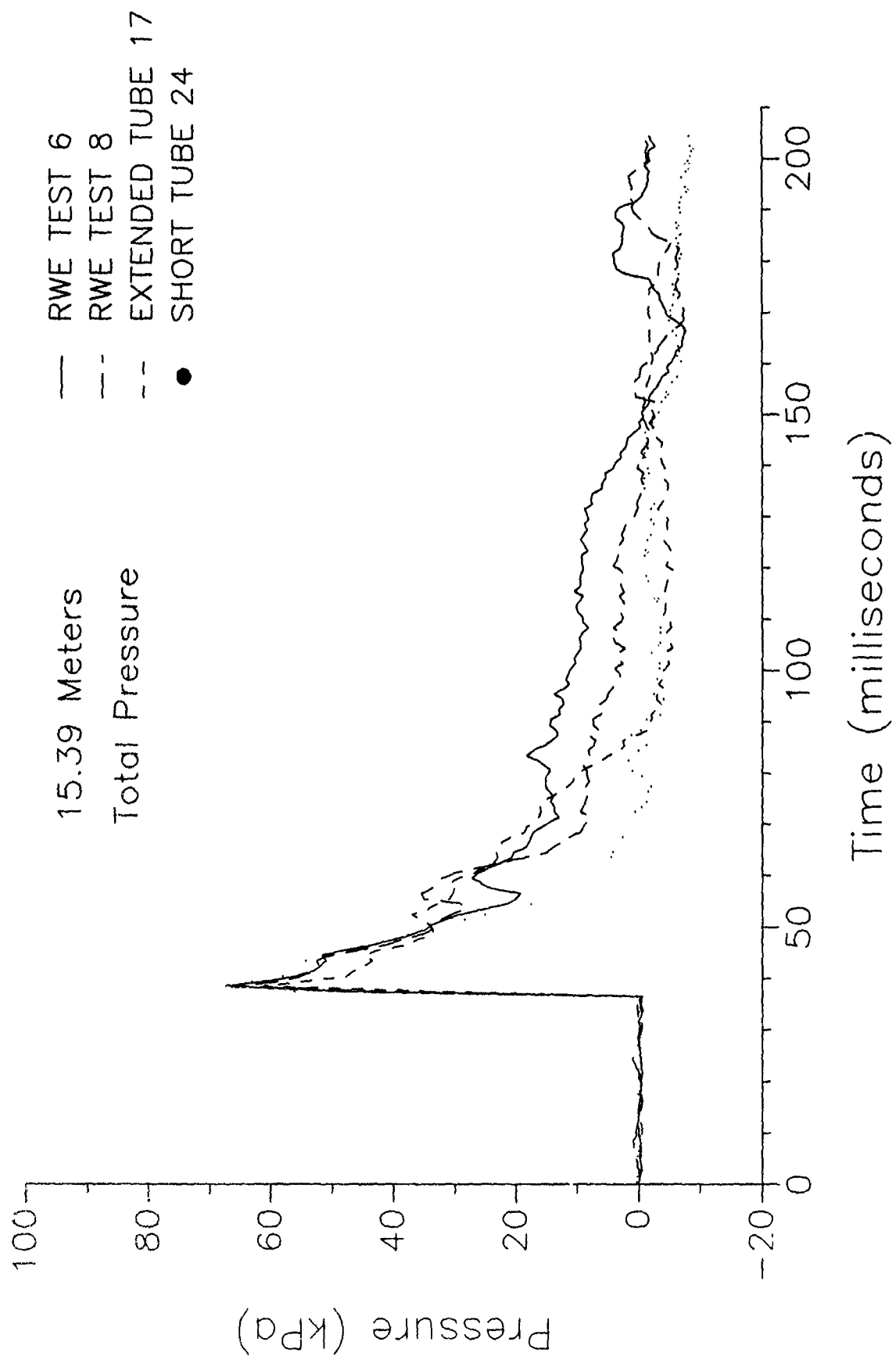


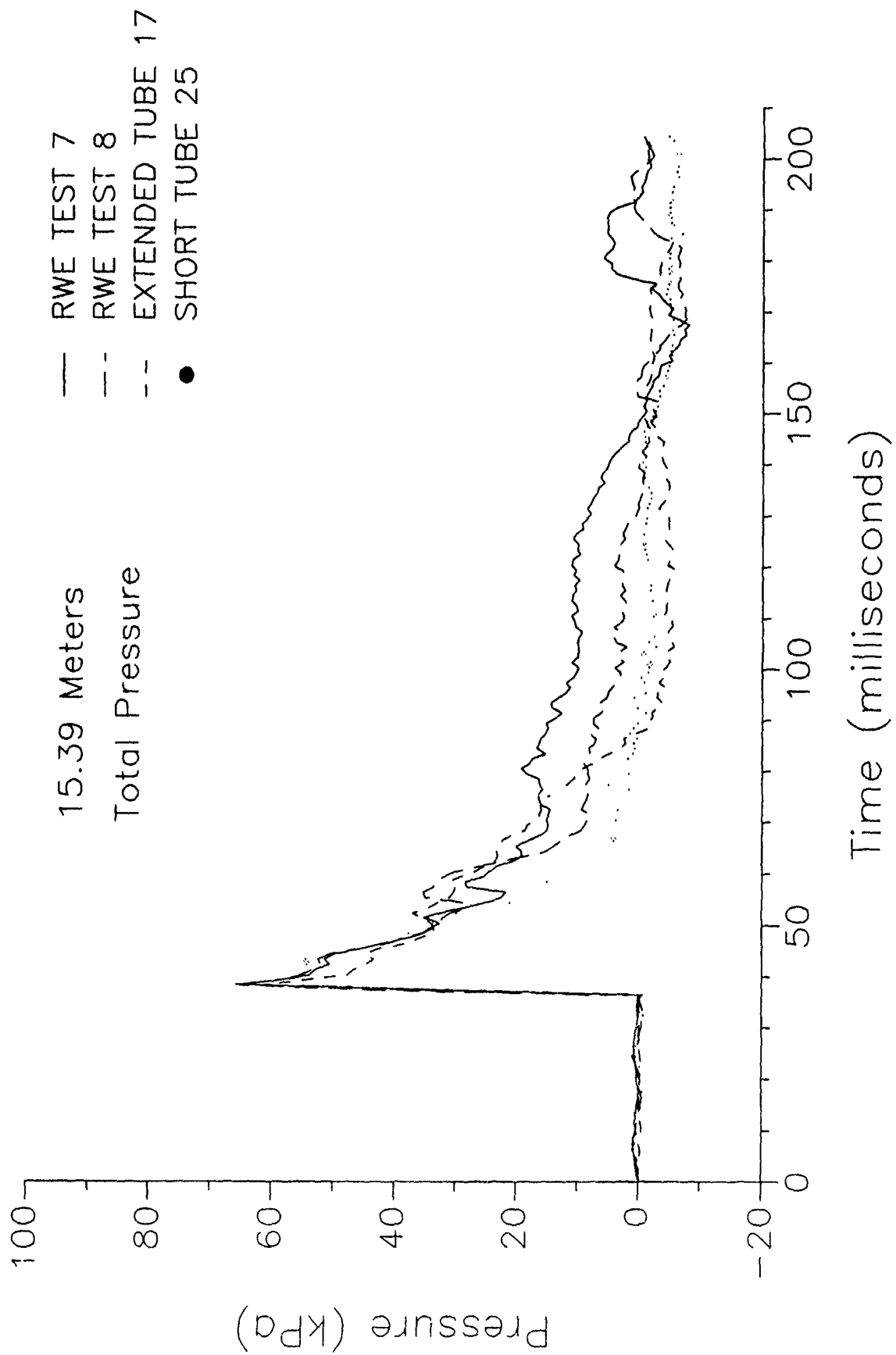








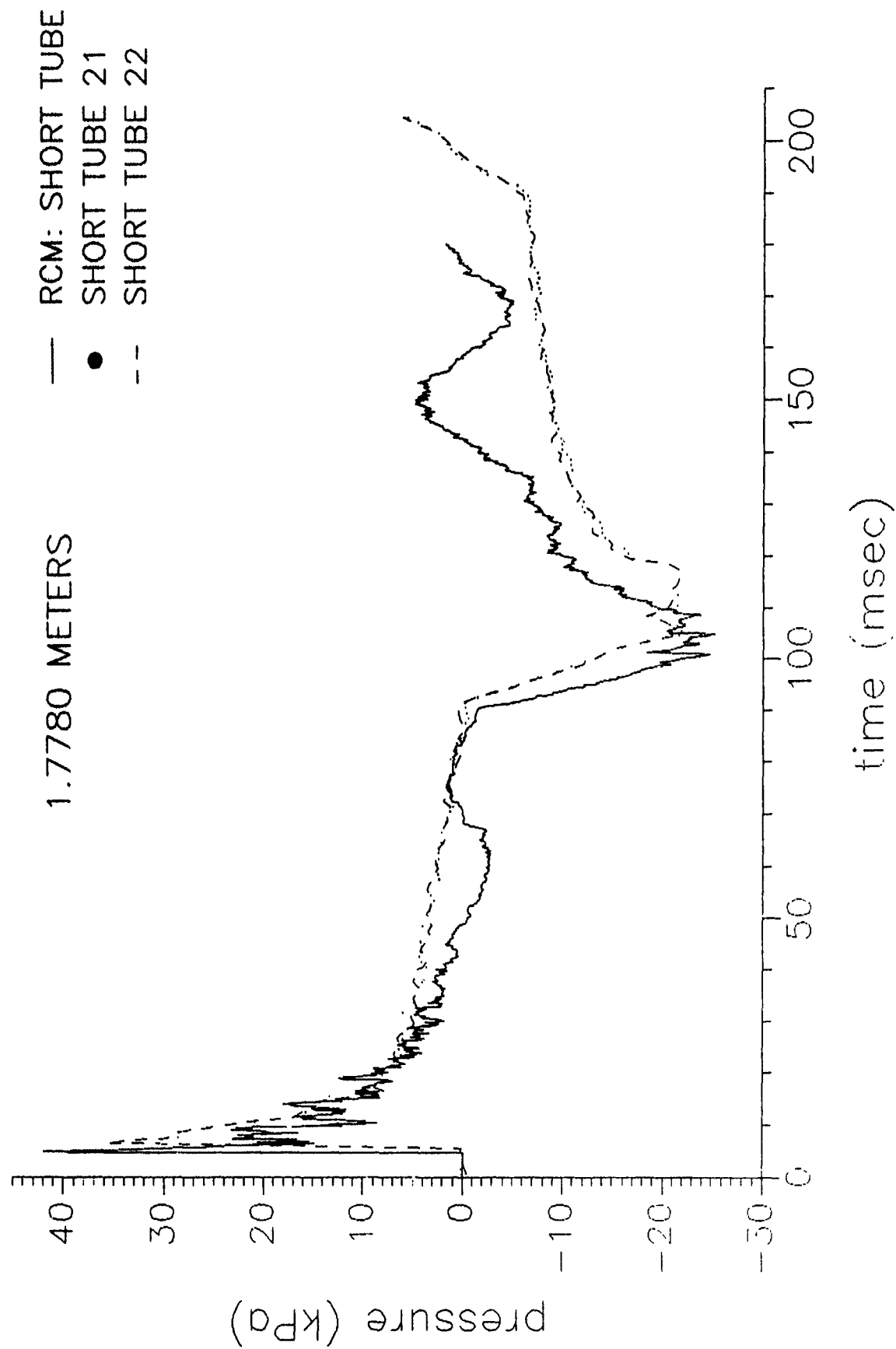


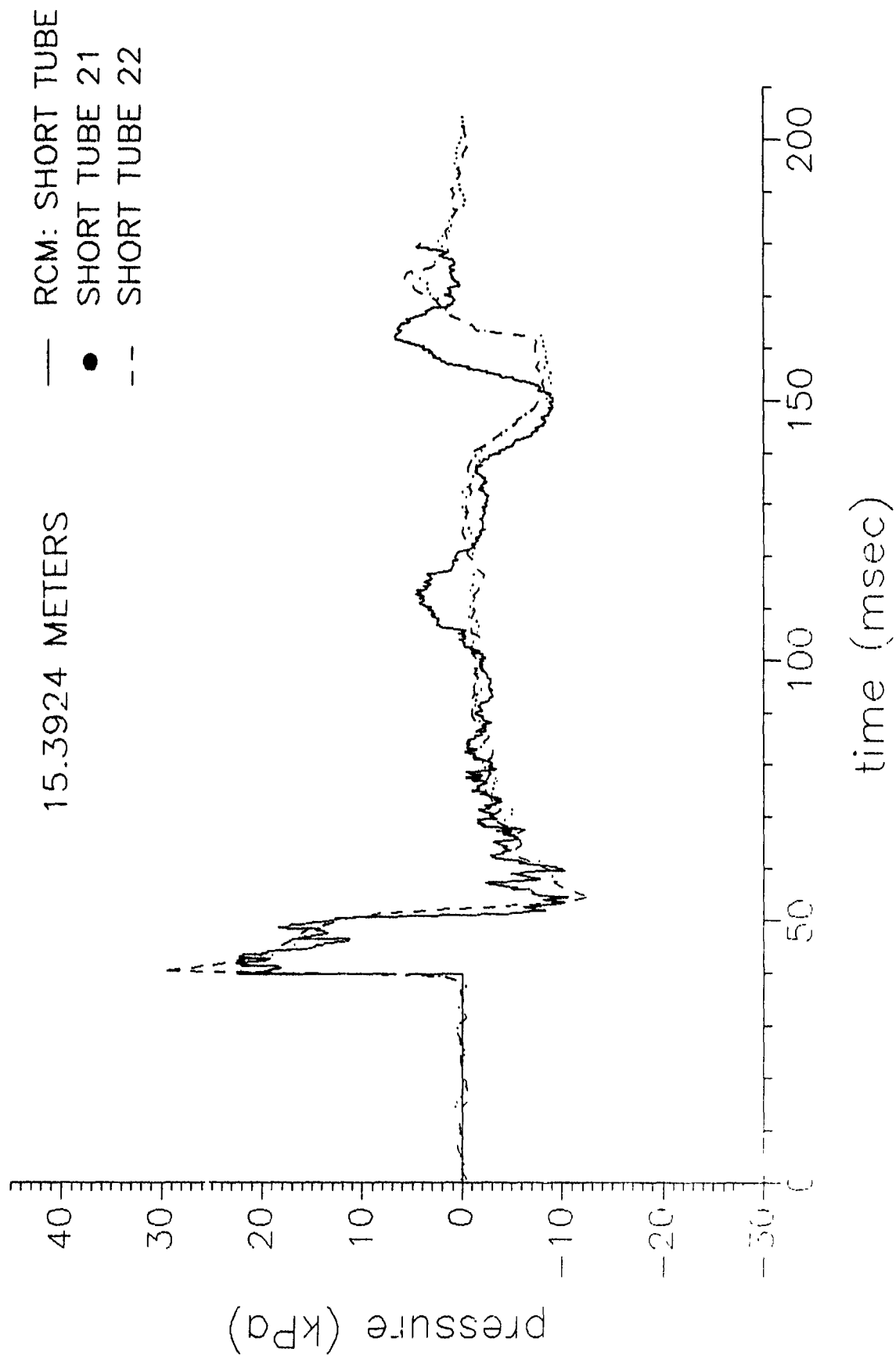


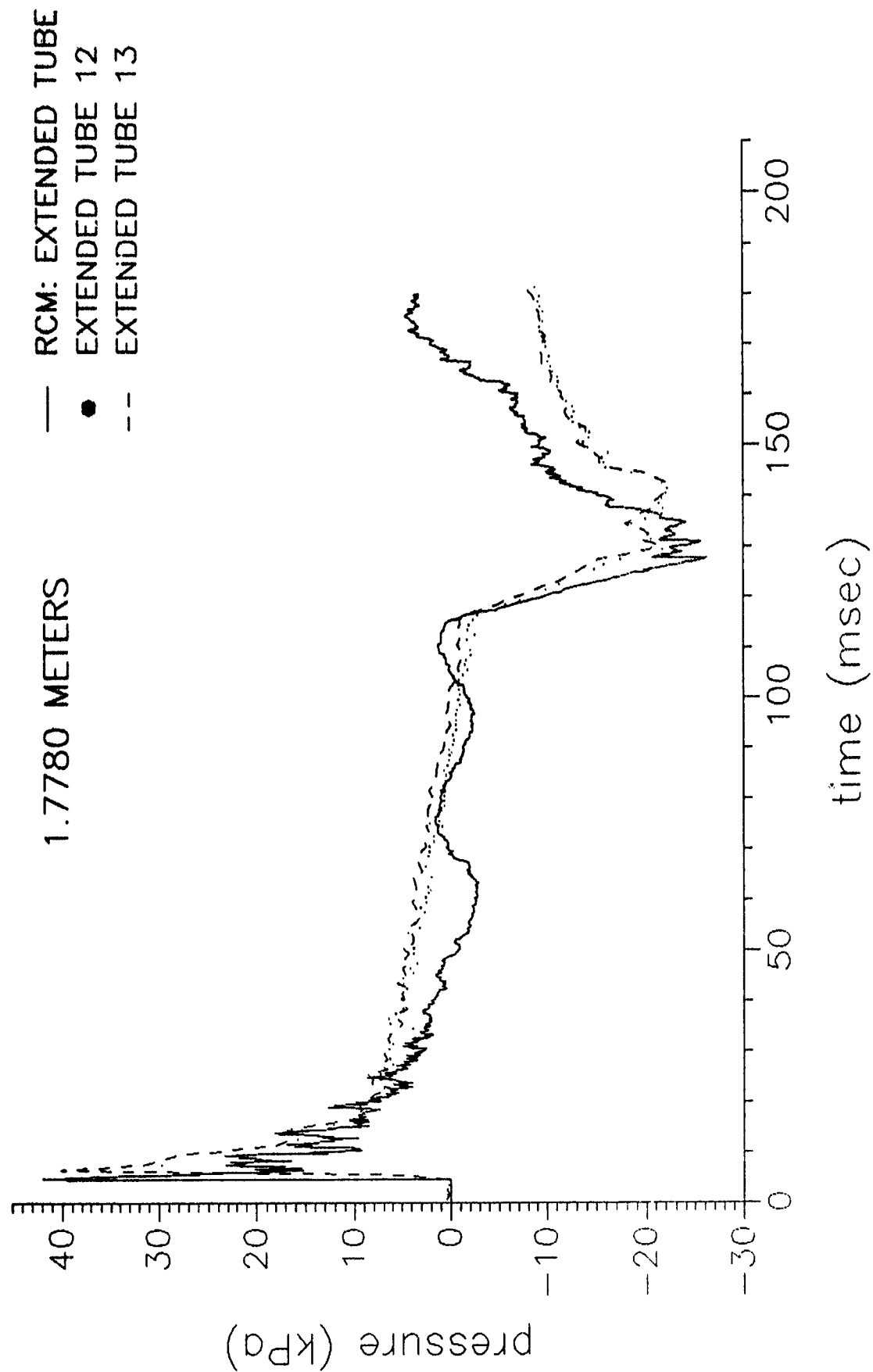
INTENTIONALLY LEFT BLANK.

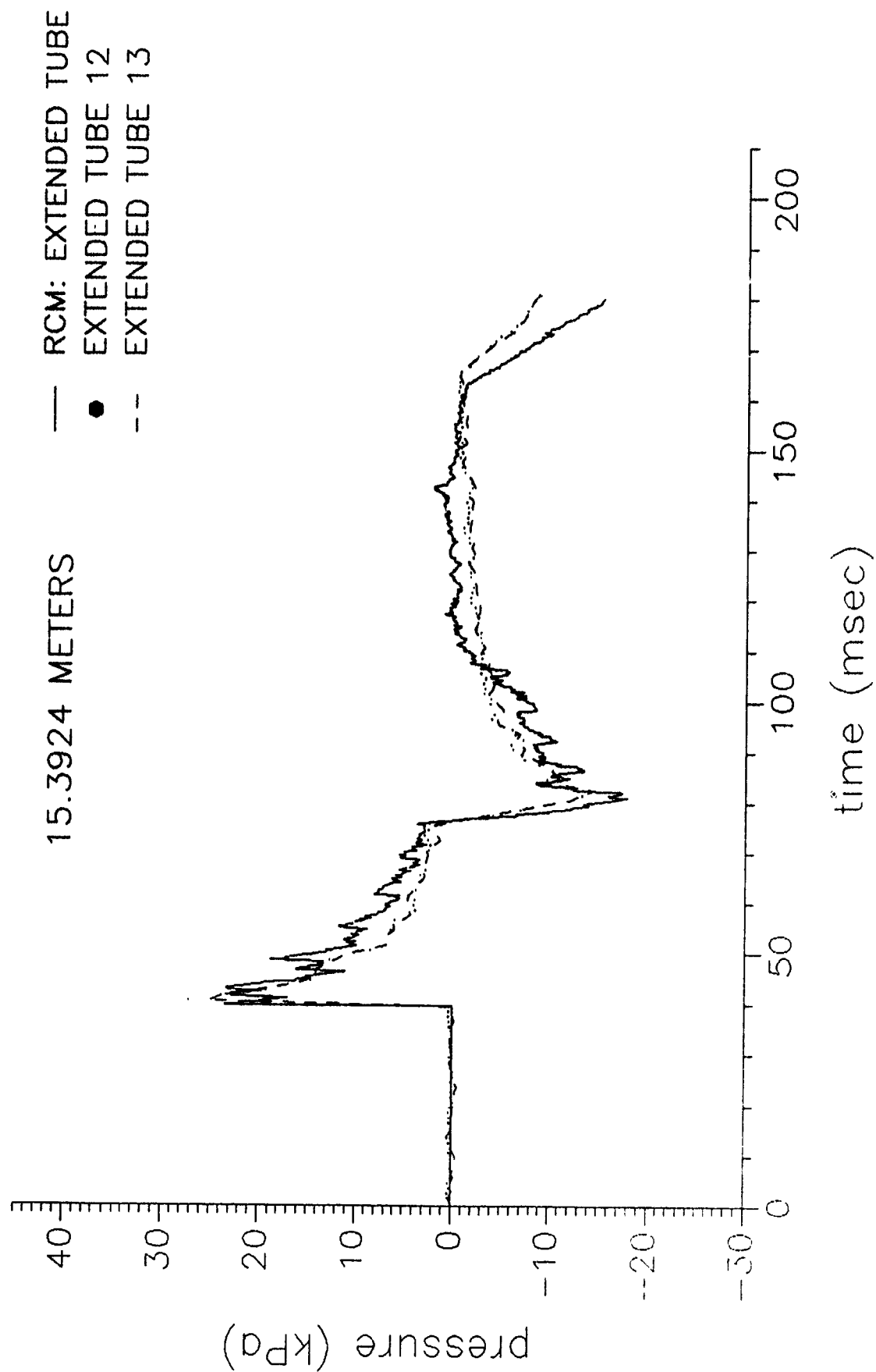
APPENDIX D
TEST DATA AND RCM CALCULATION COMPARISONS

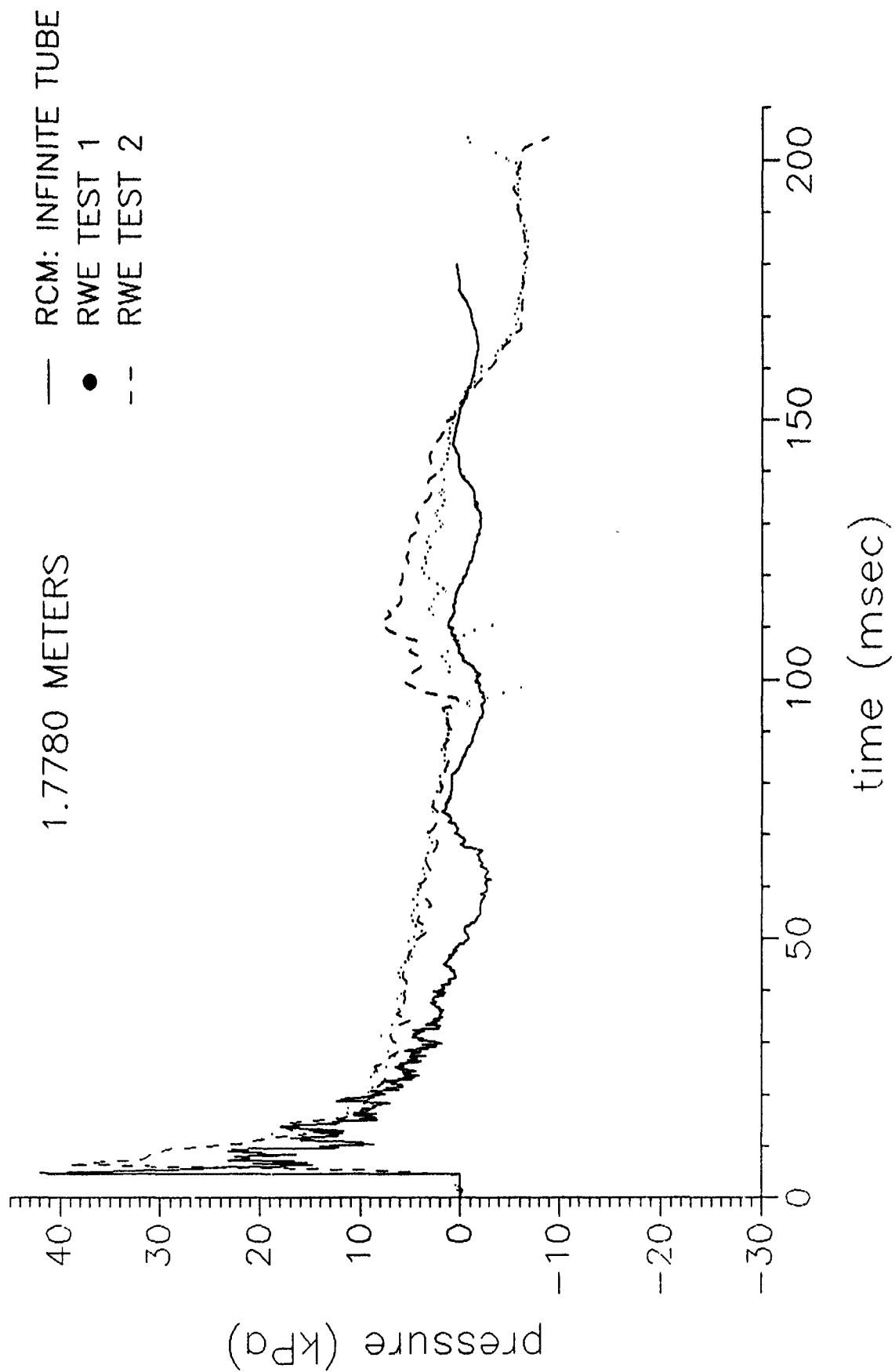
INTENTIONALLY LEFT BLANK.

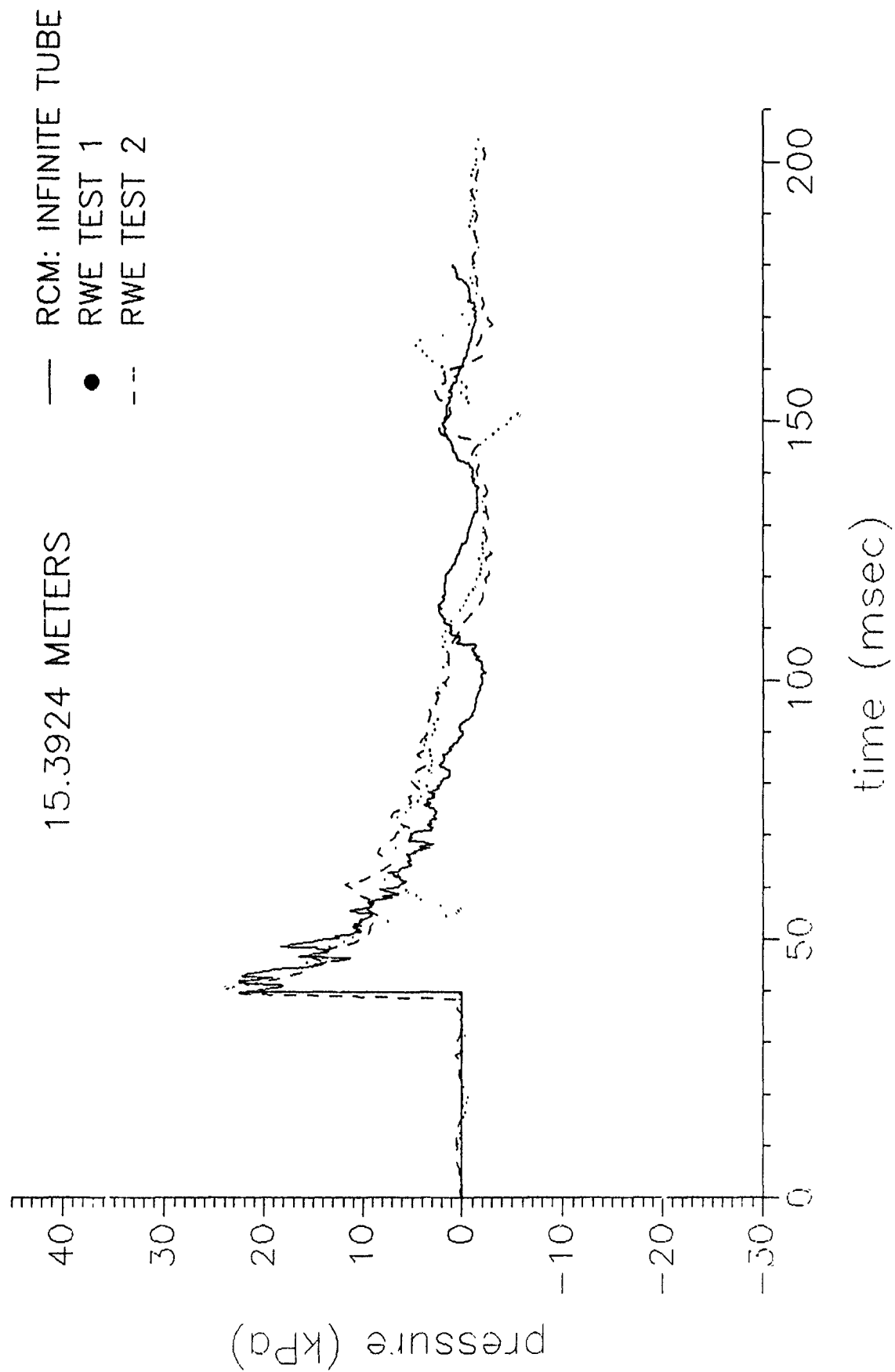


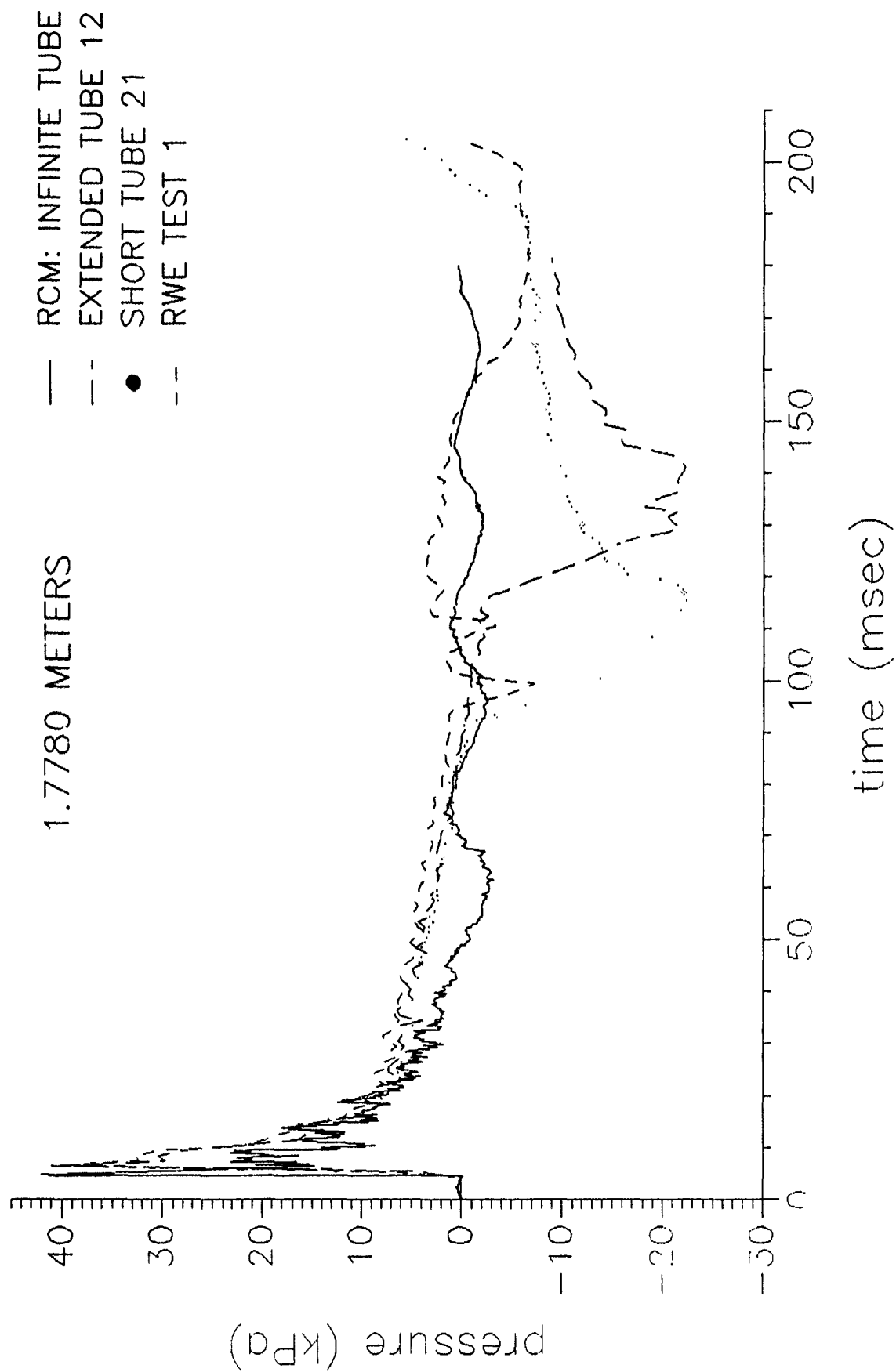


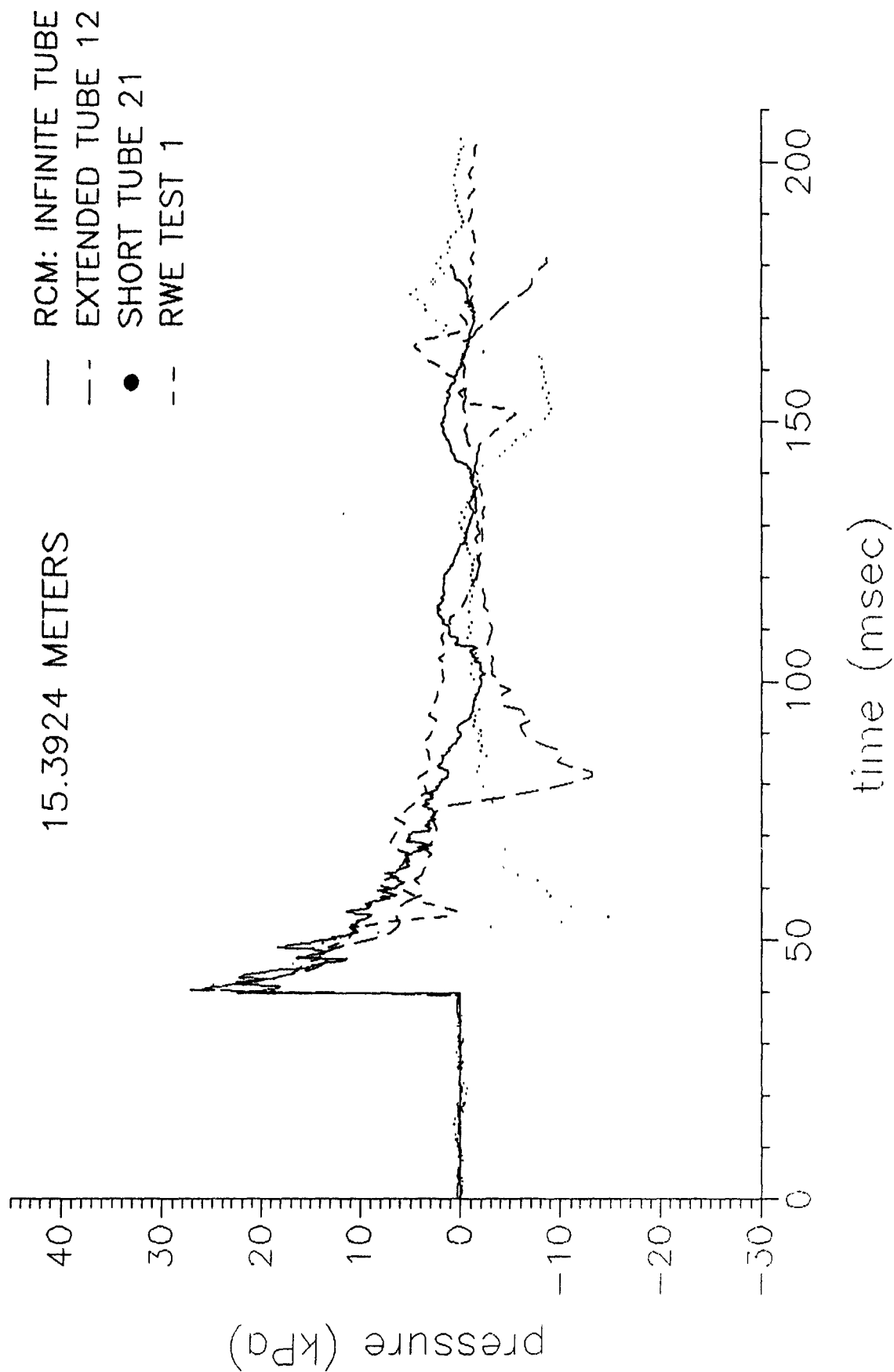


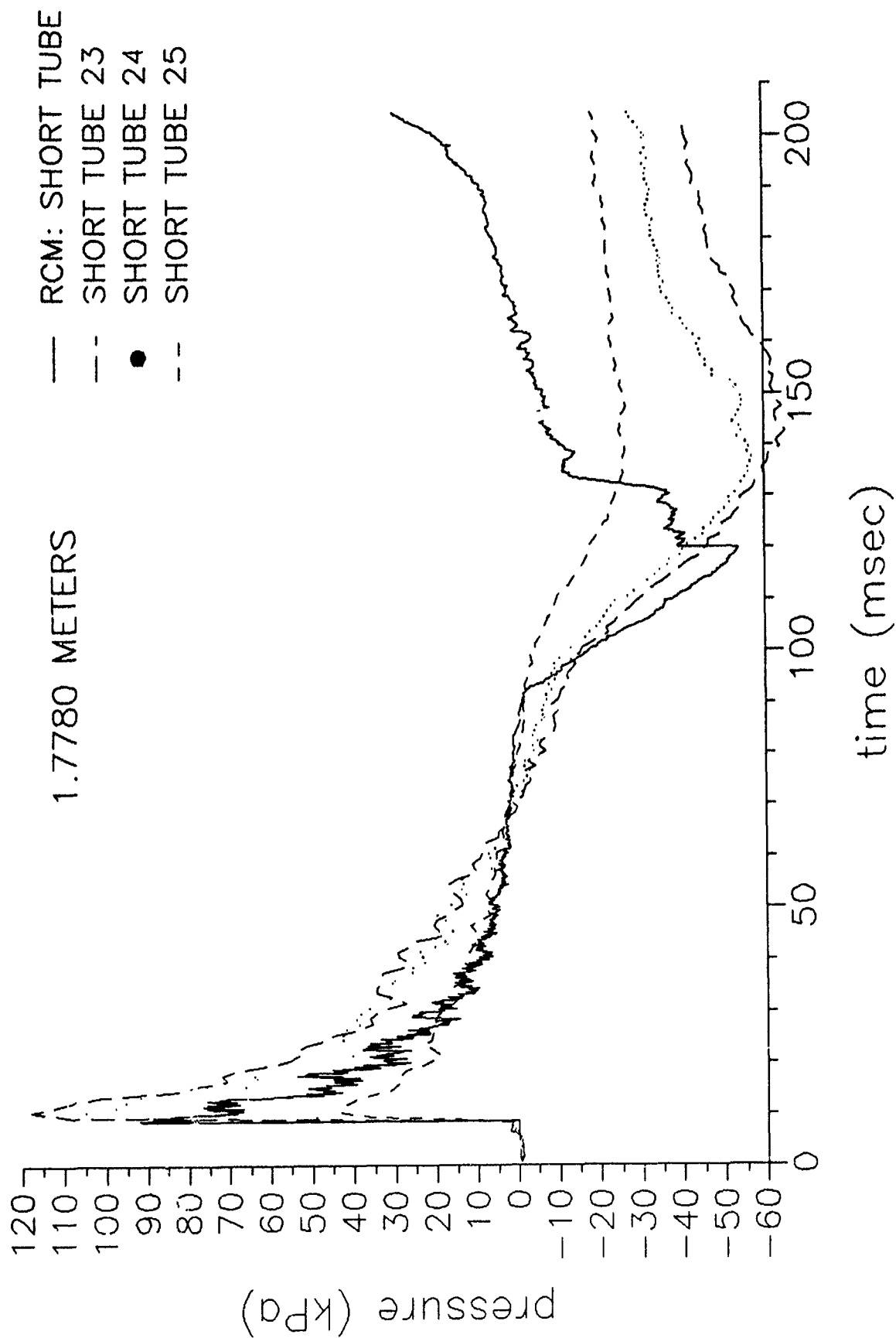


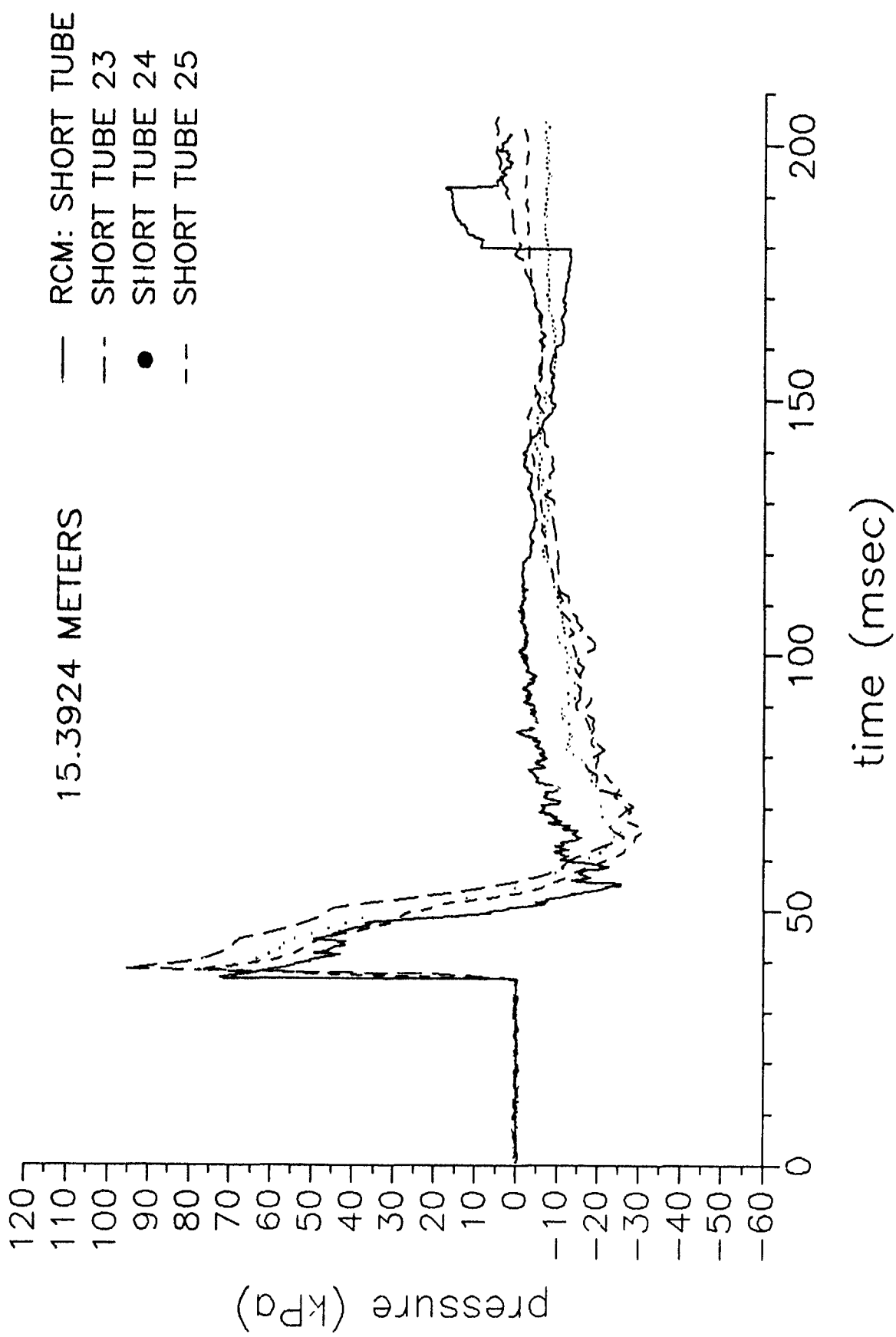


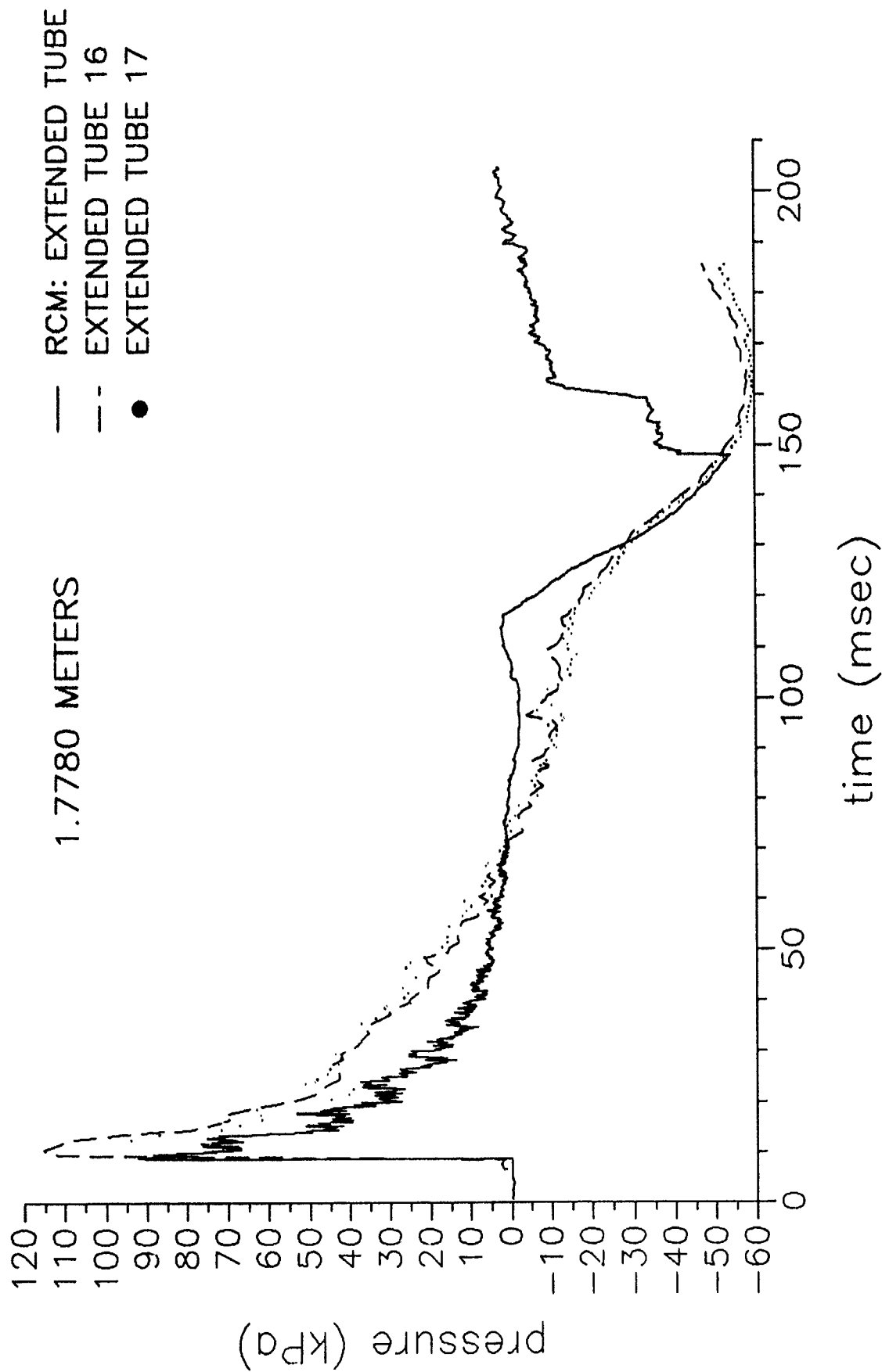


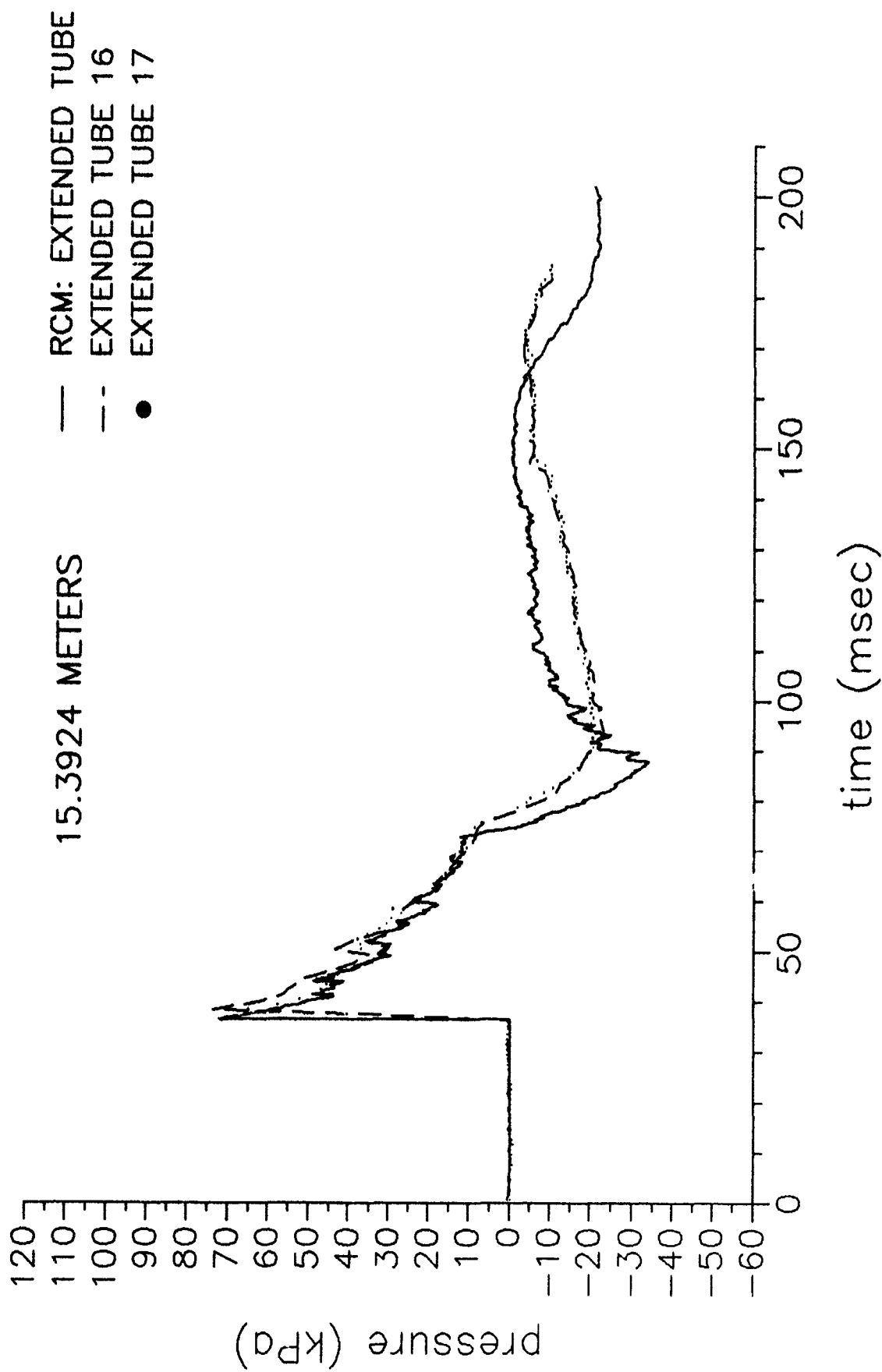


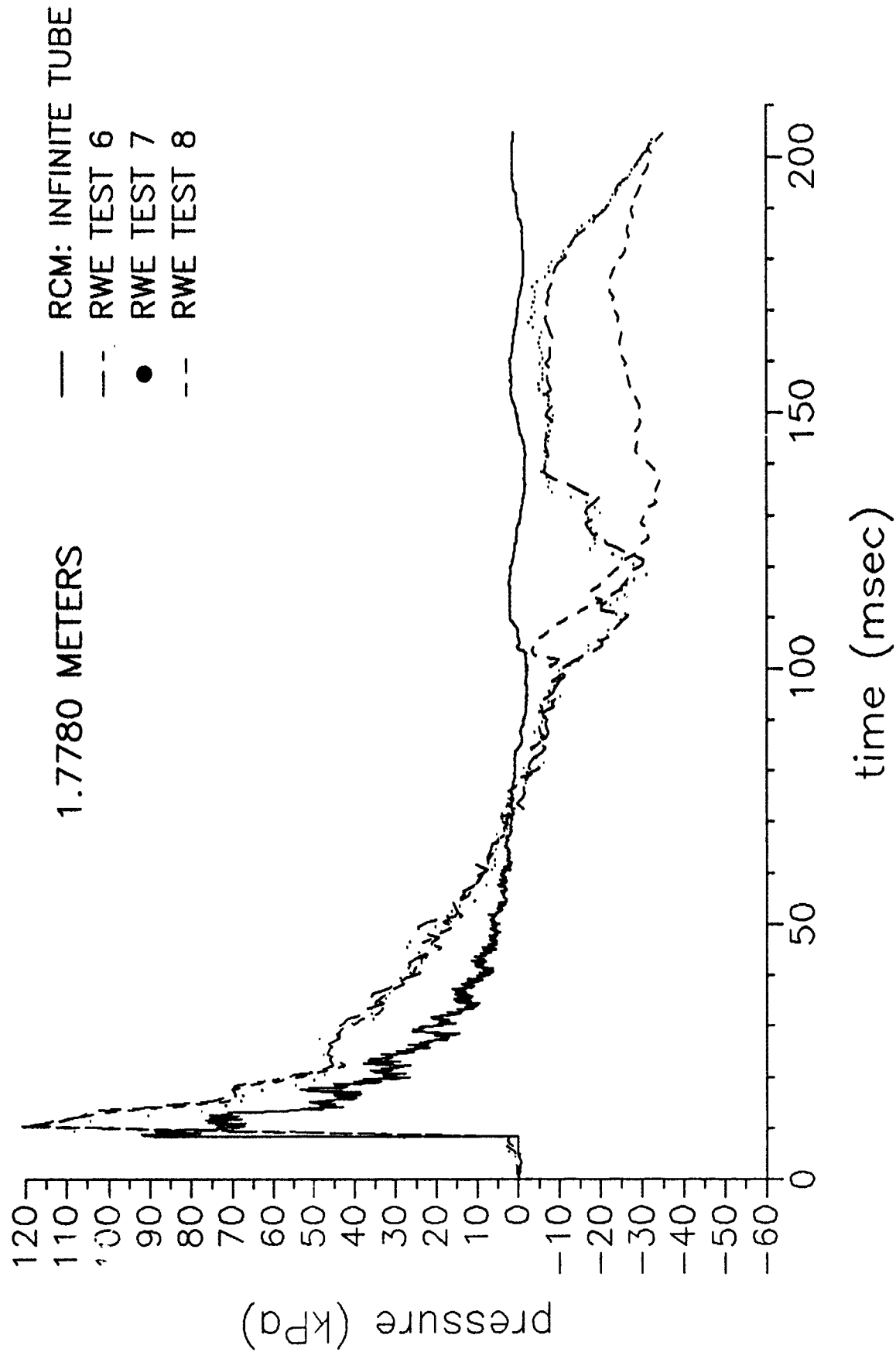


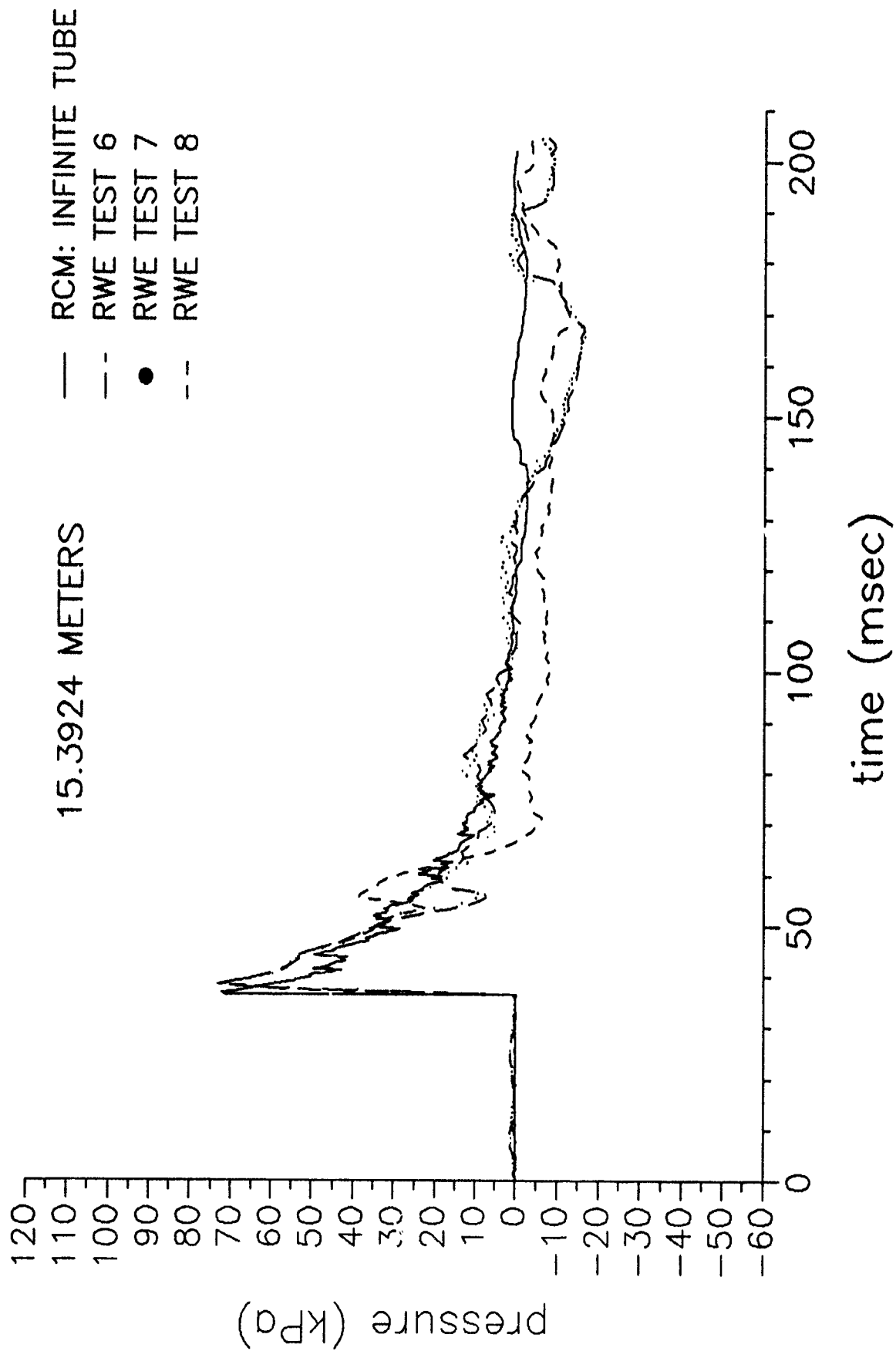


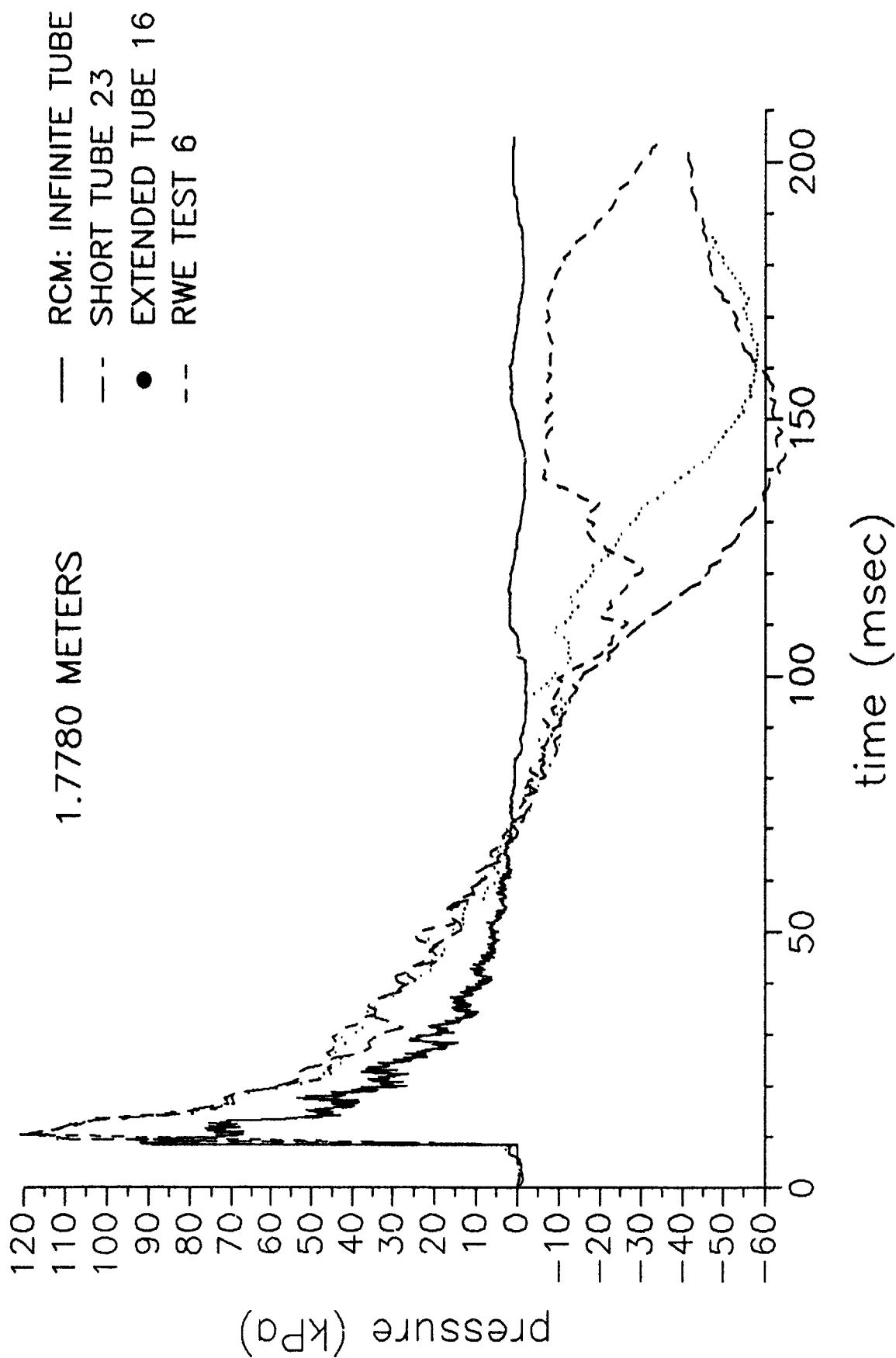


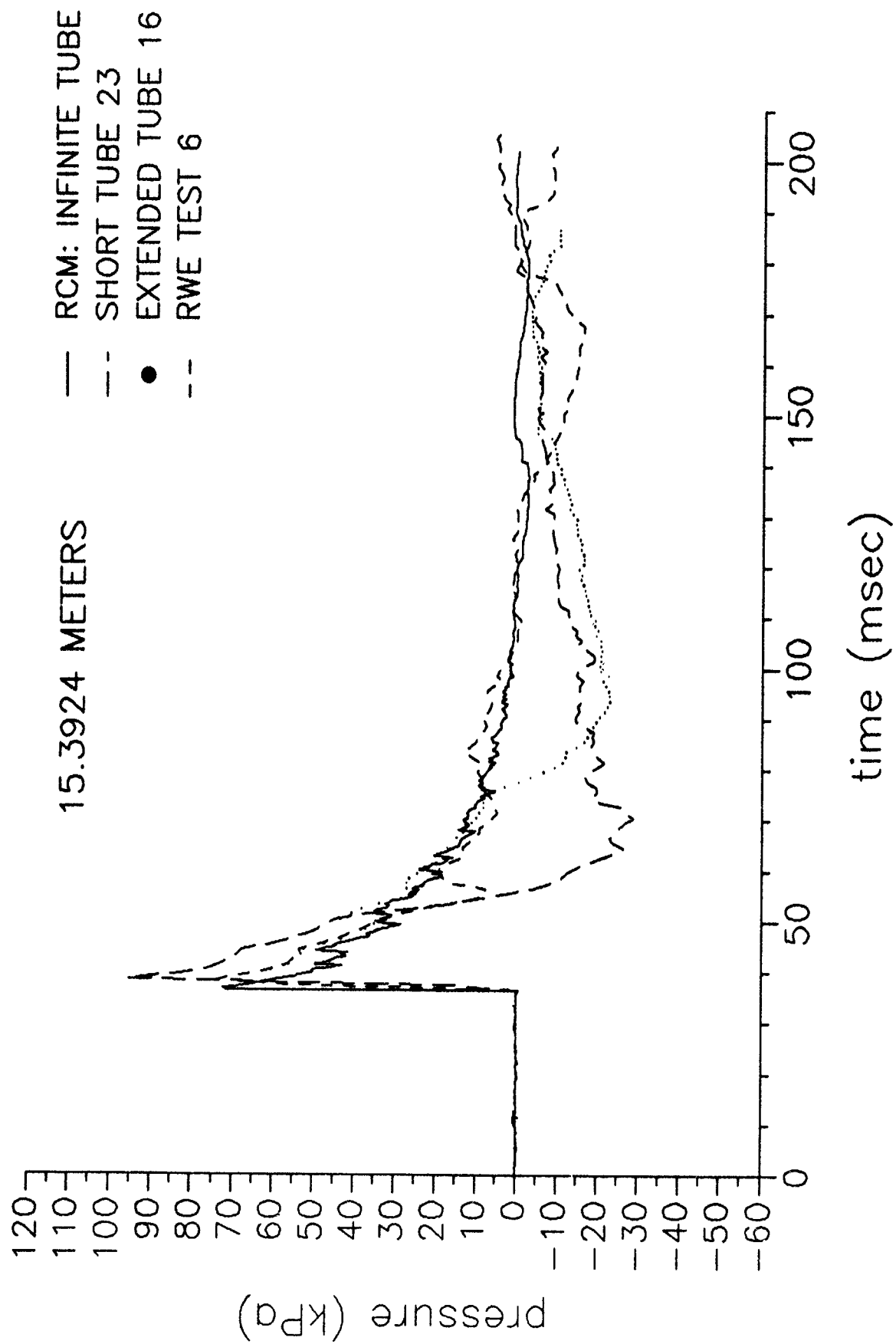


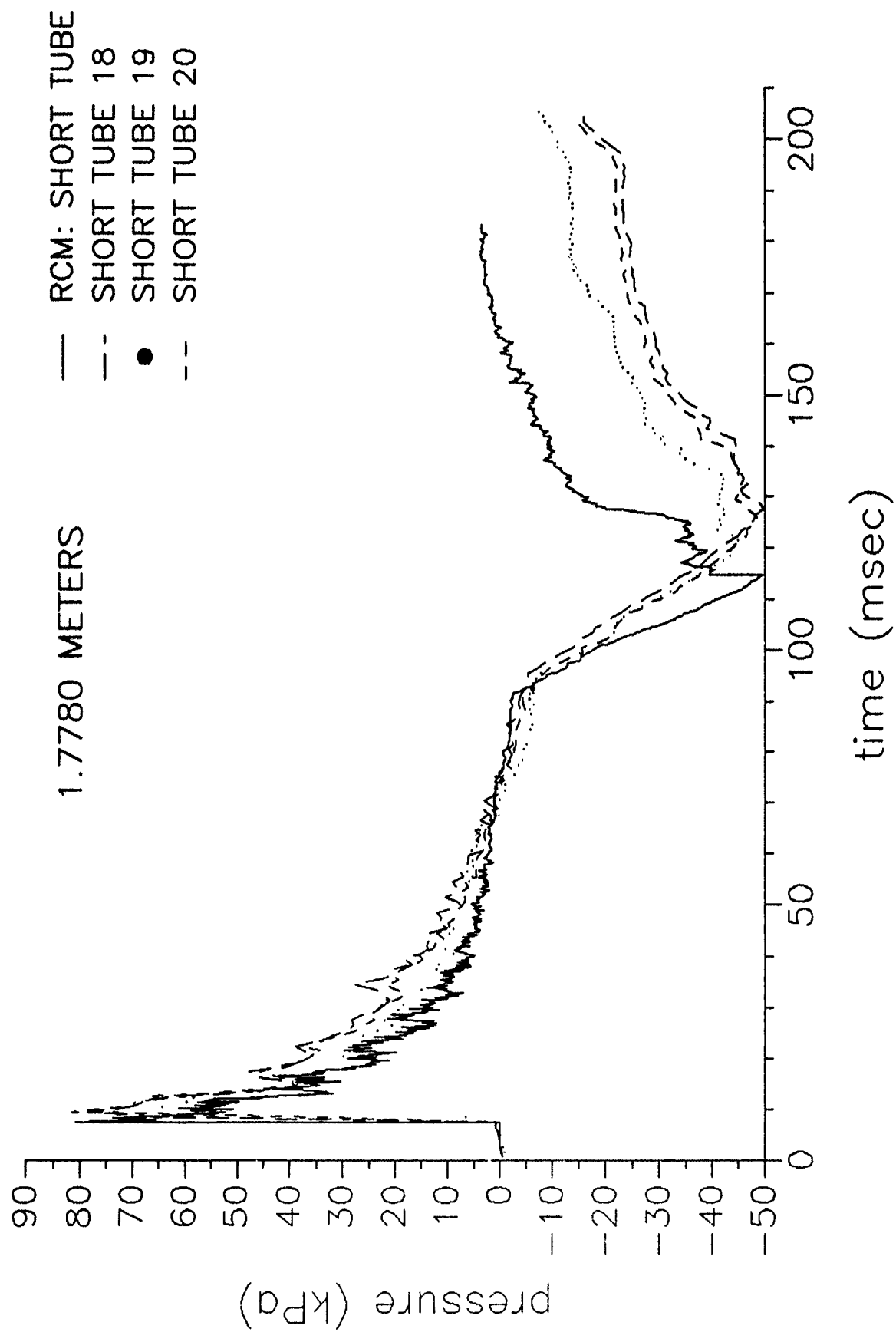


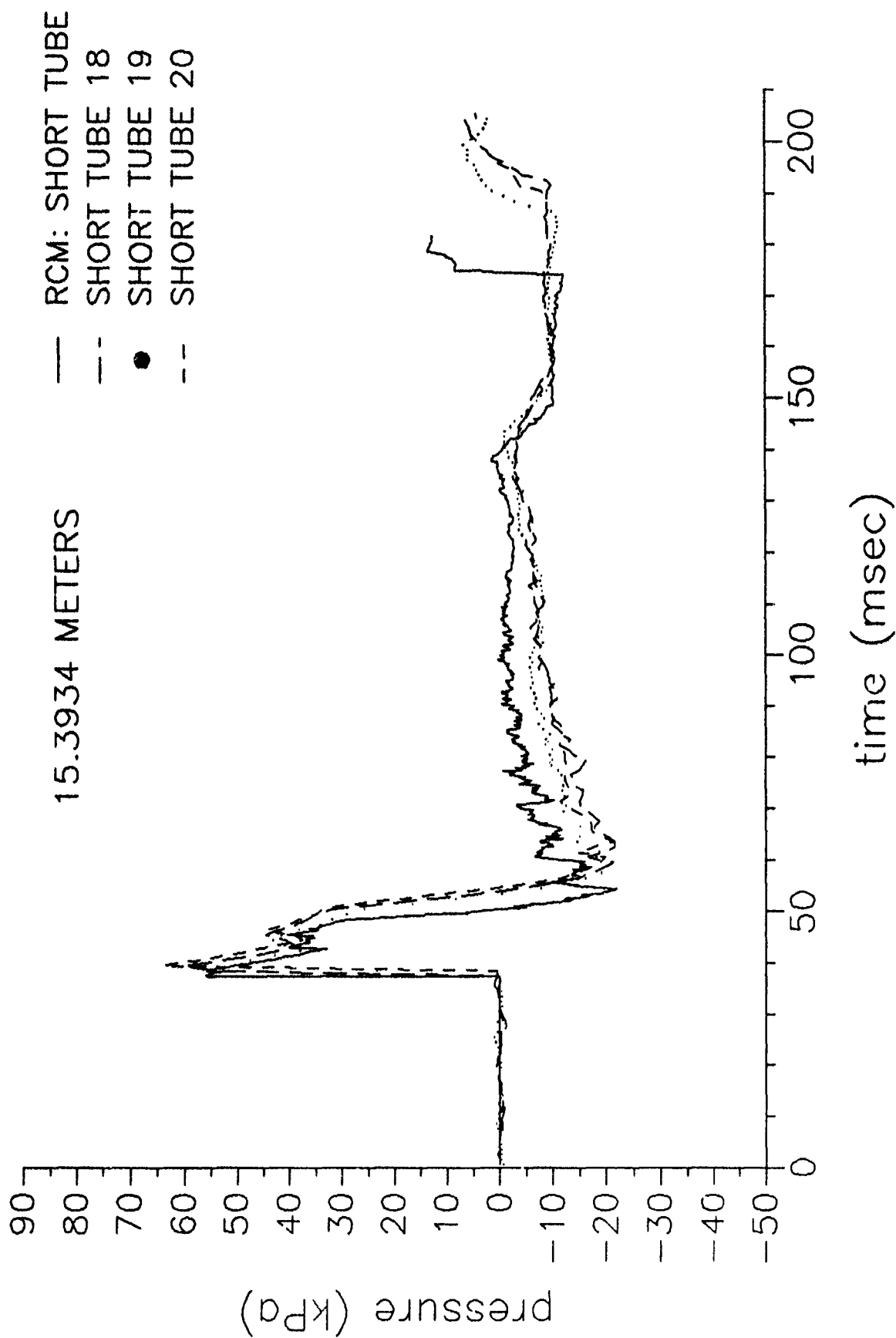


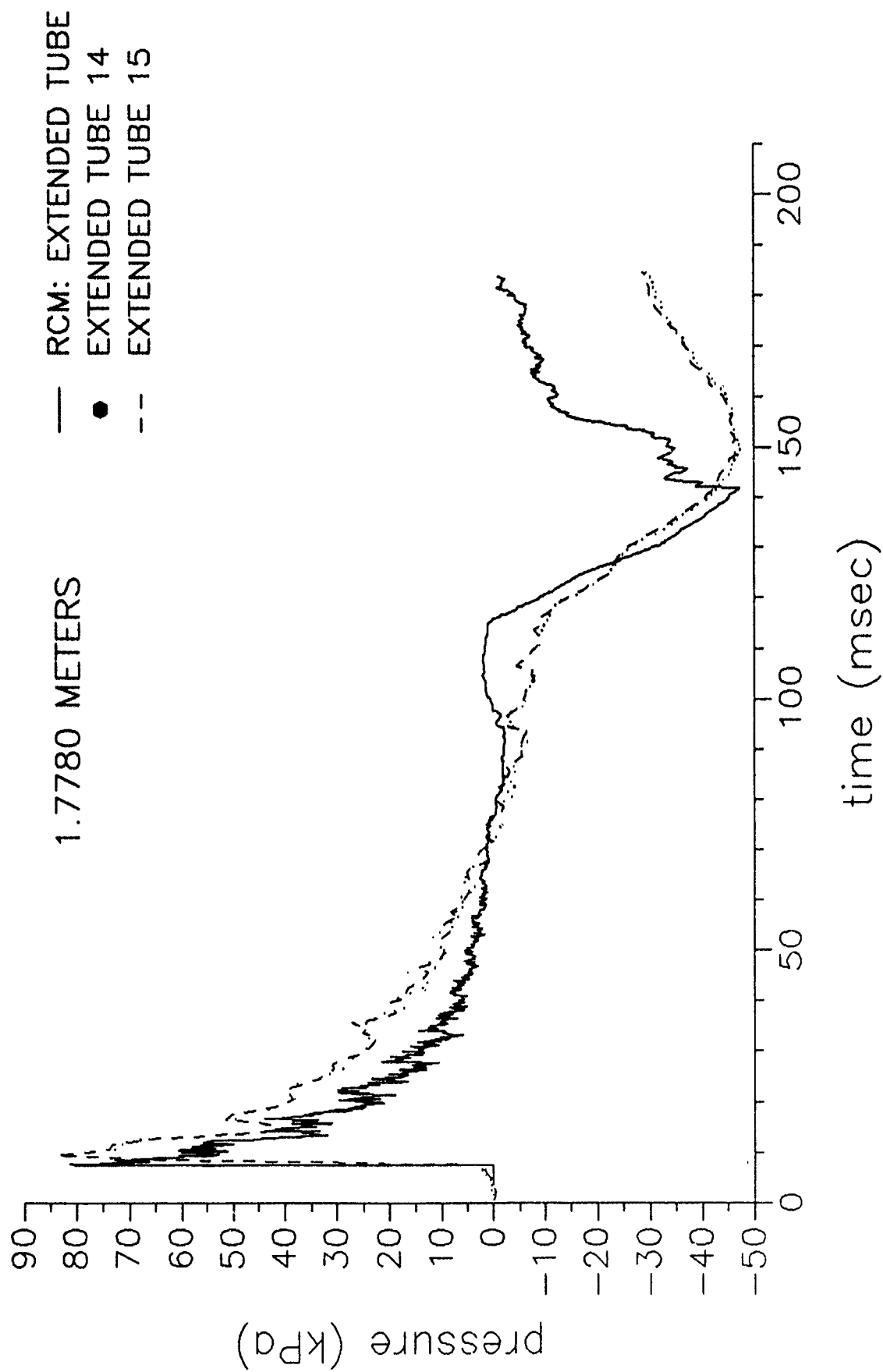


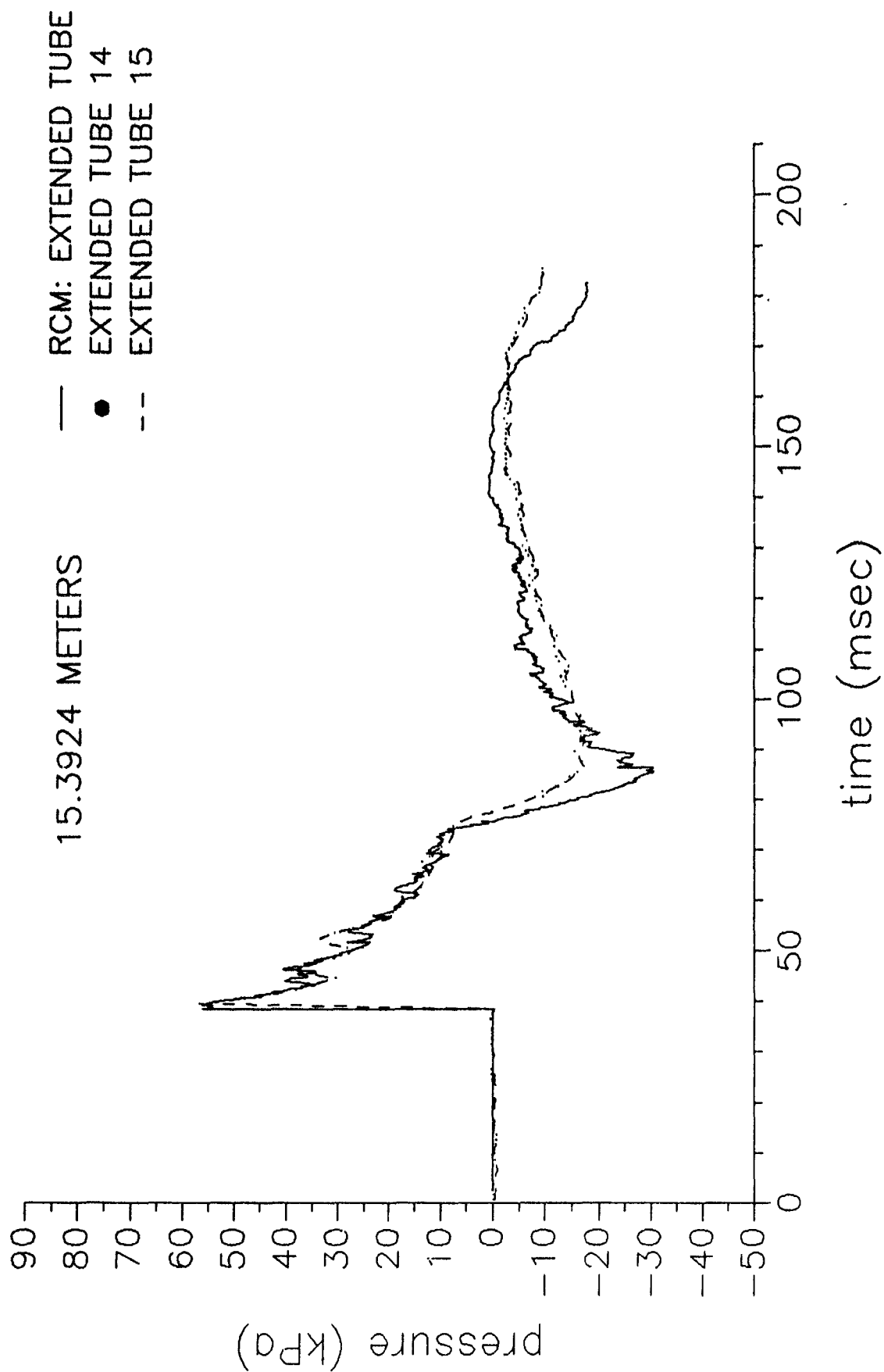


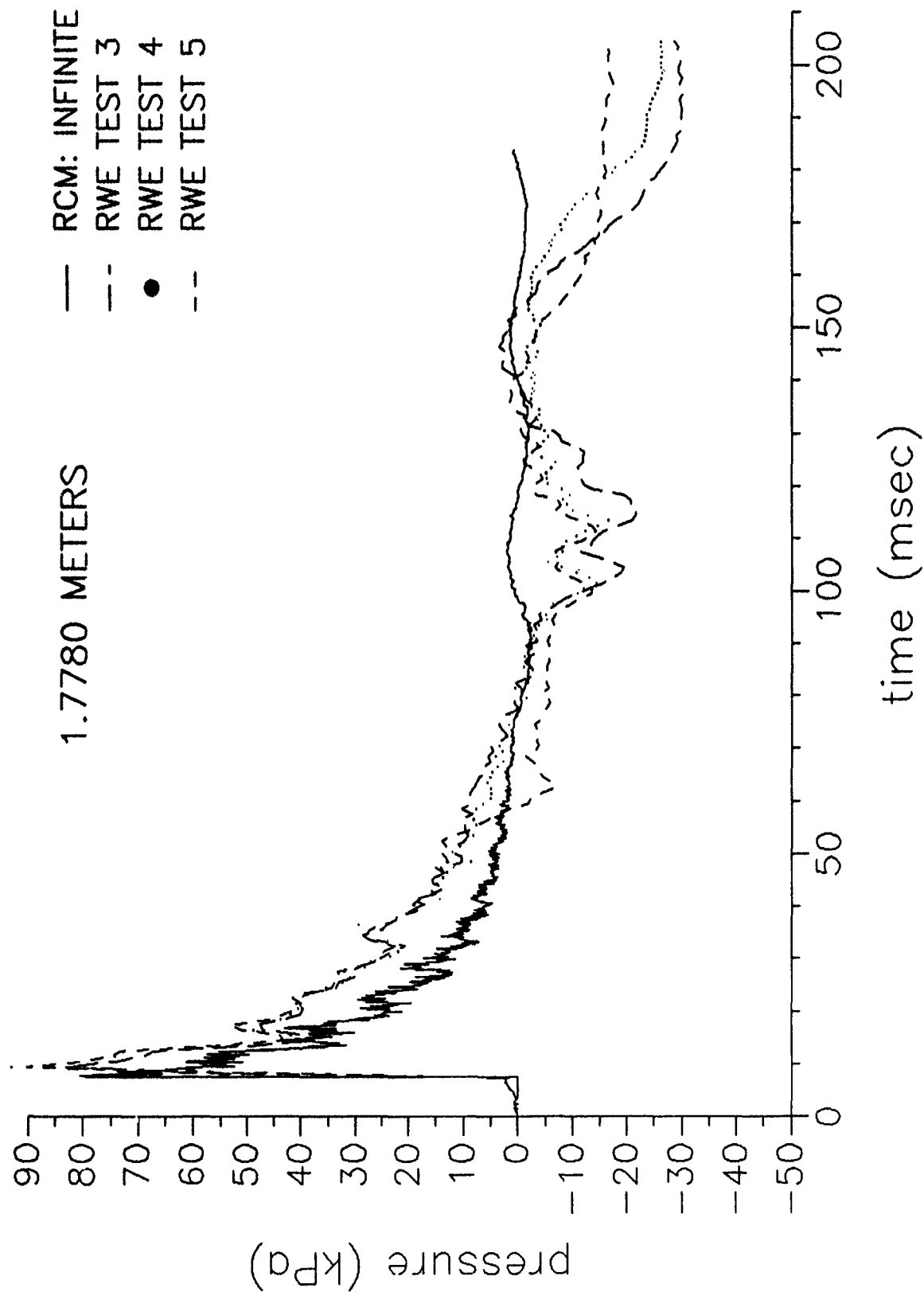


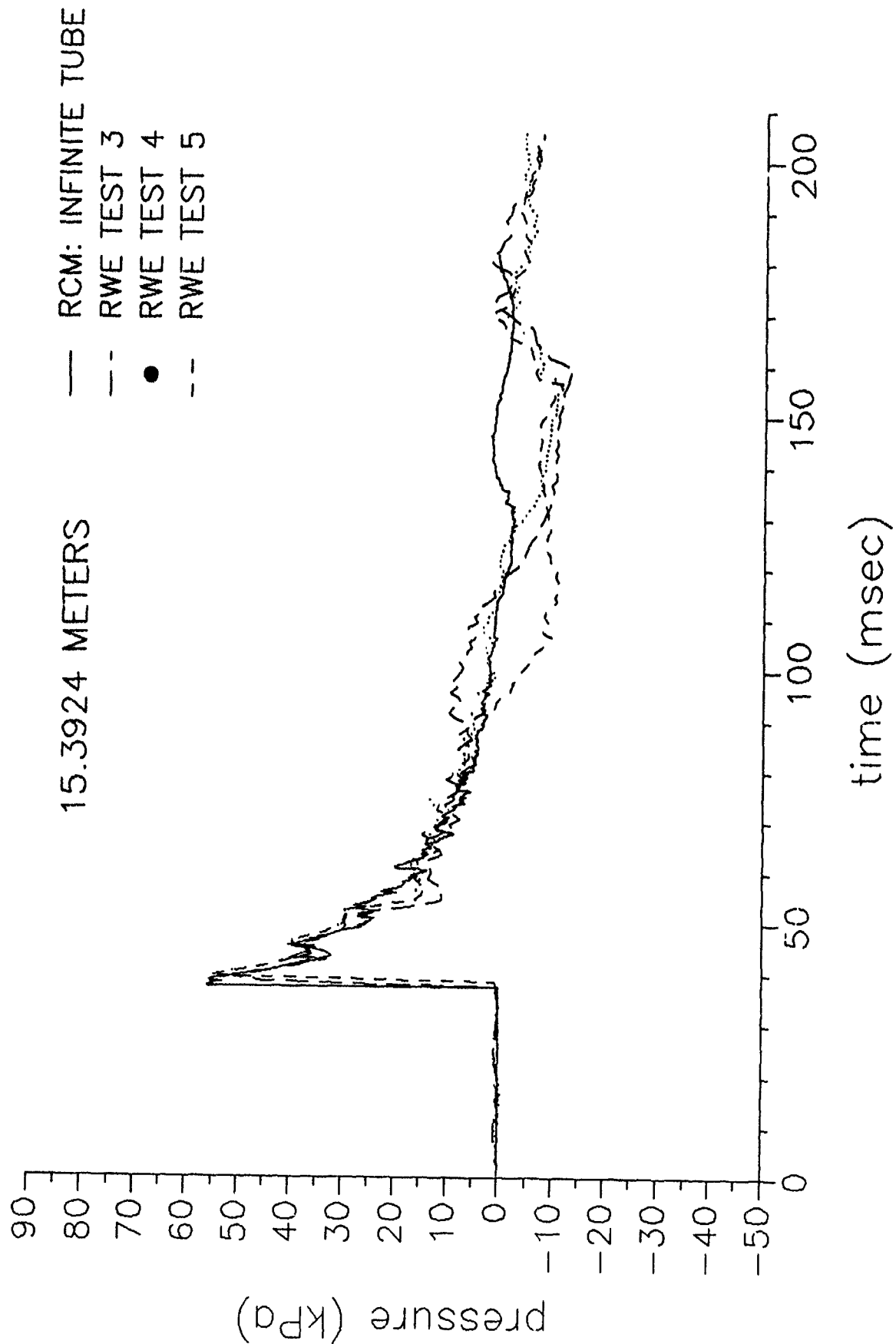


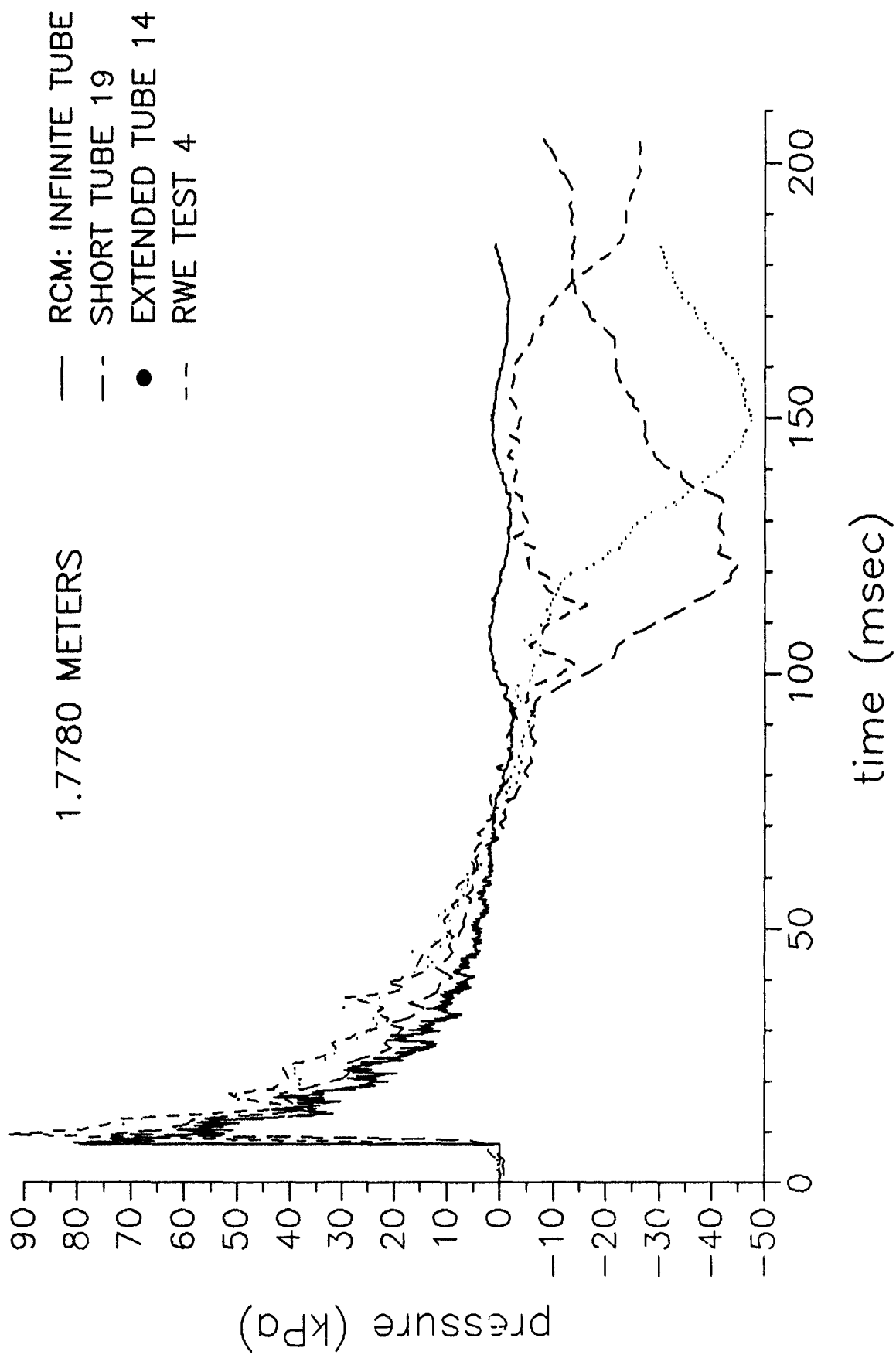


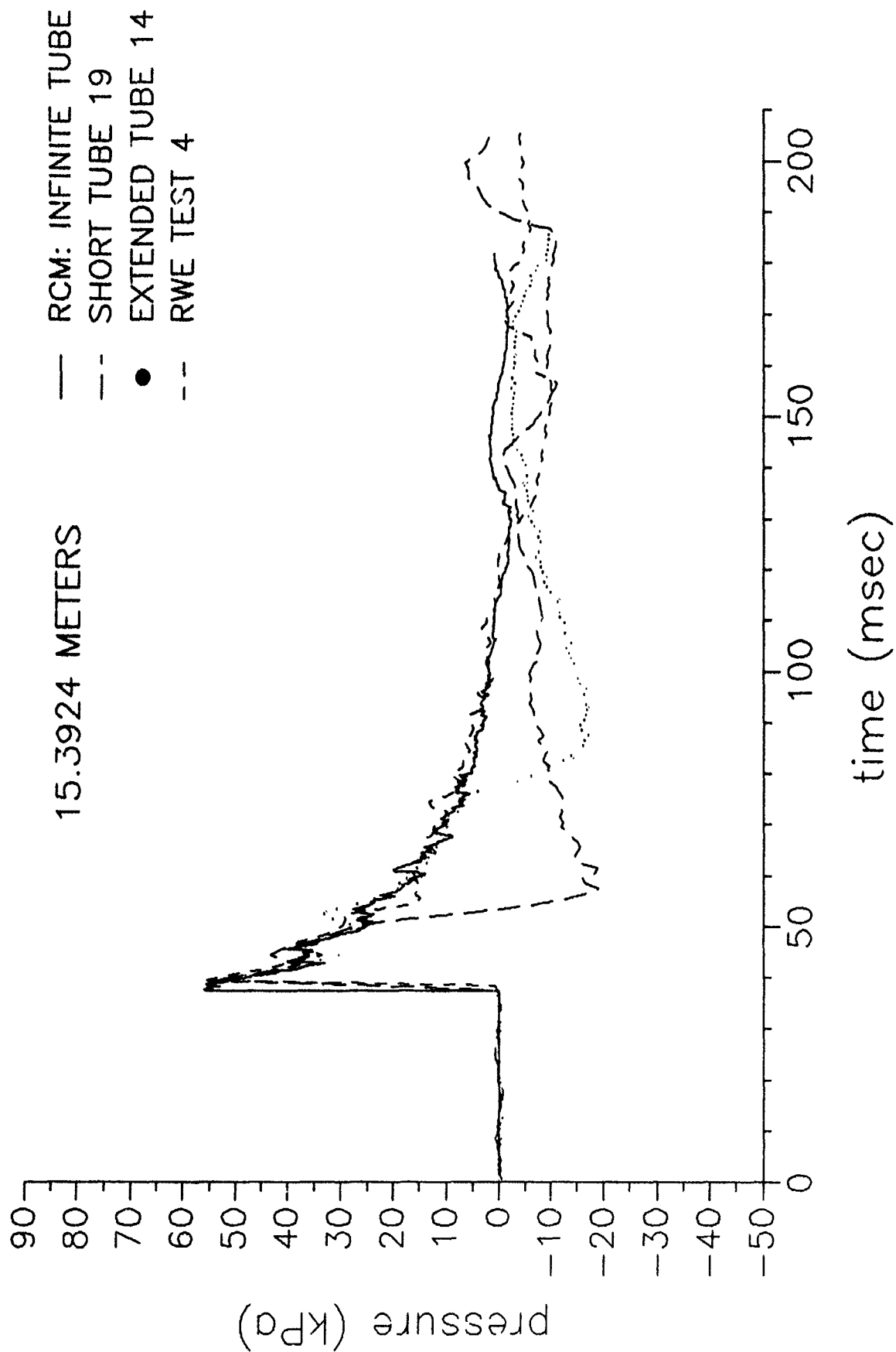












APPENDIX E
DISCHARGE COEFFICIENT FOR
FLows THROUGH LOUVERS

INTENTIONALLY LEFT BLANK.

The procedure for calculating the effective discharge coefficient for flows passing out through sharp-edged louvers of a reflection eliminator is presented herein. This presentation includes the relevant equations and the FORTRAN code listing.

The properties of the air flow upstream of the louvers must be completely known in this calculation procedure. Hence, for a perfect gas, the pressure P_3 , sound speed a_3 , and flow velocity u_3 , are sufficient to specify state 3. The temperature, density and flow Mach number can be obtained easily by means of $T_3 = a_3^2/(\gamma R)$, $\rho_3 = P_3/RT_3$, and $M_3 = u_3/a_3$, where R is the gas constant. Furthermore, the stagnation pressure of the air in state 3 can be obtained from the equation $P_{stag} = P_3 \left[1 + \frac{\gamma-1}{2} M_3^2 \right]^{\gamma/(\gamma-1)}$.

The next step is to obtain the properties of the jet emanating from the slots between adjacent louvers. The jet properties are determined from the flow properties of state 3 and the atmospheric pressure P_{atm} existing outside of the blast simulator. A critical pressure is calculated first by the expression $P_{crit} = P_{stag} \left[\frac{\gamma+1}{2} \right]^{-\gamma/(\gamma-1)}$. If $P_{crit} \leq P_{atm}$, then the jet flow is subsonic or just sonic. For this case the subcritical or critical jet pressure and flow Mach number can be summarized as

$$P_j = P_{atm} \quad \text{if } P_{crit} \leq P_{atm} \quad (1)$$

$$M_j = \sqrt{\frac{2}{\gamma-1} \left[\left(\frac{P_{stag}}{P_j} \right)^{\frac{\gamma-1}{2}} - 1 \right]}$$

On the other hand, if $P_{crit} > P_{atm}$, then the jet flow is choked with a subsequent supersonic jet. For this case, the jet pressure and flow Mach number at the minimum jet area can be summarized as

$$P_j = P_{crit} \quad \text{if } P_{crit} > P_{atm} \quad (2)$$

$$M_j = 1$$

For both unchoked and choked jets the sound speed, flow velocity and area of the jet (normalized by the channel area) follow from

$$a_j = a_3 \left[\frac{P_j}{P_3} \right]^{\frac{\gamma-1}{2\gamma}}, \quad (3)$$

$$u_j = a_j M_j, \quad (4)$$

$$A_j = \frac{M_3}{M_j} \left[\frac{P_3}{P_j} \right]^{\frac{\gamma+1}{2(\gamma-1)}}, \quad (5)$$

where the last result for the jet area is an approximation.

For the case of subsonic jet flows ($M_j < 1$), the value of the discharge coefficient is obtained approximately by the following iterative procedure. The value of the effective discharge coefficient C_d is guessed initially to have a value of unity. This permits the louver angle β_1 in degrees to be estimated by the equation

$$\beta_1 = \frac{180}{\pi} \sin^{-1} \left[0.966 \left[1 - \frac{A_j}{C_d} \right] \right]. \quad (6)$$

By using this value of angle β_1 , and known values of M_3 , M_j and $\gamma = 7/5$, all in the subroutine called ENDJETO at the end of this appendix, a value of C_{d1} can be determined. Furthermore, by using a value of angle $\beta_2 = 180^\circ - \beta_1$ along with M_3 , M_j and $\gamma = 7/5$ in the subroutine ENDJETO, a value of C_{d2} can be obtained. Then, a new value of the effective discharge coefficient can be determined from $C_d = \frac{1}{2} [C_{d1} + C_{d2}]$. The iterative process is repeated with this and subsequent values of C_d , until convergence is obtained--normally 3 to 6 cycles.

```

C=====
      SUBROUTINE ENDJET0 (MJETSQ, MFLWSQ, ANGLE, GAMMA, CDJET, ITOL)

```

```

C=====
C  ENDJET0 is a subroutine for obtaining the contraction coefficient
C  of a jet from a sharp-edged infinitely-wide slot in a vertical or
C  angled plate partly covering the otherwise open end of an infini-
C  tely wide channel of finite to infinite height, using Falkovich's
C  formulae cast into a better form and code by Picket and Gottlieb.

```

```

C-----
C  MJETSQ    square of the jet flow Mach number (minimum jet area)
C  MFLWSQ    square of the flow Mach number in duct ahead of slot
C  ANGLE     angle of plates partly covering duct end (in degrees),
C            for angles that range from fully open (0 degrees) to
C            slightly closed (45) to vertical walls (90) to partly
C            inward walls (135) to fully inward folded walls (180).
C  GAMMA     ratio of specific heats of the gas (1.002 to 5.0)
C  CDJET     contraction coefficient of the end jet (based on mass)
C  ITOL      tolerance indicator (0 -- CDJET are accurate to 5x10-5,
C                               1 -- accuracy is less than 5x10-5)
C-----

```

```

      IMPLICIT REAL*8 (A-H, M, N, O-Z)

```

```

      PARAMETER (PIBY2=3.1415926535898D0/2D0, TOL3=1D-3, TOL5=1D-5)

```

```

      PARAMETER (TOL8=1D-8, TOL10=1D-10, TOL20=1D-20, QQ=90D0)

```

```

      PARAMETER (ONEHUN=100D0, TWOHUN=200D0, RMOD51=-0.51D0)

```

```

      PARAMETER (CON=3.56359487256136D0, ROD9=0.9D0, S1S2=1D0/2D0)

```

```

      PARAMETER (C1=+0.5786165197D0, S1S3=1D0/3D0, S1S4=1D0/4D0)

```

```

      PARAMETER (C2=-0.6102248293D0, S3S4=3D0/4D0, S3S2=3D0/2D0)

```

```

      PARAMETER (C3=0.62927082761D0, S1S6=1D0/6D0, S5S6=5D0/6D0)

```

```

      DIMENSION W(0:10), R(82)

```

```

      SAVE JUMP, GAM, BET, ALFA, TAUS, RTAUS, ANG

```

```

      SAVE AE1, BE1, SUME1S, HBETMQ, QSQM1, Q

```

```

      DATA W/0D0,1D0,2D0,3D0,4D0,5D0,6D0,7D0,8D0,9D0,10D0/

```

```

      DATA (R(I),I=1,43) /0.10727017D0, 0.10888576D0, 0.11050978D0,

```

```

& 0.11214213D0, 0.11378273D0, 0.11543151D0, 0.11708838D0,

```

```

& 0.11875325D0, 0.12042605D0, 0.12210669D0, 0.12379510D0,

```

```

& 0.12549120D0, 0.12719490D0, 0.12890613D0, 0.13062481D0,

```

```

& 0.13235086D0, 0.13408420D0, 0.13582476D0, 0.13757247D0,

```

```

& 0.13932723D0, 0.14108899D0, 0.14285767D0, 0.14463319D0,

```

```

& 0.14641548D0, 0.14820446D0, 0.15000007D0, 0.15180222D0,

```

```

& 0.15361086D0, 0.15542591D0, 0.15724730D0, 0.15907496D0,

```

```

& 0.16090882D0, 0.16274882D0, 0.16459488D0, 0.16644693D0,

```

```

& 0.16830492D0, 0.17016877D0, 0.17203842D0, 0.17391381D0,

```

```

& 0.17579486D0, 0.17768152D0, 0.17957372D0, 0.18147140D0/

```

```

      DATA (R(I),I=44,82) /0.18337450D0, 0.18528295D0, 0.18719670D0,

```

```

& 0.18911568D0, 0.19103984D0, 0.19296911D0, 0.19490343D0,

```

```

& 0.19684275D0, 0.19878701D0, 0.20073615D0, 0.20269012D0,

```

```

&      0.20464886D0, 0.20661230D0, 0.20858041D0, 0.21055312D0,
&      0.21253038D0, 0.21451213D0, 0.21649833D0, 0.21848891D0,
&      0.22048384D0, 0.22248305D0, 0.22448650D0, 0.22649413D0,
&      0.22850590D0, 0.23052175D0, 0.23254164D0, 0.23456552D0,
&      0.23659335D0, 0.23862506D0, 0.24066062D0, 0.24269998D0,
&      0.24474310D0, 0.24678992D0, 0.24884041D0, 0.25089452D0,
&      0.25295220D0, 0.25501341D0, 0.25707812D0, 0.25707812D0/

```

C- - - - -

C Compute certain constants only if required because GAMMA changes.

IF (JUMP.NE.11) GOTO 10

TEST=GAMMA-GAM

IF (TEST*TEST.LT.TOL10) GOTO 20

10 JUMP=11

GAM=GAMMA

BET=W(1)/(GAM-W(1))

ALFA=C3*W(2)**(S1S2*BET+W(1))/(GAM+W(1))**(S1S2*(BET+S1S3))

TAUS=(GAM-W(1))/(GAM+W(1))

TOL3TS=TOL3*TAUS

RTAUS=DSQRT(TAUS)

GOTO 30

C- - - - -

C Compute other constants only if required because of changes in Q.

20 TEST=ANGLE-ANG

IF (TEST*TEST.LT.TOL10) GOTO 40

30 ANG=ANGLE

Q=ANG/QQ

AE1=C1*(Q*GAM+Q)**S1S3

BE1=Q*(GAM/W(10)+S1S4)

SUME1S=AE1+C2/C1-W(2)*(BE1-BE1*PIBY2)

HBETMQ=S1S2*BET-S1S4

QSQM1=Q*Q-W(1)

CQP=CON*Q**S1S6

C- - - - -

C Compute Chaplygin's variable for upstream flow TAUU and jet TAUJ,

C do checks on TAUU, TAUJ and Q, and compute often employed values.

40 ITOL=0

CDJET=W(1)

TAUJ=MJETSQ/(BET+BET+MJETSQ)

TAUU=MFLWSQ/(BET+BET+MFLWSQ)

IF (TAUU.GT.TAUJ) TAUU=TAUJ

IF (TAUJ.LT.TOL20) TAUJ=TOL20

IF (TAUJ-TAUU.LT.TOL5*TAUJ) RETURN

IF (Q*Q.LT.TOL8) RETURN

TAUUU=TAUU/(TAUS-TAUS*TAUU)

TAUJJ=TAUJ/(TAUS-TAUS*TAUJ)

TAUSU=TAUS/(TAUS-TAUS*TAUU)


```

      TAUSJ=TAUS/(TAUS-TAUS*TAUJ)
C- - - - -
C The sum of series E1 is calculated by closed form approximations,
C one for the case of subsonic jets -- when TAUS-TAUJ > 0.001*TAUS,
C and one for the case of sonic jets - when TAUS-TAUJ < 0.001*TAUS,
C The results are used to get CDJET for channel of infinite height.
      SUM=SUME1S
      IF (TAUS-TAUJ.LT.TOL3TS) GOTO 50
      A=DSQRT(TAUSJ-TAUJJ)
      B=W(0)
      IF (TAUJ.LT.ROD9*TAUS) B=S1S4*Q*(TAUJ/(TAUJ-TAUS)+TAUJJ)
      SUM=W(2)*(B*PIBY2-B)-A
50 N=W(0)
      SIHN=W(1)
      TERM=W(0)
60 N=N+W(1)
      NSQ=N/Q
      XN=W(1)
      IF (TAUJ.LT.TOL20) GOTO 80
      K=W(10)*DLOG10(NSQ)+W(2)
      IF (K.LT.10) K=10
      YM=DBLE(K+2)
      DO 70 I=K,0,-1
      YM=YM-W(1)
      DM=YM+NSQ
      Z=(BET+S1S2)*(DM-NSQ)*(DM+NSQ)/DM
      D=BET-Z/(DM+S1S2)
70 XN=W(1)-(BET-Z/(DM+S1S2))*TAUJ/(W(2)-TAUJ-TAUJ-D*TAUJ/XN)
      XN=W(1)-BET*TAUJ/(XN-XN*TAUJ)
80 SIHN=-W(1)*SIHN
      OTERM=TERM
      FACT=W(4)*N*N-W(1)
      Z=A-B/N
      IF (TAUS-TAUJ.LT.TOL3TS) Z=AE1/N**S1S3-BE1/N
      TERM=SIHN*W(4)*N*(XN/(FACT-QSQM1)-Z/FACT)
      SUM=SUM+TERM
      TEST=OTERM+TERM
      IF (TEST*TEST.GT.TOL8 .OR. N.LT.S3S2) GOTO 60
      CDJET=PIBY2/(PIBY2-DSIN(Q*PIBY2)*(SUM+S1S2*OTERM))
C- - - - -
C The sum of series E2 is calculated by closed form approximations,
C one for the case of subsonic jets -- when TAUS-TAUJ > 0.001*TAUS,
C and one for the case of sonic jets - when TAUS-TAUJ < 0.001*TAUS.
C This CDJET value from series E1 for an infinitely high channel is
C now used with series E2 to get CDJET for a finite height channel.
      IF (TAUU.LT.TOL20) GOTO 130

```

```

AU1=DSQRT(TAUS*(TAUSU-TAUUU))
AU2=DSQRT(TAUSU-TAUUU)
IF (TAUS-TAUJ.GT.TOL3TS) THEN
    AJ1=DSQRT(TAUS*(TAUSJ-TAUJJ))
    AJ2=DSQRT(TAUSJ-TAUJJ)
    HUJ1=DLOG((W(1)+AU1)*(W(1)-AJ1)/((W(1)-AU1)*(W(1)+AJ1)))
    HUJ2=DLOG((W(1)+AU2)*(W(1)-AJ2)/((W(1)-AU2)*(W(1)+AJ2)))
    XX=S1S2*(HUJ1/RTAUS-HUJ2)/Q
    IF (XX*XX.GT.ONEHUN) GOTO 130
    X=DEXP(XX)
    A=((W(1)-TAUU/TAUS)*(W(1)-TAUJ/TAUS))*S1S4
    A=A*(W(1)-TAUU)**HBETMQ/(W(1)-TAUJ)**(HBETMQ+S1S2)
    SUM=(A/X-A*X)*DATAN(X)-A
ELSE
    HU1=DLOG((W(1)+AU1)/(W(1)-AU1))
    HU2=DLOG((W(1)+AU2)/(W(1)-AU2))
    XX=S1S2*(HU1/RTAUS-HU2)/Q
    IF (XX*XX.GT.ONEHUN) GOTO 130
    IF (XX.LT.RMOD51) THEN
        X=W(1)
        A=W(0)
        SUM=W(0)
    ELSE
        X=DEXP(XX)
        A=CQP*(W(1)-TAUU)**HBETMQ*(W(1)-TAUU/TAUS)**S1S4/ALFA
        J=TWOHUN*X
        I=J-119
        SUM=A*((R(I)-R(I+1))*(TWOHUN*X-J)-R(I))
    ENDIF
ENDIF
ENDIF
N=W(0)
K=0
SIHN=W(1)
TERM=W(0)
90 N=N+W(1)
    NSQ=N/Q
    AN=NSQ+NSQ+W(1)
    CSUM=(AN-W(1)-BET)/W(2)
    BN=CSUM+DSQRT(CSUM*CSUM+BET*AN*NSQ)
    CN=CSUM+CSUM-BN
    YN=W(1)
    IF (TAUJ.LT.TOL20) GOTO 110
    ZNP=W(1)
    KK=S3S4*AN-S1S2*(BN+CN)
    NK=S1S2*AN-S1S2
    NT=NK+(CN-NK)*TAUU

```

```

        DI=DBLE(KK+15)
        DO 100 I=KK+14,0,-1
        DI=DI-W(1)
        RR=(AN-BN+DI)*(CN+DI)/((AN+DI)*(W(1)+DI))
        YN=W(1)-RR*YN*TAUJ*TAUSJ
100    ZNP=W(1)-(NT+DI+W(1))*RR*TAUU*TAUSU*ZNP/(NT+DI)
        IF (YN.LT.TOL8) THEN
            ITOL=1
            GOTO 120
        ENDIF
        YN=YN/(W(1)-TAUJ)**CN
        IF (NSQ.GT.GAM) THEN
            MU=(W(4)*NSQ+W(3)+W(1)/BET-DSQRT((NSQ+NSQ+NSQ/BET)
&            *W(8)+W(9)+(W(6)+W(1)/BET)/BET))/(NSQ+NSQ)
            MAX=(W(1)-TAUJ)**(BET*NSQ)
            IF (YN.LT.MAX**MU .OR. YN.GT.MAX) THEN
                ITOL=1
                GOTO 120
            ENDIF
        ENDIF
        ZNP=(NK-NK*TAUU+CN*TAUU)*ZNP/(W(1)-TAUU)**(W(1)+CN)
110    K=K+1
        SIHN=-SIHN
        OTERM=TERM
        FACT=W(4)*N*N-W(1)
        Z=N
        IF (TAUS-TAUJ.LT.TOL3TS) Z=N**S5S6/W(4)
        Z=A*Z*X**(K+K)/FACT
        TERM=SIHN*W(4)*(Q*(TAUU/TAUJ)**NSQ*ZNP/(YN*(FACT-QSQM1))-Z)
        SUM=SUM+TERM
        TEST=OTERM+TERM
        IF (TEST*TEST.GT.TOL8 .OR. N.LT.S3S2) GOTO 90
        SUM=SUM+S1S2*OTERM
120    Z=(TAUSU/TAUSJ)**BET*DSIN(Q*PIBY2)*SUM/PIBY2
        CDJET=CDJET/(W(1)+CDJET*Z)
130    CDJET=DMIN1(CDJET,W(1))
        RETURN
        END

```

INTENTIONALLY LEFT BLANK.

APPENDIX F
LISTING OF THE ELIM CODE

INTENTIONALLY LEFT BLANK.

```

C-----
CCCCCCCCCCCCCCCCCCCCCCCCCCCCCCCCCCCCCCCCCCCCCCCCCCCCCCCCCCCC
CCC                                     CCC
CCC      REFLECTION ELIMINATOR PROGRAM by JAMES GOTTLIEB      CCC
CCC                                     CCC
CCC      for the DENVER RESEARCH INSTITUTE   (4 January 1987)   CCC
CCC                                     CCC
CCCCCCCCCCCCCCCCCCCCCCCCCCCCCCCCCCCCCCCCCCCCCCCCCCCCCCCCCCCC

```

```

C-----
C      This is the main computer program to compute the area setting
C      for the reflection eliminator to produce no reflected wave except
C      for the transient spike, or to obtain the reflected wave strength
C      when the area setting of the reflection eliminator is specified.
C      The four special cases under consideration are summarized below:

```

- 1) flat-topped incident shock wave with a given pressure ratio, specified in the input data file called IN, which results in no wave reflection except for the transient spike (note that only one value of the final area setting will be returned to the user in the output data file called OUT for each input),
- 2) same case of a flat-topped incident shock wave as in case a, but this time it is repeated for the case of a reflected wave with a given pressure ratio in terms of a percentage of the incident shock pressure ratio (greater or less than zero for a reflected shock or rarefaction wave, respectively),
- 3) flat-topped incident shock wave with a given pressure ratio and a specified area setting for the reflection eliminator, which are given in the input data file called IN, for which a reflected shock or rarefaction wave will in general occur and the strength of this reflected wave will be computed and put in the output data file called OUT,
- 4) incident blast wave with a time varying signature for which the pressure, sound speed, flow velocity and gamma are given as a function of time in the input file called IN, which now produces no reflected wave (the same number of values of the output as input will be returned to the user in the output data file called OUT).

```

C      For each type of reflection eliminator run the first line in the
C      input data file IN must have the initial or atmospheric pressure
C      and sound speed, in units of Pa (N/m2) and m/s.

```

```

C-----
      REAL      MS,  M3,  MJ,  MFLUX
      DATA     PI/3.141592654/

```

```

C-----
      OPEN (UNIT=1, FILE='IN')
      OPEN (UNIT=2, FILE='OUT', STATUS='NEW')

```

```

C-----
C      First read in the atmospheric pressure P1 and sound speed A1 from
C      the input data file IN, and then read in the type computation to
C      be done by this computer program (choices of K = 1, 2, 3, or 4).

```

```

      READ (1,*)
      READ (1,*) P1, A1
      READ (1,*) K

```

```

C-----
C      Set up headings required for output information in data file OUT.
      IF (K.GT.0 .AND. K.LE.4) THEN

```

```

        WRITE (2,*) '                                OUTPUT FOR CASE #',K
    ENDIF
    IF (K.EQ. 1) THEN
        WRITE (2,('' P2/P1    RADIUS    WIDTH    OMEGA'',
+              ''    CD    JET AREA    RE AREA''))
    ELSE IF (K.EQ.2 .OR. K.EQ.3) THEN
        WRITE (2,('' P2/P1    RADIUS    WIDTH    RW JUMP'',
+              ''    CD    JET AREA    RE AREA''))
    ELSE IF (K.EQ. 4) THEN
        WRITE (2,(''    TIME    P/P1    U/A1    RADIUS    '',
+              ''    WIDTH    JET AREA    RE AREA''))
    ELSE
        WRITE (2,*) ' Type of data is not 1, 2, 3, or 4.'
        WRITE (2,*) ' Please correct and then try again.'
        STOP
    ENDIF

```

C- - - - -

C Read in the appropriate input data from the input data file IN.

```

10 IF (K.EQ. 1) THEN
    READ (1,*,END=110) P21,RADOUT,WIDTH,G
ELSE IF (K.EQ. 2) THEN
    READ (1,*,END=110) P21,RADOUT,WIDTH,G,RWJUMP
ELSE IF (K.EQ. 3) THEN
    READ (1,*,END=110) P21,RADOUT,WIDTH,G,AREAE
ELSE IF (K.EQ. 4) THEN
    READ (1,*,END=110) T,P2,A2,U2,RADOUT,RADIN,WIDTH,G
    GOTO 20
ENDIF
IF (P21.LE. 1.0) THEN
    WRITE (2,*) ' P21 MUST BE GREATER THAN UNITY FOR A SHOCK.'
    WRITE (2,*) ' Please correct and rerun the computer code.'
    STOP
ENDIF

```

C- - - - -

C Calculate flow properties for state 2 behind a flat-topped shock wave, if a shock wave is incident on the reflection eliminator.

```

P2=P21*P1
A2=((G+1.0)/(G-1.0)+P2/P1)/((G+1.0)/(G-1.0)+P1/P2)
A2=A1*SQRT(A2)
MS=SQRT(1.0+(G+1.0)*(P21-1.0)/(2.0*G))
U2=A1*(2.0/(G+1.0))*(MS-1.0/MS)

```

C- - - - -

C Compute the jump in flow properties across the reflected shock or rarefaction wave to state 3, if a reflected wave actually exists.

```

20 IF (K.EQ. 3) RWJUMP=0.0
    NUMRW=0
30 NUMRW=NUMRW+1
    IF (K.EQ.1 .OR. K.EQ.4) THEN
        P3=P2
        A3=A2
        U3=U2
    ELSE IF (K.EQ.2 .OR. K.EQ.3 .AND. RWJUMP.GE.1.0) THEN
        P3=P2+(P2-P1)*RWJUMP/100.0
        A3=((G+1.0)/(G-1.0)+P3/P2)/((G+1.0)/(G-1.0)+P2/P3)
        A3=A2*SQRT(A3)
        MS=-SQRT(1.0+(G+1.0)*(P3/P2-1.0)/(2.0*G))
        U3=U2+A2*(2.0/(G+1.0))*(MS-1.0/MS)
    ELSE IF (K.EQ.2 .OR. K.EQ.3) THEN
        P3=P2+(P2-P1)*RWJUMP/100.0
        A3=A2*(P3/P2)**((G-1.0)/(2.0*G))
    
```



```

      U3=U2+2.0*(A2-A3)/(G-1.0)
ENDIF
      M3=U3/A3
C- - - - -
C For outflow (from the channel through the reflection eliminator),
C M3 and P3-P1 are both positive, and the following coding is used.
  IF (M3.LE.0.0 .OR. P3-P1.LE.0.0) GOTO 50
  PCRIT=P3*((2.0+(G-1.0)*M3*M3)/(G+1.0))*((G/(G-1.0))
  IF (PCRIT .GE. P1) THEN
    PJ=PCRIT
    MJ=1.0
  ELSE
    PJ=P1
    MJ=SQRT(((PCRIT/PJ))*((G-1.0)/G)*(G+1.0)-2.0)/(G-1.0))
  ENDIF
  AJ=A3*(PJ/P3))*((G-1.0)/(2.0*G))
  UJ=MJ*AJ
  AREAJ=(M3/MJ)*(P3/PJ))*((G+1.0)/(2.0*G))
  TAU3=(G-1.0)*M3*M3/(2.0+(G-1.0)*M3*M3)
  TAUJ=(G-1.0)*MJ*MJ/(2.0+(G-1.0)*MJ*MJ)
  ZETA=TAUJ/(1.0-TAUJ)
  C0=PI/(PI+2.0-5.0*ZETA+2.0*ZETA*ZETA)
  ETA=7.0*TAUJ+1.0/(1.0+12*TAUJ)
  A=(2.0*ETA-1.0)*(1.0-C0)
  B=2.0*(1.0-ETA)*(1.0-C0)
  CDS=C0+A*(TAU3/TAUJ)+B*(TAU3/TAUJ)**2
  CD=CDS
  NUMCD=1
40 Z=-45.0*RADOUT*CD/(AREAJ*WIDTH)
  IF (ABS(Z) .GT. 78) Z=78.0*Z/ABS(Z)
  OMEGA=1.0-EXP(Z)
  CDPREV=CD
  CD=CDS+OMEGA*(1.0-CDS)
  IF (ABS(1.0-CDPREV/CD) .LT. 5.0E-05) GOTO 100
  NUMCD=NUMCD+1
  IF (NUMCD .LT. 20) GOTO 40
  WRITE (2,*) ' FAILURE OF CD ITERATION (outflow)!'
  STOP
C- - - - -
C For inflow (through the reflection eliminator to the channel), M3
C and P3-P1 are both negative and the following coding is employed.
50 IF (M3.GE.0.0 .OR. P3-P1.GE.0.0) GOTO 90
  GG=(G-1.0)/2.0
  A3=SQRT(A1*A1-GG*U3*U3)
  MFLUX=G*P3*U3/(A3*A3)
  Z=((G+1.0)/2.0))*((G+1.0)/(2.0*G-2.0))*MFLUX*A1/(G*P1)
  PCRIT=P1*(2.0/(G+1.0))*((G/(G-1.0))*(1.0-(1.0-Z)**2*G/2.0))
  IF (PCRIT .GE. P3) THEN
    MJ=-1.0
  ELSE
    KCYCL=0
    MJ=-SQRT((P1-P3)/(P1-PCRIT))
    Z=MFLUX*A1/(G*P1)
60  ZZ=MJ-Z*((1.0+GG*MJ*MJ))*((G+1.0)/(2.0*G-2.0))
    FF=P3*(1.0+GG*MJ*MJ))*((G/(G-1.0))-P1*(1.0-G*ZZ*ZZ/2.0))
    FP=G*P3*MJ*(1.0+GG*MJ*MJ))*((1.0/(G-1.0))+G*P1*ZZ*(1.0-(G
+    +1.0)*(Z/2.0)*MJ*(1.0+GG*MJ*MJ))*((3.0-G)/(2.0*G-2.0)))
    PREV=MJ
    MJ=MJ-FF/FP
    KCYCL=KCycl+1

```

```

      IF (ABS(MJ-PREV) .LT. 0.001) GOTO 70
      IF (KCYCL .LT. 30) GOTO 60
      WRITE (2,*) ' FAILURE OF MJ ITERATION (inflow)'
      STOP
    ENDIF
70  AREAJ=(Z/MJ)*(1.0+GG*MJ*MJ)**((G+1.0)/(2.0*G-2.0))
    CDS=0.5+MJ**2/8.0+(2.0-G)*MJ**4/48.0
    +   +(2.0-G)*(3.0-2.0*G)*MJ**6/384.0
      CD=CDS
      NUMCD=1
80  Z=-45.0*RADIN*CD/(AREAJ*WIDTH)
      IF (ABS(Z) .GT. 78) Z=78.0*Z/ABS(Z)
      OMEGA=1.0-EXP(Z)
      CDPREV=CD
      CD=CDS+OMEGA*(1.0-CDS)
      IF (ABS(1.0-CDPREV/CD) .LT. 5.0E-05) GOTO 100
      NUMCD=NUMCD+1
      IF (NUMCD .LT. 20) GOTO 80
      WRITE (2,*) ' FAILURE OF CD ITERATION (inflow)'
      STOP
C- - - - -
C  In the two cases when P3-P1 and M3 have the opposite signs, there
C  is no reflection elimination, and the reflection eliminator area
C  is simply set to zero.
90  AREAJ=0.0
      CD=1.0
C- - - - -
C  Print the data out into the output file called OUT.  For case 3,
C  however, we need an iteration if RWJUMP is not the right value to
C  give the reflection eliminator area as specified.
100 IF (K .EQ. 1) THEN
      AREAE=AREAJ/CD
      WRITE (2, '(F7.3,2E12.4,4F9.4)') P21, RADOUT, WIDTH,
    +   OMEGA, CD, AREAJ, AREAE
      GOTO 10
    ELSE IF (K .EQ. 2) THEN
      AREAE=AREAJ/CD
      WRITE (2, '(F7.3,2E12.4,F10.2,3F9.4)') P21, RADOUT, WIDTH,
    +   RWJUMP, CD, AREAJ, AREAE
      GOTO 10
    ELSE IF (K .EQ. 3) THEN
      IF (NUMRW .EQ. 1) THEN
        DIFF1=AREAJ/CD-AREAE
        RWJUMP=20.0*ABS(DIFF1)/DIFF1
        GOTO 30
      ELSE
        F=FAC
        FAC=DIFF1/(DIFF1-AREAJ/CD+AREAE)
        IF (MAX(FAC,F) .GE. 1.0 .AND. MIN(FAC,F) .LE. 1.0)
    +   FAC=(1.0+2.0*FAC)/3.0
        RWJUMP=RWJUMP*FAC
        IF (NUMRW .GT. 40) FAC=1.0
        IF (ABS(FAC-1.0) .GT. 5.0E-05) GOTO 30
      ENDIF
      WRITE (2, '(F7.3,2E12.4,F10.2,3F9.4)') P21, RADOUT,
    +   WIDTH, RWJUMP, CD, AREAJ, AREAE
      GOTO 10
    ELSE IF (K .EQ. 4) THEN
      AREAE=AREAJ/CD
      IF (AREAJ .LT. 0.0) AREAJ=0.0

```

```

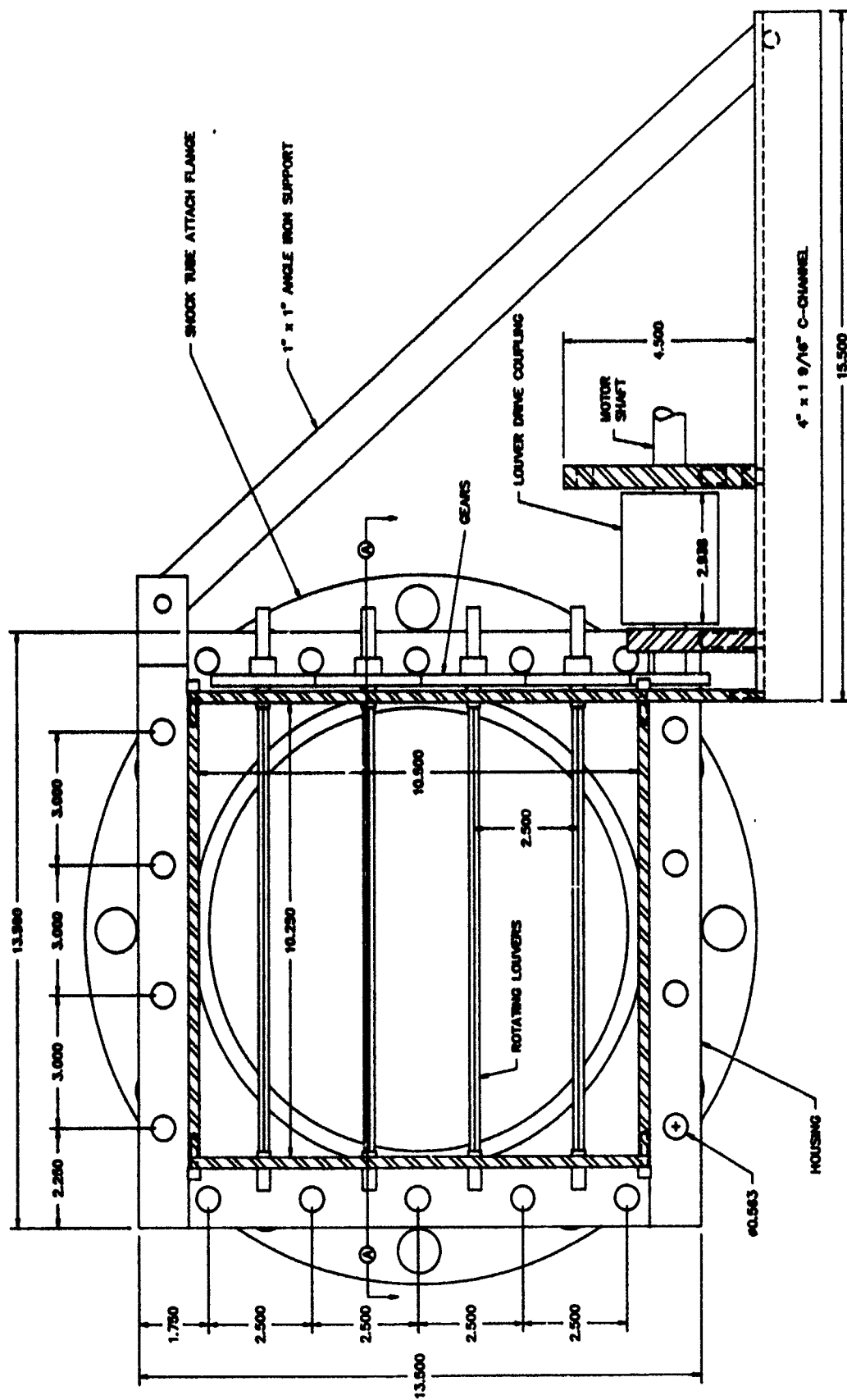
        IF (AREAJ .GT. 1.0) AREAJ=1.0
        IF (AREAE .LT. 0.0) AREAE=0.0
        IF (AREAE .GT. 1.0) AREAE=1.0
        IF (M3 .GE. 0.0) THEN
+          WRITE (2, '(E11.4,F8.3,F9.3,2E12.4,2F8.4)') T, P2/P1,
+            U2/A1, RADOUT, WIDTH, AREAJ, AREAE
        ELSE
+          WRITE (2, '(E11.4,F8.3,F9.3,2E12.4,2F8.4)') T, P2/P1,
+            U2/A1, RADIN WIDTH, AREAJ, AREAE
        ENDIF
        GOTO 10
    ENDIF
110 STOP
    END

```

INTENTIONALLY LEFT BLANK.

APPENDIX G
CONSTRUCTION DRAWINGS AND PHOTOGRAPHS
OF THE 1/57TH SCALE RWE

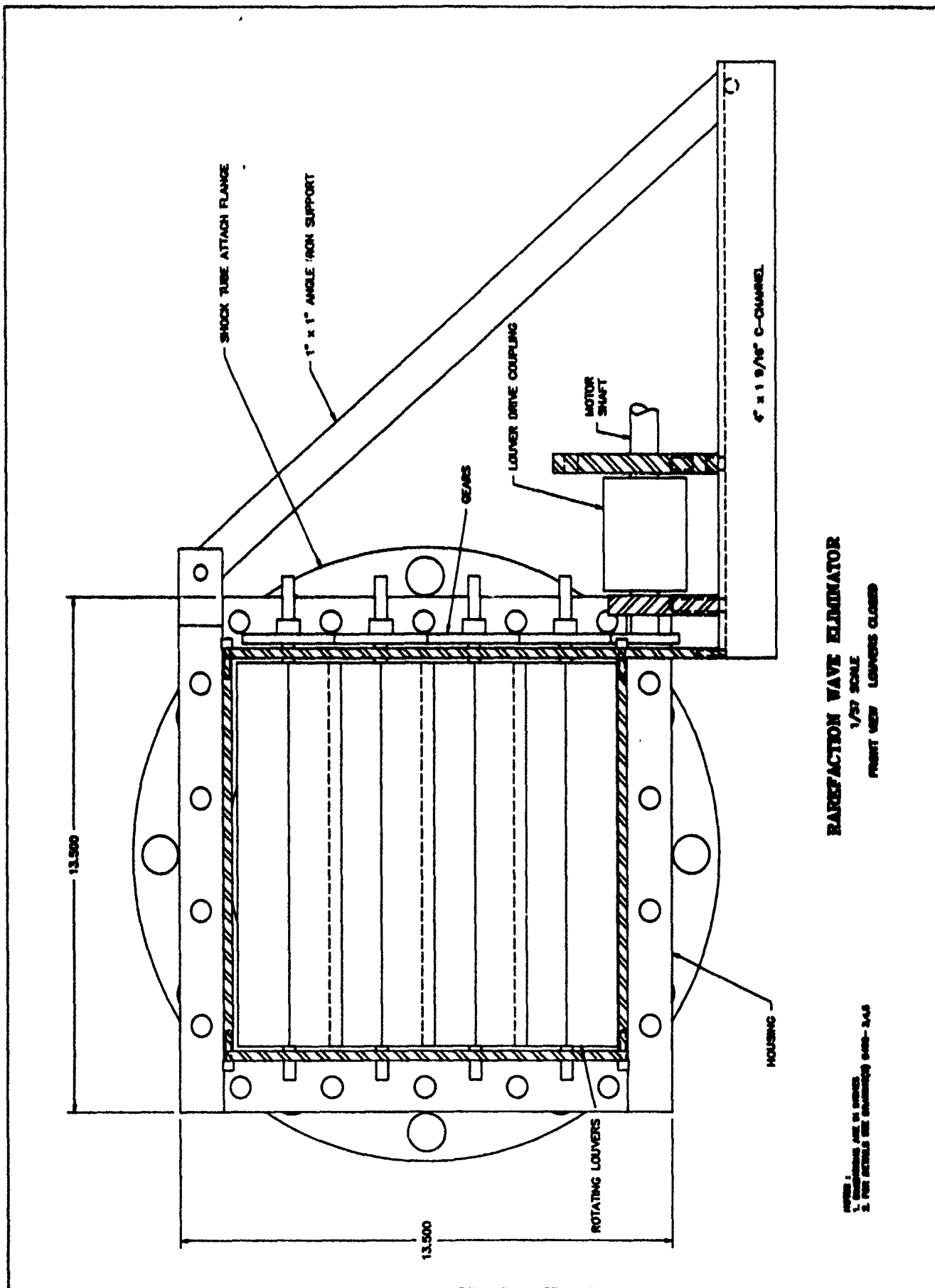
INTENTIONALLY LEFT BLANK.



RAREFACTION WAVE ELIMINATOR

1/37 SCALE
FRONT VIEW (OFD)

NOTES:
1. DIMENSIONS ARE IN INCHES
2. FOR DETAILS SEE DRAWINGS 8400-3.4.5

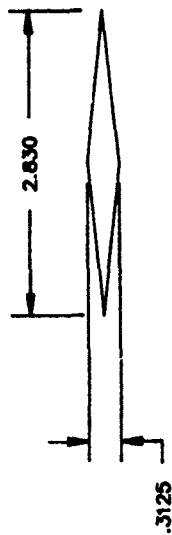


RAREFACTION WAVE ELIMINATOR

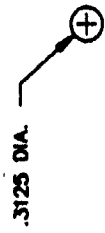
1/37 SCALE

FRONT VIEW LOUVERS CLOSED

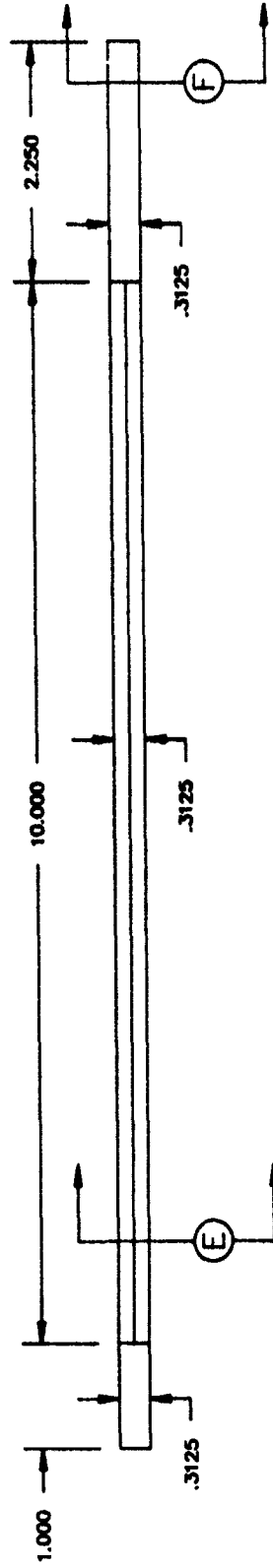
NOTES:
1. DIMENSIONS ARE IN INCHES
2. FOR DETAILS SEE DRAWINGS 6000-343



SECTION E

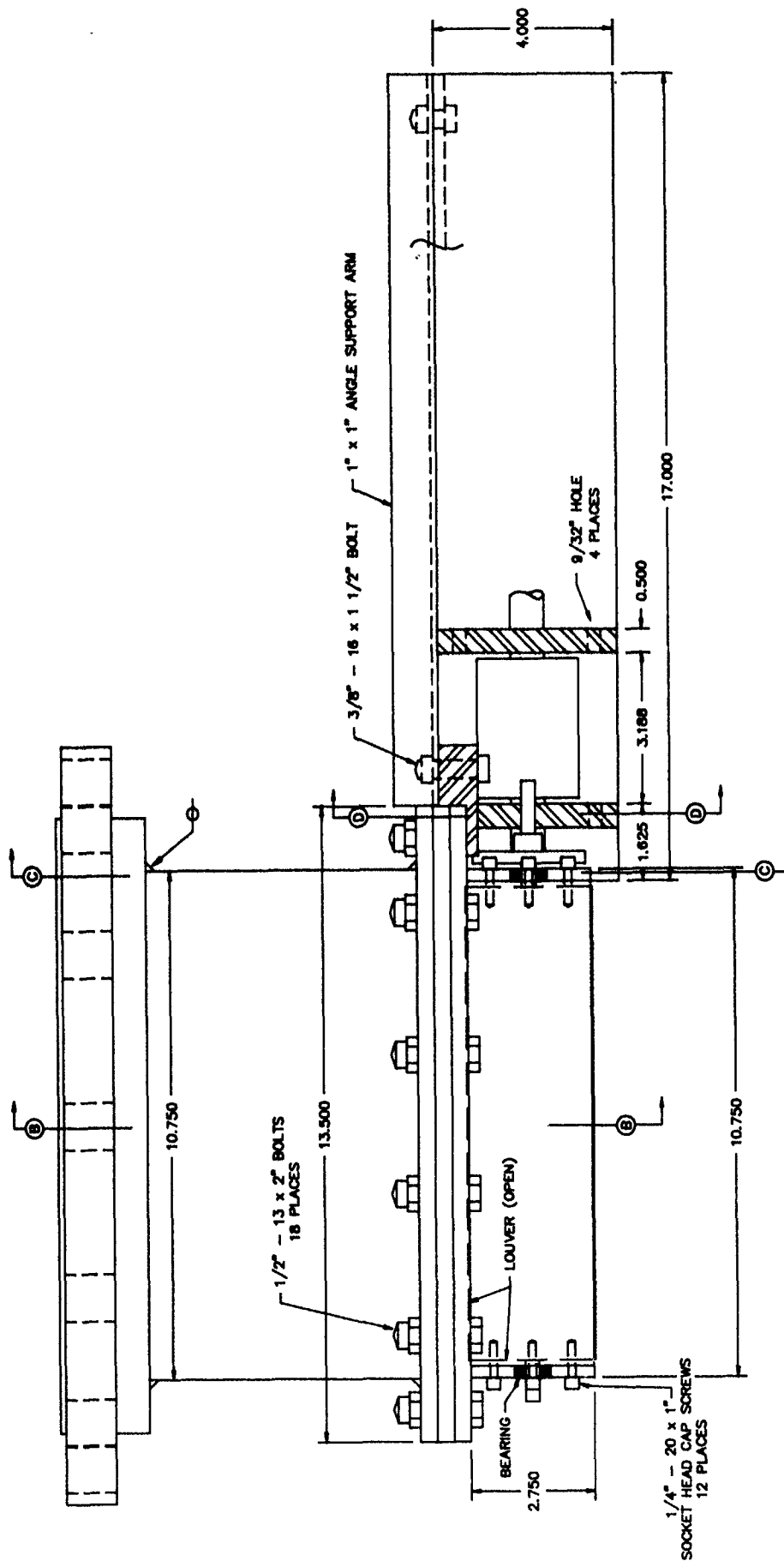


SECTION F



LOUVER DETAIL

NOTES :
1. DIMENSIONS ARE IN INCHES

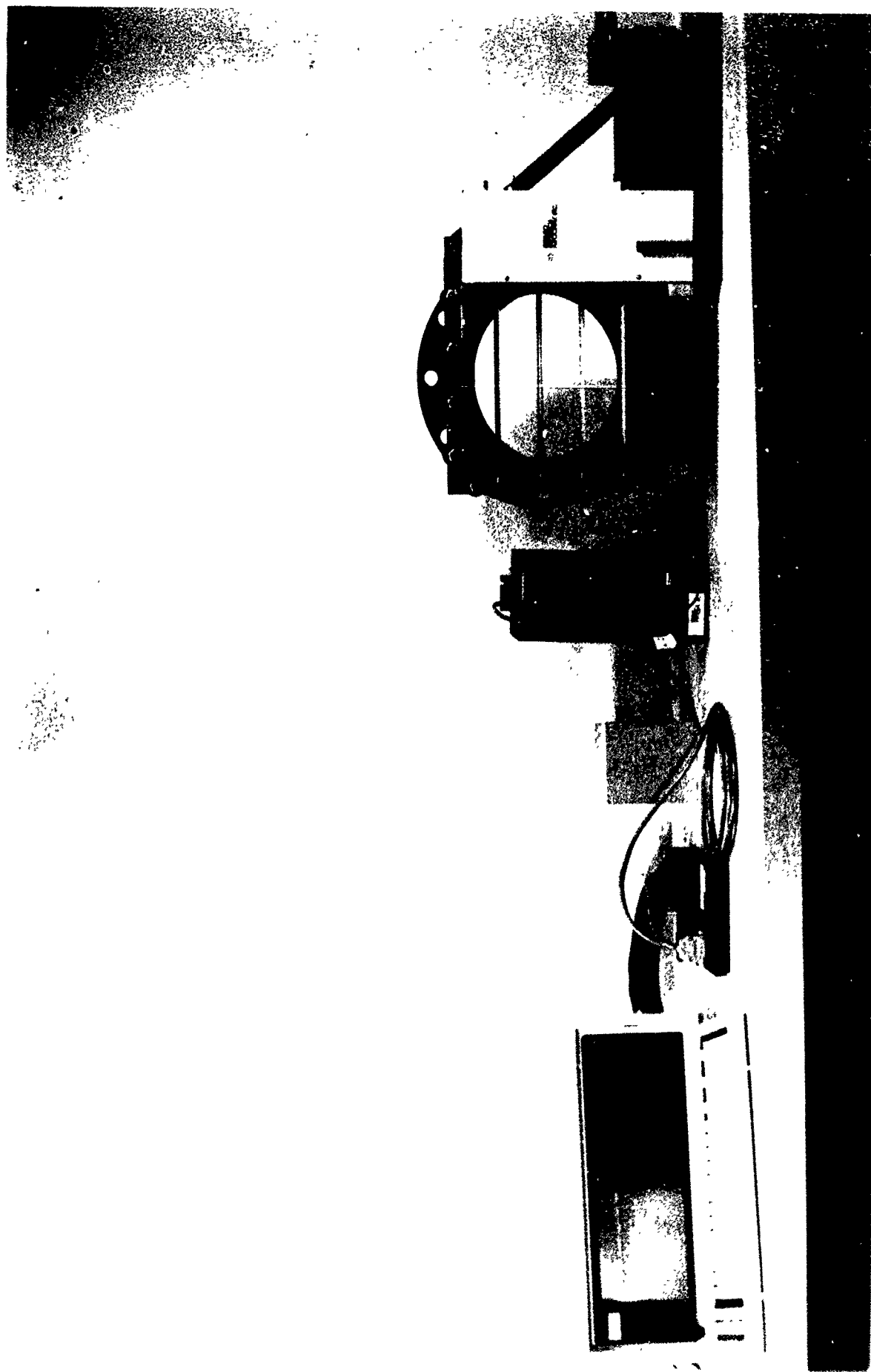


NOTES :

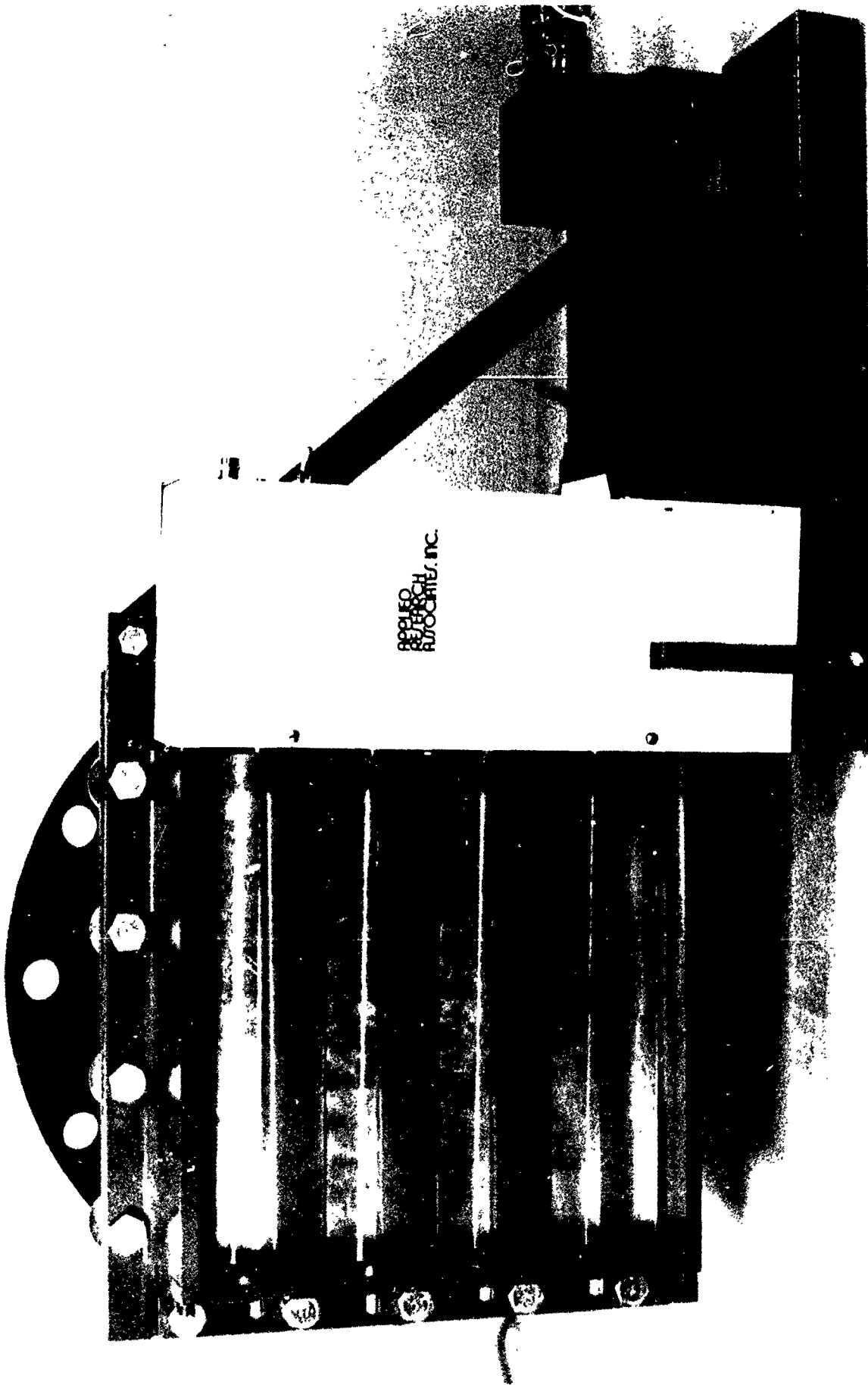
1. DIMENSIONS ARE IN INCHES
2. FOR MORE DETAILS, SEE DRAWINGS 5462- 4,5

R. W. E.

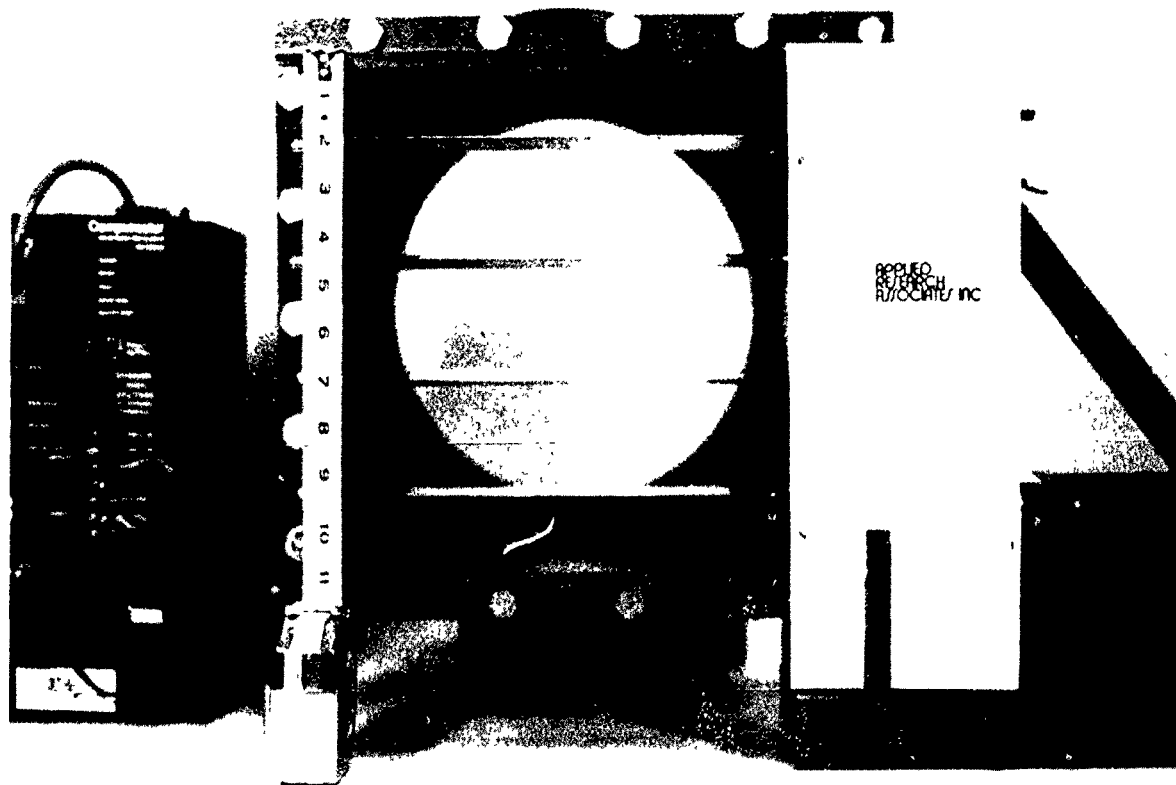
1/57 SCALE - TOP VIEW



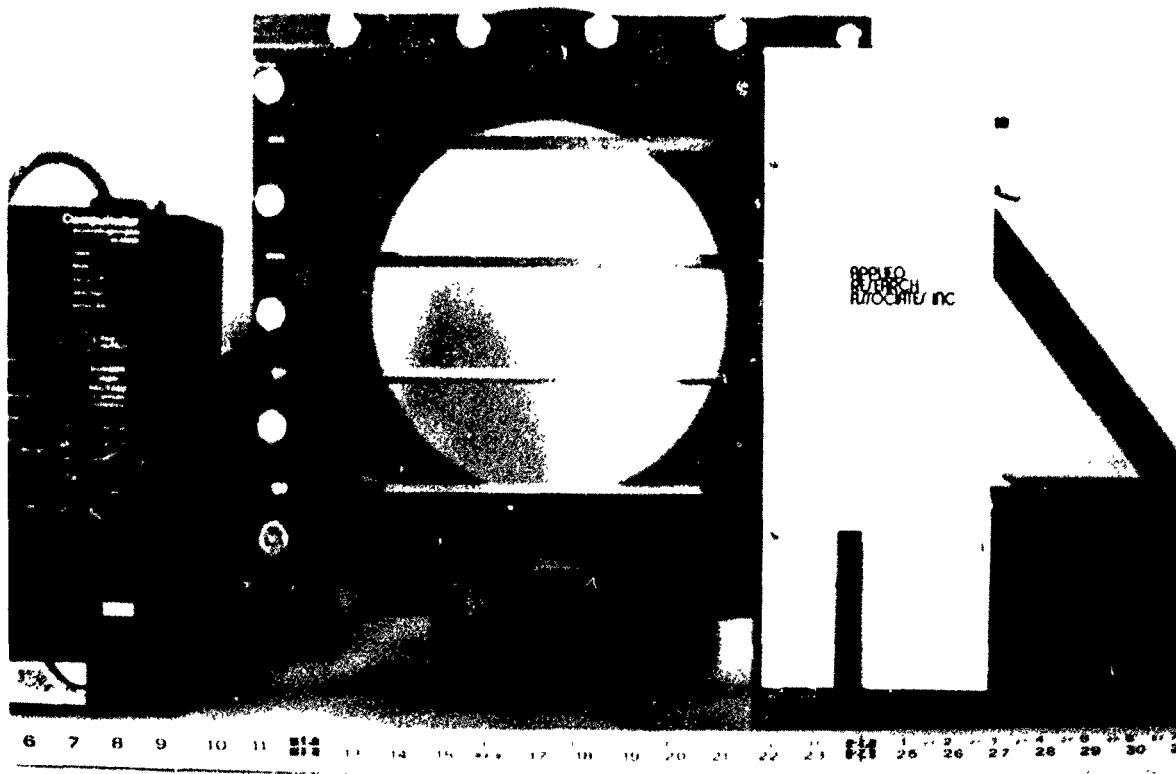
Entire 1/57th scale RWE system



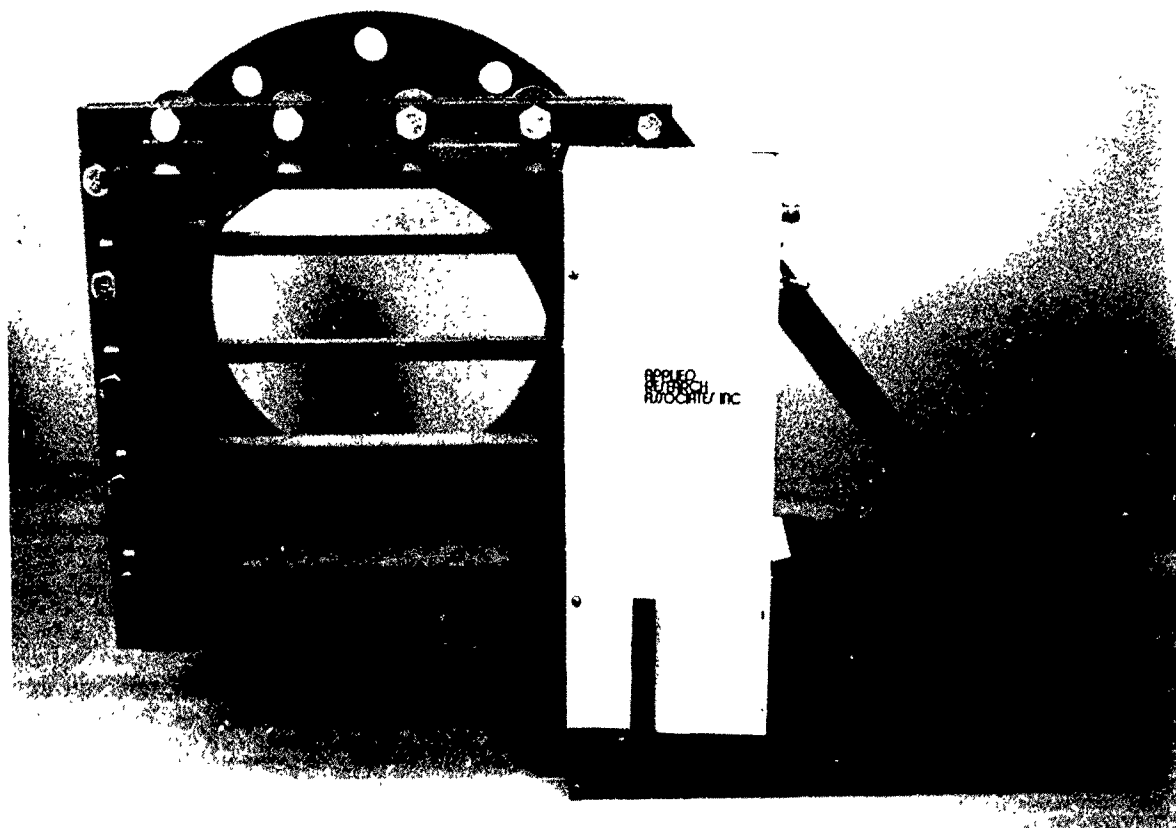
RWE and Servo Motor in closed position



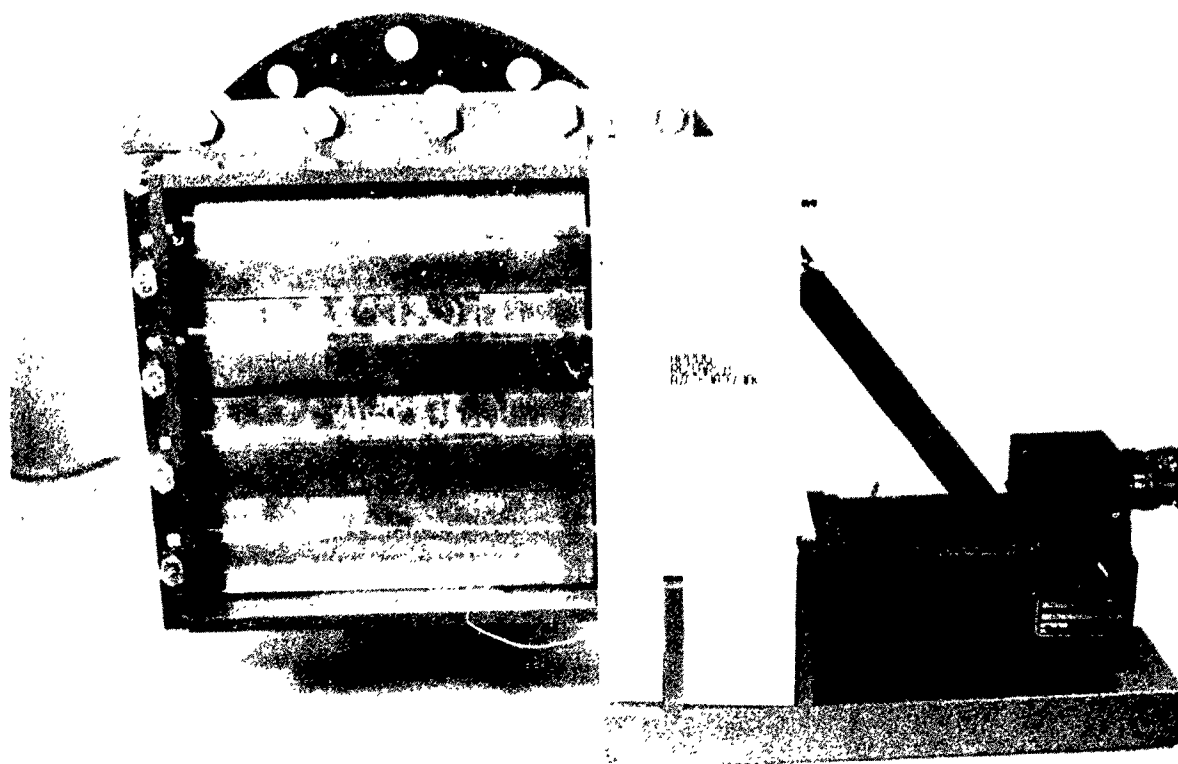
Open RWE with vertical scale



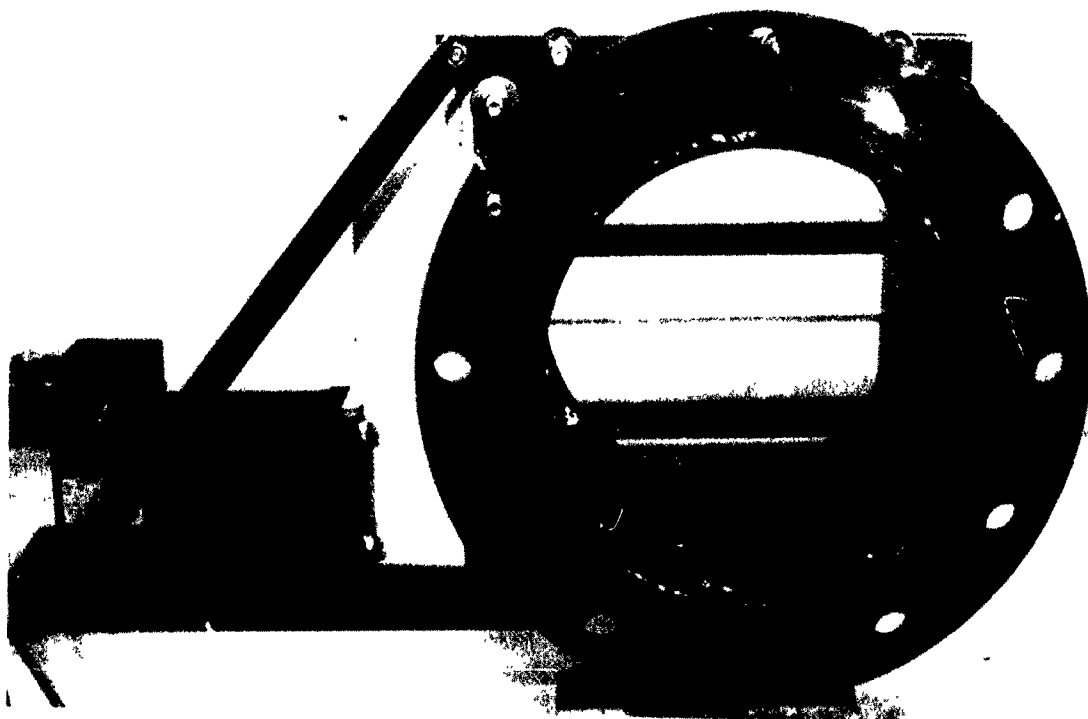
Open RWE with horizontal scale



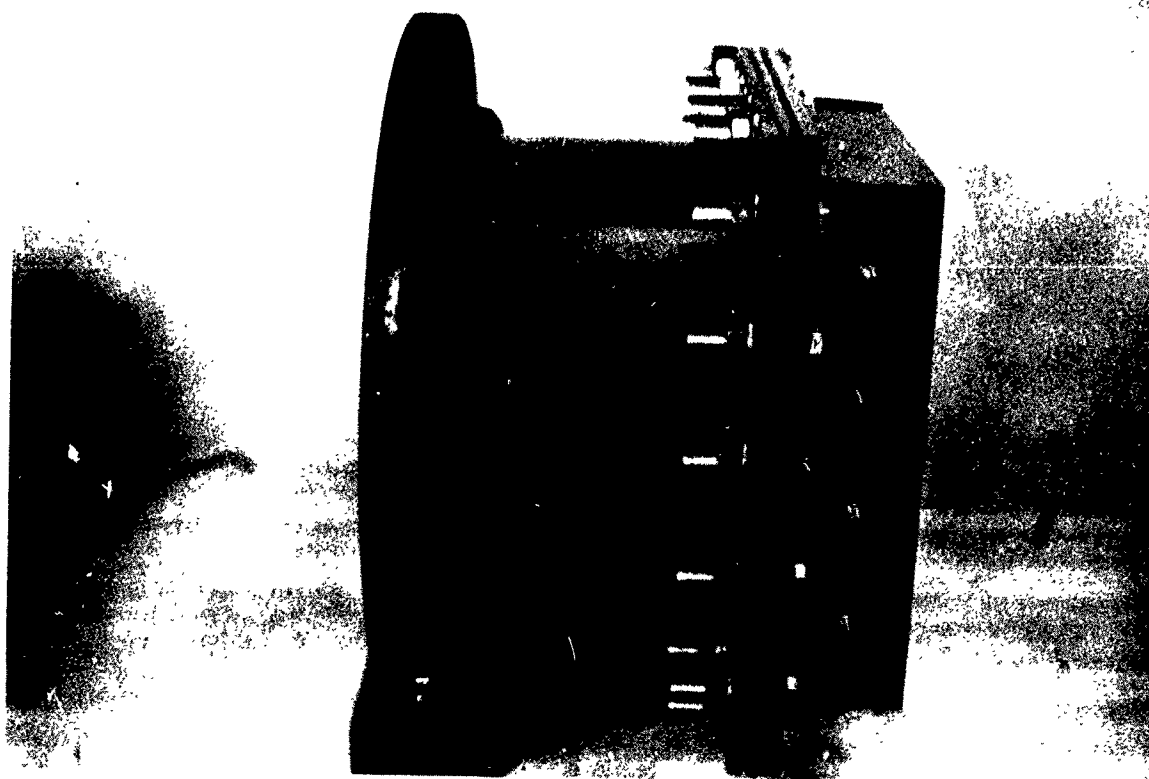
Open RWE close up



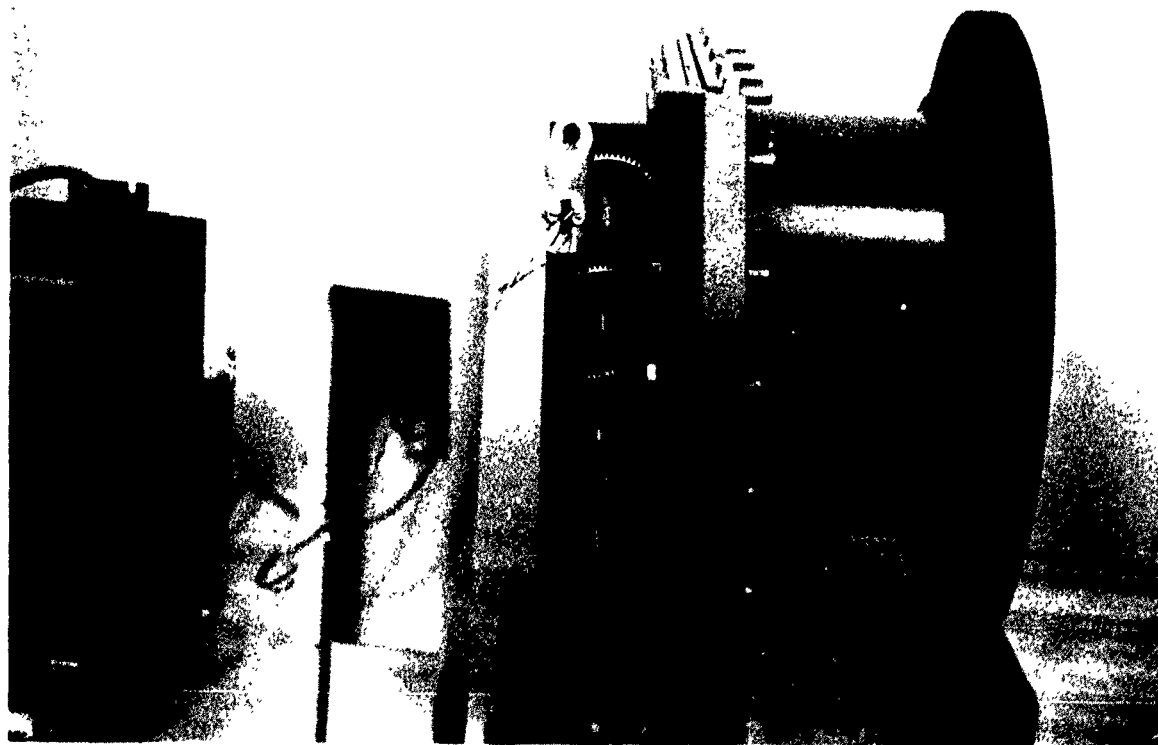
Closed RWE close up



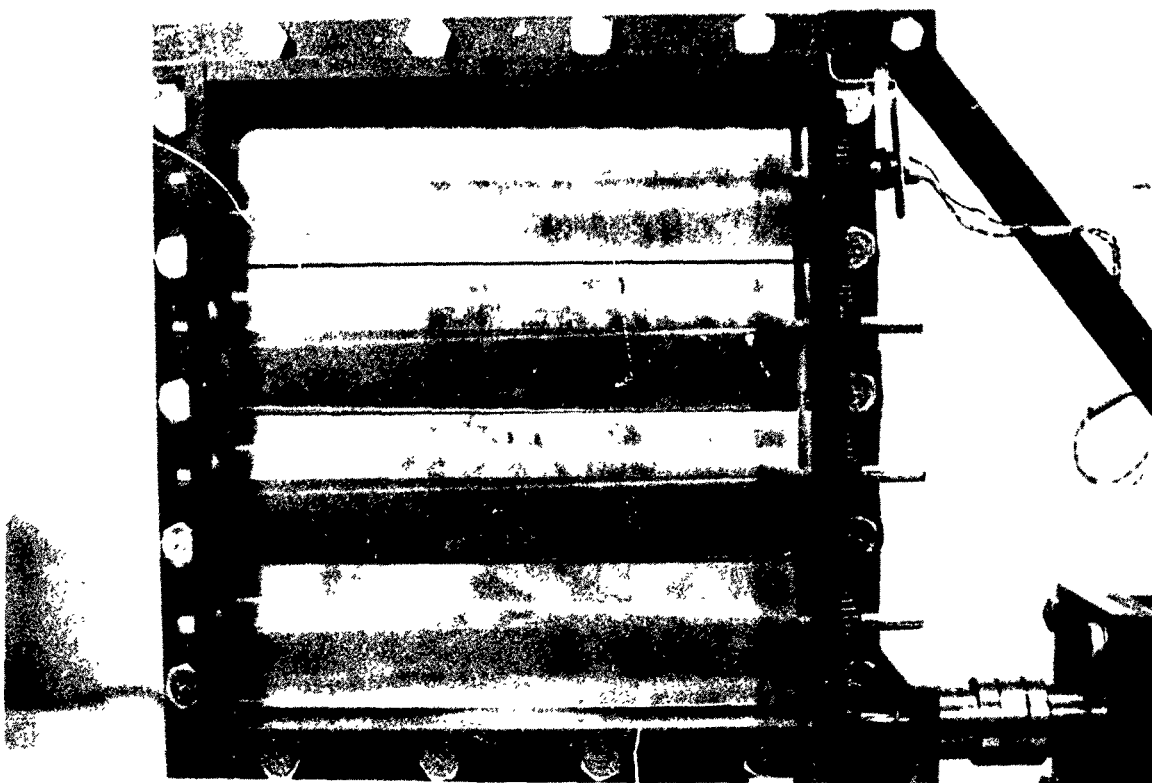
Flange face of RWE



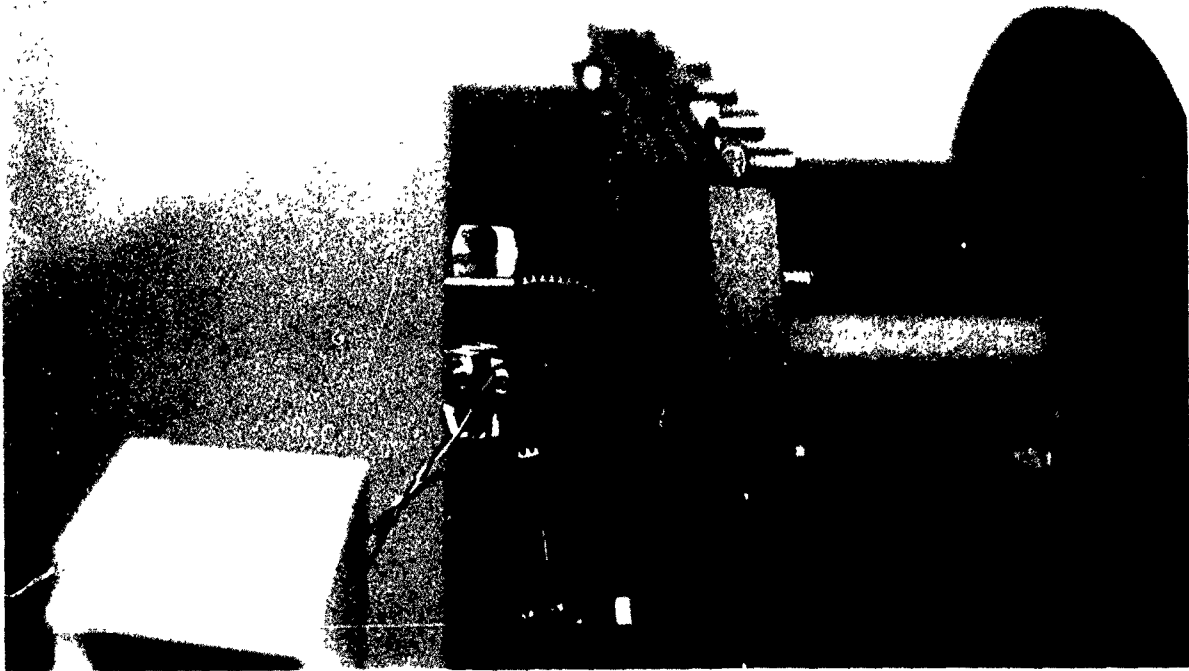
Left side of RWE



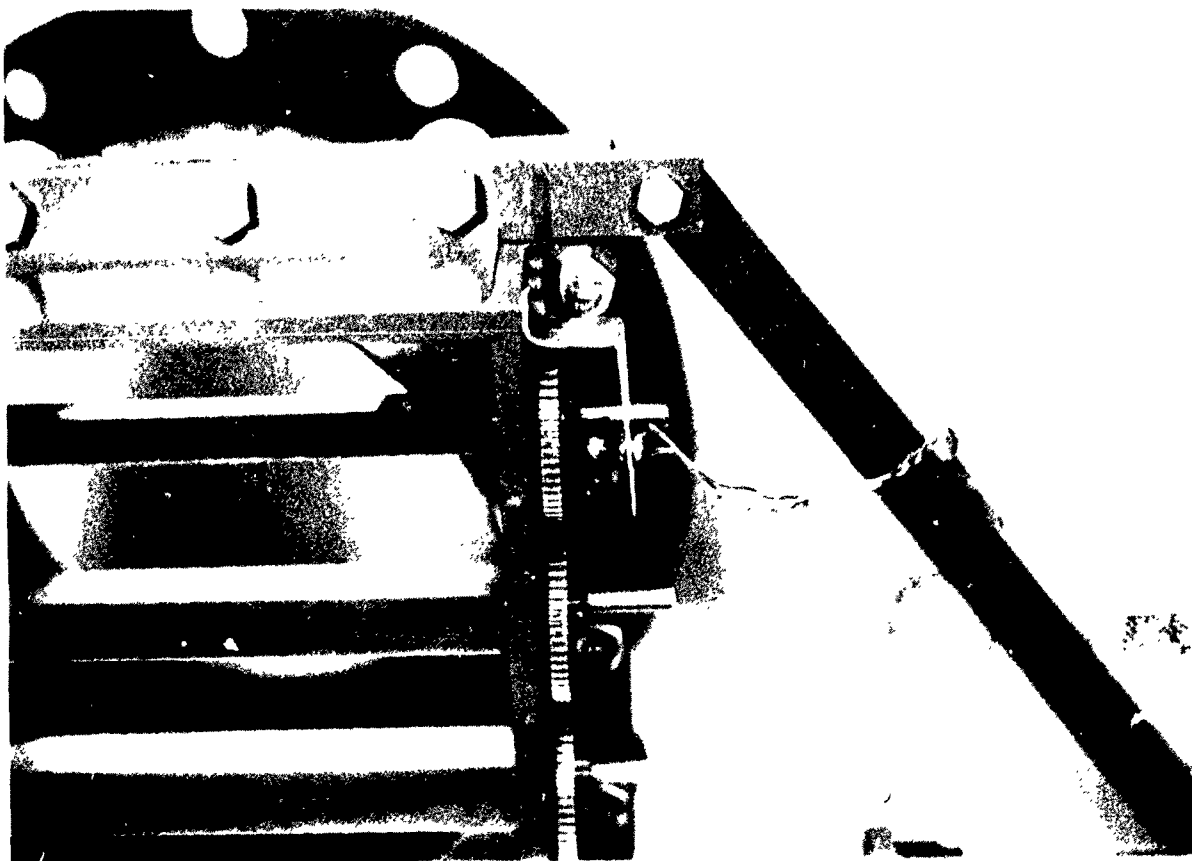
Right side of RWE showing gear train



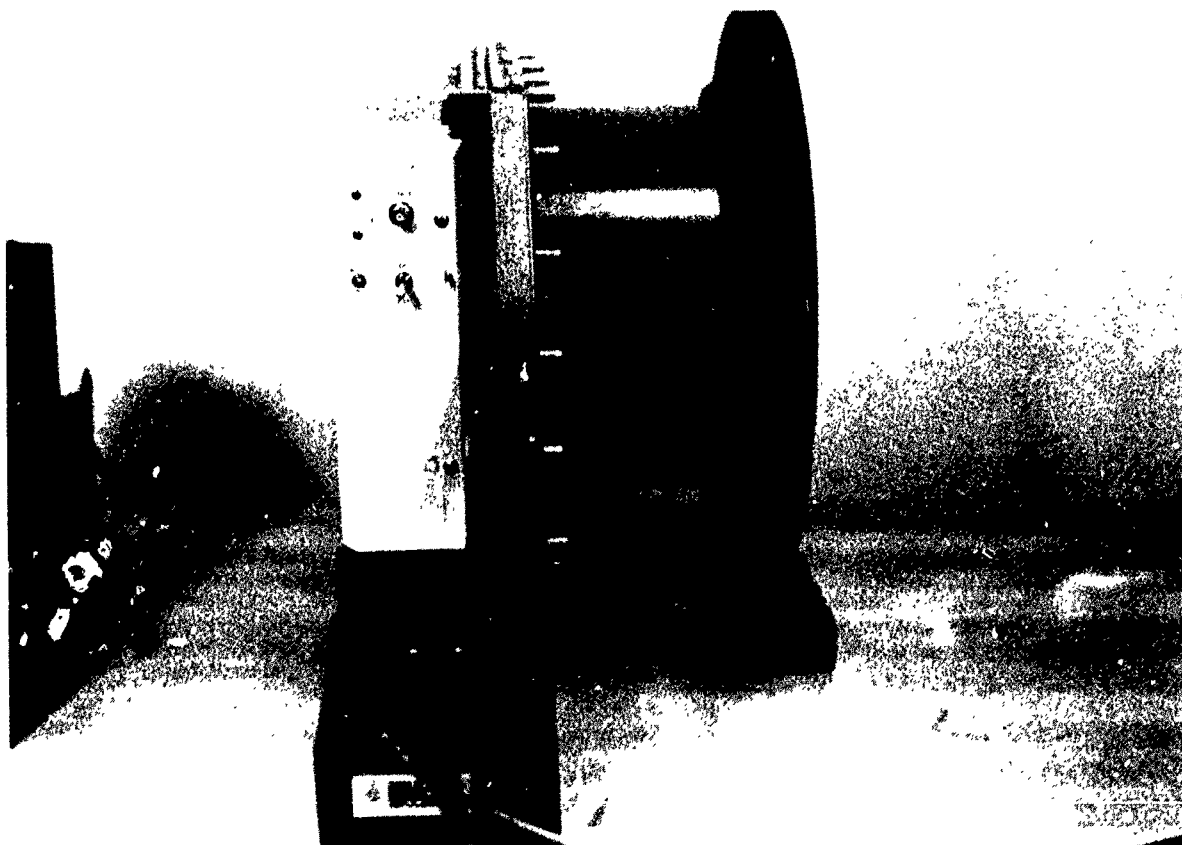
Close up of closed RWE and gear train



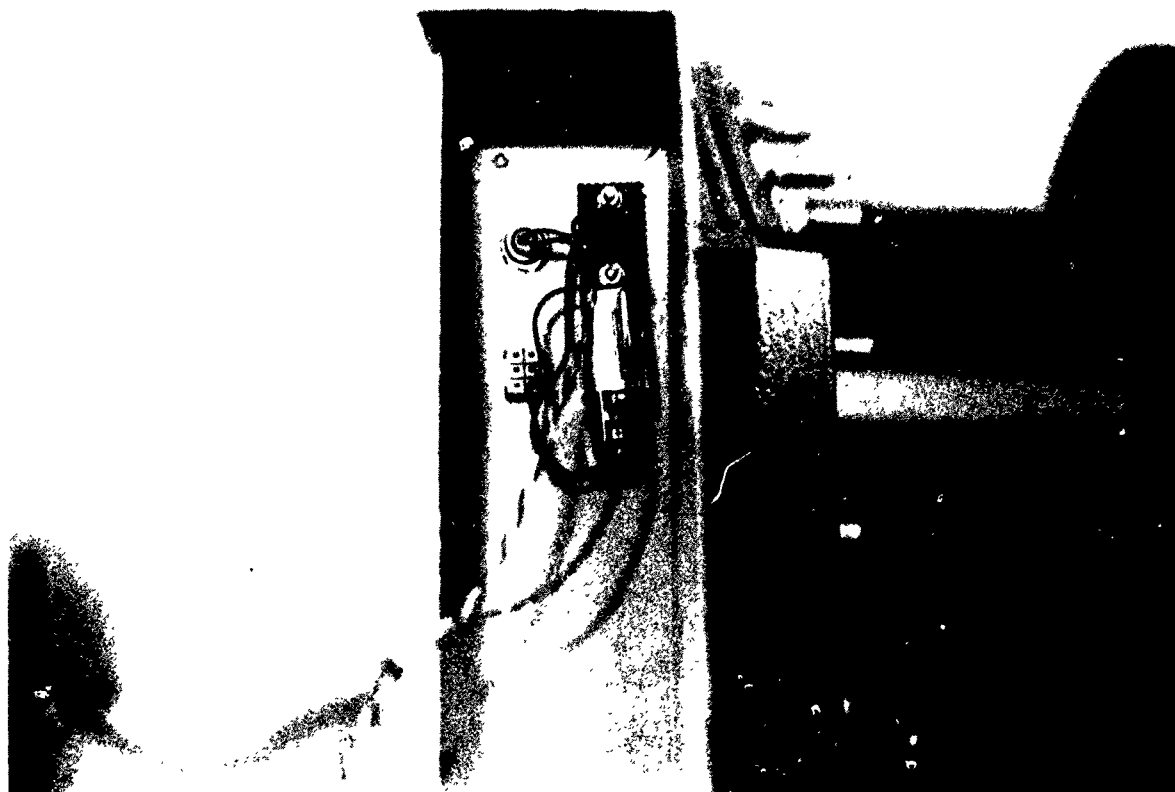
Close up side view of velocity indicator



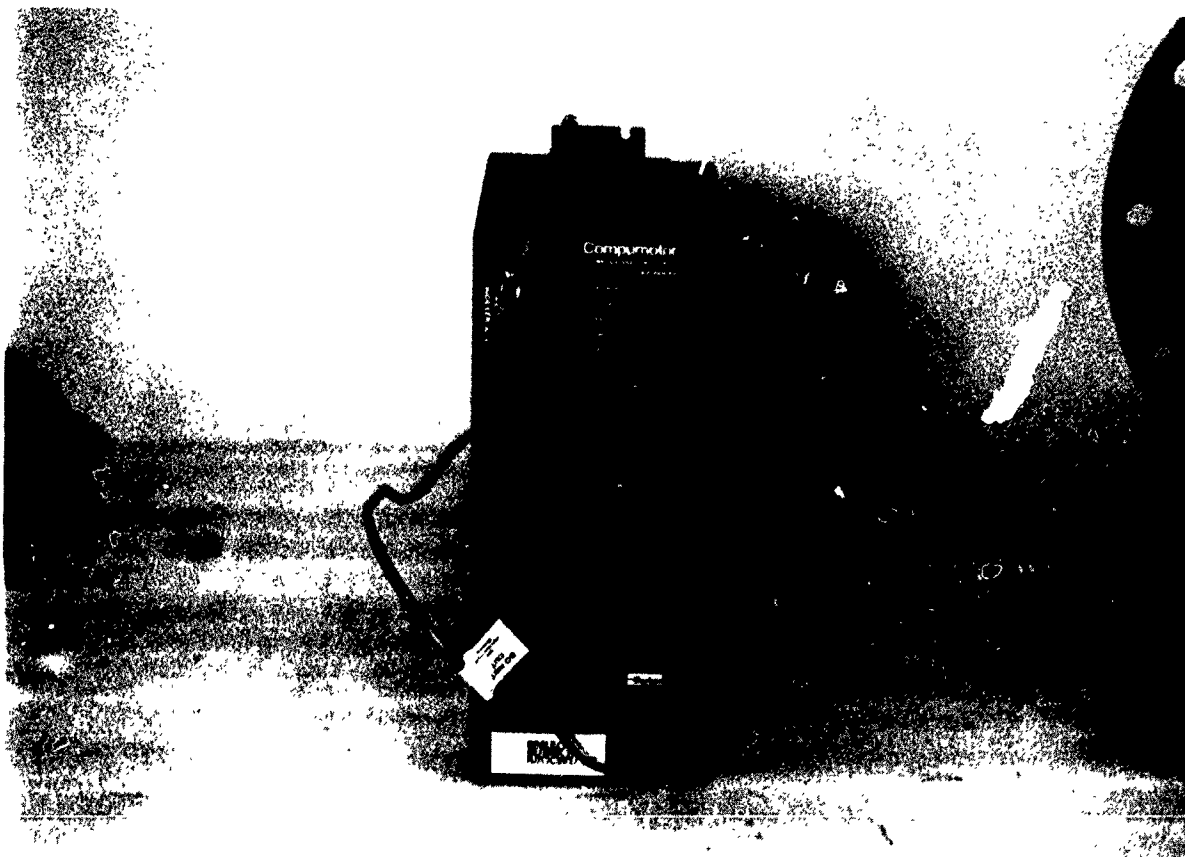
Close up front view of velocity indicator



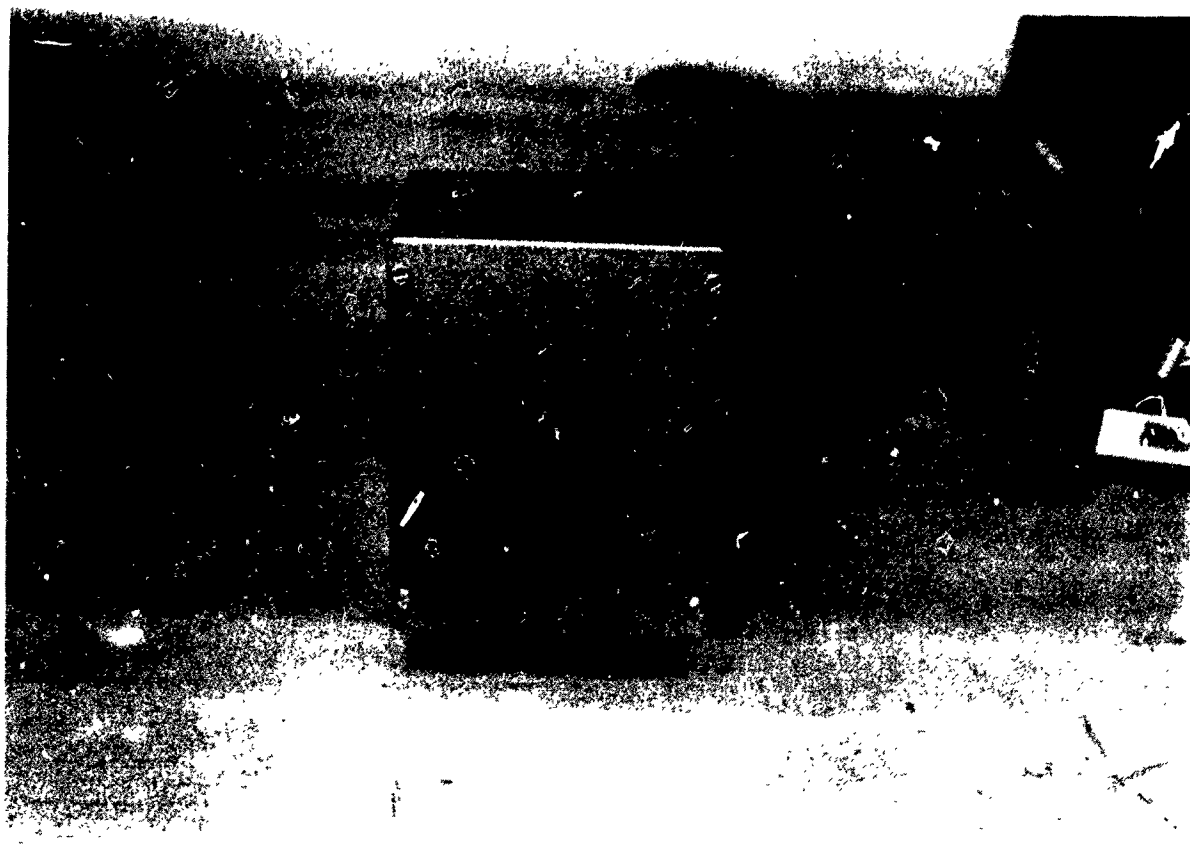
Right side of RWE with gear cover in place



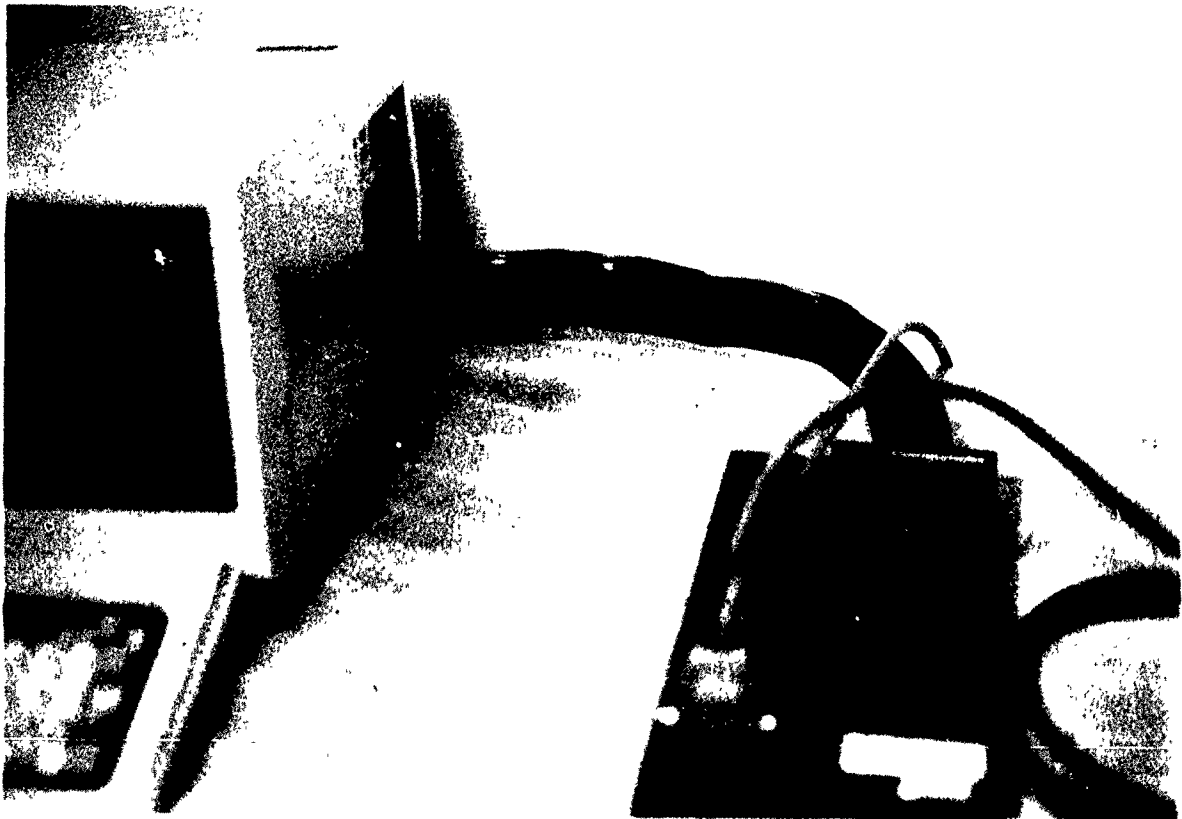
Close up of power supply for velocity indicator



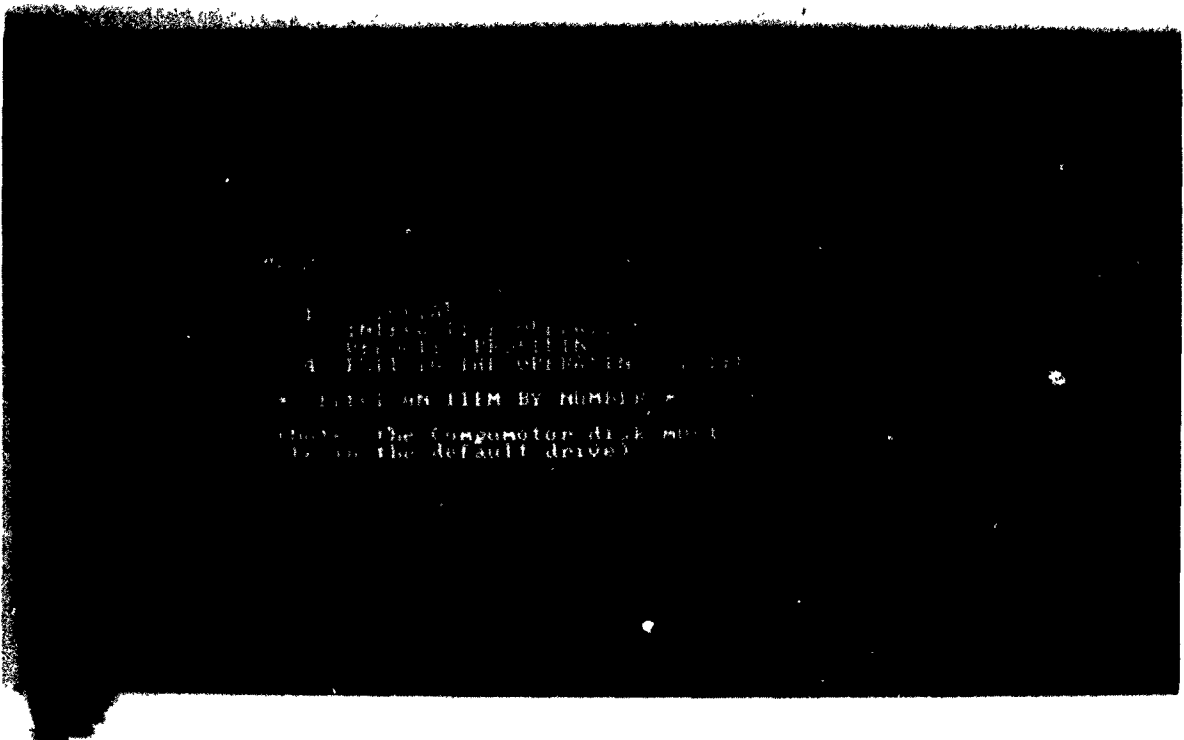
Servo motor controller



Power supply for indexer



Servo motor indexer



PC with sample motion program

INTENTIONALLY LEFT BLANK.

<u>No. of Copies</u>	<u>Organization</u>	<u>No. of Copies</u>	<u>Organization</u>
2	Administrator Defense Technical Info Center ATTN: DTIC-DDA Cameron Station Alexandria, VA 22304-6145	1	Commander U.S. Army Missile Command ATTN: AMSMI-RD-CS-R (DOC) Redstone Arsenal, AL 35898-5010
1	Commander U.S. Army Materiel Command ATTN: AMCAM 5001 Eisenhower Avenue Alexandria, VA 22333-0001	1	Commander U.S. Army Tank-Automotive Command ATTN: ASQNC-TAC-DIT (Technical Information Center) Warren, MI 48397-5000
1	Commander U.S. Army Laboratory Command ATTN: AMSLC-DL 2800 Powder Mill Road Adelphi, MD 20783-1145	1	Director U.S. Army TRADOC Analysis Command ATTN: ATRC-WSR White Sands Missile Range, NM 88002-5502
2	Commander U.S. Army Armament Research, Development, and Engineering Center ATTN: SMCAR-IMI-I Picatinny Arsenal, NJ 07806-5000	1	Commandant U.S. Army Field Artillery School ATTN: ATSF-CSI Ft. Sill, OK 73503-5000
2	Commander U.S. Army Armament Research, Development, and Engineering Center ATTN: SMCAR-TDC Picatinny Arsenal, NJ 07806-5000	(Class. only) 1	Commandant U.S. Army Infantry School ATTN: ATSH-CD (Security Mgr.) Fort Benning, GA 31905-5660
1	Director Benet Weapons Laboratory U.S. Army Armament Research, Development, and Engineering Center ATTN: SMCAR-CCB-TL Watervliet, NY 12189-4050	(Unclass. only) 1	Commandant U.S. Army Infantry School ATTN: ATSH-CD-CSO-OR Fort Benning, GA 31905-5660
(Unclass. only) 1	Commander U.S. Army Armament, Munitions and Chemical Command ATTN: AMSMC-IMF-L Rock Island, IL 61299-5000	1	Air Force Armament Laboratory ATTN: WL/MNOI Eglin AFB, FL 32542-5000 <u>Aberdeen Proving Ground</u>
1	Director U.S. Army Aviation Research and Technology Activity ATTN: SAVRT-R (Library) M/S 219-3 Ames Research Center Moffett Field, CA 94035-1000	2	Dir, USAMSAA ATTN: AMXSY-D AMXSY-MP, H. Cohen
		1	Cdr, USATECOM ATTN: AMSTE-TC
		3	Cdr, CRDEC, AMCCOM ATTN: SMCCR-RSP-A SMCCR-MU SMCCR-MSI
		1	Dir, VLAMO ATTN: AMSLC-VL-D
		10	Dir, BRL ATTN: SLCBR-DD-T

No. of	
<u>Copies</u>	<u>Organization</u>
2	Commander, USACECOM ATTN: AMSEL-RD AMSEL-RO-TPPO-P Fort Monmouth, NJ 07703-5301
1	Commander, USACECOM R & D Technical Library ATTN: ASQNC-ELC-IS-L-R, Myer Center Fort Monmouth, NJ 07703-5000
1	Director U.S. Army Missile and Space Intelligence Center ATTN: AIAMS-YDL Redstone Arsenal, AL 35898-5500
1	Commander U.S. Army Foreign Science and Technology Center ATTN: Research and Data Branch 220 7th Street, NE Charlottesville, VA 22901-5396
1	Director U.S. Army TRAC - Fort Lee ATTN: ATRC-L, Mr. Cameron Fort Lee, VA 23801-6140
1	Director U.S. Army Materials Technology Laboratory ATTN: AMXMR-ATL Watertown, MA 02172-0001
2	Commander U.S. Army Strategic Defense Command ATTN: CSSD-H-MPL, Tech Lib CSSD-H-XM, Dr. Davies P.O. Box 1500 Huntsville, AL 35807
2	Commander U.S. Army Natick Research and Development Center ATTN: AMDNA-D, Dr. D. Sieling STRNC-UE, J. Calligeros Natick, MA 01762

No. of	
<u>Copies</u>	<u>Organization</u>
1	Commander U.S. Army Engineer Division ATTN: HNDED-FD P.O. Box 1500 Huntsville, AL 35807
3	Commander U.S. Army Corps of Engineers Waterways Experiment Station ATTN: CAWES-SS-R, J. Watt CAWES-SE-R, J. Ingram CAWES-TL, Tech Lib P.O. Box 631 Vicksburg, MS 39180-0631
1	Commander U.S. Army Corps of Engineers Fort Worth District ATTN: CESWF-PM-J, R. Timmermans P.O. Box 17300 Fort Worth, TX
1	Commander U.S. Army Research Office ATTN: SLCRO-D P.O. Box 12211 Research Triangle Park, NC 27709-2211
3	Commander U.S. Army Nuclear and Chemical Agency ATTN: ACTA-NAW MONA-WE Tech Lib 7500 Backlick Rd., Bldg. 2073 Springfield, VA 22150
1	Director HQ, TRAC RPD ATTN: ATRC-RPR, Radda Fort Monroe, VA 23651-5143
1	Director TRAC-WSMR ATTN: ATRC-WC, Kirby White Sands Missile Range, NM 88002-5502

No. of Copies	Organization
1	Director TRAC-FLVN ATTN: ATRC Fort Leavenworth, KS 66027-5200
1	Commander U.S. Army Test and Evaluation Command Nuclear Effects Laboratory ATTN: STEWS-TE-NO, Dr. J. L. Meason P.O. Box 477 White Sands Missile Range, NM 88002
2	Chief of Naval Operations ATTN: OP-03EG OP-985F Department of the Navy Washington, DC 20360
1	Director Strategic Systems Projects Office ATTN: NSP-43, Tech Library Department of the Navy Washington, DC 20360
1	Commander Naval Electronic Systems Command ATTN: PME 117-21A Washington, DC 20360
1	Commander Naval Facilities Engineering Command ATTN: Technical Library Washington, DC 20360
1	Commander Naval Sea Systems Command ATTN: Code SEA-62R Department of the Navy Washington, DC 20362-5101
2	Office of Naval Research ATTN: Dr. A. Faulstick, Code 23 (2 cps) 800 N. Quincy Street Arlington, VA 22217

No. of Copies	Organization
1	Officer-in-Charge (Code L31) Civil Engineering Laboratory Naval Construction Battalion Center ATTN: Tech Lib Port Hueneme, CA 93041
1	Commanding Officer (Code L51) Naval Civil Engineering Laboratory ATTN: J. Tancreto Port Hueneme, CA 93043-5003
1	Commander Naval Surface Warfare Center ATTN: Code DX-21, Library Dahlgren, VA 22448-5000
1	Commander David Taylor Research Center ATTN: Code 522, Tech Info Ctr Bethesda, MD 20084-5000
1	Officer-in-Charge White Oak Warfare Center Detachment ATTN: Code E232, Tech Library 10901 New Hampshire Avenue Silver Spring, MD 20903-5000
1	Commanding Officer White Oak Warfare Center ATTN: Code WA501, NNPO Silver Spring, MD 20902-5000
1	Commander (Code 533) Naval Weapons Center ATTN: Tech Library China Lake, CA 93555-6001
1	Commander Naval Weapons Evaluation Fac ATTN: Document Control Kirtland AFB, NM 87117
1	Commander Naval Research Laboratory ATTN: Code 2027, Tech Library Washington, DC 20375

No. of <u>Copies</u>	<u>Organization</u>
1	Director of Defense Research and Engineering ATTN: DD/TWP Washington, DC 20301
1	Assistant Secretary of Defense (Atomic Energy) ATTN: Document Control Washington, DC 20301
1	Chairman Joint Chiefs of Staff ATTN: J-5, R & D Division Washington, DC 20301
2	Deputy Chief of Staff for Operations and Plans ATTN: Technical Library Director of Chemical and Nuclear Operations Department of the Army Washington, DC 20310
1	European Research Office USARDSG (UK) ATTN: Dr. R. Reichenbach Box 65 FPO New York 09510-1500
1	Director Defense Advanced Research Projects Agency ATTN: Tech Lib 1400 Wilson Boulevard Arlington, VA 22209
2	Director Federal Emergency Management Agency ATTN: Public Relations Office Technical Library Washington, DC 20472
1	Chairman DOD Explosives Safety Board Room 856-C Hoffman Bldg. 1 2461 Eisenhower Avenue Alexandria, VA 22331-0600

No. of <u>Copies</u>	<u>Organization</u>
1	Director Defense Intelligence Agency ATTN: DT-2/Weapons and System Div Washington, DC 20301
1	Director National Security Agency ATTN: R15, E. F. Butala Fort Meade, MD 20755
7	Director Defense Nuclear Agency ATTN: CSTI, Tech Lib DDIR DFSP NANS OPNA SPSD SPTD Washington, DC 20305
3	Commander Field Command, DNA ATTN: FCPR FCTMOF NMHE Kirtland AFB, NM 87115
10	Central Intelligence Agency DIR/DB/Standard ATTN: GE-47 HQ (10 cps) Washington, DC 20505
3	Director U.S. Army Harry Diamond Labs ATTN: SLCHD-NW-RA, Belliveau SLCHD-NW-P, Abbe SLCHD-TA-L, Tech Lib 2800 Powder Mill Road Adelphi, MD 20783-1197
1	AL/LSCF ATTN: J. Levine Edwards AFB, CA 93523-5000
1	AL/TSTL (Tech Lib) ATTN: J. Lamb Edwards AFB, CA 93523-5000

No. of Copies	Organization
2	Air Force Armament Laboratory ATTN: AFATL/DOIL AFATL/DLYV Eglin AFB, FL 32542-5000
1	RADC (EMTLD/Docu Library) Griffiss AFB, NY 13441
3	Phillips Laboratory (AFWL) ATTN: NTE NTED NTES Kirtland AFB, NM 87117-6008
1	AFESC/RDCS ATTN: Paul Rosengren Tyndall AFB, FL 32403
1	AFIT ATTN: Tech Lib, Bldg. 640/B Wright-Patterson AFB, OH 45433
1	FTD/NIIS Wright-Patterson AFB, OH 45433
1	INEL ATTN: Spec Programs, J. Patton 2151 North Blvd., MS 2802 Idaho Falls, ID 83415
2	Director Idaho National Engineering Laboratory EG&G Idaho Inc. ATTN: R. Guenzler, MS-3505 R. Holman, MS-3510 P.O. Box 1625 Idaho Falls, ID 83415
1	Director Lawrence Livermore National Laboratory ATTN: Dr. Allan Kuhl 5230 Pacific Concourse Drive, Suite 200 Los Angeles, CA 90045
1	Director Lawrence Livermore National Laboratory ATTN: Tech Info Dept L-3 P.O. Box 808 Livermore, CA 94550

No. of Copies	Organization
2	Director Los Alamos National Laboratory ATTN: Th. Dowler, MS-F602 Doc Control for Reports Library P.O. Box 1663 Los Alamos, NM 87545
3	Director Sandia National Laboratories ATTN: Doc Control 3141 C. Cameron, Div 6215 A. Chabai, Div 7112 P.O. Box 5800 Albuquerque, NM 87185-5800
1	Director Sandia National Laboratories Livermore Laboratory ATTN: Doc Control for Tech Library P.O. Box 969 Livermore, CA 94550
1	Director National Aeronautics and Space Administration ATTN: Scientific and Tech Info Fac P.O. Box 8757, BWI Airport Baltimore, MD 21240
1	Director NASA-Langley Research Center ATTN: Tech Lib Hampton, VA 23665
1	Director NASA-Ames Research Center Applied Computational Aerodynamics Branch ATTN: Dr. T. Holtz, MS 202-14 Moffett Field, CA 94035
1	ADA Technologies, Inc. ATTN: James R. Butz Honeywell Center, Suite 110 304 Inverness Way South Englewood, CO 80112

No. of Copies	Organization
1	Alliant Techsystems, Inc. ATTN: Roger A. Rausch (MN48-3700) 7225 Northland Drive Brooklyn Park, MN 55428
2	Applied Research Associates, Inc. ATTN: J. Keefer N. H. Ethridge P.O. Box 548 Aberdeen, MD 21001
1	Aerospace Corporation ATTN: Tech Info Services P.O. Box 92957 Los Angeles, CA 90009
3	Applied Research Associates, Inc. ATTN: R. L. Guice (3 cps) 7114 West Jefferson Ave., Suite 305 Lakewood, CO 80235
1	Black and Veatch, Engineers - Architects ATTN: H. D. Laverentz 1500 Meadow Lake Parkway Kansas City, MO 64114
1	The Boeing Company ATTN: Aerospace Library P.O. Box 3707 Seattle, WA 98124
1	California Research and Technology, Inc. ATTN: M. Rosenblatt 20943 Devonshire Street Chatsworth, CA 91311
1	Carpenter Research Corporation ATTN: H. Jerry Carpenter 27520 Hawthorne Blvd., Suite 263 P.O. Box 2490 Rolling Hills Estates, CA 90274
1	Dynamics Technology, Inc. ATTN: D. T. Hove 21311 Hawthorne Blvd., Suite 300 Torrance, CA 90503

No. of Copies	Organization
1	EATON Corporation Defense Valve and Actuator Div ATTN: J. Wada 2338 Alaska Ave. El Segundo, CA 90245-4896
2	FMC Corporation Advanced Systems Center ATTN: J. Drotleff C. Krebs, MDP95 Box 58123 2890 De La Cruz Blvd. Santa Clara, CA 95052
1	Goodyear Aerospace Corporation ATTN: R. M. Brown, Bldg. 1 Shelter Engineering Litchfield Park, AZ 85340
4	Kaman AviDyne ATTN: R. Ruetenik (2 cps) S. Criscione R. Milligan 83 Second Avenue Northwest Industrial Park Burlington, MA 08130
3	Kaman Sciences Corporation ATTN: Library P. A. Ellis F. H. Shelton P.O. Box 7463 Colorado Springs, CO 80933-7463
2	Kaman-Sciences Corporation ATTN: DASIAC (2 cps) P.O. Drawer 1479 816 State Street Santa Barbara, CA 93102-1479
1	Ktech Corporation ATTN: Dr. E. Gaffney 901 Pennsylvania Ave., N.E. Albuquerque, NM 87111
1	Lockheed Missile and Space Co. ATTN: J. J. Murphy, Dept. 81-11, Bldg. 154 P.O. Box 504 Sunnyvale, CA 94086

No. of	
<u>Copies</u>	<u>Organization</u>
2	McDonnell Douglas Astronautics Corporation ATTN: Robert W. Halprin K. A. Heinly 5301 Bolsa Avenue Huntington Beach, CA 92647
1	Orlando Technology, Inc. ATTN: D. Matuska 60 Second Street, Bldg. 5 Shalimar, FL 32579
1	Physics International Library P.O. Box 5010 San Leandro, CA 94577-0599
2	R&D Associates ATTN: Thomas A. Mazzola Technical Library P.O. Box 9695 Marina Del Rey, CA 90291
1	R&D Associates ATTN: G. P. Ganong P.O. Box 9377 Albuquerque, NM 87119
1	Science Applications International Corporation ATTN: J. Guest 2301 Yale Blvd., SE, Suite E Albuquerque, NM 87106
1	Science Applications International Corporation ATTN: N. Sinha 501 Office Center Drive, Apt. 420 Fort Washington, PA 19034-3211
1	Sparta, Inc. Los Angeles Operations ATTN: I. B. Osofsky 3440 Carson Street Torrance, CA 90503
1	Sunburst Recovery, Inc. ATTN: Dr. C. Young P.O. Box 2129 Steamboat Springs, CO 80477

No. of	
<u>Copies</u>	<u>Organization</u>
1	Sverdrup Technology, Inc. ATTN: R. F. Starr P.O. Box 884 Tullahoma, TN 37388
3	SRI International ATTN: Dr. G. R. Abrahamson Dr. J. Gran Dr. B. Holmes 333 Ravenswood Avenue Menlo Park, CA 94025
2	S-CUBED A Division of Maxwell Laboratories, Inc. ATTN: C. E. Needham L. Kennedy 2501 Yale Blvd., SE Albuquerque, NM 87106
3	S-CUBED A Division of Maxwell Laboratories, Inc. ATTN: Technical Library R. Duff K. Pyatt P.O. Box 1620 La Jolla, CA 92037-1620
1	Texas Engineering Experiment Station ATTN: Dr. D. Anderson 301 Engineering Research Center College Station, TX 77843
1	Thermal Science, Inc. ATTN: R. Feldman 2200 Cassens Dr. St. Louis, MO 63026
1	TRW Ballistic Missile Division ATTN: H. Korman, Mail Station 526/614 P.O. Box 1310 San Bernadino, CA 92402
1	Battelle ATTN: TACTEC Library, J. N. Higgins 505 King Avenue Columbus, OH 43201-2693

No. of

Copies Organization

- 1 California Institute of Technology
ATTN: T. J. Ahrens
1201 E. California Blvd.
Pasadena, CA 91109
- 2 Denver Research Institute
ATTN: J. Wisotski
Technical Library
P.O. Box 10758
Denver, CO 80210
- 1 Massachusetts Institute of Technology
ATTN: Technical Library
Cambridge, MA 02139
- 2 University of New Mexico
New Mexico Engineering Research
Institute (CERF)
ATTN: Dr. J. Leigh
Dr. R. Newell
P.O. Box 25
Albuquerque, NM 87131
- 1 Northrop University
ATTN: Dr. F. B. Safford
5800 W. Arbor Vitae Street
Los Angeles, CA 90045
- 3 Southwest Research Institute
ATTN: Dr. C. Anderson
S. Mullin
A. B. Wenzel
P.O. Drawer 28255
San Antonio, TX 78228-0255
- 1 Stanford University
ATTN: Dr. D. Bershader
Durand Laboratory
Stanford, CA 94305
- 1 State University of New York
Mechanical and Aerospace Engineering
ATTN: Dr. Peyman Givi
Buffalo, NY 14260

No. of

Copies Organization

- Aberdeen Proving Ground
- 1 Cdr, USATECOM
ATTN: AMSTE-TE-F (L. Teletski)
 - 1 Cdr, USATHMA
ATTN: AMXTH-TE
 - 1 Cdr, USACSTA
ATTN: STECS-PO

No. of

Copies Organization

1 University of Toronto
 Institute for Aerospace Studies
 ATTN: Dr. James Gottlieb
 4925 Dufferin Street
 Downsview, Ontario,
 Canada M3H 5T6

INTENTIONALLY LEFT BLANK.

USER EVALUATION SHEET/CHANGE OF ADDRESS

This laboratory undertakes a continuing effort to improve the quality of the reports it publishes. Your comments/answers below will aid us in our efforts.

1. Does this report satisfy a need? (Comment on purpose, related project, or other area of interest for which the report will be used.) _____

2. How, specifically, is the report being used? (Information source, design data, procedure, source of ideas, etc.) _____

3. Has the information in this report led to any quantitative savings as far as man-hours or dollars saved, operating costs avoided, or efficiencies achieved, etc? If so, please elaborate. _____

4. General Comments. What do you think should be changed to improve future reports? (Indicate changes to organization, technical content, format, etc.) _____

BRL Report Number BRL-CR-678 Division Symbol _____

Check here if desire to be removed from distribution list. _____

Check here for address change. _____

Current address: Organization _____
Address _____

DEPARTMENT OF THE ARMY
Director
U.S. Army Ballistic Research Laboratory
ATTN: SLCBR-DD-T
Aberdeen Proving Ground, MD 21005-5066

OFFICIAL BUSINESS

BUSINESS REPLY MAIL

FIRST CLASS PERMIT No 0001, APG, MD

Postage will be paid by addressee

Director
U.S. Army Ballistic Research Laboratory
ATTN: SLCBR-DD-T
Aberdeen Proving Ground, MD 21005-5066



NO POSTAGE
NECESSARY
IF MAILED
IN THE
UNITED STATES

